WOODHEAD PUBLISHING SERIES IN ENERGY

Compendium of Hydrogen Energy

Volume 1: Hydrogen Production and Purification

Edited by Velu Subramani, Angelo Basile and T. Nejat Veziroğlu

WP
WOODHEAD PUBLISHING

Compendium of Hydrogen Energy

Related titles

Polymer electrolyte membrane and direct methanol fuel cell technology Volume 1: Fundamentals and performance of low temperature fuel cells

(ISBN 978-1-74569-773-0)

Polymer electrolyte membrane and direct methanol fuel cell technology Volume 2: In situ characterization techniques for low temperature fuel cells

(ISBN 978-1-84569-774-7)

Handbook of membrane reactors Volume 1: Fundamental materials science, design and optimisation

(ISBN 978-0-85709-414-8)

Woodhead Publishing Series in Energy: Number 83

Compendium of Hydrogen Energy

Volume 1: Hydrogen Production and Purification

Edited by

Velu Subramani, Angelo Basile and T. Nejat Veziroğlu

AMSTERDAM • BOSTON • CAMBRIDGE • HEIDELBERG
LONDON • NEW YORK • OXFORD • PARIS • SAN DIEGO
SAN FRANCISCO • SINGAPORE • SYDNEY • TOKYO
Woodhead Publishing is an imprint of Elsevier

Woodhead Publishing is an imprint of Elsevier
80 High Street, Sawston, Cambridge, CB22 3HJ, UK
225 Wyman Street, Waltham, MA 02451, USA
Langford Lane, Kidlington, OX5 1GB, UK

Notice
No responsibility is assumed by the publisher for any injury and/or damage to persons or property as a matter of products liability, negligence or otherwise, or from any use or operation of any methods, products, instructions or ideas contained in the material herein. Because of rapid advances in the medical sciences, in particular, independent verification of diagnoses and drug dosages should be made.

British Library Cataloguing in Publication Data
A catalogue record for this book is available from the British Library

Library of Congress Control Number: 2015932007

ISBN 978-1-78242-361-4 (print)
ISBN 978-1-78242-383-6 (online)

Contents

List of contributors

E. Acha Department of Chemical and Environmental Engineering, University of the Basque Country (UPV/EHU), Bilbao, Spain

C. Agrafiotis German Aerospace Center (DLR), Köln, Germany

S.I. Allakhverdiev Institute of Plant Physiology, Russian Academy of Sciences, Moscow, Russia; Institute of Basic Biological Problems, Russian Academy of Sciences, Moscow Region, Russia; M.V. Lomonosov Moscow State University, Moscow, Russia

E.J. Anthony Cranfield University, Cranfield, UK

A. Basile Institute on Membrane Technology of the Italian National Research Council (ITM-CNR), Rende, Italy

B. Bensmann Gottfried Wilhelm Leibniz Universität Hannover, Hannover, Germany

P. Bernardo Institute on Membrane Technology of the Italian National Research Council (ITM-CNR), Rende, Italy

G. Bonura Istituto di Tecnologie Avanzate per l'Energia "Nicola Giordano," Messina, Italy

J.F. Cambra Department of Chemical and Environmental Engineering, University of the Basque Country (UPV/EHU), Bilbao, Spain

P.A. Charpentier Western University, London, ON, Canada

P.E. Dodds University College London, London, UK

J.L.G. Fierro Institute of Catalysis and Petroleum Chemistry, Energy and Sustainable Chemistry Group, CSIC, Cantoblanco, Madrid, Spain

F. Frusteri Istituto di Tecnologie Avanzate per l'Energia "Nicola Giordano," Messina, Italy

L. García Universidad de Zaragoza, Zaragoza, Spain

R. Guil Institute of Catalysis and Petroleum Chemistry, Energy and Sustainable Chemistry Group, CSIC, Cantoblanco, Madrid, Spain

R. Hanke-Rauschenbach Gottfried Wilhelm Leibniz Universität Hannover, Hannover, Germany

M.Z. Hossain Western University, London, ON, Canada

H. Idriss Corporate Research and Innovation (CRI), SABIC-KAUST, Thuwal, Saudi Arabia

K. Inoue Research Institute for Photobiological Hydrogen Production, Kanagawa University, Tsuchiya, Hiratsuka, Kanagawa, Japan

A. Iulianelli Institute on Membrane Technology of the Italian National Research Council (ITM-CNR), Rende, Italy

J.C. Jansen Institute on Membrane Technology of the Italian National Research Council (ITM-CNR), Rende, Italy

A.R. Koirala Sogang University, Shinsu-dong, Seoul, Republic of Korea

D.H. Lee Korea Institute of Machinery and Materials, Yuseong-Gu, Daejeon, Republic of Korea

H. Masukawa Research Institute for Photobiological Hydrogen Production, Kanagawa University, Tsuchiya, Hiratsuka, Kanagawa, Japan

P. Millet University of Paris-Sud, Orsay Cedex, France

J. Mougin CEA-Liten, Grenoble, France

N. Muradov University of Central Florida, Orlando, FL, USA

M.M. Najafpour Institute for Advanced Studies in Basic Sciences (IASBS), Zanjan, Iran

R.M. Navarro Institute of Catalysis and Petroleum Chemistry, Energy and Sustainable Chemistry Group, CSIC, Cantoblanco, Madrid, Spain

R.S. Poudyal Pusan National University, Busan, Republic of Korea; Tribhuvan University, Kirtipur, Kathmandu, Nepal

J.M. Requies Department of Chemical and Environmental Engineering, University of the Basque Country (UPV/EHU), Bilbao, Spain

M. Roeb German Aerospace Center (DLR), Köln, Germany

C. Sattler German Aerospace Center (DLR), Köln, Germany

M. Scott School of Chemical Sciences, The University of Auckland, Auckland, New Zealand

V. Subramani Refining and Logistics Technology, BP Products North America, Inc., Naperville, IL, USA

I. Tiwari Pusan National University, Busan, Republic of Korea

T. Tomo Tokyo University of Science, Kagurazaka, Shinjuku-ku, Tokyo, Japan

J. Tong Colorado School of Mines, Golden, CO, USA

T.N. Veziroğlu International Association for Hydrogen Energy, Miami, FL, USA

Woodhead Publishing Series in Energy

1 **Generating power at high efficiency: Combined cycle technology for sustainable energy production**
Eric Jeffs

2 **Advanced separation techniques for nuclear fuel reprocessing and radioactive waste treatment**
Edited by Kenneth L. Nash and Gregg J. Lumetta

3 **Bioalcohol production: Biochemical conversion of lignocellulosic biomass**
Edited by Keith W. Waldron

4 **Understanding and mitigating ageing in nuclear power plants: Materials and operational aspects of plant life management (PLiM)**
Edited by Philip G. Tipping

5 **Advanced power plant materials, design and technology**
Edited by Dermot Roddy

6 **Stand-alone and hybrid wind energy systems: Technology, energy storage and applications**
Edited by John K. Kaldellis

7 **Biodiesel science and technology: From soil to oil**
Jan C. J. Bart, Natale Palmeri and Stefano Cavallaro

8 **Developments and innovation in carbon dioxide (CO_2) capture and storage technology Volume 1: Carbon dioxide (CO_2) capture, transport and industrial applications**
Edited by M. Mercedes Maroto-Valer

9 **Geological repository systems for safe disposal of spent nuclear fuels and radioactive waste**
Edited by Joonhong Ahn and Michael J. Apted

10 **Wind energy systems: Optimising design and construction for safe and reliable operation**
Edited by John D. Sørensen and Jens N. Sørensen

11 **Solid oxide fuel cell technology: Principles, performance and operations**
Kevin Huang and John Bannister Goodenough

12 **Handbook of advanced radioactive waste conditioning technologies**
Edited by Michael I. Ojovan

13 **Membranes for clean and renewable power applications**
Edited by Annarosa Gugliuzza and Angelo Basile

14 **Materials for energy efficiency and thermal comfort in buildings**
Edited by Matthew R. Hall

15 **Handbook of biofuels production: Processes and technologies**
Edited by Rafael Luque, Juan Campelo and James Clark

16 **Developments and innovation in carbon dioxide (CO_2) capture and storage technology Volume 2: Carbon dioxide (CO_2) storage and utilisation**
Edited by M. Mercedes Maroto-Valer

17 **Oxy-fuel combustion for power generation and carbon dioxide (CO_2) capture**
Edited by Ligang Zheng
18 **Small and micro combined heat and power (CHP) systems: Advanced design, performance, materials and applications**
Edited by Robert Beith
19 **Advances in clean hydrocarbon fuel processing: Science and technology**
Edited by M. Rashid Khan
20 **Modern gas turbine systems: High efficiency, low emission, fuel flexible power generation**
Edited by Peter Jansohn
21 **Concentrating solar power technology: Principles, developments and applications**
Edited by Keith Lovegrove and Wes Stein
22 **Nuclear corrosion science and engineering**
Edited by Damien Féron
23 **Power plant life management and performance improvement**
Edited by John E. Oakey
24 **Electrical drives for direct drive renewable energy systems**
Edited by Markus Mueller and Henk Polinder
25 **Advanced membrane science and technology for sustainable energy and environmental applications**
Edited by Angelo Basile and Suzana Pereira Nunes
26 **Irradiation embrittlement of reactor pressure vessels (RPVs) in nuclear power plants**
Edited by Naoki Soneda
27 **High temperature superconductors (HTS) for energy applications**
Edited by Ziad Melhem
28 **Infrastructure and methodologies for the justification of nuclear power programmes**
Edited by Agustín Alonso
29 **Waste to energy conversion technology**
Edited by Naomi B. Klinghoffer and Marco J. Castaldi
30 **Polymer electrolyte membrane and direct methanol fuel cell technology Volume 1: Fundamentals and performance of low temperature fuel cells**
Edited by Christoph Hartnig and Christina Roth
31 **Polymer electrolyte membrane and direct methanol fuel cell technology Volume 2: *In situ* characterization techniques for low temperature fuel cells**
Edited by Christoph Hartnig and Christina Roth
32 **Combined cycle systems for near-zero emission power generation**
Edited by Ashok D. Rao
33 **Modern earth buildings: Materials, engineering, construction and applications**
Edited by Matthew R. Hall, Rick Lindsay and Meror Krayenhoff
34 **Metropolitan sustainability: Understanding and improving the urban environment**
Edited by Frank Zeman
35 **Functional materials for sustainable energy applications**
Edited by John A. Kilner, Stephen J. Skinner, Stuart J. C. Irvine and Peter P. Edwards
36 **Nuclear decommissioning: Planning, execution and international experience**
Edited by Michele Laraia
37 **Nuclear fuel cycle science and engineering**
Edited by Ian Crossland
38 **Electricity transmission, distribution and storage systems**
Edited by Ziad Melhem

39 **Advances in biodiesel production: Processes and technologies**
Edited by Rafael Luque and Juan A. Melero
40 **Biomass combustion science, technology and engineering**
Edited by Lasse Rosendahl
41 **Ultra-supercritical coal power plants: Materials, technologies and optimisation**
Edited by Dongke Zhang
42 **Radionuclide behaviour in the natural environment: Science, implications and lessons for the nuclear industry**
Edited by Christophe Poinssot and Horst Geckeis
43 **Calcium and chemical looping technology for power generation and carbon dioxide (CO_2) capture: Solid oxygen- and CO_2-carriers**
Paul Fennell and E. J. Anthony
44 **Materials' ageing and degradation in light water reactors: Mechanisms, and management**
Edited by K. L. Murty
45 **Structural alloys for power plants: Operational challenges and high-temperature materials**
Edited by Amir Shirzadi and Susan Jackson
46 **Biolubricants: Science and technology**
Jan C. J. Bart, Emanuele Gucciardi and Stefano Cavallaro
47 **Advances in wind turbine blade design and materials**
Edited by Povl Brøndsted and Rogier P. L. Nijssen
48 **Radioactive waste management and contaminated site clean-up: Processes, technologies and international experience**
Edited by William E. Lee, Michael I. Ojovan, Carol M. Jantzen
49 **Probabilistic safety assessment for optimum nuclear power plant life management (PLiM): Theory and application of reliability analysis methods for major power plant components**
Gennadij V. Arkadov, Alexander F. Getman and Andrei N. Rodionov
50 **The coal handbook: Towards cleaner production Volume 1: Coal production**
Edited by Dave Osborne
51 **The coal handbook: Towards cleaner production Volume 2: Coal utilisation**
Edited by Dave Osborne
52 **The biogas handbook: Science, production and applications**
Edited by Arthur Wellinger, Jerry Murphy and David Baxter
53 **Advances in biorefineries: Biomass and waste supply chain exploitation**
Edited by Keith Waldron
54 **Geological storage of carbon dioxide (CO_2): Geoscience, technologies, environmental aspects and legal frameworks**
Edited by Jon Gluyas and Simon Mathias
55 **Handbook of membrane reactors Volume 1: Fundamental materials science, design and optimisation**
Edited by Angelo Basile
56 **Handbook of membrane reactors Volume 2: Reactor types and industrial applications**
Edited by Angelo Basile
57 **Alternative fuels and advanced vehicle technologies for improved environmental performance: Towards zero carbon transportation**
Edited by Richard Folkson

58 **Handbook of microalgal bioprocess engineering**
Christopher Lan and Bei Wang
59 **Fluidized bed technologies for near-zero emission combustion and gasification**
Edited by Fabrizio Scala
60 **Managing nuclear projects: A comprehensive management resource**
Edited by Jas Devgun
61 **Handbook of Process Integration (PI): Minimisation of energy and water use, waste and emissions**
Edited by Jiří J. Klemeš
62 **Coal power plant materials and life assessment**
Edited by Ahmed Shibli
63 **Advances in hydrogen production, storage and distribution**
Edited by Ahmed Basile and Adolfo Iulianelli
64 **Handbook of small modular nuclear reactors**
Edited by Mario D. Carelli and Dan T. Ingersoll
65 **Superconductors in the power grid: Materials and applications**
Edited by Christopher Rey
66 **Advances in thermal energy storage systems: Methods and applications**
Edited by Luisa F. Cabeza
67 **Advances in batteries for medium and large-scale energy storage**
Edited by Chris Menictas, Maria Skyllas-Kazacos and Tuti Mariana Lim
68 **Palladium membrane technology for hydrogen production, carbon capture and other applications**
Edited by Aggelos Doukelis, Kyriakos Panopoulos, Antonios Koumanakos and Emmanouil Kakaras
69 **Gasification for synthetic fuel production: Fundamentals, processes and applications**
Edited by Rafael Luque and James G. Speight
70 **Renewable heating and cooling: Technologies and applications**
Edited by Gerhard Stryi-Hipp
71 **Environmental remediation and restoration of contaminated nuclear and NORM sites**
Edited by Leo van Velzen
72 **Eco-friendly innovation in electricity networks**
Edited by Jean-Luc Bessede
73 **The 2011 Fukushima nuclear power plant accident: How and why it happened**
Yotaro Hatamura, Seiji Abe, Masao Fuchigami and Naoto Kasahara. Translated by Kenji Iino
74 **Lignocellulose biorefinery engineering: Principles and applications**
Hongzhang Chen
75 **Advances in membrane technologies for water treatment: Materials, processes and applications**
Edited by Angelo Basile, Alfredo Cassano and Navin Rastogi
76 **Membrane reactors for energy applications and basic chemical production**
Edited by Angelo Basile, Luisa Di Paola, Faisal Hai and Vincenzo Piemonte
77 **Pervaporation, vapour permeation and membrane distillation: Principles and applications**
Edited by Angelo Basile, Alberto Figoli and Mohamed Khayet
78 **Safe and secure transport and storage of radioactive materials**
Edited by Ken Sorenson

79 **Reprocessing and recycling of spent nuclear fuel**
Edited by Robin Taylor
80 **Advances in battery technologies for electric vehicles**
Edited by Bruno Scrosati, Juergen Garche and Werner Tillmetz
81 **Rechargeable lithium batteries: From fundamentals to applications**
Edited by Alejandro A. Franco
82 **Calcium and chemical looping technology for power generation and carbon dioxide (CO_2) capture**
Edited by Paul Fennell and Ben Anthony
83 **Compendium of Hydrogen Energy Volume 1: Hydrogen Production and Purificiation**
Edited by Velu Subramani, Angelo Basile and T. Nejat Veziroğlu
84 **Compendium of Hydrogen Energy Volume 2: Hydrogen Storage, Transmission, Transportation and Infrastructure**
Edited by Ram Gupta, Angelo Basile and T. Nejat Veziroğlu
85 **Compendium of Hydrogen Energy Volume 3: Hydrogen Energy Conversion**
Edited by Frano Barbir, Angelo Basile and T. Nejat Veziroğlu
86 **Compendium of Hydrogen Energy Volume 4: Hydrogen Use, Safety and the Hydrogen Economy**
Edited by Michael Ball, Angelo Basile and T. Nejat Veziroğlu

This page intentionally left blank

Part One

Introduction to hydrogen

This page intentionally left blank

Introduction to hydrogen and its properties

1

H. Idriss[1], *M. Scott*[2], *V. Subramani*[3]
[1]Corporate Research and Innovation (CRI), SABIC-KAUST, Thuwal, Saudi Arabia;
[2]School of Chemical Sciences, The University of Auckland, Auckland, New Zealand;
[3]Refining and Logistics Technology, BP Products North America, Inc., Naperville, IL, USA

1.1 Introduction

Hydrogen, the first element on the periodic table with an atomic number of 1, is truly in a class by itself. It does not belong to any family of elements. Although hydrogen is a nonmetal, it is placed on the left side of the periodic table along with the first group alkali metals, but obviously, hydrogen does not belong to the alkali metals family. Hydrogen is the most abundant element in the universe; it is found as interstellar gas and as the chief constituent of main sequence stars. Helium is the other element similar to hydrogen in its simplicity and abundance, and is placed on the same row at the right side of the periodic table. Although helium is a noble gas, and hence it is chemically inert, hydrogen reacts with all sorts of other elements and makes variety of useful compounds. For instance, the bonding of hydrogen with carbon forms the backbone for a vast collection of organic molecules, known as hydrocarbons. Similarly, by bonding with oxygen, hydrogen makes water, the single most important compound on the Earth.

Although hydrogen is the most abundant element, it makes up only about 0.14% of the Earth's crust by weight. It occurs, however, in vast quantities as part of the water in oceans, ice packs, rivers, lakes, and the atmosphere. As part of innumerable carbon compounds, hydrogen is present in all animal and vegetable tissue and in petroleum. Even though it is often said that there are more known compounds of carbon than of any other element, the fact is that, because hydrogen is contained in almost all carbon compounds and also forms a multitude of compounds with all other elements (except some of the noble gases), it is possible that hydrogen compounds are more numerous.

Elementary hydrogen finds its principal industrial application in the manufacture of ammonia; a compound of hydrogen and nitrogen, and in the hydrogenation of carbon monoxide and organic compounds to make a variety of chemicals and fuels. Hydrogen has also been considered as a potential source of power and transportation and, perhaps in the future, as a source of abundant clean energy.

The purpose of this chapter is to provide an overview of hydrogen, its physical and chemical properties, an overview of industrial production, and uses in chemical and energy industries.

Compendium of Hydrogen Energy. http://dx.doi.org/10.1016/B978-1-78242-361-4.00001-7

1.2 Some historical events (Hoffmann, 2012 and hydrogen fact sheet)

1766	Henry Cavendish, the British scientist, first identified hydrogen as a distinct element after observing a gas evolved by the reaction of zinc metal with hydrochloric acid. In a demonstration to the Royal Society of London, Cavendish applied a spark to hydrogen gas that yielded water (H_2O). This discovery led to his later finding that H_2O is made of hydrogen and oxygen.
1783	Jacquest Alexander Cesar Charles, a French physicist, launched the first hydrogen balloon flight known as Charliere. This unmanned balloon flew to an altitude of 3 km. Three months later, Charles himself flew in his first manned hydrogen balloon.
1788	Based on the discoveries of Cavendish, the French chemist Antoine Lavoisier gave hydrogen its name, which was derived from Greek words: "hydro" and "genes," meaning "water" and "born of."
1800	English scientists William Nicholson and Sir Anthony Carlisle discovered the process of "electrolysis."
1838	Swiss chemist Christian Friedrich Schoenbein discovered the fuel cell effect that produced electric current and pure water by combining hydrogen and oxygen gases.
1845	Sir William Grove, an English scientist and judge, demonstrated Schoenbein's discovery on a practical scale by creating a "gas battery." He earned the title "father of the fuel cell" for his achievement.
1874	Jules Verne, a French author, prophetically examined the potential use of hydrogen as a fuel in his popular work of fiction entitled *The Mysterious Island*.
1889	Ludwig Mond and Charles Langer attempted to build the first fuel cell device using air and industrial coal gas.
1920	German engineer Rudolf Erren converted the internal combustion engines of trucks, buses, and submarines to use hydrogen or hydrogen mixtures. During this period, British scientist and Marxist writer, J.B.S. Haldane, introduced the concept of renewable hydrogen.
1952	The United States of America conducted its first nuclear test of a fusion device, or "hydrogen bomb" at Eniwetok in the Marshall Islands.
1958	The United States formed the National Aeronautics and Space Administration (NASA). NASA's space program currently uses the most liquid hydrogen worldwide, primarily for rocket propulsion and as a fuel for fuel cells.
1959	Francis T. Bacon of Cambridge University in England built the first practical hydrogen-air fuel cell. The 5-kW system powered a welding machine. He named his fuel cell design the "Bacon cell." Later that year, Harry Karl Ihrig, an engineer for the Allis–Chalmers Manufacturing Company, demonstrated the first fuel cell vehicle: a 20-horsepower tractor. Hydrogen fuel cells, based upon Francis T. Bacon's design, have been used to generate on-board electricity, heat, and water for astronauts aboard the Apollo spacecraft and all subsequent space shuttle missions.

1970	Electrochemist John O'M. Bockris coined the term "hydrogen economy" during a discussion at the General Motors (GM) Technical Center in Warren, Michigan. He later published Energy: The Solar-Hydrogen Alternative, describing his envisioned hydrogen economy in which he explains how could cities in the United States be supplied with energy derived from the sun.
1973	The OPEC oil embargo and the resulting supply shock suggested that the era of cheap petroleum had ended and that the world needed alternative fuels. Consequently, the development of hydrogen fuel cells for conventional commercial applications began.
1974	The International association for Hydrogen Energy (IAHE) was formed at the Hydrogen Economy Miami Energy Conference (THEME), the first international conference that Prof. T. Nejat Veziroğlu of the University of Miami, Florida, organized to discuss hydrogen energy.
1976	The International Journal of Hydrogen Energy (IJHE) was established by T. Nejat Veziroğlu as its editor-in-chief, and published by Pergamon Press, to provide a platform for hydrogen energy related scientific papers.
1977	The International Energy Agency (IEA) was established in response to global oil market disruptions. IEA activities included the research and development of hydrogen energy technologies. The U.S. Department of Energy (DOE) was also created during this time.
1989	The National Hydrogen Association (NHA) was formed in the United States with 10 members. Today, the NHA has nearly 100 members.
1990	The United Nations International Standards Organization (ISO), at the initiative of Gustar Grob of Switzerland, established the ISO/TC-197 Committee to prepare the international standards for hydrogen energy technologies.
1990	The world's first solar-powered hydrogen production plant at Solar-Wasserstoff-Bayern, a research and testing facility in Southern Germany, became operational.
1994	Daimler Benz demonstrated its first NECAR I (new electric car) fuel cell vehicle at a press conference in Ulm, Germany.
1998	Iceland unveiled a plan to create the first hydrogen economy by 2030 with Daimler−Benz and Ballard Power Systems.
1999	The Royal Dutch/Shell Company committed to a hydrogen future by forming a hydrogen division. Europe's first hydrogen fueling stations were opened in the German cities of Hamburg and Munich.
2000	Ballard Power Systems presented the world's first production-ready PEM fuel cell for automotive applications at the Detroit auto show.
2004	The world's first fuel cell-powered submarine undergoes deep-water trials (Germany navy).
2013	Honda unveiled its new FCEV concept hydrogen fuel-cell vehicle at the Los Angeles auto show, promising to market the car initially in Japan and the United States in 2015 followed by European introduction. Chiyoda Corp. plans to build what it describes as the world's first large-scale power plant fueled mainly by hydrogen (70%) and natural gas (30%).

1.3 Physical and chemical properties

Naturally, hydrogen exists in molecular form. It is a colorless, odorless, and tasteless gas. It changes from gas to liquid at a temperature of −252.77 °C (−422.99 °F) and from liquid to solid at a temperature of −259.2 °C (−434.6 °F). It is slightly soluble in water and alcohol. It has the lowest density (0.08999 g/L) of all elements and the ability to rapidly disperse and quickly ascend to the upper atmosphere.

Hydrogen is an extremely flammable gas. It burns in air and oxygen to produce water. When mixed with air and with chlorine, it can spontaneously explode by spark, heat, or sunlight. The molecular hydrogen dissociates into atomic hydrogen with a dissociation energy of around 435 kJ/mol. The atomic hydrogen is very reactive. It can bond to other atoms to make either covalent bond or ionic bond. In making covalent bond, hydrogen is unusual, because most atoms confirm to the octet rule, ending up with eight valence electrons, the bonding behavior of hydrogen follows the duet rule, resulting in just two electrons for bonding. Examples of covalent bonds with hydrogen include water (H_2O), hydrogen sulfide (H_2S), and ammonia (NH_3) as well as the many organic compounds formed on a hydrogen−carbon backbone. For making ionic bond, it gains an extra electron to become the negative ion H^-, or hydride ion. It is then able to combine with a metallic positive ion (cation). Ionic hydrides are convenient sources of hydrogen gas: for instance, calcium hydride, or CaH_2, is sold commercially and provides a very convenient means of hydrogen generation. The hydrogen gas produced by the reaction of calcium hydride with water can be used to inflate life rafts. The surfaces of metals that do not combine with hydrogen to form stable hydrides (e.g., platinum) catalyze the recombination of hydrogen atoms to form hydrogen molecules and are thereby heated to incandescence by the energy that this reaction releases.

Molecular hydrogen exists in two types; *ortho* and *para* hydrogen. They differ in the magnetic interactions of the protons due to the spinning motions of the protons. In *ortho*-hydrogen, the spins of both protons are aligned in the same direction—that is, they are parallel. In *para*-hydrogen, on the other hand, the spins are aligned in opposite directions and are therefore antiparallel. The relationship of spin alignments determines the magnetic properties of the atoms. Normally, transformations of one type into the other (i.e., conversions between *ortho* and *para* molecules) do not occur and *ortho*-hydrogen and *para*-hydrogen can be regarded as two distinct modifications of hydrogen. The two forms may, however, interconvert under certain conditions. Equilibrium between the two forms can be established in several ways. One of these is by the introduction of catalysts (such as activated charcoal or various paramagnetic substances); another method is to apply an electrical discharge to the gas or to heat it to a high temperature.

The concentration of *para*-hydrogen in a mixture that has achieved equilibrium between the two forms depends on the temperature. At 0 K (−273 °C), hydrogen presents primarily as *para*-hydrogen, which is more stable. At the temperature of liquefaction of air (around 80 K or −193 °C), the *ortho*:*para* hydrogen ratio is 1:1 and the ratio increases to 3:1 around room temperature. Essentially pure *para*-hydrogen can be produced by bringing the mixture into

contact with charcoal at the temperature of liquid hydrogen; this converts all the *ortho*-hydrogen into *para*-hydrogen. The *ortho*-hydrogen, on the other hand, cannot be prepared directly from the mixture because the concentration of *para*-hydrogen is never less than 25%.

The two forms of hydrogen have slightly different physical properties. The melting point of *para*-hydrogen is 0.10 °C lower than that of a 3:1 mixture of *ortho*-hydrogen and *para*-hydrogen. At −252.77 °C, the pressure exerted by the vapor over liquid *para*-hydrogen is 1.035 atm compared with 1.000 atm for the vapor pressure of the 3:1 *ortho*−*para* mixture. As a result of the different vapor pressures of *para*-hydrogen and *ortho*-hydrogen, these forms of hydrogen can be separated by low-temperature gas chromatography, an analytical process that separates different atomic and molecular species on the basis of their differing volatilities.

1.4 Energy content

Hydrogen has the highest combustion energy release of any commonly occurring material making it an ideal fuel. This property and its low weight make it the fuel of choice for the upper stages of multistage rockets. Hydrogen combustion is clean (producing only water) and very efficient as indicated by the very high British Thermal Unit of hydrogen (Idriss, 2004). Hydrogen possesses the highest energy content per unit of weight (120.7 kJ/g) compared with any of the known fuels (Table 1.1) (Haryanto, Fernando, Murali, & Adhikari, 2005; Sorensen, 2005). However, there are issues with the storage and transport of hydrogen that must be addressed.

Table 1.1 Energy density by weight and volume and mass density for various hydrogen storage forms (Sorensen, 2005)

Storage form	Energy density		Density (kg/m^3)
	kJ/kg	MJ/m^3	
Hydrogen gas (0.1 MPa)	120,000	10	0.090
Hydrogen gas (20 MPa)	120,000	1900	15.9
Hydrogen gas (30 MPa)	120,000	2700	22.5
Hydrogen liquid	120,000	8700	71.9
Hydrogen in metal hydrides	2000−9000	5000−15,000	−
Hydrogen in metal hydrides typical	2100	11,450	5480
Methane (natural gas) at 0.1 MPa	56,000	37.4	0.668
Methanol	21,000	17,000	0.79
Ethanol	28,000	22,000	0.79

Compressed gas storage of hydrogen typically at pressures of 10−35 MPa is the most common storage form used today; tests are ongoing to increase pressure and hence storage capacity for passenger vehicle, maintaining reasonable system weight.

Compression may take place at filling stations receiving hydrogen from a pipeline. Yet transportation, compression, and transferal are expensive operations and require a completely new, state-of-the-art infrastructure. Safety of compressed hydrogen tanks is also an area of scrutiny. Storage of liquid hydrogen requires refrigeration to a temperature of 20 K another energy expensive method first developed for space travel. Hydrogen storage as hydrides is another area of investigation; however, hydride storage has many a down side. Typical storage densities are still only 10% or less when compared with conventional fuels and low hydrogen fraction by mass (less than 10%) casting doubt on this technique for mobile applications (Lim, Kazemian, Yaakob, & Daud, 2010; Sakintuna, Lamari-Darkrim, & Hirscher, 2007). Heat is released when hydrogen enters the lattice and heat must be supplied to drive hydrogen out of the lattice causing potential for inefficient desorption of hydrogen. The cost of the metals in the hydride is an additional limiting factor of storage. Other hydrogen storage methods include cryo-adsorbed gas storage in carbon materials and storage as a hydrocarbon. In particular storing of hydrogen as formic acid is receiving considerable interest (Moret, Dyson, & Laurenczy, 2014; Wesselbaum, Hintermair, & Leitner, 2012), because decomposition of the latter (back to hydrogen) is relatively efficient.

Transportation, storage, and safety issues may be overcome if we consider the use of ethanol as the energy carrier with conversion of ethanol (obtained from biofuels) to hydrogen immediately before use as a fuel. Conversion of ethanol to hydrogen is apparently the ideal step in the efficient turnover of the petroleum economy to a hydrogen economy because there is no need of an extensive new infrastructure for fueling. Infrastructure for ethanol production and distribution is already established in many countries as ethanol is already used as an octane enhancer or oxygenate blended with gasoline. Both steam reforming and partial oxidation of ethanol appear as the processes capable of converting ethanol to hydrogen; however, these processes are still in the research and development stage.

Fuel cells being developed are electrochemical cells capable of efficiently turning hydrogen and oxygen into water creating an electric current.

$$2H_2 + O_2 \rightarrow 2H_2O + 240\ \text{kJ/mol} \tag{1.1}$$

The various cells that exist for this purpose include molten carbonate cells, solid oxide cells, acid and alkaline cells, and proton exchange membranes.

Industry currently largely produces hydrogen gas from the steam reforming of methane/natural gas. Other lesser-used methods include methanol reforming, partial oxidation, autothermal and dry reforming, water electrolysis, photodissociation, gasification of heavier fossil fuels and woody biomass, biological processes still in the research and development stage as well as direct thermal or catalytic splitting of water.

1.5 Overview of industrial production

1.5.1 Steam reforming

Steam reforming of methane is a well-established industrial technique for hydrogen production. Carbon of one form or another has long been used to extract hydrogen from water (see the water−gas shift (WGS) reaction in a following section). Catalytic steam reforming of natural gas is the most energy efficient process available for current commercial hydrogen production. Steam reforming of ethanol aims at cracking ethanol in the presence of steam over a catalyst producing as much hydrogen and CO_2 as possible. Depending on the catalyst used there are several reaction pathways that may occur in the steam reforming of ethanol. Rh/CeO_2 catalyst shows excellent activity over the temperature range 573−1073 K and shows 100% ethanol conversion (Haryanto et al., 2005). However, this catalyst is observed to produce significant amounts of CH_4 and CO even though it shows good WGS reactivity (Sorensen, 2005). In general, the selectivity to hydrogen is twice as high for the steam reforming in comparison to partial oxidation (Brown, 2001).

1.5.2 Catalytic oxidation

Total oxidation of hydrocarbons will yield CO_2 and H_2O and hence are not favorable in the interests of the production of hydrogen. Partial oxidation processes yielding H_2 are of more relevance. Combinations of steam reforming and partial oxidation processes are considered more favorable in the decomposition of hydrocarbons. Partial oxidation systems have several distinct advantages over steam reforming systems such as fast start-up and response times and the reactor is more compact than a steam reformer because it does not require the addition of a heat exchanger as partial oxidation is exothermic. Pt/CeO_2 has been reported as an efficient catalyst for partial oxidation of natural gas for hydrogen production and for ethanol partial oxidation (Mattos & Noronha, 2005).

1.5.3 Dry reforming

Carbon dioxide may also be used in the presence of a catalyst at elevated temperatures to oxidize ethanol (Tsiakaras & Demin, 2001). Use of carbon dioxide as an oxidant is known in methane reforming; however, it is a lesser-used reforming process. Dry reforming does not excel in hydrogen production as no excess hydrogen is produced from the oxidant.

$$CH_3CH_2OH + CO_2 \rightarrow 3H_2 + 3CO \quad \Delta H^\circ = 296\ \text{kJ/mol} \tag{1.2}$$

The mechanism proceeds by donation of one of the oxygen atoms of CO_2 to a carbon atom and the subsequent evolution of CO and H_2. The process is more endothermic than steam reforming and it is unclear whether using CO_2 has any positive effects in decreasing pollution by recirculating carbon-containing species as the amount of energy needed is high probably offsetting any gain.

1.5.4 Water–gas shift reaction

The water–gas shift reaction (WGSR) process is an intrinsic inclusion into the reforming process; WGS is seen to increase the H_2/CO ratio. Most catalysts in the steam reforming of ethanol produce CO. WGSR is the reaction of an equimolar mixture of steam and carbon monoxide and the process is moderately exothermic. It is an important step in the reforming process.

The mechanism of WGSR is thought to occur as follows (Gokhale, Dumesic, & Mavrikakis, 2008) (where * is a vacant site):

$$CO + O_{(a)} \rightarrow CO_2 + * \quad \Delta H^\circ = -283\ \text{kJ/mol} \tag{1.3}$$

$$H_2O + * \rightarrow H_2 + O_{(a)} \quad \Delta H^\circ = 242\ \text{kJ/mol} \tag{1.4}$$

Combining the above two reactions gives WGSR.

$$CO + H_2O \rightarrow CO_2 + H_2 \quad \Delta H^\circ = -41\ \text{kJ/mol} \tag{1.5}$$

Because WGSR is moderately exothermic, the equilibrium constant decreases with temperature, and high conversions are favored by low temperatures. The presence of steam in quantities greater than the stoichiometric quantity improves conversion. Although equilibrium favors formation of products at lower temperatures, reaction kinetics dominate at elevated temperatures. In addition to the WGSR, other processes may be at work to reduce the presence of CO. For example, methanation reaction converts any residual carbon oxides to methane and water, consuming hydrogen, and is thus not the preferred method of CO elimination. WGS kinetics on CeO_2-supported Pt, Pd, and Rh suggest the reaction mechanism proceeds via the metal adsorbed CO, oxidized by cerium and the cerium is reoxidized by water.

1.5.5 Catalytic oxidation of methane

Industry currently produces hydrogen from steam reforming of methane/natural gas.

$$CH_4 + H_2O \rightarrow CO + 3H_2 \quad \Delta H^\circ = 206\ \text{kJ/mol} \tag{1.6}$$

This reaction requires a catalyst and is typically made to proceed at temperatures of about 850 °C and a pressure of around 2.5×10^6 Pa. Methane reforming is endothermic and to obtain a high conversion efficiency, some heat inputs are taken from cooling the reactants and from the heat outputs of the subsequent WGSR.

$$CO + H_2O \rightarrow CO_2 + H_2 \quad \Delta H^\circ = -41\ \text{kJ/mol} \tag{1.7}$$

WGSR usually takes place in a second reactor where heat is recovered and recycled back to the first reaction. This involves two heat exchangers and is the main reason for

the high cost of producing hydrogen by steam reforming. A previous steam/methane ratio unity is necessary to avoid carbon and excess CO formation. Industrial steam reformers typically use total combustion of a fraction of the methane to provide the heat required for the process. Combining the above two reactions gives the overall reaction that follows.

$$CH_4 + 2H_2O \rightarrow CO_2 + 4H_2 \quad \Delta H^\circ = 164\ \text{kJ/mol} \tag{1.8}$$

Carbon dioxide reforming of methane is another investigated pathway for hydrogen production; however, the process results in rapid carbon deposition on the catalysts causing deactivation from sintering.

$$CH_4 + CO_2 \rightarrow 2CO + 2H_2 \quad \Delta H^\circ = 246\ \text{kJ/mol} \tag{1.9}$$

Partial oxidation of methane is also a pathway viable for hydrogen production from methane. It produces hydrogen from the hydrocarbon only and does not include any water in the process. The process of partial oxidation is carried out on the same type of catalyst as the steam reforming process but in the presence of oxygen.

$$CH_4 + O_2 \rightarrow 2H_2 + CO_2 \quad \Delta H^\circ = -320\ \text{kJ/mol} \tag{1.10}$$

During the proceedings of a chemical reaction, an energy exchange takes place. Energy exchanges obey the laws of thermodynamics. A reaction may gain or lose energy. Reactions that lose energy warm their surroundings and have a negative ΔH value, this type or reaction is called exothermic. A reaction that gains energy cools its surrounding and has a positive ΔH value is called endothermic. An exothermic reaction is more favorable and is thus more likely to occur than an endothermic reaction. All combustion reactions are exothermic. Entropy factors are not important in the catalytic decomposition of ethanol because more molecules are produced than are used in the reaction thus an increase in entropy is observed. The energy difference between the reactants and the activated complex may be lowered by a catalyst.

Figure 1.1 illustrates the different energy barriers that must be overcome in an exothermic process compared to an endothermic process. We see the energy barrier for an endothermic process is much bigger: an endothermic process requires a large amount of heat energy. A combination of steam reforming, an endothermic process and partial oxidation, an exothermic process, will produce a lower energy barrier than the endothermic alone.

The carbon dioxide and any remaining carbon monoxide are then removed by passing the gases through a zeolite sieve. From time to time, the vessel containing the sieve is taken out of the gas stream and flushed with hydrogen to displace carbon dioxide and regenerate the sieve. There is a significant change in the choice of fuel used in the reformer. Instead of a hydrocarbon gas, coal is more available than methane in some countries (notably China).

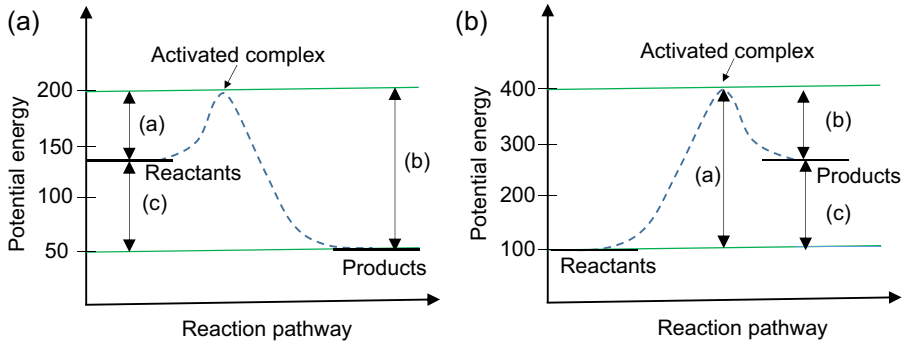

Figure 1.1 (a) Reaction scheme for an exothermic process. (b) Reaction scheme for an endothermic process.

1.6 Overview of industrial uses

Hydrogen for oil refining is used to process crude oil into refined fuels, for example, gasoline and diesel as well as for removing contaminants, in particular sulfur and nitrogen, by hydrodesulfurization and hydrodenitrification. The principal drivers of this growth in refinery hydrogen demand are: low sulfur in diesel fuel regulations, increased consumption of low-quality "heavy" crude oil (requiring more hydrogen to refine), and increased oil consumption in emerging economies such as China and India. About 75% of hydrogen consumed worldwide by oil refineries is supplied from natural gas or other hydrocarbon fuels. Hydrogen is used in a range of other industries, including chemical production, metal refining, food processing, and electronics manufacturing (Ramachandran & Menon, 1998). Hydrogen is either delivered to customers in these industries as compressed or liquid hydrogen, or generated on-site from water using electrolysis or from natural gas. In certain applications, there is a gradual shift toward on-site generation to replace delivered compressed or liquid hydrogen, largely based on the lower cost of new on-site hydrogen generation technologies when compared with delivered hydrogen. Capital cost reduction is critical to the continued expansion of the on-site hydrogen generation market using small-scale reforming technology, including cost reduction of the hydrogen purification equipment included in these systems. Hydrogen is used in the manufacture of two of the most important chemical compounds made industrially: ammonia and methanol. It is also used in the refining of crude oils; for example, reforming is a process for obtaining high-grade petrol and for removing sulfur compounds from petroleum, which would otherwise poison automotive catalytic converters. In years to come, hydrogen itself may become one of the most important fuels because it does not produce carbon dioxide emissions, the only product formed is water. However, there are major problems to be overcome including its manufacture, storage, and distribution. Annual production of hydrogen is about 50 million tons. Figure 1.2 presents the industrial uses of hydrogen, where half of the annual production is used for NH_3 synthesis.

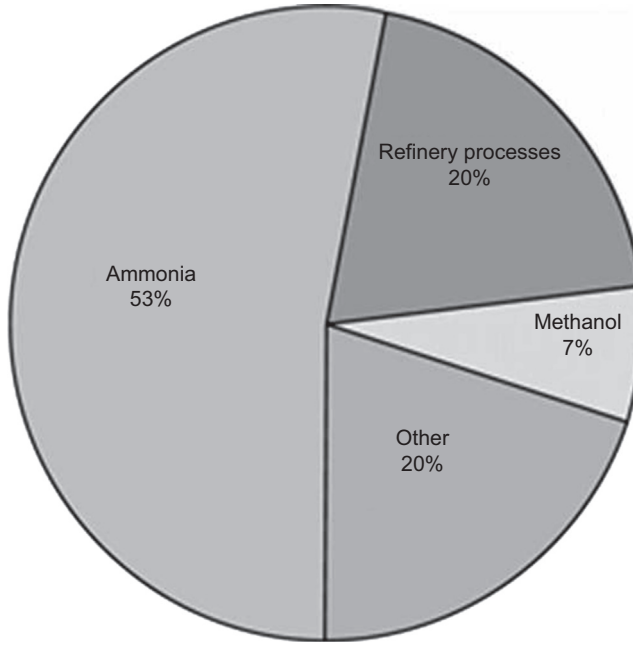

Figure 1.2 Uses of hydrogen in chemical industry.

The obvious route to produce hydrogen gas is by the reverse process, the electrolysis of water. The overall equation is:

$$2H_2O_{(l)} \rightarrow 2H_{2(g)} + O_{2(g)} \tag{1.11}$$

However, this needs electricity from power stations. If the power station uses fossil fuels, it defeats the purpose of producing a fuel without the production of carbon dioxide. Other forms of generating power, such as nuclear, wind, and geothermal, do not have this disadvantage. Fuel cells can produce electrical potential from the reaction between hydrogen and oxygen with about 50% efficiency. One such fuel cell is the PEM cell (Figure 1.3) (polymer electrolyte membrane or proton exchange membrane). A stream of hydrogen is delivered to the anode on one side of a fluorinated polymer or carbon fiber type of a membrane.

$$H_{2(g)} \rightarrow 2H^+ + 2e^- \tag{1.12}$$

The protons permeate the membrane and react with oxygen at the cathode:

$$2H^+ + {}^1\!/\!_2O_{2(g)} \rightarrow H_2O_{(l)} \tag{1.13}$$

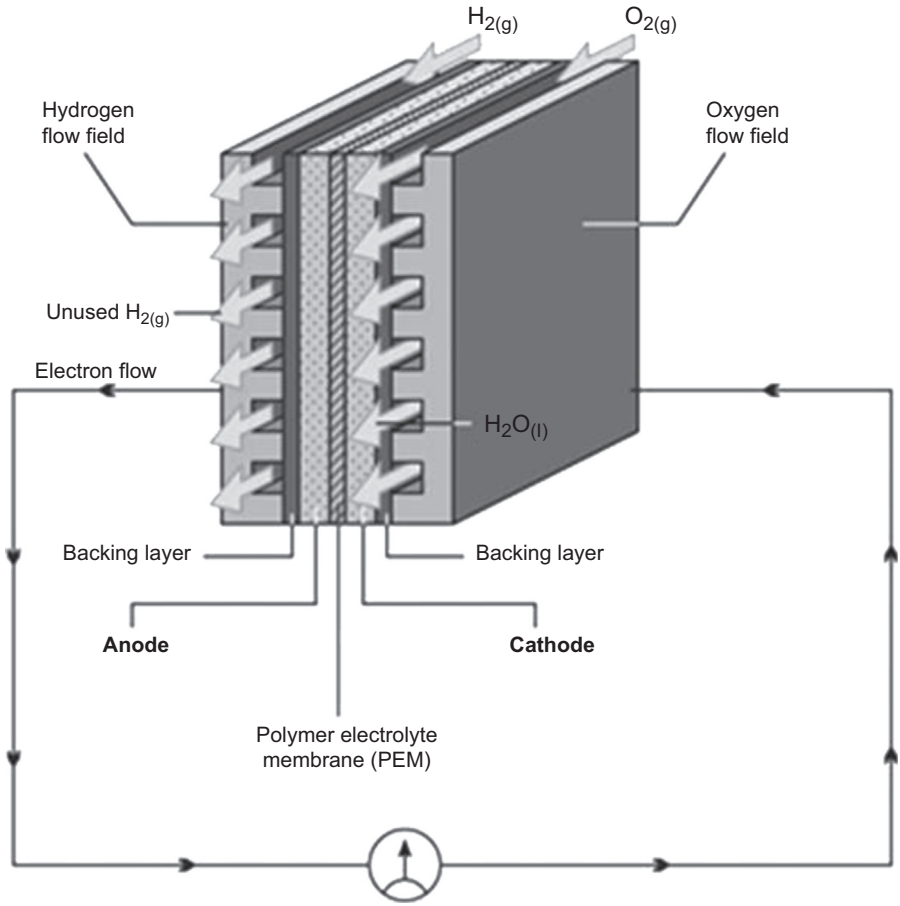

Figure 1.3 Structure of a membrane fuel cell.

The best catalysts for both reactions are nanoparticles of platinum (alone or in the form of alloy) metal deposited on the electrodes.

Because of the practical difficulties in the distribution and storage of hydrogen, hydrogen carrier organic compounds such as methanol are being used in experimental moving vehicles. Methanol is converted into hydrogen and carbon dioxide by a reforming reaction. This demands a very high level of engineering skills to produce conversion units which are light enough for a car but strong enough to withstand all the problems caused by continuous vibrations.

Syngas is an abbreviation for synthesis gas, a mixture of CO, CO_2, and H_2. It is produced by gasification of a carbon-containing fuel (coal, biomass wastes, or hydrocarbons). The name syngas is derived from its use as an intermediate in generating synthetic natural gas and to create ammonia or methanol. Because it is a gas that can be used to synthesize other chemicals, it is named synthesis gas. Syngas is also

an intermediate in creating synthetic petroleum to use as a lubricant or fuel. Syngas has 50% of the energy density of natural gas and as an intermediate to produce other chemicals. The production of syngas for use as a raw material in fuel production occurs by the gasification of coal or organic waste (Liu, Song, & Subramani, 2010). In these reactions, carbon combines with water or oxygen to give CO, CO_2, and H_2. Syngas is used as an intermediate in the industrial synthesis of ammonia and fertilizer.

Impurities in syngas are removed through further processing. For example, sulfur is recovered in the elemental form or as sulfuric acid, which is a primary source of this latter. If syngas contains a considerable quantity of nitrogen, it needs to be separated to avoid production of nitric oxides; pollutants contributing to acid rain. Because both CO and N_2 have similar boiling points, recovering requires a difficult cryogenic processing.

Hydrocarbons synthesis from CO hydrogenation was discovered in 1902 by Sabatier and Senderens (Sabatier & Senderens, 1902), to make methane by passing CO and H_2 over Ni, Fe, and Co catalysts (Liu et al., 2010). At about the same time, the first commercial hydrogen production from syngas from steam methane reforming was commercialized. Haber and Bosch discovered the synthesis of ammonia from H_2 and N_2 in 1910, and the first industrial ammonia synthesis plant was commissioned in 1913. The production of liquid hydrocarbons and oxygenates from syngas conversion over iron catalysts was discovered in 1923 by Fischer and Tropsch. Variations on this synthesis pathway followed for the selective production of methanol, mixed alcohols, and isosynthesis products (a mixture of C1−C4 alcohols and hydrocarbons with the C4 being isobutene/isobutene and isobutanol) (see Figure 1.4). Another ramification of Fischer−Tropsch synthesis (FTS) was the hydroformylation of olefins discovered in 1938.

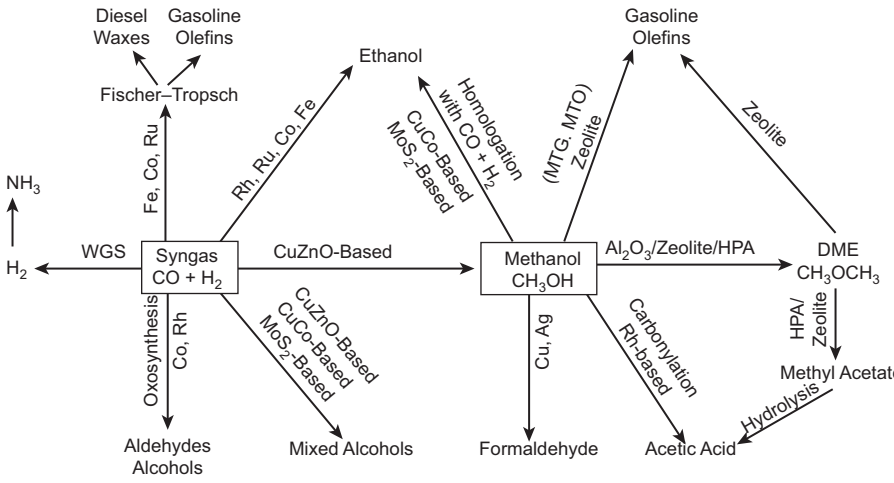

Figure 1.4 Opportunities for catalytic conversion of syngas to fuels and chemicals (Subramani & Gangwal, 2008).

Most of the syngas conversion processes were developed in the first part of the twentieth century when natural resources were becoming scarce and alternative routes for hydrogen production, ammonia synthesis, and transportation fuels were needed. With the development of the petroleum industries from the 1940s and beyond, the unattractive economics of many of these syngas routes became an issue and were replaced by petroleum-based processes. Methanol and ammonia continue to be produced from syngas using similar processes. Apart from hydrogen production, these processes constitute the major uses of syngas.

Sasol based in South Africa developed one of the most successful commercial FTS industry in the world based on syngas production from coal gasification. Increasing environmental concerns and tighter regulations surrounding fossil fuel use also provided impetus for syngas conversion technologies to produce cleaner fuels and chemicals. The use of methanol and isobutene for the production of methyl tert-butyl ether (MTBE), now seldom used, an octane enhancing oxygenated component in reformulated gasoline, also increased demand for syngas conversion technologies. MTBE is becoming an environmental concern as a watershed pollutant with uncertain future. The latest environmental driver will likely increase demand for syngas even more as the goal of establishing a hydrogen economy. The vision is that hydrogen will be the fuel of choice for transportation and electricity generation (in addition to its traditional role). In principle, syngas can be produced from any hydrocarbon feedstock. These include natural gas, naphtha, residual oil, petroleum coke, coal, and biomass. The lowest cost routes for syngas production, however, are based on natural gas.

Nevertheless, the syngas production operation in a gas-to-liquids plant amounts to greater than half of the capital cost of the plant. The choice of technology for syngas production also depends on the scale of the synthesis operation. Syngas production from solid fuels can require an even greater capital investment with the addition of feedstock handling and more complex syngas purification operations. The greatest impact on improving gas-to-liquids plant economics is to decrease capital costs associated with syngas production and improve thermal efficiency through better heat integration and utilization. Improved thermal efficiency can be obtained by combining the gas-to-liquids plant with a power generation plant to take advantage of the availability of low-pressure steam. The syngas composition, most importantly the H_2/CO ratio, varies as a function of production technology and feedstock. Steam methane reforming yields H_2/CO ratios of 3/1, whereas coal gasification yields ratios closer to unity or lower. Conversely, the required properties of the syngas are a function of the synthesis process. Fewer moles of product almost always occur when H_2 and CO are converted to fuels and chemicals. Consequently, syngas conversion processes are more thermodynamically favorable at higher H_2 and CO partial pressures. The optimum pressures depend on the specific synthesis process. With the exception of methane steam reforming, catalytic syngas conversion processes are exothermic reactions generating large excesses of heat. This highlights the specific need for removing this heat of reaction to carefully control reaction temperatures and maintain optimized process conditions.

The choice of catalysts is crucial in syngas conversion reactions. One of the fundamentals in syngas catalysis is the mode by which the CO molecule is adsorbed on the

catalyst. For C2 and above synthesis CO dissociation is necessary, whereas for methanol synthesis, the CO bond remains intact. Hydrogen has two roles in catalytic syngas synthesis reactions. In addition to being a reactant needed for CO hydrogenation, it keeps the metal surface reduced. Since the discovery of syngas conversion to fuels and chemicals, a tremendous amount of research and development has been devoted to optimizing product yields and process efficiencies. This includes the discovery of catalysts with optimized formulations containing the most active metals in combination with appropriate additives (electronic or structural promoters) to improve conversion and selectivity. Mechanistic studies have been conducted to explain the fundamentals of specific conversion processes and measure the kinetic rates of key chemical reactions (Rostrup-Nielsen, 2002). Reactor design and engineering is another active research and development area of syngas conversion technology. Temperature control and stability in conversion reactors is a critical process parameter because of the large excess heat of reaction. Detailed process engineering and integration with respect to heat integration and syngas recycle to improve conversion efficiencies is used to optimize commercial synthesis processes. A diagram highlighting the specific processes reviewed in this report is shown in Figure 1.4.

Although hydrogen is a clean burning fuel, depending upon the feedstock used, its production can generate a considerable amount of CO_2. This important association needs to be considered for CO_2 activation processes where large amounts of hydrogen are used offsetting the potential environmental gain. Additionally, steam reformers produce NO_x from fuel combustion (Baade, Parekh, & Raman, 2001). Generally, as the feedstock goes from natural gas to light hydrocarbons to heavy hydrocarbons and then to solid feedstock, there is an increase in processing difficulty and capital costs.

In addition to the direct production of hydrogen from gaseous hydrocarbon feedstock, hydrogen can be produced from liquid energy carriers such as ethanol and methanol as well as from ammonia. Methanol reforming ($CH_3OH + H_2O \rightarrow CO_2 + 3H_2$) is in practice where there are no economical sources of syngas (Suresh, Gubler, & Sasano, 2001). Conventional steam reforming catalysts are 10−33 wt% NiO on a mineral support (alumina, cement, or magnesia). Reforming catalyst suppliers include, BASF, Dycat International, Haldor Topsoe, ICI Katalco, and United Catalysts (Twigg, 1989). Heavy feedstock tends to coke the reforming catalyst but promoters (potassium, lanthanum, ruthenium, and cerium) may be used to help avoid this problem. For feedstock heavier than naphtha, nickel-free catalysts containing primarily strontium, aluminum, and calcium oxides have been successfully tested (Häussinger, Lohmüller, & Watson, 2000).

Sulfur compounds are the main poison of reforming catalysts. Even at a concentration of 0.1 ppm, the catalyst can begin to deactivate. To increase the catalyst lifetime the sulfur concentration in the reformer feed gas should be less than 0.5 ppm (Leiby, 1994). Uranium oxide and chromium oxide are used as a promoter in certain reforming catalysts resulting in a higher tolerance to sulfur poisoning (Haussinger et al., 2000). Natural gas usually contains only small amounts of sulfur compounds generally in the form of H_2S. In most steam methane reforming plants, before the steam reformer, there is a hydrogenator where sulfur compounds are converted to H_2S. A desulfurizer follows this where the H_2S in the feed gas is absorbed on a ZnO bed.

Any remaining organic sulfur compounds and carbonyl sulfide are partially cracked and absorbed on the zinc oxide bed (Haussinger et al., 2000). If the sulfur concentration in the feed gas is greater than 1%, then the sulfur must be removed by chemical or physical scrubbing. The low-temperature shift catalyst (Cu-based catalysts) is also very sensitive to sulfur and chlorides. An HTS (high-temperature shift) catalyst can tolerate sulfur concentrations up to several hundred ppm, although the activity will decline. Other HTS catalyst poisons include phosphorus, silicon, and unsaturated hydrocarbons in the presence of NO_x.

List of acronyms

DOE	Department of Energy
FCEV	Fuel cell electric vehicle
FTS	Fischer-Tropsch synthesis
HTS	High-temperature shift
IAHE	International Association for Hydrogen Energy
IEA	International Energy Association
IJHE	International Journal of Hydrogen Energy
ISO	International Organization for Standardization
LTS	Low-temperature shift
MTBE	Methyl-tertiary-butyl ether
NASA	National Aeronautics and space Administration
NECAR	New electric car
NHA	National Hydrogen Association
THEME	The Hydrogen Economy Miami Energy
WGSR	Water−gas shift reaction

References

Baade, W. F., Parekh, U. N., & Raman, V. S. (2001). *"Hydrogen." kirk-othmer encyclopedia of chemical technology*. John Wiley & Sons, Inc. British Government Panel on Sustainable Development. July 1999.

Brown, L. F. (2001). *International Journal of Hydrogen Energy, 26*, 381−397.

Gokhale, A. A., Dumesic, J. A., & Mavrikakis, M. (2008). On the mechanism of low-temperature water gas shift reaction on copper. *Journal of the American Chemical Society, 130*, 1402−1414.

Haryanto, A., Fernando, S., Murali, N., & Adhikari, S. (2005). *Energy and Fuels, 19*, 2098−2106.

Häussinger, P., Lohmüller, R., & Watson, A. M. (2000). *"Hydrogen." Ullmann's encyclopedia of industrial*. Wiley-VCH Verlag GmbH & Co.KGaA.

Hoffmann, P. (2012). *Tomorrow's energy. Hydrogen, fuel cells, and the prospects for a cleaner planet*. The MIT Press.

Hydrogen fact sheet from New York state energy and research and development authority. www.nyserda.org.

Idriss, H. (2004). *Platinum Metals Review, 48*, 105−115.

Leiby, S. M. (1994). *Options for refinery hydrogen*. Menlo Park, CA: SRI Report No. 212.
Lim, K.-L., Kazemian, H., Yaakob, Z., & Daud, W. R. W. (2010). Solid-state materials and methods for hydrogen storage: a critical review. *Chemical Engineering and Technology, 33*, 213−226.
Liu, K., Song, C., & Subramani, V. (Eds.). (2010). *Hydrogen and syngas production and purification technologies*. Wiley and AIChE.
Mattos, L. V., & Noronha, F. B. (2005). *Journal of Catalysis, 233*, 453−463.
Moret, S., Dyson, Paul J., & Laurenczy, G. (2014). Direct synthesis of formic acid from carbon dioxide by hydrogenation in acidic media. *Nature Communications, 5*, 4017, 1−7.
Ramachandran, R., & Menon, R. K. (1998). An overview of industrial production of hydrogen. *International Journal of Hydrogen Energy, 23*, 593.
Rostrup-Nielsen, J. R. (2002). Syngas in perspective. *Catalysis Today, 71*, 243−247.
Sabatier, P., & Senderens, J. B. (1902). Direct hydrogenation of oxides of carbon in presence of various finely divided metals. *Comptes Rendus Chemie, 134*, 689−691. Bulletin Societe Chimique 29, III (103) p. 294; Journal of the Chemical Society, 82, II (1902), 317.
Sakintuna, B., Lamari-Darkrim, F., & Hirscher, M. (2007). Metal hydride materials for solid hydrogen storage: a review. *International Journal of Hydrogen Energy, 32*, 1121−1140.
Sorensen, B. (2005). *Hydrogen and fuel cells: Emerging technologies and applications*. Elsevier Academic Press.
Suresh, B., Gubler, R., & Sasano, T. (2001). *"Hydrogen." chemical economics handbook product review*. Menlo Park, CA: SRI International. Report number 743.5000.
Tsiakaras, P., & Demin, A. (2001). *Journal of Power Sources, 102*, 210−217.
Twigg, M. V. (1989). *Catalyst handbook* (2nd ed.). Frome, England: Buttler and Tanner.
Subramani, & Gangwal, S. (2008). A review of recent literature to search for an efficient catalytic process for the conversion of syngas to ethanol. *Energy and Fuels, 22*, 814−839.
Wesselbaum, S., Hintermair, U., & Leitner, W. (2012). Continuous-flow hydrogenation of carbon dioxide to pure formic acid using an integrated $scCO_2$ process with immobilized catalyst and base. *Angewandte Chemie International Edition, 51*, 8585−8588.

This page intentionally left blank

Introduction to hydrogen production

2

R.M. Navarro, R. Guil, J.L.G. Fierro
Institute of Catalysis and Petroleum Chemistry, Energy and Sustainable Chemistry Group, CSIC, Cantoblanco, Madrid, Spain

2.1 Introduction

Hydrogen is the most common element on the Earth but it remains combined with other elements and is always found as part of water, biomass and fossil hydrocarbons. Hydrogen gas is currently produced from a variety of primary sources such as natural gas, naphtha, heavy oil, water and coal (Navarro, Peña, & Fierro, 2007; Peña, Alvarez-Galvan, & Fierro, 2011; Peña, Gomez, & Fierro, 1996).

Currently, industrial plants produce about 55 million metric tons of hydrogen globally each year, with its increasing demand of about 5% per year, almost all of which is for captive use in the chemical and refinery industries. Almost 50% of the world hydrogen production comes from the steam reforming (SR) of natural gas, an additional 30% from higher hydrocarbons reforming from refinery-chemical industrial off-gases, 18% from coal gasification, 3.9% from water electrolysis and a very low fraction of about 0.1% from other sources (Muradov & Veziroğlu, 2005). Almost half of this hydrogen goes into making ammonia a major component of fertilizers, whereas refineries use the second largest amount of hydrogen for chemical processes such as removing sulphur from gasoline and converting heavy hydrocarbons into gasoline or diesel fuel. Many other industries, e.g. methanol, food, metallurgy, glass, pharmaceutical consume the rest. Apart from its traditional uses, hydrogen is considered an ideal energy carrier in future energy systems that need to be economically and environmentally sustainable. The possibility of using hydrogen as an alternative energy carrier has intensified the exploration of hydrogen production processes from a wide range of primary sources such as biomass, coal, solar and nuclear.

The use of natural gas, whose major component is methane, fails to provide a solution to deal with the huge amount of carbon dioxide emissions (approximately 7 kg CO_2/kg H_2) during the reforming processes. Not only the use of fossil fuels contributes to the greenhouse gases pool but the depletion of fossil resources also threatens sustainable development (Farrel et al., 2006). It is obvious that hydrogen production can be environmentally friendly only if the precursor used to extract hydrogen is renewable. Thus, biomass, a product of photosynthesis, is an attractive alternative to fossil feedstocks as it can be considered as a renewable H_2 precursor.

Compendium of Hydrogen Energy. http://dx.doi.org/10.1016/B978-1-78242-361-4.00002-9

CO_2-neutral hydrogen production can be achieved by the conversion of biomass via gasification (Chen, Andries, Spliethoff, Fang, & van der Enden, 2004), pyrolysis of bio-oils (Taralas & Kontominas, 2006), SR of biomass-derived higher alkanes and alcohols (Navarro et al., 2007; Peña et al., 2011; Rostrup-Nielsen, 2001) and aqueous phase reforming (APR) of oxygenated hydrocarbons (Cortright, Davda, & Dumesic, 2002; Huber, Shabaker, Evans, & Dumesic, 2006; Shabaker, Simonetti, Cortright & Dumesic, 2005). These biomass conversion processes not only turn low-value feedstocks into a valuable product, but also carbon dioxide released in parallel is slowly recycled by the planting of new crops to provide the needed biomass, even though time constants of the carbon cycle are different. A biomass strategy of hydrogen generation can be the intermediate step between the current fossil fuel technology and the ultimate goal of efficient hydrogen production from water splitting using solar energy. The solar hydrogen production also attracts great attention as key technology in the future because of its potential to use the abundance of this energy and water. Solar energy can be used to produce hydrogen in the form of heat (thermochemical), light (photoelectrochemical or photocatalytic) or electricity (electrolysis).

Although hydrogen production and storage/distribution are commercially available in chemical and refining industries, the cost and efficiency of the infrastructures for the storage and distribution of H_2 for energy use is currently unacceptable compared with existing petroleum distillate facilities. A key precondition for the realization of a hydrogen economy is the development of a hydrogen infrastructure which, by definition, includes the system needed to produce hydrogen, store it and deliver it to its users. This encompasses hydrogen production systems for converting primary energy sources or other energy carriers to hydrogen; hydrogen storage needed to match time (and space, location) varying demands to hydrogen production output and finally distribution systems. The wide use of hydrogen thus necessitates resolving its storage issue. This ranges from large-scale storage of hydrogen down to small-scale use near at the point of use, for example, on board hydrogen storage in vehicles. For the large-scale storage, there are solutions and options applied today by the industry using hydrogen as a chemical commodity that could be used in future energy systems. However, it is the small-scale storage of hydrogen that poses a great number of challenges and remains a high priority. Because of the crucial problems still facing the infrastructures for the storage and distribution of hydrogen, considerable research is still needed in the short and medium term (2010–2015) and it is essential to take into account the different requirements of stationary and transport applications.

In this chapter, we report a summary of the current methods for hydrogen production, production statistics and expected future trends. In addition, this chapter includes a summary about the hydrogen production methods from less costly and abundant biomass, the advances in the conversion methods of solar energy into hydrogen via the water splitting process assisted by thermochemical, photoelectrochemical and photocatalytic processes and, finally, the challenges that need to be addressed over the coming years to verify the feasibility of hydrogen production as a competitive process in the hydrogen economy.

2.2 Industrial hydrogen production methods

2.2.1 Steam reforming of methane and light hydrocarbons

The SR process involves three reactions, namely, the splitting of hydrocarbons with steam (Eqn (2.1)), the water–gas shift (WGS) (Eqn (2.2)) and the formation of methane (Eqn (2.3))

$$C_nH_m + n\ H_2O \rightarrow n\ CO + (n + m/2)\ H_2 \tag{2.1}$$

$$CO + H_2O \rightarrow CO_2 + H_2 \tag{2.2}$$

$$CO + 3H_2 \rightarrow CH_4 + H_2O \tag{2.3}$$

It is emphasized that the H:C atom ratio of the raw feedstock is an important parameter characterizing the SR process. The higher this ratio is the lower carbon dioxide emission is formed. For methane, H:C ratio is 4, which results in the lowest CO_2 emissions, about 7 kg CO_2/kg H_2. The reaction products are controlled mainly by thermodynamics, which favours the production of methane at lower temperatures (approximately 623 K) and of hydrogen at higher values (approximately 1273 K). The SR catalysts usually contain nickel as the major metallic component. The noble Group 8 metals are also active in the reforming reaction but the cost makes them prohibitive. The catalytic activity depends on the metal area, and their properties are dictated by the severe operating conditions such as temperatures in the range 700–1250 K and steam partial pressures of up to 30 bar. The activity of the catalyst is not, in general, a limiting factor. Thus, a typical nickel catalyst is characterized by a turnover frequency of approximately 0.5 s^{-1} at 723 K under conditions approaching industrial practice, which corresponds to CH_4 conversions around 10%. The principal barrier is the equilibrium conversion which determines very high conversions only at temperatures above 1170 K. As a consequence of the strong mass and heat transfer limitations, classical reformers are limited by the effectiveness factor of pelletized catalysts, which is usually less than 10%, whereas kinetics is rarely the limiting factor (Rostrup-Nielsen, 2003). The heat efficiency of hydrogen production by the SR of methane process on an industrial scale is 80–85% (Sorensen, 2011).

The traditional SR process basically consists of several units (Figure 2.1): feed gas preheating and pretreatment units, prereformer unit, reforming unit, high- and low-temperature WGS units and hydrogen purification unit. A conventional methane steam reformer is quite large (approximately 450,000 Nm^3 H_2/day) and operates with a contact time of the order of 1 s. In the prereformer, all high hydrocarbons are converted directly into C_1 components (methane and carbon oxides) at a low temperature range, typically from 673 to 823 K. The products from prereformer could be heated to temperatures up to 1073 K, reducing the risk of carbon formation from thermal cracking of the fuel before it reaches the reforming catalyst bed. The prereforming catalyst is especially prone to carbon deactivation from the low operating temperature. Specially precipitated high nickel-loaded catalysts (Ni = 20–30 wt%) with

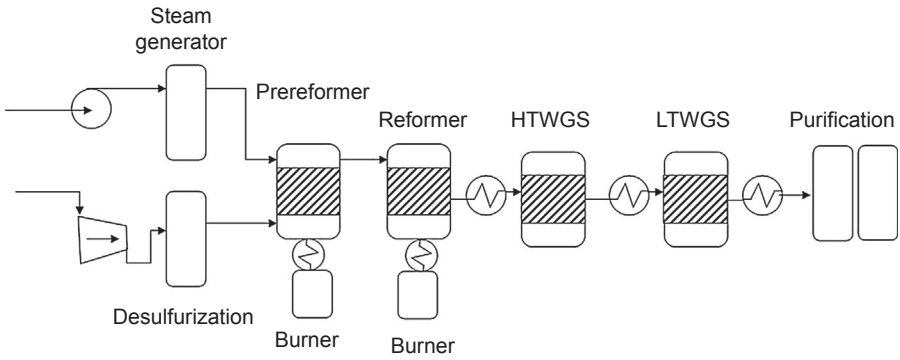

Figure 2.1 Flow diagram corresponding to conventional steam reforming of the methane/hydrocarbons process.

supports with alkaline properties (MgO = 60−70 wt%) and high surface area are used in the prereforming process.

The carbon monoxide obtained after the reforming could be converted to additional hydrogen by means of the WGS reaction (Eqn (2.2)). The WGS reaction is run in two catalytic stages: high temperature shift (HTS) and low temperature shift (LTS). These two units, which are placed downstream of the reformer, ideally reduce the CO content to less than 0.5% vol. In industrial application, the conventional catalyst formulations employed are Fe_2O_3-Cr_2O_3 and Cu-ZnO-Al_2O_3 for the HTS and LTS units, respectively (Navarro et al., 2007). For typical reformate streams (8−10% vol CO), the HTS reactor operating at near equilibrium (623−693 K) reduces the CO level to about 4% vol, whereas the LTS working at 453−613 K achieves 0.4−0.8% vol CO.

The H_2-rich stream produced after WGS still contains some contaminants, i.e. unconverted CH_4, some minor mounts of CO, etc. All of them are traditionally removed in a pressure swing adsorption unit, thus a purified H_2 stream with a typical purity of 99.99 vol% is produced. In the pressure swing adsorption units, gases other than hydrogen coming from the reformer are adsorbed at elevated pressure on activated carbon or molecular sieves. These non−H_2-containing gases are desorbed by expanding the adsorber tank to nearly atmospheric pressure and then returned to the reformer reactor as auxiliary fuel.

2.2.1.1 Catalysts and mechanism

Most SR catalysts are based on a nickel phase deposited on suitable carrier such as Al_2O_3, $MgAl_2O_4$ and ZrO_2. Cobalt and noble metals are also active phases in the SR reaction but their costs make them prohibitive for large-scale operation. A detailed description of the nature of the active phase, catalyst supports, promoter effects and strategies employed in bibliography to prepare highly active catalysts for the SR reaction can be found in our previous works (Navarro et al., 2007; Peña et al., 2011). The catalytic activity of reforming catalysts depends on the surface area of the supported

metal phase and their properties are dictated by the high temperatures, usually above 1023 K required to run the reaction. As a matter of fact, the activity of the SR catalysts is not a limiting factor. The SR is a mass-transfer limited reaction at the high working temperatures needed (Rostrup-Nielsen, 1984). Because the intrinsic activity of the catalyst is proportional to its nickel surface area, the key criterion for designing Ni reforming catalysts is maximizing the heat transfer at low pressure drop.

The mechanism of methane SR reaction on supported Ni catalysts has been studied in some detail (Bengaard et al., 2002; Wei & Iglesia, 2004). Although there have been many controversies, recent theoretical and experimental contributions have been formulated to derive a mechanism for SR of methane on Ni. From these results, it was established that the methane SR is a structure sensitive reaction and that under-coordinated Ni surface sites, i.e. corners and edges, are more active than close-packed Ni sites. It was also demonstrated that the rate-limiting step of the reforming reaction is the activation of C−H bonds of CH_4 molecule. According to these studies the following mechanism for the formation of syngas from methane was proposed:

$$H_2O_{(g)} * \rightarrow *{-}O_{(a)} + H_{2(g)} \tag{2.4a}$$

$$CH_{4(g)} + 2* \rightarrow CH_3{-}*_{(ad)} + H{-}*_{(ad)} \tag{2.4b}$$

$$CH_3{-}*_{(ad)} + * \rightarrow CH_2{-}*_{(ad)} + H{-}*_{(ad)} \tag{2.4c}$$

$$CH_2{-}*_{(ad)} + * \rightarrow CH{-}*_{(ad)} + H{-}*_{(ad)} \tag{2.4d}$$

$$CH{-}*_{(ad)} + *{-}O_{(ad)} \rightarrow *{-}CO_{(ad)} + H{-}*_{(ad)} \tag{2.4e}$$

$$CO{-}*_{(ad)} \rightarrow CO_{(g)} + * \tag{2.4f}$$

$$2H{-}*_{(ad)} \rightarrow H_{2(g)} + 2* \tag{2.4g}$$

where * denotes a Ni surface atom. According to this mechanism, H_2O reacts with surface Ni atoms, towards surface carrier adsorption, providing adsorbed oxygen and gaseous hydrogen. The mechanism proposed for methane SR (Eqn (2.4a−g)) is also generally accepted for the reforming of higher aliphatic hydrocarbons. However, hydrocarbon adsorption needs a dual site to split the α C−C bond (Eqn (2.5a and b)).

$$R{-}CH_2{-}CH_{2(g)} + 2* \rightarrow R{-}CH*{-}CH_2*_{(a)} + H_2 \tag{2.5a}$$

$$R{-}CH*{-}CH_2*_{(a)} \rightarrow R{-}CH*_{(a)} + *CH_{2(a)} \tag{2.5b}$$

In the course of the SR reactions, carbon formation usually takes place in the form of fibres or whiskers. These carbonaceous deposits accumulate progressively on the catalyst surface result with subsequent drop in the activity of the catalyst and in some cases may cause partial or complete blockage of the reformer tubes. Carbon formation from methane includes two kinds of carbonaceous deposits: (1) elemental carbon formed directly from methane decomposition (Eqn (2.6)) or (2) CO disproportionation (Eqn (2.7)):

$$CH_4 \rightarrow C + 2H_2 \tag{2.6}$$

$$2CO \rightarrow C + CO_2 \tag{2.7}$$

Carbon formation on the catalyst surfaces depends to a large extent on the reaction conditions and surface properties of the catalyst (Bengaard et al., 2002; Rostrup-Nielsen, 1984). Whisker is the most common form of carbon produced on the metal surface during steam methane reforming (SMR) reactions (Navarro et al., 2007). The mechanism involved in whisker formation includes first the dissociation of adsorbed CH_4 or CO on the metal surface, yielding C atoms that dissolve within the metal particle; then carbon diffuses through the particle and nucleates into the filament at the rear interface. These carbon whiskers have high mechanical strength and the catalyst particles might well be destroyed when the whiskers hit the pore walls of the substrate.

Given that the formation of carbon on nickel surfaces takes place in ensembles of specific sites (Trimm & Önsan, 2001) and by means of surface metal carbide formation, several approaches can be followed to minimize coke formation on Ni or other metal surfaces: (1) controlling the number of surface Ni sites in a given ensemble (ensemble size control) (Alstrup & Andersen, 1987), (2) modification of the electronic properties of the active metals limiting the possibility of metal carbide formation by alloy or surface compound formation (Nikolla, Holewinski, Schwank, & Linic, 2006; Parizotto et al., 2007; Trimm & Önsan, 2001) or by means of changes in metal-support interactions and (3) enhancement of steam adsorption using carefully engineered supports with the addition of alkali (K or Mg) or lanthanide oxides (Koo, Roh, Jung, & Yoon, 2009; Nikolla et al., 2006).

2.2.2 Gasification of coal and heavy hydrocarbons

Gasification of coal and heavy hydrocarbons is another technology for the large-scale production of hydrogen. Gasification involves the reaction at high temperatures (1200−1400 K) and moderate pressures (5−10 bar) of the source of carbon with a source of hydrogen, usually steam and/or oxygen. Gasification can be performed with or without a catalyst and in a fixed-bed or fluidized-bed reactor, with the latter reactor leading to better performance. For the production of hydrogen, the separation of oxygen from air to be used as pure oxidant in the gasifier is needed. Separation of oxygen from air is usually performed by cryogenics. The presence of oxygen in the gasification process promotes partial oxidation over pyrolysis reactions.

A combination of pyrolysis, partial oxidation and/or SR reactions of gaseous alkanes and char takes place under gasification conditions. Although gaseous products (H_2 and CO_x) are mainly obtained, the fast pyrolysis reactions can also produce bio-oils, tar (aromatic hydrocarbons) and charcoal. This conversion process can be expressed as:

$$\text{Coal/heavy HCs} + H_2O + O_2 \rightarrow H_2 + CO_x + CH_4 + \text{HCs} + \text{char} \quad (2.8)$$

Several parameters such as heating rate, temperature and residence time can be optimized to maximize the efficiency of gasification with minimum tar formation. The chemistry of gasification is quite complex, involving a combination of cracking, partial oxidation, steam gasification, WGS and methanation reactions (Velez, Chejne, Valdez, Emery, & Londoño, 2008). In the first stages of the gasification, the feedstock becomes progressively devolatilized upon increasing temperature and yielding simultaneously oils, phenols, tars and light hydrocarbon gases followed by the WGS reaction and methanation reactions. In a simple form, the basic reaction network in an oxygen and steam fed gasifier can essentially be summarized as follows:

$$\text{Pyrolysis: coal} \rightarrow \text{char (C)} + \text{volatiles (VM)} \quad (2.9a)$$

$$\text{Hydrocracking: VM} + H_2 \rightarrow CH_4 \quad (2.9b)$$

$$\text{Gasification: VM} + H_2O \rightarrow CO + H_2 \quad (2.9c)$$

$$\text{Hydrogasification: C} + H_2 \rightarrow CH_4 \quad (2.9d)$$

$$\text{Gasification: C} + H_2O \rightarrow CO + H_2 \quad (2.9e)$$

$$\text{Gasification: C} + CO_2 \rightarrow 2CO \quad (2.9f)$$

$$\text{Shift conversion: CO} + H_2O \rightarrow CO_2 + H_2 \quad (2.9g)$$

$$\text{Combustion: C} + O_2 \rightarrow CO_2 \quad (2.9h)$$

Volatile matter (VM) includes all gases, tar and light hydrocarbons. Pyrolysis and shift reactions occur under all conditions of gasification. The tar undergoes hydrocracking and gasification reactions yielding H_2, CO and CH_4 products. Similarly, the char undergoes hydrogasification and gasification reactions producing also H_2, CO and CH_4. The gasification reactions, using either H_2O or O_2, are endothermic with an enthalpy of 120−160 kJ/mol, therefore they are favoured at temperatures above 1023 K. The hydrogasification and shift reactions are moderately exothermic with an enthalpy of 32−88 kJ/mol, thus favoured at temperatures below 1023 K. The combustion reaction is highly exothermic with an enthalpy of 376 kJ/mol. For this latter reaction, the equilibrium constant shows that the reaction has not significant thermodynamic limitations up to temperatures of about 2473 K. Under practical conditions of coal gasification, the combustion reaction proceeds to completion whereas gasification and hydrogasification reactions approach pseudo-equilibrium (Sha, 2005).

One of the major issues in gasification is the tar formation that occurs during the process. The unwanted tar polymerizes to a more complex structure which is not favorable for hydrogen production through SR. Currently, three methods are available to minimize tar formation: (1) proper design of gasifier; (2) incorporation of catalysts and (3) control of operation variables. Regarding method (3) the operation parameters, such as gasifying agent, temperature and residence time, are key factors in the formation and decomposition of tar. Tar can be thermally cracked at temperature above 1273 K. In the type (2) method, the use of additives (type such as dolomite, olivine and even char), also facilitate tar reduction (Kuznetsov & Shchipko, 1996; Mondal, Piotrowski, Dasgupta, Hippo, & Wiltowski, 2005; Orio, Corella, & Narvaez, 1997). Dolomite is particularly suited because 100% elimination of tar can be achieved with this additive. Catalysts also reduce the tar content, but are particularly effective for improving gas product quality and conversion. Dolomite and CeO_2/SiO_2 supported Ni, Pt, Pd, Ru and alkaline metal oxides can be used to catalyse the gasification process to reduce tar formation and improve the product gas purity and conversion efficiency (Tomishige, Asadullah, & Kunimori, 2004). Although $Rh/CeO_2/SiO_2$ has been reported to be the most effective catalyst to reduce tar formation, Ni-based catalysts are also highly active for tar destruction (Balasubramanian, Ortiz, Kaytakuglu, & Harrison, 1999).

The gasification process consists of several units (Figure 2.2): gasification unit, high- and low-temperature WGS units and hydrogen purification unit. Under reducing conditions of the gasifier, most of the organic sulphur present in the carbon/hydrocarbon feed is converted to hydrogen sulfide (H_2S), whereas a small fraction, usually not surpassing 10%, forms carbonyl sulfide. The nitrogen present in organic heterostructures forms ammonia (NH_3) and smaller amounts of hydrogen cyanide. The presence of these impurities implies the necessity to remove them, usually by means of physical absorption (acid gases) and subsequent membrane or pressure swing adsorption units.

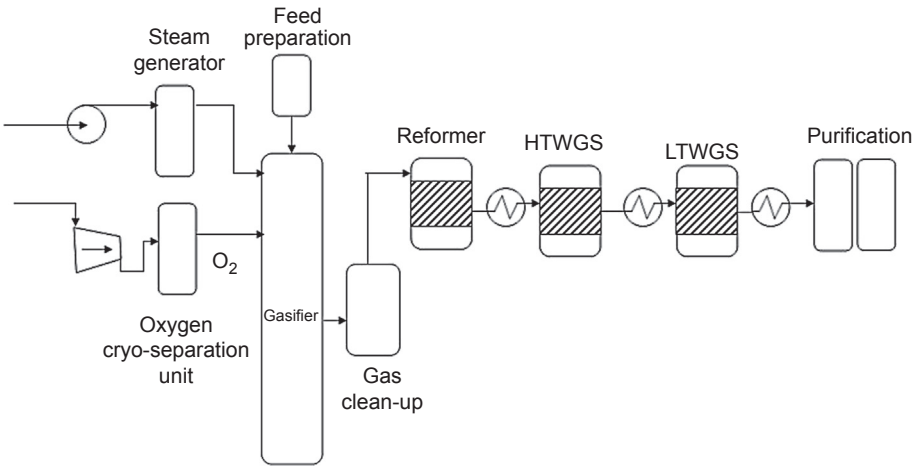

Figure 2.2 Flow diagram corresponding to gasification of the coal/heavy hydrocarbons process.

2.2.3 Electrolysis of water

Alkaline water electrolysis is one of the easiest methods for hydrogen production although it is relatively expensive technology. If relatively small quantities of hydrogen are required, on-site electrolysis of water may result more economical than other methods. This technique is very clean and produces more than 99.989% purity of hydrogen gas. In addition, electrolysis can be linked to renewable electricity-producing technologies and hence could become even more important in the future. Usually an alkaline medium is employed (25−30% KOH). The electrolytic reactions that occur on each electrode are given by the following equations:

$$\text{Cathode: } 2H_2O + 2e^- \rightarrow 2OH^- + H_2 \tag{2.10a}$$

$$\text{Anode: } 2OH^- \rightarrow {}^1/_2\, O_2 + H^+ + 2e^- \tag{2.10b}$$

$$\text{Overall: } H_2O \rightarrow H_2 + {}^1/_2\, O_2 \tag{2.10c}$$

From the overall reaction, assuming the current efficiency to be 100%, 2 F of electricity are required to produce 1 mol of H_2 gas, i.e. 0.1268 cm^3/A.s of H_2 gas at ambient conditions. The Gibbs free energy and the enthalpy change for the overall water decomposition reaction (Eqn (2.10c)) represents the reversible voltage and thermoneutral voltage, respectively. From thermochemistry, the difference between these two values arises from the entropy changes and must be balanced by either supplying or removing heat from the system. The water decomposition reaction is an endothermic reaction. If the opening cell voltage is below the thermoneutral voltage (but above the reversible voltage), then the electrolysis cell will absorb heat from the surroundings. Conversely, if the cel1 voltage is above the thermoneutral voltage, then an excess heat will be generated and this causes energy inefficiency. Thus, it is desirable to operate the cell voltage as close as possible to the thermoneutral voltage.

Cell voltage is directly proportional to the power consumption for the process because the current efficiency for alkaline electrolysis is very close to 100%. Generally, this cell voltage is composed of:

$$E = E_{rev} + \eta_a + \eta_c + \eta_{ohm} \tag{2.11}$$

where E_{rev} refers to the reversible thermodynamic decomposition voltage, η_a to the anode overpotential, η_c to the cathode overpotential and η_{ohm} to the interelectrode ohmic drop.

Present-day electrolysers have a cell voltage of 1.8−2.2 V and operate between 343 and 363 K, which means voltage efficiency from 68% to 80% only (Millet & Grigoriev, 2012). To increase this efficiency, the voltage should be reduced by lowering the overvoltages experienced (at the cathode and anode) and the interelectrode resistance from the electrolyte, the membrane and the bubbles. The cell voltage increases when the process is operated at higher current densities. Above a current density of 150 mA/cm^2, this increment is mainly due to the higher bubble population

in the electrolyte as the gas production rate increases linearly with current density. Therefore, to lower the internal ohmic drop, the bubble residence time in the interelectrode gap has to be minimized. This residence time is dependent on the characteristic bubble size as it influences the drag and buoyancy force of the bubble movement. The characteristic size itself is dependent on the cell configuration (such as cell and electrode geometry) and operational parameter (such as current density, electrolyte flow conditions, temperature and pressure).

2.2.3.1 Developments

Alkaline water electrolysis is known as the principal process for the water splitting reaction. Military applications related to the use of hydrogen isotopes boosted the development of this technology. The first plants for the electrolysis of D_2O (D_2 production) were built in Norway. Nowadays, several companies are producing alkaline electrolysers for the production of hydrogen of electrolytic grade. The production capacity of these industrial electrolysers is in the 5−500 m^3 H_2/h range.

NEL electrolysers operate at atmospheric pressure and deliver 50−485 m^3 H_2/h with energy consumption in the range 4.1−4.3 kWh/H_2 Nm^3 at current densities up to 0.3 A/cm^2. Hydrogen purity reaches 99.9%, operating temperature is 353 K and electrolyte solution is 25% KOH. Hydrogenics manufactures both monopolar and bipolar electrolysers. Monopolar electrolysers are ease to design and require low maintenance but they are heavier and larger which often reduce the application field. The Electrolysers Company developed its own electrolysers for ammonia synthesis, hydrogen peroxide synthesis, oxygen production and hydrogen isotope separation deuterium. This company built one of the first pilot stations for filling 200 buses per day fuelled with hydrogen compressed at 400 bar. The Hydrogenics Corporation manufactures electrolysers with hydrogen capacities up to 120 m^3 H_2/h at 20 bar output pressure, H_2 purity is 99.9% and O_2 purity is 99.5% and specific energy consumption is 4.8−4.9 kWh/m^3 H_2 including the energy requirement of plant infrastructure.

Alkaline water electrolysers are designed and manufactured for a wide range of applications. Major gas-consuming industries are: (1) electric power generator cooling in power plants, (2) semiconductor industry, (3) flat panel computers and television screen producing units and (4) glass plants and metallurgical industries. Other industrial applications include food processing, laboratory applications, heat treatments, meteorology and welding industries. Hydrogen as an energy carrier is opening the way to new applications such as management of smart grids for more energy flexibility, chemical storage of renewable energies and hydrogen refuelling stations for fuel cell−powered vehicles.

Alkaline water electrolysis is a mature technology. Many industrial electrolysers capable to deliver up to 650 m^3 H_2/h are installed for different end-uses. From an economic viewpoint, the lifetime of these systems, on the order of several tens of thousands hours, can be considered satisfactory for continuous operation. Notwithstanding, alkaline electrolyser cells can hardly operate at very low current densities. This is a limit in terms of flexibility in load-following operation which will be required for operation with renewable energy sources. From the material viewpoint, major

research efforts concern the development of advanced diaphragms with adapted electrode material. Most efficient diaphragms used are made from asbestos that are not permitted in many countries. The replacement of asbestos by composite ceramic/polymer materials is proposed but there is still room for improvement (Divisek & Murgen, 1983). Improved electrocatalysts are also needed. Attempts have been made to develop new electrocatalysts, and the electrocatalytic properties of some transition metal macrocycles have been studied (Pile & Daugthy, 2005). From a performance viewpoint, higher efficiencies can be obtained by using advanced alkaline electrolysers. Prototypes built to deliver up to 25 m^3 H_2/h have been developed along the last decades. Such units have been designed to operate under high current densities (1.25 A/cm^2), at 393 K and operation pressure 25−40 bar. The electrical power consumption is 3.81 kWh/m^3 H_2 at 363 K and somewhat lower 3.65 kWh/m^3 H_2 at 393 K.

2.3 Hydrogen markets

2.3.1 Current markets

Worldwide hydrogen consumption amounts nearly 50 MT per year (Shell, 2004), including intentionally produced hydrogen as well as hydrogen that is produced as a by-product in the petrochemical industry and consumed on site. Major current uses of produced hydrogen are for producing ammonia for fertilizers, for oil refining where hydrogen is used for hydrotreating of crude oil as part of the refining steps to improve the hydrogen-to-carbon ratio of the fuel, food production, metallurgical uses and metal treatment as well as other industries. Power production uses relatively small quantities of hydrogen, somewhat about 10−20 kT/y in the United States, only about 0.1% of the total. This estimate is based in the Fuel Cell Energy report that their fuel cell devices produced over 4×10^8 kWh of electricity through 2009, using about 30,000 T of hydrogen over the past several years (Fuel Cell Energy, 2011). The Fuel Cell Energy devices represent nearly 30−50% of the total installed fuel cell systems in the market (Adamson, 2008).

Table 2.1 summarizes the 2003 global consumption of produced hydrogen break down by sector and region. The Asia/Oceania region is the largest market with 39% of global production share in 2010. The region generated around 21 MT of hydrogen in 2010. This region pioneers refinery and ammonia production capacity and this makes it the largest consumer. Europe/Eurasia is the second largest producer, followed by North America which comes third. North America is the largest market for merchant hydrogen, with 60% of global merchant hydrogen production in 2010. Country-wise, the United States is the largest merchant producer, with 47% of global merchant hydrogen production share. China is the largest consumer, with 22% of global hydrogen consumption share. China's maximum demand comes from ammonia producers because it is the world's largest ammonia producer and accounts for 32% of worldwide ammonia production. The 2003 worldwide hydrogen consumption amounted to 41.09 MT with 57.5% used for ammonia production, 27% in oil refining,

Table 2.1 2003 global consumption of produced and merchant hydrogen (MT)

	US	Western Europe	Japan	Rest of the world	Total
Captive users					
Ammonia	2.59	1.78	0.23	19.02	23.63
Refineries	3.19	2.81	1.17	4.10	11.26
Methanol	0.39	0.31	0	3.29	3.99
Other	0.03	0.09	ND	0.47	
Merchant users					
Pipeline or on-site	1.16	0.44	0.03	ND	1.63
Cylinder and bulk	0.05	0.06	0.01	ND	0.12
Total	7.74	5.42	1.53	26.41	41.09

ND, not documented.
Suresh, Schlag and Igonuchi (2004).

about 10% in the methanol industry and the remainder used in a variety of industrial applications. About 95% of the total demand is captive, meaning that the hydrogen is produced at the site of consumption (air products). The remainder is produced as merchant hydrogen. Only a small portion (4−6%) of the merchant demand consumes liquid hydrogen; the remainder is compressed gas that includes a variety of industrial applications (Hafner, Karbuz, Esnault, & El Andaloussi, 2005). Although liquid merchant hydrogen is a premium product that commands higher prices, it is important to note that demand densities are such that production facilities are typically smaller, with the largest current size at about 20 kT/y. When hydrogen is produced using a centralized plant, it has to be delivered to the point of consumption by pipeline, cylinders or trailers. For large quantities, pipelines are the preferred option. Although pipeline delivery is cheaper compared with packaged options with trailers in the long term, it can only be economically justified when quantity is sufficiently high. Pipelines require significant initial investment and thus are preferred when sales are high. On the other hand, cylinders are used for small quantities and hence are preferred by industries such as glass manufacturing, metal production and fabrication, food processing, electronics, etc. On-site hydrogen generation, known as distributed generation, eliminates a number of problems associated with transportation and delivery and thus market for on-site generation system is growing significantly. Also, in recent years, small scale on-site generation option has become more attractive from the economic point of view because new on-site hydrogen generation technologies offering low cost when compared with delivered merchant hydrogen.

2.3.2 Future trends

2.3.2.1 Hydrogen for transportation

Hydrogen use in transportation might well be the main application for hydrogen in the coming decades. The full development of the use of hydrogen in transportation with the associated infrastructure is expected to take several decades because different technological advancements in fuel cell technology and storage and transportation of hydrogen will be needed. Initially, small-scale distributed hydrogen production plants, mostly natural gas-based, will be deployed to avoid the need for a new large-scale distribution infrastructure. Current hydrogen production facilities that are often near major population centres, such as oil refineries, as well as ammonia and methanol plants, could serve to overcome this transition. Hydrogen production in those facilities could be increased incrementally to serve a small, but growing, transportation hydrogen demand. Once demand reaches a critical level in larger metropolitan areas, more centralized production technologies might take a hold in the market.

Because of the long-term nature of this market deployment, some uncertainties arise. Nevertheless, using the underlying hydrogen demand scenario used in the report on the hydrogen economy by the National Academy of Sciences (National Academy of Sciences, 2004), one can estimate the growing hydrogen demand. Following such a scenario, the hydrogen demand for transport is estimated to be 1.8, 16.2, 67.1 and 100.0 MT for 2020, 2030, 2040 and 2050, respectively.

2.3.2.2 Hydrogen for oil and tar sands conversion

It is emphasized that decreasing sulphur level in petroleum products, lowering crude oil quality and rising demand of hydrogen-operated fuel cell applications, the global hydrogen production volume is forecasted to grow at annual growth rate of 5.6% during 2011−2016. One of the future hydrogen markets is the processing of oil and tar sands. Canada and Venezuela concentrate the largest deposits of oil sands. Estimates indicate that Canada's proven oil sand reserves total about 179 billion barrels, in second place after Saudi Arabia's petroleum reserves of 259 billion barrels. These oil or tar sand reserves consist of bitumen (10−12%), sand and clay (80−85%) and water (4−6%). Bitumen is heavy, viscous oil that must be hydroprocessed to convert it into synthetic crude oil through coking, hydrodesulphurization and hydrocracking. The annual hydrogen demand in 2010 for exploitation of Canada's oil and tar sands amounted 1.92 MT and projections for 2015 and 2020 are 2.86 and 3.19 MT, respectively (Yildiz, Petri, & Forsberg, 2005). Indeed, the projected hydrogen consumption in 2020 would be the same as the current captive hydrogen consumption in the US refining sector. Surface mining operations typically range from 13,000 to 274,000 barrels/day (b/d) with the median around 50,000 b/d (Alberta Department of Energy, 2004). This means that half of the oil sand production facilities require hydrogen consumptions of about 46,000 tonnes/y, which could be easily supplied by a medium-sized centralized hydrogen production facility. In terms of natural gas consumption, Canada is projected to use almost 1100 Bcf of natural gas in the production of synthetic crude oil from oil sands. The share of H_2-related gas

consumption increases over time as the share of surface mining oil sands increases. The increase in gas demand is of concern, and alternative technologies are being explored.

2.3.2.3 Hydrogen for coal and shale oil conversion

Coal can be converted into transportation liquid fuels either by indirect or direct hydrogenation processes. In direct liquefaction, coal is partially dissolved at high pressure and temperature in a liquid solvent. As coal is H_2-deficient, converting solid coal into a liquid form requires the addition of hydrogen. Hydrogen is added under pressure to the coal and solvent mixture at temperatures up to 723 K. For instance, producing 100 kg of synthetic crude oil through direct hydrogenation from 110 kg of coal requires 7.4 kg of hydrogen (Carbon Neutral Fuels, 2012). This synthetic crude requires further refining to take the hydrogen-to-carbon ratio from 1.6 to approximately 2.0 for finished liquid fuel products. Indirect liquefaction involves two consecutive steps. In the first stage, coal is heated in the presence of steam and oxygen to produce a mixture of carbon monoxide and hydrogen, or synthesis gas. Because of the low hydrogen content of coal, an additional source of hydrogen is required. This is usually supplied through the WGS reaction of CO and H_2O, with the resultant CO_2 being removed from the product stream. In the second stage, the synthesis gas is catalytically converted into a synthetic liquid fuel via Fischer−Tropsch process. Alternatively, by varying the catalyst reactor setup and operation variables, the synthesis gas can yield alcohols, such as methanol or ethanol. Notwithstanding, full-scale commercial deployment requires substantial work to improve both process stages. The first process stage requires an oxygen plant for making the synthesis gas. About 30−50% of the total investment requirements of a coal liquefaction plant are associated with the oxygen plant. This typically limits Fischer−Tropsch plants to very large operations, in the order of 100,000 b/d or more. Improved catalysts would make the process more economic. Based on the specific hydrogen needs, it is estimated that the hydrogen requirements for a coal indirect-liquefaction plant with an output of 100,000 barrels of synthetic crude oil per day to be around 370,000 T/y. This means that if the United States were to replace all its current net crude oil imports of 9.65 Mb/d with synthetic crude produced from coal liquefaction it would require about 97 such facilities consuming about 37.7 MT of hydrogen. That quantity is equivalent to about 4.5 times the current US hydrogen consumption.

Another resource to be exploited is shale oil. Recovery of oil from this resource includes pyrolysis, hydrogenation and thermal dissolution. This processes convert hydrocarbons retained in the rock into synthetic oil and gas. Total global shale oil resources have been estimated to be around 2.6×10^{12} barrels, about 75% of them are found in the United States. These resources display almost 10 times higher density as compared with the Canadian oil sands. From the technical point of view, the hydrocarbons present in oil shale are solid and do not melt and are not soluble. To convert oil shale into liquids, the hydrocarbons must be converted from a solid to a liquid state. This conversion can be done following two conventional approaches. First, the shale is fractured in situ and heated to obtain gases and liquids at wells, then the liquid

component is extracted, transported and finally hydrogenated to about 723 K, adding hydrogen to the resulting product. Commercial-scale oil shale processing plants will likely be in the 150−200,000 b/d range.

2.4 Hydrogen production from renewables

2.4.1 Hydrogen production from biomass

Biomass is an attractive alternative to fossil feedstocks as it can be considered as a renewable H_2 precursor. Biomass is available from a variety of sources, such as municipal solid wastes, crop residues, agricultural wastes, sawdust, aquatic plants, waste paper, corn and many others (Demirbas, 2006). CO_2-neutral hydrogen can be produced by the conversion of biomass via gasification, pyrolysis of bio-oils, SR of biomass-derived higher alkanes and alcohols and APR of oxygenated hydrocarbons (Figure 2.3). A brief description of the biomass-based approaches is given in the following section.

2.4.1.1 Biomass gasification

The polymeric structures of the biomass can be broken down into smaller molecular units, hydrogen and carbon oxides, according to a thermochemical process called gasification. Nowadays, this process is gaining more and more interest as a means of converting low-energy, low-density biomass feeds into hydrogen for heat and power generation. Hydrogen is produced by gasification of biomass with steam and/or oxygen. This process, including heating of the feedstock and reactants, requires energy and is described by Eqn (2.12). The high energy demand of the gasifier requires air/oxygen incorporation to the process:

$$C_xH_yO_z + H_2O/O_2 \rightarrow CO + CO_2 + H_2 + CH_4 + C_{2-4} + \text{tars} + \text{char} \quad (2.12)$$

The direct products of gasification are gases, tars, char and ash. The gases are the desired product which are further purified, subjected to secondary reactions and upgrading thus leading to syngas ($CO + H_2$) or methane. Gasification can be

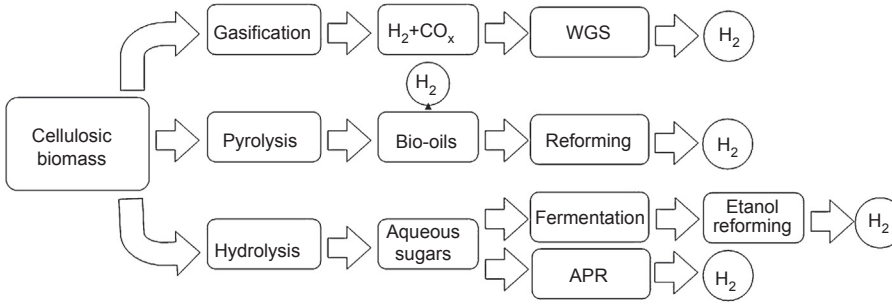

Figure 2.3 Routes to hydrogen production from biomass. WGS, water−gas shift; APR, aqueous phase reforming.

performed with or without a catalyst and in a fixed-bed or fluidized-bed reactor, with the latter reactor leading to better performance. Incorporation of steam and/or oxygen in the gasification process results in the production of 'syngas' with a H_2/CO close to 2 which can then be employed either to produce hydrocarbons via the Fische−Tropsch synthesis or coupled to a WGS reactor for hydrogen production (Duret, Friedli, & Maréchal, 2005).

It is emphasized that gasification results in the formation of a significant amount of 'tars' (mixture of higher aromatic hydrocarbons) in the gas stream, even if the reactor is operated at temperatures in the 1073−1273 K range. Typically, a secondary reactor, to which dolomite and/or nickel catalyst is incorporated, is used to clean up and upgrade the product gas. Although pure oxygen can be used in gasifiers, oxygen separation unit is cost prohibitive for small-scale plants. This limits the gasifiers to the use of air resulting in dilution of the product. Indeed, low-cost, efficient oxygen separation units are needed for this technology. If H_2 is the target product, a WGS reactor must be incorporated to increase the hydrogen concentration followed by a separation process to produce pure hydrogen (Weber, Fu, & Wu, 2006). Typically, gasification reactors are very large and require huge amounts of biomass to be continuously fed. Because Ni-based catalysts are industrially employed for the SR of natural gas and naphtha (Navarro et al., 2007), they are suitable for the SR of tars as well as for the WGS reaction to produce H_2.

Improvements in the gasification technology include the hydrogen production by reaction-integrated novel gasification (HyPr-RING) technology (Lin, Harada, Suzuki, & Hatano, 2002). This technology combines both gasification and WGS reactions in a single reactor with simultaneous absorption of CO_2 and other pollutants to increase the hydrogen yield while maintaining a relatively low temperature (923 K). One of the recent developments in gasification is the Caro-V process (CHOREN Technologies GmbH) designed to produce tar-free syngas for H_2 or liquid fuels (Rudloff, 2005). The advantage of this process over the conventional gasifier is that its efficiency is higher (>80%). A similar two-step process, called BIOLIQ, was developed by the Forchungszentrum Karlsruhe, Germany (Santo et al., 2007). A very high carbon conversion (>99%) was reported for temperatures about 1273 K.

Biomass can be also gasified under supercritical water gas (SCWG) conditions (221 bar and 647 K). At temperatures in the range 823−1023 K, dilute biomass is highly reactive however its reactivity drops sharply upon increasing its concentration. This problem may be overcome by conducting SCWG in two stages: the first involves hydrolysis of biomass into water-soluble compounds followed by gasification in the second. If model compounds are used, the H_2 yield increases by addition of alkalis such as KOH, Na_2CO_3 and $KHCO_3$ (Kruse, Meier, Rimbrecht, & Schacht, 2000). At low temperature, SCWG catalysts are required to achieve high conversions. The catalyst used for this purpose includes Ru or Ni supported on titania, zirconia and carbon (Matsumura et al., 2005) which are stable under the severe oxidizing conditions imposed by the near supercritical water. Homogeneous alkali solutions and heterogeneous alkali metals (Minowa, Zhen, & Ogi, 1998) have been also employed as catalysts in SCWG, but recovery of these catalysts at the end of gasification is a major drawback.

It is emphasized that under SCWG conditions the methanation reaction is also thermodynamically favoured and accordingly a little of the hydrogen produced is consumed to form methane. Nickel and many other metal catalysts also suffer from severe corrosion under the conditions imposed by SCWG, especially at the high temperatures required for higher H_2 production rates. Currently, the high logistics costs of gasification plants and the removal of tars to acceptable levels for pure hydrogen production limit the commercialization of biomass-based hydrogen production.

2.4.1.2 Reforming of biomass-derived products

Reforming of bio-oil

Another methodology of biomass transformation is pyrolysis. Pyrolysis is the thermochemical decomposition of biomass at temperatures in the range 673−853 K in the absence of oxidant. The decomposition process releases volatile species, while the solid, nonvolatiles are collected as bio-char. A portion of the gas-phase volatiles condense into a black, viscous fluid termed bio-oil liquor. Although pyrolysis itself is not appropriate for hydrogen production, the reforming of bio-oil is much more attractive (Dickerson & Soria, 2013). Starting with bio-oils, hydrogen can be produced by SR (Vaidya & Rodrigues, 2006) and autothermal (Vagia & Lemonidou, 2008) processes. Studies on SR of oxygenated compounds present in bio-oils demonstrated that the homogeneous thermal decomposition of that compound competes with the catalytic heterogeneous process which results in coke accumulation thus leading to catalyst deactivation and plugging the reactor. These problems can be minimized by running the reaction under autothermal conditions. Following the autothermal operation, H_2 yields obtained from model compounds reach 71−78% of the stoichiometric yield, which compares reasonably with the SR yield. It has been also reported recently that H_2 can be produced using the sequential cracking method (Vagia & Lemonidou, 2008). Bio-oil sequential cracking involves two steps in which catalytic cracking of the feed is alternated with a catalyst regeneration step. During the cracking step, the oxygenated compound decomposes on the surface of a metal catalyst, usually a Pt group metal, to produce H_2 and solid carbon on the metal surface. During the regeneration step, the coke deposited on the metal surface is combusted or gasified to produce CO_2 while the metal surface is cleaned. The advantage of this two-step process is that H_2 and CO_2 products are collected in separate steps thereby saving the energy required to purify H_2.

Reforming of bio-ethanol

Bio-ethanol, produced renewably by fermentation of biomass, is very attractive raw compound to produce H_2 because of its relatively high hydrogen content, availability, nontoxicity, and storage and handling safety. Hydrogen can be obtained directly from ethanol by SR process (Steam reforming of ethanol (SRE), Eqn (2.13))

$$CH_3CH_2OH + 3H_2O \rightarrow 6H_2 + 2CO_2 \ (\Delta H^\circ = +207.7 \text{ kJ/mol}) \tag{2.13}$$

The ethanol SR is a complex reaction in which simultaneous and consecutive reactions are involved, i.e. SR, dehydrogenation, dehydration, decomposition, Boudouard

and WGS (Vaidya & Rodrigues, 2006). In these reactions, catalysts play a major role towards complete conversion of ethanol, but each catalyst determines different pathways and therefore the selection of a suitable catalyst is essential in SRE reaction. Good catalysts should maximize H_2 selectivity and inhibit coke formation as well as CO production. Reactions that lead to C and C_2H_4 products which are precursors of coke deposition on catalysts surfaces must be avoided. Thus, catalysts for the SR of ethanol to produce H_2 selectively must be able to: (1) dehydrogenate ethanol; (2) break the C−C bonds of surface intermediates to produce CO and CH_4 and (3) reform these C_1 products to generate hydrogen. To fulfil these requirements, appropriate selection of both the metal and support constituents of the catalysts is essential. Different oxide catalysts (Llorca, de la Piscina, Sales, & Homs, 2001), non-noble metal catalysts (Ni, Co, Ni/Cu) (Fatsikostas, Kondarides, & Verykios, 2001) and noble metal-based catalysts (Pt, Pd, Rh) (Fierro, Akdim, & Mirodatos, 2003; Navarro, Alvarez-Galván, Sanchez-Sanchez, Rosa, & Fierro, 2005) have proved to be active in the ethanol-reforming reaction.

Ni catalysts are doubtless the most widely used, low-cost metal catalyst for ethanol reforming. For Ni catalysts, the influence of the support has been investigated in some detail (Sun, Qiu, Wu, & Zhu, 2005) compared with the catalytic activity of Ni catalyst supported on La_2O_3 and Al_2O_3 for H_2 production by ethanol SR at 773 K and atmospheric pressure. Under these reaction conditions, the Ni/La_2O_3 catalyst showed 99.5% ethanol conversion and 48.5% H_2 selectivity, and simultaneously exhibited a high stability during on-stream. The high stability of this catalyst was explained in terms of formation of a lanthanum oxycarbonate species ($La_2O_2CO_3$) which could react with surface coke deposited during reaction and thus these residues become gasified and hence catalyst deactivation is prevented (Sánchez-Sánchez, Navarro, & Fierro, 2007). For comparison, selectivity of hydrogen for Ni/Al_2O_3 catalyst reached the maximum H_2 selectivity of 47.7% at 573 K. This relatively low H_2 selectivity is probably due to the relatively low steam/ethanol molar ratio used (3:1) because increasing water/ethanol molar ratio could significantly increase selectivity of hydrogen. Other oxides, such as CeO_2 and MgO, have also been employed as supports for Ni catalysts. It was found that Ni supported on high surface area CeO_2 support displays good performance in the SR of ethanol with high resistance towards coke deposition and better product selectivity compared with Ni/Al_2O_3 catalyst (Laosiripojana, Assabumrungrat, & Charojrochkul, 2007). Cobalt-based catalysts also exhibited good performance in the ethanol SR reaction. This behaviour may be related to the presence of both acid and basic sites on the ZnO surface and also to the relatively high activity of cobalt for cracking of C−C bonds and WGS reactions (Chiou et al., 2013). The Co/ZnO catalysts exhibited very high catalytic performance within the temperature range 573−773 K (Mattos, Jacobs, Davis, & Noronha, 2012). Using an EtOH/H_2O = 1/13 (molar ratio) mixture, total conversion of ethanol and the high values of H_2 and CO_2 were obtained, and in absence of deactivation. Noble metals supported on porous oxide substrates (Al_2O_3, SiO_2, CeO_2, TiO_2 and MgO) (Birot, Epron, Descorme, & Duprez, 2008; Breen, Burch, & Coleman, 2002; Liguras, Kondarides, & Verykios, 2003) are highly active in the SR of ethanol to CO_x and H_2. The nature of the support plays an important role in

the SR of ethanol over noble metal catalysts. In a study on the effect of both the metal and the support in the SR of ethanol, it was observed that at 973 K the hydrogen yield on alumina-supported metal catalysts decreased in the following order: Rh > Pd > Pt > Ru (Auprête, Descorme, & Duprez, 2003). From this study, it was concluded that the high activity of the metals in ethanol SR and their poor efficiency in the WGS reaction would give active and selective catalysts for ethanol reforming.

So far, the development of catalyst for ethanol reforming is basically a trial-and-error approach. Although there is an important body of work, detailed analyses of reactant species, intermediate product species, and final product species are lacking. Therefore, commercial catalysts for this reaction have not yet been achieved.

2.4.1.3 Aqueous phase reforming

This method involves the conversion of biomass-derived oxygenated hydrocarbons with C:O ratio of 1:1, such as methanol, ethylene glycol, glycerol, glucose and sorbitol, into H_2, CO, CO_2 and light alkanes using heterogeneous metal catalysts (Cortright et al., 2002; Huber et al., 2006; Shabaker et al., 2005). The APR is carried out within the temperature range 473−523 K and pressures in the 10−50 bar range. The overall APR reaction by starting with oxygenated compounds, whose carbon-to-oxygen ratio is 1, is represented by the following equation:

$$C_xH_{2x}O_x + x\ H_2O \rightarrow 2x\ H_2 + x\ CO_2 \tag{2.14}$$

The main advantages of this method of production include: (1) moderate reaction temperature and pressure which favour the WGS reaction in the same reactor; (2) low CO level in the gas stream (100−1000 ppm), which is ideal for fuel cell application and (3) lower energy requirement compared to SR because the oxygenated hydrocarbon feed and water are in the liquid phase. Additionally, the feedstock is nonhazardous which makes its storage relatively easier. The reaction pathways involved in the formation of H_2, CO, CO_2 and alkanes in the aqueous phase ethylene glycol reforming reaction is similar to the SR reaction. Once C−C bond cleavage occurs, the CO produced remains adsorbed on the metal site and then the WGS reaction produces H_2 and CO_2. The reaction pathway for the production of H_2 and CO_2 by APR of oxygenated hydrocarbons involves cleavage of C−C bonds as well as C−H and/or O−H bonds to form adsorbed species on the catalyst surface. Therefore, a good catalyst for production of H_2 by APR must be highly selective for C−C bond breaking and promote removal of adsorbed CO species by the WGS reaction. However the catalyst must not catalyse C−O bond cleavage and hydrogenation of CO and CO_2 into CH_4.

Many metal catalysts such as Pt, Pd, Rh, Sn, Ni, Co, Cu, Zn as well as their combinations (Davda, Shabaker, Huber, Cortright, & Dumesic, 2003) are active in C−C bond breaking. Catalysts based on noble metals have a lower sensitivity to carbon deposition and higher activity. Nevertheless, considering the high cost and limited availability of the noble metals, it is more economical to develop catalysts based on non-noble metals such as nickel, with good performance and high resistance to carbon deposition (Jun, Roh, & Chary, 2007). It is emphasized that alumina is one of

the most widely used supports because of its high surface area which allows a great dispersion of the active ingredient. In addition, alumina has relevant characteristics such as high porosity, good mechanical strength and high thermal stability, forming a diffusion barrier that prevents the active phase migration to form clusters of larger particles with lower activity (Suzuki et al., 2002). There is evidence that the support has a significant effect on the overall catalytic behavior and the use of reducible oxides, such as ZrO_2 and CeO_2, can result in additional benefits when compared to irreducible oxides, such as Al_2O_3. The reducibility and oxygen transfer capacity of ZrO_2 and CeO_2 have shown to be fundamental in keeping the active phase surface free of carbon deposits (Souza, Aranda, & Schmal, 2001), thereby decreasing the carbon deposition and promoting the stability of the catalyst during the reforming of hydrocarbons.

2.4.2 Solar hydrogen production

The conversion of solar energy into a clean fuel (H_2) is the most promising technology for the future because large quantities of hydrogen can potentially be generated in a clean and sustainable manner. Undoubtedly, the conversion of solar energy into H_2 is one of the greatest challenges facing scientists in the twenty-first century. Solar energy can be used to produce hydrogen in the form of heat (thermochemical), light (photoelectrochemical or photocatalytic) or electricity (electrolysis). Among these, thermochemical, photoelectrochemical or photocatalytic are the most efficient solar paths to hydrogen because they do not have the inefficiencies associated with the conversion of solar energy to electricity followed by electrolysis. Thermochemical water splitting and photolytic water splitting and are examined briefly in next sections.

2.4.2.1 Thermochemical splitting of water

The most direct method for using solar energy to derive hydrogen from water is one-step thermolysis of the water molecule. However, the thermodynamics of the thermolysis of water demands very high temperatures to dissociate the molecule (e.g. 3000 K for 64% dissociation at 1 bar) (Perkins & Weilmer, 2004). These temperatures not only require extremely high solar concentrations ($\times$38,000 for 50% efficiency), but material selection for reactor construction at these temperatures proves challenging. Additionally, direct thermolysis produces a mixture of H_2 and O_2 that requires high-temperature separation based on the use of porous ceramic membranes. Due to materials limitations at the high-temperatures required, direct water splitting is not expected to be economically viable in the near future.

An alternative to direct thermolysis is to use a series of processes for the production of hydrogen by multistep thermochemical cycles that bypass the H_2/O_2 separation problem and further allow operating at relatively moderate upper temperatures. Analysis of the most promising thermochemical cycles (Abanades, Charvin, Flamant, & Neveu, 2006; Perret et al., 2005) indicates that two-step water-splitting cycles using metal-oxide redox pair are the most attractive cycles for practical solar applications taking into account its simplicity and efficiency.

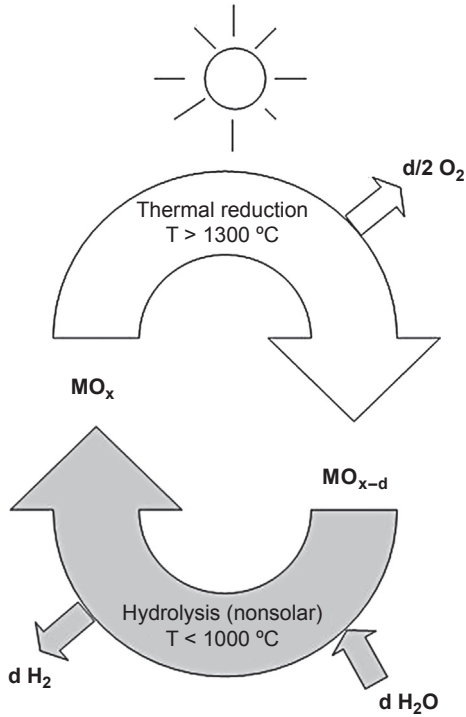

Figure 2.4 Schematic representation of the two-step water-splitting metal-oxide redox cycle.

The two-step metal-oxide redox cycle (Figure 2.4) proceeds with the endothermic solar thermal dissociation of the metal oxide to the metal or the lower-valence oxide (Eqn (2.15)) followed by a second, nonsolar, exothermic step corresponding to the hydrolysis of the metal/lower-valence oxide to form H_2 and regenerating the metal oxide (Eqn (2.16)). The net reaction is H_2O + thermal energy $\rightarrow$ $H_2 + {}^1/_2\ O_2$.

$$\text{First step (solar): } MO_x + \text{thermal energy} \rightarrow MO_{x-d} + d/2\ O_2 \tag{2.15}$$

$$\text{Second step (nonsolar): } MO_{x-d} + d\ H_2O \rightarrow MO_x + d\ H_2 \tag{2.16}$$

This cycle was originally proposed by Nakamura (1977) using the redox pair Fe_3O_4/FeO. Subsequently, the redox pair ZnO/Zn was also considered as a potential candidate for two-step thermochemical water-splitting (Palumbo et al., 1998). Based on a thermal reduction at 2273 K, the energy efficiency of ZnO/Zn cycle is about 45% and the maximum exergy without heat recovery is 29% (Miller et al., 2008). Consequently, ZnO/Zn is considered the most favourable cycle given its potential for reaching high energy and exergy efficiencies, but strong technical challenges are remaining associated with the very high temperature necessary for the thermal reduction of solids. The very high thermal reduction temperature used for the ZnO/Zn (>2235 K) and also for Fe_3O_4/FeO (>2500 K) redox pairs means severe sintering,

melting and vaporization of materials decreasing the efficiency and durability in the cyclic operation. In addition, in such systems it is necessary to quench the reduction products (FeO or Zn) to avoid reoxidation, a fact introducing irreversibilities and complexities in large-scale utilization.

To thermodynamically favour the thermal reduction of Fe_3O_4 to FeO, solid solutions between the Fe_3O_4 and M_3O_4 forming ferrites with spinel-type structure have been examined using an approach that involves the possibility of combining the high H_2 yield associated with the Fe_3O_4/FeO redox pair with the high reduction of the M_3O_4/MO pair. In the past several years, research effort have focused on various types of ferrites MFe_2O_4 (M = Co (Kodama, Kondoh, Yamamoto, Andou, & Satou, 2005; Miller et al., 2008), Ni (Kodama, Gokon, & Yamamoto, 2008) and Zn (Kaneko et al., 2004) Ni-Mn (Tamaura, Steinfeld, Kuhn, & Ehrensberger, 1995), Ni-Zn and Mn-Zn (Agrifiotis et al., 2005)). These ferrites showed a thermal reduction step that proceeds at lower temperature than in the case of pure Fe_3O_4. However, the reduction temperature of these ferrites are close with their melting points and therefore the reduced ferrites sinter after this step, decreasing the H_2 generation in the subsequent hydrolysis cycle. To prevent the sintering or melting of ferrites during thermal reduction, the supporting of ferrites on monoclinic ZrO_2 that have good sintering resistance in the temperature range from 1273 to 1673 K have been studied. Partially stabilized tetragonal ZrO_2 and yttria-stabilized cubic zirconia are also studied as supports to suppress the ferrite high temperature sintering (Gokon, Mizuno, Nakamuro, & Kodama, 2008).

To find redox pairs alternative to Fe_3O_4 or ZnO that work at lower temperatures, different metal oxides have been recently examined. A thermochemical cycle based on CeO_2/Ce_2O_3 has been recently reported by Abanades and Flamant (2006). Thermochemical cycles based on SnO_2/SnO (Abanades, Charvin, Lemont, & Flamant, 2008) and GeO_2/GeO (Kang et al., 2009) are the latest redox pairs studied as alternatives to perform the water-splitting reaction at low temperature. Thermal reduction of GeO_2 was demonstrated at low temperature (below 1773 K), but melting of GeO_2 and disproportionation of GeO restricted the practical application of this cycle.

As has been observed, strong technical challenges for solar thermal water splitting remain associated with the very high temperature necessary for the thermal reduction of solids. Consequently, the progress in material science and engineering applied to the development of materials with lower reduction temperature and high water-splitting ability is still a challenge in this scientific area.

2.4.2.2 *Photocatalytic splitting of water*

Water splitting into H_2 and O_2 is classified as an 'uphill' photocatalytic reaction because it is accompanied by a large positive change in Gibbs free energy. The reaction involves the standard Gibbs free energy change (ΔG°) greater than 237 kJ/mol, equivalent to 2.46 eV per molecule (1 eV/molecule = 96.1 kJ/mol). This energy is equivalent to the energy of photons with wavelengths between 1010 and 500 nm. Because pure water does not absorb solar radiation, the water splitting needs a photo-semiconductor able to efficiently absorb solar energy and then to split the

molecule in an indirect way. Because the electrochemical decomposition of water to hydrogen and oxygen is a two electron stepwise process, it is possible to use photo-semiconductor surfaces capable to absorb solar energy to generate electrons and holes that can respectively reduce and oxidize the water molecules adsorbed on photocatalysts. In this reaction, photon energy is converted into chemical energy, as seen in photosynthesis by green plants. This reaction is therefore sometimes referred to as artificial photosynthesis.

$$H_2O_{(l)} \rightarrow H_{2(g)} + {}^{1}/_{2}\, O_{2(g)} \tag{2.17}$$

Figure 2.5 depicts the basic principle of overall water splitting on a solid photocatalyst. Under irradiation with energy greater than the bandgap (E_g) of the semiconductor photocatalyst, the electrons (e^-) of the valence band are excited into the conduction band, whereas the holes (h^+) are left in valence band. The electrons and holes which did not suffer recombination migrate towards the surface of the semiconductor where they respectively reduce and oxidize the water molecules adsorbed on the semiconductor surface.

Photocatalysts

The photocatalysts used for the water-splitting reaction must satisfy several functional requirements with respect to semiconducting and electrochemical properties (Navarro, del Valle, Villoria, & Fierro, 2009, chap. 4): (1) appropriate visible light absorption with band gap around 2.0−2.2 eV and band edge potentials suitable for overall water splitting; (2) ability to separate photo-excited electrons from reactive holes once formed; (3) minimization of energy losses related to charge transport and electron−hole recombination; (4) chemical stability to corrosion and photo-corrosion in aqueous environments; (5) kinetically suitable electron transfer properties from photocatalysts surface to water and (6) low production cost. Apart of the electronic properties of the photo-semiconductors, the precise design of the bulk and surface

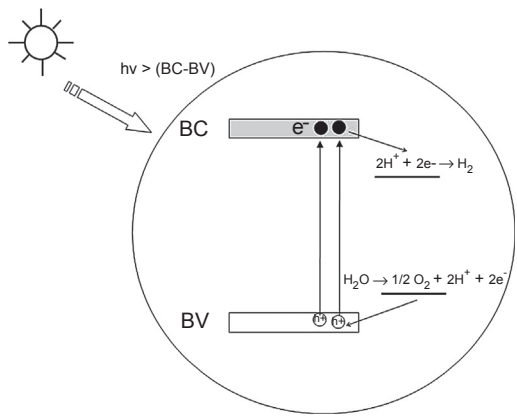

Figure 2.5 Schematic basic principle of overall water splitting on a solid photocatalyst.

properties from the semiconductor is essential to control the interrelation between its electronic, microstructural and surface properties. In the search for more efficient photocatalysts for water splitting, the control of the synthesis of the material to tailor its crystallinity and morphology at nanometric scale is very important, because these properties have a major influence on the rate of water-splitting reaction. Transport of electrons and holes towards the catalyst surface strongly depends on the microstructure and surface properties of photocatalysts. As a general rule, the photoactivity increases in highly crystalline photocatalysts because the density of defects caused by grain boundaries, which act as recombination centres of electrons and holes, decreases when increasing crystallinity of particles (Ikeda et al., 1997). Surface area, determined by the size of the photocatalyst particles, also influences on the efficiency of carriers transport. An efficient charge transport implies necessarily diffusion lengths longer than the size of the particles. Therefore, the possibility for the charge carrier to reach the surface increases upon decreasing the particle size of photocatalysts (Ashokkumar, 1998). Nevertheless, the improvement on the efficiency associated to a high crystalline degree of the photocatalyst has much larger effect on the efficiency than that associated with low crystal sizes (Kudo, Kato, & Tsuji, 2004).

Research in this field was initiated by the pioneering work conducted by Honda and Fujishima in 1972 in a photoelectrochemical cell that demonstrated that hydrogen generation via splitting of water was possible using photocatalysts based on *n*-type TiO_2 semiconductor capable to absorb light energy. This work stimulated the research for water splitting using particulate photocatalysts that was first realized by Lehn, Sauvage, and Ziessel (1980), Sato and White (1980) and Domen, Naito, Soma, Onishi, and Tamaru (1980). Over the past 40 years, many types of photo-semiconductors, with over 130 materials including oxides, nitrides, sulfides, carbides and phosphides, have been reported to act as efficient particle photocatalysts for hydrogen evolution via water splitting. Among these photocatalysts, the higher quantum yields are reported under ultraviolet light for $NiO/NaTaO_3$ (56% quantum yield) (Kato, Asakura, & Kudo, 2003). Although this yield is very high, results have only a limited value for practical H_2 production because ultraviolet light accounts for only about 3–4% of solar radiation energy. Therefore, a large utilization of solar energy requires the development of photocatalysts capable to split water efficiently under visible light ($\lambda \sim 600$ nm). Currently, the number of visible light-driven photocatalysts is limited. However, many oxides, sulfides, oxynitrides and oxysulfides have recently been found to be active for H_2 and O_2 evolution under visible light irradiation (Table 2.2). So far, the maximum apparent quantum efficiency (hydrogen yield per number of incident photons) for overall water splitting over visible light-driven particle photocatalysts records only a few percent – 5.9% apparent quantum efficiency over $Rh_{2-y}Cr_yO_3/(Ga_{1-x}Zn_x)(N_{1-x}Zn_x)$ photocatalysts applied to pure water under visible irradiation (Hisatomi et al., 2009). The low quantum efficiency is still the current 'bottleneck' of the hydrogen production from solar light. The efficiency values achieved is still far from the quantum efficiency of 10% marked as the initial starting point for practical application. Consequently, progress in material science and engineering applied to the development of efficient semiconductors used as photocatalysts is still a major issue, being the design of efficient photo-semiconductor systems for production of molecular

Table 2.2 Overview of photocatalysts developed in past several years for a water-splitting reaction under visible light

Photocatalysts
Titanium oxide and titanates
TiO_2-Cr-Sb
TiO_2-N
$SrTiO_3$-Cr-Ta
$SrTiO_3$-Cr-Sb
$La_2Ti_2O_7$-Cr
$La_2Ti_2O_7$-Fe
$Sm_2Ti_2S_2O_5$
Tantalates and niobiates
TaON
$CaTaO_2N$
$SrTaO_2N$
$BaTaO_2N$
$Sr_2Nb_2O_{7-x}N_x$
Other transition metal oxides
$BiVO_4$
Ag_3VO_4
Metal oxynitrides
$(Ga_{1-x}Zn_x)(N_{1-x}O_x)$
$(Zn_{1+x}Ge)(N_2O_x)$
Metal sulfides
CdS
CdS-CdO-ZnO
CdS-Zn
ZnS-Cu
ZnS-Ni
ZnS-Pb
$(AgIn)_xZn_{2(1-x)}S_2$
$(CuIn)_xZn_{2(1-x)}S_2$
$(CuAg\ In)_xZn_{2(1-x)}S_2$
$Na_{14}In_{17}Cu_3S_{35}$

hydrogen from water splitting one of the foremost challenges in the development of a solar hydrogen economy.

Configurations

Photocatalysts for photochemical water splitting can be used for this purpose according to two types of configurations: (1) photoelectrochemical cells and (2) particulate photocatalytic system. The photoelectrochemical cell for water decomposition (Figure 2.6) involves two electrodes immersed in an aqueous electrolyte, of which one is a photocatalyst exposed to light (photo-anode in Figure 2.6). The photo-generated electron−hole pairs, produced as a result of light absorption on the photo-anode, are separated by an electric field within the semiconductor. On the one hand, the photo-generated holes migrate to the surface of the semiconductor where they oxidize water molecules to oxygen. On the other hand, the photo-generated electrons move through an electrical circuit to the counter electrode and there reduce H^+ to hydrogen. In order to achieve practical current densities, an additional potential driving-force is usually required through the imposition of external bias voltage or the imposition of an internal bias voltage by using different concentrations of hydrogen ions in the anode/cathode compartments. Water splitting using a photoelectrochemical cell was first reported by Fujishima and Honda (1972) using an electrochemical system consisting of a TiO_2 semiconductor electrode connected through an electrical load to a platinum black counter electrode. Photo-irradiation of the TiO_2 electrode under a small electric bias leads to the evolution of H_2 and O_2 at the surface of the Pt counter electrode and TiO_2 photoelectrode, respectively.

The principles of photochemical water splitting can be extended to the design of systems using photocatalytic semiconductors in the form of particles or powders suspended in aqueous solutions (Bard, 1979, 1980). In this system, each photocatalyst particle functions as a microphotoelectrode performing both oxidation and the

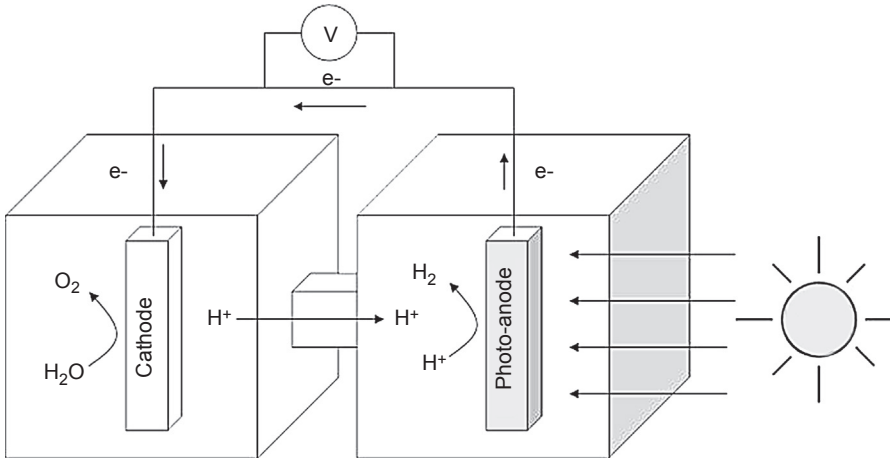

Figure 2.6 Diagram of photoelectrochemical cell for water splitting.

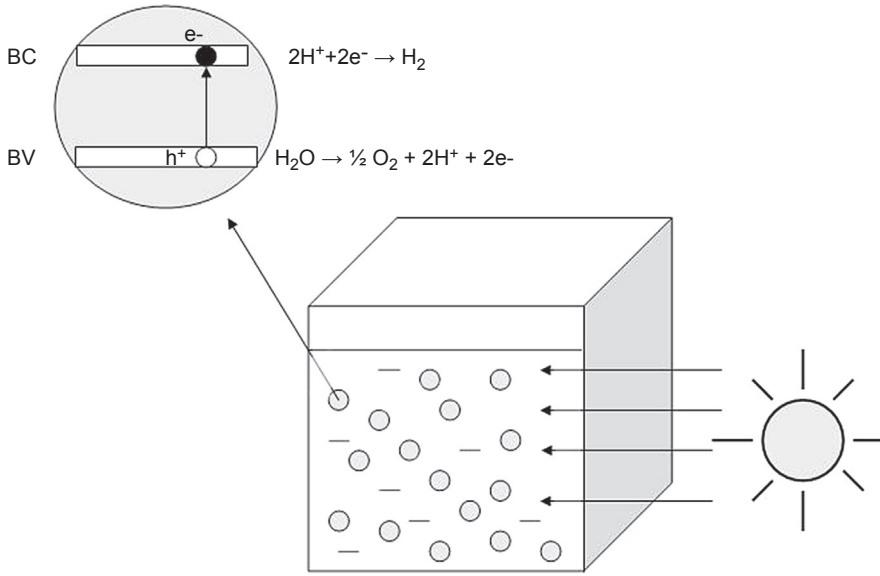

Figure 2.7 Scheme of the photocatalyst particulate suspension system for water splitting.

reduction of water on its surface (Figure 2.7). Such particulate systems have the advantage of being much simpler and less expensive to construct and use compared with photoelectrochemical cells. Furthermore, a wide variety of materials can be used as photocatalysts in particulate systems that may be difficult to prepare in single crystals or the high quality polycrystalline form necessary in the case of photoelectrodes. Another advantage is that electrical conductivity does not need to be as high as that required for photoelectrodes. Moreover, the efficiency of light absorption in suspensions or slurries of powders can be very high because of the high semiconductor surface exposed to light (100 mg of the photocatalysts powder of particle diameter $\sim$0.1 μm consists of more than 10^{11} particles that are mobile and independent of each other). However, particulate photocatalytic systems also have disadvantages: the separation of charge carriers is not as efficient as with a photoelectrode system and the difficulty associated with the effective separation of the stoichiometric mixture of oxygen and hydrogen to avoid the backward reaction.

2.4.3 Hydrogen as storage of renewable energy

Renewable energy sources such as solar and wind energy have a great potential, but their utilization is difficult because of their fluctuating and intermittent nature. In large electricity networks, renewable power sources with a low output can be balanced by conventional power generation, but a higher percentage of renewables needs improved energy storage. Whereas batteries, compressed air, flywheels or capacitors are suited for the short-term storage of electricity, long-term storage could be realized with hydrogen as energy vector.

Up to now, problems with fluctuating and intermittent electricity from renewable power sources have only occurred in local power grids with a high percentage of renewables. In the future, high percentage of renewable electricity is expected to be fed into larger power grids. With power-to-gas, electricity is converted into hydrogen by water electrolysis as a way to store the excess of electricity. The hydrogen produced can be stored in pressure tanks and when needed can be reconverted into electricity with fuel cells or hydrogen combustion engines. Figure 2.8 shows the main components of a power-to-gas system. Alkaline electrolysers are mainly used for hydrogen production because they are commercially available. In most systems, DC-to-DC converters connect the components via DC bus and thus enable the optimal operation of each component. Hydrogen storage is mainly done with pressure tanks, because they are commercially available and high capacities can be achieved with them. The design and sizing of the components of the power-to-gas plants considerably influences their efficiency, reliability and economics. The overall efficiency of power-to-gas plants strongly depends on the control strategy and can be improved by higher efficient components, improved heat management and optimal system integration.

The first power-to-gas system for storing renewable electricity by means of electrolysis and subsequent storage was realized in 1991 (Szyszka, 1998), and the number of installations increased in the past several years. Most of the plants correspond to laboratory or demonstration purpose with an installed capacity from 50 to 800 kWe. Until now more than 40 pilot plants have been evaluated and operated around the world (Gahleitner, 2013). In most power-to-gas pilot plants, wind or solar energy is used to generate electricity. Most of the projects (95%) are situated in Europe (Germany, Spain and the United Kingdom) and North America (the United States and Canada). One critical aspect of the power-to-gas projects that have been evaluated is that most of them have only been operated for a short time and it has only been possible to gather long-term experience from a small number of projects. The application of the hydrogen as storage of renewable energy is still under development and further developments are necessary. In many of the plants, it was concluded that design and sizing, control strategy and system integration have a great influence on their overall efficiency, reliability and economics. Topics for further research are the improvement of efficiency, reliability, lifetime, maintenance, costs of hydrogen components (electrolyser and fuel cell) and better ways of dealing with fluctuating power sources. In order to improve the overall performance, the reduction of auxiliary equipment and the continuous long-term operation will be necessary. The further developments about system integration, system configurations and control strategy with respect to the available infrastructure and type of application are also recommended.

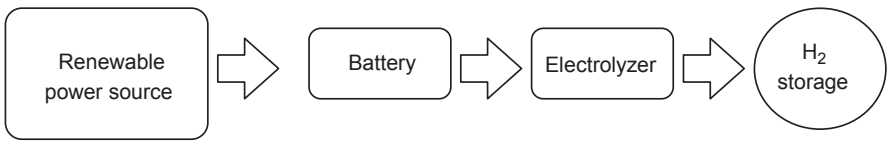

Figure 2.8 Components of a power-hydrogen storage system.

2.5 Hydrogen infrastructures and distribution

2.5.1 Present situation

Although micro-scale hydrogen production systems are being developed for domestic use by some companies, it is likely that a distribution network of hydrogen would be required to supply hydrogen to end-users. Small-scale hydrogen production from electrolysis or biomass would be possible but large plants would otherwise be required for fossil fuel feedstocks so that the CO_2 by-product could be captured and stored. In the short-term, small-scale SMR could also be deployed at refuelling stations to facilitate the transition to a hydrogen economy but these would not be compatible with decarbonization in the long-term (Usher & Strachan, 2012).

Hydrogen consumption is expected to grow rapidly because of the development of fuel cells, and specifically for the transport sector. As stated previously, SMR, coal and residues gasification are mature technologies for H_2 production. However, as long as natural gas remains at low or even moderate cost, SMR will continue to be the technology of choice for massive H_2 production. This trend is expected to continue because of the rapidly growing interest in fuel cells in stationary and mobile applications. Accordingly, distributed hydrogen production via small-scale reforming at refueling stations could be an attractive near to mid-term option for supplying hydrogen to vehicles. A brief account of the present status and/or commercialization of H_2 production technologies based in fossil precursors have been examined in some detail (Navarro et al., 2007). Hydrogen is relatively difficult to store and transport in comparison with petroleum fuels. Hydrogen gas has two principle drawbacks: (1) the unusually low volumetric energy density of gaseous hydrogen means that the gas must be compressed to extremely high pressure to be used as a transport fuel and (2) the tiny molecules have a higher propensity to leak than other gases and require particularly complex storage materials. One method of avoiding these two difficulties is to compress the hydrogen into a liquid, but this is energetically expensive and difficult to handle because liquid hydrogen boils at around 20 K. Other forms of hydrogen, for example metal hydrides, are being researched but are at an early stage of development. Three methods are commonly used to deliver hydrogen to refuelling stations (Yang & Ogden, 2007). Pipelines to transport H_2 gas require large up-front capital investments but can transport large amounts of hydrogen very cheaply over short and sometimes long distances. The most cost-effective method of delivering small amounts of H_2 gas over short distances is using gaseous tube trailers, but for longer distances, liquid H_2 delivery by road tanker becomes optimal.

Refineries, chemicals and petrochemicals industries consume large amounts of hydrogen with a large-scale production and supply infrastructure. Regarding transportation of hydrogen, along with conventional means such as high-pressure or cryogenic tankers as well as cylinders, transportation via pipelines has been employed to cater to a specific range of mass-consuming users. The main difference in the delivery and supply aspects for hydrogen as a source of energy and hydrogen as an industrial gas lies in the fact that the former element has to deal with supplying an unspecified range of general consumers. For this reason, successful dissemination of the new technology

necessarily requires not only development of technologies for producing and supplying hydrogen as energy but also examination into methods of transportation for its supply. From these points of view, after the turn of the century, various projects have been launched in Europe and the USA for technical as well as economic examinations regarding a method of transporting hydrogen by mixing it into the existing natural gas pipeline system wherein hydrogen is separated at the end users.

2.5.2 Future infrastructure prospects: centralized and distributed options

Central, semi-central and distributed production facilities are expected to play a role in the evolution and long-term use of hydrogen as an energy carrier. The different resources and processes used to produce hydrogen may be suitable to one or more of these scales of production. Large central hydrogen production facilities (750,000 kg/day) that take advantage of economies of scale will be needed in the long term to meet the expected large hydrogen demand. Compared with distributed production, centralized production will require more capital investment as well as a substantial hydrogen transport and delivery infrastructure. Intermediate-size hydrogen production facilities (5000−50,000 kg/day) located in close proximity (30−140 km) to the point of use may play an important role in the long-term use of hydrogen as an energy carrier. These facilities can provide not only a level of economy of scale but also minimize hydrogen transport costs and infrastructure. Hydrogen can also be produced in small units where it is needed, such as vehicle refueling stations, in a manner known as 'distributed production'. Distributed production may be the most viable approach for introducing hydrogen in the near term in part because the initial demand for hydrogen will be low. Two distributed hydrogen production technologies that may offer potential for development and commercialization are (1) reforming natural gas or liquid fuels, including renewable liquids, such as ethanol and bio-oil and (2) small-scale water electrolysis.

Distributed hydrogen production via small-scale reforming is less costly than centralized production until a large geographically concentrated hydrogen demand has built up. Distributed hydrogen production would be attractive especially in the early stages of a hydrogen economy. Hydrogen could be provided where it was needed, allowing supply to match demand, as more hydrogen vehicles were added to the fleet. On the other hand, once a large enough hydrogen energy demand is developed, central hydrogen production would become cost competitive with distributed production. Many analysts see eventual production of hydrogen in large centralized plants, with local hydrogen pipeline distribution similar to that for natural gas. At this time, decarbonized fossil hydrogen or other low carbon sources of hydrogen could be phased in (hydrogen from renewables). If hydrogen is produced at a large centralized energy complex, the added costs for CO_2 capture and disposal are quite small. In contrast, with distributed small-scale hydrogen production from fossil fuels, capture, collection and sequestration of CO_2 from many dispersed small reformers is prohibitively expensive (Muradov, 2003). Thus, implementing the fossil hydrogen/CO_2 sequestration scenario for hydrogen supply supposes that

hydrogen is produced in large plants. The cost of hydrogen from biomass or wastes is also lower at large scale.

Development of hydrogen infrastructure requires the identification of potential markets for the related technologies which are not always easy to identify especially when the technology is still in its infancy. However, hydrogen's versatility through its use in proton exchange membrane fuel cells makes it applicable in a wide variety of end-user applications. This versatility also provides a basis for the assessment of the market requirements (Ajayi-Oyakhire, 2012).

The markets for hydrogen include fuel cell devices such as portable consumer electronics, micro-cooling, heat and power (CHP) for power generation and transport. It has been suggested (Mathur, 2013) that the major future markets for hydrogen as fuel will depend primarily on four factors: (1) cost of hydrogen; (2) the rate of advance of various H_2-consuming technologies; (3) the cost of competing energy systems and (4) the potential long-term restrictions on greenhouse gases.

Hydrogen has the potential to become a very important transport fuel for proton exchange membrane-powered vehicles. However, for hydrogen to have a stable and long-term market share in the automotive sector, several technological factors that influence the costs of vehicles will need to be addressed. The costs of fuel cell electric vehicles are determined by their automotive fuel cell systems e.g. the on-board storage tanks, the fuel cell stack itself, the electric drive motor. Another even more critical factor that drives the market for hydrogen as a transport fuel is the amount of greenhouse gas reduction achievable with hydrogen as opposed to other low emissions fuel options, e.g. bio-fuels. As a transport fuel, bio-fuels have the potential to be the most cost-effective, low-carbon option to conventional transport fuels simply because they are easy to produce and use, and may not require a radical infrastructure overhaul. However, despite their massive potential, sources of bio-fuels are surrounded by controversy.

If all the uncertainties around hydrogen as a fuel are resolved, there are still issues to do with aligning investment in refuelling infrastructure, investment in new vehicle technology and incentives to buy hydrogen vehicles to make them cost-effective until they are mass-produced. It is believed that to achieve a successful transition to hydrogen as a transport fuel, government policy will play a prominent role by maintaining incentives that can promote the uptake and mass-market appeal of the next generation of zero-emission vehicles in an effort to decarbonize the road transport system.

There are numerous niche markets for hydrogen in stationary applications, some of which include medium scale stationary fuel cell systems (200−1000 kW) and CHP or combined CHP plants that could be used for neighbourhood-scale power generation. These could also be useful for off-grid or remote micro-generation of power. The Energy Saving Trust (2009) suggested that micro-generation products such as fuel cell micro-CHP units could meet up to 30−40% of the UK's electricity needs and make a vital contribution to reaching targets of 80% reduction in carbon emissions by 2050.

New markets for hydrogen in the areas of light duty vehicles, forklifts, buses, scooters and back-up power units are also growing. Besides this, the gas industry is interested in hydrogen because of dwindling gas reserves and the need to limit emissions of CO_2 to meet target reductions in greenhouse gases. One way of possibly

incorporating hydrogen would be adding it to natural gas and distributing it in the existing infrastructure. Studies performed for the International Gas Union (Slim, 2006) indicate that replacing 10% v/v of a natural gas supply stream with hydrogen reduces CO_2 emissions by 3%. It has been also suggested that CO_2 reductions of up to 15% could be achieved with hydrogen gas addition up to 50% v/v. This small CO_2 reduction compared with the volumetric amount of hydrogen added is due to the low density and low calorific value of hydrogen.

2.6 Other hydrogen production methods

2.6.1 Plasma reforming

The energy and free radicals used for the reforming reaction are provided by plasma typically generated with electricity or heat, but the network of reforming reactions is the same as that in conventional reforming. When water or steam is injected with the fuel, H•, OH• and O• radicals in addition to electrons are formed, thus creating conditions for both reductive and oxidative reactions to occur.

Plasma devices referred to as plasmatrons can generate very high temperatures (approximately 2000 °C) with a high degree of control using electricity (Bromberg, Cohn, Rabinovich, & Alexeev, 1999; Paulmier & Fulcheri, 2005). The heat generated is independent of reaction chemistry, and optimal operating conditions can be maintained over a wide range of feed rates and gas compositions. Compactness of the plasma reformer is ensured by high energy density associated with the plasma itself, and by the reduced reaction times, resulting in short residence times. H_2-rich gas streams can be efficiently produced in plasma reformers from a variety of precursors (biomass, bio-oils or natural gas) with conversion efficiencies close to 100% (Bromberg et al., 1999; Paulmier & Fulcheri, 2005). Plasma-reforming technology has potential advantages over conventional technologies of hydrogen manufacturing. The high temperatures, high degree of dissociation and substantial degree of ionization achieved by plasmas can be used to accelerate thermodynamically favourable chemical reactions without a catalyst or to accelerate endothermic reforming reactions. Plasmas could be used to produce H_2 for a variety of stationary applications, such as distributed and low-pollution electricity generation for fuel cells. Besides, it could be used for mobile applications, such as for on-board generation of H_2 for fuel cell powered vehicles, and for refueling stations (stationary sources of hydrogen for vehicles).

The disadvantages of plasma reforming are the dependence on electricity and the difficulty of high-pressure operation required for high-pressure processes. High pressure, if achievable, increases electrode erosion due to decreased arc mobility and, therefore, it decreases electrode lifetime.

2.6.2 Ion transport membrane reforming

Ion transport membranes (ITM) are nonporous multicomponent oxides suited to work at temperatures above 973 K and have high oxygen flux and selectivity

(Dyer, Richards, Russek, & Taylor, 2000). The initial design was carried out for a hydrogen refuelling station dispensing about 12,000 Nm^3 H_2/day. Initial cost estimations show significant reduction in the cost of on-site high-pressure H_2 produced according to ITM technology in a plant of capacity in the range 3000−30,000 Nm^3 H_2/day. For instance, the cost of the H_2 produced via ITM methodology appears approximately 27% cheaper than the liquid H_2 transported by road.

In this approach, oxygen is separated from air fed to one side of the membrane at temperatures around 300 K and moderate pressure (0.03−0.20 bar) and reacts on the other side with methane and steam at higher pressure (3−20 bar) to form a mixture of CO and H_2. Then this mixture can be processed downstream to produce H_2 or liquid fuels. Among the different geometries employed for the ITM reactor, the flat-plate system offers some advantages because it reduces the number of seals and thus makes safer operation.

2.6.3 Sorbent enhanced reforming

Sorbent enhanced SMR is an emerging technology for the production of high-purity hydrogen from hydrocarbons reforming with in situ CO_2 capture (Broda et al., 2013). In this concept, calcium oxide is mixed with the SR catalyst, removing the CO_2 (and CO) via carbonation of calcium oxide. The resulting H_2/CO mixture produced according to this methodology is H_2-enriched. Thus, a syngas composition of 90% H_2, 9.5% CH_4, 0.5% CO_2 and CO levels below 50 ppm has been reported. This reduces the need for downstream processing (WGS and preferential oxidation) which are expensive in a small-scale steam reformer. In addition, removal of CO_2 by calcium oxide makes the reaction to occur at lower temperature (673−773 K vs 1073−1273 K), reducing heat losses and material costs. Sorbent-enhanced reforming technology is still at the demonstration scale, and shows promise for low-cost H_2 production. Critical issues in this methodology are sorbent lifetime and system design.

2.6.4 Microchannel reactors

Over the past few years, there has been great interest in finding an improved process that decreases both the investment and operating costs of hydrogen production via SR reaction. Microchannel reactors are one of the most attractive options to reduce capital cost by intensifying reactor equipment and reducing operating costs by improving heat and mass transfer (Hu et al., 2005; Wihite et al., 2013). A conventional methane steam reformer is quite large (approximately 450,000 Nm^3 H_2/day) and operates with a contact time of the order of 1 s. However, a microchannel plant with the same capacity operates with a contact time below 10 ms which corresponds to a plant volume around 88 Nm^3, much lower than the 2700 Nm^3 required in conventional methane steam reformer plants (Tonkovich et al., 2004). Recently, methane SR experiments have been conducted on a prototype with a channel width of 0.7 mm and wash-coated with 0.03 mm of a Ni-based catalyst is operated at 1023 K and 11 bar with feed composition of 25% CH_4 and balance H_2O. Results indicate that volumetric heat

fluxes greater than 150 W/cm^3 are achievable at residence times of 6.9 ms, whereas volumetric heat fluxes greater than 100 W/cm^3 were observed at overall thermodynamic efficiencies above 70%. Design simulations revealed that 20−100% improvements in volumetric heat transfer rates may be achieved by reducing channel widths from 0.7 to 0.3 mm. The use of microchannel reactors demonstrates that a highly active catalyst allows methane SR to be carried out with a contact time of less than 1 ms. Further reduction in contact time may be reasonably achieved by increasing the catalyst thickness in a manner that minimizes heat and mass transport limitations through careful design.

2.7 Future trends

There is a tremendous body of work pursued towards the development of H_2-generation technologies. The large-scale production of hydrogen from natural gas and other available hydrocarbons through catalytic reforming processes remains the cheapest source of hydrogen. Methane SR is the standard technology employed in industrial production of H_2, but it produces massive amounts of CO_2 which have some impact on global warming. One approach to reduce CO_2 emissions is to apply reforming methods to alternative renewable precursors. Biomass precursors derived from plant crops, agricultural residues, woody biomass, etc., are being used for generating heat, electricity and liquid transportation fuels (ethanol, sugars). Clean biomass precursors are converted to a gas mixture from which hydrogen is extracted by means of reforming processes. Because these technologies are already advanced from decades of research and development, it is unlikely that there will be a substantial improvement in the performance of these technologies in the coming years. Improvements in the performance can however come from new catalytic developments and new reactor designs such as catalytic membrane reactors which enhance syngas conversion by shifting the equilibrium of the reaction.

There is a need to develop nonconventional processes for renewable H_2 production outside the C-cycle. One of the most promising renewable energy technologies is the production of H_2 by water splitting using solar energy. Two-step metal-oxide redox cycles are considered one of the most attractive thermochemical cycles for practical solar H_2 production taking into account its simplicity and potential for reaching high energy and exergy efficiencies, but strong technical challenges remain associated with the very high temperature necessary for the thermal reduction of solids. Consequently, the progress in material science applied to the development of materials with lower reduction temperature and high water-splitting ability is still a challenge. Water-splitting reaction using photonic energy technology on semiconductor surfaces offers the most promising renewable energy technology in the production of H_2. However, more than three decades after the initial reports of photoinduced water splitting on semiconductor electrodes, efficient solar-powered hydrogen production based on this concept remains a challenge. Improving the efficiency of photocatalysts requires developments based on an understanding of the sophisticated factors that determine the photoactivity for the water-splitting reaction. On the other hand, the

search for new photocatalytic materials with improved semiconducting and electrochemical properties is still likely to be the key to success. These areas represent significant opportunities for improving water-splitting photocatalysts.

2.8 Sources of further information and advice

Ball, M., Wietschef, M. (Eds.) (2009). *The hydrogen economy- opportunities and challenges*. New York, NY: Cambridge University Press, USA.

Gandia, L.M., Arzamendi, G., Dieguez, P.M. (Eds.) (2013). *Renewable hydrogen technologies - production, purification, storage, applications and safety.* Philadelphia, PA: Elsevier Science, USA.

Liu, V., Song, C., Subramani, V. (Eds.) (2010). *Hydrogen and syngas production and purification technologies*. Hoboken, NJ: John Wiley & Sons, USA

Rajeshwar, K., McConnell, R., Licht, S. (2008). *Solar hydrogen generation - toward renewable energy future.* New York, NY: Springer, USA.

Nomenclature

η_a	Anode overpotential
APR	Aqueous-phase reforming
E_g	Band gap
Bcf	Billion cubic feet
η_c	Cathode overpotential
COS	Carbonyl sulfide
E	Cell voltage for water electrolysis
CCHP	Combined cooling, heat and power
CB	Conduction band
DC	Direct current
FC	Fuel cell
FCEVs	Fuel cell electric vehicles
LTS	Low temperature shift
HCN	Hydrogen cyanide
HTS	High temperature shift
HyPr-RING	Hydrogen production by reaction-integrated novel gasification
η_{ohm}	Interelectrode ohmic drop
ITM	Ion transport membranes
kWh	Kilowatts/hour
MSR	Methane steam reforming
MT	Million tonnes
PSA	Pressure swing adsorption
QY	Quantum yield
E_{rev}	Reversible thermodynamic decomposition voltage
ΔG°	Standard Gibbs free energy
SR	Steam reforming
SRE	Steam reforming of ethanol

SCWG	Supercritical water gasification
TOF	Turn-over frequency
UV	Ultraviolet light
VB	Valence band
VM	Volatile matter
λ	Wavelength
WGS	Water−gas shift

Acknowledgements

The authors gratefully acknowledge the Ministry of Science and Innovation (Spain) and the Autonomous Government of Madrid, Madrid (Spain) under grants CTQ2013-48669-P, PIB2010BZ-00531 and S2013/MAE-2882, respectively.

References

Abanades, S., & Flamant, G. (2006). Thermochemical hydrogen production from a two-step solar-driven water-splitting cycle based on cerium oxides. *Solar Energy, 80*, 1611−1623.

Abanades, S., Charvin, P., Flamant, G., & Neveu, P. (2006). Screening of water-splitting thermochemical cycles potentially attractive for hydrogen production by concentrated solar energy. *Energy, 31*, 2805−2822.

Abanades, S., Charvin, P., Lemont, F., & Flamant, G. (2008). Novel two-step SnO_2/SnO water-splitting cycle for solar thermochemical production of hydrogen. *International Journal of Hydrogen Energy, 33*, 6021−6030.

Adamson, K. A. (August 2008). *Fuel cell today*.

Agrifiotis, C., Roeb, M., Konstandopoulos, A. G., Nalbandian, L., Zaspalis, V. T., Sattler, C., et al. (2005). Solar water splitting for hydrogen production with monolithic reactors. *Solar Energy, 79*, 409−421.

Ajayi-Oyakhire, O. (2012). *IGEM report*. UK: Institution of Gas Engineers & Managers.

Alberta Department of Energy Report (2004).

Alstrup, I., & Andersen, N. T. (1987). Statistical models for ensemble control by alloying and poisoning of catalysts: II. Comparisons with Monte Carlo simulations and with experimental results. *Journal of Catalysis, 104*, 466−479.

Ashokkumar, M. (1998). An overview on semiconductor particulate systems for photoproduction of hydrogen. *International Journal of Hydrogen Energy, 23*, 427−438.

Auprête, G., Descorme, C., & Duprez, D. (2003). Bio-ethanol catalytic steam reforming over supported metal catalysts. *Catalysis Communications, 3*, 263−267.

Balasubramanian, B., Ortiz, A. L., Kaytakuglu, S., & Harrison, D. P. (1999). Hydrogen from methane in a single step process. *Chemical Engineering Science, 54*, 3543−3552.

Bard, A. J. (1979). Photoelectrochemistry and heterogeneous photo-catalysis at semiconductors. *Journal of Photochemistry, 10*, 59−75.

Bard, A. J. (1980). Photoelectrochemistry. *Science, 207*, 139−144.

Bengaard, H. S., Norskov, J. K., Sehested, J., Clausen, B. S., Nielsen, L. P., Molenbroek, A. M., et al. (2002). Steam reforming and graphite formation on Ni catalysts. *Journal of Catalysis, 209*, 365−384.

Birot, A., Epron, F., Descorme, C., & Duprez, D. (2008). Steam reforming of ethanol. 2. Preliminary kinetic investigation of Pt/CeO_2 catalysts. *Applied Catalysis B: Environmental, 79*, 17−25.

Breen, J. P., Burch, R., & Coleman, H. M. (2002). Metal-catalysed steam reforming of ethanol in the production of hydrogen for fuel cell applications. *Applied Catalysis B: Environmental, 39*, 65−74.

Broda, M., Manovic, V., Imtiaz, Q., Kierzkowska, A. M., Anthony, E. J., & Muller, C. R. (2013). High-purity hydrogen via the sorption-enhanced steam methane reforming reaction over a synthetic CaO-based sorbent and a Ni catalysts. *Environmental Science & Technology, 47*, 6007−6014.

Bromberg, L., Cohn, D. R., Rabinovich, A., & Alexeev, N. (1999). Plasma catalytic reforming of methane. *International Journal of Hydrogen Energy, 24*, 1131−1137.

Chen, G., Andries, J., Spliethoff, H., Fang, M., & van der Enden, P. J. (2004). Biomass gasification integrated with pyrolysis in a circulating fluidised bed. *Solar Energy, 76*, 345−349.

Chiou, J. Y. Z., Wang, W. Y., Yang, S. Y., Lai, C. L., Huang, H. H., & Wang, C. B. (2013). Ethanol steam reforming to produce hydrogen over Co/ZnO and PtCo/ZnO catalysts. *Catalysis Letters, 143*, 501−507.

Cortright, R. D., Davda, R. R., & Dumesic, J. A. (2002). Hydrogen from catalytic reforming of biomass-derived hydrocarbons in liquid water. *Nature, 418*(6901), 964−966.

Davda, R. R., Shabaker, J. W., Huber, G. W., Cortright, R. D., & Dumesic, J. A. (2003). Aqueous-phase reforming of ethylene glycol on silica-supported metal catalysts. *Applied Catalysis B: Environmental, 43*, 13−26.

Demirbas, M. F. (2006). Hydrogen from various biomass species via pyrolysis and steam gasification processes. *Energy Sources A, 28*, 245−252.

Dickerson, T., & Soria, J. (2013). Catalytic fast pyrolysis: a review. *Energies, 6*, 514−538.

Divisek, J., & Murgen, J. (1983). US Patent 4,394,244.

Domen, K., Naito, S., Soma, M., Onishi, T., & Tamaru, K. (1980). Photocatalytic decomposition of water vapour on an $NiO{-}SrTiO_3$ catalyst. *JCS Chemical Communications*, 543−544.

Duret, A., Friedli, C., & Maréchal, F. (2005). Process design of production using wood gasification. *Journal of Cleaner Production, 13*, 1434−1446.

Dyer, P. N., Richards, R. E., Russek, S. L., & Taylor, D. M. (2000). ITM technology for oxygen separation and syngas production. *Solid State Ion, 134*, 21−33.

Energy Saving Trust (2009). http://www.publications.uk/pa/cm200910/cmselect/cmenvaud/159/159we23.htm.

Farrell, A. E., Plevin, R. J., Turner, B. T., Jones, A. D., O'Hare, M., & Kammen, D. M. (2006). Ethanol can contribute to energy and environmental goals. *Science, 311*, 506−508.

Fatsikostas, A. N., Kondarides, D. I., & Verykios, X. E. (2001). Steam reforming of biomass-derived ethanol for the production of hydrogen for fuel cell applications. *Chemical Communications*, 851−852.

Fierro, V., Akdim, O., & Mirodatos, C. (2003). On-board hydrogen production in a hybrid electric vehicle by bio-ethanol oxidative steam reforming over Ni and noble metal based catalysts. *Green Chemistry, 5*(1), 20−24.

Fuel Cell Energy. (2011). *Fact sheet*. www.fuelcellenergy.com.

Fujishima, A., & Honda, K. (1972). Electrochemical photolysis of water at a semiconductor electrode. *Nature, 238*, 37−38.

Gahleitner, G. (2013). Hydrogen from renewable electricity: an international review of power-to-gas pilot plants for stationary applications. *International Journal of Hydrogen Energy, 38*, 2039−2061.

Gokon, N., Mizuno, T., Nakamuro, Y., & Kodama, T. (2008). Application of an internally circulating fluidized bed for windowed solar chemical reactor with direct irradiation of reacting particles. *Journal of Solar Energy Engineering, 130*(1), 1−8.

Hafner, M., Karbuz, S., Esnault, B., & El Andaloussi, H. (2005). *OME report*.

Hisatomi, T., Maeda, K., Takanabe, K., Kubota, J., Sakata, Y., & Domen, K. (2009). Aspects of the water splitting mechanism on $(Ga_{1-x}Zn_x)(N_{1-x}O_x)$ photocatalyst modified with $Rh_{2-y}Cr_yO_3$ co-catalyst. *Journal of Physical Chemistry C, 113*, 21458−21466. http://www.publications.uk/pa/cm200910/cmselect/cmenvaud/159/159we23.htm.

Hu, J., Wang, Y., Cao, C., Elliott, D. C., Stevens, D. J., & White, J. F. (2005). Conversion of biomass syngas to DME using a microchannel reactor. *Industrial & Engineering Chemistry Research, 44*, 1722−1727.

Huber, G. W., Shabaker, J. W., Evans, S. T., & Dumesic, J. A. (2006). Aqueous-phase reforming of ethylene glycol over supported Pt and Pd bimetallic catalysts. *Applied Catalysis B: Environmental, 62*, 226−235.

Ikeda, S., Tanaka, A., Shinohara, K., Hara, M., Kondo, J. N., Maruya, K., et al. (1997). Effect of the particle size for photocatalytic decomposition of water on Ni-loaded $K_4Nb_6O_{17}$. *Microporous Materials, 9*, 253−258.

Jun, K. W., Roh, H. S., & Chary, K. V. R. (2007). Structure and catalytic properties of ceria-nickel catalyst for CO_2 reforming of methane. *Catalysis Surveys from Asia, 11*, 97−113.

Kaneko, H., Kodama, T., Gokon, N., Tamaura, Y., Lovegrove, K., & Luzzi, A. (2004). Decomposition of Zn ferrite for O_2 generation by concentrated solar radiation. *Solar Energy, 76*, 317−322.

Kang, K.-S., Kim, C.-H., Cho, W.-C., Bae, K.-K., Kim, S.-H., & Park, C.-S. (2009). Novel two-step thermochemical cycle for hydrogen production from water using germanium oxide: KIER 4 thermochemical cycle. *International Journal of Hydrogen Energy, 34*, 4283−4290.

Kato, H., Asakura, K., & Kudo, A. (2003). Highly efficient water splitting into H_2 and O_2 over lanthanum-doped $NaTaO_3$ photocatalysts with high crystallinity and surface nanostructure. *Journal of American Chemical Society, 125*, 3082−3089.

Kodama, T., Kondoh, Y., Yamamoto, R., Andou, H., & Satou, N. (2005). Thermochemical hydrogen production bi a redox system of ZrO_2-supported Co(II) ferrites. *Solar Energy, 78*, 623−631.

Kodama, T., Gokon, N., & Yamamoto, R. (2008). Thermochemical two-step water splitting by ZrO_2-supported $Ni_xFe_{3-x}O_4$ for solar hydrogen production. *Solar Energy, 82*, 73−79.

Koo, K. Y., Roh, H. S., Jung, U. H., & Yoon, W. L. (2009). CeO_2 promoted Ni/Al_2O_3 catalyst in combined steam and carbon dioxide reforming of methane for gas to liquid (GTL) process. *Catalysis Letters, 130*, 217−221.

Kruse, A., Meier, D., Rimbrecht, P., & Schacht, M. (2000). Gasification of pyrocatechol in supercritical water in the presence of potassium hydroxide. *Industrial & Engineering Chemistry Research, 39*, 4842−4848.

Kudo, A., Kato, H., & Tsuji, I. (2004). Strategies for the development of visible-light-driven photocatalysts for water splitting. *Chemistry Letters, 33*, 1534−1535.

Kuznetsov, B., & Shchipko, M. L. (1996). Chemical processing of coal for sustainable development. *Chemistry for Sustainable Development, 4*, 403−412.

Laosiripojana, N., Assabumrungrat, S., & Charojrochkul, S. (2007). Catalytic dry reforming of methane over high surface area ceria. *Applied Catalysis A: General, 327*, 180−188.

Lehn, J. M., Sauvage, J. P., & Ziessel, R. (1980). Photochemical water splitting. Continuous generation of hydrogen and oxygen on irradiation of aqueous suspensions of metal loaded strontium titanate. *New Journal of Chemistry, 4*(11), 623−628.

Liguras, D. K., Kondarides, D. I., & Verykios, X. E. (2003). Production of hydrogen for fuel cells by steam reforming of ethanol over supported noble metal catalysts. *Applied Catalysis B: Environmental, 43*, 345−354.

Lin, S., Harada, M., Suzuki, Y., & Hatano, H. (2002). Effect of coal rank on steam gasification of coal/CaO mixtures. *Energy Fuels, 81*, 2079−2085.

Llorca, J., de la Piscina, P. R., Sales, J., & Homs, N. (2001). Direct production of hydrogen by steam reforming of aqueous solutions over oxide catalysts. *Chemical Communications*, 641−642.

Mathur, V. K. (2013). *Energy and transport processes*, 13 AIChE annual meeting, San Francisco.

Matsumura, Y., Minowa, T., Potic, B., Kersten, S. R. A., Prins, W., & van Swaaij, W. P. M. (2005). Evaluation of biomass gasification in supercritical water. Evaluation and prospects. *Biomass Bioenergy, 29*, 269−292.

Mattos, L. V., Jacobs, G., Davis, B. H., & Noronha, F. B. (2012). Production of hydrogen from ethanol: review of reaction mechanism and catalyst deactivation. *Chemical Reviews, 112*, 4094−4123.

Miller, J. E., Allendorf, M. D., Diver, R. B., Evans, L. R., Siegel, N. P., & Stuecker, J. N. (2008). Metal oxide composites and structures for ultrahigh temperature solar thermochemical cycles. *Journal of Material Science, 43*, 4714−4728.

Millet, P., & Grigoriev, S. (2012). Water electrolysis technologies. In J. M. Gandia, G. Arizmendi, & P. M. Dieguez (Eds.), *Renewable hydrogen technologies* (pp. 19−41). Elsevier.

Minowa, T., Zhen, F., & Ogi, T. (1998). Cellulose decomposition in hot-compressed water with alkali or nickel catalyst. *Journal of Supercritical Fluids, 13*, 253−259.

Mondal, K., Piotrowski, K., Dasgupta, D., Hippo, E., & Wiltowski, T. (2005). Hydrogen from coal in a single step. *Industrial & Engineering Chemical Research, 44*, 5508−5517.

Muradov, N. Z., & Veziroğlu, T. N. (2005). From hydrocarbon to hydrogen−carbon to hydrogen economy. *International Journal of Hydrogen Energy, 30*, 225−237.

Muradov, N. Z. (2003). Emission-free fuel reformers for mobile and portable fuel cell applications. *Journal of Power Sources, 118*, 320−324.

Muradov, N. Z., & Veziroğlu, T. N. (Eds.). (2012). *Carbon neutral fuels and energy carriers*. FL: CRC Press/Taylor and Francis.

Nakamura, T. (1977). Hydrogen production from water utilizing solar heat at high temperatures. *Solar Energy, 19*, 467−475.

National academy of sciences report.(February 11, 2004).

Navarro, R. M., Alvarez-Galván, M. C., Sanchez-Sanchez, M. C., Rosa, F., & Fierro, J. L. G. (2005). Production of hydrogen by oxidative reforming over Pt supported on Al_2O_3 modified with Ce and La. *Applied Catalysis B: Environmental, 55*(4), 229−241.

Navarro, R. M., Peña, M. A., & Fierro, J. L. G. (2007). Hydrogen production reactions from carbon feedstocks: fossil fuels and biomass. *Chemical Reviews, 107*, 3952−3991.

Navarro, R. M., del Valle, F., Villoria, J. A., & Fierro, J. L. G. (2009). In B. Serrano, & H. de Lasa (Eds.), *Advances in chemical engineering-progress in photocatalytic reaction engineering* (pp. 111−143). Elsevier Science Publishers.

Nikolla, E., Holewinski, A., Schwank, J., & Linic, S. (2006). Controlling carbon chemistry by alloying: carbon tolerant reforming catalyst. *Journal of American Chemical Society, 128*, 11354−11355.

Orio, A., Corella, J., & Narvaez, I. (1997). Performance of different dolomites on hot raw gas cleaning from biomass gasification with air. *Industrial & Engineering Chemistry Research, 36*, 3800−3808.

Palumbo, R., Lédé, J., Boutin, O., Elorza Ricart, E., Steinfeld, A., Möller, S., et al. (1998). The production of Zn from ZnO in a high-temperature solar decomposition quench process I. The scientific framework for the process. *Journal of Chemical Engineering Science, 53*(14), 2503−2517.

Parizotto, N. V., Rocha, K. O., Damyanova, S., Passos, F. B., Zanchet, D., Marques, C. M. P., et al. (2007). Alumina-supported Ni catalysts modified with silver for the steam reforming of methane: effect of Ag on the control of coke formation. *Applied Catalysis A: General, 330*, 12−22.

Paulmier, T., & Fulcheri, L. (2005). Use of non-thermal plasma for hydrocarbon reforming. *Chemical Engineering Journal, 106*, 59−71.

Peña, M. A., Gomez, J. P., & Fierro, J. L. G. (1996). New catalytic routes for syngas and hydrogen production. *Applied Catalysis A: General, 144*, 7−57.

Peña, M. A., Alvarez-Galvan, M. C., & Fierro, J. L. G. (2011). Supported metals in the production of hydrogen. In J. A. Anderson, & M. Fernandez (Eds.), *Supported metal catalysts* (pp. 301−405). London: ICP.

Perkins, C., & Weimer, A. (2004). Likely near-term solar-thermal water splitting technologies. *International Journal of Hydrogen Energy, 29*(15), 1587−1599.

Perret, T., Chen, Y., Besenbruch, G., Diver, R., Weimer, A., Lewandowski, A., et al. (2005). *Solar hydrogen generation research*. Annual Progress Report US DOE IV.I.1.

Pile, D. L., & Daugthy, D. H. (2005). *Sandia national laboratory*. Report on DOE Contract DE-AC04-94AL85000.

Rostrup-Nielsen, J. R. (1984). Catalytic steam reforming. In J. R. Anderson, & M. Boudart (Eds.), *Catalysis science and technology* (pp. 1−117). Berlin: Springer Verlag.

Rostrup-Nielsen, J. R. (2001). Conversion of hydrocarbons and alcohols for fuel cells. *Physical Chemistry Chemical Physics, 3*, 283−288.

Rostrup-Nielsen, J. R. (2003). Hydrogen generation by catalysis. In I. T. Horvath (Ed.), *Encyclopedia of catalysis*. Wiley Interscience.

Rudloff, M. (2005). *SYNBIOS second generation automotive biofuel conference*. Sweden: Stockholm.

Sánchez-Sánchez, M. C., Navarro, R. M., & Fierro, J. L. G. (2007). Ethanol steam reforming over Ni/La-Al_2O_3 catalysts: influence of lanthanum loading. *Catalysis Today, 129*, 336−345.

Santo, U., Seifert, H., Kolb, T., Krebs, L., Kuhn, D., & Wiemer, H. J. (2007). Conversion of biomass based slurry in an entrained flow gasifier. *Chemical Engineering & Technology, 30*, 967−969.

Sato, S., & White, J. M. (1980). Photodecomposition of water over Pt/TiO_2 catalysts. *Chemical Physics Letters, 72*, 83−86.

Sha, X. (2005). Coal gasification. In G. Jinsheng (Ed.), *Encylopedia of life support systems* (pp. 380−396).

Shabaker, J. W., Simonetti, D. A., Cortright, R. D., & Dumesic, J. A. (2005). Sn-modified Ni catalysts for aqueous-phase reforming: characterization and deactivation studies. *Journal of Catalysis, 231*(1), 67−76.

Shell. (2004). http://www.roads2hy.com.

Slim, K. B. (2006). Should we add hydrogen to the natural gas grid to reduce CO_2-emissions. In *23rd world gas conference, Amsterdam*.

Sorensen, B. (2011). *Hydrogen and fuel cells* (2nd ed.). Academic Press. Emerging Technologies and Applications.

Souza, M. M. V. M., Aranda, D. A. G., & Schmal, M. (2001). Reforming of methane with carbon dioxide over Pt/ZrO_2/Al_2O_3 catalyst. *Journal of Catalysis, 204*, 498−511.

Sun, J., Qiu, X. P., Wu, F., & Zhu, W. T. (2005). H_2 from steam reforming of ethanol at low temperature over Ni/Y_2O_3, Ni/La_2O_3 and Ni/Al_2O_3 catalysts for fuel-cell application. *International Journal of Hydrogen Energy, 30*, 437–445.

Suresh, B., Schlag, S., & Igonuchi, Y. (2004). *Hydrogen marketing research report. Chemical Economics Handbook-SRI consulting*. Ref. 743.5000A.

Suzuki, T., Morikawa, A., Suda, A., Sobukawa, H., Sugiura, M., Kanazawa, J., et al. (2002). Alumina-ceria-zirconia composite oxides for three way catalysts. *R&D Review Toyota CRDL, 37*, 28.

Szyszka, A. (1998). Ten years of solar hydrogen demonstration project at Neunburg Vorm Wald, Germany. *International Journal of Hydrogen Energy, 23*(10), 849–860.

Tamaura, T., Steinfeld, A., Kuhn, P., & Ehrensberger, K. (1995). Production of solar hydrogen by a novel, two-step water splitting thermochemical cycle. *Energy, 20*(4), 325–330.

Taralas, G., & Kontominas, M. G. (2006). Pyrolysis of solid residues commencing from the olive oil food industry for potential hydrogen production. *Journal of Analytical and Applied Pyrolysis, 76*, 109–116.

Tomishige, K., Asadullah, M., & Kunimori, K. (2004). Syngas production by biomass gasification using Rh/CeO_2-SiO_2 catalysts and fluidized bed reactor. *Catalysis Today, 89*, 389–403.

Tonkovich, A. Y., Perry, S. T., Wang, Y., Qiu, D., LaPlante, T., & Rogers, W. A. (2004). Microchannel process technology for compact. Methane steam reforming. *Chemical Engineering Science, 59*, 4819–4824.

Trimm, D. L., & Önsan, Z. I. (2001). Onboard fuel conversion for hydrogen-fuel-cell-driven vehicles. *Catalysis Reviews: Science and Engineering, 43*, 30–84.

Usher, W., & Strachan, N. (2012). Critical mid-term uncertainties in long-term decarbonisation pathways. *Energy Policy, 41*, 433–444.

Vagia, E. C., & Lemonidou, A. A. (2008). Thermodynamic analysis of hydrogen production via steam reforming of selected components of aqueous bio-oil fraction. *International Journal of Hydrogen Energy, 33*, 2489–2500.

Vaidya, P. D., & Rodrigues, A. E. (2006). Insight into steam reforming of ethanol to produce hydrogen for fuel cells. *Chemical Engineering Journal, 117*, 39–49.

Velez, J. F., Chejne, F., Valdez, C. F., Emery, E. J., & Londoño, C. A. (2008). Biomass in fluidized bed: an experimental study. *Fuel, 88*, 424–430.

Weber, G., Fu, Q., & Wu, H. (2006). Energy efficiency of an integrated process based on gasification for hydrogen production from biomass. *Developments in Chemical Engineering and Mineral Processing, 14*, 33–48.

Wei, J. M., & Iglesia, E. (2004). Proposed rate expressions for CH_4-reforming reactions on Ni-based catalysts. *Journal of Catalysis, 224*, 370–383.

Wilhite, B. A., Breziner, L., Mettes, J., & Bossard, P. (2013). Radial microchannel reactors (RMRs) for efficient and compact steam reforming of methane: experimental demonstration and design simulations. *Energy Fuels, 27*, 4403–4410.

Yang, C., & Ogden, J. M. (2007). Determining the lowest-cost hydrogen delivery mode. *International Journal of Hydrogen Energy, 32*, 268.

Yildiz, B. M., Petri, G., & Forsberg, C. (July 31, 2005). *ANL-05 report*. Argon.

This page intentionally left blank

Economics of hydrogen production

3

P.E. Dodds
University College London, London, UK

3.1 Introduction

The cost of producing hydrogen, and in particular low-carbon 'green' hydrogen, will be a critical factor in the success of hydrogen-powered technologies in the future. At the moment, steam methane reforming (SMR) is used to produce most of the 50 Mt hydrogen that is produced globally each year (Hydrogen Production Expert Panel, 2013). SMR produces substantial CO_2 emissions and alternative routes will be needed in the future to produce low-carbon hydrogen. Electrolysis using low-carbon electricity is one option that produces hydrogen with very high purity. Otherwise, carbon-based feedstocks (natural gas, coal and biomass) could also be used in conjunction with carbon capture and storage (CCS) technologies. More speculative photochemical and biological production routes are also under development. Although the economics of SMR are understood (Schoots, Ferioli, Kramer, & van der Zwaan, 2008), the economics of low-carbon hydrogen production are more uncertain, particularly for nascent technologies.

This chapter examines the costs of hydrogen production, both now and in the future. It considers how these costs are affected by commodity prices and environmental externalities. Finally, it compares the levelised costs of hydrogen production for a range of technologies.

The chapter is structured as follows. The levelised cost of hydrogen production is introduced in Section 3.2. This section also examines cost data sources and discusses some of the methodological issues that should be addressed when assessing the economics of hydrogen production. The cost components of the principal hydrogen production technologies are examined in Section 3.3, starting with steam reforming, gasification of coal and biomass and electrolysis. The costs from different technologies are compared in Section 3.4 and some conclusions are drawn in Section 3.5. Those readers interested in further information and advice can consult Section 3.6.

3.2 Levelised cost of hydrogen production

The costs of producing hydrogen using different technologies can be compared using the levelised cost of hydrogen production. The levelised cost accounts for the initial plant investment (annualised capital cost (ACC) over the economic lifetime of the plant), fixed and variable annual operations and maintenance costs (FOM and

Compendium of Hydrogen Energy. http://dx.doi.org/10.1016/B978-1-78242-361-4.00003-0

VOM, respectively) and the cost of feedstocks (e.g. electricity, natural gas; denoted FUEL). It can be summarised using this equation:

$$\text{Levelised cost} = \text{ACC} + \text{FOM} + (\text{VOM} + \text{FUEL}) \times \text{FCONSUM} \tag{3.1}$$

where FCONSUM is the annual fuel consumption. In this chapter, each of these costs is estimated for each technology and they are then combined to calculate the levelised cost for each technology over time.

3.2.1 Sources of plant cost data

Schoots et al. (2008) analyse the actual construction costs of numerous SMR, coal gasification and electrolysis plants, and these data are used to estimate plant capital costs in this chapter.

Production costs for these technologies have been estimated using a self-consistent methodology by two research programmes and these are primarily used to estimate plant costs in the future. The H2A programme of the US Department of Energy (Steward, Ramsden, & Zuboy, 2008) produced estimates in 2005 and updated most of these in 2012, so can be used to understand how cost projects have evolved in the intervening period. The TECHPOL programme estimated costs in 2004 (Krewitt & Schmid, 2004). Further data are extracted from studies in the literature (Acar & Dincer, 2014; Cormos, 2010, 2014; DEA, 2010; Gray & Tomlinson, 2002; Iaquaniello, Giacobbe, Morico, Cosenza, & Farace, 2008; Khamis & Malshe, 2010; Kreutz, Williams, Consonni, & Chiesa, 2005; NRC, 2004, 2008).

Four general obstacles must be overcome when estimating plant costs. First, it can be difficult to estimate the capital and operating and maintenance (O&M) costs for each technology using a consistent approach as different studies use different assumptions (e.g. whether the cost of licensing or land is included). Second, costs tend to vary between countries as a result of variations in labour costs, environmental regulations, currency exchange rates, supply chains, banking practices and other factors. Third, it is necessary to convert the costs into consistent monetary units for a single currency and year. Fourth, the feedstock conversion efficiency of each technology should be calculated consistently across the model. The following sections expand on these obstacles.

3.2.1.1 Estimating plant investment and operating and maintenance costs

The direct plant investment costs are the cost of the installed equipment. All plant construction projects also have substantial indirect costs as well. System costs include design, site preparation, contingency costs and profits for the construction contractor (direct costs implicitly include profits for equipment manufacturers). The cost of land, licensing and permits vary between countries. Some plants have additional financial costs to cover financing for up-front fees.

All studies estimate direct technology costs, but some indirect costs are often omitted. Because indirect costs are often around a third of the total cost, the inclusion or omission of indirect costs can be one of the principal drivers of cost differences between studies.

O&M cost estimates vary as they can include equipment, feedstock(s), outage costs, running costs, licensing costs and labour. Some are fixed each year (e.g. for annual outages and for licensing), whereas other variable O&M costs are proportional to the plant output. We separately consider fixed and variable O&M costs in this chapter, and we further separate feedstock costs which are a large proportion of the overall cost.

3.2.1.2 Cost variations between countries

Large-plant construction costs in North America tend to be lower than those in Europe as a result of less restrictive environmental regulations, lower taxes and lower labour and land costs (Schoots, Rivera-Tinoco, Verbong, & van der Zwaan, 2010). Similar cost variations occur in most regions of the world. Unfortunately, there is no simple way of comparing costs in different countries. Cost variations between countries should be taken into account both when interpreting cost projections from different studies and when applying the cost projections in this chapter to a particular country.

3.2.1.3 Converting costs into consistent monetary units

Investment costs in the literature are specified in both dollars and euros, with different base years used in different studies, so it is necessary to account for both currency conversion and inflation. In this chapter, all costs are converted to US dollars in the year 2013. There are two methods for this conversion: (1) adjust for inflation in the original currency and then apply the year 2013 currency exchange rate or (2) use the exchange rate in the study base year and then to adjust for inflation using the inflation rate of that country. Exchange rates are more volatile than inflation rates, so the first option produces a more consistent conversion factor. In this chapter, in common with Lemus and Duart (2010) and Bartels, Pate, and Olson (2010), the first approach is adopted. Because plant cost inflation data are difficult to obtain, average economy-wide inflation rates are used in this chapter as a proxy. It is possible that these inflation rates could diverge over time, for example from variations in the global price cost of building supplies such as steel.

3.2.1.4 Estimating feedstock conversion efficiency

The energy that can be extracted from a fuel is measured as the energy released as heat when the fuel undergoes complete combustion or electrochemical conversion with oxygen. The energy content can be measured using two reference points depending on whether the water product is treated as a liquid or steam. The higher heating value (HHV) is the strict thermodynamic definition of energy content, whereas the lower heating value (LHV) excludes the latent heat used to evaporate the water products

Table 3.1 Heat of combustion of several fuels (MJ/kg)

	Higher heating value	Lower heating value	HHV:LHV ratio
Hydrogen	142	121	1.17
Methane	56	50	1.12
Gasoline	47	44	1.07
Coal (anthracite)	27	27	1.00
Wood	15	15	1.00

from combustion (Petchers, 2002). The more practical LHV definition became prominent in the nineteenth century as the heat from sulphur-rich coal combustion below 150 °C could not be recovered and put to economic use. It is possible for the LHV efficiency to exceed 100%, which reflects an antiquated accounting convention rather than a violation of the first law of thermodynamics (Dodds & Hawkes, 2014). LHV efficiencies are commonly quoted in Europe, whereas HHV efficiencies are used in the United States.

In this chapter, efficiencies are quoted using HHV. Table 3.1 compares the LHV and HHV heat of combustion for several common fuels. For solid fuels with higher carbon content (e.g. coal and biomass), the HHV and LHV can vary substantially depending on the exact fuel composition. For example, the efficiency of coal gasification is different for anthracite, lignite and other types of coal.

3.2.2 Learning curves for hydrogen production technologies

The costs of new technologies tend to reduce over time through industrial 'learning by doing' (Grübler, Nakićenović, & Victor, 1999). As companies gain experience manufacturing a product, they optimise the design and production process, and so costs gradually decrease as the number of manufactured products increases (Staffell, 2014).

There are limited opportunities for technology learning to reduce the costs of producing hydrogen from carbonaceous feedstocks. Natural gas and coal technologies are mature and are unlikely to change substantially over the coming decades. Biomass gasification is an evolution of coal gasification, whereas nuclear technologies are also evolutions of current technologies. Moreover, the rate of learning for large plants tends to be lower as there are relatively few opportunities to optimise the production process compared with smaller, high-volume technologies.

Electrolysis has more potential for cost reductions and efficiency improvements in the future as much research is targeted at reducing the costs of fuel cells and electrolysers, whereas the modular nature of the technology makes it more suitable for low-cost assembly line production. Some novel technologies are also being researched

with very high capital costs but low running costs, for example algal hydrogen production, and these would have significant potential for cost reductions if they were shown to be economically viable.

This chapter considers both the current and future costs of hydrogen production. Cost reductions are considered where appropriate in the future costs, but it is important to remember that these could change because of technology learning. The presented costs for each technology are an average when building numerous plants and so represent the 'nth-of-a-kind' plant rather than a 'first-of-a-kind' plant that would be expected to have substantially higher costs.

3.2.3 Feedstock commodity price forecasts

The most important operating cost for most plants is the cost of the feedstock(s) from which the hydrogen is produced. Feedstock prices in the future are highly uncertain and could cause substantial variations in the overall levelised costs of producing hydrogen from different technologies. The electricity price is particularly difficult to forecast as it depends on the generation portfolio and on the design of the electricity system (for example, the electricity price can reduce below zero if intermittent renewable generation exceeds demand). The projections used in this chapter are shown in Table 3.2.

Feedstock prices are likely to be affected by taxes and/or subsidies. For example, a carbon tax would increase the cost of fossil fuels unless the CO_2 emissions were captured and stored using CCS technologies. Other environmental externalities, for example sulphur and other emissions from coal, might be taxed in some jurisdictions and not in others. In this chapter, the impact of a carbon tax on the levelised costs is examined in a sensitivity study.

Table 3.2 Feedstock prices projections used in this study

	Price projections in 2010	Price projections in 2050		
	Central	Low	Central	High
Coal	4	4	5	7
Gas	10	7	12	17
Biomass	10	6	10	14
Electricity	14	14	29	33

The gas and coal projections are from DECC (2013). Biomass cost projections are from Howes et al. (2011). Electricity costs are average annual wholesale costs; this is currently around £50/MWh in the United Kingdom and future costs depend on the choice of generation technology (National Grid, 2014). The costs from 2030 are assumed to be £90/MWh which is the strike price agreed for two new nuclear reactors that are being constructed in the United Kingdom and is taken as a typical long-term low-carbon electricity price. All costs have been converted to US dollars in 2013 and are expressed per GJ of embodied energy.

3.3 Cost components of principal hydrogen production technologies

This section examines cost and operating efficiency estimates for hydrogen production technologies. Estimates of the capital costs of the most prominent hydrogen production technologies are compared in Figure 3.1. Fixed O&M costs are often best expressed as a function of the capital costs; we take this approach in Figure 3.2. The feedstock conversion efficiency for hydrogen production by each technology is compared in Figure 3.3. In all three of these figures, the costs for large centralised and small distributed plants are compared, as are the costs for centralised fossil plants both with and without CCS technologies.

3.3.1 Hydrogen production from carbonaceous feedstocks

3.3.1.1 Steam methane reforming

Most hydrogen for industrial applications is currently produced by cracking carbonaceous fossil fuels. Methane is the most common feedstock but coal has also been used. It would be necessary to deploy CCS systems on these plants to produce low-carbon hydrogen which would only be economic for large-scale production.

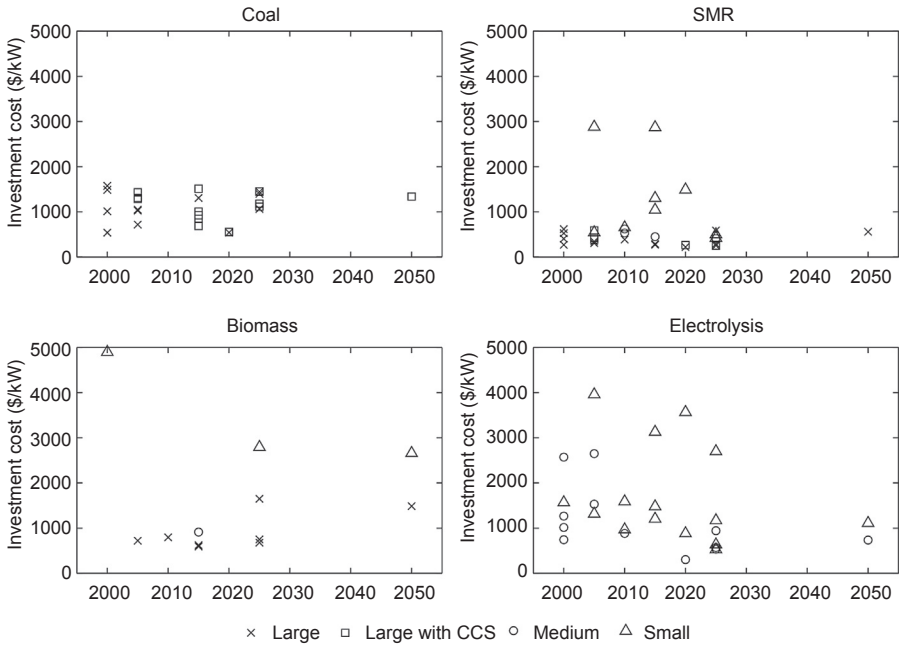

Figure 3.1 Capital costs for hydrogen production technologies. Costs are from the studies cited in Section 3.2.1 and have been converted to US dollars in 2013.

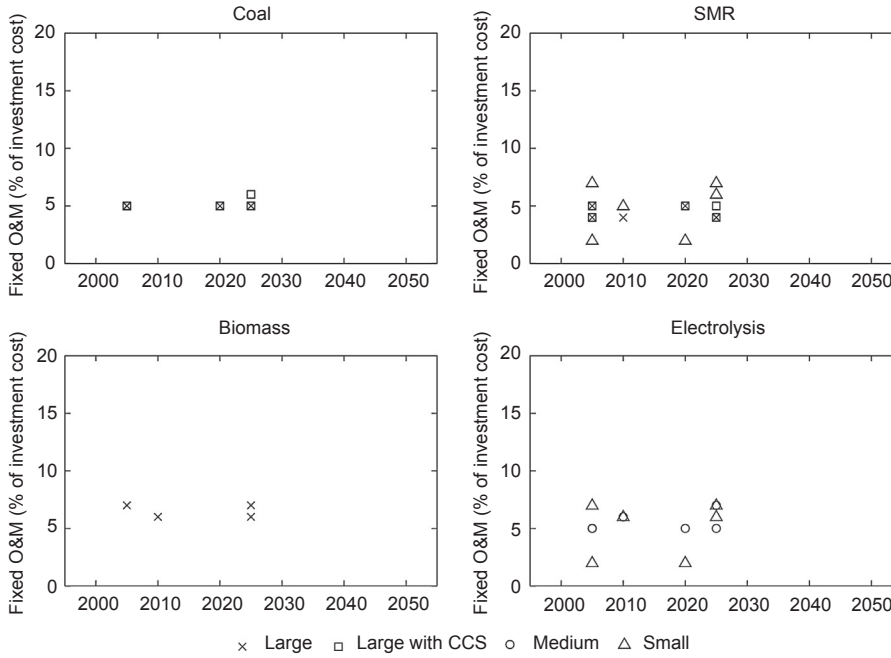

Figure 3.2 Fixed operating and management (O&M) costs for hydrogen production technologies. Costs are from the studies cited in Section 3.2.1 and are presented as a percentage of the capital costs in each study.

Natural gas reforming is currently the most efficient, economical and widely used process for producing hydrogen and has been used globally for many decades in the oil refinery and fertiliser industries. Steam reforming is the standard method but membrane reforming has also been demonstrated in small-scale plants (Iaquaniello et al., 2008; Shirasaki et al., 2009). Figure 3.1 shows that SMR has the lowest capital costs of the principal hydrogen production technologies.

Compact, small-scale reformers, suitable for refuelling stations, have been proposed as one option for a hydrogen economy (Ogden, 2001). Although this option would remove the requirement for expensive delivery infrastructure in the early stages of a transition to hydrogen, the systems would be too small for CCS to be used so substantial CO_2 emission savings would be not be achieved.

SMR efficiencies are currently in the range 60−80%, with larger plants being more efficient (Figure 3.3). Efficiencies are expected to rise only slightly in the future, but the gap between central and distributed plant efficiencies should reduce. Membrane plants are likely to only slightly increase the conversion efficiencies (Shirasaki et al., 2009). Despite the high energy efficiency, feedstock costs are already the most important economic factor; moreover, these will rise substantially in the future if CO_2 emissions become heavily taxed. CCS would reduce the impact of such taxes, but are more expensive to build and would reduce plant energy efficiencies.

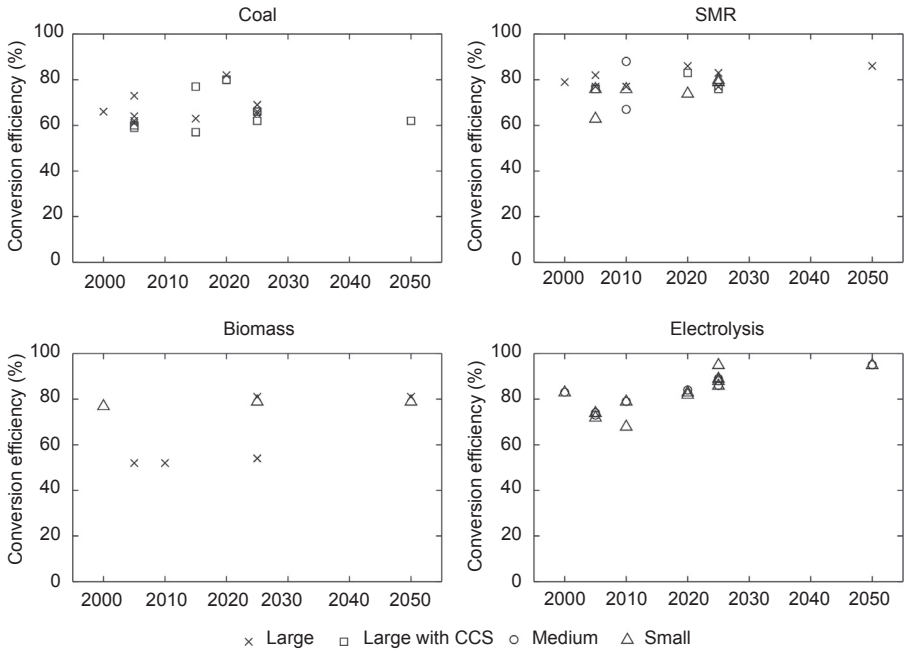

Figure 3.3 Energy efficiencies of the principal hydrogen production technologies. The data are from the studies cited in Section 3.2.1.

The magnitude of the reduction would depend on the energy required to capture, compress and transport the CO_2 to the underground storage site.

3.3.1.2 Coal and oil gasification

Before the development of electricity networks, coal gasification was used to produce gas for lighting purposes. The technology is mature but is less widely used than SMR, despite having lower feedstock costs, because the conversion efficiency is lower and the capital investment costs are higher and more variable. Only large-scale plants are envisaged in the literature.

Although the conversion efficiency of coal gasification is lower than that of SMR (Figure 3.3), the differential has been reduced historically by lower coal prices. Efficiencies range from 50% to 80%, which could represent both technological differences and the wide variations in the quality of different types of coal. Any future conversion efficiency improvements will be reduced by the incorporation of CCS. Because a greater quantity of CO_2 is produced by coal gasification than by SMR for each unit of produced hydrogen, one might expect a greater conversion efficiency reduction to capture the CO_2. On the other hand, membrane technology could reduce the efficiency loss from CO_2 capture (Amelio, Morrone, Gallucci, & Basile, 2007).

Coal-fuelled plants produce emissions other than CO_2 that impact air quality. The costs of such environmental externalities are not often incurred by plant owners but

this might change in the future, either through legislation requiring abatement measures or through the imposition of emissions taxes.

Oil is a more valuable commodity than coal, particularly for transport applications, so is unlikely to be used for hydrogen production unless the transport sector broadly switches to alternative fuels. Although light oils can be reformed in a similar way to natural gas, heavy oils must be gasified to produce hydrogen. The costs of hydrogen production from oil are not generally considered in the literature.

3.3.1.3 Biomass-fuelled technologies

Biomass accounts for 15% of global primary energy consumption and is particularly important in less-developed countries. Saxena, Seal, Kumar, and Goyal (2008) identify three broad methods for producing hydrogen from biomass: thermochemical conversion (gasification or pyrolysis), biochemical/biological conversion and mechanical extraction. Biomass-fuelled technologies are most strongly characterised by their diversity in terms of both the types of technology and the range of different biomass fuels that are used. The data in Figures 3.1–3.3 are only for gasification technologies as the other methods are still at the laboratory stage of development.

All biomass technologies suffer from low yields because of the low hydrogen content of biomass (approximately 6%) and the 40% oxygen content which lowers the overall available energy; as a result, there are no completed industrial-scale demonstrations of any biomass technology for producing hydrogen (Kalinci, Hepbasli, & Dincer, 2009), and cost and energy efficiency data must be considered speculative. Efficiencies are higher for biomass-derived biofuels (e.g. bioethanol) that are processed prior to the hydrogen production plant; the principal advantage of such feedstocks would be to reduce the feedstock transport costs from the farm gate to the hydrogen plant. Biofuel production has increased substantially in recent years, with the loss of land for food production and high land use emissions causing controversy.

Capital costs are similar to coal gasification costs because the conversion processes and plant requirements are broadly similar (Figure 3.1). The range of conversion efficiencies in Figure 3.3 reflects the range of potential feedstocks; the conversion efficiency of wood is unlikely to exceed 50% because of the low heat of combustion (Table 3.1), whereas the higher values represent steam reforming of biofuels. The latter efficiencies are artificially high because they do not account for the energy that is required to produce biofuel from the feedstock. None of the sources in Section 3.2.1 consider biomass technologies with CCS, despite such plants having negative lifecycle emissions. Biomass with CCS has been identified as a key technology for electricity production by several energy system models and hydrogen production from biomass offers similar advantages to the energy system.

3.3.2 Hydrogen production from water

3.3.2.1 Electrolysis

Electrolysis is the only widely used method for producing hydrogen by cracking water and has the important advantage of producing very pure hydrogen with no CO_2

Table 3.3 Capital costs of hydrogen production plants for the levelised cost comparison

	Capital costs in 2010			Capital costs in 2050		
	Low	**Central**	**High**	**Low**	**Central**	**High**
Coal	722	1056	1391	694	1056	1418
Coal + CCS	1045	1344	1642	926	1272	1618
Gas	288	409	530	233	409	585
Gas + CCS	361	468	575	321	409	585
Biomass	667	759	852	261	759	1257
Electricity	737	1522	2308	457	696	935

These costs are based on the data in Figure 3.1 and are US dollars in 2013. All costs are presented per kW of installed hydrogen output.

emissions. The principal drawback of this method is the high cost of electricity relative to other feedstocks. Alkaline electrolysis has been used to produce hydrogen since the eighteenth century and is the basis of most commercially available electrolysers. Extremely pure hydrogen is produced but at a substantially higher cost than from SMR. Low-temperature polymer electrolyte membrane (PEM) electrolysers and high-temperature solid oxide electrolysers (SOE) have been proposed as more efficient and flexible technologies for the future (DEA, 2010). PEM electrolysers are suited to small-scale hydrogen production and varying loads, for example from intermittent renewable electricity generation, whereas SOEs can reduce electricity requirements by the use of high-temperature heat in a process called thermal cracking.

Figure 3.1 shows that electrolysis systems have a wide range of capital investment costs in the literature. One surprising aspect is that several estimates are higher that the average costs of plants that are already in operation, which range from $750/kW to $2500/kW (Schoots et al. 2008). Costs for small systems are particularly high but all systems are expected to become substantially cheaper in the future through technological breakthroughs and learning.

Twentieth-century electrolysers achieved energy efficiencies in the 58−72% range (Levene, Mann, Margolis, & Milbrandt, 2007) and it is reasonable to assume that new electrolysers will be at the upper end of this range. Efficiencies in the 85−95% range are expected to be achieved for both small- and medium-sized plants in the future, particularly if PEM electrolysers and SOEs can be successfully developed.

3.3.2.2 Thermochemical cracking of water

High-temperature thermal cracking could reduce the cost of hydrogen production from water. Hundreds of high-temperature chemical cycles have been identified for producing hydrogen (Rosen, 2010). Studies have primarily concentrated on two technologies

to produce the energy for these thermochemical cycles. First, high-temperature nuclear reactors could supply both electricity and high-temperature waste heat to an adjacent production plant (Lubis, Dincer, & Rosen, 2010; Utgikar & Thiesen, 2006). Second, concentrated solar power (CSP) plants could produce both electricity and the required temperatures in a central tower for hydrogen production (Coelho, Oliveira, & Mendes, 2010; Felder & Meier, 2008).

The cost of hydrogen production from fourth-generation nuclear reactors has been examined as part of the US Department of Energy Nuclear Hydrogen Initiative program (Bartels et al., 2010). Cost evaluation tools are now being developed (e.g. Khamis & Malshe, 2010). Costs are not presented in this chapter as they are still very uncertain, but more authoritative estimates might become available in future.

The costs of CSP are even more speculative. Most authoritative studies are relatively old (e.g. Glatzmaier, Blake, & Showalter, 1998) and both the costs and efficiencies are uncertain at the moment as the technology is at a relatively early stage of development (Steinfeld, 2005), so no data are presented here. The conversion efficiencies would be strongly influenced by the location of the CSP plant because of the variations in solar radiation across the planet.

3.4 Comparison of costs from different production routes

In this section, we compare the levelised costs of hydrogen production from the more mature technologies discussed above. We calculate the levelised costs using Eqn (3.1). The capital costs that we use in this comparison are shown in Table 3.3 for 2010 and 2050. Capital costs are annualised using an interest rate on capital of 10% and assuming that all plants have an economic lifetime of 30 years. The fixed O&M costs are shown in Table 3.4 and are the same for all years. With the exception of feedstocks, variable O&M costs tend to be very small, so these are incorporated into the fixed O&M costs in these calculations. Table 3.4 also summarises the assumed conversion efficiencies for each plant type, whereas feedstock prices are summarised in Table 3.2.

Figure 3.4 shows the best-estimate levelised cost projections for the principal technologies. Coal gasification and SMR technologies with CCS are shown separately, although CCS only slightly increases the overall cost. Coal gasification is slightly cheaper than SMR, reflecting recent high gas prices and the high gas commodity price forecasts for the longer term. It is notable that some coal gasification plants are under construction in China to supply hydrogen for new industrial plants. Biomass gasification is substantially more expensive than SMR and coal gasification, reflecting the higher commodity cost, and electrolysis is the most expensive technology. Electrolysis produces hydrogen with higher purity that is more valuable as a transport fuel (but has no additional value as an industrial feedstock), so the hydrogen produced by electrolysis potentially has a higher value that would partially offset the higher production cost.

Table 3.4 Fixed O&M costs and assumed conversion efficiencies for the levelised cost comparison, as a function of the capital costs

	Fixed O&M costs	Energy efficiency in 2010	Energy efficiency in 2050
Coal	5%	65%	65%
Gas	4%	80%	85%
Biomass	7%	50%	50%
Electricity	5%	75%	85%

O&M, operating and maintenance.

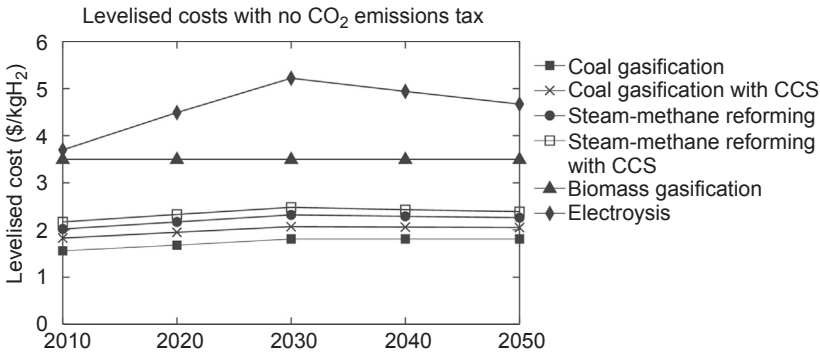

Figure 3.4 Best-estimate levelised cost projections for the principal hydrogen production technologies. Costs are expressed in $/kg hydrogen using US dollars in 2013.

3.4.1 Uncertainties in technology costing

The cost projections in Figure 3.4 are inherently uncertain. In Figure 3.5, cost ranges are estimated for the principal technologies in 2050. These ranges are calculated as follows:

1. The high- and low-capital costs are assumed to be one standard deviation from the best central cost, with the standard deviation calculated from the data presented in Figure 3.1.
2. The fixed O&M cost ranges are calculated from the capital cost ranges using the factors in Table 3.4.
3. Commodity cost ranges are summarised in Table 3.2.
4. The upper and lower energy efficiencies of the plants are assumed to increase or decrease by 5% from the central estimates in Table 3.4.

Figure 3.5(a) shows that the cost range is substantially higher for biomass and electrolysis technologies than for coal gasification and SMR. For electrolysis, the uncertainty over the future price of electricity is particularly important. There is

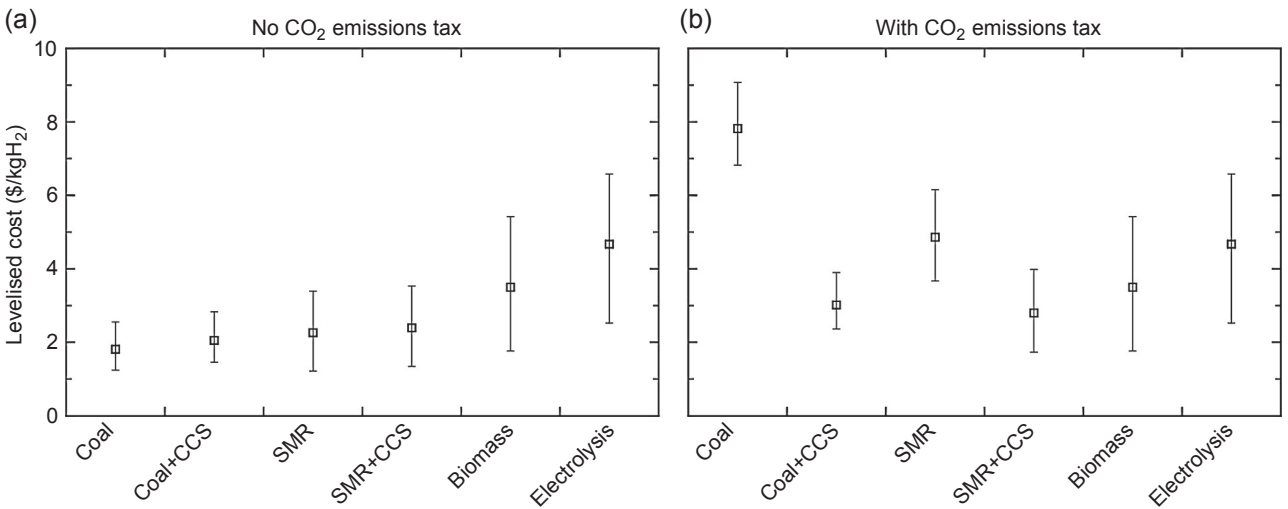

Figure 3.5 Levelised cost ranges for the principal hydrogen production technologies. Costs are presented (a) without and (b) with a CO_2 emissions tax, in units \$/kgH_2.

substantial crossover between the ranges of all the technologies, which suggests that the most economic technology in the future is likely to depend on the success of technological developments and the evolution of feedstock prices.

In a climate of decarbonisation, one method of reducing CO_2 emissions is to apply a carbon tax. Such a tax might increase from \$0/tCO_2 in 2010 to \$300/tCO_2 in 2050 to sufficiently reduce emissions across OECD (Organisation for Economic Cooperation and Development) economies to meet emission reduction targets. Figure 3.5(b) examines the impact of imposing a \$300/tCO_2 tax on hydrogen production costs in 2050. Unabated coal gasification becomes very expensive and the cost of gas SMR is also much higher as well. Coal and gas CCS technologies are also more expensive because the CCS system is assumed to capture only 85% of the CO_2 emissions, so tax must be paid for the remaining 15% that is released to the atmosphere. Biomass feedstocks are assumed to be carbon-neutral so biomass costs are not affected by this tax.

Figure 3.5(b) shows that coal and SMR with CCS are the cheapest production methods when this tax is applied. It is reasonable to conclude that hydrogen production from unabated fossil fuels is uneconomic with this level of taxation. However, the ranges of the other technologies overlap strongly, so it is not possible to identify a technology that is clearly cheaper than the others. The most economic technology in the long term will depend on whether capital and operating costs can be reduced through improved technologies, but will also be sensitive to commodity price variations and to environmental legislation and taxation policies in each country.

3.4.2 Other cost factors

These costs cannot be interpreted as a projection of the future price of hydrogen. The costs will vary by country as they are affected by environmental legislation, taxes, land prices and other influences. They include neither the delivery cost, presumably using a pipeline network, nor profits for plant operators.

3.5 Conclusions

Hydrogen production from SMR is a mature and widely used technology. Production from coal gasification and electrolysis is also increasing; electrolysis in particular serves markets such as vehicles where hydrogen with few impurities is required. These are mature technologies and are expected to have an important role in the future. Yet there is uncertainty in the literature about the future costs of these technologies. This is amplified by commodity price uncertainties and by the potential impacts of environmental legislation and taxation.

Biomass gasification is a potential low-carbon alternative to these more mature technologies. Although the economics of using biomass have been examined by several studies, none of these has examined biomass with CCS, despite it having the potential to produce hydrogen while simultaneously removing large quantities

of CO_2 from the atmosphere. More generally, CCS is a key enabling technology for hydrogen production from carbonaceous fuels in a low-carbon energy system. Although unabated hydrogen production from fossil fuels continues to be the most economic approach at the moment, the imposition of a substantial CO_2 emissions tax would tend to greatly favour plants with CCS or with non-carbonaceous feedstocks.

Electrolysis is the most difficult of the mature technologies to forecast future costs. Both capital and feedstock costs are currently higher than for other technologies. However, there is much more potential for electrolysis costs to reduce through innovation than for the other technologies. There is also much more uncertainty about the future price of electricity; although it is expected to rise as renewables replace fossil fuel generation, there are already periods in some countries when the price reduces to zero as renewable supply exceeds demand.

Numerous other technologies are being developed to produce hydrogen from water. These are as yet at an early stage of development and it is difficult to produce a realistic estimate of their levelised costs at the moment. Performing economic appraisals and reducing costs will be key challenges for the development of these technologies in the future.

3.6 Sources of further information and advice

The H2A Production Analysis programme of the US Department of Energy has developed comprehensive technoeconomic methodologies for costing hydrogen production (http://www.hydrogen.energy.gov/h2a_production.html).

Several less mature technologies are being developed at the US National Renewable Energy Laboratory (http://www.nrel.gov/hydrogen/proj_production_delivery.html).

Many research articles that examine the economics of hydrogen production are cited in Section 3.2.1.

List of acronyms

CCS	Carbon capture and storage
CSP	Concentrated solar power
DOE	USA Department of Energy
H2A	US Department of Energy Hydrogen Analysis Project
HHV	Higher heating value
LHV	Lower heating value
O&M	Operations and maintenance
PEM	Polymer electrolyte membrane
SMR	Steam methane reforming
SOE	Solid oxide electrolyser
TECHPOL	Hydrogen technology database developed by the Cascade Mints project

References

Acar, C., & Dincer, I. (2014). Comparative assessment of hydrogen production methods from renewable and non-renewable sources. *International Journal of Hydrogen Energy, 39*(1), 1−12.

Amelio, M., Morrone, P., Gallucci, F., & Basile, A. (2007). Integrated gasification gas combined cycle plant with membrane reactors: technological and economical analysis. *Energy Conversion and Management, 48*(10), 2680−2693.

Bartels, J. R., Pate, M. B., & Olson, N. K. (2010). An economic survey of hydrogen production from conventional and alternative energy sources. *International Journal of Hydrogen Energy, 35*(16), 8371−8384.

Coelho, B., Oliveira, A. C., & Mendes, A. (2010). Concentrated solar power for renewable electricity and hydrogen production from water − a review. *Energy & Environmental Science, 3*(10), 1398−1405.

Cormos, C.-C. (2010). Evaluation of energy integration aspects for IGCC-based hydrogen and electricity co-production with carbon capture and storage. *International Journal of Hydrogen Energy, 35*(14), 7485−7497.

Cormos, C.-C. (2014). Techno-economic and environmental evaluations of large scale gasification-based CCS project in Romania. *International Journal of Hydrogen Energy, 39*(1), 13−27.

DEA. (2010). *Technology data for energy plants*. Copenhagen, Denmark: Danish Energy Agency.

DECC. (2013). *DECC fossil fuel price projections*. London, UK: Department of Energy and Climate Change.

Dodds, P. E., & Hawkes, A. (2014). *The role of hydrogen and fuel cells in providing affordable, secure low-carbon heat*. London, UK: H2FC SUPERGEN.

Felder, R., & Meier, A. (2008). Well-to-wheel analysis of solar hydrogen production and utilization for passenger car transportation. *Journal of Solar Energy Engineering, 130*(1), 011017-10.

Glatzmaier, G., Blake, D., & Showalter, S. (1998). *Assessment of methods for hydrogen production using concentrated solar energy*. Golden, CO, USA: NREL.

Gray, D., & Tomlinson, G. (2002). *Hydrogen from coal*. Falls Church, VA, USA: Mitretek.

Grübler, A., Nakićenović, N., & Victor, D. G. (1999). Dynamics of energy technologies and global change. *Energy Policy, 27*(5), 247−280.

Howes, P., Bates, J., Landy, M., O'Brien, S., Herbert, R., Matthews, R., et al. (2011). *UK and global bioenergy resources and prices*. Didcot, UK: AEA Technology, Oxford Economics and Forest Research.

Hydrogen Production Expert Panel. (2013). *Report of the hydrogen production expert panel: A subcommittee of the hydrogen & fuel cell technical advisory committee*. Washington, DC, USA: US Department of Energy.

Iaquaniello, G., Giacobbe, F., Morico, B., Cosenza, S., & Farace, A. (2008). Membrane reforming in converting natural gas to hydrogen: production costs, part II. *International Journal of Hydrogen Energy, 33*(22), 6595−6601.

Kalinci, Y., Hepbasli, A., & Dincer, I. (2009). Biomass-based hydrogen production: a review and analysis. *International Journal of Hydrogen Energy, 34*(21), 8799−8817.

Khamis, I., & Malshe, U. D. (2010). HEEP: a new tool for the economic evaluation of hydrogen economy. *International Journal of Hydrogen Energy, 35*(16), 8398−8406.

Kreutz, T., Williams, R., Consonni, S., & Chiesa, P. (2005). Co-production of hydrogen, electricity and CO_2 from coal with commercially ready technology. part B: economic analysis. *International Journal of Hydrogen Energy, 30*(7), 769−784.

Krewitt, W., & Schmid, S. A. (2004). *Fuel cell technologies and hydrogen production/distribution options*. Stuttgart, Germany: CASCADE MINTS. DLR Institute of Vehicle Concepts.

Lemus, R. G., & Duart, J. M. M. (2010). Updated hydrogen production costs and parities for conventional and renewable technologies. *International Journal of Hydrogen Energy, 35*(9), 3929−3936.

Levene, J. I., Mann, M. K., Margolis, R. M., & Milbrandt, A. (2007). An analysis of hydrogen production from renewable electricity sources. *Solar Energy, 81*(6), 773−780.

Lubis, L. L., Dincer, I., & Rosen, M. A. (2010). Life cycle assessment of hydrogen production using nuclear energy: an application based on thermochemical water splitting. *Journal of Energy Resources Technology, 132*(2).

National Grid. (2014). *UK future energy scenarios*. Warwick, UK.

NRC. (2004). *The hydrogen economy: Opportunities, costs, barriers, and R&D needs*. Washington, DC, USA: National Research Council of the National Academies.

NRC. (2008). *Transitions to alternative transportation technologies − A focus on hydrogen*. Washington, DC, USA: National Research Council of the National Academies.

Ogden, J. M. (2001). *Review of small stationary reformers for hydrogen production*. Princeton, USA: Princeton University.

Petchers, N. (2002). Chapter 5 − heating value and combustion of fuel. In *Combined heating, cooling and power handbook: Technologies and applications*. New York, USA: Fairmont Press.

Rosen, M. A. (2010). Advances in hydrogen production by thermochemical water decomposition: a review. *Energy, 35*(2), 1068−1076.

Saxena, R. C., Seal, D., Kumar, S., & Goyal, H. B. (2008). Thermo-chemical routes for hydrogen rich gas from biomass: a review. *Renewable & Sustainable Energy Reviews, 12*(7), 1909−1927.

Schoots, K., Ferioli, F., Kramer, G. J., & van der Zwaan, B. C. C. (2008). Learning curves for hydrogen production technology: an assessment of observed cost reductions. *International Journal of Hydrogen Energy, 33*(11), 2630−2645.

Schoots, K., Rivera-Tinoco, R., Verbong, G. P. J., & van der Zwaan, B. C. C. (2010). *The cost of pipelining climate change mitigation: An overview of the economics of CH_4, CO_2 and H_2 transportation*. SSRN eLibrary.

Shirasaki, Y., Tsuneki, T., Ota, Y., Yasuda, I., Tachibana, S., Nakajima, H., et al. (2009). Development of membrane reformer system for highly efficient hydrogen production from natural gas. *International Journal of Hydrogen Energy, 34*(10), 4482−4487.

Staffell, I. (2014). Fuel cell technologies. In P. E. Dodds, & A. Hawkes (Eds.), *The role of hydrogen and fuel cells in providing affordable, secure low-carbon heat*. London, UK: H2FC SUPERGEN.

Steinfeld, A. (2005). Solar thermochemical production of hydrogen − a review. *Solar Energy, 78*(5), 603−615.

Steward, D., Ramsden, T., & Zuboy, J. (2008). *H2A production model, version 2 user guide*. Golden, Colorado: National Renewable Energy Laboratory, Department of Energy.

Utgikar, V., & Thiesen, T. (2006). Life cycle assessment of high temperature electrolysis for hydrogen production via nuclear energy. *International Journal of Hydrogen Energy, 31*(7), 939−944.

This page intentionally left blank

Part Two

Conventional hydrogen production methods

This page intentionally left blank

Hydrogen production by steam reforming of natural gas and other nonrenewable feedstocks

4

L. García
Universidad de Zaragoza, Zaragoza, Spain

4.1 Introduction

Steam reforming is a mature technology. Currently the main process for hydrogen production is steam reforming of natural gas. Other nonrenewable feedstocks for hydrogen production by steam reforming are methanol, liquefied petroleum gas (LPG) (mainly propane and butane), naphtha, jet fuel, and diesel. The best selection of feedstock should consider the global economy of the process; the price of feedstock is relevant and an adequate operation is significant.

Catalyst deactivation by coking and the presence of sulfur in feed can decrease hydrogen production in steam reforming processes. In this field, extensive research is being carried out to develop more stable and cheaper catalysts.

Because of the high production of hydrogen by steam reforming and some inconveniences derived from the complexity of the processes, such as the high number of stages, thermodynamic constraints, and low energy efficiency, among other, new processes are being developed.

This chapter presents a global vision of hydrogen production by steam reforming of nonrenewable feedstocks, including fundamentals, conventional plants, and new process development.

4.2 Natural gas steam reforming: fundamentals

Natural gas steam reforming is a mature technology that currently generates 48% of the world's hydrogen production (Ferreira-Aparicio, Benito, & Sanz, 2005).

After treatment of natural gas from wells, it contains mainly one chemical compound, methane. The typical composition of natural gas is as follows (expressed as volume percentage): CH_4: 95%, C_{2+}: 3.5%, N_2: 1%, CO_2: 0.5%, and small amounts of sulfur compounds.

In steam reforming, steam reacts with the feedstock in a set of reactions to produce mainly hydrogen, carbon dioxide, and carbon monoxide. Natural gas is the most

Compendium of Hydrogen Energy. http://dx.doi.org/10.1016/B978-1-78242-361-4.00004-2

important feedstock for steam reforming. Main reactions of natural gas steam reforming are:

$$CH_4 + H_2O \leftrightarrow CO + 3H_2 \quad \Delta H^{\circ}_{298\ K} = 206.4\ kJ/mol \tag{4.1}$$

$$C_nH_{2n+2} + nH_2O \rightarrow nCO + (2n+1)H_2 \quad \Delta H^{\circ}_{298\ K} > 0 \tag{4.2}$$

$$CO + H_2O \leftrightarrow CO_2 + H_2 \quad \Delta H^{\circ}_{298\ K} = -41.2\ kJ/mol \tag{4.3}$$

C_nH_{2n+2} in reaction (4.2) represents hydrocarbons higher than methane contained in natural gas. Reaction (4.3) is called a water gas shift (WGS) reaction. Reactions (4.1) and (4.2) are endothermic and reaction (4.3) is slightly exothermic. Globally, the process is endothermic.

$$CH_4 + CO_2 \rightarrow 2CO + 2H_2 \quad \Delta H^{\circ}_{298\ K} = 247.3\ kJ/mol \tag{4.4}$$

Reaction (4.4) may also occur, and it is called CO_2 reforming or dry reforming. Other secondary reactions involved in natural gas steam reforming are:

$$CH_4 \rightarrow C + 2H_2 \quad \Delta H^{\circ}_{298\ K} = 74.9\ kJ/mol \tag{4.5}$$

$$2CO \rightarrow C + CO_2 \quad \Delta H^{\circ}_{298\ K} = -172.5\ kJ/mol \tag{4.6}$$

Reaction (4.5) is methane decomposition and reaction (4.6) is the Boudouard reaction. These reactions produce carbon deposits.

The main operating variables that influence natural gas steam reforming are temperature, pressure, and the molar steam-to-carbon ratio (S/C). The selection of operating variables must consider kinetics, economics, and gas use in addition to thermodynamics. The reaction bed in which natural gas steam reforming occurs normally contains a catalyst. This catalyst, mainly based on nickel, facilitates kinetic reactions (4.1) and (4.2), decreasing the reforming temperature. The main causes of catalyst deactivation are poisoning by sulfur and deposition of carbon. Halogen compounds and heavy metals such as lead, arsenic, and vanadium are also catalyst poisons (Häussinger, Lohmüller, & Watson, 1989). Useful information about catalysts in steam reforming can be found in Rostrup-Nielsen (2008).

Owing to the endothermic nature of natural gas steam reforming, a heat input is required for the process. As a consequence, other reforming processes have been developed for hydrogen production, such as partial oxidation, autothermal reforming, and combining reforming. Carbon dioxide reforming is a related process.

In partial oxidation, oxygen is used under a stoichiometric combustion ratio. Oxygen reacts with natural gas in an exothermic reaction; as a consequence, there is no need for external heat. Autothermal reforming is a combination of steam reforming and partial oxidation. In this process, the energy for reforming is produced by partial oxidation of the hydrocarbon feedstock (Ferreira-Aparicio et al., 2005).

Combining reforming refers to a combination of previously mentioned processes. As an example, a primary steam reformer is combined in series with an oxygen reformer, partial oxidation, or autothermal reformer. These arrangements allow a reduction in the size of the primary reformer and softens operating conditions (Ferreira-Aparicio et al., 2005).

In CO_2 reforming, CO_2 reacts with the hydrocarbon. For example, using natural gas, the reaction (4.4) is involved mainly, which is more endothermic than steam reforming of methane (reaction (4.1)). This reaction has attracted a great deal of attention recently because of the reduction in greenhouse gas emissions. Operating temperatures are usually above 900 °C. Two commercial technologies based on this reaction have been developed. Usually this process is combined with steam reforming or partial oxidation (Ferreira-Aparicio et al., 2005).

Carbon dioxide reforming of methane is a promising option for the conversion of natural gas into syngas. Reaction (4.4) produces a gas with a H_2/CO ratio of approximately 1:1, which is lower than that obtained in steam reforming. The syngas generated in CO_2 reforming of methane is a valuable feedstock for many chemical processes, such as liquid hydrocarbons in Fischer−Tropsch reaction and aldehydes and alcohols in oxo-synthesis, where alkenes react with syngas.

The main drawback of CO_2 reforming of methane is the catalyst deactivation resulting from carbon deposition. A wide number of references exist in the literature focused on the study of catalyst stability in CO_2 reforming of methane. Nickel-based catalysts and supported noble metal catalysts have promising catalytic performance. Research in nickel-based catalysts is wide owing to its low price compared with supported noble catalysts. However, more carbon formation is observed in nickel-based catalysts than in noble metal catalysts.

Wang and Lu (1998) studied the influence of the nature of catalyst support in nickel-based catalysts. They concluded that the support structure, metal−support interaction and acidity−basicity of support affect metal dispersion and carbon deposition. The high stability of the Ni/MgO catalyst was attributed to the formation of a solid−solid solution and more basic property. A strong interaction between metal and support produced a significant reduction in carbon formation on Ni/TiO_2 and Ni/CeO_2 catalysts.

Bradford and Vannice (1999) studied SiO_2- and TiO_2-supported transition metals to elucidate the role of metal−support interactions in CO_2 reforming of CH_4. They found that catalyst activity depends on both the support and the band occupancy (i.e., %d-character) of the metal. Using SiO_2 as support, the maximum activity was observed with Pt, whereas with TiO_2 the optimum performance was obtained with Rh.

In the review of Ross (2005) Pt supported on zirconia was identified as a catalyst for the CO_2 reforming of methane superior to Pt on alumina or Pt on titania catalysts. The addition of a variety of promoters to zirconia, such as La or Y, improves the behavior of the resultant catalysts. The addition of CeO_2 to the support showed a positive effect because ceria is a source of additional labile oxygen species. Because of the cost of Pt, several carbides have been proposed as catalysts for dry reforming. The catalyst of Mo_2C supported on ZrO_2 and promoted with Bi showed high activity compared with other Mo_2C catalysts.

Recently, Fidalgo and Menéndez (2011) reviewed CO_2 reforming of methane using carbon materials as catalysts. They explained that dry reforming can be considered a combination of methane decomposition and gasification of the carbon deposits by CO_2; the latter step is a crucial reaction in the process. Fidalgo, Domínguez, Pis, and Menéndez (2008) studied microwave-assisted dry reforming using activated carbon as catalyst. They proved that enhancement is produced when microwave heating is used instead of conventional heating.

Aqueous-phase reforming is a recent process developed by Dumesic and coworkers (Cortright, Davda, & Dumesic, 2002). This process uses pressures in the range of 2.5−6 MPa and low temperatures around 227 °C, with the purpose of maintaining water in liquid phase, avoiding evaporation costs. Aqueous-phase reforming has application in residual organic streams with high water content.

4.3 Conventional plants for natural gas steam reforming

In Figure 4.1 a block diagram shows a conventional steam reforming plant for hydrogen production from natural gas. There are four main blocks: desulfurization, reforming, WGS, and H_2 purification.

4.3.1 Desulfurization

This section is required because of the high sulfur sensitivity of catalysts in the reformer and in the low-temperature shift reactor. Natural gas usually contains small amounts of sulfur compounds, normally in form of hydrogen sulfide, but can also contain carbonyl sulfide and higher organic sulfur compounds such as mercaptans and thiophene.

For low-content sulfur compounds in natural gas, a zinc oxide bed can remove it. However, for high-content sulfur compounds with higher organic sulfur compounds, one hydrogenation stage is required previous to the zinc oxide bed (Häussinger et al., 1989). The hydrogen required for the hydrogenation reaction is taken from the product stream and uses amounts of around 5% for natural gas. Hydrogenation also lowers the amount of olefins in the feed to the reformer, which decreases catalyst deactivation by coking. The excess of hydrogen in the feed helps maintain the reforming catalyst at the top of the tube in a reduced state.

The gas leaves this section with a sulfur content lower than 1 ppm at a temperature between 350 °C and 400 °C.

4.3.2 Reforming

In the reforming section, steam reforming reactions of natural gas are carried out. Operation conditions are high temperatures of 800−900 °C, the process pressure varies between 1.5 and 3.0 MPa, and common values for natural gas are S/C ratios of 2.5−3.

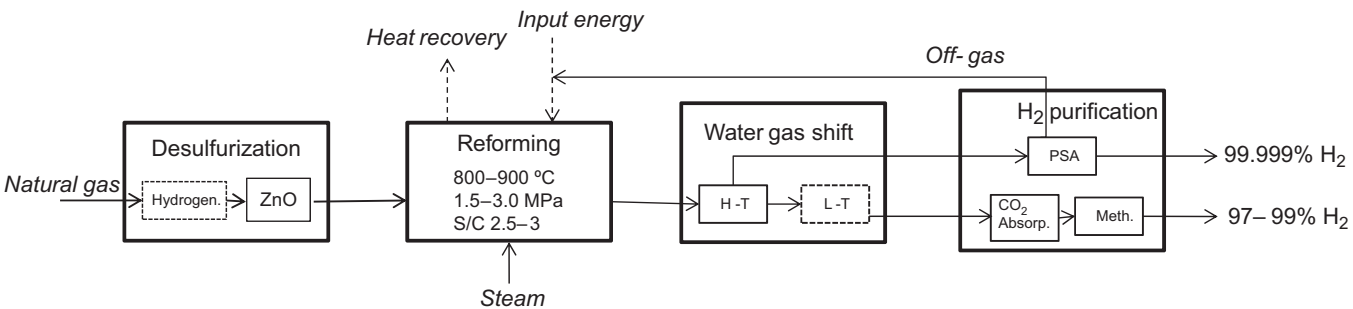

Figure 4.1 Block diagram of a conventional plant of hydrogen production using natural gas steam reforming.

The reactions are catalyzed by supported nickel catalysts that contain 15−25 wt% nickel oxide on a carrier such as α-Al_2O_3, aluminosilicates, or magnesia, among others. Despite the high temperatures used in steam reforming, a catalyst is still required to accelerate the reaction because of the high stability of methane. Previous to the reforming reaction the catalyst has to be activated, reducing the nickel oxide to metallic nickel. This is done with hydrogen but also can be performed with the feeding gas.

The catalyst is placed in the steam reformer tubes as a fixed bed. Other properties required for the catalyst are low pressure drop and high mechanical resistance at temperatures up to 1000 °C. The catalysts are usually in the form of rings with an outer diameter of 16 mm, inner diameter of 8 mm, and height of 16 mm (Häussinger et al., 1989). This relatively large size decreases the reaction rate as a result of internal mass transfer control.

In the absence of oxidation reactions, the heat input for endothermic reforming reactions is provided by indirect heating. A fuel is fired outside the reformer tubes. Heat distribution in a conventional reformer is influenced by the geometry of burner arrangements, the pitch of tubes, the type and length of the flame, the radiation of the flames, the flue gas and refractory walls, and the size, shape, and thickness of the tubes and materials.

The steam reformer consists of two sections: radiant and convection. In the radiant section reforming reactions occur. In the convection section the natural gas feed and process steam are preheated and superheated steam is generated by heat recovered from the flue gases (Moulijn, Makkee, & van Diepen, 2008). The overall thermal efficiency of a reformer is normally expected to be around 92%. Heat loss and the recovery of excess heat in the flue gas used to produce export steam significantly influence that value (Häussinger et al., 1989).

A furnace may contain 500−600 tubes with a length of 7−12 m and an inside diameter between 70 and 130 mm (Moulijn et al., 2008).

The objective of a reformer is to optimize fuel use, achieving the maximum degree of reforming and, as a consequence, a high amount of hydrogen after WGS and purification sections. Different types of steam reformer for hydrogen production with furnace and convection zone configurations can be found in the literature (Häussinger et al., 1989).

4.3.3 WGS reaction

In this section it is possible to find two WGS reactors. In high-temperature shift conversion, the gas cooled down to 350 °C with a high content of carbon monoxide is converted to hydrogen by WGS reaction (4.3) using iron oxide-based catalysts. The catalysts usually contain 8−12 wt% Cr_2O_3. Because of the exothermicity of this reaction, the exit gas temperature is around 400−450 °C and the conversion is incomplete. The CO content in the exit gas is around 3 vol%, which is close to equilibrium (Hinrichsen, Kochloefl, & Muhler, 2008).

The gas is cooled to around 220 °C and fed into the low-temperature shift reactor. Cu-Zn or Cu-Zn-Al catalysts are used and the CO content of the exit gas is about

0.05−0.5 vol%, corresponding to 95−99% conversion. The temperature rises progressively through the converter and should not exceed 260 °C. The maximum H_2S concentration in the inlet gas of a low-temperature shift reactor should not exceed 0.5 ppm (Hinrichsen et al., 2008).

4.3.4 Hydrogen purification

Two main options can be found. The first uses pressure-swing adsorption (PSA). After high-temperature shift conversion, the gas is cooled down to ambient temperature. Water is condensed and removed before the gas is fed to the adsorption step. Hydrogen product from this purification process has purity up to 99.999%. The hydrogen losses of the PSA off-gas are burned in the reformer to provide input heat and decrease fuel requirements.

The second option is called the classical process. High-temperature shift conversion and a low-temperature shift reactor are employed. The product gas is cooled down to ambient temperature and fed to a carbon dioxide scrubber using monoethanolamine or hot potash. The remaining impurities in the hydrogen, traces of carbon monoxide and carbon dioxide, are removed by a catalytic methanation step. Using this process hydrogen purity of 97−99% can be attained (without considering the inert gases).

The classical route is used only in special cases, such as (Häussinger et al., 1989):

1. Expensive natural gas
2. Cheap fuel is available to fire the reformer
3. Carbon dioxide is a desired product
4. Hydrogen purity lower than 99.9% can be tolerated.

4.4 New processes

4.4.1 Steam reforming with membranes

Industrial fixed-bed steam reformers present the following problems (Adris, Lim, & Grace, 1997):

- Low catalyst effectiveness factors, which is a consequence of severe diffusional limitations with large catalyst particles. Smaller particle sizes are not practicable because of the high pressure drop.
- Low heat transfer rates that produce radial and axial profiles and large temperature gradients.
- Thermodynamic equilibrium constraints. Reforming and WGS reactions are equilibrium limited and it is not possible to have total conversion of natural gas to CO_2 and H_2.

These inconveniences can be solved using a fluidized-bed membrane reactor. Main advantages of this reactor are:

- Fluidized beds with small catalyst particles achieve elimination of diffusional limitations and catalyst bed temperature uniformity.
- Permselective membrane technology can produce in situ separation that removes hydrogen shifting equilibrium favoring methane conversion (as a main component of natural gas) and

allow obtain a hydrogen stream of high purity. The last fact simplifies hydrogen purification compared with conventional installations.

Integration of membranes in the steam reforming process occurs in two configurations (De Falco, Iaquaniello, & Salladini, 2011). In the first, a membrane reactor, the membrane is placed directly inside the reaction environment. In the second, the reformer and membrane module, the membrane is assembled into separate modules downstream of the reactor. The main advantage in membrane reactor configuration is the shift of equilibrium, which improves conversion and hydrogen production, whereas in reformer and membrane module configuration is the selection of different and optimized temperatures in the reactor and in the membrane module. The use of lower temperatures in the membrane avoids possible damage.

Table 4.1 presents the most relevant facts of some types of work steam reforming with membranes. Adris, Lim, and Grace (1994) found reaction conversions in the fluidized-bed membrane reactor beyond conventional limits as a result of hydrogen

Table 4.1 Examples of research work with membranes

	H_2 production capacity	Operating conditions	Membrane/catalyst/ reactor dimensions
Adris et al. (1994)	6 m^3(STP)/h	450–640 °C 0.7–1.0 MPa S/C 2.3–4.1	Pd membranes NiO/α-Al_2O_3 Reactor: 97-mm diameter, 1.143-m length
Jarosch and de Lasa (1999)	–	750 °C 2.2 MPa S/C 2.2	Pd membrane 20 wt%Ni/α-Al_2O_3 Riser simulator: 2.54-cm diameter
Patil et al. (2007)	0.09 m^3(STP)/h	550–650 °C 0.2–0.4 MPa 1.5–6 umf	Pd membrane Highly active noble metal-based CPO Reactor: 100-mm diameter, 60-cm length
Mahecha-Botero et al. (2008)	1.0 m^3(STP)/h	550 °C 0.6–0.9 MPa S/C 3.0	Pd/Ag membrane NiO/Al_2O_3 Reactor: 48.4-cm^2 and 2-m length
De Falco et al. (2011)	20 m^3(STP)/h	550–650 °C (reformer) Up to 2.1 MPa 450 °C (separation)	Pd and Pd/Ag membranes Ru-Pt/Al_2O_3 supported on SiC foam

permeation through the membrane that shifts the reaction equilibrium. Also, they demonstrated that temperature shows the strongest dependence on the reaction conversion. This last result is a consequence of faster kinetics and an increase in the permeation rate when the bed temperature increases. The experimental data showed good agreement with the model developed (Adris et al., 1997). Inconel supported palladium membranes and fluidizable supported nickel catalysts were successfully developed in the work of Jarosch and de Lasa (1999).

In the experimental work of Patil, van Sint Annaland, and Kuipers (2007), optimal operating conditions were 650 °C, 0.3−0.4 MPa, and 1.5−2 umf. This indicates that the best reactor performance is achieved at a high temperature within the boundaries imposed by membrane stability (700 °C) and high pressure. Roses, Gallucci, Manzolini, and van Sint Annaland (2013) concluded that in terms of hydrogen yield, it would be convenient to use an S/C ratio in the range of 2.5−3.0 but not higher. No trace of CO was detected in the permeate hydrogen even at temperatures of 630 °C using Pd membranes. Also, stable performance in the reactor was obtained over 260 h.

Mahecha-Botero et al. (2008) concluded that the overall performance of the reactor primarily depended on the area of the installed membrane. Hydrogen permeate purity was up to 99.994%, with an H_2/CH_4 yield of 3.03 with the full membrane and under steam reforming conditions. A cumulative reforming time of 395 h was reached (Mahecha-Botero et al., 2011). Also, the results confirmed the ability of the reactor to use different natural gases containing up to 9.9 mol% of non-methane hydrocarbons. Hydrogen purity exceeded 99.99% for all tests.

Three concepts of reforming reactors with membranes are proposed and deserved to be mentioned. In the catforming process (Figure 4.2), the continuous movement of catalyst occurs between the reforming reactor and regenerator (Jarosch & de Lasa, 1999). The regenerated catalyst and the reactant gas fall down the reactor where steam reforming and WGS reactions take place and the hydrogen thus generated is continuously removed through a membrane. The formation of coke on the catalyst is expected owing to the low S/C ratios employed.

A fluidized-bed bimembrane reactor (Figure 4.3) was proposed by Patil, van Sint Annaland, and Kuipers (2005). At the bottom, perovskite membranes operating at 900−1000 °C allow selective addition for partial oxidation, whereas at the top section steam reforming/WGS reactions take place at 500−600 °C with permselective Pd metallic membranes for hydrogen removal.

The sorbent-enhanced/membrane reforming process was modeled by Chen et al. (2008). Figure 4.4 shows a schematic of the process. In this, a circulation fluidized-bed membrane reformer is coupled with a catalyst/sorbent regenerator. In the reformer H_2 is removed by membranes and CO_2 is captured by sorbents.

The process of natural gas steam reforming performed at low temperatures, such as for membrane reformers, requires active and stable catalysts for these conditions. Angeli, Monteleone, Giaconia, and Lemonidou (2014) reviewed the state-of-the-art in this field, considering temperatures lower than 550 °C. Three main groups of catalysts were considered: Ni catalysts, noble metals catalysts, and bimetallic catalysts. The influence of support dopants and promoters of the active phase on metal dispersion, particle size, and reducibility was relevant in catalyst performance and in

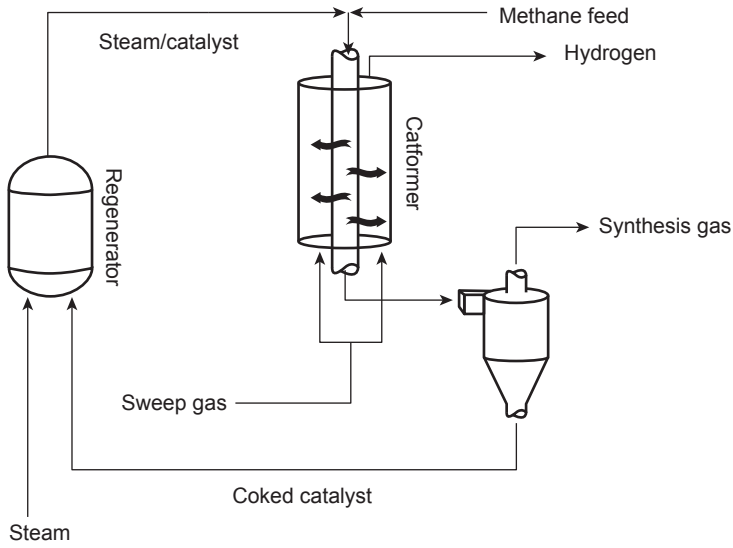

Figure 4.2 Schematic flow diagram of the Catformer concept.
Reprinted from Jarosch, K., & de Lasa, H. I. (1999). Novel riser simulator for methane reforming using high temperature membranes. *Chemical Engineering Science, 54*, 1455−1460, Copyright (1999), with permission from Elsevier.

resistance to carbon formation. CeO_2 as a catalyst support or support dopant with high oxygen storage capacity and redox properties significantly improved coke resistance.

4.4.2 Sorption-enhanced reforming

Some inconveniences of conventional natural gas steam reforming are:

- The complexity of the process, which requires a high number of stages with different catalysts.
- The primary reformer operates at 800−850 °C and needs high energy input to maintain these temperatures with supplemental fuel. In addition, expensive high-alloy steels are required in the tubes.
- Thermodynamic constraints in the reformer result from CH_4 reforming and WGS reactions, which limit CH_4 conversion and hydrogen yield.
- H_2 losses in the purification steps. These losses are associated with both methanation and preferential oxidation. Also in the PSA units, H_2 losses are 10% or more.

In the sorption-enhanced reforming (SER) process the reforming catalyst is mixed with a CO_2 sorbent. In the same vessel, reforming, shift, and CO_2 separation occur simultaneously. The CO_2 capture reaction when using CaO as sorbent is shown as reaction (4.7). The normal equilibrium limits of the reforming and shift reactions are removed and a product gas with 97% H_2 (dry basis) is possible (Balasubramanian, Lopez Ortiz, Kaytakoglu, & Harrison, 1999). From thermodynamic analysis at 650 °C, the equilibrium hydrogen yield with CO_2 acceptor is 3.46 mol per mol of

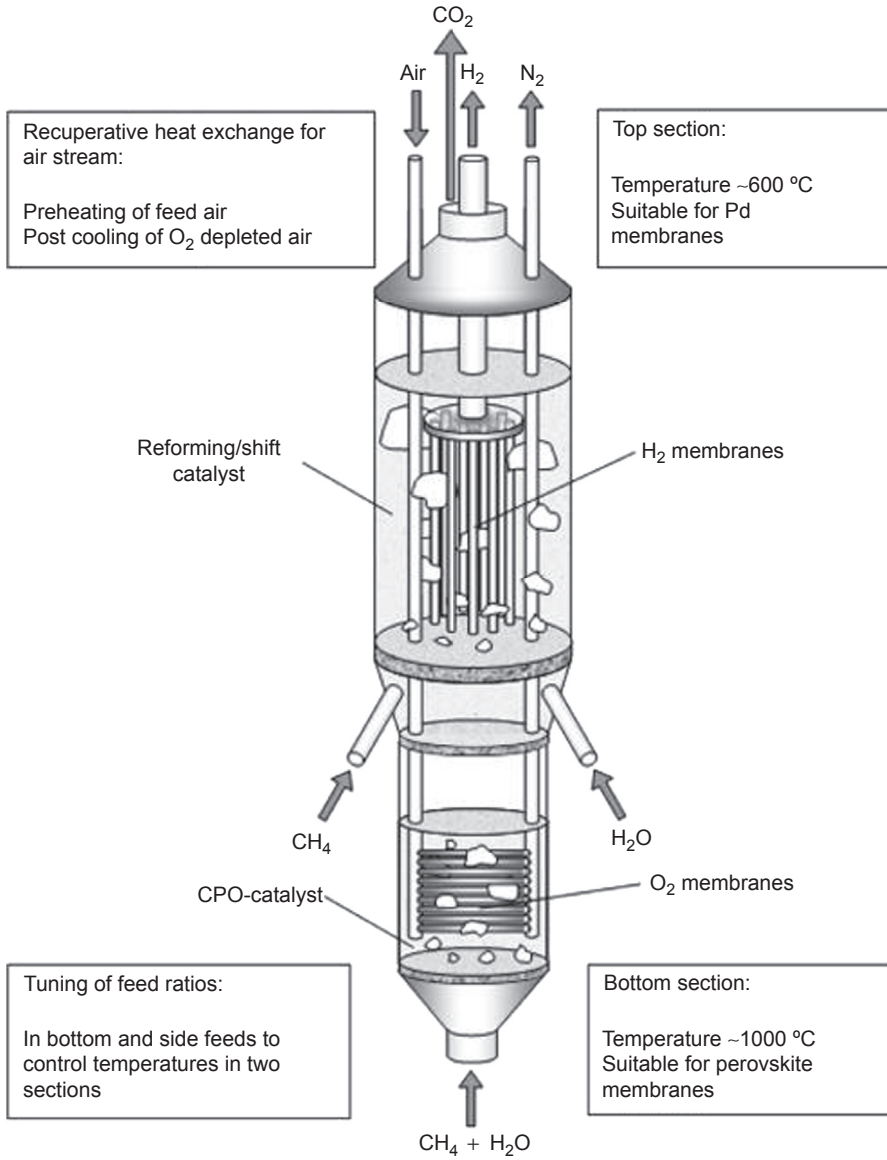

Figure 4.3 Schematic of the novel fluidized-bed bimembrane reactor.
Reprinted with permission from Patil, C. S., van Sint Annaland, M., & Kuipers, J. A. M. (2005). Design of a novel autothermal membrane-assisted fluidized-bed reactor for the production of ultrapure hydrogen form methane. *Industrial and Engineering Chemistry Research, 44*, 9502−9512, Copyright (2005), American Chemical Society.

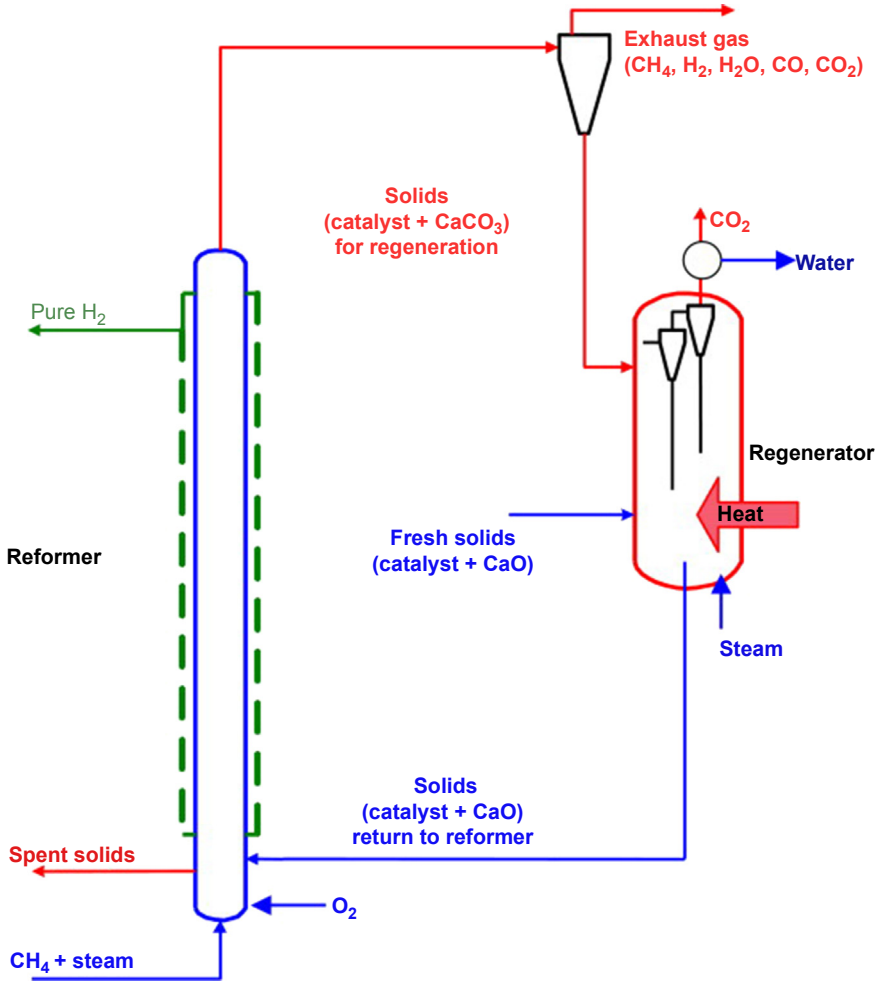

Figure 4.4 Schematic of a circulating fluidized-bed membrane reformer coupled with a catalyst/sorbent regenerator.
Reprinted with permission from Chen, Z., Po, F., Grace, J. R., Lim, C. J., Elnashaie, S., Mahecha-Botero, A., et al. (2008). Sorbent-enhanced/membrane-assited steam-methane reforming. *Chemical Engineering Science, 63*, 170−182, Copyright (2008), with permission from Elsevier.

CH_4 compared with a maximum yield of 4.0 (Balasubramanian et al., 1999). Because of the exothermic nature of CO_2 sorption, coupling in the reformer of the endothermic reforming reaction and the exothermic shift and CO_2 sorption reactions improve energy efficiency.

$$CO_2(g) + CaO(s) \rightarrow CaCO_3(s) \tag{4.7}$$

The main advantages of SER are the simplified process, energy efficiency, and the use of lower temperatures in the reformer, and as consequence, lower cost construction materials. However, this new process presents some inconveniences, such as the high temperature required for acceptor regeneration and the low purity of the hydrogen product (Balasubramanian et al., 1999).

Balasubramanian et al. (1999) carried out a comparative study of conventional and SER processes based on complete material and energy balances. They concluded that simplification of the potential process is evident. In the SER process two major vessels (primary reactor and regenerator) replace five vessels (reformer, two shift reactors, and the CO_2 scrubber and stripper) in the conventional process. Also, energy efficiency is improved because 0.5 mol of supplemental methane fuel is required per mole of process methane in conventional process compared with 0.37 mol of supplemental methane fuel in the SER process.

Martínez, Romano, Chiesa, Grasa, and Murillo (2013) simulated an H_2 production plant based on the SER process and compared the results with a conventional plant using commercially available amine absorption for CO_2 capture. In the SER process, the reformer and calciner are circulating fluidized-bed reactors operating at the same low pressure and at different temperatures. The temperature in the reformer varied in the range of 600−675 °C whereas in the calciner the temperature was modified between 885 and 950 °C. The authors demonstrated the significance of developing high active sorbents because the lower the solid circulation that was assumed (low Ca-to-C molar ratio), the higher were the hydrogen efficiencies reported for the SER plant.

Requirements for the CO_2 sorbent are large CO_2 capacity, which reduces the quantity of sorbent needed and increases the duration of the reaction−sorption cycle, and low regeneration temperatures, which should reduce sintering, increase sorbent durability, and possibly reduce energy input for regeneration (Harrison, 2008).

Carbon dioxide sorbents can be classified as Ca-based oxides, hydrotalcites (HTC), and metal oxides of Li and Na. Table 4.2 shows the main characteristics of these sorbents (Harrison, 2008).

Naturally inexpensive precursors such as limestone and dolomite have been studied. Limestone has a higher theoretical capacity (0.79 g CO_2/g CaO) than dolomite (0.46 g CO_2/g CaO.MgO). However, dolomite has improved performance in multicycle tests. The importance of pore volume and the stabilization effects of Mg have been identified in retention of the initial CO_2 sorption capacity (Harrison, 2008). Using limestone, reactivation in steam significantly increases the degree of carbonation; an explanation for this is that $Ca(OH)_2$ decomposition is effective in maintaining the inventory of small pores.

To carry out the SER process at an industrial scale, Harrison (2008) proposed a schematic showed in Figure 4.5, which included two circulating fluidized beds with sorbent hydration for maintenance of activity. In his review, Harrison (2008) cited the Zero Emission Gas Power Project and Pratt and Witney Rocketdyne as processes in which H_2 is produced by SER of natural gas.

Table 4.2 Main characteristics of CO_2 sorbents (Harrison, 2008)

Type	Ca-based oxides	K-HTC	Metal oxides of Li and Na
Examples/ explanation	CaO, limestone, and dolomite as precursors	Double-layered hydroxides doped with K_2CO_3	Li_2ZrO_3, Li_4SiO_4, Na_2ZrO_3
Advantages	Natural materials are wide available and inexpensive High CO_2 capacity Equilibrium favorable with high H_2 content Fast kinetics of CO_2 sorption	Regeneration at low temperature and improved sorbent durability	Regeneration at low temperature Higher CO_2 capacity than HTC Better durability in multi-cycle experiments than Ca-based oxides
Disadvantages	High temperature for sorbent regeneration Sorbent durability owing to loss of activity	Lower CO_2 capacity than Ca-based and considerably more expensive	Little information available for SER Less favorable thermodynamic properties (product with lower H_2 content) than Ca-based sorbents

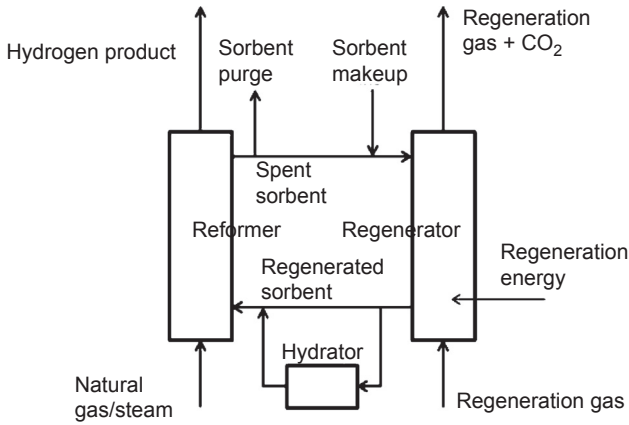

Figure 4.5 Schematic of a possible sorption-enhanced hydrogen production process. Reprinted with permission from Harrison, D. P. (2008). Sorption-enhanced hydrogen production: a review. *Industrial and Engineering Chemistry Research, 47*, 6486−6501, Copyright (2008), American Chemical Society.

4.4.3 Microreactors

In general, microreactors are miniaturized chemical reaction systems that contain parallel reaction channels with typical diameters between 10 and 500 μm. These reaction systems are fabricated by use of the methods of microtechnology and precision engineering. A solid catalyst may be present as a coating on the channel walls. Because of these small channel dimensions, an increase in the ratio of the surface area to volume is produced and, as a consequence, an increase in the driving forces for heat and mass transport (Löwe & Ehrfeld, 1999).

Some benefits of microreactors are (Delsman, Laarhoven, de Croon, Kramer, & Schouten, 2005):

- When in conventional reactors the reaction rate is limited by either mass transport to the catalyst or through an interface or by heat transport to or from the reaction zone.
- One may safely carry out reactions in the explosive regime, which can open up new reactions pathways or avoid the use of large dilution streams.
- Large batch vessels filled with possibly dangerous chemicals are replaced by small continuous flow reactors.

Specifically in hydrogen production by steam reforming, two advantages of using microreactors can be cited (Izquierdo et al., 2012):

- The process intensification allows the combination of reforming reactions and the required input energy in a small space. This achieves better heat transfer than in conventional reactors, which has a key role.
- This technology contributes to the development of distributed and portable power generation systems. Currently there are several applications ranging from portable electronic devices, such as laptops and cell phones, to onboard power production in vehicles (Stefanidis & Vlachos, 2010). These advanced reactions systems can be used for the decentralized production of hydrogen from natural gas.

Izquierdo et al. (2012) compared experimental results of methane and natural gas steam reforming in conventional and microreactor reaction systems. The microreactor was composed of 14 microchannels with 500 × 250-μm (width × depth) dimensions, made of stainless steel. In the reactor microchannels the catalyst was deposited by impregnation. The catalysts used two Ni-based catalysts (over MgO and Al_2O_3) and two noble metal-based catalysts (Pd and Pt over Al_2O_3). For all catalysts, at the same weight hourly space velocity, higher hydrocarbon conversions and higher hydrogen yields were achieved in the microreactors than in the fixed-bed reactor.

Stefanidis and Vlachos (2010) conducted a simulation study of steam reforming of natural gas focused on the choice of combustible fuel and reforming catalyst. A schematic of the simulated multifunctional microreactor is shown in Figure 4.6. This multifunctional microreactor combines a catalytic combustion channel and a steam reforming channel. The catalytic combustion channel is coated with Pt, and propane or methane together with air are fed. The steam reforming channel is coated with Rh or Ni, and methane and steam are fed. The solid wall that separates the two channels acts as a heat exchanger between the two processes. Some dimensions of the microreactor are: $d_w = 750$ μm, $d_1 = 300$ μm, $d_2 = 200$ μm, and a reactor length of 5 cm.

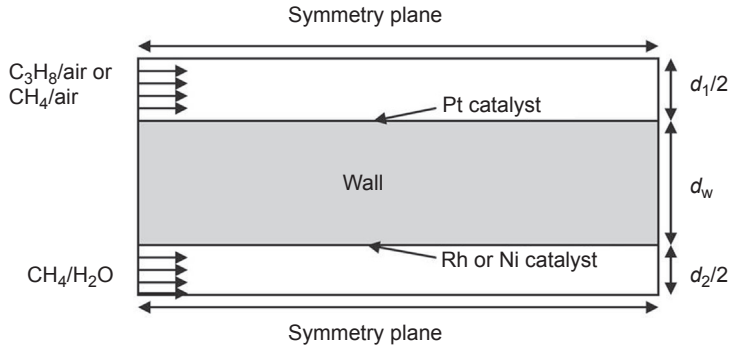

Figure 4.6 Schematic of the simulated multifunctional microreactor.
Reprinted with permission from Stefanidis, G. D., & Vlachos, D. (2010). Intensification of steam reforming of natural gas: choosing combustible fuel and reforming catalyst. *Chemical Engineering Science, 65*, 398−404, Copyright (2010), with permission from Elsevier.

Some advantages of this microreactor are its compactness, the possibility of scaling up the process by stacking together many plates, and the flexibility of using different configurations as well as different catalysts in the two channels (Stefanidis & Vlachos, 2010).

One conclusion of the study indicates (Stefanidis & Vlachos, 2010) that using propane as a combustible fuel, maximum power and hydrogen yield can be obtained using high steam reforming flow rates. Another conclusion is that steam reforming on Rh becomes 3−20 times faster than on Ni over the temperature range 730−1230 °C. An Ni catalyst in steam reforming at microscale with millisecond contact times is in principle feasible at increased catalyst loadings. The stability of the Ni catalyst owing to sintering and poisoning must be also considered for practical realization of an Ni steam reforming process.

Tonkovich, Yang, Perry, Fitzgerald, and Wang (2007) experimentally and theoretically studied the use of low contact times, between 90 and 900 μs, in methane steam reforming using a microchannel reactor. The active catalyst in the reforming channel was Rh whereas the catalyst in the combustion channel was Pd. The experimental results showed that steam reforming of methane at a contact time of 900 μs approached 99% to equilibrium whereas at a contact time of 90 μs the approach to equilibrium was 19.7%. Appropriate model agreement for both contact times was obtained.

4.5 Other nonrenewable feedstocks

A wide variety of nonrenewable feedstocks can be used for hydrogen production by steam reforming. The best option should consider availability and price. Perhaps natural gas is the best option in most cases. This section explains steam reforming of methanol, LPG, naphtha, jet fuel, and diesel.

4.5.1 Methanol

Although methanol can be produced from renewable sources, it is mainly produced by synthesis gas from fossil fuels such as natural gas, oil, or coal. Methanol is a promising energy vector without the problems of storage and transportation created by hydrogen.

Methanol can be converted into hydrogen by steam reforming according to the following chemical reactions:

$$CH_3OH + H_2O \leftrightarrow CO_2 + 3H_2 \quad \Delta H^{\circ}_{298\ K} = 49.7\ kJ/mol \tag{4.8}$$

$$CH_3OH \leftrightarrow CO + 2H_2 \quad \Delta H^{\circ}_{298\ K} = 90.7\ kJ/mol \tag{4.9}$$

Reaction (4.8) represents methanol steam reforming and reaction (4.9) represents the methanol decomposition reaction. Also, WGS reaction (4.3) occurs.

Methanol steam reforming can be carried out in conventional fixed-bed reactors and membrane reactors. Iulianelli, Ribeirinha, Mendes, and Basile (2014) compared these types of reactors. They observed from a high amount of research in the literature that in membrane reactors methanol conversion higher than 50% was reported to be between 200 and 300 °C whereas in conventional reactors the reaction temperature ranged from 300 to 400 °C for the same methanol conversion.

Methanol steam reforming is carried out in membrane reactors at relatively low temperatures, about 240−260 °C (Iulianelli et al., 2014). These temperatures are significantly lower than those used in conventional natural gas steam reformers, with considerably energy savings. The main drawback of this process is CO formation as a byproduct, which can poison the anodic catalyst of the proton exchange membrane fuel cells (PEMFC) as well as negatively affect the permeation of Pd-based membrane reactors.

The most common catalysts for this process are based on copper, such as Cu/ZnO/Al_2O_3. Catalyst deactivation can occur because of sintering, coke deposition, and poisoning (chloride and sulfur), among others (Iulianelli et al., 2014). The S/C molar ratio generally used is 1.5.

Areas of catalyst development in methanol steam reforming are activity, stability, and low CO production, especially for operating at temperatures around 180 °C. These temperatures favor WGS reaction to H_2 and CO_2, and then low CO content. Moreover, endothermic steam reforming can be coupled with high-temperature PEMFC, which works exothermally. Two approaches can be followed in copper-based catalysts development: adding promoters such as ZnO, ZrO_2, Mn, CeO_2, or Al_2O_3 and changing the preparation method (Iulianelli et al., 2014).

Another concern is the concentration of CO in the hydrogen-rich stream for the PEMFC supply. The CO level coming from conventional reformers is not adequate to supply low-temperature PEMFC directly but it can be useful for high-temperature PEMFC. The CO level required for low-temperature PEMFC has to be lower than 10 ppm, whereas for high-temperature PEMFC it has to be lower than 20,000 ppm. The CO level coming from membrane reformers depends on the kind of membrane. Thus, dense, self-supported, Pd-based membranes allow high-purity permeated

hydrogen, making the direct supply to low-temperature PEMFC possible. The last case presents the inconvenience of the high cost of dense Pd-based membranes.

4.5.2 Liquefied petroleum gas

LPG is a mixture of hydrocarbons, predominantly propane and *n*-butane. LPG can be liquefied under relatively low pressures and is an abundant feedstock from refinery operations. Some advantages of propane and *n*-butane as feedstocks for hydrogen production are easy storage and an existing infrastructure.

Natural gas is the most favored feedstock for hydrogen production because of its availability, advantageous price, and catalyst stability. However, higher hydrocarbons may be preferred in many places, depending on local availability and local prices relative to natural gas. Also, for onboard hydrogen generation or distributed hydrogen filling stations, a feedstock with a high volumetric hydrogen density is required, preferably at atmospheric or near-ambient pressures; under these conditions, higher hydrocarbons are more favorable than natural gas. LPG is preferred instead of heavier hydrocarbon feedstock such as naphtha or diesel because of its higher weight percentage of hydrogen and low coke formation.

In refineries LPG is fed first to a pre-reformer, operated at temperatures around 450−550 °C, where all hydrocarbons heavier than methane are converted; this produces a methane-rich gas that is introduced to the steam reformer, which operates at temperatures around 850−950 °C (Rakib, Grace, Lim, Elnashaie, & Ghiasi, 2010). Another specific characteristic of steam reforming of propane as a representative hydrocarbon in LPG is the higher S/C ratio used, with values around 4 and 6 and the promotion of the Ni catalyst with earth alkaline metals such as Mg and Ca to improve stability and selectivity. This is a consequence of the higher tendency of propane to coke formation compared with methane.

Rakib et al. (2010) carried out an experimental work with the purpose of studying propane steam reforming in a fluidized-bed membrane reactor. They selected a commercial steam reforming catalyst (RK-212 naphtha steam reforming catalyst from Haldor Topsoe A/S). This catalyst contains Mg, K, and Ca, as well as Ni and Al. From this study they concluded that it is possible to produce a high yield of hydrogen with only one reactor at moderate temperatures around 500 °C. Use of these temperatures has several advantages, among which are energy savings, the ability to avoid expensive alloys, and the stability of the catalyst. The authors also indicated flexibility of the reactor for a high variety of feedstocks because propane is fully consumed near the bottom of the reactor, and then the reactor predominantly acts as a methane steam reformer.

Rhodium is a more effective catalyst than nickel in terms of activity and stability. However, because of the costs and availability, currently rhodium is not widely used in industrial applications. Zapf et al. (2013) studied the application of rhodium nanoparticles in Rh/Al_2O_3 catalyst preparation with the aim of reducing the rhodium content of the catalyst, and consequent costs. The results obtained in a microreactor indicated that it was possible to reduce the noble metal content of the catalyst from 5% to 1% with no significant loss of activity for steam reforming of propane, and the stability of the catalyst was observed during 140 h of time-on-stream.

4.5.3 Naphtha

Naphtha is not a single compound; its composition varies with the source and refinery operating conditions (Moulijn et al., 2008). Naphtha is composed of a mixture of compounds in the range C_3−C_{15} (mainly C_5−C_9) with a boiling range between 52 and 187 °C.

For this feedstock, in industrial processes, a pre-reformer is installed upstream the steam reformer (Moulijn et al., 2008). In the pre-reformer, which is a catalytic fixed-bed reactor operating adiabatically at about 497 °C, the higher hydrocarbons are converted to methane and carbon dioxide, as in reaction (4.10):

$$C_nH_{2n+2} + \frac{1}{2}(n-1)\,H_2O \rightarrow \frac{1}{4}(3n+1)\,CH_4 + \frac{1}{4}(n-1)\,CO_2 \quad \Delta H^{\circ}_{298\ K} < 0 \tag{4.10}$$

The product of the pre-reformer enters the steam reformer, which operates at higher temperatures similar to those found in conventional reformers of natural gas to convert CH_4 to hydrogen.

The higher hydrocarbons found in naphtha have a great tendency to form carbon, which is enhanced by a low S/C ratio and high temperature. The low temperature in the pre-reformer minimizes carbon formation. The presence of the pre-reformer allows the steam reformer to operate at a lower S/C ratio without the danger of carbon deposition.

In the research field, Melo and Morlanés (2005) studied catalysts, mixed oxides obtained by hydrotalcite-type material thermal decomposition, with different nickel contents in the steam reforming of a mixture of *n*-heptane and *n*-hexane, simulating a naphtha. A comparison of these catalysts with a commercial steam reforming catalyst (Haldor-Topsoe R67-7H) indicates a higher specific area of mixed oxides than the commercial catalyst. Also, greater conversion of mixed oxides than the commercial catalyst for a similar nickel content was observed at 450 °C, 10 bar, and an S/C ratio of 4. Catalytic activity increases as nickel content increases until approximately 30 wt%; after that, catalytic activity diminishes with nickel content. As the nickel content decreases, the interaction of nickel with support increases and a small nickel particle size and high dispersion are obtained, which is helpful in avoiding carbon formation. This last result can be influenced by a high magnesium content in the mixed oxide.

4.5.4 Jet fuel and diesel

The advantages of gasoline, diesel, and jet fuel for hydrogen production are their availability and relatively low cost, and the existing infrastructure for delivery and transportation. Moreover, these liquid hydrocarbon fuels contain more chemical energy per unit volume than hydrogen, and thus it is better to carry hydrocarbon fuels than hydrogen (Xu, Li, & Shen, 2013).

Diesel is a common fuel source for transportation application worldwide and in some places is the main source for the generation of electricity. Conversion of the

chemical energy of diesel in combustion engines generates greenhouse gases (CO_2), unwanted byproducts such as nitrogen oxides and particulate matter (Parmar, Kundu, & Karan, 2009). To solve these inconveniences, a hydrogen-rich stream can be generated from diesel reforming and used as a fuel for low-temperature PEMFC for automotive applications and for high-temperature solid oxide fuel cells to generate electricity remotely.

Fuel cells are devices with high energy use efficiency; to avoid storing high-pressure hydrogen, the fuel can be generated in an onboard fuel processor. Several catalytic reaction processes, including steam reforming, partial oxidation, and autothermal reforming, can be carried out to convert liquid hydrocarbons to hydrogen (Cheekatamarla & Lane, 2005).

Steam reforming has the advantage of a high concentration of hydrogen compared with the other two routes (Lakhapatri & Abraham, 2011). Autothermal reforming has attracted considerable attention owing to its higher energy efficiency compared with other processes and its low investment (Cheekatamarla & Lane, 2005).

Disadvantages in the design and operation of a reforming system for heavy hydrocarbon fuels are (Xu et al., 2013):

- The problem exists of making a fuel reformer compatible with various fuels owing to the different additives in diesel and jet fuel.
- The large carbon content may cause coking.
- Sulfur components could deactivate reforming catalysts.

Parmar et al. (2009) carried out a thermodynamic analysis of the diesel reforming process to identify operating conditions that avoid carbon formation, maximize the production of hydrogen, and minimize reactor energy input. In the case of steam reforming for an entire range of temperatures the S/C ratio should be ≥ 2. An increase in S/C ratio increases the hydrogen yield but also the reactor input energy. Partial oxidation of diesel is the least favorable option because it forms a high amount of carbon. Recommended autothermal reforming operating conditions are 750 °C with an O_2/C ratio of 0.25 or slightly higher, an S/C greater than 1.25 (ideally 1.75), and a constant heat supply.

A wide number of works focus on catalyst development. For example, Fauteux-Lefebvre, Abatzoglou, Braidy, and Achouri (2011) efficiently tested an Al_2O_3/YSZ-supported $NiAl_2O_4$ catalyst in diesel steam reforming with no deactivation for more than 15 h at high space velocity. No significant coking occurred on the catalyst surface after the experiment and no sulfur poisoning was observed. Achouri, Abatzoglou, Fauteux-Lefebvre, and Braidy (2013) evaluated the efficiency of Ni-Al catalysts supported on alumina synthesized by wet impregnation and co-precipitation in diesel steam reforming. The impregnated catalyst exhibited a higher catalytic performance and stability over time compared with the co-precipitated catalyst.

Xu et al. (2011) prepared rare earth (La, Ce, Yb) promoted an Ni/γ-Al_2O_3 catalyst by the impregnation method and tested it in diesel steam reforming. Experimental results showed that rare earth promoters, especially Yb, improved the activity and carbon formation resistance of the Ni/γ-Al_2O_3 catalyst. The Yb-Ni catalyst demonstrated higher performance than several commercial catalysts.

Cheekatamarla and Lane (2005) studied bimetallic catalysts for hydrogen generation. Experimental results of autothermal reforming of synthetic diesel fuel revealed that bimetallic catalysts had a higher hydrogen yield than monometallic catalysts. The impregnation of Ni or Pd (in addition to Pt) on ceria-supported catalysts improved the resistance of poisoning from sulfur present in feed.

Lakhapatri and Abraham (2011) studied catalyst deactivation during steam reforming of jet fuel on an Ni-(PdRh)/γ-Al_2O_3 catalyst. They concluded that addition of Rh to the catalyst formulation had a positive effect on catalyst activity in terms of hydrogen yield and inhibited the growth of Ni crystallites. They also showed that sulfur preferentially adsorbed onto Ni sites, which blocked these sites and reduced the performance of the catalyst.

Other works focused on the diesel steam reforming process. Boon, van Dijk, de Munck, and van der Brink (2011) tested commercial catalysts and commercially obtained diesel fuels. For 118 h, a commercial nickel catalyst did not show deactivation at an S/C ratio of 2.6 with the route of pre-reforming sulfur-free diesel at around 475 °C. No deactivation was observed when sulfur concentration in the route of direct steam reforming was increased to temperatures of 800 °C using a commercial precious metal catalyst for 1190 h. Diesel containing biodiesel components resulted in poor spray quality and eventually caused a decrease in catalyst performance (Boon et al., 2011).

Kolb, Hofmann, O'Connell, and Scürer (2009) developed and tested three microstructured reactors on the kilowatt scale. These microstructured reactors were an oxidative diesel steam reformer, a WGS reactor, and a preferential oxidation reactor. The experiments proved the potential of microstructured plate heat exchanger technology for improved heat management and system integration for portable, mobile, and distributed stationary fuel processors.

4.6 Conclusions

Although natural gas steam reforming is a mature technology, new processes exist to solve the inconveniences of conventional plants. In these new processes, membranes and sorption enhanced will improve thermodynamic constraints, increasing hydrogen yield among other benefits.

There is a large variety of nonrenewable feedstocks for hydrogen production by steam reforming, ranging from natural gas to diesel. Jet fuel and diesel are complex feedstocks with problems in the stability of catalysts as a result of coking and sulfur poisoning. A huge amount of research is being carried out to develop more stable catalysts. Bimetallic catalysts and the addition of Rh as promoter are two options in this field.

Microreactors are promising chemical reactions systems for application in portable electronic devices and onboard power production in vehicles. Some advantages of microreactors in hydrogen production result from process intensification that combines the reforming reaction and its required energy input in a small place.

4.7 Future trends

Despite problems from nonrenewable feedstocks such as environmental pollution and the depletion of resources, currently the main process for hydrogen production is steam reforming of natural gas. This situation might not change in the short term.

Probably, in the long term, the contribution to hydrogen production by steam reforming of renewable feedstocks such as bio-oil, bio-ethanol, biodiesel, and glycerine will be higher.

Fuel cells are devices with high energy efficiency, much higher than internal combustion engines. Because of the high cost of energy, an increase in the use and development of new fuel cells is expected. The main fuel for existing fuel cells is hydrogen. Purity requirements of new fuel cells will have an influence on reforming processes from different feedstocks. Moreover, whether derived problems with hydrogen storage and distribution are solved will have an effect on the development of onboard hydrogen generation processes from liquid fuels.

Another expected trend in steam reforming is the implementation of membranes and/or sorption enhanced in industrial processes. Sorbent regeneration may be the main inconvenience in applying SER. The high energy efficiency of autothermal reforming will influence industrial use. Microreactors are chemical reaction systems with a high impact on hydrogen production by steam reforming in the future.

List of acronyms

FBMR	Fluidized-bed membrane reactor
HTC	Hydrotalcites
LPG	Liquefied petroleum gas
PEMFC	Proton exchange membrane fuel cells
PROX	Preferential oxidation
PSA	Pressure-swing adsorption
S/C	Molar steam-to-carbon ratio
SER	Sorption enhanced reforming
WGS	Water gas shift
ZEG	Zero emission Gas power

Acknowledgments

The author wish to express gratitude to the Spanish Ministry of Science and Innovation (MICINN) (Research Project Ref. No. ENE2010-18985). Permission for figures reprinted from the American Chemical Society and Elsevier is also acknowledged.

References

Achouri, I. E., Abatzoglou, N., Fauteux-Lefebvre, C., & Braidy, N. (2013). Diesel steam reforming: comparison of two nickel aluminate catalysts prepared by wet-impregnation and co-precipitation. *Catalysis Today, 207*, 13−20.

Adris, A. M., Lim, C. J., & Grace, J. R. (1994). The fluidized bed membrane reactor system: a pilot scale experimental study. *Chemical Engineering Science, 49*, 5833−5843.

Adris, A. M., Lim, C. J., & Grace, J. R. (1997). The fluidized-bed membrane reactor for steam reforming: model verification and parametric study. *Chemical Engineering Science, 452*, 1609−1622.

Angeli, S. D., Monteleone, G., Giaconia, A., & Lemonidou, A. A. (2014). State-of the-art catalysts for CH_4 steam reforming at low temperature. *International Journal of Hydrogen Energy, 39*, 1979−1997.

Balasubramanian, B., Lopez Ortiz, A., Kaytakoglu, S., & Harrison, D. P. (1999). Hydrogen from methane in a single-step process. *Chemical Engineering Science, 54*, 3543−3552.

Boon, J., van Dijk, E., de Munck, S., & van der Brink, R. (2011). Steam reforming of commercial ultra-low sulphur diésel. *Journal of Power Sources, 196*, 5928−5935.

Bradford, M. C. J., & Vannice, M. A. (1999). The role of metal-support interactions in CO_2 reforming of CH_4. *Catalysis Today, 50*, 87−96.

Cheekatamarla, P. K., & Lane, A. M. (2005). Efficient bimetallic catalysts for hydrogen generation from diesel fuel. *International Journal of Hydrogen Energy, 30*, 1277−1285.

Chen, Z., Po, F., Grace, J. R., Lim, C. J., Elnashaie, S., Mahecha-Botero, A., et al. (2008). Sorbent-enhanced/membrane-assisted steam-methane reforming. *Chemical Engineering Science, 63*, 170−182.

Cortright, R. D., Davda, R. R., & Dumesic, J. A. (2002). Hydrogen from catalytic reforming of biomass-derived hydrocarbons in liquid water. *Nature, 418*, 964−967.

De Falco, M., Iaquaniello, G., & Salladini, A. (2011). Experimental tests on steam reforming of natural gas in a reformer and membrane modules (RMM) plant. *Journal of Membrane Science, 368*, 264−274.

Delsman, E. R., Laarhoven, B. J. P. F., de Croon, M. H. J. M., Kramer, G. J., & Schouten, J. C. (2005). Comparison between conventional fixed-bed and microreactor technology for a portable hydrogen production case. *Transactions IChemE, Part A, Chemical Engineering Research and Design, 83*(A9), 1063−1075.

Fauteux-Lefebvre, C., Abatzoglou, N., Braidy, N., & Achouri, I. E. (2011). Diesel steam reforming with a nickel-alumina spinel catalyst for solid oxide fuel cell application. *Journal of Power Sources, 196*, 7673−7680.

Ferreira-Aparicio, P., Benito, M. J., & Sanz, J. L. (2005). New trends in reforming technologies: from hydrogen industrial plants to multifuel microreformers. *Catalysis Reviews: Science and Engineering, 47*, 491−588.

Fidalgo, B., Domínguez, A., Pis, J. J., & Menéndez, J. A. (2008). Microwave-assisted dry reforming of methane. *International Journal of Hydrogen Energy, 33*, 4337−4344.

Fidalgo, B., & Menéndez, J. A. (2011). Carbon materials as catalysts for decomposition and CO_2 reforming of methane: a review. *Chinese Journal of Catalysis, 32*, 207−216.

Harrison, D. P. (2008). Sorption-enhanced hydrogen production: a review. *Industrial and Engineering Chemistry Research, 47*, 6486−6501.

Häussinger, P., Lohmüller, R., & Watson, A. M. (1989). Hydrogen. In B. Elvers, S. Hawkins, M. Ravenscroft, & G. Schulz (Eds.), *Ullmann's encyclopedia of industrial chemistry* (Vol. A13, pp. 297−442). Weinheim: VCH.

Hinrichsen, K. O., Kochloefl, K., & Muhler, M. (2008). Water gas shift and COS removal. In G. Ertl, H. Knözinger, F. Schüth, & J. Weitkamp (Eds.), *Handbook of heterogeneous catalysis* (Vol. 6, pp. 2905−2920). Weinheim: Wiley-VCH.

Iulianelli, A., Ribeirinha, P., Mendes, A., & Basile, A. (2014). Methanol steam reforming for hydrogen generation via conventional and membrane reactors: a review. *Renewable and Sustainable Energy Reviews, 29*, 355−368.

Izquierdo, U., Barrio, V. L., Cambra, J. F., Requies, J., Güemez, M. B., Arias, P. L., et al. (2012). Hydrogen production from methane and natural gas steam reforming in conventional and microreactor reaction systems. *International Journal of Hydrogen Energy, 37*, 7026−7033.

Jarosch, K., & de Lasa, H. I. (1999). Novel riser simulator for methane reforming using high temperature membranes. *Chemical Engineering Science, 54*, 1455−1460.

Kolb, G., Hofmann, C., O'Connell, M., & Scürer, J. (2009). Microstructured reactors for diesel steam reforming, water-gas shift and preferential oxidation in the kilowatt power range. *Catalysis Today, 147S*, S176−S184.

Lakhapatri, S. L., & Abraham, M. A. (2011). Analysis of catalyst deactivation during steam reforming of jet fuel on Ni-(PdRh)/γ-Al_2O_3 catalyst. *Applied Catalysis A: General, 405*, 149−159.

Löwe, H., & Ehrfeld, W. (1999). State-of-the-art in microreaction technology: concepts, manufacturing and applications. *Electrochimica Acta, 44*, 3679−3689.

Mahecha-Botero, A., Boyd, T., Gulamhusein, A., Comyn, N., Lim, C. J., Grace, J. R., et al. (2008). Pure hydrogen generation in a fluidized-bed membrane reactor: experimental findings. *Chemical Engineering Science, 63*, 2752−2762.

Mahecha-Botero, A., Boyd, T., Gulamhusein, A., Grace, J. R., Lim, C. J., Shirasaki, Y., et al. (2011). Catalytic reforming of natural gas for hydrogen production in a pilot fluidized-bed membrane reactor: mapping of operating and feed conditions. *International Journal of Hydrogen Energy, 36*, 10727−10736.

Martínez, I., Romano, M. C., Chiesa, P., Grasa, G., & Murillo, R. (2013). Hydrogen production through sorption enhanced steam reforming of natural gas: thermodynamic plant assessment. *International Journal of Hydrogen Energy, 38*, 15180−15199.

Melo, F., & Morlanés, N. (2005). Naphtha steam reforming for hydrogen production. *Catalysis Today, 107−108*, 458−466.

Moulijn, J. A., Makkee, M., & van Diepen, A. (2008). *Chemical process technology*. Chichester: Wiley.

Parmar, R. D., Kundu, A., & Karan, K. (2009). Thermodynamic analysis of diesel reforming process: mapping of carbon formation boundary and representative independent reactions. *Journal of Power Sources, 194*, 1007−1020.

Patil, C. S., van Sint Annaland, M., & Kuipers, J. A. M. (2005). Design of a novel autothermal membrane-assisted fluidized-bed reactor for the production of ultrapure hydrogen from methane. *Industrial and Engineering Chemistry Research, 44*, 9502−9512.

Patil, C. S., van Sint Annaland, M., & Kuipers, J. A. M. (2007). Fluidised bed membrane reactor for ultrapure hydrogen production via methane steam reforming: experimental demonstration and model validation. *Chemical Engineering Science, 62*, 2989−3007.

Rakib, M. A., Grace, J. R., Lim, C. J., Elnashaie, S. S. E. H., & Ghiasi, B. (2010). Steam reforming of propane in a fluidized bed membrane reactor for hydrogen production. *International Journal of Hydrogen Energy, 35*, 6276−6290.

Roses, L., Gallucci, F., Manzolini, G., & van Sint Annaland, M. (2013). Experimental study of steam methane reforming in a Pd-based fluidized bed membrane reactor. *Chemical Engineering Journal, 222*, 307−320.

Ross, J. R. H. (2005). Natural gas reforming and CO_2 mitigation. *Catalysis Today, 100*, 151−158.

Rostrup-Nielsen, J. R. (2008). Steam reforming. In G. Ertl, H. Knözinger, F. Schüth, & J. Weitkamp (Eds.), *Handbook of heterogeneous catalysis* (Vol. 6, pp. 2882−2905). Weinheim: Wiley-VCH.

Stefanidis, G. D., & Vlachos, D. (2010). Intensification of steam reforming of natural gas: choosing combustible fuel and reforming catalyst. *Chemical Engineering Science, 65*, 398−404.

Tonkovich, A. L., Yang, B., Perry, S. T., Fitzgerald, S. P., & Wang, Y. (2007). From seconds to milliseconds through tailored microchannel reactor design of a steam methane reformer. *Catalysis Today, 120*, 21−29.

Wang, S., & Lu, G. Q. (1998). Catalytic activities and coking characteristics of oxides-supported Ni catalysts for CH_4 reforming with carbon dioxide. *Energy Fuels, 12*, 248−256.

Xu, L., Mi, W., & Su, Q. (2011). Hydrogen production through diesel steam reforming over rare-earth promoted Ni/Al_2O_3 catalysts. *Journal of Natural Gas Chemistry, 20*, 287−293.

Xu, X., Li, P., & Shen, Y. (2013). Small-scale reforming of diesel and jet fuels to make hydrogen and syngas for fuel cells: a review. *Applied Energy, 108*, 202−217.

Zapf, R., Thiele, R., Wichert, M., O'Connell, M., Ziogas, A., & Kolb, G. (2013). Application of rhodium nanoparticles for steam reforming of propane in microchannels. *Catalysis Communications, 41*, 140−145.

This page intentionally left blank

Hydrogen production by reforming of bio-alcohols

5

F. Frusteri, G. Bonura
Istituto di Tecnologie Avanzate per l'Energia "Nicola Giordano," Messina, Italy

5.1 Introduction

Hydrogen is an energy carrier that will continue to be produced mainly from fossil fuels. In this respect, natural gas represents one of the most attractive hydrocarbon fuels currently used as a feedstock for hydrogen gas (H_2) production, with high conversion efficiency, low impact in terms of carbon dioxide (CO_2) emissions, and a wide distribution network (Armor, 1999; Avcı, Trimm, & Önsan, 2002; Ma & Trimm, 1996). However, the expected increased demand for hydrogen for fuel cell applications is pushing the development of new methods for hydrogen production, especially from renewable feedstocks. Among oxygenated fuels, methanol has received considerable attention as a hydrogen carrier because its conversion can be achieved with high efficiency under relatively mild conditions (Asprey, Wojciechowski, & Peppley, 1999; Avcı, Önsan, & Trimm, 2003; Ma, Jiang, Adesina, Trimm, & Wainwright, 1996; Peppley, Amphlett, Kearns, & Mann, 1999a, 1999b). Although technology dealing with methanol production is well-established (i.e., conversion of syngas via reforming of natural gas), several limitations are currently slowing down its distribution as a consequence of issues related to toxicity and volatility. From this point of view, ethanol derived from the fermentation of biomass has the advantages of being much less toxic and safer to handle and transport. Furthermore, hydrogen production from bio-ethanol offers an attractive route to CO_2 recycling because the CO_2 produced is consumed for biomass growth (Auprêtre, Descorme, & Duprez, 2002).

n-Butanol represents another promising source of H_2. Similar to other biomass-derived oxygenated hydrocarbons, *n*-butanol is a renewable resource obtainable by fermenting sugar beet, sugar cane, corn, wheat (Brum Pereira, Ramirez de La Piscina, & Homs, 2011; Cai et al., 2008), and potentially lignocellulosic biomass (Jesse, Ezeji, Qureshi, Blaschek, & Ind, 2002). *n*-Butanol has higher H_2 content (13.5 wt%) than ethanol (13.0 wt%) and methanol (12.5 wt%), lower vapor pressure, tolerance to water contamination, low corrosiveness, high energy density, low hygroscopicity ,and ease of handling and distribution to existing fuel pipelines. To date, there are few studies published in the literature on *n*-butanol reforming, such as steam reforming (SR) (Bimbela et al., 2009; Nahar & Madhani, 2010), partial oxidation (POX) (Wang & Cao, 2010), dry reforming (Wang et al., 2011), autothermal reforming (ATR), and aqueous phase reforming (APR) (Roy, Sullivan, & Leclerc, 2011).

Recently, increased production of biofuel by the fatty acid methyl ester process has motivated consideration of glycerol as a renewable source of hydrogen. In fact, SR is a

Compendium of Hydrogen Energy. http://dx.doi.org/10.1016/B978-1-78242-361-4.00005-4

promising way to use the diluted glycerol aqueous solution to produce hydrogen. Stoichiometrically, the glycerol SR reaction should produce from 1 mol to 7 mol of hydrogen, although it has been observed that the production/yield of hydrogen rarely exceeds 6 mol (Tran & Kamali Kannangara, 2013). In any case, the expected cost of hydrogen produced from SR of glycerol could vary from US$2.6 to US$3.8/kg (Tran & Kamali Kannangara, 2013), so that co-production of hydrogen via these processes could become economical if the price of natural gas increases. However, from a catalytic point of view, with respect to current market value, hydrogen production from glycerol will need catalyst optimization to achieve higher productivity as well as higher purity of hydrogen.

On the whole, the development of technology based on reforming bio-derived oxygenated compounds appears to be a challenging research topic, considering that hydrogen yield depends significantly on both the type of catalyst and the reaction conditions adopted (Comas, Marino, Laborde, & Amadeo, 2004; Haryanto, Fernando, Murali, & Adhikari, 2005; Mas, Kiproes, Amadeo, & Laborde, 2006; Vaidya & Rodrigues, 2006).

5.2 Reforming of ethanol

5.2.1 Reaction mechanism

Several steps are generally considered in the ethanol SR (ESR) reaction: (1) dehydrogenation of ethanol, (2) cleavage of the carbon−carbon bond of C2 intermediates to produce CO and CH_4, and (3) water reforming of C1 products to generate additional hydrogen.

Figure 5.1 shows the reaction scheme generally accepted by several authors as describing how SR of ethanol can evolve.

Although the ESR reaction has been widely investigated in past years, only a few attempts to provide information about the reaction steps are found in the literature (Erdohelyi et al., 2006; Fatsikostas & Verykios, 2004; Llorca, Homs, & de la Piscina, 2004; Rasko, Hancz, & Erdohelyi, 2004; Sheng, Bowmaker, & Idriss, 2004; Yee, Morrison, & Idriss, 2000). Despite these studies, many questions remain dealing with mechanisms operating in catalyst deactivation, the role of active phases and supports on the reaction network, metal interactions in bimetallic catalysts leading to synergetic effects, and so forth.

Depending on reaction conditions and the catalytic system used, the ESR reaction can proceed through two main pathways: (1) dehydration to produce ethylene (2) dehydrogenation to produce acetaldehyde. Both ethylene and acetaldehyde can react further with water to produce carbon oxides and methane and/or dehydrogenate to form carbon deposits. To maximize hydrogen production, the formation of by-products such as CO, CH_4, C_2H_4, C_2H_6, and carbon deposits must be minimized.

Moreover, if a dual acid-dehydrogenating catalyst is used, it is reasonable to think that the main reactions will be those described in the scheme shown in Figure 5.2.

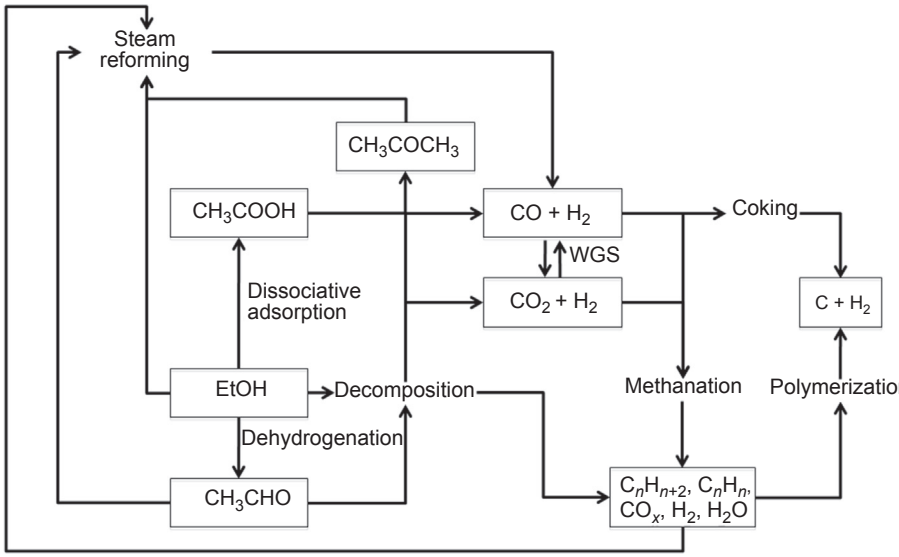

Figure 5.1 Proposed reaction scheme of ethanol steam reforming over metal catalysts.

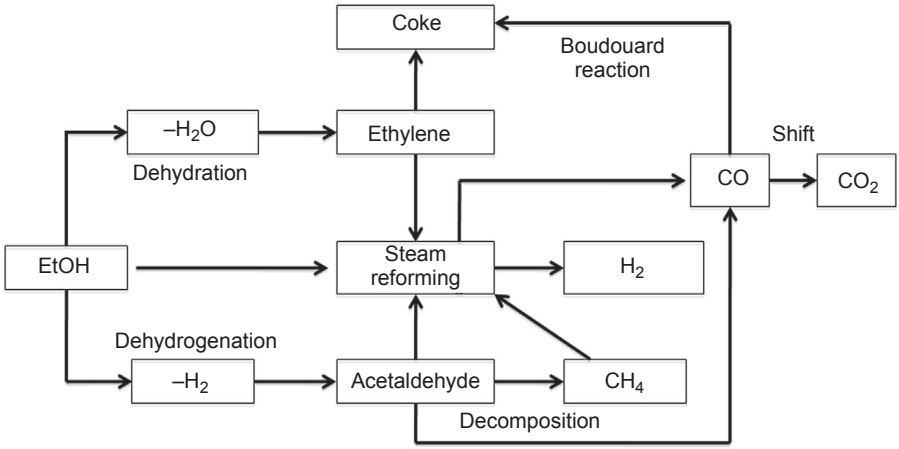

Figure 5.2 Pathways for the steam reforming of ethanol over bifunctional catalysts.

5.2.2 Different approaches proposed: SR, ATR, and APR

Currently, for most feedstocks, three main technologies are proposed to produce hydrogen from alcohols: SR, POX, and ATR. SR is the process most applied in the industry owing to its higher hydrogen yield (Ahmed & Krumpelt, 2001). The SR of ethanol is a strongly endothermic reaction (5.1):

$$C_2H_5OH + 3H_2O \rightleftarrows 2CO_2 + 6H_2 \quad \Delta H = +374\ \text{kJ/mol} \tag{5.1}$$

Although ethanol POX (5.2) leads to heat generation, H_2 yield per carbon in the fuel is lower (Krumpelt, Krause, Carter, Kopasz, & Ahmed, 2002). Carbon monoxide can be converted into carbon dioxide by the water gas shift (WGS) reaction, completing the hydrogen production (5.3):

$$C_2H_5OH + 2O_2 \rightleftarrows 2CO + 3H_2O \quad \Delta H = -517\ \text{kJ/mol} \tag{5.2}$$

$$CO + H_2O \rightleftarrows CO_2 + H_2 \quad \Delta H = -41\ \text{kJ/mol} \tag{5.3}$$

ATR combines the effects of exothermic POX and endothermic SR by feeding fuel, oxidant, and water together inside the reactor without the need for an external energy supply. Therefore, a new generation of fuel processors based on ATR is emerging because they can be more energy-efficient and the equipment can be smaller and lighter (Ahmed & Krumpelt, 2001; Krumpelt et al., 2002).

5.2.2.1 Steam reforming

SR of hydrocarbons is a highly endothermic reaction that requires high reaction temperatures, typically above 500 °C. Moreover, because the reaction is characterized by large fluctuations in adiabatic temperature (Semelsberger, Brown, Borup, & Inbody, 2004), external energy has to be supplied to sustain reformation of the fuel. Thermodynamic calculations reveal that reforming oxygenated hydrocarbons requires much less energy per moles of H_2 formed.

5.2.2.2 Autothermal reforming

ATR is the most promising reforming technology for fuel cell systems because the combination of SR, WGS, and preferential oxidation reactions allows the design of more compact adiabatic reactors characterized by low pressure drop (Farrauto et al., 2003; Hochmuth, 1992). Exit temperatures and fuel conversion depend strictly on the inlet temperature, reactor pressure, and on steam-to-carbon (S/C) and oxygen-to-carbon (C/O) ratios in the feed. Indeed, H_2 yield is favored by high inlet temperature and a high S/C ratio; under such conditions a lower O/C ratio is required to sustain the reaction (Doss, Kumar, Ahluwalia, & Krumpelt, 2001; Hagh, 2003) whereas a higher S/C ratio reduces coke formation (Seo, Shirley, & Kolaczkowski, 2002). For ethanol, the optimal S/C ratio is reported to be 2.0 (Semelsberger et al., 2004).

5.2.2.3 Aqueous phase reforming

APR produces hydrogen from biomass-derived oxygenated compounds such as glycerol, sugars, and sugar alcohols. The process generates hydrogen without losing water, which represents major energy savings. Furthermore, it occurs at a temperature and pressure at which the WGS reaction is favorable, which makes it possible to generate hydrogen with low amounts of CO in a single reactor. At a low temperature, undesirable decomposition reactions typically encountered when carbohydrates are heated to an elevated temperature are minimized.

5.2.3 Oxides and supported catalysts: activity, selectivity, and stability

The consideration of ethanol as a hydrogen source is new compared with methanol. Indeed, ethanol conversion and hydrogen yields vary significantly with the type of catalyst, method of catalyst preparation, and reaction conditions. Hydrogen production by ESR proceeds at atmospheric pressure but it requires a high reaction temperature and a high water-to-ethanol ratio. Complete EtOH conversion is essential to achieve an economic process and the catalyst has an important role because it increases the rate of reaction in such a way that the system tends toward thermodynamic equilibrium (Fishtik & Datta, 2002; Freni, Cavallaro, Mondello, Spadaro, & Frusteri, 2003; Haryanto et al., 2005; Li & Leung, 2007). The design of a suitable catalyst for the production of H_2 should involve the following assessments: (1) the choice of active metal, (2) the kind of support with suitable surface properties, (3) the preparation method, (4) the need for additives/dopants, (5) the water-to-ethanol ratio, and (6) the optimal reaction temperature considering the formation of coke and by-products (CH_4, CO, CO_2, and C_2H_4). Fuel versatility, cost, durability, and operation under transient conditions are also critical aspects to be taken into account.

Non-noble metals (i.e., Ni, Co, Cu, Ni-Cu) or noble metals (i.e., Pt, Pd, Ru, Rh, Ir) over suitable supports are promising for obtaining high hydrogen yield; main difficulties are related to by-product formation and a short catalyst lifetime. Among the non-noble metals, so far, Ni is the best catalyst for H_2 production by ESR, whereas among all noble metals, Rh produces the best activity and selectivity to H_2 because this metal favors C−C bond rupture (Cavallaro, Chiodo, Freni, Mondello, & Frusteri, 2003; Liguras, Kondarides, & Verykios, 2003).

The supports provide metal dispersion and promote the migration of surface OH groups toward metal in the presence of water at a high temperature (Li & Leung, 2007). Al_2O_3 is a common support for non-noble or noble metals. The Lewis acid sites of Al_2O_3 favor the synthesis of ethylene, which explains coke formation generally associated with Al_2O_3-supported catalysts. The addition of alkali elements can partially decrease acidity and increase catalyst stability. With regard to MgO, ZnO, CeO_2, and hydrotalcites, their basicity can inhibit ethanol dehydration to ethylene, greatly reducing coke formation. La_2O_3 also promotes dehydrogenation without producing coke. Deactivation by coke deposition on acid supports and the metal sintering of these catalysts represent main obstacles of a stable operation. Other supports such as ZrO_2, CeO_2−ZrO_2, SiO_2, and zeolite-Y have shown adequate synergy with active metals.

5.2.3.1 Catalysts based on non-noble metals

For Ni catalysts, several supports and catalytic formulations have been studied (Guo, Wang, Guo, & Li, 2011; Inokawa, Nishimoto, Kameshima, & Miyake, 2011; Liberatori, Ribeiro, Zanchet, Noronha, & Bueno, 2007; Liu et al., 2011; Vizcaìno, Lindo, Carrero, & Calles, 2012; Yang, Ma, & Wu, 2007). It is generally accepted that Ni is responsible for C−C bond cleavage as well as the role of additives (i.e., Cu, Cr) crucial in promoting ethanol oxidation to H_2 and CO.

Freni et al. (2003) stated that Ni-based catalysts exhibit higher activity and selectivity to H_2 than Co catalysts owing to the low tendency of the metallic Ni to oxidize during reaction.

Frusteri et al. (2006) found that the presence of oxygen in the reaction stream contributes to depressed coke formation on Ni/MgO and Ni/CeO_2 catalysts, but in some cases CH_3CHO forms at a high rate. Under equilibrium conditions, both catalytic systems allow H_2 selectivity to be obtained close to 70%.

Nickel-based catalysts supported on Al_2O_3, MgO, La_2O_3, ZnO, and zeolites with the addition of Cu, Zn, Na, or K have been investigated in ESR in the range 250−600 °C (Comas et al., 2004; Fatsikostas, Kondarides, & Verykios, 2002; Sun et al., 2004; Sun, Qiu, Wu, Zhu, 2005). Among the supports used, La_2O_3 contributes to enhance catalyst stability (Yang et al., 2007). The addition of La and Mg is also essential to enhance H_2 yield (Liberatori et al., 2007) although the formation of a high amount of CH_4 continues to be a problem.

Liu et al. (2011) found total ethanol conversion of around 325 °C for the $LaNiO_x$ nanotubes; their results indicated that $LaNiO_x$ nanotubes produced H_2 selectivity of 70%.

Zeolites have been also tested in ESR. Using Ni/zeolite-Y catalysts, Inokawa et al. (2011) showed that H_2 production mainly takes place via the ethanol dehydrogenation reaction path as the result of zeolite basicity, which prevents coke deposition especially if Na^+ is exchanged with K^+ or Cs^+.

The Ni^{2+} reducibility in mixed oxides was improved by realizing multi-metallic systems, such as NiMgN catalysts (with N = La or Ce) prepared by co-precipitation (Vizcaìno et al., 2012). With this catalytic system, high H_2 yield (5.1 mol H_2/mol EtOH) was reached.

Guo et al. (2011) and Biswas and Kunzru (2007) investigated Ni/CeO_2−ZrO_2 catalysts and found that Ni/$Ce_{0.74}Zr_{0.26}O_2$ catalyst with 30 wt% Ni exhibited the highest H_2 selectivity, close to 96%.

Also, cobalt has been largely studied as an active metal in ESR. In this respect, Llorca, Homs, Sales, and Ramìrez (2002) and Llorca, Dalmon, Ramìrez, and Homs (2003) prepared and tested differently supported Co catalysts (ZnO, Al_2O_3, SiO_2-TiO_2, ZrO_2, and CeO_2), observing that Co/ZnO catalyst was the best for reaching total conversion and 42% of H_2 selectivity at 450 °C after 50 h. Characterization of the used catalyst revealed that Co particles were covered by high-disorder carbon phases and carbon was deposited on the support.

Using Co/Al_2O_3, Batista, Santos, Assaf, Assaf, and Ticianelli (2004) found the presence of Co_3O_4 to be the main phase and reported complete ethanol conversion and H_2 selectivity of 65% at 400 °C. The CO concentration in the gaseous mixture was reduced to 800 ppm using a Co/Al_2O_3 catalyst with 18 wt% cobalt. The low amount of CO produced in the reaction mainly resulted from the high activity of cobalt in the WGS reaction.

Song, Zhang, Watson, Braden, and Ozkan (2007) studied Co-based catalysts supported on Al_2O_3, TiO_2, ZrO_2 and found that high Co dispersion is necessary to prepare active systems. Over the 10% Co/ZrO_2 catalyst, using an H_2O:EtOH:inert molar ratio of 10:1:75 and a gas hourly space velocity (GHSV) of 5000 h^{-1}, total ethanol conversion and yield of 5.5 mol H_2/mol EtOH were obtained at 550 °C.

Banach et al. (2011) prepared a trimetallic Co/ZnO-Al_2O_3 catalyst and obtained total ethanol conversion and 95% H_2 selectivity at 480 °C, owing to stabilization of the ZnO support operated by Al_2O_3.

Pang, Chen, Dai, and Cui (2012) studied the influence of CaO in ESR using Co/CeO_2 catalysts: high H_2 yield (90%) under optimized conditions ($T_R = 550$ °C; GHSV = 50,000 mL/g/h; S/C = 3.0) was obtained.

A combined effect of ZrO_2 and CeO_2 to promote high ethanol conversion and inhibit methanation was claimed when $CeZrO_4$ was used as a support for Co (Lin, Kim, & Ha, 2008). The Co/$CeZrO_4$ catalysts showed higher activity and H_2 selectivity with respect to Co/ZrO_2 catalyst, which produced more CH_4.

Regarding Cu catalysts, ethanol dehydrogenation to acetaldehyde followed by decarbonylation to CH_4 and CO, or by SR to H_2 and CO normally takes place. The type of support influences selectivity to H_2 and catalyst stability. Because of this, the promoting effect of ceria on copper oxide catalysts has been reported: The formation of a solid solution by incorporating Cu atoms into the CeO_2 lattice is responsible for the synergistic interaction (Shan et al., 2004). For example, the CuO-CeO_2/γ-Al_2O_3 catalyst showed constant H_2 production for more than 10 h, attaining total ethanol conversion and H_2 selectivity close to 80% at 350 °C (Snytnikov et al., 2012).

When Cu and Ni metals were supported on SiO_2, total conversion and H_2 selectivity of 90% were obtained at 700 °C (Fierro, Klouz, Akdim, & Mirodatos, 2002). First, ethanol was converted to acetaldehyde (predominantly on Cu-based catalytic centers); second, acetaldehyde was converted to H_2-rich gas. In the presence of Ni the second step proceeded at a high temperature (around 600 °C) and reaction products besides H_2 and CO contained significant amounts of CH_4 and CO_2.

The most interesting results published in ESR have been rationalized in terms of H_2 yield (mol H_2/mol EtOH) as a function of the reaction temperature (Figure 5.3).

From a first overall evaluation of the data, hydrogen yields >5 can be obtained in a wide temperature range (from 300 to 800 °C). In this respect, nickel works well at a temperature >600 °C owing to its activity in the hydrocarbon reforming process. The use of Co in place of Ni allows operation at a lower temperature, around 500 °C, reaching H_2 yields >5.5 when Co is supported in ZnO-Al_2O_3. Certainly, for both metals (Ni and Co), the nature of the carrier used can significantly affect catalytic behavior because the carrier influences the mechanisms of coke formation to further stabilize the active metal, which, as is well-known, depend on the acidity/basicity balance and surface mobility or storage of surface oxidizing species.

5.2.3.2 Noble metal catalysts

In an attempt to rationalize the numerous data reported in literature, the performance of various systems based on noble metals has been compared in terms of H_2 yield as a function of the reaction temperature.

Among the noble metals (i.e., Pt, Pd, Ru, Rh, and Ir), Rh and Ru appear to be active in ESR reaction and exhibit high selectivity to H_2 (Auprêtre et al., 2002). In the case of Rh supported on Al_2O_3, Auprêtre et al. (2002) found total conversion of ethanol and high selectivity to H_2 (73.5%) at 600 °C. The presence of ZrO_2 alone or in

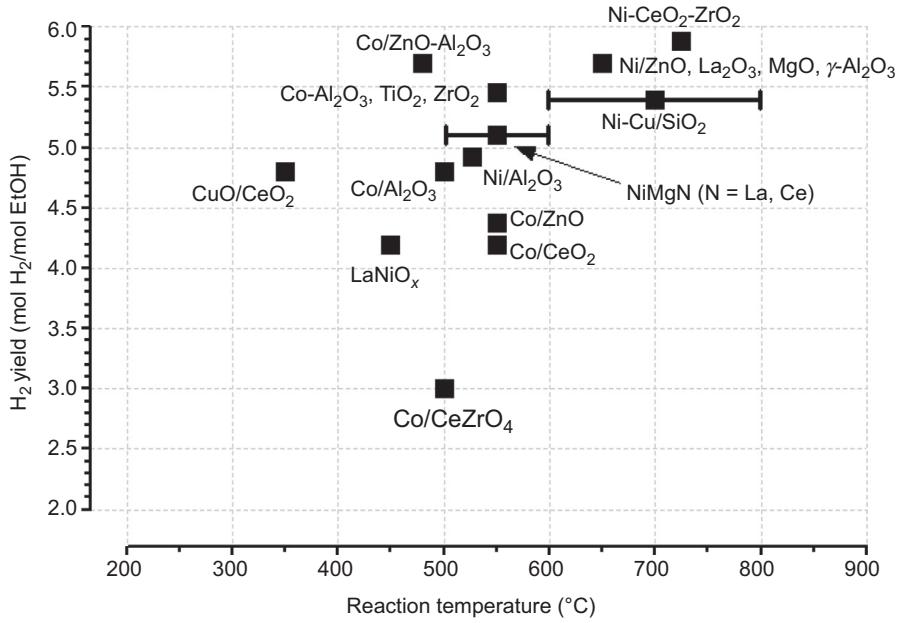

Figure 5.3 Main results of non-noble metal catalysts in ethanol steam reforming.

combination with CeO_2 decreases the formation of CO. The CO_2/CO ratio is sensitive not only to the reaction temperature but also to the relative amount of ZrO_2 or CeO_2 (Auprêtre et al., 2002; Diagne, Idriss, & Kiennemann, 2002; Diagne, Idriss, Pearson, Gòmez, & Kiennemann, 2004; Gutierrez, Karinen, Airaksinen, Kaila, & Krause, 2011; Karim et al., 2010; Roh, Wang, King, Platon, & Chin, 2006). It appears that the best catalyst (higher CO_2/CO ratio) contains equal amounts of Ce and Zr. The use of CeO_2-based supports, highly active in WGS reaction, leads to thermodynamic CO/CO_2 equilibrium. As a result, activity in the ESR reaction and selectivity to CO_2 vary in opposite directions (Auprêtre et al., 2002; Breen, Burch, & Coleman, 2002; Da Silva et al., 2011; Huang et al., 2013; Karim et al., 2010).

Rhodium/magnesium oxide shows good performance in terms of activity and stability, with a low coke formation rate (Frusteri, Freni, Spadaro, et al., 2004). However, it seems not to be as selective toward H_2 production, although in terms of metals' specific activity, Rh sites were 2.2, 3.7, and 5.8 times more active than Pd, Co, and Ni, respectively. (Frusteri, Freni, Spadaro, et al., 2004)

High catalytic performance associated with low coke deposition rate has been reported in the case of bimetallic catalysts such as Rh-Ni (Le Valant, Can, Bion, Duprez, & Epron, 2010) Rh-Co, (Churakova et al., 2010; Moura et al., 2012), Rh-Pd (Lòpez et al., 2013; Lòpez, Divins, & Llorca, 2012), and Rh-Pt (Cobo et al., 2013; Gutierrez et al., 2011) supported on CeO_2, ZrO_2, or La_2O_3.

Platinum-based catalysts have good catalytic properties and catalyze the WGS reaction, which is important for CO removal, but they are not as selective toward

H_2 formation. In particular, Pt/Al_2O_3 catalysts have high selectivity to CO_2 (Auprêtre et al., 2002); Al_2O_3 was active in the dehydration reaction to C_2H_4, even when CeO_2/ZrO_2 supported catalysts exhibited higher activity (Breen et al., 2002).

In accordance with the conversion data, some authors ordered the activity trend of each noble metal as follows: Rh » Pt > Pd > Ru (Ghita, Rosca, & Ezeanu, 2012; Liguras et al., 2003).

Platinum/ceric oxide catalysts also show high activity in ESR, likely owing to the O_2 storage properties of CeO_2 (Ciftci, Ligthart, Pastorino, & Hensen, 2013; De Lima et al., 2008; He, Yang, Wang, Zhao, & Duan, 2012). Because of this, the Pt/CeO_2 catalyst attained the best ethanol conversion with respect to CeO_2-supported Pd, Ir, and Co catalysts (Chiou, Siang, Ho, Lee, & Yeh, 2012). For these catalysts, the ethanol dehydrogenation and decomposition of acetaldehyde occur at a low temperature (300 °C); therefore, high concentrations of CH_4 (29%) and CO (8%) prevent a high H_2 yield.

In the case of Pt/ZrO_2, a strong synergistic interaction between Pt and oxygen vacancies (De Lima et al., 2008; Yamazaki et al., 2010) was indicated as responsible for favoring acetaldehyde and ethane formation. The effect of a combination of ZrO_2 and CeO_2 carriers has been studied in $CeZrO_2$ and $Pt/CeZrO_2$ catalysts at 500 °C (De Lima et al., 2008): EtOH conversion and H_2 selectivity reached 100% and 70%, respectively. Unpromoted $CeZrO_2$ was active and stable, whereas $Pt/CeZrO_2$ catalyst deactivated for all feed compositions investigated. Considering that decomposition of the dehydrogenated products and the formation of acetate species are promoted by the presence of Pt, high selectivity to CH_4, CO, and CO_2 was observed over $Pt/CeZrO_2$ (De Lima et al., 2008).

Ethanol dehydrogenation to CH_3CHO and ethanol decomposition to CH_4 and CO were the primary reactions over CeO_2-supported Pt-Co, Ir, and Pt-Ni catalysts; however, they were significantly active and selective for H_2 production by ESR at a high temperature (Palma, Castaldo, Ciambelli, & Iaquaniello, 2013, 2012a, 2012b; Palma, Palo, Castaldo, Ciambelli, Iaquaniello, 2012). Intermediate compounds such as CH_3CHO and CH_3COCH_3 were completely converted into H_2, CO, and CO_2 as the result of the major reactions of CH_4 SR and reverse WGS.

Palladium catalysts have shown suitable catalytic activity when supported on Al_2O_3 (Auprêtre et al., 2002; Breen et al., 2002; Goula, Kontou, & Tsiakaras, 2004; Liguras et al., 2003) and CeO_2/ZrO_2 (Breen et al., 2002). In particular, high H_2 selectivity was obtained (98%) with a Co_xO_y-Pd/zeolite-Y catalyst (Kwak, Kim, & Kang, 2010). This high performance at 600 °C was observed for 45 h with an H_2O/ethanol ratio of 3 and a GHSV of 8400 h^{-1}. An optimal H_2/CO molar ratio was found at a reaction temperature of about 450 °C because of low CO formation (Goula et al., 2004).

The behavior of Ru catalysts with high loading is comparable to Rh catalysts (Ciftci et al., 2013; Koh et al., 2008; Liguras et al., 2003a). However, Ru produces ethylene, which is a coke precursor. Their catalytic performance is significantly improved with increased metal loading (at least 5 wt% Ru) (Liguras et al., 2003), leading to total EtOH conversion and H_2 selectivity close to 90% at 750 °C. Indeed, 5% Ru/MgO

and 5% Ru/TiO_2 catalysts showed total conversion and high H_2 selectivity (80% and 70%, respectively). Using cluster-derived 2.5% Ru/γ-Al_2O_3 catalysts at 550 °C, a hydrogen yield close to that expected from the stoichiometry (5.8 mol of H_2) was also reported (Koh et al., 2008).

Using Ir as active phase, CeO_2 (Cai et al., 2008, 2012; Chiou et al., 2012; Wang et al., 2012; Zhang, Cai, Li, Xu, & Shen, 2008) and CeO_2-Pr_xO_y (Wang et al., 2011) were considered the most suitable supports. For example, Chiou et al. (2012) prepared Ir/CeO_2 catalysts and found that CeO_2 prevents highly dispersed Ir particles from sintering by a strong Ir−CeO_2 interaction. This may reflect the inhibition of coke formation.

By comparing CeO_2-supported metals in terms of H_2 yield, the following order was found: Ir/CeO_2 (88%, 475 °C) > Pt/CeO_2 (56.6%, 500 °C) > Co/CeO_2 (45%, 425 °C). This trend was explained on the basis of a structural sensitivity established on two types of sites: the ceria surface sites, as well as interfacial sites between Ir and CeO_2 phases.

In the case of $Ce_{0.9}Pr_{0.1}O_2$, Wang et al. (2011) studied ESR over Ir/$Ce_{0.9}Pr_{0.1}O_2$ catalyst. They found that Ir/$Ce_{0.9}Pr_{0.1}O_2$ promotes the incorporation of O_2 into the CeO_2 lattice, enhancing the storage capacity and thermal stability of the catalysts.

Catalysts that cause higher yield to hydrogen (>5 mol H_2/mol EtOH) are essentially based on rhodium or ruthenium. Depending on the substrate used, the performance of the catalyst significantly depends on the reaction temperature. For example, Rh/CeO_2 is active at a low temperature (450 °C) whereas Rh/MgO requires a reaction temperature of 700 °C. This is because the nature of the substrate has an important role in promoting or inhibiting unwanted reactions leading to the formation of methane.

Even Pd catalysts are active in ESR reaction. In particular, a surprising result (5.8 mol of H_2) was obtained at 400 °C using M_xO_x-Pd/zeolite. The authors justified this result on the basis of high dispersion of the noble metal, Pd, on the surface of the transition-metal oxides. As a result, catalytic performance was improved and catalytic deactivation was simultaneously retarded during ESR.

Results obtained from ESR reaction over noble metal catalysts are summarized in Figure 5.4.

5.2.4 Catalyst deactivation

The mechanism of catalyst deactivation is one of the most important issues for investigation under reforming conditions. Erdohelyi et al. (2006) attributed the deactivation of catalysts during ESR to the accumulation of acetate-like species on the supports. The high stability of these acetate species might block the migration of ethoxide intermediates from the support to the metal particles, where they are decomposed to produce hydrogen. On the other hand, Platon, Roh, King, and Wang (2007) suggested that the intermediates ethylene and acetone were the species responsible for the strong deactivation of catalysts observed at low reforming temperatures (250 °C). Despite these studies, the catalyst deactivation process is still not entirely understood, although coke formation and metal sintering are usually addressed as the main reasons for the short catalyst lifetime.

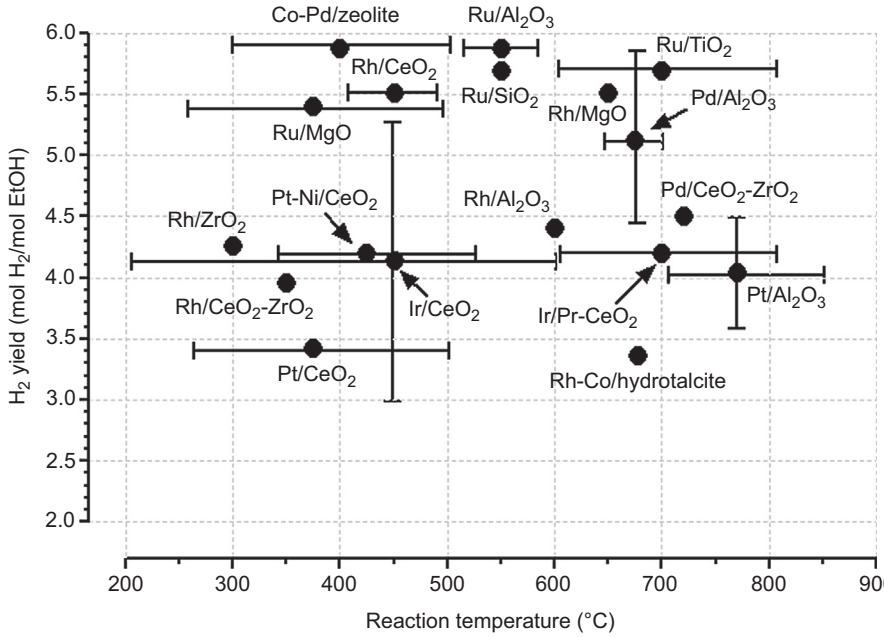

Figure 5.4 Main results of noble metal catalysts in ethanol steam reforming.

5.2.4.1 Coke formation

Carbon formation in reforming reactions of alcohols is one of the most challenging problems. The problem is mainly related to both the low thermal stability of alcohols and their propensity to dehydrate to form olefins, which are coke precursors (Trimm & Önsan, 2001).

Coke is likely formed through one of the following mechanisms (Trimm, 1997):

$$2CO = C_s + CO_2 \tag{5.4}$$

$$CO + H_2 = C_s + H_2O \tag{5.5}$$

$$CH_4 = C_s + 2H_2 \tag{5.6}$$

$$C_nH_{2n+2} = nC_s + (n+1)H_2 \tag{5.7}$$

In SR, the amount of coke formation is determined by the rates of coke formation and coke removal; thus, increasing H_2O concentrations can reduce coking by increasing the steam gasification rate.

In addition to its dependence on steam concentration, the coking rate is also dependent on the reactivity of carbon species (C_s). The typology of coke formed is a function of several factors, such as the reactor temperature, feed content, and contact time. Time on stream (TOS) can also affect the carbon morphology and thus its reactivity

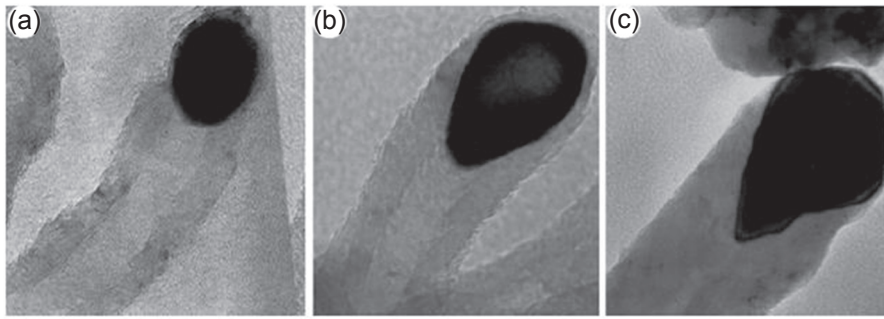

Figure 5.5 Transmission electron microscopy images showing the correlation between Ni particle shape and filament growth. Spherical particle (a); pear-shaped particle (b), triangular particle (c).

(Lakhapatri & Abraham, 2009). For instance, weakly adsorbed atomic carbon can form carbides during TOS and become more difficult to remove (Farrauto & Bartholomew, 2006).

Coke commonly deactivates catalysts by fouling, according to the mechanism of condensation of CH_x species on the catalyst surface, covering active sites and plugging pores (Heck, Farrauto, & Gulati, 2009). Surface carbon species can also become increasingly dehydrogenated and form graphitic coke (Bartholomew, 2001; Farrauto & Bartholomew, 2006). Graphitic coke can encapsulate active sites and catalyst quickly deactivates; it is hard to remove this type of coke (Bartholomew, 2001; Farrauto & Bartholomew, 2006).

The most well-studied catalysts are Ni-based, because Ni is active in reforming reactions of hydrocarbons, but these catalysts usually promote the formation of huge amounts of coke. One main problem of an Ni catalyst is that when hydrocarbon is adsorbed on its surface to be activated or decomposed, the elementary C can easily diffuse within the Ni particle with enlargement of the particle and subsequent precipitation from the opposite side (Figure 5.5) (Frusteri, Italiano, Espro, Cannilla, & Bonura, 2012). This phenomenon prevents the possible gasification by water of carbon deposited on metal particles, and thus favors the formation of filamentous carbon, which can cause the detachment of Ni particles from the support (destruction of the catalyst).

Frusteri et al. (2012) showed that the growth of carbon is closely related to the particle size of Ni, and therefore to the degree of interaction of metal and the support: Strong metal−support interaction (SMSI) limits the formation of filamentous carbon. The most commonly reported mechanism for SMSI is decoration of the active metal with the support (Ito & Tomishige, 2010).

Moreover, coke can also encapsulate the particles over Ni catalysts, resulting in immediate catalyst deactivation. As shown in Figure 5.6, the formation of encapsulating carbon results in the coverage of a great number of metallic sites (Frusteri et al., 2012). Usually, coke deposition is initially high and the rate of deposition decreases with time, because most metallic sites become inactive.

Generally, a fundamental factor in determining the type of coke formed is the reaction temperature (Alberton, Souza, & Schmal, 2007): the more reactive, amorphous

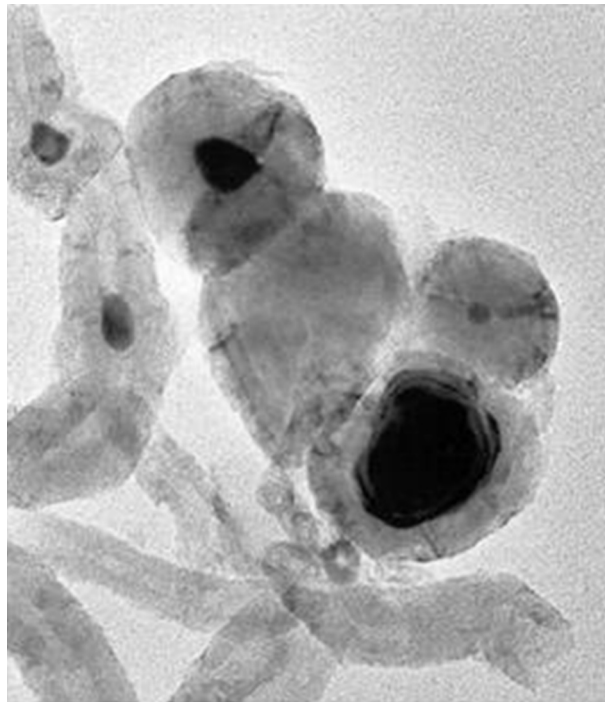

Figure 5.6 Transmission electron microscopy images of Ni catalyst affected by encapsulating coke formation.

forms of carbons formed at low temperatures (200−500 °C) are converted at high temperatures (>500 °C) to less reactive, graphitic forms.

Moreover, a low reaction temperature favors the high formation of filamentous carbon because the gasification rate with steam is slow. Generally, by increasing the reaction temperature the total amount of coke decreases; instead, the formation of encapsulating carbon increases.

Another factor that affects coke formation during ESR is the olefin production grade (i.e., ethylene), likely promoted by dehydration on acidic sites. It is well-documented that alumina, an acidic carrier, promotes the production of ethylene. It has also been shown that by decreasing the acidity of the carrier with promoters (i.e., alkaline metals), coking can be reduced (Le Valant, Can, Bion, Duprez, & Epron, 2010; Liguras et al., 2003). In addition, ethylene formation can be minimized by adding basic compounds to the reactants. For instance, the addition of diethylamine was shown to improve catalyst stability during ESR, whereas the addition of acidic compounds such as acetic acid decreased stability (Le Valant, Garron, Bion, Epron, & Duprez, 2008).

The use of noble metal catalysts such as rhodium has been seen to limit coke formation significantly, mainly because these catalysts are more active than Ni in the gasification processes of carbon. For example, using 5 wt% Rh/γ-Al_2O_3, characterized by large Rh particles, coke formation was prevented by operating at a high temperature in

the presence of a large excess of water; in particular, at 650 °C, only C1 products were found at the exit of the reaction stream, and less coke was formed when O_2 was added together with water.

According to evidence from the literature, several reactions can take place during ESR: for example, acetaldehyde formed by the dehydrogenation of ethanol is decomposed to CH_4 and CO (Eqn (5.8)) or undergoes SR (Eqn (5.9)). Then, water reforms the C1 products to hydrogen (Eqns (5.3) and (5.10)). In addition, when O_2 is present, the reactions in Eqns (5.11)−(5.14) occur (Cavallaro et al., 2003):

$$CH_3CHO \rightleftarrows CH_4 + CO \tag{5.8}$$

$$CH_3CHO + H_2O \rightleftarrows 2CO + 3H_2 \tag{5.9}$$

$$CH_4 + H_2O \rightleftarrows CO + 3H_2 \tag{5.10}$$

$$CO + 0.5O_2 \rightleftarrows CO_2 \tag{5.11}$$

$$C_2H_5OH + 0.5O_2 \rightleftarrows CH_3CHO + H_2O \tag{5.12}$$

$$CH_4 + 2O_2 \rightleftarrows CO_2 + 2H_2O \tag{5.13}$$

$$C + O_2 \rightleftarrows CO_2 \tag{5.14}$$

The regeneration of coked catalysts is typically achieved by oxidizing or gasifying the carbonaceous deposits with air, O_2, or H_2O, but treatment with CO_2 and H_2 may be attempted (Farrauto & Bartholomew, 2006). The minimum temperature required to remove coke deposits is a function of the type and location of the coke formed and the oxidizing agent used during regeneration. The graphitic forms of coke may require temperatures up to 900 °C to be fully oxidized (Farrauto & Bartholomew, 2006).

5.2.4.2 Metal sintering

Sintering leads to a reduction in the metal active surface area. In general, small particles have higher surface energy than larger particles. Once sufficient activation energy is supplied, there is a tendency for smaller particles to agglomerate into larger ones so as to decrease surface free energy. Sehested (2006) proposed three mechanisms for metal particle growth: (1) particle migration, in which entire crystallites migrate over the support followed by coalescence; (2) Ostwald ripening (atom migration), in which metal atoms emitted from one crystallite migrate over the support and are captured by another crystallite; and (3) vapor transport among particles (at high temperatures) (Sehested, 2006). Sintering is influenced by the temperature, composition of the gas over the catalyst, structure and composition of the catalyst support, and as metal−support interactions. Increasing the temperature and vapor pressure accelerates the sintering process (Bartholomew, 1993; Prasad et al., 2012; Zhang et al., 2014).

As is known, despite the relatively lower cost, Ni-based catalysts are normally affected by metal sintering. In particular, calcination and reduction temperatures of Ni-based catalysts are as mainly responsible for deactivation (Remiro et al., 2014; Valle, Aramburu, Remiro, Bilbao, & Gayubo, 2014). For example, the formation of $NiAl_2O_4$ spinel-type structures upon calcination of Ni/Al_2O_3 catalysts favors the formation of large metal crystallites. Calcination at a low temperature (<550 °C) minimizes the formation of spinel and produces a larger amount of highly dispersed nickel oxides which, after reduction, form highly dispersed metal nanoparticles that are strongly linked to support and so are more resistant to sintering (Valle et al., 2014).

The preparation method can have a significant role in preventing catalyst deactivation. Because of this, adding surfactants during the co-precipitation method of Ni-based catalysts helps to increase the surface area and resistance to Ni sintering (Nahar & Dupont, 2014).

Bimetallic catalysts exhibit better anti-sintering ability. For example, bimetallic catalysts (like Ni-Co/hydrotalcites) exhibit better resistance to sintering, because the addition of cobalt contributes to an increase in the dispersion state of nickel (Wang, Wang, Chen, & Liu, 2014). Also, the addition of Rh and Ir to Co/ZnO catalysts decreases cobalt sintering by stabilizing the Co° phase (Cai, Ramìrez de la Piscina, & Homs, 2014).

To enhance the stability of Ni supported catalysts, dissolution of an appropriate amount of Yb^{3+} ions in a zirconia host results in the formation of the highly stable *c*-(Zr-Yb)O_z phase, which inhibits the transformation of *c*-ZrO_2 to thermodynamically more stable *m*-ZrO_2 during the ESR reaction, thus avoiding sintering of the (Zr-Yb)O_z composite (Hou, Liu, Lin, & Zhang, 2014).

A common strategy for improving the stability of the active component is promotion of SMSI. (Chiou et al., 2014; Rossetti et al., 2014) In this context, TiO_2 was used as support for Ni, Co, and Cu to prepare catalysts for ESR, characterized by SMSI (Rossetti et al., 2014). According to this, the calcination temperature and in general the preparation procedure for the catalyst are key factors for promoting SMSI. In particular, calcination of Ni-based catalysts at a relatively low temperature (i.e., 500 °C) induces initially a higher dispersion of the active phase (mean Ni crystal size 7 nm); however, it is not accompanied by sufficient stabilization during activity testing (mean Ni crystal size increased to 44 nm). By contrast, calcination at a higher temperature (i.e., 800 °C) favors the instauration of an SMSI and the formation of a mixed oxide ($NiTiO_3$) which, after activation, allows the coexistence of smaller particles that are more active and resistant to deactivation and sintering, together with larger ones (up to 27 nm in size) (Fang, Paul, Capron, Dumeignil, & Jalowiecki-Duhamel, 2014; Rossetti et al., 2014).

With regard to the influence of the carrier oxide, the basic MgO leads to the formation of Ni crystallites resistant to sintering by achieving close contact between Ni and MgO. The strong interaction between NiO and MgO evidenced by the formation of the $Ni_xMg_{1-x}O_2$ solid solution can explain inhibition of the sintering of Ni during the calcination and reduction processes (Romero, Jobbágy, Laborde, Baronetti, & Amadeo, 2014). However, because of weak metal−support interaction, it was observed that at 650 °C Pd/MgO catalyst drastically deactivates during reaction owing to metal sintering (Frusteri, Freni, Chiodoet, al., 2004).

Recently, CeO_2-based support was investigated for ESR and increasing attention has been paid to the role of oxygen storage capacity in improving catalytic activity. However, modification of the ceria lattice by elements belonging to the transition-metal series is needed to confer resistance to sintering. Also, the presence of a cubic phase in the support improves reducibility of the catalyst and prevents metal sintering (Cai et al., 2014).

Interestingly, perovskite-type oxide supported Ni catalysts, namely NiO/$LaFe_yNi_{1-y}O_3$, also exhibit a good performance in ESR, owing to good resistance to nickel sintering (Wang et al., 2014).

On the whole, irrespective of the experimental conditions adopted, to minimize the effects of metal sintering and ensure a long catalyst lifetime, several crucial factors should be considered: (1) the preparation method to obtain high surface area and metal dispersion; (2) loading of active phase (below 15−20%); (3) activation temperature; (4) addition of promoters (formation of alloys); (5) SMSI.

5.3 Reforming of butanol

Butanol has been proposed as a representative compound of alcohols present in bio-oils (Bimbela et al., 2009; Nahar & Madhani, 2010). Moreover, *n*-butanol can be produced from biomass by fermentation (Marchal, Ropars, Pourquie, Fayolle, & Vandecasteele, 1992; Qureshi et al., 2008).

Compared with other alcohols (e.g., ethanol and methanol), *n*-butanol exhibits a series of advantages including higher hydrogen content (13.5 wt%) than ethanol (13.0 wt%) or methanol (12.5 wt%), lower vapor pressure, and greater tolerance to water. Furthermore, *n*-butanol can be transported by conventional fuel distribution pipelines (Wang & Cao, 2010).

From the point of view of H_2 production, by SR, up to 12 mol of H_2 can be obtained from 1 mol of butanol, according to the following reaction:

$$C_4H_{10}O + 7H_2O \rightleftarrows 4CO_2 + 12H_2 \tag{5.15}$$

In the few articles published dealing with the SR of higher alcohols, cobalt-based systems were reported to be efficient catalysts for C−C bond cleavage (Ramírez de la Piscina & Homs, 2008). A relevant role in the performance of Co-based catalysts (Karim et al., 2010; Kim & Lee, 2010; Llorca, Ramírez de la Piscina, Sales, & Homs, 2001; Ramírez de la Piscina & Homs, 2008) was exerted by Co supports characterized by different acid−base and redox properties (ZnO, CeO_2 and TiO_2). Nevertheless, the addition of noble metals to the catalyst was suggested to be beneficial for the catalytic performance of Co-based catalysts for alcohol reforming (Brum Pereira et al., 2011; Brum Pereira, Homs, Marti, Fierro, & Ramírez de la Piscina, 2008; Brum Pereira, Ramírez de la Piscina, Marti, & Homs, 2010; Profeti, Ticianelli, & Assaf, 2008). In fact, the addition of noble metals should enhance the electronic properties of cobalt, because the active sites are more resistant to deactivation phenomena (Profeti et al., 2008).

On the basis of thermodynamic calculations, some authors (Nahar & Madhani, 2010) suggested optimal reaction conditions of butanol SR for H_2 production using a water-to-butanol molar feed ratio between 1 and 18, pressure and temperature ranging from 1 to 50 bar and 300−900 °C, respectively. Under these conditions, authors reported that the yield of H_2 and CO would be maximized while methane formation should be limited. In particular, the yield of H_2 would result close to 75−80% whereas theoretically, the formation of coke would be completely inhibited under these operating conditions (Nahar & Madhani, 2010).

A few scientific papers showed that, as for ESR, the main problem in butanol SR is the formation of coke. Unfortunately, butanol is not thermally stable; before reaching the catalytic surface, it may decompose to form different intermediates can promote the formation of coke by different mechanisms once they reach the surface of the catalyst. To limit this phenomenon, the addition of oxygen to the reaction stream was proposed (Cai, Ramirez de la Piscina, & Homs, 2012). Of course, under such drastic reaction conditions (oxidation processes occurring on the catalyst surface), sintering of the active phase become important with negative repercussions for catalyst stability. However, interesting results have been obtained at 500 °C using CoRh/ZnO catalyst (Cai et al., 2014) in terms of butanol conversion (84%), hydrogen yield (65%), and stability (100 h on stream). In any case, coke formation has not been resolved and continues to represent a problem for this reaction.

5.4 Reforming of glycerol

An attractive platform chemical from biomass is glycerol, which was identified as a top 12 bio-based chemicals in recent studies by the Department of Energy of the United States (Werpy & Petersen, 2004). Currently, glycerol represents the main by-product of the biodiesel industry. The global increase in the production of biodiesel (in 2010 the European output of biodiesel was 9.57 million tons) (European Biodiesel Board, 2011) has led to a simultaneous increase in the amount of crude glycerol, causing prices to drop. Therefore, identification of high value−added outlets for crude glycerol, such as the production of energy carriers (H_2 and CH_4) or other chemicals and chemical intermediates (acrolein, methanol, or syngas) has become an active research topic and development area for increasing the overall economics of the biodiesel process (Ayoub & Abdullah, 2012; De Souza & Silveira, 2011; Rahmat, Abdullah, & Mohamed, 2010).

5.4.1 Different approaches proposed: SR, ATR, and APR

Glycerol can be converted into hydrogen or syngas (synthesis gas) through catalytic POX with O_2 (Wang, 2010), reforming with H_2O (Adhikari et al., 2008; Pompeo, Santori, & Nichio, 2010) or CO_2 (Fernandez, Arenillas, Bermudez, Menendez, & Anal, 2010; Wang et al., 2009), and pyrolysis (Kale & Kulkarni, 2010). Among these reactions, catalytic reforming of glycerol in the gaseous or aqueous phase is much more attractive because hydrogen has wide applications in many industries and is a clean fuel;

syngas, a mixture of CO and H_2, can be converted commercially into alcohols (particularly methanol) and liquid hydrocarbons (James, Mesubi, Ako, & Maity, 2010).

5.4.1.1 Catalytic SR

The SR of glycerol has some similarities to the catalytic SR of natural gas or liquid hydrocarbons in which supported metal catalysts have been used (Holladay, Hu, King, & Wang, 2009). Accordingly, similar catalysts are often explored for the SR of glycerol (Adhikari, Fernando, & Haryanto, 2009; Lin, 2013; Vaidya & Rodrigues, 2009). Many studies have confirmed that metallic species, such as Pt (Kunkes, Soares, Simonetti, & Dumesic, 2009), Rh (Chiodo, Freni, Galvagno, Mondello, & Frusteri, 2010), Ru (Byrd, Pant, & Gupta, 2008), Ir (Zhang, Tang, Li, Xu, & Shen, 2007), Ni (Cui, Galvita, Rihko-Struckmann, Lorenz, & Sundmacher, 2009; Iriondo et al., 2008), and Co (Cheng, Foo, & Adesina, 2010) are active catalysts for the SR of glycerol.

Regarding the reaction mechanism, it is a common opinion that the SR of glycerol involves at least two main reactions. Glycerol first undergoes direct splitting to form H_2 and CO (Eqn (5.16)); then the WGS reaction occurs: namely, the resultant CO reacts with steam (H_2O), thus yielding additional H_2 (Eqn (5.17)) (Adhikari et al., 2009; Chen & Syu, 2010). The overall reaction may be depicted as shown in Eqn (5.18) (Vaidya & Rodrigues, 2009):

$$C_3H_8O_3 \rightarrow 3CO + 4H_2 \quad \Delta H = 251\ \text{kJ/mol} \tag{5.16}$$

$$H_2O + CO \rightarrow H_2 + CO_2 \quad \Delta H = -41\ \text{kJ/mol} \tag{5.17}$$

$$C_3H_8O_3 + 3H_2O \rightarrow 7H_2 + 3CO_2 \quad \Delta H = 128\ \text{kJ/mol} \tag{5.18}$$

The splitting of glycerol (Eqn (5.16)) is highly endothermic and the quantity of heat required for this reaction is more than that released by the consecutive WGS reaction (Eqn (5.17)). Thus, for the SR of glycerol, the overall reaction is endothermic (Eqn (5.18)) (Chen & Syu, 2010). According to Eqn (5.16), in principle, high temperatures, low pressure, and high ratios of water to glycerol favor the production of hydrogen (Adhikari et al., 2007). In addition, by setting optimal reaction conditions and promoting the splitting of glycerol and the WGS reaction, the SR of glycerol can proceed with high hydrogen or syngas productivity.

5.4.1.2 Partial oxidation

POX is the process by which glycerol is reacted with oxygen at a sub-stoichiometric ratio:

$$C_3H_8O_3 + 1.5O_2 \rightarrow 3CO_2 + 4H_2 \quad \Delta H^\circ = -603\ \text{kJ/mol} \tag{5.19}$$

Currently, only a few articles have dealt with the POX of glycerol in gaseous phase. According to a thermodynamic analysis performed by Wang (Wang, 2010), with a $O_2/C_3H_8O_3$ molar ratio ranging from 0 to 4, reaction temperature from 200 to

1200 °C, and pressure from 1 to 20 atm, only CH_4 and C thermodynamically coexist with H_2, H_2O, CO, and CO_2, whereas other products are suppressed at essentially zero. Maximum H_2 efficiency can be achieved at atmospheric pressure whereas carbon tends to form at low temperatures and low $O_2/C_3H_8O_3$ molar ratios.

Rennard, Kruger, and Schmidt (2009) performed catalytic POX of glycerol using a nebulizer to mix droplets with air at room temperature for reactive flash volatilization. The oxidation of glycerol was carried out over noble-metal catalysts at temperatures as high as 600 °C in only a few milliseconds. The addition of water to the glycerol increased selectivity to H_2, mainly by WGS reaction. However, water also quenched the reaction, resulting in maximum H_2 yield at an S/C ratio of 2:3 over an Rh-Ce catalyst.

On the whole, selectivity for a specific product strongly depends on the reaction conditions: the concentration of reactants, the temperature, and the ratio of glycerol and catalyst.

5.4.1.3 Autothermal reforming

ATR combines the effect of POX and SR by feeding fuel, air, and water together into the reactor:

$$C_3H_8O_3 + O_2 + H_2O \rightarrow 3CO_2 + 5H_2 \quad \Delta H^\circ = -269\ \text{kJ/mol} \tag{5.20}$$

Dauenhauer, Salge, and Schmidt (2006) found that the addition of steam ($H_2O/C = 4.5$) shifted the reaction equilibrium toward a higher formation of H_2 (+30−40%). However, H_2 selectivity from glycerol can reach a maximum value of 80% when oxygen is co-fed with a C/O ratio higher than 1. Swami and Abraham (2006) performed ATR at an S/C ratio of 3 and an O/C ratio of 0.3 in the range of 550−850 °C using Pd/Ni/Cu/K catalysts. Their results showed that the hydrogen yield obtained under autothermal conditions was higher than that obtained under SR; however, hydrogen yield in both cases increased with reaction temperature. Douette, Turn, Wang, and Keffer (2007) performed a series of tests using a factorial experimental design to determine the effects of the operating parameters, including O/C and S/C ratio: 4.5 mol of hydrogen was produced per mole of glycerol, with an S/C ratio of 2.2 and temperature of 800 °C. Initially, similar hydrogen yield was obtained with crude glycerin, the by-product of biodiesel production. However, because of catalyst deactivation and coke formation in the reformer, hydrogen yield quickly decreased. This may be correlated with the presence of contaminants, chloride, and sodium cations, in crude glycerin.

5.4.1.4 Aqueous phase reforming

The APR process was established by Cortright, Davda, and Dumesic (2002) using platinum-based catalysts and mild reaction conditions (200−250 °C and 20−25 bar) for the production of hydrogen and light alkanes from oxygenated hydrocarbons:

$$C_3H_8O_{3(1)} + 3H_2O \rightarrow 3CO_2 + 7H_2 \quad \Delta H^\circ = 123\ \text{kJ/mol} \tag{5.21}$$

Lehnert and Claus (2008) investigated several platinum-based catalysts for catalytic conversion of glycerol to hydrogen by APR. Their studies indicated that catalytic reaction selectivity to hydrogen increased with increasing particle size from 78% to 95%, whereas the conversion of glycerol remained almost constant at 20%. Furthermore, a mixture of *c*-, *δ*-, and *θ*-phase alumina can increase hydrogen production to 7.6 mol/min/kg_{cat} compared with pure *γ*-alumina (1.2 mol/min/kg_{cat}). Crude glycerol can also be used as a starting material. However, the rate of hydrogen production was lower than for pure glycerol because of impurities such as NaCl.

5.4.2 Catalysts for hydrogen production from glycerol reforming

Currently, a commercial catalyst to perform glycerol SR efficiently is unavailable. Czernik, French, Feik, and Chornet (2002) and Garcia, French, Czernik, and Chornet (2000) produced hydrogen via SR of crude glycerol using a commercial nickel-based naphtha reforming catalyst. Nickel is the base catalyst for SR of hydrocarbons mainly because of its high activity and low cost.

Iriondo et al. (2008) studied glycerol SR over alumina supported nickel catalysts modified with Ce, Mg, Zr, and La. The catalytic activity of the samples clearly evidenced the different catalyst functionalities necessary to carry out the reaction. As a rule, the use of Ce, La, Mg, and Zr as promoters of Ni-based catalysts increases the hydrogen selectivity compared with the reference catalyst supported on bare alumina. Differences in activity were explained in terms of enhancement in the surface nickel concentration (Mg), the capacity to activate steam (Zr), and the stability of nickel phases under reaction conditions (Ce and La).

Hirai, Ikenaga, Miyake, and Suzuki (2005) reported the performance of noble metal−based catalyst for glycerol reforming. Catalysts loaded with group 8−10 metals were prepared using Y_2O_3, ZrO_2, CeO_2, La_2O_3, SiO_2, MgO, and Al_2O_3 as supports. The order of activity was: Ru = Rh > Ni > Ir > Co > Pt > Pd > Fe. Y_2O_3-supported ruthenium catalysts exhibited the highest glycerin conversion and H_2 yield whereas ruthenium on basic MgO had very low conversion of glycerin compared with Y_2O_3- and ZrO_2-supported catalysts. Although Al_2O_3 is usually employed as a favorable support for SR of hydrocarbons, ruthenium on Al_2O_3 showed the lowest conversion in the SR of glycerin. Higher selectivity to CH_4 and low selectivity to CO_2 were indicated as possible reasons for obtaining low H_2 yield. In all experiments, high CO_2 selectivity was obtained. These results may have been achieved because a high S/C molar ratio under reaction conditions and basic support materials promoted of the WGS reaction.

Simonetti, Kunkes, and Dumesic (2007) reported results of the conversion of glycerol to synthesis gas over various Pt-based catalysts. Catalytic measurements at 400 °C by operating with glycerol in the vapor phase demonstrated the good behavior of Pt/C catalyst in terms of stability for a long reaction time.

Zhang et al. (2007) examined the catalytic performance of M/CeO_2 catalysts (M = Ir, Ni, or Co) in SR of glycerol. The Ir/CeO_2 catalyst showed the highest catalytic activity and complete conversion of glycerol at 400 °C, reaching hydrogen yield

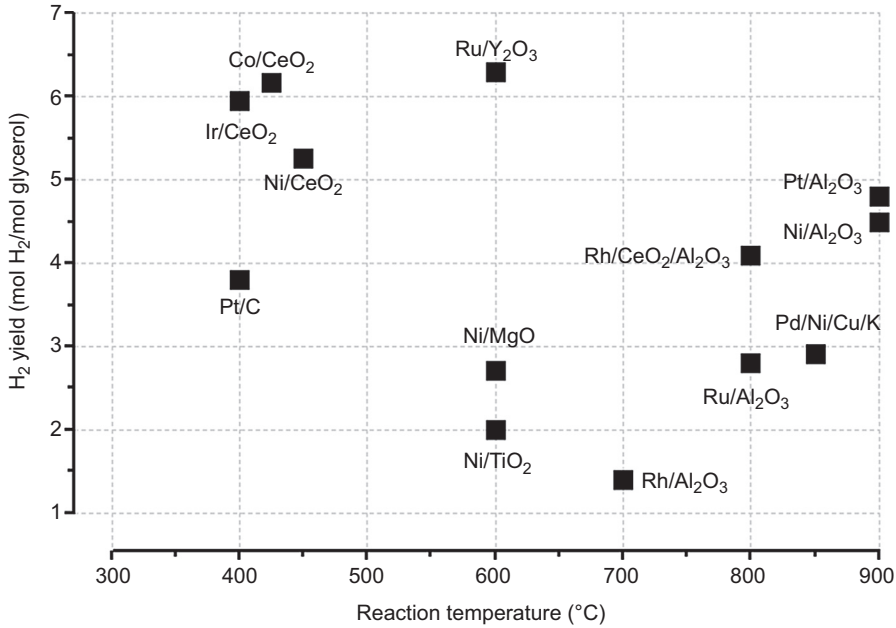

Figure 5.7 Steam reforming of glycerol: hydrogen yield as a function of reaction temperature on different catalytic systems.

close to 6 mol H_2/mol glycerol. Complete conversion of glycerol over Co/CeO_2 and Ni/CeO_2 catalysts was obtained at 425 °C and 450 °C with hydrogen selectivity of 6.16 and 5.25 mol H_2/mol glycerol, respectively.

Figure 5.7 shows the main results reported for SR of glycerol in terms of H_2 yield as a function of reaction temperature.

Surprisingly, by operating at a high temperature (>700 °C), even though hydrocarbon SR processes are thermodynamically favored, hydrogen yields are lower than those obtained at lower temperatures. It seems that independent of the active metal used, the nature of support becomes a determinant in glycerol reforming. In fact, mainly at a low reaction temperature, the best results were obtained using CeO_2 as carrier. The reason could be the oxygen storage capability of such an oxide. Maintenance of a high surface oxygen concentration during reforming processes becomes fundamental for accelerating the combustion of coke deposited on a metal surface during the reaction.

Figure 5.7 shows that at 600 °C, Ru/Y_2O_3 attains high hydrogen yield (Hirai et al., 2005). This result was explained by the high S/C molar ratio used under the reaction conditions and the use of a basic support material (i.e., Y_2O_3), causing promotion of the WGS reaction.

Although full comparability of the obtained results is not easy because of the different reaction conditions adopted, data analysis suggests the presence of a strong influence of the support on catalytic performance for all metals investigated.

In particular, Ni may be a promising metal despite catalytic activity and costs. Because of this, commonly used Ni/Al_2O_3, La_2O_3, and CeO_2 doped systems usually show superior performance in terms of activity and stability. Regarding the use of noble metals, Pt commonly demonstrates strong deactivation phenomena under SR conditions whereas Rh and Ru evidence better stability.

5.5 Conclusions

The need for hydrogen as a clean energy carrier is relatively strong worldwide. Its production by reforming bio-alcohols is a topic of environmental and energetic interest that deserves to be investigated.

Significant efforts to date allowed some efficient and stable catalytic systems to be developed for reforming ethanol or butanol, but the results obtained seem not to fit the required target mainly because these oxygenated compounds are not thermally stable and easily decompose or dehydrate to form many intermediates that can evolve with different reaction pathways to form several undesirable products. Also, the formation of coke is not easily manageable, mainly when operating at a low reaction temperature. By increasing the reaction temperature, coke formation can be reduced but the outlet streams will contain high concentrations of CO and the catalyst may rapidly deactivate owing to metal sintering.

Generally, both at low and high temperatures catalysts based on noble metals are efficient; however, catalysts based on Ni and Co also show satisfying activity but low stability.

Hydrogen production by SR of glycerol remains controversial in view of the economy, although SR of hydrocarbons appears to be the most economic and efficient technology used in industry primarily for commercial-scale production of hydrogen. Main difficulties are that each glycerol molecule contains fewer hydrogen atoms than each hydrocarbon molecule and that glycerol is a carbohydrate and there are more sophisticated reaction networks during SR, which necessitates the costly purification of hydrogen. As a result, production of hydrogen from glycerol reforming remains uneconomical.

List of acronyms

APR	Aqueous phase reforming
ATR	Autothermal reforming
C_s	Surface carbon
CO	Carbon monoxide
CO_2	Carbon dioxide
ESR	Ethanol steam reforming
EtOH	Ethanol
GHSV	Gas hourly space velocity
O/C	Oxygen to carbon ratio

POX	Partial oxidation
P_R	Reaction pressure
S/C	Steam to carbon ratio
SMSI	Strong metal support interaction
SR	Steam reforming
T_R	Reaction temperature
TOS	Time on stream
WGS	Water gas shift reaction

References

Adhikari, S., Fernando, S., Gwaltney, S. R., To, S. D. F., Bricka, R. M., Steele, P. H., et al. (2007). *International Journal of Hydrogen Energy, 32*, 2875−2880.

Adhikari, S., Fernando, S. D., & Haryanto, A. (2009). *Energy Conversion and Management, 50*, 2600−2604.

Adhikari, S., Fernando, S. D., To, S. D. F., Bricka, R. M., Steele, P. H., & Haryanto, A. (2008). *Energy Fuels, 22*, 1220−1226.

Ahmed, S., & Krumpelt, M. (2001). *International Journal of Hydrogen Energy, 26*, 291−301.

Alberton, A. L., Souza, M. M. V. M., & Schmal, M. (2007). *Catalysis Today, 123*, 257−264.

Armor, J. N. (1999). *Applied Catalysis A: General, 176*, 159−176.

Asprey, S. P., Wojciechowski, B. W., & Peppley, B. A. (1999). *Applied Catalysis A: General, 179*, 51−70.

Auprêtre, F., Descorme, C., & Duprez, D. (2002). *Catalysis Communications, 3*, 263−267.

Avcı, A. K., Trimm, D. L., & Önsan, Z. I. (2002). *Chemical Engineering Journal, 90*, 77−87.

Avcı, A. K., Önsan, Z. I., & Trimm, D. L. (2003). *Topics in Catalysis, 22*, 359−367.

Ayoub, M., & Abdullah, A. Z. (2012). *Renewable and Sustainable Energy Reviews, 16*, 2671−2686.

Banach, B., MacHocki, A., Rybak, P., Denis, A., Grzegorczyk, W., & Gac, W. (2011). *Catalysis Today, 176*, 28−35.

Bartholomew, C. H. (1993). *Applied Catalysis A: General, 107*, 1−57.

Bartholomew, C. H. (2001). *Applied Catalysis A: General, 212*, 17−60.

Batista, M., Santos, R., Assaf, E., Assaf, J., & Ticianelli, E. (2004). *Journal of Power Sources, 134*, 27−32.

Bimbela, F., Olive, M., Ruiz, J., Garcia, L., Arauzo, J., & Anal, J. (2009). *Applied Pyrolysis, 85*, 204−213.

Biswas, P., & Kunzru, D. (2007). *International Journal of Hydrogen Energy, 32*, 969−980.

Breen, J., Burch, R., & Coleman, H. (2002). *Applied Catalysis B: Environmental, 39*, 65−74.

Brum Pereira, E., Homs, N., Marti, S., Fierro, J. L. G., & Ramírez de la Piscina, P. (2008). *Journal of Catalysis, 257*, 206−214.

Brum Pereira, E., Ramirez de La Piscina, P., & Homs, N. (2011). *Bioresource Technology, 102*, 3419−3423.

Brum Pereira, E., Ramírez de la Piscina, P., Marti, S., & Homs, N. (2010). *Energy and Environmental Science, 3*, 487−493.

Byrd, A. J., Pant, K. K., & Gupta, R. B. (2008). *Fuel, 87*, 2956−2960.

Cai, W., Ramirez de la Piscina, P., & Homs, N. (2012). *Bioresource Technology, 107*, 482−486.

Cai, W., Ramìrez de la Piscina, P., & Homs, N. (2014). *Applied Catalysis B: Environmental, 145*, 56−62.

Cai, W., Wang, F., Daniel, C., Van Veen, A. C., Schuurman, Y., & Descorme, C. (2012). *Journal of Catalysis, 286*, 137−152.
Cai, W., Wang, F., Zhan, E., Van Veen, A. C., Mirodatos, C., & Shen, W. (2008). *Journal of Catalysis, 257*, 96−107.
Cavallaro, S., Chiodo, V., Freni, S., Mondello, N., & Frusteri, F. (2003). *Applied Catalysis A: General, 249*, 119−128.
Chen, W.-H., & Syu, Y.-J. (2010). *International Journal of Hydrogen Energy, 35*, 10179−10189.
Cheng, C. K., Foo, S. Y., & Adesina, A. A. (2010). *Catalysis Communications, 12*, 292−298.
Chiodo, V., Freni, S., Galvagno, A., Mondello, N., & Frusteri, F. (2010). *Applied Catalysis A: General, 381*, 1−7.
Chiou, J. Y. Z., Lee, C.-L., Fu Ho, K., Hua Huang, H., Wei Yu, S., & Bin Wang, C. (2014). *International Journal of Hydrogen Energy, 39*, 5653−5662.
Chiou, J. Y. Z., Siang, J. Y., Ho, K. F., Lee, C. L., & Yeh, C. T. (2012). *International Journal of Hydrogen Energy, 37*, 13667−13673.
Churakova, E. M., Badmaev, S. D., Snytnikov, P. V., Gubanov, A. I., Filatov, E. Y., & Plyusnin, P. E. (2010). *Kinetics and Catalysis, 51*, 893−897.
Ciftci, A., Ligthart, D. A. J. M., Pastorino, P., & Hensen, E. J. M. (2013). *Applied Catalysis B: Environmental, 130−131*, 325−335.
Cobo, M., Pieruccini, D., Abello, R., Ariza, L., Còrdoba, L. F., & Conesa, J. A. (2013). *International Journal of Hydrogen Energy, 38*, 5580−5593.
Comas, J., Marino, F., Laborde, M., & Amadeo, N. (2004). *Chemical Engineering Journal, 98*, 61−68.
Cortright, R. D., Davda, R. R., & Dumesic, J. A. (2002). *Nature, 418*, 964−966.
Cui, Y., Galvita, V., Rihko-Struckmann, L., Lorenz, H., & Sundmacher, K. (2009). *Applied Catalysis B: Environmental, 90*, 29−37.
Czernik, S., French, R., Feik, C., & Chornet, E. (2002). *Industrial and Engineering Chemistry, 41*, 4209−4215.
Da Silva, A. M., de Souza, K. R., Jacobs, G., Graham, U. M., Davis, B. H., & Mattos, L. V. (2011). *Applied Catalysis B: Environmental, 102*, 94−109.
Dauenhauer, P. J., Salge, J. R., & Schmidt, L. D. (2006). *Journal of Catalysis, 244*, 238−247.
De Lima, S. M., Silva, A. M., da Cruz, I. O., Jacobs, G., Davis, B. H., & Mattos, L. V. (2008). *Catalysis Today, 138*, 162−168.
De Souza, A. C. C., & Silveira, J. L. (2011). *Renewable and Sustainable Energy Reviews, 15*, 1835−1850.
Diagne, C., Idriss, H., & Kiennemann, A. (2002). *Catalysis Communications, 3*, 565−571.
Diagne, C., Idriss, H., Pearson, K., Gòmez, G. M. A., & Kiennemann, A. (2004). *Comptes Rendus Chimie, 7*, 617−622.
Doss, E., Kumar, R., Ahluwalia, R. K., & Krumpelt, M. (2001). *Journal of Power Sources, 102*, 1−15.
Douette, A. M. D., Turn, S. Q., Wang, W., & Keffer, V. I. (2007). *Energy Fuel, 21*, 3499−3504.
Erdohelyi, A., Rasko, J., Kecskes, T., Toth, M., Domok, M., & Baan, K. (2006). *Catalysis Today, 116*, 367−376.
European Biodiesel Board (EBB) 2010−2011 (October 2011). EU biodiesel industry production forecasts show first decrease in 2011 since data is gathered. Press Release. Bruxelles. Report No. 664/COM/11.
Fang, W., Paul, S., Capron, M., Dumeignil, F., & Jalowiecki-Duhamel, L. (2014). *Applied Catalysis B: Environmental, 152−153*, 370−382.
Farrauto, R. J., & Bartholomew, C. H. (2006). (2nd ed.). Hoboken, N.J: Wiley.

Farrauto, R., Hwang, S., Shore, L., Ruettinger, W., Lampert, J., Giroux, T., et al. (2003). *Annual Review of Materials Research, 33*, 1−27.
Fatsikostas, A. N., & Verykios, X. E. (2004). *Journal of Catalysis, 225*, 439−452.
Fatsikostas, A. N., Kondarides, D. I., & Verykios, X. E. (2002). *Catalysis Today, 75*, 145−155.
Fernandez, Y., Arenillas, A., Bermudez, J. M., Menendez, J. A., & Anal, J. (2010). *Applied Pyrolysis, 88*, 155−159.
Fierro, V., Klouz, V., Akdim, O., & Mirodatos, C. (2002). *Catalysis Today, 75*, 141−144.
Fishtik, I., & Datta, R. (2002). *Chemical Engineering Science, 209*, 306−317.
Freni, S., Cavallaro, S., Mondello, N., Spadaro, L., & Frusteri, F. (2003). *Catalysis Communications, 4*, 259−268.
Frusteri, F., Freni, S., Chiodo, V., Donato, S., Bonura, G., & Cavallaro, S. (2006). *International Journal of Hydrogen Energy, 31*, 2193−2199.
Frusteri, F., Freni, S., Chiodo, V., Spadaro, L., Di Blasi, O., Bonura, G., et al. (2004). *Applied Catalysis A: General, 270*, 1−7.
Frusteri, F., Freni, S., Spadaro, L., Chiodo, V., Bonura, G., & Donato, S. (2004). *Catalysis Communications, 5*, 611−615.
Frusteri, F., Italiano, G., Espro, C., Cannilla, C., & Bonura, G. (2012). *International Journal of Hydrogen Energy, 37*, 16367−16374.
Garcia, L., French, R., Czernik, S., & Chornet, E. (2000). *Applied Catalysis A: General, 201*, 225−239.
Ghita, D., Rosca, P., & Ezeanu, D. S. (2012). *Revista de Chimie, 63*, 1056−1061.
Goula, M., Kontou, S., & Tsiakaras, P. (2004). *Applied Catalysis B: Environmental, 49*, 135−144.
Guo, Z., Wang, S., Guo, L., & Li, X. (2011). *BioResources, 6*, 4092−4102.
Gutierrez, A., Karinen, R., Airaksinen, S., Kaila, R., & Krause, A. O. I. (2011). *International Journal of Hydrogen Energy, 36*, 8967−8977.
Hagh, B. (2003). *International Journal of Hydrogen Energy, 28*, 1369−1377.
Haryanto, A., Fernando, S., Murali, N., & Adhikari, S. (2005). *Energy Fuels, 19*, 2098−2106.
He, Z., Yang, M., Wang, X., Zhao, Z., & Duan, A. (2012). *Catalysis Today, 194*, 2−8.
Heck, R. M., Farrauto, R. J., & Gulati, S. T. (2009). (3rd ed.). Hoboken, N.J: John Wiley.
Hirai, T., Ikenaga, N., Miyake, T., & Suzuki, T. (2005). *Energy Fuels, 19*, 1761−1762.
Hochmuth, J. K. (1992). *Applied Catalysis B: Environmental, 1*, 89−100.
Holladay, J. D., Hu, J., King, D. L., & Wang, Y. (2009). *Catalysis Today, 139*, 244−260.
Hou, J., Liu, Z.-M., Lin, G.-D., & Zhang, H.-B. (2014). *International Journal of Hydrogen Energy, 39*, 1315−1324.
Huang, L., Choong, C., Chen, L., Wang, Z., Zhong, Z., & Campos-Cuerva, C. (2013). *ChemCatChem, 5*, 220−234.
Inokawa, H., Nishimoto, S., Kameshima, Y., & Miyake, M. (2011). *International Journal of Hydrogen Energy, 36*, 15195−15202.
Iriondo, A., Barrio, V. L., Cambra, J. F., Arias, P. L., Guemez, M. B., Navarro, R. M., et al. (2008). *Topics in Catalysis, 49*, 46−58.
Ito, S.-i., & Tomishige, K. (2010). *Catalysis Communications, 12*, 157−160.
James, O. O., Mesubi, A. M., Ako, T. C., & Maity, S. (2010). *Fuel Processing Technology, 91*, 136−144.
Jesse, T. W., Ezeji, T. C., Qureshi, N., Blaschek, H. P., & Ind, J. (2002). *Applied Microbiology and Biotechnology, 29*, 117−123.
Kale, G. R., & Kulkarni, B. D. (2010). *Fuel Processing Technology, 91*, 520−530.
Karim, A. M., Su, Y., Sun, J., Yang, C., Strohm, J. J., & King, D. L. (2010). *Applied Catalysis B: Environmental, 96*, 441−448.

Kim, K. S., & Lee, Y. K. (2010). *International Journal of Hydrogen Energy, 35*, 5378−5382.
Koh, A. C. W., Leong, W. K., Chen, L., Ang, T. P., Lin, J., & Johnson, B. F. G. (2008). *Catalysis Communications, 9*, 170−175.
Krumpelt, M., Krause, T. R., Carter, J. D., Kopasz, J. P., & Ahmed, S. (2002). *Catalysis Today, 77*, 3−16.
Kunkes, E. L., Soares, R. R., Simonetti, D. A., & Dumesic, J. A. (2009). *Applied Catalysis B: Environmental, 90*, 693−698.
Kwak, B. S., Kim, J., & Kang, M. (2010). *International Journal of Hydrogen Energy, 35*, 11829−11843.
Lakhapatri, S. L., & Abraham, M. A. (2009). *Applied Catalysis A: General, 364*, 113−121.
Le Valant, A., Bion, N., Can, F., Duprez, D., & Epron, F. (2010). *Applied Catalysis B: Environmental, 97*, 72−81.
Le Valant, A., Can, F., Bion, N., Duprez, D., & Epron, F. (2010). *International Journal of Hydrogen Energy, 35*, 5015−5020.
Le Valant, A., Garron, A., Bion, N., Epron, F., & Duprez, D. (2008). *Catalysis Today, 138*, 169−174.
Lehnert, K., & Claus, P. (2008). *Catalysis Communications, 9*, 2543−2546.
Li, M., & Leung, D. (2007). *International Journal of Hydrogen Energy, 32*, 3238−3247.
Liberatori, J. W. C., Ribeiro, R. U., Zanchet, D., Noronha, F. B., & Bueno, J. M. C. (2007). *Applied Catalysis A: General, 327*, 197−204.
Liguras, D. K., Kondarides, D. I., & Verykios, X. E. (2003). *Applied Catalysis B: Environmental, 43*, 345−354.
Lin, S. S. Y., Kim, D. H., & Ha, S. Y. (2008). *Catalysis Letters, 122*, 295−301.
Lin, Y. C. (2013). *International Journal of Hydrogen Energy, 38*, 2678−2700.
Liu, S. W., Liu, J. Y., Liu, Y. H., Huang, Y. H., Yeh, C. T., & Wang, C. B. (2011). *Catalysis Today, 164*, 246−250.
Llorca, J., Dalmon, J. A., Ramìrez, P., & Homs, N. (2003). *Applied Catalysis A: General, 243*, 261−269.
Llorca, J., Homs, N., & de la Piscina, P. R. (2004). *Journal of Catalysis, 227*, 556−560.
Llorca, J., Homs, N., Sales, J., & Ramìrez, P. (2002). *Journal of Catalysis, 209*, 306−317.
Llorca, J., Ramírez de la Piscina, P., Sales, J., & Homs, N. (2001). *Chemical Communications, 7*, 641−642.
Lòpez, E., Divins, N. J., Anzola, A., Schbib, S., Borio, D., & Llorca, J. (2013). *International Journal of Hydrogen Energy, 38*, 4418−4428.
Lòpez, E., Divins, N. J., & Llorca, J. (2012). *Catalysis Today, 193*, 145−150.
Ma, L., Jiang, C., Adesina, A. A., Trimm, D. L., & Wainwright, M. S. (1996). *Chemical Engineering Journal and the Biochemical Engineering Journal, 62*, 103−111.
Ma, L., & Trimm, D. L. (1996). *Applied Catalysis A: General, 138*, 265−273.
Marchal, R., Ropars, M., Pourquie, J., Fayolle, F., & Vandecasteele, J. P. (1992). *Bioresource Technology, 42*, 205−217.
Mas, V., Kiproes, R., Amadeo, N., & Laborde, M. (2006). *International Journal of Hydrogen Energy, 31*, 21−28.
Moura, J. S., Souza, M. O. G., Bellido, J. D. A., Assaf, E. M., Opportus, M., & Reyes, P. (2012). *International Journal of Hydrogen Energy, 37*, 3213−3224.
Nahar, G., & Dupont, V. (2014). *Renewable and Sustainable Energy Reviews, 32*, 777−796.
Nahar, G. A., & Madhani, S. S. (2010). *International Journal of Hydrogen Energy, 35*, 98−109.
Palma, V., Castaldo, F., Ciambelli, P., & Iaquaniello, G. (2012). *Clean Technologies and Environmental Policy, 14*, 973−987.

Palma, V., Castaldo, F., Ciambelli, P., & Iaquaniello, G. (2012). *Chemical Engineering Transactions, 29*, 109−114.
Palma, V., Castaldo, F., Ciambelli, P., & Iaquaniello, G. (2013). *Applied Catalysis B: Environmental, 145*, 73−84.
Palma, V., Palo, E., Castaldo, F., Ciambelli, P., & Iaquaniello, G. (2012). *Chemical Engineering Transactions, 29*, 109−114.
Pang, X., Chen, Y., Dai, R., & Cui, P. (2012). *Cuihua Xuebao/Chinese Journal of Catalysis, 33*, 281−289.
Peppley, B. A., Amphlett, J. C., Kearns, L. M., & Mann, R. F. (1999a). *Applied Catalysis A: General, 176*, 21−30.
Peppley, B. A., Amphlett, J. C., Kearns, L. M., & Mann, R. F. (1999b). *Applied Catalysis A: General, 176*, 31−49.
Platon, A., Roh, H. S., King, D., & Wang, Y. (2007). *Topics in Catalysis, 46*, 374−379.
Pompeo, F., Santori, G., & Nichio, N. N. (2010). *International Journal of Hydrogen Energy, 35*, 8912−8920.
Prasad, D. H., Park, S. Y., Ji, H., Kim, H. R., Son, J. W., Kim, B. K., et al. (2012). *Applied Catalysis A: General, 411−412*, 160−169.
Profeti, L. P. R., Ticianelli, E. A., & Assaf, E. M. (2008). *Journal of Power Sources, 175*, 482−489.
Qureshi, N., Ezeji, T. C., Ebener, J., Dien, B. S., Cotta, M. A., & Blaschek, H. P. (2008). *Bioresource Technology, 99*, 5915−5922.
Rahmat, N., Abdullah, A. Z., & Mohamed, A. R. (2010). *Renewable and Sustainable Energy Reviews, 14*, 987−1000.
Ramírez de la Piscina, P., & Homs, N. (2008). *Chemical Society Reviews, 37*, 2459−2467.
Rasko, J., Hancz, A., & Erdohelyi, A. (2004). *Applied Catalysis A: General, 269*, 13−25.
Remiro, A., Valle, B., Oar-Arteta, L., Aguayo, A. T., Bilbao, J., & Gayubo, A. G. (2014). *International Journal of Hydrogen Energy, 39*, 6889−6898.
Rennard, D. C., Kruger, J. S., & Schmidt, L. D. (2009). *ChemSusChem, 2*, 89−98.
Roh, H. S., Wang, Y., King, D. L., Platon, A., & Chin, Y. H. (2006). *Catalysis Letters, 108*, 15−19.
Romero, A., Jobbágy, M., Laborde, M., Baronetti, G., & Amadeo, N. (2014). *Applied Catalysis A: General, 470*, 398−404.
Rossetti, I., Lasso, J., Finocchio, E., Ramis, G., Nichele, V., Signoretto, M., et al. (2014). *Applied Catalysis A: General, 477*, 42−53.
Roy, B., Sullivan, H., & Leclerc, C. A. (2011). *Journal of Power Sources, 196*, 10652−10657.
Sehested, J. (2006). *Catalysis Today, 111*, 103−110.
Semelsberger, T. A., Brown, L. F., Borup, R. L., & Inbody, M. A. (2004). *International Journal of Hydrogen Energy, 29*, 1047−1064.
Seo, Y.-S., Shirley, A., & Kolaczkowski, S. T. (2002). *Journal of Power Sources, 108*, 213−225.
Shan, W. J., Feng, Z. C., Li, Z. L., Jing, Z., Shen, W. J., & Can, L. (2004). *Journal of Catalysis, 228*, 206−217.
Sheng, P. Y., Bowmaker, G. A., & Idriss, H. (2004). *Applied Catalysis A: General, 261*, 171−181.
Simonetti, D. A., Kunkes, E. L., & Dumesic, J. A. (2007). *Journal of Catalysis, 247*, 298−306.
Snytnikov, P. V., Badmaev, S. D., Volkova, G. G., Potemkin, D. I., Zyryanova, M. M., & Belyaev, V. D. (2012). *International Journal of Hydrogen Energy, 37*, 16388−16396.
Song, H., Zhang, L., Watson, R. B., Braden, D., & Ozkan, U. S. (2007). *Catalysis Today, 129*, 346−354.

Sun, J., Qiu, X. P., Wu, F., & Zhu, W. T. (2005). *International Journal of Hydrogen Energy, 30*, 437−445.
Sun, J., Qiu, X. P., Wu, F., Zhu, W. T., Wang, W. D., & Hao, S. J. (2004). *International Journal of Hydrogen Energy, 29*, 1075−1081.
Swami, S. M., & Abraham, M. A. (2006). *Energy Fuel, 20*, 2616−2622.
Tran, N. H., & Kamali Kannangara, G. S. (2013). *Chemical Society Reviews, 42*, 9454−9479.
Trimm, D. L. (1997). *Catalysis Today, 37*, 233−238.
Trimm, D. L., & Önsan, Z. I. (2001). *Catalysis Reviews: Science and Engineering, 43*, 31−84.
Vaidya, P. D., & Rodrigues, A. E. (2006). *Chemical Engineering Journal, 117*, 39−49.
Vaidya, P. D., & Rodrigues, A. E. (2009). *Chemical Engineering and Technology, 32*, 1463−1469.
Valle, B., Aramburu, B., Remiro, A., Bilbao, J., & Gayubo, A. G. (2014). *Applied Catalysis B: Environmental, 147*, 402−410.
Vizcaìno, A. J., Lindo, M., Carrero, A., & Calles, J. A. (2012). *International Journal of Hydrogen Energy, 37*, 1985−1992.
Wang, W. J. (2010). *Fuel Processing Technology, 91*, 1401−1408.
Wang, F., Cai, W., Provendier, H., Schuurman, Y., Descorme, C., & Mirodatos, C. (2011). *International Journal of Hydrogen Energy, 36*, 13566−13574.
Wang, W. J., & Cao, Y. Y. (2010). *International Journal of Hydrogen Energy, 35*, 13280−13289.
Wang, F., Cai, W. T., Provendier, H., Schuurman, Y., Descorme, C., & Mirodatos, C. (2012). *Applied Catalysis B: Environmental, 125*, 546−555.
Wang, X. D., Li, M. S., Wang, M. H., Wang, H., Li, S. R., Wang, S. P., et al. (2009). *Fuel, 88*, 2148−2153.
Wang, Z., Wang, C., Chen, S., & Liu, Y. (2014). *International Journal of Hydrogen Energy, 39*, 5644−5652.
Werpy, T., & Petersen, G. (2004). *Added top value chemicals from biomass*. U.S. Department of Energy.
Yamazaki, T., Kikuchi, N., Katoh, M., Hirose, T., Saito, H., & Yoshikawa, T. (2010). *Applied Catalysis B: Environmental, 99*, 81−88.
Yang, Y., Ma, J., & Wu, F. (2007). *International Journal of Hydrogen Energy, 31*, 877−882.
Yee, A., Morrison, S. J., & Idriss, H. J. (2000). *Journal of Catalysis, 191*, 30−45.
Zhang, B. C., Tang, X. L., Li, Y., Xu, Y. D., & Shen, W. J. (2007). *International Journal of Hydrogen Energy, 32*, 2367−2373.
Zhang, B., Cai, W., Li, Y., Xu, Y., & Shen, W. (2008). *International Journal of Hydrogen Energy, 33*, 4377−4386.
Zhang, J., Zhong, Z., Cao, X.-M., Hu, P., Sullivan, M. B., & Chen, L. (2014). *ACS Catalysis, 4*, 448−456.

Hydrogen production by gasification of biomass and opportunity fuels

6

M.Z. Hossain, P.A. Charpentier
Western University, London, ON, Canada

6.1 Introduction: what is gasification of biomass and opportunity fuels?

The three major Es of sustainability (energy, environment, and the economy) are well known to be highly interrelated, requiring us to consider all three simultaneously when considering approaches to alternative energy (Figure 6.1). According to the Renewables Global Energy Report 2013, approximately 78% of global energy supplies come from nonrenewable, carbon-based fossil fuels; the remainder is obtained from combustible and renewable sources (Figure 6.2) (Renewables Global Status Report, 2013). As the worldwide energy demand and consumption of our finite fossil fuels increases, we need to consider the substitution of petroleum-based fuels and products with renewable sources for a sustainable future. Foremost among environmental concerns is the issue of release and accumulation of carbon dioxide (CO_2) and other climate-changing gases from current fossil fuel usage into the atmosphere. Although climate change is controversial, CO_2 emissions are rapidly increasing, which in part is responsible for raising the world's average temperature, leading to global warming. One of the current megachallenges is how to find a highly efficient route to generate, deliver, and use energy that improves our lifestyles while providing a limited environmental impact and CO_2 emissions.

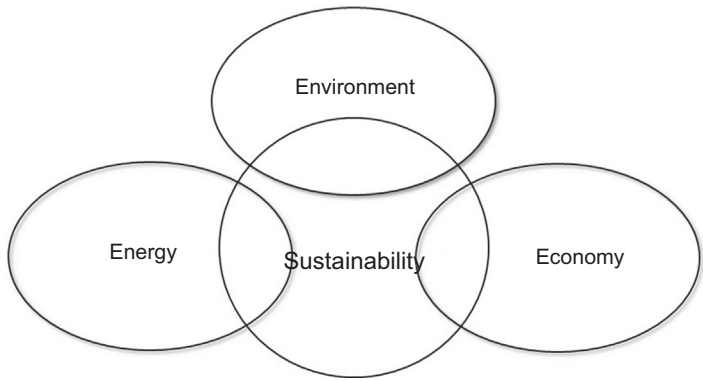

Figure 6.1 Schematic of sustainability for sustainable development.

Compendium of Hydrogen Energy. http://dx.doi.org/10.1016/B978-1-78242-361-4.00006-6

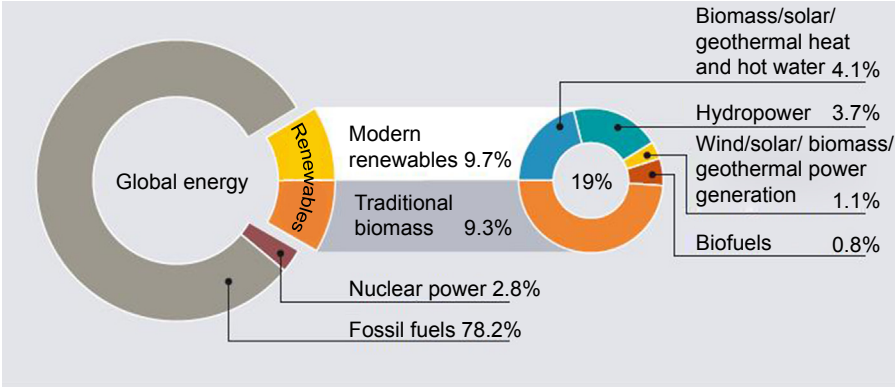

Figure 6.2 Share of world primary energy supply 2011.
Adapted from Renewables Global Status Report (2013).

Hydrogen (H_2) is widely viewed as a potential replacement for conventional fossil fuels for various types of fuel cells, transportation in cars and light trucks, and electricity production for personal electronics and other applications (Berry, Pasternak, Rambach, Smith, & Schock, 1996; Crabtree & Dresselhaus, 2008; Marbán & Valdés-Solís, 2007). Hydrogen can be obtained from renewable sources (hydro, wind, wave, solar, geothermal, and opportunity fuels) or nonrenewable sources (coal, natural gas, and nuclear) (Alternatives, C.o. and Strategies, 2004). Among the renewable sources of energy, a substantial focus of research is being directed toward the use of opportunity fuels (usually derived from waste or waste byproducts). Toward the goal of sustainability, biomass use is generally considered not to increase the net amount of CO_2 released into the atmosphere; i.e., burning biomass is part of the natural carbon cycle.

Among emerging techniques for converting opportunity fuels into a sustainable source of H_2, gasification is a promising technology. Gasification is a thermochemical technology that converts carbonaceous materials such as coal, petroleum coke, biomass, and opportunity fuels at high pressure ($\geq$33 bar) and temperatures (between 500 and 1400 °C) into a mixture of combustible gases including hydrogen, carbon monoxide, and CO_2 called syngas (Demirbaş, 2002; Morrin, Lettieri, Chapman, & Mazzei, 2012). Gasification is regarded as one of the most promising synthesis methods for using opportunity fuels because it produces fewer contaminants while forming more fuel than traditional combustion processes (Saxena, Seal, Kumar, & Goyal, 2008); i.e., it enables higher electric performance (30–32% using gas engines compared with 22% achieved with a conventional Rankine cycle) (Hernández, Aranda-Almansa, & Bula, 2010) and lower NO_x and SO_x emissions, and provides the possibility of CO_2 capture and storage (Maschio, Lucchesi, & Stoppato, 1994). Hence, gasification can add value to low- or negative-value feedstocks by converting them into marketable fuels such as hydrogen. However, commercial implementation requires several barriers to be overcome, including pretreatment of the feedstocks, gasifier operating conditions on gas quality and gasifier performance, and the removal of tars and chars (Lapuerta, Hernández, Pazo, & López, 2008).

This chapter on gasification is divided into several sections. In the first section, we will examine the basic chemistry of gasification, with the types of feedstock used for gasification and feedstocks pretreatment. Operating variables that mainly affect gasification performance and product gas generation, types of gasifiers, will be discussed in Section 2. Section 3 will focus on why gasification is preferred to all other processes as a conversion technology for generating fuel from opportunity fuel feedstocks, and the major drawbacks of using this technology and how to address these challenges. Future perspectives of opportunity fuels or biomass will be discussed in Section 4, whereas Section 5 will provide the reader with additional sources of information.

6.2 Principles and feedstocks

6.2.1 Basic chemistry

Gasification is a complex thermochemical decomposition process consisting of a number of elementary chemical reactions, beginning with the partial oxidation of a lignocellulosic feedstock (cellulose, hemicelluloses, and lignin) when using biomass as feedstock with a gasifying agent such as air, oxygen, or steam. The fundamental reaction of gasification is generally considered to be:

$$\begin{aligned}&\text{Biomass/opportunity fuels} + O_2\ (H_2O) \rightarrow CO, CO_2, H_2O, H_2, CH_4\\ &+ \text{other CHs} + \text{tar} + \text{char} + \text{ash} + HCN + NH_3 + HCl + H_2S\\ &+ \text{other sulfur gases}\end{aligned} \tag{6.1}$$

Volatile compounds released from burning the feedstock partially oxidize to yield combustion products such as H_2O and CO_2, plus heat to continue the endothermic gasification process. Water vaporizes and feedstock pyrolysis continues with burning feedstock. Higher gasification temperatures provide a product gas mixture such CO, CO_2, H_2O, H_2, CH_4, other gaseous hydrocarbons (including oxygenated hydrocarbons from some processes), tars, char, inorganic constituents, and ash owing to thermal decomposition and partial oxidation of the pyrolysis vapors. The gas composition of the products depends heavily on the gasification process, the gasifying agent, and the feedstock composition (Balat, 2008), which will be examined in detail in this chapter. Possible reactions taking place in the gasifier can be summarized as follows:

$$\text{Partial Oxidation} \quad C + \frac{1}{2}O_2 \rightleftarrows CO;\ \Delta H = -268\ \text{MJ/kmole} \tag{6.2}$$

$$\text{Complete Oxidation} \quad C + O_2 \rightleftarrows CO_2;\ \Delta H = -406\ \text{MJ/kmole} \tag{6.3}$$

$$\text{Water}-\text{gas reaction} \quad C + H_2O \rightleftarrows CO + H_2;\ \Delta H = +118\ \text{MJ/kmole} \tag{6.4}$$

The heat of reaction for the three possible reactions shows that the highest energy release is derived from the complete oxidation or combustion reaction, whereas the

partial oxidation of carbon to CO accounts for only about 65% of energy released during oxidation. Char formed during gasification is also minimized by converting carbon according to reactions (6.2)–(6.4). Carbon monoxide can undergo further reactions during gasification, as follows:

$$\text{Water–gas shift reaction} \quad CO + H_2O \rightleftarrows CO_2 + H_2;\ \Delta H = -42\ \text{MJ/kmole} \tag{6.5}$$

$$\text{Methanation reaction} \quad CO + 3H_2 \rightleftarrows CH_4 + H_2O;\ \Delta H = -88\ \text{MJ/kmole} \tag{6.6}$$

$$\text{Boudouard reaction} \quad 2CO \rightleftarrows C + CO_2;\ \Delta H = +173\ \text{MJ/kmole} \tag{6.7}$$

When H_2O and CO_2 interact with char, the water gas (6.4) and Boudouard (6.7) endothermic reactions are also favored. Because the main products of gasification at elevated temperatures are CO and H_2, the water–gas shift (WGS) reaction (6.5) becomes a crucial part of the hydrogen production process. The ratio of CO and H_2 can be adjusted by enhancing the WGS reaction. To achieve the desired conversion of CO, thermodynamic considerations necessitate the WGS reaction to be carried out at temperatures <500 °C (Yu, Tian, McKenzie, & Li, 2006). The use of a catalyst is normally required to achieve reasonable reaction rates at these low temperatures. The methanation reaction (6.6) normally needs to be reduced to maximize H_2 production.

The cracking of hydrocarbons and tars occurs in the catalytic reactor at high temperatures during the gasification process. Throughout the process, tar molecules are adsorbed onto the catalyst surface, subsequent cracking and polymerization of free-radical chemical reactions takes place, and finally they are decomposed into small molecules by catalysts. These reactions are as follows:

$$\text{Steam reforming reaction} \quad C_nH_m + nH_2O \rightleftarrows nCO + (n + m/2)H_2 \tag{6.8}$$

$$\text{Dry reforming reaction} \quad C_nH_m + n_2CO \rightleftarrows 2nCO + (m/2)H_2 \tag{6.9}$$

$$\text{Thermal cracking reaction} \quad C_nH_m \rightleftarrows nC + (m/2)H_2 \tag{6.10}$$

$$\text{Hydrocracking reaction} \quad C_nH_m + (4n - m)H_2 \rightleftarrows n_4CH \tag{6.11}$$

Reactions (6.8)–(6.11) are equilibrium-based, which can proceed in either direction depending on reactor conditions such as temperature, pressure, and the concentration of the reacting species, which is strongly influenced by both the feedstock and the reactor design. The content of H_2 increases with increasing temperature whereas the CO content initially increases and then decreases. The CH_4 content reduces significantly with an increase in the cracking reaction temperature. According to Le Chatelier's principle, higher temperatures favor reactants in exothermic reactions and products in endothermic reactions (Mahishi & Goswami, 2007). It is known

that the steam reforming reaction of CH_4 (6.8) and the reforming reaction of CO_2 (6.9) are endothermic (Hernandez, Aranda, Barba, & Mendoza, 2012; Pu, Zhou, & Hao, 2008). Therefore, reactions (6.8) and (6.9) are enhanced with increasing temperature, which results in an increase in H_2 and CO content and a decrease in CH_4. When the temperature varies from 700 °C to 900 °C, the CO content decreases because the exothermic reactions between carbon and oxygen are weakened (Franco, Pinto, Gulyurtlu, & Cabrita, 2003).

6.2.2 Gasification feedstocks

As with any chemical engineering process, the feedstock is critical to the design and operation of the gasifier. The composition of the fuel produced during gasification as outlined above depends heavily on the composition of the feedstock used. For example, lignin is known to be hard to gasify compared with cellulose because of its ordered aromatic structure, which provides high chemical stability (Alves & Figueiredo, 1988). Of most current interest for gasification are opportunity fuel feedstocks, which can be categorized into three classes including biomass fuels, industrial byproducts, and industrial or commercial waste products (Combined heat and power market, 2004).

6.2.2.1 Biomass fuels

Biomass fuels are derived from carbon-based materials contained in living organisms, which can be gasified. Current biomasses of interest for gasification include microalgae, crop residues, animal waste, food processing waste, municipal solid waste, sludge waste, and wood—wood waste. Currently, microalgae are of significant interest and are considered a versatile biomass source because of their higher photosynthetic efficiency and biomass productivities (Campbell & Duncan, 1997; Chisti, 2008). Crop residues include bagasse (sugarcane residue), corn stalks, rice hulls, rice straw, wheat straw, nutshells, and prunings from orchards and vineyards. Animal waste includes animal excrement (manure) and animal byproducts from processing. Food processing waste (FPW) includes any type of waste generated in the food processing industry that can potentially be used for fuel. Potato waste, cheese whey waste, fruit pits, leftover sludge, animal parts, and other energy-rich FPW all can be converted into a solid biomass fuel that can be gasified. Municipal solid waste includes garbage items produced from humans' everyday activities, which are of tremendous interest as feedstocks. Sludge wastes include the solid waste extracted from a process whereas wood waste includes any type of wood or wood-based product that can be burned to generate power. Most of these opportunity fuels are found in dry form except sludge waste, animal waste, and some types of food processing waste, which contain a large amount of moisture. Figure 6.3 shows the sources of biomass fuels.

On November 21, 2013, Ontario, Canada announced a ban on coal-fired electricity, making it illegal to burn coal in Ontario. Two Ontario power generation stations were fueled by coal in 2013 but planned to burn biomass instead. At its peak, Nanticoke produced 21 million tons of greenhouse gas.

Figure 6.3 Sources of biomass.

6.2.2.2 Industrial byproduct feedstocks

Industrial byproduct feedstocks include black liquor, coke oven gas, industrial volatile organic compounds, waste process heat, and so forth. Black liquor, a byproduct of the pulping process, is usually directly burned in boilers or gasified because of its high heat content. One-third of all pulping mills in the United States produce 6 million lb/day of black liquor each. The black liquor typically contains 15–20 wt% solids, which have about half the energy of the original woodchips. A gasification system can feed the liquor into a high-pressure gasifier to produce electricity or steam. The steam reforming gasification system of Thermochem Recovery International (Baltimore, Maryland) was commissioned and designed to handle 115 metric tons/day of black liquor solids. Georgia–Pacific Corporation (Big Island, Virginia) is one of the world's largest paper companies and the Big Island mill produces 900 metric tons/day of linerboard and 600 metric tons/day of corrugating medium. Thermochem Recovery International's steam reforming gasification system was commissioned to process 200 metric tons/day of black liquor solids (www.netl.doe.gov/research/coal/energy-systems/gasification/gasifipedia/blackliquor). Coke oven gas is a fuel gas with a medium calorific value that is produced during the manufacture of metallurgical coke by heating bituminous coal to temperatures of 900–1000 °C in a chamber from which air is excluded (Zhang et al., 2008). The main constituents are, by volume, about 50% H_2, 30% CH_4, and 3% higher hydrocarbons; and 7% CO, 3% CO_2, and 7% N_2. Coke oven gas is currently used only in mills and refineries as an additional source of heat, and sometimes electricity.

6.2.2.3 Commercial or industrial waste

Commercial or industrial waste includes landfill gas, construction waste, combustible production waste, and tire-derived fuel. Landfill gas is a complex mixture of different gases generated through the action of microorganisms within a landfill (a site for the disposal of waste materials by burial; the oldest form of waste treatment). Landfill gas is simply collected and used to produce heat and power. Construction waste includes

Figure 6.4 Sources of industrial or commercial waste.

all types of wood, plastic, metal debris, and assorted fluids that are produced as byproducts of a construction project. These wastes vary greatly in composition and location, and are typically disposed of in landfills. The source of combustible wastes is mainly industrial production processes and includes textile waste, wood scrap/trimmings, plastic scraps, and non-reusable solvents. Textile waste can consist of excess yarn, thread, cloth, carpet, or any other fabric. The excess material waste can be used as an energy source with about the same heat content as biomass. Although the waste contains many more pollutants and contaminants than biomass fuels, it can be gasified to produce heat and power for textile mills. Tire-derived fuel is made from shredding and processing scrap tires, and it works nearly as well as coal for boiler fuel. Figure 6.4 shows several sources of industrial or commercial waste of interest for commercial gasification feedstocks.

6.2.3 Feedstock pretreatment

6.2.3.1 Biomass fuels

Biomass fuels require pretreatment of the feedstocks, which largely depends on the gasification technology used. Key problem areas are as follows.

Drying

It is well-recognized that water has a high heat capacity; it is energy-intensive to remove by drying. Freshly cut wood contains 30–60% moisture and sometimes may exceed 90%. As much as 2260 kJ energy is required to remove 1 kg of moisture; that energy cannot be recovered. Fuel with moisture content >30% reduces the calorific value of the product gas because of the need to evaporate additional moisture before combustion/gasification can occur (Plis & Wilk, 2011; Wu, Yin, Ma, Zhou, & Chen, 2009). High-moisture content also add an extra load on any cooling and filtering equipment by raising the pressure drop across these units because of condensing liquid. For gasification, the moisture content should be between 10% and 15% (Basu, 2010).

The lower the moisture content is, the higher is the gasification efficiency (Calzavara, Joussot-Dubien, Boissonnet, & Sarrade, 2005). Perforated bin dryers, band conveyor dryers, and rotary cascade dryers have been used to dry feedstocks (Cummer & Brown, 2002). However, for low-moisture content feedstocks (less than 10%), drying stages may be required (Brammer & Bridgwater, 2002).

Size reduction

Smaller particles have larger surface areas and larger pore sizes that provide faster heat transfer and gasification rates (Kirubakaran et al., 2009). Lv et al. reported higher gas yields with smaller sawdust particles and lower amounts of CO_2, gas energy content (low heating value (LHV)), and carbon conversion efficiency (Lv et al., 2004). Luo et al. found higher H_2 and CO content with lower CO_2 content as well as gas yield and carbon conversion efficiencies by reducing sawdust particle size from 1.2 to 0.08 mm (Luo et al., 2009). Pérez, Melgar, and Benjumea (2012) found that pine bark behaves differently inside a gasifier according to its size. They observed that an increase in particle size from 2 to 6 mm during pine bark gasification in a downdraft gasifier led to lower pine bark consumption rates, fuel/air equivalent ratios, maximum process temperatures, and consequently lower flame front velocities. Hammer mills, knife mills, and tub grinders are typical units used to reduce the size of agricultural and forestry residue (Kumar, Jones, & Hanna, 2009). Energy consumption during size reduction depends on the moisture content, initial size of feedstock, feedstock properties, and screen size and properties of the mill.

Fractionation and leaching

The ash-forming elements, Al, Ca, Fe, K, Mg, Na, and Si, occur in biofuels as internal or external mineral grains or simple salts such as KCl and $CaSO_4$, or are associated with the organic parts of the fuel. Depending on the gas/particle temperature and the conditions used during the reaction process, these elements may vaporize if they are in the form of simple salts, whereas mineral grains may undergo phase transformation, forming fly ash particles. Leaching and fractionation can be used to treat materials by decreasing the amounts of alkali metal, chlorine, and sulfur and also the total ash amount at variable levels (Arvelakis & Koukios, 2002; Turn, Kinoshita, & Ishimura, 1997). Small particles have a tendency to contain less nitrogen and alkalis, so fractionation into fine particles helps to produce a gas with fewer impurities. The nitrogen and alkali content of the biomass can be reduced by prior leaching with water. Link et al. (2012) used leaching as a pretreatment process of olive residue and olive residue mixed with reed, pine pellets, and Douglas fir wood chips targeted to eliminate alkali metals such as K and Na as well as chlorine. A lower total tar yield of the product gas when leached olive residue was used was observed compared with untreated olive residue.

6.2.3.2 Industrial byproducts and waste

No special pretreatment is normally required for gaseous industrial byproducts, which can be used directly as a fuel. Construction waste contains a large percentage of inert

materials that must be removed before generating a usable fuel steam. Incineration could be a possible solution to gasify these types of waste. Incineration of waste materials converts waste into ash, flue gas, and heat. The ash is mostly formed by the inorganic constituents of the waste and may take the form of solid lumps or particulates carried by the flue gas. The flue gases must be cleaned of gaseous and particulate pollutants before they are dispersed into the atmosphere. In some cases, the heat generated by incineration can be used to generate electric power (Knox, 2005).

6.3 Process of gasification of biomass and opportunity fuels

6.3.1 Gasification plant

Figure 6.5 shows the basic process steps of a biomass gasification plant and supporting equipment.

The production of combustible gas from carbonaceous materials is a mature technology that was first introduced using blast furnaces to produce combustible gases from organic feedstocks over 200 years ago (Susta, Luby, & Mat, 2009). Furthermore, gasification has such excellent environmental performance that some state public utility commissions have identified integrated gasification combined cycle (IGCC) plants for power generation as the best available control technology (Breault, 2010).

6.3.2 Types of gasifiers

A gasifier is a reactor unit in which the feedstock fuel and gasifying agent are mixed together with catalysts or additives, and where the various reactions described in Section 6.2 occur. It is sometimes called the heart of a gasification plant, which is mainly responsible for keeping syngas/producer gas production as steady as possible. Distinct types of gasifiers have been developed depending on the way in which the reagents, feedstocks, and gasifying agents come into contact with each other (Balat, Balat, Kırtay, & Balat, 2009); the most important types used for gasification are fixed-bed, fluidized-bed, and entrained flow gasifiers (Figure 6.6). Table 6.1 shows the relative advantages and disadvantages of the major types of gasifiers used in gasification (Rampling & Gill, 1993a, 1993b).

6.3.2.1 Fixed-bed gasifier

The fixed-bed gasifier is the most useful method for gasification and involves reactor vessels in which the feed material is either packed in or moves slowly as a plug, with gases flowing between the feedstock and catalyst particles (Munzinger & Lovegrove, 2006). Fixed-bed gasifiers are subdivided into two general classes according to the way in which the feedstocks come into contact with the gasifying agents: i.e., downdraft and updraft gasifiers.

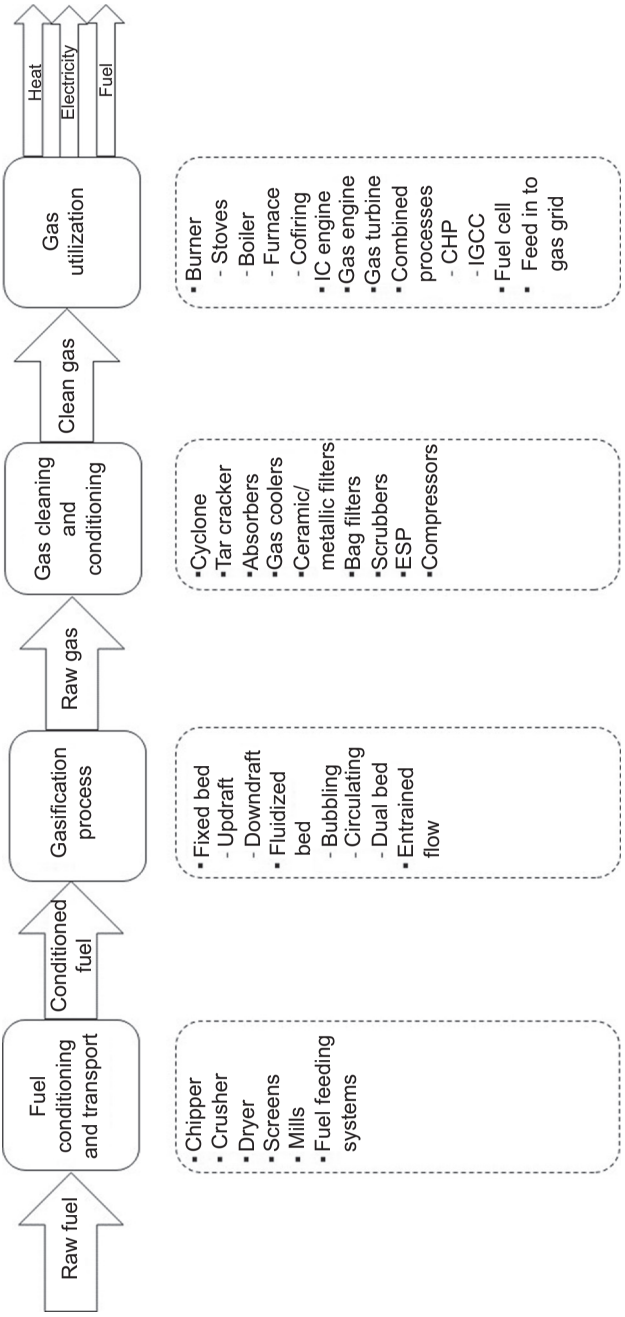

Figure 6.5 Basic process steps of a biomass gasification plant.

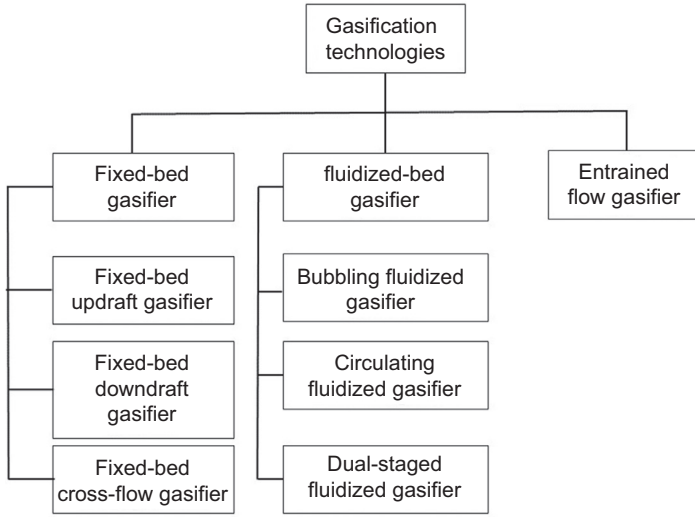

Figure 6.6 Overview of the principal gasification technologies.

Fixed-bed updraft gasifier

In a fixed-bed updraft gasifier (Figure 6.7), the gasifying agent is introduced at the bottom of the reactor, with the reactant gas flowing upward through a hot reactive zone near the bottom of the gasifier in a countercurrent direction to the flow of feedstock material (Stevens, 2001). The bottom zone collects and then discharges the ash produced in the process. Higher up the gasifier, the feedstocks are pyrolyzed, the feed is dried in the top zone, and the gases are cooled down at 200−300 °C. In the pyrolysis zone, the volatile compounds are released, while considerable quantities of tar are formed that condense partly on the feedstocks higher up and partly leave the gasifier with the product gas. Formation of considerable amounts of tar occurs during gasification, which is a major disadvantage of this gasifier type and creates a gas cleaning problem (Beenackers, 1999). Because the product gas leaves the gasifier at a low temperature, the overall energy efficiency of this process is high.

Fixed-bed downdraft gasifier

In a fixed-bed downdraft gasifier (Figure 6.7), the feed and gasifying agent move in a cocurrent direction. The product gases leave the gasifier after passing through the hot zone, enabling the partial cracking of tars formed during gasification and giving off a gas with minimum tar content. Although the tar content of the product gas is lower than for an updraft gasifier, the particulates content of the gas is higher. Because the gases leave the gasifier unit at temperatures ∼900−1000 °C, the overall energy efficiency of a downdraft gasifier is low because of the high heat content removed by the hot gas. The tar content of the product gas is lower than for an updraft gasifier but the particulate content of the gas is high. This type of gasifier is limited in scale and requires a well-defined fuel, which makes them not fuel-flexible (Boerrigter, Drift, Hazewinkel, & Küpers, 2004).

Table 6.1 Relative advantages and disadvantages of different gasifiers (McKendry, 2002)

Gasifier	Advantages	Disadvantages
Updraft fixed bed	Mature for small-scale heat applications Can handle high moisture No carbon in ash	Feed size limits High tar yields Scale-up limitations Low heating value gas Slagging potential
Downdraft fixed bed	Small-scale applications Low particulates Low tar	Feed size limits Scale limitations Low heating value gas Moisture-sensitive
Bubbling fluidized bed	Large-scale applications Feed characteristics Direct/indirect heating Can produce higher heating value gas	Medium tar yield Higher particle loading
Circulating fluidized bed	Large-scale applications Feed characteristics Can produce higher heating value gas	Medium tar yield Higher particle loading
Dual-staged fluidized bed	Oxygen not required High methane owing to low bed temperature Temperature limit in the oxidizer	More tar owing to low bed temperature Difficult to operate under pressure
Entrained flow	Can be scaled Potential for low tar Potential for low methane Can produce higher heating value gas	Large amount of carrier gas Higher particle loading Particle Size limits

6.3.2.2 Fluidized-bed gasifier

Fluidized beds are attractive compared with fixed-bed gasifiers because of their excellent mixing characteristics, low cost, good scale-up potential, ease of operation, and high reaction rates during gas–solid contact (Warnecke, 2000). Additional advantages relate to the flexibility of fluidized beds when dealing with a range of solid biomass feedstocks of varying composition. Fluidized-bed gasifiers normally operate below the ash melting point so as to avoid agglomeration; their operation is limited by the melting properties of the bed materials. It cannot achieve full conversion of char because of the continuous mixing of solids. The high degree of mixing of solids helps maintain an even bed temperature but the close mixture of gasified and partially

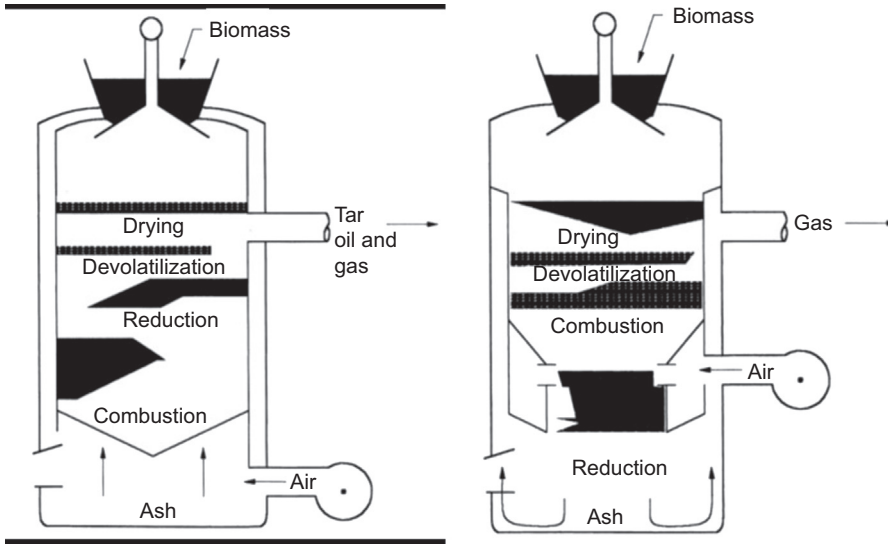

Figure 6.7 Schematic of updraft and downdraft gasifier.
Adapted from McKendry (2002).

gasified particles means that any solids that leave the bed contain partially gasified char. The typical operation temperature of a fluidized-bed gasifier is between 800 and 1000 °C. Therefore, this type of gasifier is not suitable for coal gasification because of the lower reactivity of coal compared with biomass and the required higher temperature (>1300 °C) (Boerrigter et al., 2004). Examples of fluidized-bed gasifier systems are bubbling fluidized bed (BFB), circulating fluidized bed, and dual-staged gasifiers, which will be briefly examined.

Bubbling fluidized bed

Bubbling bed gasifiers (Figure 6.8) consist of a vessel in which the gasifying agent is introduced into the system at the bottom of the reactor. The feedstocks are introduced through a continuous feeding system at the top of the gasifier. This fluidized bed contains fine-grained materials (usually silica or alumina) that have high specific heat capacity and can operate at high temperatures (Kumar et al., 2009). The bed temperature is maintained at 700−900 °C by controlling the ratio of gasifying agent to feedstocks. The feedstocks are pyrolyzed in the hot bed to produce a gas with a tar content between that of the updraft and downdraft gasifiers (Balat et al., 2009). Some pyrolysis products are swept out of the fluid bed with the gasification products, but are then cracked by contact with the hot bed materials, giving a product gas with a low tar content, typically <1 to 3 g/Nm^3 (McKendry, 2002; Warnecke, 2000).

Circulating fluidized bed

Circulating fluidized-bed gasifiers (Figure 6.9) consist of a riser (operates either in turbulent or fast fluidization regime) in which feedstocks undergo moisture evaporation,

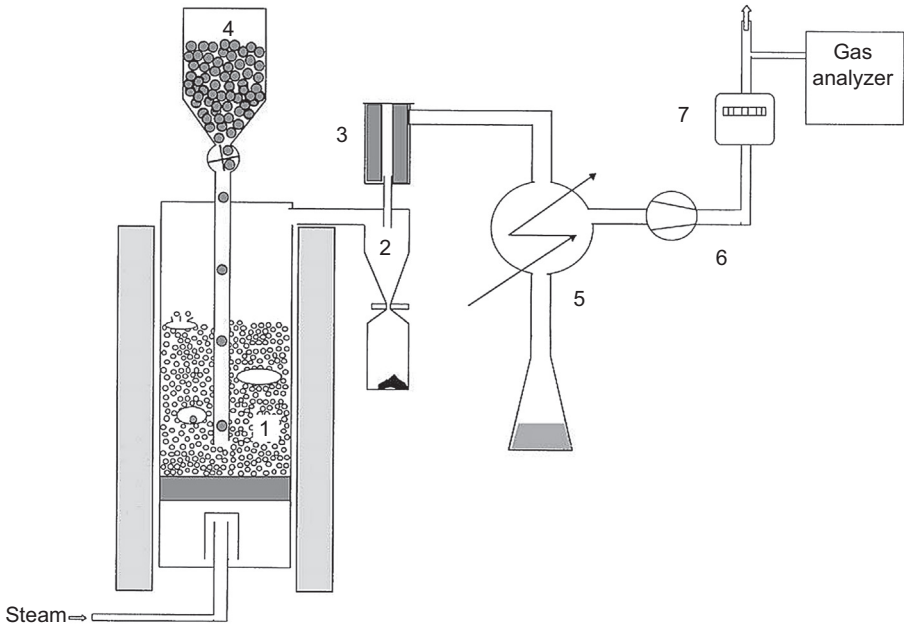

Figure 6.8 Schematic of BFB gasifier (1) Fluidized-bed gasifier; (2) cyclone; (3) ceramic candle filter; (4) feedstock feeder; (5) water and tar condensation system; (6) blower; (7) volumetric gas meter.
Adapted from Rapagna, Jand, Kiennemann, and Foscolo (2000).

pyrolysis, and char gasification, a high-temperature cyclone separator in which coarser particles are captured from the product gas and are recycled to the bottom of the riser through an air-driven loop seal, and a ceramic fiber filter unit for gas cleaning. Circulating fluidized-bed gasifiers have the ability to deal with high-capacity throughput by having a higher flow rate of fluidizing agent, and are useful for converting waste feedstocks into energy.

Dual fluidized-bed gasifier

A two-stage dual fluidized-bed gasifier (T-DFBG) was developed to incorporate gas upgrading functions into a gasifier to avoid fuel loss based on the principle shown in Figure 6.10. Here, a single fluidized bed is divided into two zones including a gasification zone (BFB) and a combustion zone or fluidized-bed combustor (FBC). The combination of a BFB and FBC is called a two-stage fluidized bed (TFB), which makes it more flexible for different feedstocks and operating conditions while suppressing tar formation (Paisley, Litt, & Creamer, 1990; Pfeifer, Rauch, & Hofbauer, 2004; Xu, Murakami, Suda, Matsuzawa, & Tani, 2006; Zschetzsche, Hofbauer, & Schmidt, 1998). Because it isolates the combustion reaction for endothermic heat required for gasification reactions, the T-DFBG has the advantage of producing N_2-free feedstock for chemical synthetic processes and CO_2-captured, H_2-rich product gases (Bridgwater, 1995; Marquard-Möllenstedt et al., 2004; Paisley, Farris, Black, Irving, & Overend, 2000).

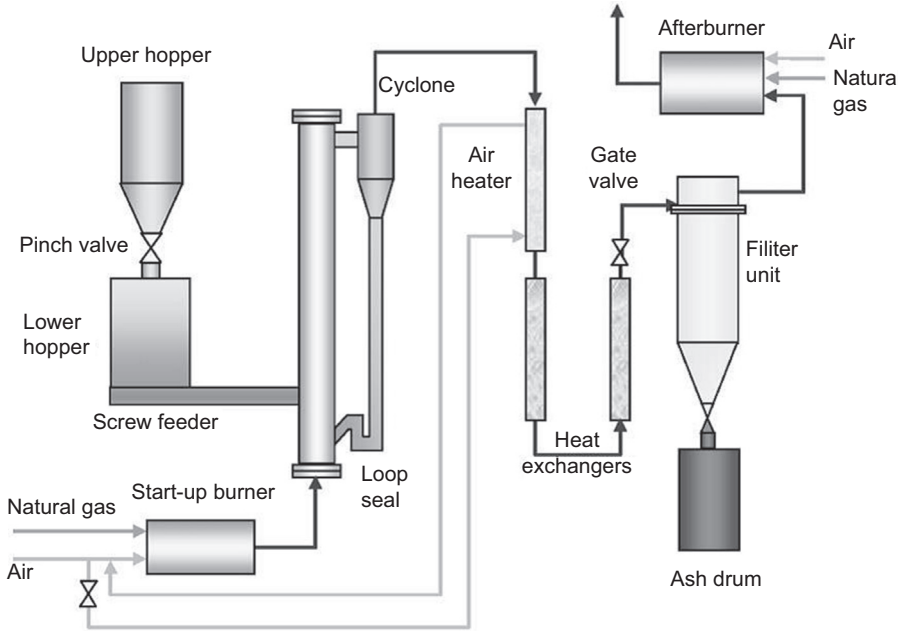

Figure 6.9 Schematic of circulating fluidized-bed gasifier.
Adapted from Li et al. (2004).

In a T-DFBG (Figure 6.11), the fuel feed is introduced into the lower stage of the TFB. The circulated heat carrier particles (HCPs) enter first the TFB's upper stage and move into its lower stage via overflow. Fuel pyrolysis and gasification occur in the lower stage of the TFB by contacting the HCPs from the upper stage and interacting with the gasifying agent (air + steam) fed into this stage. The generated gas, mixed with overfed gasification reagent, then flows up and passes through the upper stage where gas upgrading reactions, including tar/hydrocarbon reforming and the WGS occur via interacting with hot particles. Consequently, the tar and hydrocarbon reforming and WGS proceed in the upper stage.

The T-DFBG depicted in Figure 6.11 sends gasification particles to the lower endothermic reaction zone. Gas upgrading helps increase the conversion of tars into gas and enhances the WGS reaction, thus increasing the efficiency of gasification and causing the product gas to have more H_2 and less tar. The high reaction temperature in the upper stage facilitates the catalytic reactions (Xu, Murakami, Suda, Matsuzawa, & Tani, 2009), which enhances the gasification reactions and lowers tar evolution (Corella, Herguido, & Alday, 1988).

6.3.2.3 *Entrained flow gasifier*

Because of the low reaction temperatures used, fixed-bed and fluidized-bed gasifiers have several disadvantages, such as lower rates of feedstock conversion, lower calorific values, and higher tar yields. The entrained flow gasifier is a promising technology that operates at high temperatures (around 1200−1500 °C) with small particles and

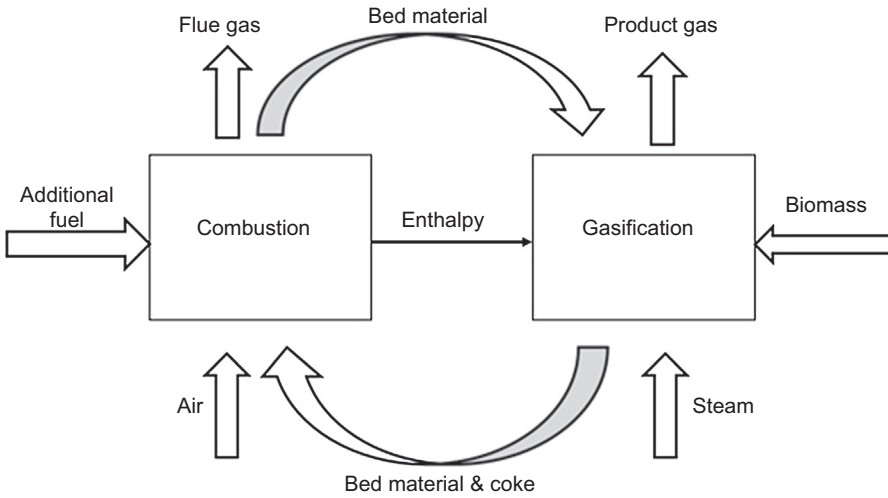

Figure 6.10 Principle of the dual fluidized-bed gasifier (Hofbauer et al., 2002).

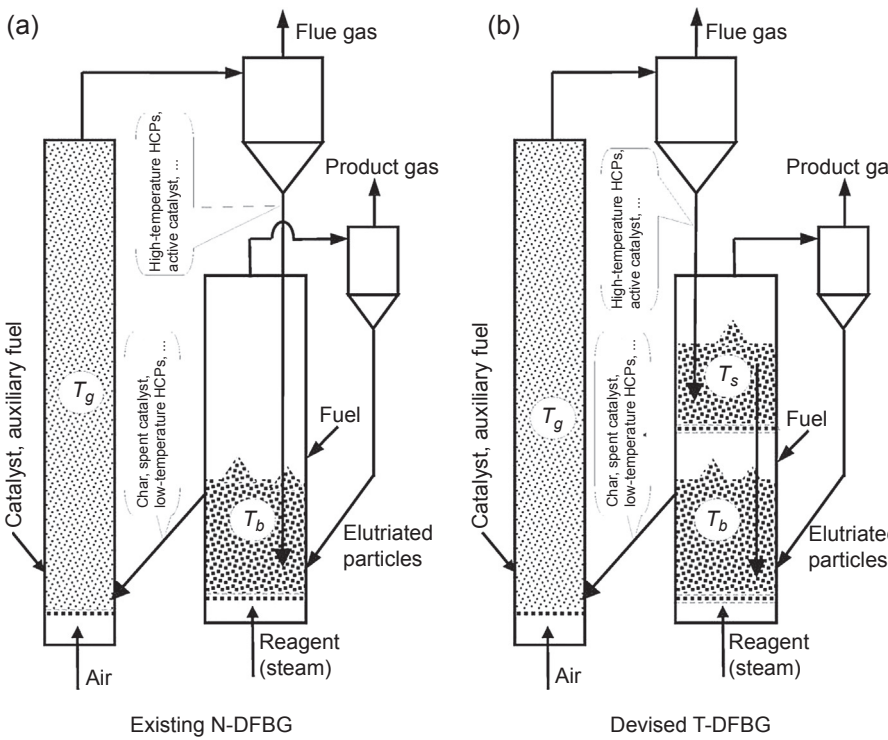

Figure 6.11 Two-stage dual fluidized-bed gasifier: (a) N-DFBG; (b) T-DFBG. Adapted from Xu et al. (2009).

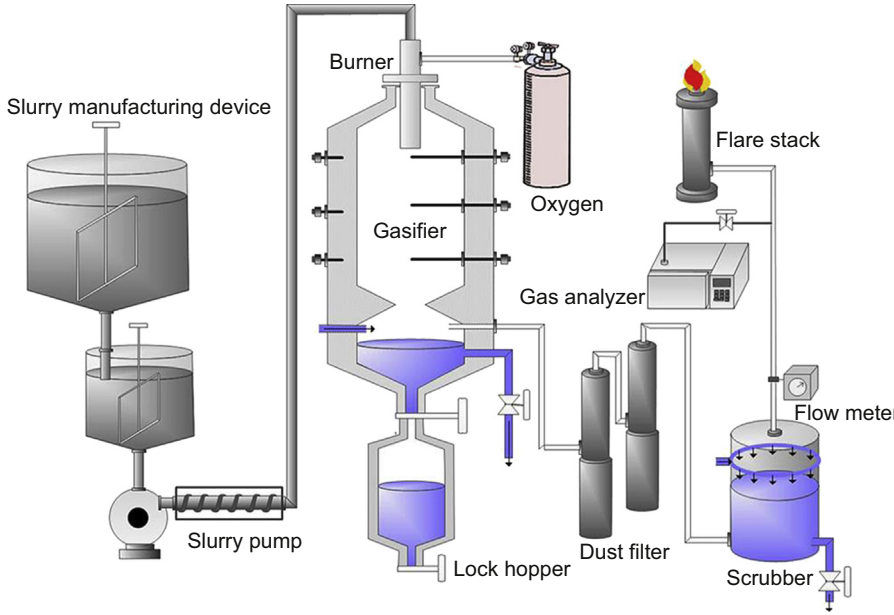

Figure 6.12 Schematic of entrained flow gasifier.
Adapted from Bae et al. (2012).

high heating rates and can achieve a high conversion rate with low residence time, providing this gasifier with a high capacity (Henrich & Weirich, 2004; Liu, Kaneko, Luo, Kato, & Kojima, 2004; Van der Drift, Boerrigter, Coda, Cieplik, & Hemmes, 2004). Moreover, the higher temperatures help secondary cracking of tar to reduce tar production (Quaark, Knoef, & Stassen, 1999). From 2005 until today, 94% of all registered gasifiers worldwide, in operation or planned, are based on entrained flow gasification (Öhrman et al., 2013).

Figure 6.12 shows an entrained flow gasifier consisting of a feedstock slurry manufacturing device, a gasifier (operating at 1800 °C temperature and 25 bar pressure) whose upper part is connected with a slurry injecting burner and an LPG burner; the lower part is connected to an ash lock hopper for slag removal. The syngas is passed through a refiner and then sent to a flare stack after its flow and other characteristics are analyzed.

6.3.2.4 Rotary kiln gasifiers

This type of gasifier is used mainly for industrial waste incineration. The advantage of using this gasifier is that it carries out two tasks simultaneously, including moving solids in and out of a high-temperature reaction zone and mixing solids during reaction. The reaction is carried out at 450 °C in a gasification drum and converted into gas and char with other residue of metals, ash, and debris. After separation and recovery of aluminum, iron, and other residue, the exit stream is fed into a high-temperature combustion chamber and burned at 1300 °C and a low excess air ratio (about 1.2) (California U.o., 2009). The waste is gasified with high-temperature air obtained in a high-temperature air heater

with no additional external fuel needed. The recovery of iron, aluminum, and slag, which can be sold, leads to a high waste volume reduction ratio, which can reach 1/200 of the original waste volume (Mitsui Recycling 21 Pyrolysis Gasification, 2011).

6.3.2.5 Plasma gasifiers

Plasma gasification is a gasification process that decomposes biomass into basic components such as H_2, CO, and CO_2 in an oxygen-starved environment at extremely high temperatures, e.g., from 2000 to 30,000 °C (Fabry, Rehmet, Rohani, & Fulcheri, 2013). Plasma is any gas in which at least part of the atoms or molecules are partially or fully ionized when an electric arc is generated by running an electric current through the gas. This results in high temperatures in the plasma current, facilitating feedstock bond breaking and thus generating a syngas. Under such extremely elevated temperatures, the injected biomass stream can be gasified within a few milliseconds with no intermediate reactions (Zhang, Xu, & Champagne, 2010). Plasma gasifiers are used mainly for gasifying organic municipal solid waste and other waste such as paper, plastics, glass, metals, textiles, wood, and rubber. (Arena, 2012). At the same time, melting of inorganic components (glass, metal, silicates, and heavy metals) gives rise to slag that vitrifies on cooling. Plasma gasification is believed to be a clean technique with little environmental impact.

6.3.2.6 Supercritical water gasifiers

Supercritical water (SCW) gasification (SCWG) is carried out in a gasifier in which the conditions of the critical point of water (374 °C and 22.1 MPa pressure) (Figure 6.13) are used as a favorable atmosphere for opportunity fuel feedstocks with no prior drying (Chen, Lu, Guo, Zhang, & Xiao, 2010; Kruse, 2008; Kruse, Forchheim, Gloede, Ottinger, & Zimmermann, 2010; Liao, Guo, Lu, & Zhang, 2013). Supercritical water has some exceptional properties that make it an exclusive solvent for opportunity fuel feedstock gasification (Chowdhury, Hossain, & Charpentier, 2011; Savage, 1999; Watanabe et al., 2004; Youssef, Chowdhury, Nakhla, & Charpentier, 2010; Youssef, Elbeshbishy, Hafez, Nakhla, & Charpentier, 2010; Youssef, Nakhla, & Charpentier,

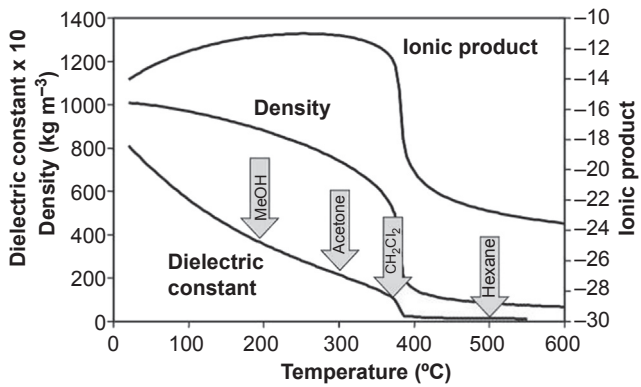

Figure 6.13 Physical properties of high-temperature water (Kritzer, 2004).

2011; Youssef, Nakhla, & Charpentier, 2012). Mass transfer resistance in SCW becomes insignificant because of the high solubility and diffusivity of gases and organic material. Under supercritical conditions, the dielectric constant of water and hydrogen bonding drops sharply, thus providing high solvating power for organic compounds. This results in SCW acting as a single-phase, nonpolar, dense gas that has solvation properties similar to low-polarity organics. Moreover, the increased value of the ionic product increases the concentration of both H^+ and OH^- ions, which leads to a significant increase in the power of the hydrolysis reaction. Hence, hydrocarbons and gases such as CO_2, N_2, and O_2 are highly soluble whereas ionic species such as inorganic salts are practically insoluble in SCW. This enhances the oxidation kinetics of organic species, especially because of the absence of mass transfer limitations. Therefore, although SCW is applicable to a wide range of feed mixtures and is not limited to aqueous organics, organic waste containing carbon, hydrogen, oxygen, and nitrogen atoms are of particular interest and oxidized primarily to CO_2, H_2O, N_2, respectively, and other small molecules.

Various reactor designs and modifications have been reported to address problems such as reactor plugging. Huang described a vertical cylindrical reactor with internal rotatable scraper blades for SCW oxidation of wastewater, which helped dissolve inorganic salts during the cooling of the effluent mixture (Huang, 1992).

The use of wet opportunity fuels without drying offers a great potential for this technology because these feedstocks often have a high water content. Hydrothermal gasification combines these aspects and offers some other additional advantages such as the nearly complete conversion of feedstocks to H_2, CH_4, and CO_2 at relatively low temperatures of 600−700 °C. The produced CO_2 can be easily separated because of its high solubility in water under pressure.

6.3.3 Operating variables of gasification reactors

As described in Section 6.2, biomass or opportunity fuel gasification consists of a large number of complex chemical reactions such as pyrolysis, partial oxidation, gasification of char, conversion of tars/hydrocarbons, and WGS reaction. These reactions are strongly controlled by both the feedstock and the process parameters including the gasifying agent used, the gasification temperature and pressure, the type of feedstock, bed materials, residence time, the air−fuel and equivalent ratio, and the design of the particular gasifier system (as described in the last section) (McKendry, 2002; Suresh Kumar Reddy, Al Shoaibi, & Srinivasakannan, 2012; Srinivas, Gupta, & Reddy, 2009). The advantages and technical challenges of different operating conditions of biomass gasification are summarized in Table 6.2; the variables effects are described in more detail below (Wang, Weller, Jones, & Hanna, 2008).

6.3.3.1 Effect of gasifying agent

Air, oxygen, steam, CO_2, or mixtures of these have been widely used as gasifying agents in the gasification process and have an important role in the resulting product gas composition and the economics of the overall process (Gil, Corella, Aznar, & Caballero, 1999). Air is the most commonly used gasifying agent for heat and power generation because it

Table 6.2 Advantages and challenges of different gasifying agents, designs, and operation (Wang et al., 2008)

	Main advantages	Main technical challenges
Gasifying agent		
Air	Partial combustion for heat supply of gasification Moderate char and tar content	Low heating value (3−6 MJ/Nm^3) Large amount of N_2 in syngas (e.g., 50% by volume) Difficult determination of ER (Usually 0.2−0.4)
Steam	High heating value syngas (10−15 MJ/Nm^3) H_2-rich syngas (e.g., 50% by volume)	Require indirect or external heat supply for gasification High tar content in syngas Require catalytic tar reforming
Carbon dioxide	High heating value syngas High H_2 and CO in syngas and low CO_2 in syngas	Require indirect or external heat supply Required catalytic tar reforming
Gasifier design		
Fixed/moving bed	Simple and reliable design Capacity for wet biomass gasification Favorable economics on a small scale	Long residence time Nonuniform temperature distribution in gasifiers High char or/and tar contents Low cold gas energy efficiency Low productivity (e.g., 5 GJ/(m^2h))
Fluidized bed	Short residence time High productivity (e.g., 20−30 GJ/(m^2h)) Uniform temperature distribution in gasifiers Low char or/and tar contents High cold gas energy efficiency Reduced ash-related problems	High particulate dust in syngas Favorable economics on a medium- to large scale

Table 6.2 Continued

	Main advantages	Main technical challenges
Gasifier operation		
Increase of temperature	Decreased char and tar content Decreased methane in syngas Increased carbon conversion Increased heating value of syngas	Decreased energy efficiency Increased ash-related problems
Increase of pressure	Low char and tar content No costly syngas compression required for downstream use of syngas	Limited design and operational experience Higher costs of a gasifier at a small scale
Increase of ER	Low char and tar content	Decreased heating value of syngas

is readily available and cost-effective (Srinivas, Reddy, & Gupta, 2012; Yin, Wu, Zheng, & Chen, 2002). Because air is highly diluted with nitrogen (80%), poor-quality gas is produced with a lower H_2 content (8−14 vol.%) and calorific value (4−7 MJ/m^3) (Alauddin et al., 2010; Cao, Wang, Riley, & Pan, 2006; Wang et al., 2008;). Oxygen as a gasifying agent produces a higher quality, nitrogen-free gas with an LHV of 10−18 MJ/m^3 (Kaiser, Weigl, Aichernig, Friedl, & Hofbauer, 2001). However, the use of oxygen requires an air separation unit, which results in a more expensive process, particularly for small-scale operations (Kirkels & Verbong, 2011; McKendry, 2002). Steam as a gasifying agent produces a syngas with higher H_2 content (30−60 vol%) and a moderate calorific value (10−16 MJ/m^3) comparable to that obtained when pure oxygen is used as a gasifying agent (Shen, Gao, & Xiao, 2008). However, the use of steam requires an external energy supply because of the endothermic reactions involved in the process, which adds complexity to the system. Carbon dioxide can also be used as a gasifying agent, as can a mixture of all the above (Wang et al., 2008).

Pu, Zhou, and Hao (2013) studied the effect of gasifying agents during pine gasification in a downdraft gasifier and compared air, oxygen, and steam as gasifying agents. They showed that the H_2 content increased with increasing air flow from 300 to 400 mL/min at 750 °C. This was attributed to an enhancement of the oxidation reactions resulting in a higher H_2 yield because the WGS and steam reforming reactions are endothermic.

6.3.3.2 *Effect of gasification temperature*

Temperature is the most significant parameter influencing the performance of a gasifier because the main gasification reactions are endothermic. With increasing temperature,

the concentration of produced syngas increases and that of CO_2, CH_4, and H_2O decreases (Emami Taba, Irfan, Wan Daud, & Chakrabarti, 2012). Lowering the temperature often helps reduce char conversion, leading to lower process efficiency and increasing the tar content in the syngas produced during gasification (Gómez-Barea, Ollero, & Leckner, 2013).

The equilibrium constant of the WGS reaction (Eqn (6.5)) decreases with increasing temperature, which favors the high conversion of CO and steam to H_2 and CO_2. The reaction is thermodynamically favored at low temperatures and kinetically favored at high temperatures. Therefore, the WGS reaction is favorable at low temperatures in the presence of catalysts that enhance the reaction rate (Bustamante et al., 2004).

Zhao et al. (2010) investigated the temperature effect on the gasification of sawdust in the presence of air as the gasifying agent in the temperature range 700−1000 °C. The formation of H_2 and CO_2 was enhanced with increased temperature, whereas the concentration of CO was decreased and that of CH_4 reached a maximum at 800 °C. The effect of temperature on the low heating value, cold gas efficiency, and carbon conversion was comparable to the concentration of CH_4, reaching a maximum at 800 °C. Similarly, Wu et al. (2009) studied the effect of temperature on the gas composition and heating rate during rice husk gasification in a fluidized-bed gasifier. The same trends were observed for H_2, CO, and CO_2 when increasing temperature; i.e., H_2 and CO_2 increased whereas CO decreased. On the other hand, CH_4 and the low heating value decreased with increasing temperature, in disagreement with the trends observed by Zhao et al. (2010).

Many of the problems encountered during the gasification process arise from temperature. If the temperature increases considerably, there may be the problems of sintering, buildup, erosion, and corrosion. Alkaline metals such as potassium can give rise to alkaline silicates and sulfates, which have melting points below 700 °C; these may become attached to the reactor walls, forming deposits that reduce process efficiency. Furthermore, the presence of these compounds in the syngas may cause similar problems in the electricity conversion equipment receiving the generated gas (Wang et al., 2008).

6.3.3.3 *Effect of gasification pressure*

High-pressure gasification reactions have two advantages. One is that the size of the gasifier can be greatly reduced depending on the applied pressure. Another is that the gas compression steps can be integrated when using processes such as Fischer−Tropsch synthesis and methanol and dimethylether synthesis, which are also carried out at high pressure. In addition, the gas cleaning step before synthesis can be performed at high pressure (Güell, Sandquist, & Sørum, 2013). Pressurized systems are mainly useful for large plants but often are not economical on a small scale (Kirkels & Verbong, 2011).

Fryda et al. modeled a gasification system combined with a solid oxide fuel cell and gas turbine and showed that increasing the pressure (atmospheric to 4 bar) did not have a major impact on the gasification process, although it affected turbine efficiency and the unit's overall efficiency (from 23% to 35%) (Fryda, Panopoulos, & Kakaras, 2008). Changing pressure does not have a major effect on the WGS reaction because

volume does not change from reactants to products. Valin et al. studied the effect of pressure (ranging from 2 to 10 bar) during wood sawdust gasification in a steam fluidized-bed gasifier at 800 °C and showed that the yields of H_2, CO_2, and CH_4 increased and that of CO decreased with increasing pressure. The evolution of H_2, CO, and CO_2 with pressure was attributed to an increase of the WGS constant owing to acceleration of the reaction kinetics with pressure and enhanced catalytic activity of the char. The increase in CH_4 with pressure was linked to an increase in secondary pyrolysis reactions (Valin, Ravel, Guillaudeau, & Thiery, 2010).

6.3.3.4 Effect of catalysts

Catalysts influence several of the reaction steps described in Section 6.2. Catalysts also have an important role in tar and char destruction during gasification, which ultimately improves the quality of the product gases. Two major types of catalysts are used in gasification processes: natural and synthetic (Sutton, Kelleher, & Ross, 2001). Dolomite and olivine are the most widely used natural catalysts. Dolomite is inexpensive and reduces the tar content effectively compared with olivine but olivine is more attrition-resistant than dolomite, which makes it convenient for fluidized-bed gasifiers (Alauddin, Lahijani, Mohammadi, & Mohamed, 2010; Devi, Craje, Thüne, Ptasinski & Janssen, 2005). Yu, Brage, Nordgreen, and Sjöström (2009) investigated several dolomites for gasification of birch to enhance tar cracking efficiency. The tar yield was found to decrease significantly from 12 to 23 mg/g_{birch} to 5 to 9 mg/g_{birch} when using dolomite catalysts.

Kirnbauer, Wilk, Kitzler, Kern, and Hofbauer (2012) investigated olivine as a bed material in a pilot-scale dual fluidized-bed gasifier for biomass gasification. The olivine used in an industrial-scale plant was reused in a pilot-scale plant and compared the fresh and used olivine, which had a significant influence on the gas composition and catalytic effects on tar conversion. The difference between the effects of fresh olivine and used olivine on the gasification properties is affected by the formation of a calcium-rich layer on the formed ash. The calcium-rich catalytic bed material enhances the exothermic WGS reaction, which increases H_2 formation while the CO content is decreased.

De Andres, Narros, and Rodríguez (2011) studied the effect of different bed materials such as olivine, alumina, and dolomite on the products of sewage sludge gasification with air and air−steam mixtures in a fluidized-bed gasifier. Tar production was significantly reduced by using dolomite compared with olivine. Alumina and dolomite increased the production of H_2 and CO and decreased the production of CH_4, CO_2, and C_nH_m owing to cracking reactions and steam and CO_2 reforming reactions. The combined use of a catalyst and steam increased H_2 and CO_2 and decreased the CH_4, CO, and C_nH_m content of the gases by enhancing the WGS and reforming reactions. Additional tar elimination was found when steam was used in the presence of a catalyst, but in these catalyzed tests, steam improved the quality of the gas (higher hydrogen production and lower tar content) and had no significant influence on cold gas efficiency or carbon conversion.

Three main classes of synthetic heterogeneous catalysts are used in gasifiers: alkali-based, nickel-based, and noble metal-based. Alkali-based catalysts are expensive but have the capacity to enhance gasification rates (Weerachanchai, Horio, &

Tangsathitkulchai, 2009). Nickel-based catalysts have been widely used owing to their high activity for steam reforming of hydrocarbons and tars at relatively low temperatures and because they lead to high percentages of H_2 and CO in the product gas mixtures. However, the major problems of nickel-based catalysts are that they have a high thermodynamic potential for coke formation in a high-temperature gasifier, which blocks the catalyst active sites; they are easily deactivated during longer reaction times and are not thermodynamically stable; and nickel sintering occurs, i.e., nickel particles grow, resulting in a decrease in the catalytic active sites (Hou, Yokota, Tanaka, & Yashima, 2003; Zhang, Xu, & Champagne, 2012). Noble metal-based catalysts are highly resistant to carbon deposition but are less attractive in view of their higher cost (Li et al., 2007; Mukainakano et al., 2007).

Lin, Peng, and Chen (2013) investigated the effect of Na and K on gas production in a fluidized-bed gasifier during gasification of sawdust, polypropylene plastic granules, and polyethylene plastic; results showed that the molar percentage of H_2 and CO increased. The total gas yield, carbon conversion efficiency, and cold gas efficiency also increased. Moreover, the addition of 0.7 wt% Na and K increased the molar percentages of H_2 from 12% to 23.6% and from 12% to 29%, respectively. Kuchonthara, Vitidsant, and Tsutsumi (2008) found a trend similar to that of Lin et al. (2013) when they used K_2CO_3 as the bed material for lignin gasification. K_2CO_3 also promoted the conversion of tars, resulting in higher carbon conversion efficiency.

Ammendola et al. (2010) compared the catalytic performance of a novel $Rh/LaCoO_3/Al_2O_3$ catalyst with that of dolomite, olivine, and Ni/Al_2O_3 during gasification of maple wood chips in a dual fluidized-bed laboratory scale gasifier. The $Rh/LaCoO_3/Al_2O_3$ catalyst showed the highest reforming activity toward tars, methane, and light hydrocarbons while increasing CO formation and decreasing CO_2 production. This catalytic system also showed the lowest total oxidation and cracking activities in tar conversion compared with the other catalysts. Among all catalysts, only the $Rh/LaCoO_3/Al_2O_3$ sample was able to oxidize methane emitted from biomass pyrolysis in the range 390−660 °C to CO_2. Ni/Al_2O_3 and dolomite favored coke formation and increased CO_2 production. The comparison between Ni/Al_2O_3 and dolomite also showed that the Ni catalyst had a slightly higher reforming activity, which led to a decrease in CO_2, CH_4, and light hydrocarbons and an increase in CO production. Compared with dolomite and Ni/Al_2O_3, olivine showed much less oxidation, reforming, and cracking activity.

6.4 Advantages and disadvantages of gasification of biomass and opportunity fuels

6.4.1 Advantages of gasification

Gasification has several advantages that make it attractive as a conversion technology for biomass and opportunity fuels.

6.4.1.1 Gasification occurs at lower temperatures than combustion

Because gasification is a lower-temperature process compared with combustion, gasifiers can have longer lifetimes and lower maintenance costs than combustors such as wood-fired boilers. Because the formation of NO_x and SO_x is enhanced at higher temperature, environmental pollution is minimized by using a gasification process.

6.4.1.2 Gasification produces different types of products

The gasification of biomass produces syngas, bio-oils, biochar, and ash. Syngas can be used as a feedstock to produce synthetic fuels such as ethanol, methanol, naphtha, gasoline, and diesel. The bio-oils, biochar, and ash may sometimes be used for products such as soil amendments, filtration media, and cement additives.

6.4.1.3 Gasification has synergies with existing fossil fuel infrastructure

Gasification has synergies with fossil fuel use that can facilitate our transition to renewable energy. As an example of a synergistic opportunity, liquid transportation fuels produced from syngas can be distributed throughout our current fueling infrastructure. Also, syngas and producer gas can be cofired with natural gas in conventional turbines and fuel cells or cofired in coal-fired boilers to generate electricity. Biohydrogen produced from syngas can be used in conjunction with hydrogen produced from natural gas. Facilities that currently use coal syngas in the production of chemicals can supplement it with syngas obtained from biomass using existing infrastructure.

6.4.1.4 Transportation of gaseous fuels is more convenient compared with solid biomass

If a gasifier is situated in a location with ready availability of feedstocks, gaseous fuels can be distributed directly from the gasification plant to consumers through pipelines. On the other hand, available space within a manufacturing facility may prohibit locating a biomass-fired boiler or furnace and its ancillary equipment within the facility. In that case, a gasifier could be located elsewhere with the product gas piped to the point of use.

6.4.1.5 Use of turbines, engines, and fuel cells increases the efficiency of electricity generation

Higher efficiency and lower emissions of pollutants during gasification compared with combustion make gaseous fuels suitable for use in reciprocating engines, gas turbines, and fuel cells to generate electricity. Syngas-fueled engines and turbines can achieve 30–40% efficiency whereas 20–25% efficiencies are achieved by a biomass-fired steam turbine.

6.4.1.6 Gasification makes biomass-fired integrated combined cycles possible

Gasification can provide a highly efficient technology for generating electricity, referred to as an IGCC. Such a system can achieve high electrical efficiencies of 42–48%. Sometimes 60–90% efficiency can be achieved if low-pressure steam is also recovered from the steam turbine. IGCC systems are cost-effective only on larger scales because of the high capital cost of the gasifier, gas turbine, boiler, and steam turbine, plus ancillary equipment.

6.4.2 Disadvantages of gasification and possible measures

When choosing an energy-efficient technology for converting feedstocks into heat and energy in the form of H_2, the main problem is the formation of byproducts such as fly ash, NO_x, SO_x, and tar. Before using the syngas or producer gas for other applications, these impurities must be removed to avoid further problems. Tar removal and ash agglomeration are two major disadvantages of commercializing the gasification process, which will be examined below.

6.4.2.1 Tar removal

Tar production in gasification can be minimized by using primary and secondary methods. In the primary method, operating variables such as the gasifying agent, temperature, equivalence ratio, residence time, and type of catalyst have an important role in the formation and destruction of tar (Cao et al., 2006). Warnecke (2000) achieved 99% removal of tar using dolomite- and nickel-based and other catalysts at temperatures of 802–902 °C. Chaiprasert and Vitidsant (Chaiprasert & Vitidsant, 2009) reported that the tar yield decreased from 19.6% to 1.4% at 802 °C during coconut shell gasification in the presence of a nickel–dolomite catalyst.

A great amount of effort concerning tar reduction during gasification has been reported (Han & Kim, 2008). Hasler used a venturi scrubber to purify product gases from a countercurrent rice husk gasifier and obtained tar separation efficiencies ranging from 51% to 91% (Hasler, 1997). Bridgwater (1995) reduced tar concentration in product gases to lower than 20–40 mg/Nm^3 using a high-efficiency scrubber system. Jansen, Jonsson, and Hagman (2002) lowered tar levels to 20–40 mg/m^3 and particulate levels to 10–20 mg/m^3 using a water scrubber.

Table 6.3 shows tar reduction efficiency in various gas cleaning systems (Hasler & Nussbaumer, 1999).

In 2001, the Energy Research Center of the Netherlands (ECN) started developing a new technology called OLGA (*OLGA* is the Dutch acronym for oil-based gas washer) to establish tar removal from syngas on the basis of a nonwater scrubbing liquid (Bergman, van Paasen, & Boerrigter, 2002).

Table 6.4 shows the typical tar content in producer gas depending on the type of technology used (Morf, 2001).

Table 6.3 Reduction efficiency of particle and tar in various gas cleaning systems (Hasler & Nussbaumer, 1999)

	Particle reduction (%)	Tar reduction (%)
Sand bed filter	70–99	50–97
Wash tower	60–98	10–25
Venture scrubber	–	50–90
Wet electrostatic precipitator	>99	0–60
Fabric filter	70–95	0–50
Rotational particle separator	85–90	30–70
Fixed-bed tar adsorber	–	50

Table 6.4 Tar content in different gasifiers (Han & Kim, 2008)

	Fixed bed		Fluidized bed	
	Updraft	Downdraft	Bubbling	Circulating
Mean tar content (g/Nm^3)	50	0.5	12	8
Range of tar (g/Nm^3)	10–150	0.01–6	1–23	1–30

Pan, Roca, Velo, and Puigjaner (1999) reported that secondary air injection above the feeding point in a fluidized-bed gasifier reduced the total tar by 88.7 wt% from 840 to 880 °C. Sun, Zhao, Ling, and Su (2009) conducted a similar study for rice husk gasification and reported that tars were thermally cracked in the high temperature zone. Higher gasification temperatures almost always achieve high conversion efficiency and low tar content in syngas (Lucas, Szewczyk, Blasiak, & Mochida, 2004). Narvaez, Orio, Aznar, and Corella (1996) observed a drastic decrease in tar content from 19 g/Nm^3 at 700 °C to 5 g/Nm^3 at 800 °C during biomass gasification in a BFB gasifier. However, too high of an operating temperature will reduce energy efficiency and increase the possibility of ash sintering and agglomeration (Devi, Ptasinski, & Janssen, 2003). Pressurized gasification has also been studied for tar reduction (Knight, 2000). Kinoshita, Wang, and Zhou (1994) and Narvaez et al. (1996) studied the effect of the equivalence ratio (ER) on reducing tar concentration during biomass gasification and reported the optimum ER value ranges from 0.2 to 0.4. Increasing the ER value enhances the availability of O_2 into the gasifier to react with volatiles of tar. However, a high ER may also cause low concentrations of H_2 and CO with high CO_2 content in the product gas, resulting in a low heating value of the product gas.

Thermal and catalytic cracking

Thermal cracking occurs during gasification at high temperatures when tar molecules are decomposed into lighter gases. Biomass-derived tar is hard to crack by thermal

Table 6.5 Main catalysts for tar reforming (Wang et al., 2008)

Catalyst types	Representative catalysts	Main advantages	Technical challenges
Natural catalysts	Dolomite, olivine, Clay, Zeolite	Cheap	Moderate reforming efficiency Easily eroded and broken
Alkali and salts	KOH, $KHCO_3$, K_2CO_3	High reforming efficiency Increased hydrogen in syngas	Increased plugging and deactivation of other metal catalysts at a high temperature
Stable metal with oxide support	NiO/Al_2O_3, $Ni/CeO_2/Al_2O_3$, $RhCeO_2SiO_2$, $LaNi_{0.3}Fe_{0.7}O_3$	High reforming efficiency Increased hydrogen content in syngas	Stable metals are expensive Metals are easily deactivated by coke, poisoned by H_2S, and sintered by ash melting Require hot water−resistant support materials

treatment alone. To decompose the tar effectively, it has been suggested to increase the gasifier residence time (Bridgwater, 1995). Partial oxidation by adding air or oxygen can increase CO levels at the expense of decreasing conversion efficiency while increasing operational costs (Bridgwater, 1995). Brandt and Henriksen (2000) reported that the necessary temperature and residence time were 1250 °C and 0.5 s, respectively, to achieve the highest tar cracking efficiency in an updraft gasifier with a flow of tar loaded gas as input. Houben (2003) also carried out thermal tar cracking experiments using naphthalene as a model compound for tar at temperatures from 900 to 1150 °C and residence times between 1 and 12 s; the researcher achieved 98−99% tar reduction efficiency at 900 °C with an excess air ratio of 0.5.

Catalytic cracking of tars has been of interest since the mid-1980s, when both pilot and demonstration plants gave encouraging results (Han & Kim, 2008). Tar conversion in excess of 99% has been achieved using dolomite- and nickel-based and other catalysts at elevated temperatures typically of 800−900 °C. Table 6.5 shows the main catalysts used in gasifiers for reducing tar.

6.4.2.2 Ash agglomeration mechanism and reduction

The other major problem with gasifiers is sintering, agglomeration, deposition, erosion, and corrosion if ash is present in the system. Alkali metals such as potassium

react readily with silica, even at temperatures far below 900 °C, by breaking the Si−O−Si bond and forming silicates or reacting with sulfur to produce alkali sulfates. The alkali silicates and sulfates have melting points even lower than 700 °C and tend to deposit on the reactor walls and leave a sticky deposit on the surface of the bed particles, causing sintering and defluidization (Arvelakis, Gehrmann, Beckmann, & Koukios, 2002, 2005). Fluidized-bed gasification performs better than fixed-bed gasification to reduce ash-related problems because the bed temperature of fluidized beds can be kept uniformly below the ash slagging temperature. The low gasification temperature can also reduce the volatilization of ash elements such as sodium and potassium into the syngas, thus improving the quality of syngas (Gabra, Pettersson, Backman, & Kjellström, 2001).

6.4.3 Conditions for commercial application

Gasification has been considered close to commercialization. However, many issues still need to be addressed:

1. Gasification technology must have a better theoretical framework with proven prototypes and long-term duration testing.
2. A sustainable feedstock supply is required.
3. Motivated and skilled labor forces are required.
4. Scale-up, demonstration, replication, and optimization are required to commercialize the technology. Demonstration and familiarity with technology are critical whereas replication and optimization will help reduce capital costs.
5. Information and knowledge exchange between universities and companies are important for pursuing this technology.
6. Clear regulations on emission standards and other health and safety aspects are needed.

6.5 Future trends

Hydrogen gas will be used worldwide as an energy carrier complementing electricity in the foreseeable future, but the production technology for H_2 needs to be economically feasible and environmental friendly and ensure H_2 quality criteria. To overcome the challenges to enabling commercialization (stated in Section 6.4.3), multiple collaborators need to have an active role in promoting the industrialization of biorefinery systems. Biorefineries may have an important role in minimizing global warming by supplementing demand for sustainable energy, chemicals, and materials, potentially aiding energy security and independence, and creating new opportunities and markets in a move toward bio-based manufacturing. The growth of a partially bio-based economy will help foster economic growth and job creation opportunities, particularly in rural areas where incomes and economic prospects are limited.

Future biorefineries will be analogous to modern oil refineries, using biomass or opportunity fuels as feedstocks, thereby causing a transition from fossil carbon to more sustainable bio-based production across all industries. This could fundamentally

reshape the industrial landscape and have particular impact on energy security and climate change, creating markets and collaboration.

The basic principle of biorefinery is that each biorefinery should convert its corresponding feedstock into a multitude of valuable products that may be produced in an oil refinery, but also those that may not be accessible in oil refineries.

6.6 Sources of further information and advice

The following resources are available for more information on opportunity fuels or biomass-fired combined heat and power systems.

6.6.1 International Energy Agency

The International Energy Agency is an excellent online source for current updates on the status of thermal gasification technology and projects worldwide, including North America. The main Web page for their Task 33: Thermal Gasification program can be found at http://www.ieatask33.org/

6.6.2 National Renewable Energy Laboratory

The National Renewable Energy Laboratory's biomass research Web site is: http://www.nrel.gov/biomass/

6.6.3 United States (US) Department of Energy

Information about types of opportunity fuels and conversion technologies are available at the Department of Energy's Web site: http://www.maceac.psu.edu/clean_energy_opportunity_fuels_biomass.html.

6.6.4 United States Environmental Protection Agency

Information about combined heat and power (CHP) technologies and CHP policies and incentives are available in the US Environmental Protection Agency Web site: http://www.epa.gov/chp/index.html.

6.6.5 Biomass Magazine

Information about current updates on biomass are available at this Web site: http://www.biomassmagazine.com/

6.6.6 Oak Ridge National Laboratory

Oak Ridge National Laboratory has a database of biomass characteristics available at http://cta.ornl.gov/bedb/appendix_b.shtml.

6.6.7 Energy Research Center of The Netherlands

The ECN https://www.ecn.nl/ has compiled a number of resources on renewable energy. Among them, Phyllis 2 is an extensive database of information on the composition of biomass and waste at https://www.ecn.nl/phyllis2/.

6.6.8 Sustainable Development Technology Canada

Canada is a world leader in the production and use of energy from renewable resources, which currently provides about 16% of Canada's total primary energy supply. Information is available at the Sustainable Development Technology Canada Web site: http://www.sdtc.ca/index.php?page=alias-9

6.6.9 Natural Resources Canada

The overall scenario of Canada's bioenergy is available at the Natural Resources Canada Web site: http://www.nrcan.gc.ca/energy/renewable/1297#bio.

6.6.10 Clean Energy

Information about biomass in Canada is available at the Clean Energy Web site: http://www.cleanenergy.gc.ca/index.cfm?action=cantechdir_techsub.summary&sid=39.

6.6.11 European Biomass Industry Association

Biomass status in Europe is available at the European Biomass Industry Web site: http://www.eubia.org/

6.6.12 Biomass Energy Europe

Methodologies for biomass resource assessments for energy purposes in Europe and its neighboring countries are available at the Biomass Energy Europe Web site: http://www.eu-bee.com/.

6.6.13 Clean Energy Application Centers

The US Department of Energy's Industrial Technologies Program and its eight regional Clean Energy Application Centers provide assistance to facilities considering CHP, district energy, and waste energy recovery. These centers offer technology, application, and project development information, case studies and other publications, workshops and other educational opportunities, and contacts for local resources.

1. US Clean Heat and Power Association
   http://www.uschpa.org
2. Gulf Coast Clean Energy Application Center
   Texas, Louisiana, and Oklahoma
   http://www.gulfcoastchp.org

3. Intermountain Clean Energy Application Center
   Arizona, Colorado, New Mexico, Utah, and Wyoming
   http://www.intermountainchp.org
4. Mid-Atlantic Clean Energy Application Center
   Delaware, Maryland, New Jersey, Pennsylvania, Virginia, West Virginia, and Washington, DC
   http://www.chpcenterma.org
5. Midwest Clean Energy Application Center
   Illinois, Indiana, Iowa, Michigan, Minnesota, Missouri, Ohio, and Wisconsin
   http://www.chpcentermw.org
6. Northeast Clean Energy Application Center
   Connecticut, Maine, Massachusetts, New Hampshire, New York, Rhode Island, Vermont, Alaska, Idaho, Montana, Oregon, and Washington
   http://www.northeastchp.org
7. Pacific Region Clean Energy Application Center
   California, Hawaii, and Nevada
   http://www.chpcenterpr.org
8. Southeast Clean Energy Application Center
   Alabama, Arkansas, Florida, Georgia, Kentucky, Mississippi, South Carolina, North Carolina, and Tennessee
   http://www.chpcenterse.org

List of acronyms

BFB	Bubbling fluidized bed
CHP	Combined heat and power
ECN	Energy Research Center of The Netherlands
FBC	Fluidized-bed combustor
FPW	Food processing waste
HCPs	Heat carrier particles
IGCC	Integrated gasification combined cycle
LHV	Low heating value
LPG	Liquefied petroleum gas
SCW	Supercritical water
SCWG	Supercritical water gasification
T-DFBG	Two-stage dual fluidized-bed gasifier
TFB	Two-stage fluidized bed
TRI	Thermochem Recovery International, Baltimore, Maryland
WGS	Water gas shift reaction

References

Alauddin, Z. A. B. Z., Lahijani, P., Mohammadi, M., & Mohamed, A. R. (2010). Gasification of lignocellulosic biomass in fluidized beds for renewable energy development: a review. *Renewable and Sustainable Energy Reviews, 14*(9), 2852−2862.

Alternatives, C.o. and Strategies. (2004). *The hydrogen economy: Opportunities, costs, barriers, and R&D needs*. United States: Department of Energy. Office of Energy Efficiency and Renewable Energy.

Alves, S., & Figueiredo, J. (1988). Pyrolysis kinetics of lignocellulosic materials by multistage isothermal thermogravimetry. *Journal of analytical and applied pyrolysis, 13*(1), 123−134.

Ammendola, P., Piriou, B., Lisi, L., Ruoppolo, G., Chirone, R., & Russo, G. (2010). Dual bed reactor for the study of catalytic biomass tars conversion. *Experimental Thermal and Fluid Science, 34*(3), 269−274.

Arena, U. (2012). Process and technological aspects of municipal solid waste gasification. A review. *Waste management, 32*(4), 625−639.

Arvelakis, S., Gehrmann, H., Beckmann, M., & Koukios, E. G. (2002). Effect of leaching on the ash behavior of olive residue during fluidized bed gasification. *Biomass and Bioenergy, 22*(1), 55−69.

Arvelakis, S., Gehrmann, H., Beckmann, M., & Koukios, E. G. (2005). Preliminary results on the ash behavior of peach stones during fluidized bed gasification: evaluation of fractionation and leaching as pre-treatments. *Biomass and Bioenergy, 28*(3), 331−338.

Arvelakis, S., & Koukios, E. (2002). Physicochemical upgrading of agroresidues as feedstocks for energy production via thermochemical conversion methods. *Biomass and Bioenergy, 22*(5), 331−348.

Bae, J.-S., Lee, D.-W., Park, S.-J., Lee, Y.-J., Hong, J.-C., Ra, H. W., et al. (2012). High-pressure gasification of coal water ethanol slurry in an entrained flow gasifier for bioethanol application. *Energy & Fuels, 26*(9), 6033−6039.

Balat, M. (2008). Mechanisms of thermochemical biomass conversion processes. Part 2: reactions of gasification. *Energy Sources, Part A, 30*(7), 636−648.

Balat, M., Balat, M., Kırtay, E., & Balat, H. (2009). Main routes for the thermo-conversion of biomass into fuels and chemicals. Part 2: gasification systems. *Energy conversion and management, 50*(12), 3158−3168.

Basu, P. (2010). *Biomass gasification and pyrolysis: Practical design and theory*. Academic Press.

Beenackers, A. (1999). Biomass gasification in moving beds, a review of European technologies. *Renewable Energy, 16*(1), 1180−1186.

Bergman, P. C., van Paasen, S. V., & Boerrigter, H. (2002). The novel "OLGA" technology for complete tar removal from biomass producer gas. In *Pyrolysis and gasification of biomass and waste, expert meeting, Strasbourg, France*.

Berry, G. D., Pasternak, A. D., Rambach, G. D., Smith, J. R., & Schock, R. N. (1996). Hydrogen as a future transportation fuel. *Energy, 21*(4), 289−303.

Boerrigter, H., Drift, A. V. D., Hazewinkel, J. H. O., & Küpers, G. (2004). *Biosyngas: Multi-functional intermediary for the production of renewable power, gaseous energy carriers, transportation fuels, and chemicals from biomass*. Petten, Netherlands: Energy Research Centre of the Netherlands. Final report of the OTC Project (ECN-04-112).

Brammer, J., & Bridgwater, A. (2002). The influence of feedstock drying on the performance and economics of a biomass gasifier−engine CHP system. *Biomass and Bioenergy, 22*(4), 271−281.

Brandt, P., & Henriksen, U. B. (2000). Decomposition of tar in gas from updraft gasifier by thermal cracking. *Proceedings of 1st World Conference on Biomass for Energy and Industry in Sevilla, Spain, 5−9 June 2000*. London: James & James (Science Publishers) Ltd.

Breault, R. W. (2010). Gasification processes old and new: a basic review of the major technologies. *Energies, 3*(2), 216−240.

Bridgwater, A. (1995). The technical and economic feasibility of biomass gasification for power generation. *Fuel, 74*(5), 631−653.

Bustamante, F., Enick, R. M., Cugini, A. V., Killmeyer, R. P., Howard, B. H., Rothenberger, K. S., et al. (2004). High-temperature kinetics of the homogeneous reverse water−gas shift reaction. *AIChE Journal, 50*(5), 1028−1041.

California, U.o. (2009). *Evaluation of emissions from thermal conversion technologies processing municipal solid waste and biomass*. Final report for Bioenergy Producers Ass. Available on: www.bioenergyproducers.org/documents/ucr_emissions_report.pdf.

Calzavara, Y., Joussot-Dubien, C., Boissonnet, G., & Sarrade, S. (2005). Evaluation of biomass gasification in supercritical water process for hydrogen production. *Energy Conversion and Management, 46*(4), 615−631.

Campbell, C. J., & Duncan, R. C. (1997). *The coming oil crisis*. Multi-Science Publishing.

Cao, Y., Wang, Y., Riley, J. T., & Pan, W. (2006). A novel biomass air gasification process for producing tar-free higher heating value fuel gas. *Fuel Processing Technology, 87*(4), 343−353.

Chaiprasert, P., & Vitidsant, T. (2009). Promotion of coconut shell gasification by steam reforming on nickel-dolomite. *American Journal of Applied Sciences, 6*(2), 332.

Chen, J., Lu, Y., Guo, L., Zhang, X., & Xiao, P. (2010). Hydrogen production by biomass gasification in supercritical water using concentrated solar energy: system development and proof of concept. *International Journal of Hydrogen Energy, 35*(13), 7134−7141.

Chisti, Y. (2008). Biodiesel from microalgae beats bioethanol. *Trends in Biotechnology, 26*(3), 126−131.

Chowdhury, M. B., Hossain, M. M., & Charpentier, P. A. (2011). Effect of supercritical water gasification treatment on Ni/La_2O_3-Al_2O_3-based catalysts. *Applied Catalysis A: General, 405*(1), 84−92.

Combined heat and power market potential for opportunity fuels. (2004). Resourcr Dynamics Co-operation, US Department of Energy.

Corella, J., Herguido, J., & Alday, F. (1988). Pyrolysis and steam gasification of biomass in fluidized beds. Influence of the type and location of the biomass feeding point on the product distribution. In *Research in thermochemical biomass conversion* (pp. 384−398). Springer.

Crabtree, G. W., & Dresselhaus, M. S. (2008). The hydrogen fuel alternative. *Mrs Bulletin, 33*(04), 421−428.

Cummer, K. R., & Brown, R. C. (2002). Ancillary equipment for biomass gasification. *Biomass and Bioenergy, 23*(2), 113−128.

De Andres, J. M., Narros, A., & Rodríguez, M. E. (2011). Behaviour of dolomite, olivine and alumina as primary catalysts in air−steam gasification of sewage sludge. *Fuel, 90*(2), 521−527.

Demirbaş, A. (2002). Gaseous products from biomass by pyrolysis and gasification: effects of catalyst on hydrogen yield. *Energy Conversion and Management, 43*(7), 897−909.

Devi, L., Craje, M., Thüne, P., Ptasinski, K. J., & Janssen, F. J. J. G. (2005). Olivine as tar removal catalyst for biomass gasifiers: catalyst characterization. *Applied Catalysis A: General, 294*(1), 68−79.

Devi, L., Ptasinski, K. J., & Janssen, F. J. (2003). A review of the primary measures for tar elimination in biomass gasification processes. *Biomass and Bioenergy, 24*(2), 125−140.

Emami Taba, L., Irfan, M. F., Wan Daud, W. A. M., & Chakrabarti, M. H. (2012). The effect of temperature on various parameters in coal, biomass and CO-gasification: a review. *Renewable and Sustainable Energy Reviews, 16*(8), 5584−5596.

Fabry, F., Rehmet, C., Rohani, V., & Fulcheri, L. (2013). Waste gasification by thermal plasma: a review. *Waste and Biomass Valorization, 4*(3), 421−439.

Franco, C., Pinto, F., Gulyurtlu, I., & Cabrita, I. (2003). The study of reactions influencing the biomass steam gasification process. *Fuel, 82*(7), 835−842.

Fryda, L., Panopoulos, K., & Kakaras, E. (2008). Integrated CHP with autothermal biomass gasification and SOFC−MGT. *Energy Conversion and Management, 49*(2), 281−290.

Gabra, M., Pettersson, E., Backman, R., & Kjellström, B. (2001). Evaluation of cyclone gasifier performance for gasification of sugar cane residue—part 1: gasification of bagasse. *Biomass and Bioenergy, 21*(5), 351−369.

Gil, J., Corella, J., Aznar, M. P., & Caballero, M. A. (1999). Biomass gasification in atmospheric and bubbling fluidized bed: effect of the type of gasifying agent on the product distribution. *Biomass and Bioenergy, 17*(5), 389−403.

Gómez-Barea, A., Ollero, P., & Leckner, B. (2013). Optimization of char and tar conversion in fluidized bed biomass gasifiers. *Fuel, 103*, 42−52.

Güell, B. M., Sandquist, J., & Sørum, L. (2013). Gasification of biomass to second generation biofuels: a review. *Journal of Energy Resources Technology-Transactions of the ASME, 135*(1), 014001, (1−9).

Han, J., & Kim, H. (2008). The reduction and control technology of tar during biomass gasification/pyrolysis: an overview. *Renewable and Sustainable Energy Reviews, 12*(2), 397−416.

Hasler, P. (1997). *Evaluation of gas cleaning technologies for small scale biomass gasifiers*. Zurich: Swiss Federal Office of Energy and Swiss Federal Office for Education and Science.

Hasler, P., & Nussbaumer, T. (1999). Gas cleaning for IC engine applications from fixed bed biomass gasification. *Biomass and Bioenergy, 16*(6), 385−395.

Henrich, E., & Weirich, F. (2004). Pressurized entrained flow gasifiers for biomass. *Environmental Engineering Science, 21*(1), 53−64.

Hernández, J. J., Aranda-Almansa, G., & Bula, A. (2010). Gasification of biomass wastes in an entrained flow gasifier: effect of the particle size and the residence time. *Fuel Processing Technology, 91*(6), 681−692.

Hernandez, J. J., Aranda, G., Barba, J., & Mendoza, J. M. (2012). Effect of steam content in the air−steam flow on biomass entrained flow gasification. *Fuel Processing Technology, 99*, 43−55.

Hofbauer, H., Rauch, R., Loeffler, G., Kaiser, S., Fercher, E., & Tremmel, H. (2002). Six years experience with the FICFB-gasification process. In *12th European conference and technology exhibition on biomass for energy, industry and climate protection*.

Hou, Z., Yokota, O., Tanaka, T., & Yashima, T. (2003). Characterization of Ca-promoted Ni/α-Al_2O_3 catalyst for CH_4 reforming with CO_2. *Applied Catalysis A: General, 253*(2), 381−387.

Houben, M. (2003). *Analysis of tar removal in a partial oxidation burner*. Technische Universiteit Eindhoven.

Huang, C.-Y. (1992). Apparatus and method for supercritical water oxidation. Google Patents.

Jansen, J. L., Jonsson, K., & Hagman, M. (2002). Biological detoxification of tar-water. *Water Science & Technology, 46*(4−5), 59−65.

Kaiser, S., Weigl, K., Aichernig, Ch., Friedl, A., & Hofbauer, H. (2001). Simulation of a highly efficient dual fluidized bed gasification process. In *3rd European congress on chemical engineering, Nürnberg*.

Kinoshita, C., Wang, Y., & Zhou, J. (1994). Tar formation under different biomass gasification conditions. *Journal of Analytical and Applied Pyrolysis, 29*(2), 169−181.

Kirkels, A. F., & Verbong, G. P. (2011). Biomass gasification: still promising? A 30-year global overview. *Renewable and Sustainable Energy Reviews, 15*(1), 471−481.

Kirubakaran, V., Sivaramakrishnan, V., Nalini, R., Sekar, T., Premalatha, M., & Subramanian, P. (2009). A review on gasification of biomass. *Renewable and Sustainable Energy Reviews, 13*(1), 179−186.

Kirnbauer, F., Wilk, V., Kitzler, H., Kern, S., & Hofbauer, H. (2012). The positive effects of bed material coating on tar reduction in a dual fluidized bed gasifier. *Fuel, 95*, 553−562.

Knight, R. A. (2000). Experience with raw gas analysis from pressurized gasification of biomass. *Biomass and Bioenergy, 18*(1), 67−77.

Knox, A. (2005). *An overview of incineration and EFW technology as applied to the management of municipal solid waste (MSW)*. ONEIA Energy Subcommitte.

Kritzer, P. (2004). Corrosion in high-temperature and supercritical water and aqueous solutions: a review. *The Journal of Supercritical Fluids, 29*(1−2), 1−29.

Kruse, A. (2008). Supercritical water gasification. *Biofuels, Bioproducts and Biorefining, 2*(5), 415−437.

Kruse, A., Forchheim, D., Gloede, M., Ottinger, F., & Zimmermann, J. (2010). Brines in supercritical biomass gasification: 1. Salt extraction by salts and the influence on glucose conversion. *The Journal of Supercritical Fluids, 53*(1), 64−71.

Kuchonthara, P., Vitidsant, T., & Tsutsumi, A. (2008). Catalytic effects of potassium on lignin steam gasification with γ-Al_2O_3 as a bed material. *Korean Journal of Chemical Engineering, 25*(4), 656−662.

Kumar, A., Jones, D. D., & Hanna, M. A. (2009). Thermochemical biomass gasification: a review of the current status of the technology. *Energies, 2*(3), 556−581.

Lapuerta, M., Hernández, J. J., Pazo, A., & López, J. (2008). Gasification and co-gasification of biomass wastes: effect of the biomass origin and the gasifier operating conditions. *Fuel Processing Technology, 89*(9), 828−837.

Liao, B., Guo, L., Lu, Y., & Zhang, X. (2013). Solar receiver/reactor for hydrogen production with biomass gasification in supercritical water. *International Journal of Hydrogen Energy, 38*(29), 13038−13044.

Li, X. T., Grace, J. R., Lim, C. J., Watkinson, A. P., Chen, H. P., & Kim, J. R. (2004). Biomass gasification in a circulating fluidized bed. *Biomass and Bioenergy, 26*(2), 171−193.

Li, B., Kado, S., Mukainakano, Y., Miyazawa, T., Miyao, T., Naito, S., et al. (2007). Surface modification of Ni catalysts with trace Pt for oxidative steam reforming of methane. *Journal of Catalysis, 245*(1), 144−155.

Link, S., Arvelakis, S., Paist, A., Martin, A., Liliedahl, T., & Sjöström, K. (2012). Atmospheric fluidized bed gasification of untreated and leached olive residue, and co-gasification of olive residue, reed, pine pellets and Douglas fir wood chips. *Applied Energy, 94*, 89−97.

Lin, C.-L., Peng, T.-H., & Chen, H. (2013). Effect of Na and K on gas production during simulated municipal waste gasification process. *Energy & Fuels, 27*(9), 5307−5312.

Liu, H., Kaneko, M., Luo, C., Kato, S., & Kojima, T. (2004). Effect of pyrolysis time on the gasification reactivity of char with CO_2 at elevated temperatures. *Fuel, 83*(7), 1055−1061.

Lucas, C., Szewczyk, D., Blasiak, W., & Mochida, S. (2004). High-temperature air and steam gasification of densified biofuels. *Biomass and Bioenergy, 27*(6), 563−575.

Luo, S., Xiao, B., Guo, X., Hu, Z., Liu, S., & He, M. (2009). Hydrogen-rich gas from catalytic steam gasification of biomass in a fixed bed reactor: influence of particle size on gasification performance. *International Journal of Hydrogen Energy, 34*(3), 1260−1264.

Lv, P., Chang, J., Wang, T., Fu, Y., Chen, Y., & Zhu, J. (2004). Hydrogen-rich gas production from biomass catalytic gasification. *Energy & Fuels, 18*(1), 228−233.

Mahishi, M. R., & Goswami, D. (2007). Thermodynamic optimization of biomass gasifier for hydrogen production. *International Journal of Hydrogen Energy, 32*(16), 3831−3840.

Marbán, G., & Valdés-Solís, T. (2007). Towards the hydrogen economy? *International Journal of Hydrogen Energy, 32*(12), 1625−1637.

Marquard-Möllenstedt, T., Sichler, P., Specht, M., Michel, M., Berger, R., Hein, K. R. G., et al. (2004). New approach for biomass gasification to hydrogen. In *2nd world conference on biomass for energy, industry and climate protection*.

Maschio, G., Lucchesi, A., & Stoppato, G. (1994). Production of syngas from biomass. *Bioresource Technology, 48*(2), 119−126.

McKendry, P. (2002). Energy production from biomass (part 3): gasification technologies. *Bioresource Technology, 83*(1), 55−63.

Mitsui recycling 21 pyrolysis gasification and melting process for municipal waste. (2011). Japanese Advanced Environment Equipment.

Morf, P. O. (2001). *Secondary reactions of tar during thermochemical biomass conversion* (Technical Sciences thesis). Zürich: Swiss Federal Institute of Technology.

Morrin, S., Lettieri, P., Chapman, C., & Mazzei, L. (2012). Two stage fluid bed-plasma gasification process for solid waste valorisation: technical review and preliminary thermodynamic modelling of sulphur emissions. *Waste management, 32*(4), 676−684.

Mukainakano, Y., Li, B., Kado, S., Miyazawa, T., Okumura, K., Miyao, T., et al. (2007). Surface modification of Ni catalysts with trace Pd and Rh for oxidative steam reforming of methane. *Applied Catalysis A: General, 318*, 252−264.

Munzinger, M., & Lovegrove, K. (2006). Biomass gasification using solar thermal energy. In *Proceedings of ANZSES annual conference*. Solar.

Narvaez, I., Orio, A., Aznar, M. P., & Corella, J. (1996). Biomass gasification with air in an atmospheric bubbling fluidized bed. Effect of six operational variables on the quality of the produced raw gas. *Industrial & Engineering Chemistry Research, 35*(7), 2110−2120.

Öhrman, O. G., Weiland, F., Pettersson, E., Johansson, A., Hedman, H., & Pedersen, M. (2013). Pressurized oxygen blown entrained flow gasification of a biorefinery lignin residue. *Fuel Processing Technology, 115*, 130−138.

Paisley, M. A., Farris, M. C., Black, J. W., Irving, J. M., & Overend, R. P. (2000). Preliminary operating results from the battelle/FERCO gasification demonstration plant in Burlington, Vermont, USA. In *1st world conference and exhibition on biomass for energy and industry in Seville, Spain*.

Paisley, M., Litt, R., & Creamer, K. (1990). *Gasification of refuse derived fuel in a high throughput gasification system*. Lake Buena Vista, Florida: Energy from Biomass and Wastes XIV.

Pan, Y., Roca, X., Velo, E., & Puigjaner, L. (1999). Removal of tar by secondary air in fluidised bed gasification of residual biomass and coal. *Fuel, 78*(14), 1703−1709.

Pérez, J. F., Melgar, A., & Benjumea, P. N. (2012). Effect of operating and design parameters on the gasification/combustion process of waste biomass in fixed bed downdraft reactors: an experimental study. *Fuel, 96*, 487−496.

Pfeifer, C., Rauch, R., & Hofbauer, H. (2004). In-bed catalytic tar reduction in a dual fluidized bed biomass steam gasifier. *Industrial & Engineering Chemistry Research, 43*(7), 1634−1640.

Plis, P., & Wilk, R. (2011). Theoretical and experimental investigation of biomass gasification process in a fixed bed gasifier. *Energy, 36*(6), 3838−3845.

Pu, G., Zhou, H-p., & Hao, G-t. (2008). Air-steam gasification of biomass in a fluidized bed: process optimization by enriched air. *Fuel Processing Technology, 90*, 677−685.

Pu, G., Zhou, H-p., & Hao, G-t. (2013). Study on pine biomass air and oxygen/steam gasification in the fixed bed gasifier. *International Journal of Hydrogen Energy, 38*(35), 15757−15763.

Quaark, P., Knoef, H., & Stassen, H. E. (1999). *Energy from biomass: A review of combustion and gasification technologies* (Vol. 23). World Bank-free PDF.

Rampling, T., & Gill, P. (1993). *Fundamental research of the thermal treatment of wastes and biomass: Literature review of past research on thermal treatment of biomass and waste*. ETSU.

Rampling, T., & Gill, P. (1993). *Fundamental research on the thermal treatment of wastes and biomass: Thermal treatment characteristics of biomass* (Vol. 208). Harwell Laboratory, Energy Technology Support Unit.

Rapagna, S., Jand, N., Kiennemann, A., & Foscolo, P. U. (2000). Steam-gasification of biomass in a fluidised-bed of olivine particles. *Biomass and Bioenergy, 19*(3), 187−197.

Renewables global status report (2013). Available online: http://www.ren21.net/Portals/0/documents/Resources/GSR/2013/GSR2013_lowres.pdf.

Savage, P. E. (1999). Organic chemical reactions in supercritical water. *Chemical Reviews, 99*(2), 603−622.

Saxena, R. C., Seal, D., Kumar, S., & Goyal, H. B. (2008). Thermo-chemical routes for hydrogen rich gas from biomass: a review. *Renewable and Sustainable Energy Reviews, 12*(7), 1909−1927.

Shen, L., Gao, Y., & Xiao, J. (2008). Simulation of hydrogen production from biomass gasification in interconnected fluidized beds. *Biomass and Bioenergy, 32*(2), 120−127.

Srinivas, T., Gupta, A., & Reddy, B. (2009). Thermodynamic equilibrium model and exergy analysis of a biomass gasifier. *Journal of Energy Resources Technology, 131*, 031801.

Srinivas, T., Reddy, B., & Gupta, A. (2012). Thermal performance prediction of a biomass based integrated gasification combined cycle plant. *Journal of Energy Resources Technology, 134*(2), 021002-(1-9).

Stevens, D. J. (2001). *Hot gas conditioning: Recent progress with larger-scale biomass gasification systems*. NREL subcontractor report (NREL/SR-510-29952).

Sun, S., Zhao, Y., Ling, F., & Su, F. (2009). Experimental research on air staged cyclone gasification of rice husk. *Fuel Processing Technology, 90*(4), 465−471.

Suresh Kumar Reddy, K., Kannan, P., Al Shoaibi, A., & Srinivasakannan, C. (June 08, 2012). Thermal pyrolysis of polyethylene in fluidized beds: review of the influence of process parameters on product distribution. *Journal of Energy Resources Technology, 134*(3), 034001−034006.

Susta, M. R., Luby, P., & Mat, S. (2009). *Biomass energy utilization and environment protection commercial reality and outlook*. Power Gen Asia. http://www.powergeneration.siemens.com/download/pool/industrialheatpower_02. pdf. Accessed.

Sutton, D., Kelleher, B., & Ross, J. R. (2001). Review of literature on catalysts for biomass gasification. *Fuel Processing Technology, 73*(3), 155−173.

Turn, S. Q., Kinoshita, C. M., & Ishimura, D. M. (1997). Removal of inorganic constituents of biomass feedstocks by mechanical dewatering and leaching. *Biomass and Bioenergy, 12*(4), 241−252.

Valin, S., Ravel, S., Guillaudeau, J., & Thiery, S. (2010). Comprehensive study of the influence of total pressure on products yields in fluidized bed gasification of wood sawdust. *Fuel Processing Technology, 91*(10), 1222−1228.

Van der Drift, A., Boerrigter, H., Coda, B., Cieplik, M. K., & Hemmes, K. (2004). Entrained flow gasification of biomass - Ash behaviour, feeding issues, and system analyses. The Netherlands: ECN.

Wang, L., Weller, C. L., Jones, D. D., & Hanna, M. A. (2008). Contemporary issues in thermal gasification of biomass and its application to electricity and fuel production. *Biomass and Bioenergy, 32*(7), 573−581.

Warnecke, R. (2000). Gasification of biomass: comparison of fixed bed and fluidized bed gasifier. *Biomass and Bioenergy, 18*(6), 489−497.

Watanabe, M., Sato, T., Inomata, H., Smith, R. L., Arai, K., Kruse, A., et al. (2004). Chemical reactions of C1 compounds in near-critical and supercritical water. *Chemical Reviews, 104*(12), 5803−5822.

Weerachanchai, P., Horio, M., & Tangsathitkulchai, C. (2009). Effects of gasifying conditions and bed materials on fluidized bed steam gasification of wood biomass. *Bioresource Technology, 100*(3), 1419−1427.

Wu, C., Yin, X., Ma, L., Zhou, Z., & Chen, H. (2009). Operational characteristics of a 1.2-MW biomass gasification and power generation plant. *Biotechnology Advances, 27*(5), 588−592.

Xu, G., Murakami, T., Suda, T., Matsuzawa, Y., & Tani, H. (2006). The superior technical choice for dual fluidized bed gasification. *Industrial & Engineering Chemistry Research, 45*(7), 2281−2286. www.netl.doe.gov/research/coal/energy-systems/gasification/gasifipedia/blackliquor.

Xu, G., Murakami, T., Suda, T., Matsuzaw, Y., & Tani, H. (2009). Two-stage dual fluidized bed gasification: its conception and application to biomass. *Fuel Processing Technology, 90*(1), 137−144.

Yin, X. L., Wu, C. Z., Zheng, S. P., & Chen, Y. (2002). Design and operation of a CFB gasification and power generation system for rice husk. *Biomass and Bioenergy, 23*(3), 181−187.

Youssef, E. A., Chowdhury, M. B. I., Nakhla, G., & Charpentier, P. A. (2010). Effect of nickel loading on hydrogen production and chemical oxygen demand (COD) destruction from glucose oxidation and gasification in supercritical water. *International Journal of Hydrogen Energy, 35*(10), 5034−5042.

Youssef, E. A., Elbeshbishy, E., Hafez, H., Nakhla, G., & Charpentier, P. A. (2010). Sequential supercritical water gasification and partial oxidation of hog manure. *International Journal of Hydrogen Energy, 35*(21), 11756−11767.

Youssef, E. A., Nakhla, G., & Charpentier, P. A. (2011). Oleic acid gasification over supported metal catalysts in supercritical water: hydrogen production and product distribution. *International Journal of Hydrogen Energy, 36*(8), 4830−4842.

Youssef, E. A., Nakhla, G., & Charpentier, P. A. (2012). Co-gasification of catechol and starch in supercritical water for hydrogen production. *International Journal of Hydrogen Energy, 37*(10), 8288−8297.

Yu, J., Tian, F.-J., McKenzie, L. J., & Li, C.-Z. (2006). Char-supported nano iron catalyst for water-gas-shift reaction: hydrogen production from coal/biomass gasification. *Process Safety and Environmental Protection, 84*(2), 125−130.

Yu, Q.-Z., Brage, C., Nordgreen, T., & Sjöström, K. (2009). Effects of Chinese dolomites on tar cracking in gasification of birch. *Fuel, 88*(10), 1922−1926.

Zhang, Y., Li, Q., Shen, P., Liu, Y., Yang, Z., Ding, W., et al. (2008). Hydrogen amplification of coke oven gas by reforming of methane in a ceramic membrane reactor. *International Journal of Hydrogen Energy, 33*(13), 3311−3319.

Zhang, L., Xu, C. C., & Champagne, P. (2010). Overview of recent advances in thermo-chemical conversion of biomass. *Energy Conversion and Management, 51*(5), 969−982.

Zhang, L., Xu, C. C., & Champagne, P. (2012). Activity and stability of a novel Ru modified Ni catalyst for hydrogen generation by supercritical water gasification of glucose. *Fuel, 96*, 541−545.

Zhao, Y., Sun, S., Zhou, H., Sun, R., Tian, H., Luan, J., et al. (2010). Experimental study on sawdust air gasification in an entrained-flow reactor. *Fuel Processing Technology, 91*(8), 910−914.

Zschetzsche, A., Hofbauer, H., & Schmidt, A. (1998). Biomass gasification in an internal circulating fluidized bed. In *Proceedings of the eighth European conference on biomass for agriculture and industry*.

This page intentionally left blank

Part Three

Production of hydrogen through electrolysis

This page intentionally left blank

Hydrogen production using high-pressure electrolyzers

7

R. Hanke-Rauschenbach[1], *B. Bensmann*[1], *P. Millet*[2]
[1]Gottfried Wilhelm Leibniz Universität Hannover, Hannover, Germany;
[2]University of Paris-Sud, Orsay Cedex, France

7.1 Introduction

The concept of hydrogen economy is based on the use of hydrogen as an energy carrier for the purpose of storing transient renewable energy sources. The water splitting reaction can be used for that purpose:

$$H_2O(liq) \rightleftarrows H_2(g) + \frac{1}{2}O_2(g) \tag{7.1}$$

Main advantages of Eqn (7.1) for the implementation of a hydrogen economy are: (1) electrochemical reversibility of the reaction at ambient temperatures; (2) the abundance of water on Earth; (3) high energy density and (4) the possibility of storing oxygen in the atmosphere (although dilution in air substantially reduces cycle efficiency). Main disadvantages are (1) the paradoxical fact that energy is stored in the form of gaseous chemicals that are not easily stored; (2) insufficient reversibility of the water–oxygen redox couple at close to ambient temperatures, a source of energy loss and (3) safety issues. Implementation of this energy cycle on a large scale requires a compression step for the storage and distribution of hydrogen. Basically, there are three different approaches to produce pressurized hydrogen of electrolytic grade from water electrolysis: first, by performing water electrolysis (Figure 7.1(a)) at atmospheric pressure and then pressuring the gas in a second step (using, for example, a conventional gas compressor or electrochemical compressor, as shown in Figure 7.1(b)); second, by performing water electrolysis under pressure (self-pressurization or pressurization using an inert gas) and third, by combining pressurized electrolysis and external compression. Because the compression of liquid water requires less power than the compression of hydrogen, it can be expected that the second process requires less power than the first one. Also, in terms of investment cost, when hydrogen is pressurized directly in the electrolyzer, the additional cost owing to the high-pressure structure may balance the need for an external hydrogen compressor. The focus of this chapter is on different options from a thermodynamic and technical viewpoint.

Compendium of Hydrogen Energy. http://dx.doi.org/10.1016/B978-1-78242-361-4.00007-8

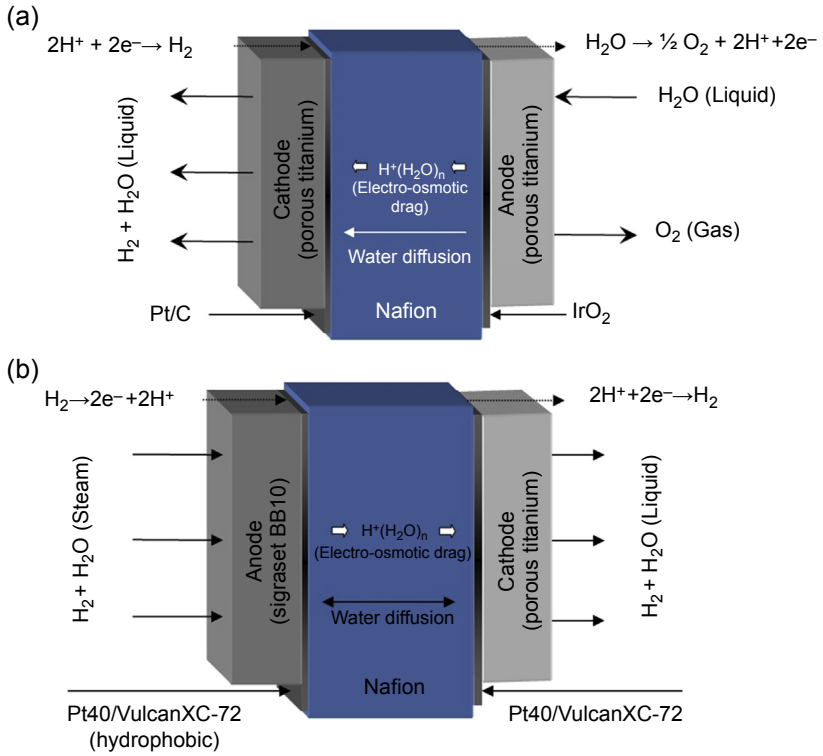

Figure 7.1 Schematic diagrams of (a) a PEM water electrolysis cell and (b) a PEM compression cell.

7.2 Thermodynamic aspects and high-pressure electrolyzer configurations

When considering high-pressure electrolysis as a potential pathway to convert excess electricity into chemical energy, the specific electric energy demand of the electrolyzer and the amount of heat released per unit-mole product are important variables. Independent of the electrolyzer type and its specific technical realization, some instructive relations for these quantities can be derived and should be discussed at the beginning of this chapter.

7.2.1 Minimum required energy: reversible conditions

Initially, an expression for the minimal required energy to drive the electrolysis reaction (Eqn (7.1)) should be discussed. It is convenient to apply for a brief derivation the first and second laws of thermodynamics to the electrolyzer.

$$0 = P_{\mathrm{el}} + Q + \sum_{j} G^{j} h\left(T^{j}, p^{j}, x_{\alpha}^{j}\right) \tag{7.2}$$

$$0 = \frac{Q}{T} + \sum_j G^j s\left(T^j, p^j, x_\alpha^j\right) + \dot{S}_{\text{irr}} \tag{7.3}$$

The variables P_{el} (in W) and Q (in W) stand for the electric power and the heat fed to the electrolyzer. G^j (in mol/s) is the total molar flow crossing the boundary j of the electrolyzer (with $j =$ anode inlet, anode outlet, cathode inlet and cathode outlet). The variables h (in J/mol) and s (in J/mol/K) stand for the specific enthalpy and the specific entropy of these streams, respectively. Both quantities are functions of the temperature T (in K), pressure p (in Pa) and mole fractions x_α of the species α within the corresponding stream. Finally, $\dot{S}_{\text{irr}}$ (J/K) is the entropy production rate.

The minimal required energy to carry out electrolysis can be determined when considering an isothermal operation of the electrolyzer ($T^j = T \forall j$) under reversible conditions ($\dot{S}_{\text{irr}} = 0$). When using the following caloric state equations (valid for ideal gases)

$$h(T, p, x_\alpha) = \sum_\alpha x_\alpha \left(h_\alpha\left(T^\theta\right) + \int_{T^\theta}^{T} c_{p,\alpha}(\tau)\, \mathrm{d}\tau \right) \tag{7.4}$$

$$s(T, p, x_\alpha) = \sum_\alpha x_\alpha \left(s_\alpha\left(T^\theta, p^\theta\right) + \int_{T^\theta}^{T} \frac{c_{p,\alpha}(\tau)}{\tau}\, \mathrm{d}\tau - R \ln a_\alpha \right) \tag{7.5}$$

$$\text{with } a_\alpha = p_\alpha / p^\theta \text{ (for } \alpha = \mathrm{H_2}, \mathrm{O_2}) \text{ and } a_\alpha = 1 \text{ (for } \alpha = \mathrm{H_2O})$$

and making the simplification that the product streams leave the electrolyzer in dry form, Eqns (7.2) and (7.3) and some simple mass balances can be combined to find the well-known result:

$$\underbrace{\frac{P_{\text{el}}^{\text{rev}}}{G_{\mathrm{H_2}}^{\text{out}}}}_{= w_{\mathrm{H_2}}^{\text{rev}}} = \Delta_R g\left(T, p^\theta\right) + RT \ln\left[\left(\frac{p^A}{p^\theta}\right)^{0,5} \left(\frac{p^C}{p^\theta}\right) \right] \tag{7.6}$$

$$\underbrace{\frac{Q^{\text{rev}}}{G_{\mathrm{H_2}}^{\text{out}}}}_{= q_{\mathrm{H_2}}^{\text{rev}}} = T\Delta_R s\left(T, p^\theta\right) - RT \ln\left[\left(\frac{p^A}{p^\theta}\right)^{0,5} \left(\frac{p^C}{p^\theta}\right) \right] \tag{7.7}$$

The quantity $q_{\mathrm{H_2}}^{\text{rev}}$ (in $\mathrm{J/mol_{H_2}}$) represents the heat that needs to be supplied (if positive) or released (if negative) per mole of evolved hydrogen to maintain the electrolyzer under isothermal conditions. The symbol $w_{\mathrm{H_2}}^{\text{rev}}$ (in $\mathrm{J/mol_{H_2}}$) stands for the minimal required electric energy demand to evolve 1 mol of hydrogen under these

conditions. The quantities $\Delta_R s(T, p^\theta)$ and $\Delta_R g(T, p^\theta)$ are the entropy (in J/(mol K)) and the Gibbs enthalpy (in J/mol) of the electrolysis reaction (Eqn (7.1)). It is worth mentioning that P_{el}^{rev} and Q^{rev} can also refer to the oxygen flow rate $G_{O_2}^{out}$ leaving the electrolyzer. Under reversible conditions, we thus find $w_{O_2}^{rev} = 2 \cdot w_{H_2}^{rev} (\text{in J/mol}_{O_2})$ and $q_{O_2}^{rev} = 2 \cdot q_{H_2}^{rev} (\text{in J/mol}_{O_2})$.

The thick lines in Figures 7.2 and 7.3 graphically represent the results (7.6) and (7.7), showing $w_{H_2}^{rev}$ and $q_{H_2}^{rev}$ as functions of the electrolyzer pressure p (with $p^A = p$, $p^C = p$). The pressure dependence of both quantities comes solely from the last term of Eqns (7.6) and (7.7). When increasing p, the heat demand is reduced whereas the electric energy demand is increased by the same amount. However, the extra energy required to evolve product gases at elevated pressure takes only a small portion of the overall energy demand. For example, at 100 bar we find 231.5 kJ/mol for the first term and 15.9 kJ/mol for the last term on the right-hand side of Eqn (7.6); i.e. only 6.4% of electric energy is assigned to the high-pressure operation whereas the rest of the energy is required to drive the water-splitting reaction.

It is worth reviewing the two classical simplifications that have to be made to obtain the well-known correlations for $w_{H_2}^{rev}$ and $q_{H_2}^{rev}$ (Eqns (7.6) and (7.7)). First, the assumption of dry product streams should be discussed. In reality, both gas streams leave the

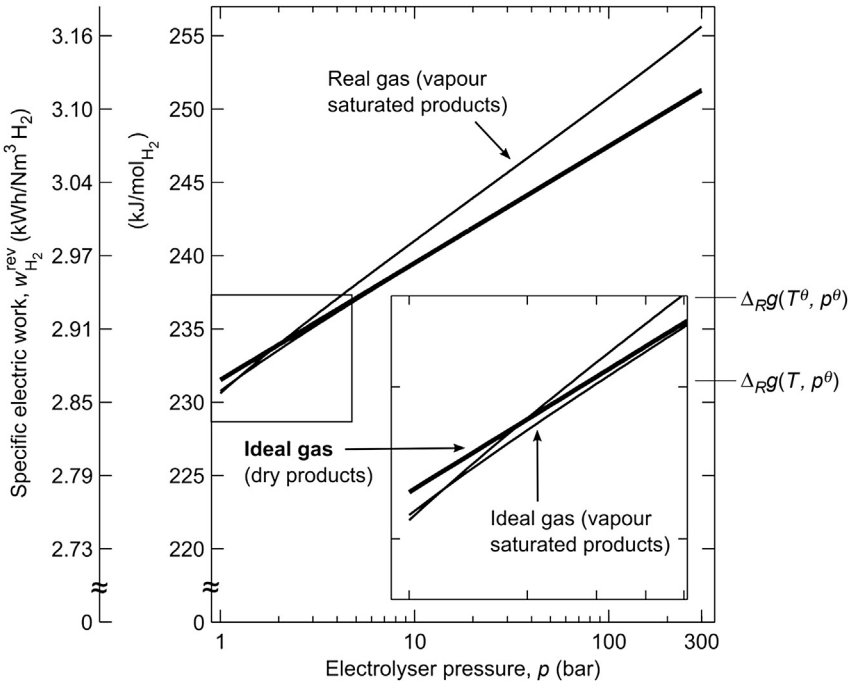

Figure 7.2 Specific reversible electric energy demand for water electrolysis as a function of electrolyzer pressure ($p = p^A = p^C$, symmetric high-pressure system) at $T = 60\ ^\circ$C. Further parameters: $p_{H_2O}^{sat}(T = 60\ ^\circ C) = 0.1961$ bar, $h_\alpha(T^\theta)$, $s_\alpha(T^\theta, p^\theta)$, $c_{p,\alpha}(T)$ according to VDI-GVC (2010).

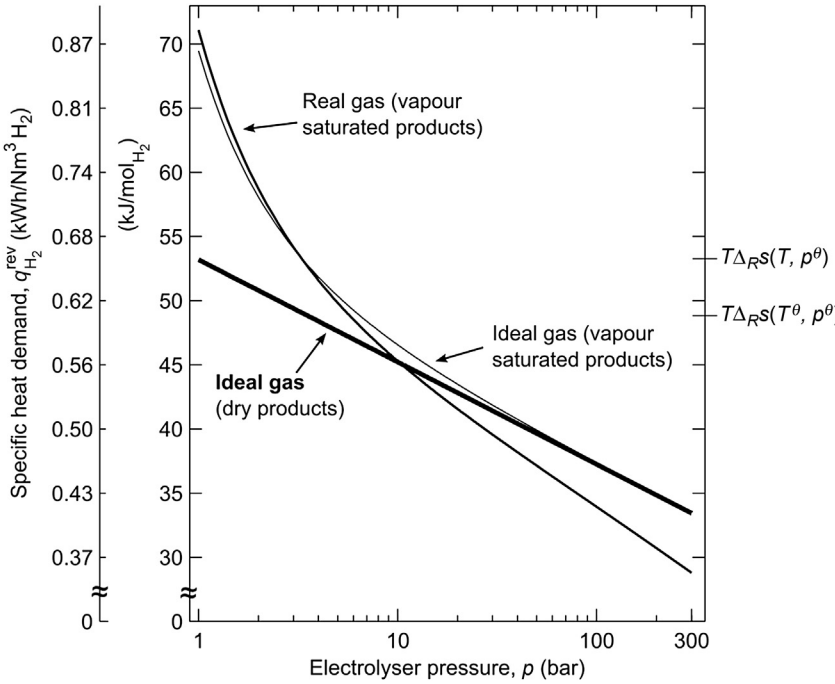

Figure 7.3 Specific reversible heat demand for water electrolysis as function of electrolyzer pressure ($p = p^A = p^C$, symmetric high-pressure system) at $T = 60\ °C$. Further parameters: $p^{sat}_{H_2O}(T = 60\ °C) = 0.1961$ bar, $h_\alpha(T^\theta)$, $s_\alpha(T^\theta, p^\theta)$, $c_{p,\alpha}(T)$ according to VDI-GVC (2010).

electrolyzer saturated with water vapour. When considering this aspect in the material balances, which are then again combined with Eqns (7.2)–(7.5), the following correlations can be derived:

$$w^{rev}_{H_2} = \Delta_R g\left(T, p^\theta\right) + RT \ln\left[\left(\frac{p^A - p^{sat}_{H_2O}(T)}{p^\theta}\right)^{0,5}\left(\frac{p^C - p^{sat}_{H_2O}(T)}{p^\theta}\right)\right] \tag{7.8}$$

$$q^{rev}_{H_2} = T\Delta_R s\left(T, p^\theta\right) - RT \ln\left[\left(\frac{p^A - p^{sat}_{H_2O}(T)}{p^\theta}\right)^{0,5}\left(\frac{p^C - p^{sat}_{H_2O}(T)}{p^\theta}\right)\right] + \left(\frac{1}{2} \cdot \frac{p^{sat}_{H_2O}(T)/p^A}{1 - p^{sat}_{H_2O}(T)/p^A} + \frac{p^{sat}_{H_2O}(T)/p^C}{1 - p^{sat}_{H_2O}(T)/p^C}\right)\left(h^V_{H_2O}(T) - h^L_{H_2O}(T)\right) \tag{7.9}$$

Comparison of this result with Eqns (7.6) and (7.7) shows two differences. First, the heat demand $q^{rev}_{H_2}$ is increased by the energy required to evaporate the amount of water

required to saturate the outflows (c.f. the last term in Eqn (7.9)). Second, reduction of the product partial pressures by the water vapour leads to a reduction in the electric energy demand (c.f. the last term in Eqn (7.8)). The error made when using Eqns (7.6) and (7.7) instead of Eqns (7.8) and (7.9) would be largest for an operation of the electrolyzer under ambient pressure conditions (c.f. Figures 7.2 and 7.3). At 1 bar and, for example, 60 °C, we find from our derivations that Eqn (7.6) overestimates the electric energy demand by 0.3% and Eqn (7.7) underestimates the heat demand by 23.4%.

Finally, relaxation of the second assumption (ideal gas behaviour) should be discussed. For this purpose we have used the GERG-2004 equation of state (Kunz, Klimeck, Wagner, & Jaeschke, 2007) instead of Eqns (7.4) and (7.5) to evaluate the caloric quantities $h(T, p, x_\alpha)$, $s(T, p, x_\alpha)$. GERG-2004 is valid for $p \leq 300$ bar and $90\ \mathrm{K} \leq T \leq 450\ \mathrm{K}$ and represents the caloric state variables with an error of less than 0.5% (Kunz et al., 2007). When combining GERG-2004 with Eqns (7.2) and (7.3) and the material balances again $w_{H_2}^{rev}(T, p^A, p^C)$ and $q_{H_2}^{rev}(T, p^A, p^C)$ can be calculated. Figures 7.2 and 7.3 show the results. Not surprisingly, the deviation from the curve assuming ideal gas behaviour grows with increasing pressure. At 100 bar and 60 °C, Eqn (7.8) underestimates the electric energy demand by 1.3% and Eqn (7.9) overestimates the heat demand by 9.7%.

7.2.2 Technical electrolysis in high-pressure systems: irreversible conditions

To realize reversible conditions it would be required to operate the electrolyzer at an infinite small current density ($i = I/A_{cell} \rightarrow 0$). The voltage of the single cells of the electrolyzer would then adjust to the reversible cell voltage, which can be calculated from the reversible electric energy demand through:

$$V^{rev} = \frac{w_{H_2}^{rev}}{2F} \tag{7.10}$$

However, as a consequence the specific productivity of the electrolyzer would be poor ($G_{H_2}^{out}/A_{cell},\ G_{O_2}^{out}/A_{cell} \rightarrow 0$). Therefore, in a technical application the device is always operated at a finite current density ($i > 0$), which requires a cell voltage above V^{rev}:

$$V = V^{rev} + \Delta V(i, \ldots) \tag{7.11}$$

The actual value of the cell polarization ΔV (in V) depends on the applied current density and some other parameters to be discussed further below.

A second aspect to be considered in a technical electrolysis, especially in high-pressure systems, is crossover of the product gases. Hydrogen, whose partial pressure is higher at the cathode, is transported towards the anode and recombines there partially with oxygen to water. Similarly, oxygen will be driven from the anode towards the cathode. As a consequence, the hydrogen and oxygen outflows will deviate from their stoichiometric values. The ratio between the actual molar flow rate of the

product and the stoichiometric expected value is quantified through the Faradaic efficiencies ε_{H_2} and ε_{O_2}:

$$\varepsilon_{H_2} = \frac{G_{H_2}^{out}}{I/2F} \tag{7.12}$$

$$\varepsilon_{O_2} = \frac{G_{O_2}^{out}}{I/4F} \tag{7.13}$$

Both quantities are related through the material balances with the crossover flows $G_{H_2}^{cross}$, $G_{O_2}^{cross}$ (in mol/s) by:

$$\varepsilon_{H_2} = 1 - \frac{2F}{I}\left(G_{H_2}^{cross} + 2\zeta_{rec}^{C} G_{O_2}^{cross}\right) \tag{7.14}$$

$$\varepsilon_{O_2} = 1 - \frac{4F}{I}\left(G_{O_2}^{cross} + 0.5\zeta_{rec}^{A} G_{H_2}^{cross}\right) \tag{7.15}$$

Here, ζ_{rec}^{C} and ζ_{rec}^{A} stand for the extent of the recombination reaction ($H_2 + 0.5O_2 \rightleftarrows H_2O$) at the cathode and the anode side, respectively. ζ_{rec}^{C}, $\zeta_{rec}^{A} \to 1$ corresponds to a full recombination and ζ_{rec}^{C}, $\zeta_{rec}^{A} \to 0$ corresponds to no recombination.

To find a relation for the specific electric energy demand under irreversible conditions, the following equation

$$P_{el} = V \cdot I \tag{7.16}$$

can be combined with Eqns (7.10)–(7.12) to find the final result

$$\underbrace{\frac{P_{el}}{G_{H_2}^{out}}}_{=w_{H_2}} = \frac{w_{H_2}^{rev} + 2F \cdot \Delta V\left(i, T(i), c_\alpha\left(i, p^A\right), \ldots\right)}{\varepsilon_{H_2}\left(p^A, p^C, \ldots\right)} \tag{7.17}$$

Here, w_{H_2} stands for the specific electric energy demand per mole of evolved hydrogen. In the braces behind the variables ΔV and ε_{H_2} their determining factors are indicated. It is worth discussing them briefly especially in the context of high-pressure electrolysis. Cell polarization ΔV is the driving force for the electrode reactions and the ion transport through the electrolyte. In general it is a function of the current density i, the temperature field T and concentration field c_α within the electrolyzer. The last ones are functions of the current density as well. In high-pressure systems, the concentration field also depends on at least the anode pressure p^A. This variable has a direct influence on the two-phase conditions on the anode side as the oxygen bubble volume scales with $1/p$. Especially at high current densities, where two-phase mass transport on the anode side limits the performance of the electrolyzer, an increase

in anode pressure will lead to a decrease in the required cell polarization. So far, no quantifying experimental data exist for this aspect in the literature for either alkaline electrolyzers (AEL) or polymer electrolyte membrane electrolyzers (PEMEL). Therefore, for the plot given in Figure 7.4 the pressure dependence of ΔV was neglected. Under these conditions, cell polarization ΔV simply causes a constant shift in the curve $w_{H_2}^{rev}(p)$ by the value of $2F \cdot \Delta V$ (c.f. Eqn (7.17), Figure 7.4 thin curve for $\varepsilon_{H_2} = 1$).

In contrast to ΔV, the pressure dependence of the Faradaic efficiency ε_{H_2} can be quantified more easily. As can be seen from Eqn (7.14), ε_{H_2} is a function of the crossover flows $G_{H_2}^{cross}$ and $G_{O_2}^{cross}$. The main driving forces for these quantities are the difference in the hydrogen and oxygen partial pressures between the anode and cathode. As a consequence, the crossover flows will increase with increasing pressure and therefore ε_{H_2} will decrease. Figure 7.4 (thick line) shows the final effect on the specific electric energy demand w_{H_2}.

Finally, a few comments should be made on the specific heat demand under irreversible conditions. For this purpose it is instructive to rearrange Eqn (7.17) into

$$w_{H_2} = w_{H_2}^{rev} + \frac{2F}{\varepsilon_{H_2}} \cdot (V^{rev}(1 - \varepsilon_{H_2}) + \Delta V) \tag{7.18}$$

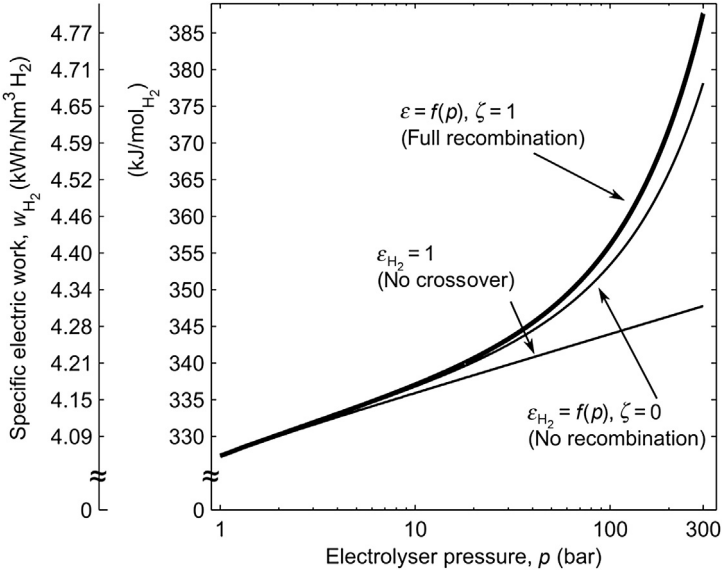

Figure 7.4 Specific electric energy demand for water electrolysis as a function of electrolyzer pressure ($p = p^A = p^C$, symmetric high-pressure system) at $T = 60\ °C$, $\Delta V = 0.5$ V and $I = 1$ A/cm^2. Further parameters: $w_{H_2}^{rev}(p)$ calculated according to Eqn (7.8), $G_{H_2}^{cross} = k_{H_2} \cdot (p^C - p_{H_2O}^{sat})/t^M$, $G_{O_2}^{cross} = k_{O_2} \cdot (p^A - p_{H_2O}^{sat})/t^M$, $p_{H_2O}^{sat}(T = 60\ °C) = 0.1961$ bar, $t^M = 180$ µm, $k_{H_2} = 2.5 \times 10^{-9}$ mol/(m s bar) (Bensmann, Hanke-Rauschenbach, & Sundmacher, 2014), $k_{O_2} = 3.5 \times 10^{-10}$ mol/(m s bar) (Ito, Maeda, Nakano, & Takenaka, 2011).

This result can be inserted together with the material balances into the energy balance (7.2) to find after some rearrangement:

$$q_{H_2} = q_{H_2}^{rev} - \frac{2F}{\varepsilon_{H_2}} \cdot \left(V^{rev}(1-\varepsilon_{H_2}) + \Delta V\right) + q_{H_2}^{*}\left(\varepsilon_{O_2}, \varepsilon_{H_2}, \zeta_{rec}^{A}, \zeta_{rec}^{C}\right) \tag{7.19}$$

A comparison of Eqns (7.18) and (7.19) shows that the additional electric energy (last term in Eqn (7.18)) is completely dissipated into heat (the mentioned term from Eqn (7.18) appears with the opposite sign in Eqn (7.19)). Depending on the value of ΔV this reduces the heat demand or leads to a typical situation in which the electrolyzer needs to be cooled (q_{H_2} then has a negative sign, c.f. Figure 7.5). The last term in Eqn (7.19), $q_{H_2}^{*}$, mainly represents the heat demand for splitting the extra water to make up the hydrogen crossover. It takes a maximum positive value in the case of $\zeta_{rec}^{A}, \zeta_{rec}^{C} = 0$, i.e. when no recombination of hydrogen and oxygen occurs. For $\zeta_{rec}^{A}, \zeta_{rec}^{C} = 1$, i.e. full recombination, the term $q_{H_2}^{*}$ disappears as the heat required for splitting extra water is delivered by the exothermic recombination reaction.

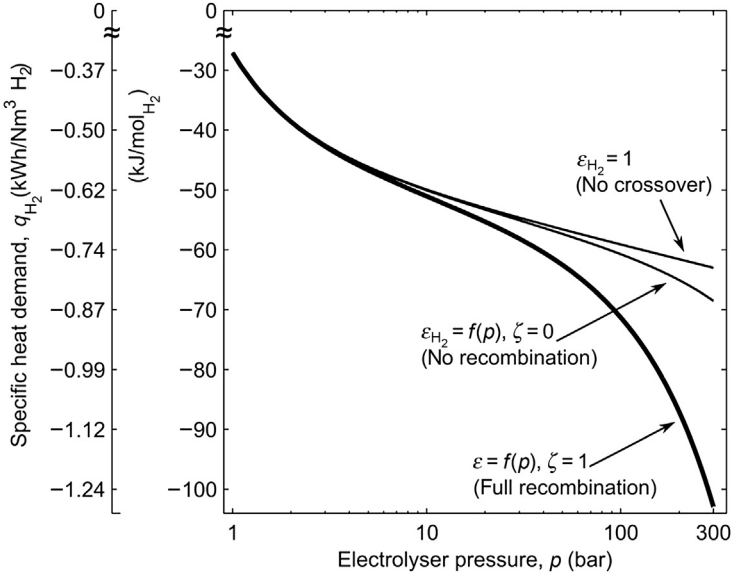

Figure 7.5 Specific heat demand for water electrolysis as a function of electrolyzer pressure ($p = p^A = p^C$, symmetric high-pressure system) at $T = 60\ °C$, $\Delta V = 0.5$ V and $i = 1$ A/cm^2. Further parameters: $q_{H_2}^{rev}(p)$ calculated according to Eqn (7.9), $G_{H_2}^{cross} = k_{H_2} \cdot (p^C - p_{H_2O}^{sat})/t^M$, $G_{O_2}^{cross} = k_{O_2} \cdot (p^A - p_{H_2O}^{sat})/t^M$, $p_{H_2O}^{sat}(T = 60\ °C) = 0.1961$ bar, $t^M = 180\ \mu m$, $k_{H_2} = 2.5 \times 10^{-9}$ mol/(m s bar) (Bensmann et al., 2014), $k_{O_2} = 3.5 \times 10^{-10}$ mol/(m s bar) (Ito et al., 2011).

7.2.3 Possible configurations for high-pressure electrolyzers and advantages compared with ambient electrolysis and subsequent product compression

High-pressure electrolyzers can be designed in different configurations. The classic is the symmetric configuration discussed so far. It is also referred to as balanced high-pressure configuration. Here, at the outlet of both gas streams control valves and back-pressure controllers are installed (Figure 7.6(a)). By this means the desired delivery pressure can build up on the anode and the cathode of the electrolyzer ($p^A = p^C = p$). In this configuration the feed water is to be pressurized to the electrolyzer operating pressure by the feed water pump (Figure 7.6(a)).

As an alternative to the symmetric configuration, an asymmetric or unbalanced, high-pressure configuration also can be realized. Here anode and cathode are maintained at different pressure levels. Such a configuration can be only realized with

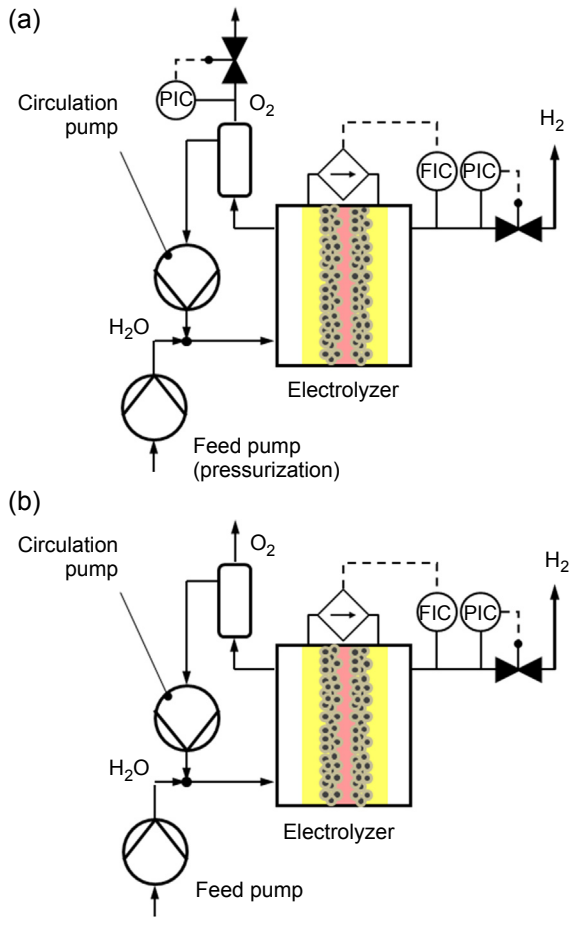

Figure 7.6 Selected high-pressure configurations using the example of a PEM electrolyzer. (a) Symmetric configuration and (b) asymmetric configuration.

membrane electrolyzers, in which the membrane can mechanically withstand the pressure difference. Typically the anode side is operated at ambient conditions whereas the cathode is kept at an elevated pressure (Figure 7.6(b); see, e.g. Degiorgis, Santarelli, & Cali, 2007; Marangio, Santarelli, & Cali, 2009). By this means hydrogen can be delivered at high pressure while the feed water is supplied and the oxygen is evolved under ambient conditions. The inverse configuration also exists, i.e. anode at elevated pressure and cathode under ambient conditions (see, e.g. Myles et al., 2012). Here, the oxygen is delivered at a high pressure whereas the hydrogen is produced at atmospheric conditions.

Asymmetric configurations are potentially advantageous whenever either hydrogen or oxygen needs to be pressurized while the other product can be delivered under atmospheric conditions. A typical case would be a power-to-gas application in which the oxygen is not considered a product and is vented into the atmosphere. The general energetic advantage of an asymmetric configuration above a symmetric configuration can be directly seen from Eqn (7.6). For the symmetric configuration we have $p^A = p$, $p^C = p$ and find

$$w_{\mathrm{H_2}}^{\mathrm{rev}} = \Delta_R g\left(T, p^\theta\right) + RT \ln\left[\left(\frac{p}{p^\theta}\right)^{1,5}\right] \tag{7.20}$$

For the asymmetric configuration, e.g. with a high-pressure cathode, we can set $p^A = p^\theta$, $p^C = p$ and find from Eqn (7.6):

$$w_{\mathrm{H_2}}^{\mathrm{rev}} = \Delta_R g\left(T, p^\theta\right) + RT \ln\left[\left(\frac{p}{p^\theta}\right)\right] \tag{7.21}$$

However, under asymmetric conditions the product crossover is higher because a difference in total pressure exists between the anode and cathode. This will drive an additional convective material flux through the membrane. Consequently, at large pressure differences the energetic advantage disclosed by Eqns (7.20) and (7.21) will be consumed by a reduced Faradaic efficiency (c.f. Eqn (7.17)).

To compare different high-pressure configurations and the configurations with atmospheric electrolyzers, the energy required for the feed water pump and product compression would have to be considered. There have been several attempts in this direction (Laoun, 2007; Onda, Kyakuno, Hattori, & Ito, 2004; Roy, Watson, & Infield, 2006). These contributions focused on comparing the balanced high-pressure configuration with an atmospheric electrolysis and subsequent mechanical compression. Unfortunately, the different contributions had different results. Onda et al. (2004) and Laoun (2007) found the balanced high-pressure pathway to be superior to the atmospheric pathway. Onda et al. (2004) calculated a difference in the electric energy demand of 5%, whereas Laoun (2007) found a difference of up to 20% between the two configurations. In contrast, Roy et al. (2006) found the opposite and stated that energy consumption for the balanced high-pressure electrolyzer was up to 16% higher compared with the atmospheric pathway. The main reason for the contradicting results

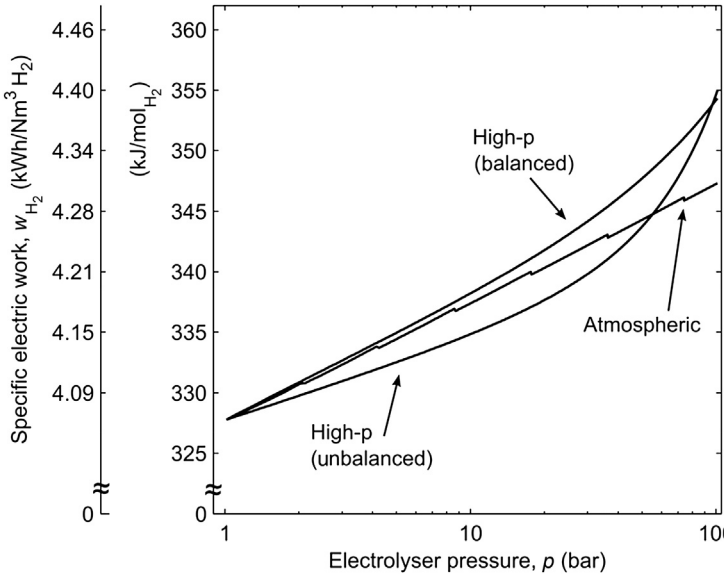

Figure 7.7 Specific energy demand for three different pathways to produce high-pressure hydrogen at $T = 60$ °C according to Bensmann et al. (2013). The atmospheric pathway involves an atmospheric electrolysis with subsequent product compression. The other two pathways involve high-pressure electrolysis in the balanced as well as unbalanced configuration. For further details, see Bensmann et al. (2013).

is the difference in thermodynamic data employed in the studies and different model assumptions being made. In another effort, Bensmann, Hanke-Rauschenbach, Pena Arias, and Sundmacher (2013) reevaluated these studies and compared all three pathways, i.e. (1) atmospheric electrolysis with subsequent product compression, (2) balanced high-pressure electrolysis and (3) unbalanced high-pressure electrolysis on a common model basis. The authors qualitatively confirmed the results of Roy et al. (2006). In addition, they found that up to a pressure of 40 bar, unbalanced high-pressure electrolysis is superior to the other two pathways (Figure 7.7). However, the relative differences in the energy demand are small (Figure 7.7), which means that other arguments than energetic ones might govern the decision about the configuration to be realized.

7.3 High-pressure electrolysis with alkaline systems

Alkaline electrolyzers have been in use since the beginning of the twentieth century. At that time the main driver was the use of cheap energy from hydroelectricity to produce hydrogen, especially for the fertilizer industry (Millet & Grigoriev, 2013). The current rediscovered interest in alkaline electrolysis has mainly been triggered by an increase in the share of electricity from renewable energy. Because of the need for long-term energy

storage, hydrogen production by alkaline electrolysis is a required building block in the future energy system, in which the conversion of electrical to chemical energy (also often summarized as power-to-gas) is considered important. This also reflects in the amount of demonstration projects related to this field. A summary of international electrolysis projects in the context of power to gas, installed and planned between 1991 and 2013, is given in Gahleitner (2013). In addition, platforms give up-to-date information about projects set up in Europe (NSPtG) and Germany (DENA).

When evaluating power-to-gas projects from these sources, 40 projects can be identified in which alkaline electrolyzers of various sizes are installed or planned. Hydrogen production rates range from 0.7 to 1300 Nm^3/h. The smallest plant was installed in the framework of the PVFC-SYS project, finished in 2004. The objective of this project was to supply remote sites with heat and electricity. Hydrogen was produced by a 3-kW alkaline electrolyzer operated at 10 bar, which was provided with electricity from photovoltaics. Storage tanks and a fuel cell completed the hybrid plant. The biggest plant was finished in 2013 and is located in Werlte, Germany. It consists of three 2-MW alkaline electrolyzers that operate at atmospheric conditions. The goal of the related project is to combine hydrogen production from electrolysis with a methanation unit to produce synthetic natural gas that is fed to the local gas grid.

The electrolyzers installed in the reviewed demonstration projects have a pressure level ranging from atmospheric up to 32 bar. Whereas five electrolyzers are operated at atmospheric conditions, two other distinct pressures levels are 10 bar (13 of 40 projects) and 30 bar (seven projects). These demonstration projects also mainly reflect the typical pressure level of commercially available alkaline electrolyzers. Devices of considerable scale (>60 Nm^3/h) are available in the range from atmospheric pressure to 32 bar. Only one company sells electrolyzers with an operating pressure of up to 450 bar (NOW, 2011). Pressure levels of 60 bar are reported to be in preparation but the currently available system design is expected to dominate in the near future, with a trend towards an average pressure level closer to 30 bar (FCH-JU, 2014).

One motivation for the increase in operation pressure is related to the new fields of application. The produced gas can be stored in or distributed through the existing natural gas grid. Its pressure level varies with location and dimension of the grid section. However, the main grid operating pressure varies between 10 and 70 bar. Hydrogen can be fed directly or after methanation from natural gas. Methanation is typically realized at pressures of up to 30 bar. Therefore, hydrogen production at 10−30 bar can avoid the installation of mechanical hydrogen compressors or at least reduce the number of compression stages. Although this technology is well-established, its replacement would be favourable because it has a high energy requirement and worse reliability; often at least two compressors are installed in parallel to guarantee safe operation (Tzimas & Filiou, 2003). Therefore, hydrogen compressors make up a significant share of the investment costs of high-pressure hydrogen production routes and a significant reduction in system cost is expected with increasing pressure (FCH-JU, 2014).

Of course, elevated hydrogen production pressure increases the cost of the electrolyzer because of additional peripheral components and higher requirements for electrolyzer material as well as a necessary increase in wall thickness to fulfill the higher

safety demands. On the other hand, the linear reduction of gas volume with pressure enables smaller pipe diameters and a smaller peripheral component size, which allows finally a more compact system design.

In addition, the operating pressure is interesting with regard to the electricity demand of the electrolyzer, which influences the operating cost. The increase in system pressure is manifold but it may finally reduce the cell over-potential and allow higher current densities. For example, higher pressure could allow a higher operating temperature, above 100 °C, favourable because of the positive influence on electrolyte resistance and reaction over-potentials. Because the temperature has to be kept below the electrolyte bubble point, it is limited to approximately 80 °C under atmospheric conditions. An increase in pressure would significantly increase the bubble point of the electrolyte and is currently gaining interest in research (e.g. Allebrod, Chatzichristodoulou, & Mogensen, 2013; Ganley, 2009). Another advantage in terms of efficiency is a reduction in the gas volume in the electrolyte and the related reduction in ohmic losses. This issue and the influence of the operating pressure on the apparent processes in alkaline electrolyzers will be discussed more intensively in the subsequent section. Afterwards the influence of pressure on the cell, stack and system design will be reviewed and compared with conventional atmospheric design.

7.3.1 Influence of operating pressure on governing processes

Alkaline electrolyzers use liquid electrolytes such as potassium or sodium hydroxide as ion-conductive media. Two gas evolving electrodes are directly placed in the electrolyte and separated by a gastight diaphragm. The evolved gases, oxygen at the anode and hydrogen at the cathode, make up two-phase conditions in both compartments. An important variable to characterize these conditions is the void fraction ε, defined as

$$\varepsilon = \frac{V_g}{V_g + V_l} \tag{7.22}$$

where V_g and V_l (in m^3) are the total volume of the gas and the volume of the liquid, respectively. Another important variable is the gas coverage, θ, of the electrode. Especially at high current densities a gas film can form on the electrode surface. Both variables are potentially pressure dependent and have an influence on the polarization behaviour of the cell. This aspect will be elucidated first. Afterwards, the pressure influence on product crossover will be discussed. It has an important effect on the Faradaic efficiency and product contamination.

Influence of pressure on void fraction and electrode coverage. The total volume occupied by gas bubbles in the two-phase mixture at both electrodes decreases with increasing pressure. Neglecting in a first approximation the pressure dependence of the bubble rising velocity, the total bubble volume scales according to ideal gas law with $1/p$. As a consequence the void fraction (Eqn (7.22)) also scales with $1/p$. We find

$$\varepsilon_p = \varepsilon_{p0} \cdot \frac{p_0}{p} \tag{7.23}$$

where ε_{p0} is the initial void fraction under atmospheric conditions $p_{0,}$ and ε_p the void fraction at elevated pressure p.

The void fraction has a strong influence on electrolyte conductivity. Several correlations exist in the literature (Sequeira, Santos, Sljukic, & Amaral, 2013). A well-excepted approach is the so-called Maxwell-relation:

$$k_\varepsilon = k_0 \frac{(1-\varepsilon)}{(1+0.5\cdot\varepsilon)} \tag{7.24}$$

where k_0 is the gas-free electrolyte conductivity. This relation is highly accurate at low void fractions. For higher values of ε and non-spherical bubbles, the Bruggemann relation might be used:

$$k_\varepsilon = k_0(1-\varepsilon)^{1.5} \tag{7.25}$$

Combining Eqn (7.23) and, e.g. (7.25), the change of the conductivity with regard to pressure is

$$\frac{k_\varepsilon(p)}{k_\varepsilon(p_0)} = \frac{\left(1-\varepsilon_{p0}\cdot\frac{p_0}{p}\right)^{1.5}}{\left(1-\varepsilon_{p0}\right)^{1.5}} \tag{7.26}$$

Figure 7.8 illustrates the conductivity increase with pressure resulting from changes in the void fraction according to Eqn (7.26). For high initial void fractions ε_{p0} the pressure increase has a strong influence. In the case of $\varepsilon_{p0} = 0.2$, conductivity is increased by 40% at a pressure of 20 bar.

The change in electrolyte conductivity will finally cause a change in the ohmic voltage drop of the cell. From Ohms law we have

$$\varphi_{\text{ohm}} = i \cdot \frac{x_{\text{gap}}}{k_\varepsilon} \tag{7.27}$$

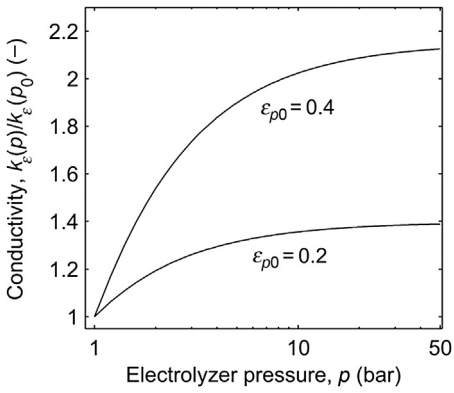

Figure 7.8 Dependence of conductivity on electrolyzer pressure. Initial void fractions at atmospheric conditions (ε_{p0}) are 0.2 and 0.4.

where x_{gap} (in m) is the distance between the two electrodes. Inserting (7.25), we finally find

$$\varphi_{ohm}(p) = i \cdot \frac{x_{gap}}{k_0\left(1 - \varepsilon_{p0} \cdot \frac{p_0}{p}\right)^{1.5}} \tag{7.28}$$

Figure 7.9 represents this correlation for a current density of 0.4 A/cm^2 and typical values for x_{gap} and k_0. The ohmic voltage drop can be decreased with pressure. For the given parameters we find for an initial void fraction of 0.2 a reduction in the ohmic drop of about 70 mV when increasing the pressure to 20 bar.

Next, the influence of the electrolyzer pressure on the electrode coverage will be discussed. An increase in the electrode coverage will occur with an increase in the activation over-potential (Zeng & Zhang, 2010). For an approximation of the corresponding voltage loss, the Tafel equation may be used (Vogt, 2012). If the reduced surface is considered by using the coverage factor and mass transport is neglected, it reads (Vogt, 2012):

$$\varphi_{act} = \frac{2.3 \cdot R \cdot T}{\alpha \cdot n \cdot F} \cdot \ln\left(\frac{i}{(1-\theta) i_0}\right) \tag{7.29}$$

where α is the charge transfer factor and i_0 is the exchange current density. After some rearrangement, the influence of the coverage on the over-potential φ_{act}^{θ} can easily be quantified:

$$\varphi_{act}^{\theta} = \frac{2.3 \cdot R \cdot T}{\alpha \cdot n \cdot F} \cdot (-\ln(1-\theta)) \tag{7.30}$$

Although investigation of the electrode coverage in two-phase processes is an intensively studied subject, its pressure dependence is still not completely clear owing to the

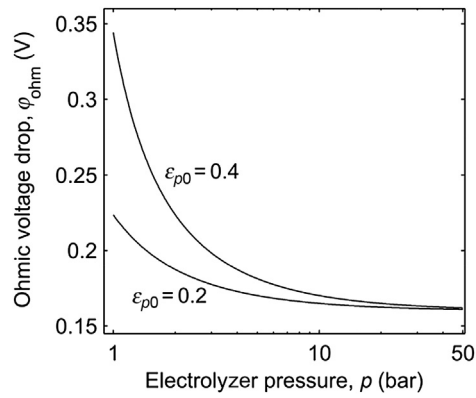

Figure 7.9 Dependence of ohmic voltage drop on electrolyzer pressure. φ_{ohm} calculated according to Eqn (7.28), $x_{gap} = 2$ mm, $k_0 = 0.5$ S/cm, $i = 0.4$ A/cm^2. Initial void fractions at atmospheric conditions (ε_{p0}) are 0.2 and 0.4.

large amount of influencing parameters (Mandin, Derhoumi, Roustan, & Rolf, 2014). Vogt and Balzer (2005) found the following correlation describing electrode coverage in stagnant electrolytes under the assumptions of small contact angles, as is typical for industrial electrolyzers:

$$\theta = \frac{\pi}{2} \cdot \frac{\dot{V}_G}{A} \cdot \frac{t_r}{V_r} R_r^2 \tag{7.31}$$

According to this equation the bubble detachment radius R_r, bubble residence time t_r, bubble volume V_r and volumetric flux density of the produced gas $\dot{V}_G/A$ remain the main influencing parameters. These parameters in turn depend on the operating conditions, such as current density, pressure or temperature, the properties of the electrolyte, and the produced gases and electrode materials. A comprehensive discussion can be found, for example, in Vogt and Balzer (2005) as well as in Eigeldinger and Vogt (2000).

The pressure influence on the coverage is manifold and is controversial. In Ursua, Martin, Barrios, and Sanchis (2013) an increase in coverage with pressure is expected owing to the higher residence time of bubbles on the electrode. Janssen (1978) and Janssen, Sillen, Barendrecht, and Van Stralen (1984) found the coverage of the hydrogen electrode to be almost independent of pressure whereas the coverage of the oxygen electrode increased with pressure. This observation is explained by the different coalescence behaviours of the two gases, which are also influenced by pressure.

Another direct influence of pressure on cell potential comes from the Nernst equation (c.f. Section 7.2). At a temperature of 60 °C a pressure increase to 2 bar is related to a difference in voltage of approximately 22 mV. With a further increase in pressure its influence is eased and for pressures of 20 and 100 bar a difference of 72 and 107 mV, respectively, is obtained.

If the three described effects are combined, this short-cut approach shows that under certain conditions the single contributions counteract each other and can easily level off. For the observed parameters the contributions level off at a pressure of 20 bar. Because the magnitude of both influence decreases strongly with pressure, this would not change at higher pressure levels. Of course, owing to the complexity of the overall pressure effect on cell voltage and the counteracting effects, this approach is just a rough approximation, but it can give a first phenomenological insight into the influence of pressure. This is important because the influence of pressure is rarely observed and published theoretical and experimental results are partly contradictory. From experimental results of a project by the Juelich Research Center with an alkaline prototype designed to operate at pressures up to 120 bar, it can be seen that even in the wide pressure range of 25 to 120 bar no clear trend in cell voltage was observed (Figure 7.10) and no correlation between pressure and specific current demand is possible (Janssen, Emonts & Stolten, 2008). Ursua et al. (2013) also reported that a variation in the operating pressure of a commercial Hydrogenics system between 5 and 25 bar had no influence on cell voltage. The experimental results were explained by the counteracting effects of lesser void fraction and higher electrode bubble coverage of the electrodes on the cell voltage.

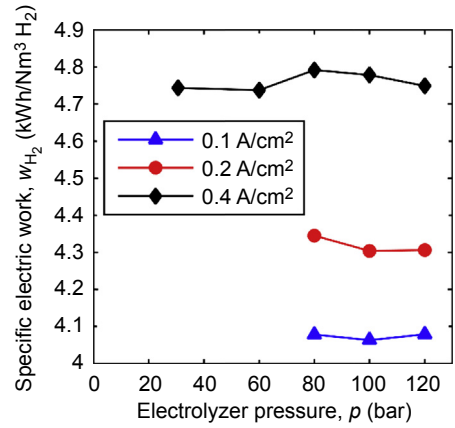

Figure 7.10 Specific energy demand of a high-pressure electrolyzer. Figure was reproduced from data of a project from the Jülich research center with a 5-kW alkaline electrolyzer (Janssen et al., 2008).

Currently, a general statement about the overall influence of pressure on cell voltage seems to be difficult. On the one hand this is because of a lack of sufficient data from experimental analyses. On the other hand, comparability of results is difficult because of the amount of influencing parameters on electrolyzer performance. An electrolyzer will be most efficient in the region of its nominal current density and nominal pressure, because for each set an optimal design exists. That means that if an electrolyzer with a design pressure of 30 bar is operated at 15 bar, its performance will not be a benchmark for maximal efficiency at this pressure. An electrolyzer designed for this specific pressure will probably be more efficient.

Influence of pressure on gas solubility and product crossover – Another important aspect is the influence of pressure on the solubility of gases in the electrolyte as well as diffusion through the separator. If Henry's law is applied the amount of solute gas is approximately linear dependent on pressure. As reported by Pray, Schweickert, and Minnich (1952), the solubility of hydrogen in water at a temperature of 60 °C changes from 0.1 to 0.7 mL_{H_2}/g_{H_2O} for a pressure increase from 6 to 40 bar. The solubility of oxygen is on the same order of magnitude.

According to Tham, Walker, and Gubbins (1970), the diffusion coefficient of hydrogen is two to three times higher than that of oxygen. Typical values for hydrogen are around 4×10^{-5} cm^2/s at 60 °C. Because the driving force is the concentration gradient of the gas, this leads to an almost linear increase of diffusion with pressure (Janssen, Bringmann, Emonts, & Schroeder, 2004).

In Janssen et al. (2004) a linear increase of hydrogen content in oxygen product gas was reported that was mainly attributed to diffusion. An increase in the molar fraction from 1.5% to 2.5% for a pressure change of 70 to 130 bar was observed. These fractions are already close to the lower explosion limit for hydrogen in oxygen, which is around 5.5% in this pressure range (Janssen et al., 2004). This clearly indicates increasing safety issues at elevated pressures.

Even more severe is when the electrolyzer is operated at part load (Ziems, Tannert, & Krautz, 2012). The lower boundary of the operation range in conventional plants is not

below 20% of the nominal current density. This is because of reduced oxygen flux but current independent hydrogen crossover flux and gas solubility, which lead to a further increase in hydrogen content at the anode. In addition to safety issues, this reduces production efficiency because of increased gas loss in the deoxidizer.

Especially at high current densities, local gas accumulation may occur in the electrolyte, which will induce a rise in differential pressures across the separator. This has to be avoided because it further increases gas crossover and leads to higher mechanical stress on the separator.

7.3.2 Design considerations for high-pressure alkaline systems

In this section, the influence of pressure on electrolyzer design considerations at the cell, stack and system levels will be discussed.

Cell level. As stated before, differential pressures as well as the driving force for gas crossover across the separator increase with elevated system pressure. In addition, a high-pressure environment is more challenging in terms of corrosion. Therefore, more gastight and mechanically resistant separators are necessary for high-pressure applications (Roy et al., 2006). In the past, the commercially most used separator was asbestos. It is no longer allowed owing to health concerns. One alternative is NiO, but the research is still ongoing; possible candidates are other porous composites or ceramics (Smolinka, 2009; Ursua, Gandia, & Sanchis, 2012).

Nickel (Ni) or Ni-coated iron and Ni-based alloys, especially Raney nickel, were identified as the most suitable electro-catalysts in terms of the tradeoff between good performance and low cost. For temperatures up to 80 °C and slightly elevated pressure they showed good ability to resist the highly alkaline environment of KOH or NaOH solutions (Zeng & Zhang, 2010). However, there is still a need for improvement, especially because operating conditions are expected to become more demanding in future. The danger of corrosion and deactivation of the electrode will be more severe with an increase in pressure and temperature. One example is the deactivation of Ni in a hydrogen environment. With an increase in pressure, the hydrogen concentration in the vicinity of the electrode will become higher and hydrogen be adsorbed. This will lead to the formation of less active Ni hydride. Several projects have been started that focus on enhancing the electro-catalyst, the separator material and the cell design under these conditions (e.g. RESlyser, Elygrid).

In past years, triggered by the need for higher efficiency, the so-called micro- or zero-gap cell design has gained interest. In this setup perforated (porous) electrodes are directly attached to the separator, sometimes spaced by thin felt, soaked with electrolyte (e.g. Marini et al., 2012). This setup has an advantage in that electrolyte resistance, and with it ohmic losses, can be minimized. The gases, oxygen, at the anode and hydrogen at the cathode are produced mainly at the rear of the electrodes, which reduces the gas volume between the electrodes and separator and further decreases ohmic losses in the electrolyte (Caspersen & Kirkegaard, 2012; Wendt, 1984). In this setup the positive effect of pressure on ohmic losses, mentioned before, is diminished as a result of the already reduced void fraction. However, in this setup the electrodes have to be properly modified with slits or holes to provide easy escape for the

produced gases and avoid blocking the electrode and separator with hydrogen or oxygen. The required porosity and structure of the electrode have to be optimized according to the bubble size of the produced gas and depend, in addition to other parameters, on the applied pressure (Fischer, Hofmann, Luft, & Wendt, 1980). Also, the zero-gap design is demanding with regard to the materials and prone to corrosion or mechanical failure. Direct contact between the separator and electrode, e.g. hydride, produced on the electrodes, could damage the separator (Häussinger, Lohmüller, & Watson, 2000). A comprehensive overview on the issues of the zero-gap geometry and material selection is given in Pletcher and Li (2011).

Stack level. At the stack level, the use of a bipolar filter-press design is important for the realization of large modules and high operating pressures. It allows for a compact serial connection (low current and high voltage) of several hundreds of single cells, each separated by a current collector (cell spacer) that serves as the anode for one compartment and the cathode for the other (Ursua et al., 2012). Using this setup, thinner cells and larger cell areas can be realized. Today, it is used in almost all commercially available electrolyzers, although the investment costs and construction efforts are higher (Zeng & Zhang, 2010). Therefore, there are basically no significant pressure-dependent differences in the stack design. However, the requirement for materials is much higher with regard to leak tightness and clamping pressure (NOW, 2011). Therefore, an interesting approach is casting of the whole stack, and sometimes parts of the peripheral components, in a water-filled pressure vessel (e.g. Janssen et al., 2004). This eliminates the pressure difference between the stack and its enclosure and reduces the complexity of the stack sealing. In addition, the demands on the materials of the stack and the peripheral components, including in the vessel, are reduced because these are not exposed to the difference between atmospheric and operating pressure.

System level. For atmospheric and pressurized plants, two separators for the lye−gas mixture and deoxidizers are required. Separators in pressurized systems are orientated horizontally, in contrast to the atmospheric design in which they are oriented vertically. The horizontal design is required to maintain a constant lye level despite lower gas volumes.

In a pressurized system a feed water pump is required because, different from atmospheric systems, water feed cannot be realized purely by gravity. Also, a circulation pump for the electrolyte may be required at pressures around 30 bar to maintain uncritical operating conditions (Roy et al., 2006). Whereas at atmospheric conditions the electrolyte circulates naturally as a result of buoyancy forces, the increased weight of the bubbles at elevated pressure reduces vertical velocity and circulation may be insufficient to avoid problematic local gas accumulation (Ziems et al., 2012).

This external circulation has a considerable influence on the void fraction and electrode coverage; in addition to reduced safety issues, it has a positive influence on overpotential. The gas volume scales almost linear with the electrolyte flow velocity. Therefore, a smaller decreased void fraction and less ohmic loss can be assumed with external electrolyte flow. In Janssen, Geraets, Barendrecht, and Stralen (1982), a voltage drop of almost 10% was observed when the velocity was increased from

0.2 to 1 m/s. In Eigeldinger and Vogt (2000), the influence of a rise in velocity on coverage was described as:

$$\theta = \frac{\theta_0}{\left(1 + (C \cdot v)^2\right)^2} \tag{7.32}$$

where C is a design parameter that is constant for a specific system, θ_0 is the coverage without external circulation and v is the electrolyte velocity. At velocities of 0.3 m/s the coverage was considerably reduced to a few percent of the value obtained without circulation. However, the results also depend strongly on the applied current density, and an increase in velocity can intensify corrosion and even lead to erosion of the electrode.

Another influence on safety issues is an increase in the minimal required wall thickness of pipes or cylindrical vessels that are exposed to elevated pressure conditions. It can be described by (IACS, 2012):

$$t = t_0 + b + c \tag{7.33}$$

$$t_0 = \frac{p \cdot D}{20 \cdot K \cdot e + p} \tag{7.34}$$

where p is the inner pressure, D the outer diameter of the device or tube and K the material-specific permissible stress. Parameters e, b and c reflect safety margins related to seams, mechanical tolerances and corrosion. Owing to the high values of K for, e.g. stainless steel (on the order of 100 MPa), the thickness t_0 scales almost linear with pressure. In turn, an increase in pressure reduces the gas volume and smaller device diameters can be realized. Because the inner diameter of the devices also has a linear influence on wall thickness, this partly reduces the direct pressure effect. Both effects may influence the dynamic behaviour of the electrolyzer. On the one hand, temperature dynamics are negatively influenced by the thicker walls that increase the heat capacity of the system and can lead to longer startup times after shutdown. On the other hand, the gas volume of the product gases is significantly reduced. This has a positive influence on the pressure and composition dynamics because volume changes in the system are smaller and its response time is shorter (Roy et al., 2006).

The higher pressure and resulting gas crossover in combination with the increase in solubility have consequences for the system design. In conventional systems lye streams are often recombined to simplify the setup. However, because of safety problems and higher gas loss caused by recombination, in advanced systems the streams are split, despite the related increase in system cost and complexity. Furthermore, local gas accumulation and crossover impede proper pressure control of the cell. Additional consumers such as the pressure control, the additional circulation pump for lye streams, the feed water pump and the extra safety arrangements or necessary control systems increase the effort of maintenance and the specific energy demand, as well as the investment costs of the pressurized system (Roy et al., 2006).

However, with increasing system size the specific cost of the system and specific energy demand are reduced. In pressurized systems this dependence is stronger and the potential of reducing the system's specific energy demand is higher than in atmospheric systems (Smolinka, 2009).

7.4 High-pressure electrolysis with solid polymer electrolyzers

A cross-section of a conventional polymer electrolyte membrane (PEM) water electrolysis cell is provided in Figure 7.11 (thicknesses of individual components are not to scale) (Millet et al., 2011; Rozain & Millet, 2014). The polytetrafluoroethylene-reinforced solid polymer electrolyte (SPE) at the center (1) and its two catalytic layers (2 and 2′) are clamped between two porous titanium current distributors (3 and 3′). Two grid spacers (4 and 4′) placed close to the end plates (5 and 5′) are used to manage a cavity through which liquid water is pumped and gases are collected during operation.

During operation, a fraction of the liquid water pumped through the anodic compartment (4′) diffuses across the porous anodic current distributor (3′) up to the anode (2′), where it is decomposed into protons, oxygen and electrons. Bubbles of gaseous oxygen

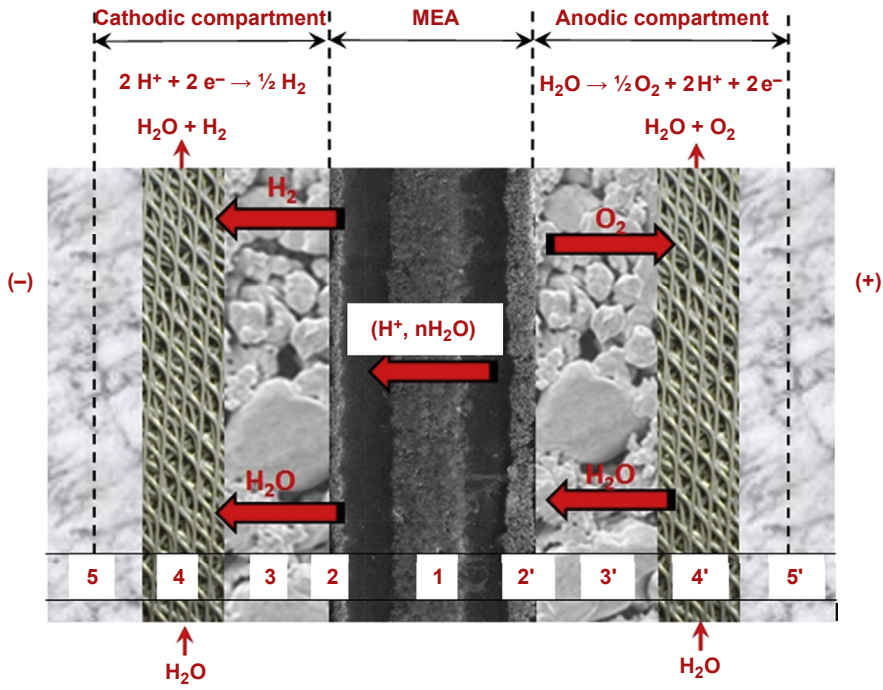

Figure 7.11 Cross-section of a PEM water electrolysis cell.

diffuse back to the anodic compartment (4′), where the liquid−gas mixture that forms is then carried out of the cell by circulating water. Electrons are collected and transferred out to the external DC generator. Hydrated protons (this flow of water is usually referred to as electro-osmotic drag; the number of solvation water molecules dragged along the proton flux is a function of the equivalent weight (EW) of the membrane and operating temperature) diffuse through the SPE (1) down to the cathode (2). At the cathode, protons are reduced by incoming electrons into gaseous hydrogen and solvation water molecules are released there as liquid water. The liquid−gas biphasic mixture formed of hydrogen gas bubbles and the water electro-osmotic flow diffuse through the pores of the cathodic current distributor (3) up to the cathodic compartment (4), where it is carried out of the cell by circulating water.

7.4.1 Pressure dependence of electrochemical reaction kinetics in pressurized PEM water electrolysis

In PEM water electrolyzers, half-cell reactions are:

$$\text{Anode}: \quad H_2O \rightarrow \frac{1}{2}O_2 + 2H^+ + 2e^- \tag{7.35}$$

$$\text{Cathode}: \quad 2H^+ + 2e^- \rightarrow H_2^- \tag{7.36}$$

Equation (7.36) is the hydrogen evolution reaction (HER) and Eqn (7.35) is the oxygen evolution reaction (OER).

Concerning the HER, only two reactions paths involving two steps each are regarded as likely to occur in acidic media (H_{ad} denotes a surface ad-atom, and M a surface metal site) (Millet & Ngameni, 2011):

Mechanism 1 (Volmer-Tafel)

$$H^+ + 1e^- + M \leftrightarrow MH_{ad} \tag{7.37}$$

$$2MH_{ad} \leftrightarrow 2M + H_2(g) \tag{7.38}$$

Mechanism 2 (Volmer-Heyrovsky)

$$H^+ + 1e^- + M \leftrightarrow MH_{ad} \tag{7.39}$$

$$H^+ + 1e^- + MH_{ad} \leftrightarrow M + H_2(g) \tag{7.40}$$

The first step (Volmer step) is shared by both mechanisms. They differ only by the desorption step (chemical desorption for mechanism 1 via the Tafel desorption step (7.38), which implies surface-diffusion of H_{ad} species, or electrochemical desorption for mechanism 2 via the Heyrovsky desorption step (7.40)). In the literature, there is general agreement that on platinum (in acidic media), the HER mechanism is that of a fast proton discharge followed by rate-determining chemical desorption (mechanism 1) but there is no experimental evidence that an increased hydrogen pressure can affect

the kinetics of the rate-determining step. In some cases, at high current density, mass transport effects are sometimes observed, but this usually results from mass transport across porous current collectors, the porosity of which is inappropriately open (Millet, de Guglielmo, Grigoriev, & Porembskiy, 2012).

Concerning the OER, several different mechanisms have been reported in the literature to account for the kinetics of the OER in acidic media on metallic oxides (Bockris, 1956). The most frequently quoted are:

Mechanism 1 (oxide path on Pt)

$$4Pt + 4H_2O \rightarrow 4PtOH + 4H^+ + 4e^- \tag{7.41}$$

$$4PtOH \rightarrow 2PtO + 2PtH_2O \tag{7.42}$$

$$2PtO \rightarrow O_2 + 2Pt \tag{7.43}$$

Mechanism 2 (Krasil'shchikov path on IrO_2 (Krasil'shchikov, 1963), where S denotes a reaction site)

$$S + H_2O \rightarrow S\text{-}OH + H^+ + 1e^- \tag{7.44}$$

$$S\text{-}OH \rightarrow S\text{-}O^- + H^+ \tag{7.45}$$

$$S\text{-}O^- \rightarrow S\text{-}O + e^- \tag{7.46}$$

$$S\text{-}O \rightarrow S + {}^1\!/_2\, O_2 \tag{7.47}$$

IrO_2 is commonly used in PEM water electrolyzers. Mechanism 2 prevails and the oxide oxidation step is usually considered to be rate-determining. The effect of oxygen pressure on the kinetics is negligible.

All of these observations have been confirmed experimentally (Figure 7.12). PEM water electrolysis polarization curves measured at different operating pressures are shifted to higher cell voltage values. A 100- to 120-mV shift is observed when the pressure is raised from 1 to 50 bars. Therefore, the extra energy cost required to perform pressurized water electrolysis comes only from the thermodynamics of the water-splitting reaction and not from the kinetics of half-cell reactions.

7.4.2 Gas cross-permeation phenomena in PEM water electrolyzers

Mass transport mechanisms across the SPE. Investigation of gas cross-permeation during PEM water electrolysis has only recently begun. A few years ago, the inverse proportionality between the contamination level and operating current density was proved experimentally and a model was proposed to account for experimental observations (Grigoriev et al., 2009; Grigoriev et al., 2011). A more detailed analysis of gas cross-permeation phenomena in PEM water electrolysis was proposed by Schalenbach, Carmo, Fritz, Mergel, and Stolten (2013). Ideally, the SPE should be

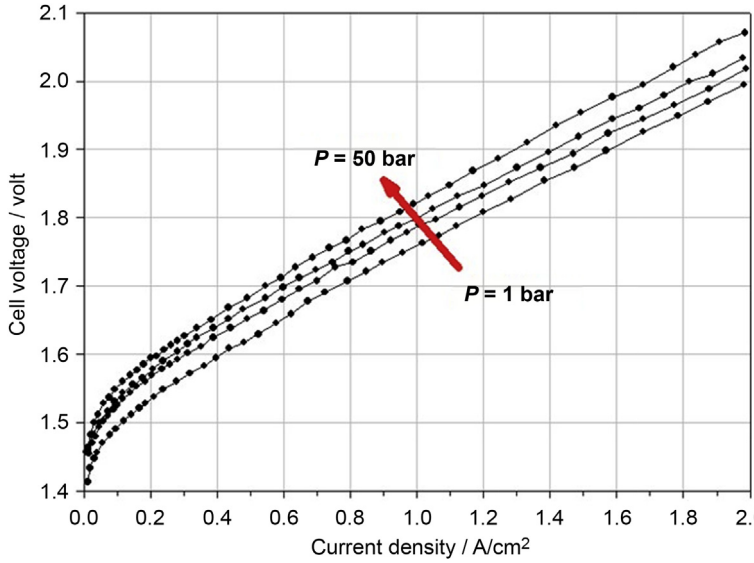

Figure 7.12 Role of operating pressure on polarization curves of a PEM water electrolysis cell using platinum as cathodic catalyst and iridium as anodic catalyst.

totally impermeable to gases. Only water-saturated pure gases should be produced during electrolysis and should be collected at the exhaust of the PEM water electrolysis cell (hydrogen from the cathodic compartment and oxygen from the anodic compartment). However, such an ideal situation is a limiting case not observed experimentally. Several microscopic mechanisms contribute to gas cross-permeation phenomena (Figure 7.13).

As a result, hydrogen can be detected in oxygen at concentration levels sometimes above the lower explosive limit; likewise, oxygen is found in hydrogen. For a given SPE material (chemical composition, water content and thickness), the extent of this contamination is a function of operating temperature, pressure and current density. Because lower flammable and explosive limits of hydrogen in air (and oxygen) can easily be reached during PEM water electrolysis operation, for safety reasons there is a need to monitor the hydrogen content continuously in oxygen and to gain a good understanding of the mechanisms involved in the contamination process.

Main microscopic mass transport mechanisms during PEM water electrolysis that can contribute to the contamination of oxygen by hydrogen are (Figure 7.13):

- Mechanism A: Hydrogen produced at the cathode of the PEM water electrolysis cell is soluble in the SPE. The concentration of dissolved hydrogen is at equilibrium with the gas phase. For a given SPE material, the concentration of dissolved hydrogen is mainly a function of temperature and pressure.
- Mechanism B: Because hydrogen can dissolve in the SPE, it can also be transported along a concentration gradient. This is what happens across the SPE membrane during water electrolysis. Fickian diffusion-controlled transport of dissolved hydrogen formed at the cathode

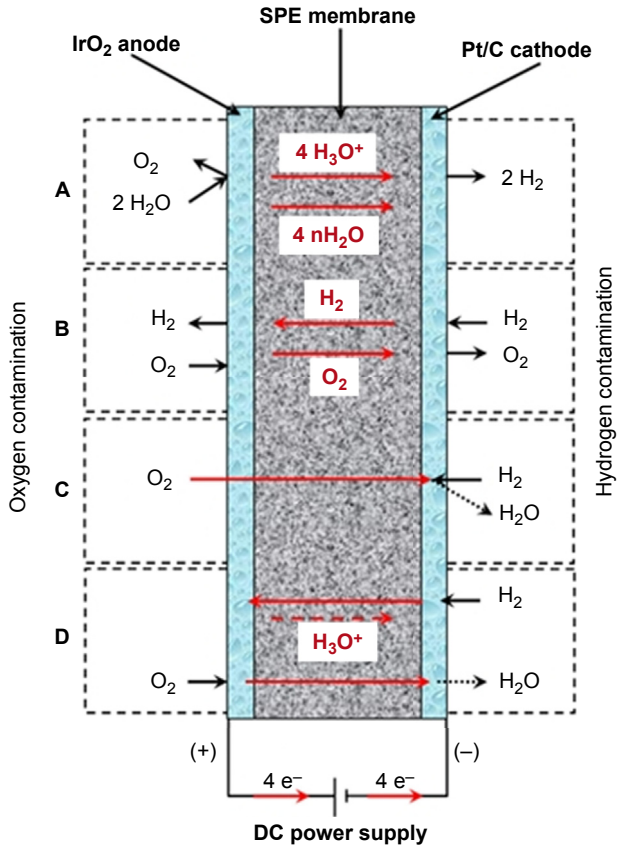

Figure 7.13 Microscopic mass transport mechanisms during PEM water electrolysis: A: water splitting (electrolysis); B: Fickian diffusion cross-permeation; C: H_2 and O_2 chemical recombination; D: H_2 and O_2 electrochemical recycling.

towards the anode is the predominant transport mechanism (there are few if any experimental indications that convection may exist in perfluorosulphonic acid (PFSA) materials owing to their specific nanostructure). The gradient of chemical potential (concentration) set across the SPE is the driving force to cross-permeation.

- Mechanism C: Chemical recombination of dissolved hydrogen and oxygen into hydrogen peroxide or even water inside the SPE may occur. These reactions can be catalyzed at the cathode by Pt/C particles used for the HER. The process tends to reduce the faradaic efficiency of the electrochemical process but can potentially reduce cross-permeation of gases and subsequent contamination.
- Mechanism D: Electrochemical oxidation of hydrogen into protons can take place at the anode. During water electrolysis, the anode is operating at a high potential, close to 1.8 V, a value at which hydrogen is supposed to be easily reoxidized.
- The electro-osmotic flow of water that drives solvation water molecules from the anode down to the cathode during electrolysis (mechanism A) tends to bring hydrogen back to

the cathode and does not favour hydrogen crossover. This electro-osmotic flow of water is a function of the operating current density.

Main microscopic mass transport mechanisms during PEM water electrolysis that can contribute to the contamination of hydrogen by oxygen are (Figure 7.13):

- Mechanism A: Oxygen produced at the anode of the PEM water electrolysis cell is also soluble in the SPE. There is also a solubility equilibrium between the gas phase and the SPE (with a solubility constant different from hydrogen) and for a given SPE material, the concentration of dissolved hydrogen is a function of temperature and pressure.
- Mechanism B: Oxygen is also transported across the SPE by Fickian diffusion-controlled transport of dissolved molecules. The gradient of chemical potential (concentration) set across the SPE is the driving force. However, oxygen is less soluble and less mobile than hydrogen (by approximately a factor of 2) and hydrogen crossover is usually larger than oxygen crossover.
- Mechanism C: Chemical recombination of dissolved oxygen and hydrogen into hydrogen peroxide or even water inside the SPE may occur at the cathode, catalyzed by the Pt/C catalyst particles. The process tends to reduce cross-permeating flows of hydrogen and oxygen.
- Mechanism D: Electrochemical reduction of oxygen at the cathode occurs. During operation, the cathode operates at a potential close to −0.1 V/RHE, which is sufficiently low to reduce oxygen. The process contributes to lowering the flow of cross-permeating oxygen.
- The electro-osmotic flow of water that drives solvation water molecules from the anode down to the cathode (mechanism A) tends favour oxygen cross-permeation. This mechanism of oxygen transport is a function of the operating current density because the electro-osmotic flow of water is a function of current density.

In conclusion, gas crossover phenomena result from different microscopic mechanisms that have either positive or negative roles in cross-permeation phenomena. In addition, a fraction of the gas cross-permeating flow is lost by either chemical or electrochemical recombination, thus reducing the faradic efficiency of each interface, a situation that adds complexity to the analysis of the problem. More details are provided in the following paragraphs.

Microstructure of PFSA materials. In PEM water electrolysis technology, chemically stable sulphonated tetrafluoroethylene-based fluoropolymer copolymer membranes (W. Grot, E.I. DuPont Co., Nafion® products) are commonly used as SPE (Figure 7.14). Nafion® products gather a number of physical properties necessary for operation in PEM water electrolysis cells: (1) high ionic conductivity (>10 mS/cm); (2) poor electronic conductivity; (3) good chemical and mechanical stability; (4) high thermal conductivity (>0.1 J/s m K) and (5) limited permeability to hydrogen and oxygen. Proton conductivity, water management, relative affinity to water, hydration stability at high temperatures, electro-osmotic drag and mechanical, thermal and oxidative stability of these materials are directly determined by their chemical microstructure.

The cluster-network model of Gierke, Munn, and Wilson (1981) has been used for many years to interpret the properties of Nafion® membranes (especially ion and water transport and ion permselectivity). In this model (Figure 7.15), it is assumed that there are approximately 40 Å-diameter clusters of sulphonate-ended perfluoroalkyl ether groups organized as inverted micelles and arranged on a lattice. These micelles are

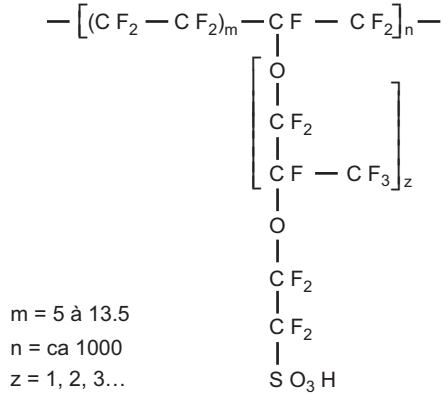

Figure 7.14 Structure unit of Nafion®.

connected by pores or channels that are approximately 10 Å in size. These $-SO_3^-$-coated channels were invoked to account for inter-cluster transfer of cations and ion conductivity. The model has then be refined (e.g. by Yeager and Steck (1981)). Compared with the model of Gierke et al. (1981), the clusters do not have a strict geometry and their geometrical distribution has a lower degree of order. Most important, intermediate interphase domains are found between hydrophobic and hydrophilic regions. For the development of PEM water electrolysis applications, Nafion® can be considered a homogeneous two-phase medium, a mixture of hydrophobic regions concentrating fluorocarbon backbones and hydrophilic regions containing water, in which proton conductivity takes place.

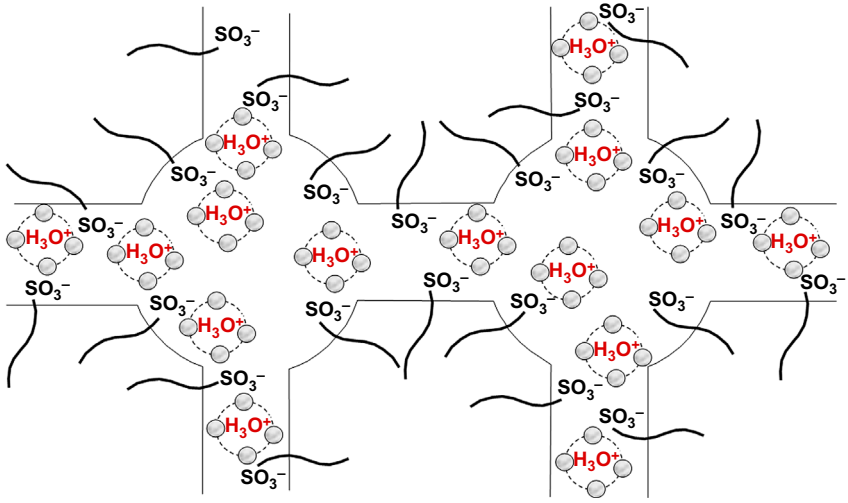

Figure 7.15 Gierke model of sulphonate nanoclusters in perfluorosulphonic acid materials.

Gas solubility in PFSA materials. All gases including hydrogen and oxygen can dissolve in PFSA materials. Gas solubility is at the origin of gas cross-permeation during water electrolysis. The solubility is a function of several parameters, among which the EW of the polymer, the water content, the operating temperature and the pressure are the most significant. At equilibrium, the quantitative relationship between concentration C_i (in mol/cm^3) of gas species i in the polymer and its partial pressure p_i (in Pa) in the gas phase is given by Henry's law:

$$p_i = H_i C_i \tag{7.48}$$

where H_i is the solubility coefficient (Henry's constant) of species i in Pa cm^3/mol. In PEM water electrolysis experiments, the partial pressure of gases must be considered because both hydrogen and oxygen released by the electrolyzer are saturated with water vapour. Different reports are available in the literature on gas (H_2 and O_2) solubility in PFSA (Nafion) materials (Ogumi, Takehara, & Yoshizawa, 1984; Sakai, Takenaka, & Torikai, 1986; Yeo & McBreen, 1979). For H_2, the following relations can be used in the 0−100 °C temperature range and the 1−10 atm pressure range (Mann, Amphlett, Peppley, & Thurgood, 2006): for 0 °C < T < 45 °C:

$$H_{H_2}^{H_2O} = 7.9 \times 10^6 \exp(-545/T) \times \left(1 + 0.000071 P_{H_2}^3\right) \text{ in atm cm}^3/\text{mol} \tag{7.49}$$

for 45 °C < T < 100 °C:

$$H_{H_2}^{H_2O} = 8.3 \times 10^5 \exp(-170/T) \times \left(1 + 0.000071 P_{H_2}^3\right) \text{ in atm cm}^3/\text{mol} \tag{7.50}$$

For O_2, the following relations can be used in the 0−100 °C temperature range, at 1 atm: for 0 °C < T < 45 °C:

$$H_{O_2}^{H_2O} = 1.3 \times 10^8 \exp(-1540/T) \text{ in atm cm}^3/\text{mol} \tag{7.51}$$

for 45 °C < T < 100 °C:

$$H_{O_2}^{H_2O} = 5.1 \times 10^6 \exp(-500/T) \text{ in atm cm}^3/\text{mol} \tag{7.52}$$

Measurement of gas cross-permeation. Accurate measurement of cross-permeation flow is critical for a correct and detailed analysis of cross-permeation phenomena at microscopic levels. This is usually performed under stationary conditions, when concentrations are time independent and easier to measure. Gas cross-permeation fluxes can be measured during electrolysis under stationary conditions by measuring the hydrogen concentration in oxygen and vice versa, using, for example, a gas chromatograph (see, e.g. Bensmann et al. (2014) for a survey of other

available methods). Bensmann et al. (2014) suggested a method for measuring hydrogen crossover in PEM water electrolysis cells. The measurement principle is based on the electrochemical compensation of the crossover flux, which translates the mass flux determination into an electric current measurement. The technique is especially suitable for high-pressure PEM electrolyzers operated under asymmetric pressure conditions. It allows for measurement with a fully assembled cell at normal water electrolysis conditions using standard equipment also installed in industrial electrolysis plants.

7.4.3 Simplified model for gas cross-permeation

A simplified model of gas cross-permeation processes in PEM water electrolysis cells can be developed by considering the Fickian diffusion transport of dissolved gases as the main contribution to gas crossover flows.

Transport equations. In a first approximation, the SPE is considered an isotropic medium with uniform distribution of physical properties. Gas transport is a diffusion-controlled process that follows Fick's law of diffusion:

$$f_i = D_i \frac{\partial C_i}{\partial x} \tag{7.53}$$

where f_i is the flow of species i in mol cm^2/s across the SPE, D_i is the diffusion coefficient of species i and x is the distance coordinate along the membrane thickness in cm. Under stationary conditions (constant current density at constant temperature and pressure), the stationary flux of gas transported across the SPE of thickness L is:

$$f_i = D_i \frac{\Delta C_i}{L} \tag{7.54}$$

A combination of Eqns (7.48) and (7.54) yields:

$$f_i = \frac{D_i}{H_i} \frac{(p_1 - p_2)}{L} \text{ in mol/s cm}^2 \tag{7.55}$$

where p_1 and p_2 are the partial pressures of the diffusing species in both cell compartments.

Gas permeability and diffusivity in PFSA materials. The permeability P_i of a gaseous species i across an SPE membrane of thickness L (in m) and surface area A (in m^2) is defined as:

$$P_i = \frac{u_i}{\Delta P} \frac{L}{A} \text{ in cm}^2/\text{Pa s} \tag{7.56}$$

where u_i is the rate of permeation of species i in Nm^3/s and ΔP is the difference of pressure set across the membrane. The permeability of PFSA materials with different

water content towards different gaseous species has been studied extensively. The temperature dependence of hydrogen and oxygen permeability of Nafion 117 equilibrated with different water contents are plotted in Figure 7.16 (Sakai, Takenaka, Wakabayashi, Kawami, & Torikai, 1985).

Permeability varies markedly with both the temperature and water content of the polymer membrane, bracketing values measured on poly(tetrafluoroethylene) (PTFE) and liquid water. These data show that the transport of dissolved gases across hydrated PFSA materials (Nafion®) is similar to that across liquid water. This is an indication that transport of dissolved gases takes place mainly through the ionic (hydrated) clusters. The permeability P_i of species i is related to its diffusion coefficients D_i (in cm^2/s) through:

$$D_i = P_i^m RTC_i \tag{7.57}$$

where R is the ideal gas constant; T is the operating temperature (in K) and C_i is the concentration of species i (in mol/cm^3). Hydrogen and oxygen diffusion coefficients in

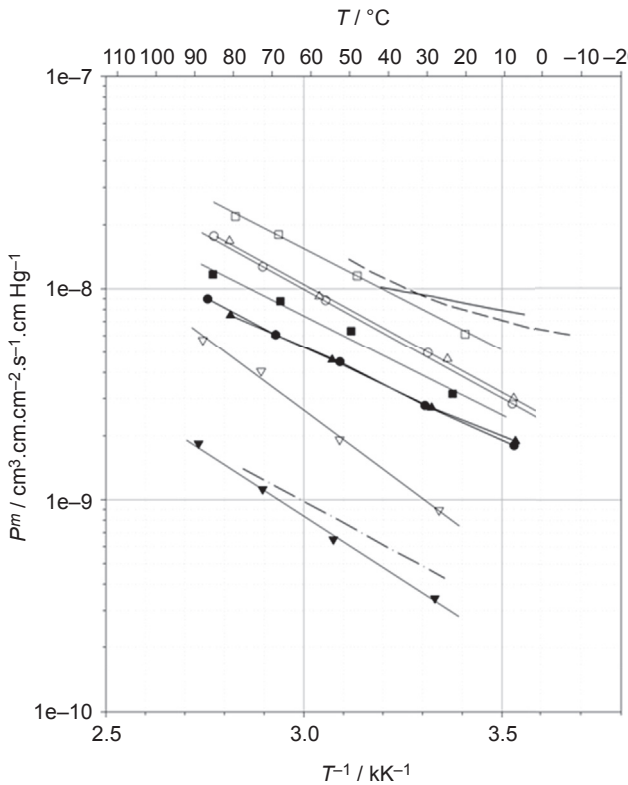

Figure 7.16 Hydrogen (open symbols) and oxygen (close symbols) permeability of Nafion® 117 with temperature and water content: (--) H_2 in pure water; — O_2 in pure water. □, ■ Nafion 117, 100% H_2O; △, ▲ Nafion 117, 50% H_2O; ○, ● Nafion 117, 34% H_2O; ▽, ▼ Dry Nafion 117; (- · -), PTFE.

Table 7.1 H_2 and O_2 permeability and diffusion coefficient in fully hydrated Nafion 117 at different temperatures

T/°C	10	20	40	60	85
$P^m_{O_2}$/cm^2/Pa s	2.1×10^{-12}	2.3×10^{-12}	3.7×10^{-12}	5.3×10^{-12}	8.4×10^{-11}
D_{O_2}/cm^2/s	2.1×10^{-7}	2.5×10^{-7}	4.2×10^{-7}	6.5×10^{-7}	1.1×10^{-6}
$P^m_{H_2}$/cm^2/Pa s	3.8×10^{-12}	4.6×10^{-12}	7.6×10^{-12}	1.2×10^{-11}	2.0×10^{-11}
D_{H_2}/cm^2/s	3.9×10^{-7}	4.9×10^{-7}	8.7×10^{-7}	1.5×10^{-6}	2.6×10^{-6}
D_{H_2}/D_{O_2}	1.9	2.0	2.1	2.3	2.4

Nafion® 117 at different operating temperatures are compiled in Table 7.1. D_{H_2} is larger than D_{O_2} by a factor of 2 over the conventional 0−100 °C temperature range of operation of PEM water electrolyzers. Thus, hydrogen concentration in oxygen at constant pressure of operation is twice as high as the oxygen concentration in hydrogen. For safety reasons, this is why the concentration of hydrogen in oxygen is usually scrutinized during operations.

The value of D_{H_2} can also be determined using the empirical relationship proposed by Ogumi et al. (1984):

$$D_i\ (\mathrm{cm}^2/\mathrm{s}) = 4.1 \times 10^{-3} \exp\left(-\frac{2602}{T}\right) \tag{7.58}$$

Calculation of contamination levels. Let j be the operating current density in A/cm^2. During water electrolysis, the flux f_{O_2} of oxygen produced at the anode (in mol/cm^2 s) is:

$$f_{O_2} = j/2F \tag{7.59}$$

where F is the Faraday constant (96,470 C/mol). The mole fraction n_{H_2} (in %) of hydrogen in oxygen is therefore given by:

$$n_{H_2}(\%) = \frac{f_{H_2}}{f_{H_2} + f_{O_2}} \times 100 \tag{7.60}$$

Combining Eqns (7.55), (7.59) and (7.60), one finally obtains:

$$n_{H_2}(\%) = \frac{2FD_{H_2}\Delta P_{H_2}}{(2FD_{H_2}\Delta P_{H_2}) + (jLH_{H_2})} \times 100 \tag{7.61}$$

In Eqn (7.61), the hydrogen flux across the membrane (at constant temperature and pressure) is a function of hydrogen diffusivity (D_{H_2}), hydrogen solubility (H_{H_2}) and pressure gradient $(\Delta P/L)$. The hydrogen content in oxygen n_{H_2} is also inversely

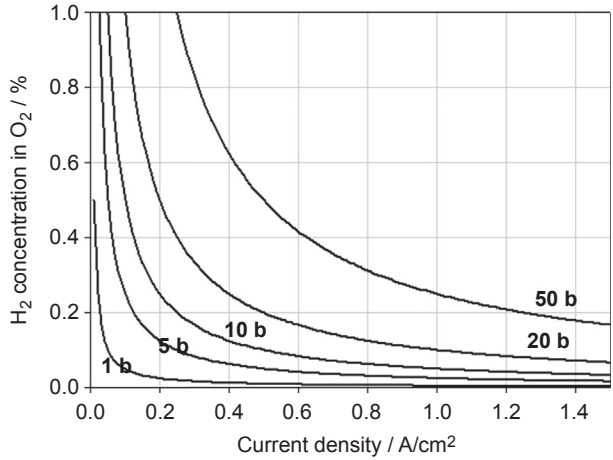

Figure 7.17 Role of operating pressure on contamination level.

proportional to the current density. The operating current density is the parameter that sets the level of dilution of hydrogen in oxygen. Assuming that the Fickian transport of hydrogen across the SPE is the main contribution to hydrogen cross-permeation, the effect of operating pressure on the hydrogen contamination level in oxygen is plotted in Figure 7.17 and the effect of membrane thickness on the hydrogen contamination level in oxygen is plotted in Figure 7.18 (the reference case is that of Table 7.2). As expected, the higher the operating pressure and the thinner the membrane, the higher the contamination is at a given operating current density. These results clearly show that contamination problems occur in PEM water electrolyzers operating at low current densities.

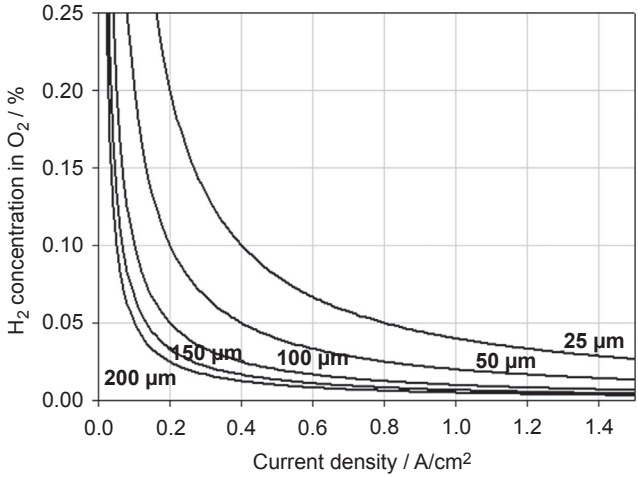

Figure 7.18 Role of operating pressure on contamination level.

Table 7.2 Reference parameters value used to model hydrogen cross-permeation

SPE thickness (μm)	Temperature (°C)	Pressure (bar)	D_{H_2} (cm^2/s)	H_{H_2} ($Pa/mol\ cm^3$)
200	85	1	2.6×10^{-6}	5×10^{10}

Analysis of experimental results. Gas cross-permeation experiments indicate that the general trend dictated by Eqn (7.61) is globally satisfied. The hydrogen content in oxygen is inversely proportional to the operating current density and the contamination level tends to increase with the operating pressure (Figure 7.19). When internal catalytic promoters are used (for example, by applying a platinum surface coating on the current collectors), the situation at low current density is improved. However, Eqn (7.61) is based on different simplifying assumptions, among which the crudest one is that the faradaic efficiency remains equal to unity. A difficult experimental problem is to prove the different mechanisms listed in Figure 7.13 and evaluate their contribution as a function of operating conditions. The problem has not yet been totally solved; additional work is required to clarify the situation fully.

Limitation of gas cross-permeation effects. As discussed above, it is necessary for safety reasons but also for the satisfaction of downstream process requirements to maintain the hydrogen concentration in oxygen and oxygen concentration in

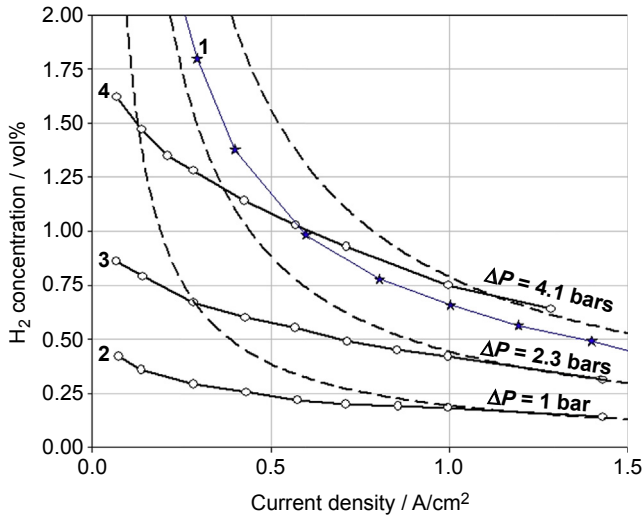

Figure 7.19 H_2 content (vol%) in the anodic oxygen−water vapour mixture, measured at different pressures as a function of operating current density. $T = 85$ °C. (1) 6 bars (from Schalenbach et al., 2013); (2−4) measures with platinized current collector 1.0, 2.3 and 4.1 bars. Dotted lines: model curves using Eqn (7.61) (see text).

hydrogen below critical threshold values. Because gas cross-permeation phenomena are inherently caused by the microstructure and physical properties of PFA materials used as cell electrolyte and by Fickian diffusion, gas crossover phenomena can be limited either by modifying the solubility and gas transport properties of the SPE or by the catalytic promotion of a catalytic recombination of hydrogen and oxygen into water. Different approaches can be followed. First, thicker SPEs can be used to reduce gas transport by cross-permeation through the SPE. In particular, Nafion-reinforced membranes (in which a PTFE cloth is clamped between two conventional perfluorinated membranes) developed for the chlorine-alkali industry are commercially available. These membranes are thicker and less permeable to gas crossover.

Second, it is possible to reduce either the diffusion coefficient or the solubility of the gas. This can be obtained by incorporating inorganic fillers inside the SPE, such as silica or zirconium oxide. Some experiments made with zirconium dioxide have shown that D_i and H_i can be reduced up to a factor of 10, depending on the filler concentration added to the SPE (Millet, Dragoe, Grigoriev, Fateev, & Etievant, 2009). Usually, such fillers are incorporated into the SPE by impregnating cationic precursor species followed by chemical precipitation using an adequate chemical.

Third, it is possible to maintain the final purity of hydrogen at levels >99.99%, i.e. at values well above the thresholds of explosion mixtures, by using passive catalytic gas (H_2/O_2) recombiners. In such recombiners, dry gases are chemically recombined into water at a platinum surface with a large surface area and subsequently re-dried. This can be done outside the electrolyzer: for example, in the liquid−gas separators. Recombiners can also be implemented directly in PEM cells using internal gas recombiners (Grigoriev et al., 2009). For example, titanium current collectors can be surface platinized to promote gas recombination and reduce pollution levels, with the additional advantage that current collectors are then less prone to surface oxidation, a factor that contributes to increase the durability of PEM water electrolyzers. The price of any of these improvements is often a reduction in the ionic conductivity of the SPE, an additional ohmic term during electrolysis, lower cell efficiency and higher cost. A balance has to be made between cost considerations and safety issues.

7.4.4 Technology developments

PEM water electrolysis stacks can be either self-pressurized (polymer-based peripheral gaskets of individual PEM cells are used for that purpose) or pressurized in a pressurization vessel. The first technique is simpler but usually is limited to operating pressures less than 100 bars. The second technique can be used to potentially reach several 100 bars. The electrolysis stack is introduced in a stainless-steel pressurization vessel.

Commercial pressurized PEM water electrolyzers. Most commercial PEM water electrolyzers use self-pressurized PEM cells. The maximum rating pressure available on large PEM electrolyzers ($\approx$60 Nm^3 H_2/h) is 35−40 bars. A list of technical performance provided by different manufacturers of PEM and alkaline water electrolyzers is provided in Table 7.3 for comparison. Higher pressure levels can be reached using

Table 7.3 **List of electrolyzer manufacturers and selection of key performance indicators (FCH-JU, 2014)**

Company	Country	Technology	Product	Capacity (Nm^3/h)	H_2 output pressure (barg)	H_2 purity (%)	Electricity consumption (kWh/kg)	Electric LHV efficiency (%)
Acta	Italy	AEM	ELI1000	1	29	99.94	53.2	63%
AREVA	France	PEM	Development	20	35	99.9995	55.6	60%
CETH2	France	PEM	E60 cluster	240	14	99.9	54.5	61%
ELT Elektrolyse Technik	Germany	Alkaline	Customized	330	Atmospheric	99.85	51	65%
Erredue s.r.l	Italy	Alkaline	G256	170	30	99.5	59.5	56%
H_2 Nitidor	Italy	Alkaline	200-Nm^3/h	200	30	99.9	52.3	64%
H-TEC Systems	Germany	PEM	EL30/144	3.6	29	N/A	55.6	60%
Hydrogenics	Belgium, Canada	Alkaline (PEM in dev.)	HyStat60	60	10	99.998	57.8	58%
Idroenergy	Italy	Alkaline	Model120	80	5	99.5	52.4	64%
IHT Industrie Haute Technologie	Switzerland	Alkaline	Customized	760	31	N/A	51.2	65%
ITM Power	UK	PEM (AEM in dev.)	HPac40	2.4	15	99.99	53.4	62%
NEL Hydrogen	Norway	Alkaline	Customized	485	Atmospheric	>99.8	50	67%
McPhy	Germany	Alkaline	60-Nm^3/h container	60	10	>99.3	57.8	58%
Proton OnSite	USA	PEM	Hogen C30	30	30	99.9998	64.5	52%
Siemens	Germany	PEM	SILV2ER200	~250	N/A	N/A	~60	~55%
Teledyne Energy Systems	USA	Alkaline	SLM 1000	56	10	99.9998	N/A	N/A
Wasserelektrolyse Hydrotechnik	Germany	Alkaline	EV150	225	Atmospheric	99.9	58.7	57%

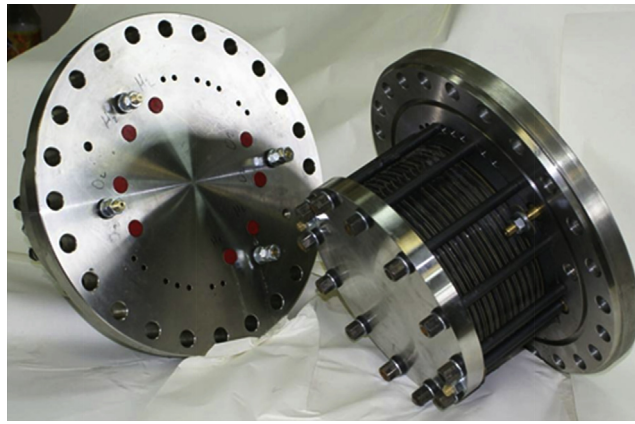

Figure 7.20 Photograph of two individual PEM stacks.

mechanical compressors. There is little information available in the literature concerning the effect of elevated operating pressure on performance and degradation processes. This is because for civil applications, PEM water electrolysis is a recent technology. There are indications, however, that the durability of PEM water electrolyzers is not significantly altered by operation under pressure.

Research and development on high-pressure PEM electrolyzers. Some research and development (R&D) projects are also investigating the possibility of operating PEM water electrolyzers at pressures much higher than those available commercially. The driving force for this kind of R&D development is that emerging markets of hydrogen as an energy carrier are calling for higher compression levels (for example, 800 bars is required for application in the automotive industry). In this pressure range, the use of pressurization vessels is mandatory. A picture of a pressurized PEM water electrolysis bi-stack is shown in Figure 7.20 (each stack can deliver up to 1.0 Nm^3 H_2/h at 1.2 A/cm^2). Each stack is made of eight membrane–electrode assemblies (MEAs), each with a 250-cm^2 active area, series connected in a filter-press configuration to reach the targeted hydrogen production capacity (Millet, Grigoriev, & Porembskiy, 2013). MEAs contain conventional noble metal electro-catalysts: $\approx$0.4 mg/cm^2 of metallic platinum for the HER and $\approx$2.0 mg/cm^2 of mixtures of metallic platinum and iridium for the OER. Nafion®-reinforced membranes from EI. DuPont Co. are used as SPE. Porous titanium disks (1.2 mm thick and 40% open porosity) are used as current collectors; titanium grids are used as cell spacers and titanium foil is used for bipolar plates. Carbon-based gaskets are used as cell sealants.

The two stacks are mounted on a cylindrical pressurization vessel (Figure 7.21). The dimensions of the unit are adjusted to minimize the open volume inside the pressurization cylinder. During electrolysis experiments, the pressure inside the stacks (because of the gaseous production of hydrogen and oxygen) is counterbalanced by a continuous flow of nitrogen into the pressurization cylinder. The pressure of nitrogen is set at a few hundred millibars above the internal pressure in the stacks to reduce the effect of pressure on the MEAs, reduce gas leaks during high-pressure measurements,

Figure 7.21 Photograph of a high-pressure bi-stack with its pressurization vessel.

and avoid H_2 and/or O_2 accumulation in the pressurization vessel. Alternatively, it is possible to inject liquid water into the pressurization vessel for thermal management. The efficiency of the electrolyzer (calculated on the higher heating value of hydrogen) is approximately 80% at 400 mA/cm^2 and 80 °C. Some results obtained in the 1−130 bar pressure range reproduced from Millet et al. (2013) are compiled in Table 7.4. Tests have been performed under stationary conditions at a current density of ≈500 mA/cm^2 and mean operating temperature of 88 °C. Here, the main operating parameter is the operating pressure. During operation, individual cell voltages are homogeneous and stable during operation.

Figure 7.22, shows that specific energy consumption (expressed in kWh/Nm^3 H_2) tends to increase with pressure. As discussed above, this mainly results from the effect of operating pressure on the thermodynamics of the water-splitting reaction. Also, although the current density remains stable, the hydrogen production rate (in Nm^3 H_2/h) tends to decrease. This is an indication that the current (faradaic) efficiency decreases significantly with pressure, owing to hydrogen crossover through the SPE membrane. Measurements show that the current (faradic) efficiency ε_j drops to almost 90% at 130 bars (Table 7.4) and that both the hydrogen purity (falling from 99.98% at atmospheric pressure to 97.34% at 130 bars) and oxygen purity are strongly altered. From these results, it can be concluded that whereas higher operating pressures negatively affect energy consumption, the extra energy cost remains significantly less than the energy required to compress hydrogen from atmospheric pressure with a mechanical (piston or membrane) compressor. Therefore, direct production of pressurized hydrogen with a pressurized electrolyzer remains attractive, at least from the energy

Table 7.4 Main test results obtained with the high-pressure PEM water electrolysis stack under stationary operating conditions

Parameter	Unit	Measured value at operating pressure, bar					
		1	**25**	**50**	**75**	**100**	**130**
Electric current	A	123.5	126.5	125.5	124.5	125.0	124.0
Operating temperature	°C	86	87	85	89	84	88
H_2 production rate	Nm^3/h	0.42	0.43	0.42	0.40	0.38	0.36
H_2 purity before recombiner	% vol.	99.98	99.76	99.18	98.56	98.01	97.34
H_2 purity after recombiner	% vol.	99.999	99.999	99.997	99.995	99.993	99.991
Individual cell voltage	V						
1		1.70	1.70	1.71	1.71	1.72	1.73
2		1.68	1.69	1.70	1.71	1.71	1.72
3		1.71	1.71	1.71	1.72	1.71	1.71
4		1.70	1.71	1.71	1.73	1.74	1.74
5		1.71	1.70	1.71	1.71	1.73	1.74
6		1.69	1.69	1.70	1.71	1.73	1.73
7		1.70	1.69	1.69	1.70	1.72	1.73
8		1.68	1.70	1.70	1.73	1.74	1.74
Stack voltage	V	13.57	13.59	13.63	13.72	13.80	13.84
Power consumption	kW	1.676	1.719	1.711	1.708	1.725	1.716
Specific energy	kWh/Nm^3	3.99	4.00	4.07	4.27	4.54	4.77
Current efficiency	%	99.98	99.68	98.13	96.57	92.91	90.45
Energy efficiency $\varepsilon_{\Delta G}$	%	72.5	72.4	72.2	71.7	71.3	71.0

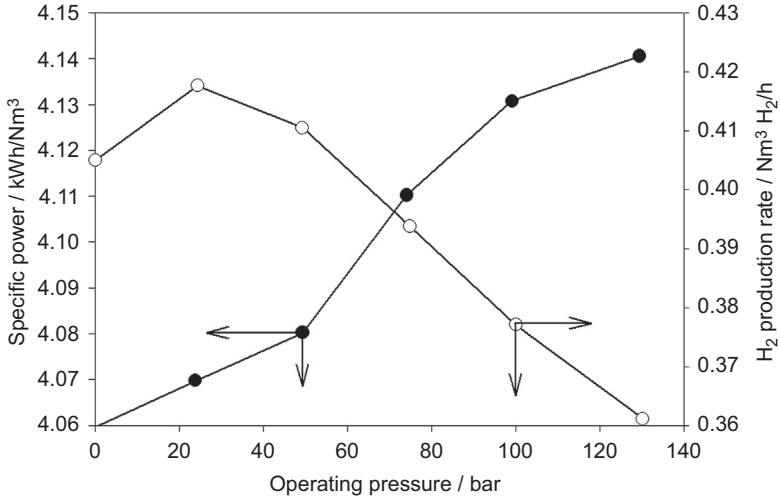

Figure 7.22 Mean specific power consumption and hydrogen production rate versus operation pressure for the pressurized PEM bi-stack in Figure 7.21.

(operating expense) viewpoint. However, progress is required to manage cross-permeation issues that have an increasingly strong negative impact on performance as the operating pressure is raised.

7.5 Future trends

Pressurized PEM water electrolyzers are being developed and made commercially available because some emerging hydrogen markets (e.g. hydrogen refueling stations for mobility applications, services offered to electrical grids or electricity storage) require compressed hydrogen of electrolytic grade. Self-pressurized stacks are available at no significant capital expenditure extra cost up to approximately 30–50 bars, but higher pressures require pressurization vessels and specific equipment (pressurized pumps, etc.) that tend to make the process economically less interesting. Therefore, pressurized PEM water electrolysis alone is usually not sufficient to reach appropriate levels of pressure required by downstream processes (e.g. 800 bars in hydrogen refueling stations) and electrolyzers need to be coupled with additional (either mechanical or electrochemical) pressurization units. Main effects of increasing operating pressure on the performance of PEM electrolyzers are: (1) increasing electrolysis voltage owing to the effects of pressure on the thermodynamics of the water-splitting reaction ($\approx$100 mV from 1 to 50 bars); however, there is a logarithmic relationship between cell voltage and pressure: cell voltage tends to increase less rapidly when the pressure is further raised; (2) no specific effects on the kinetics of the hydrogen and OERs and (3) increasing cross-permeation effects that tend to make contamination levels (mainly hydrogen concentration in oxygen) higher and eventually unacceptable for safety

reasons. Therefore, innovation in polymer science remains critical. So far, the literature does not have a report that high operating pressure could have a negative impact on durability issues, but the development of pressurized PEM water electrolyzers is still at an early stage and additional experiments will be needed to gain a more detailed picture of the situation, especially in the long-term when joint pressurization−thermal cycles will be applied because of operation under transient power loads.

Nomenclature

Latin symbols

a_α	Activity of species α (1)
A_{cell}	Cell area (m^2)
A	Surface area solid polymer electrolyte (m^2)
c_α	Concentration of species α (mol/m^3)
$c_{p,\alpha}$	Heat capacity of species α (J/mol K)
C	Design parameter (s/m)
C_i	Concentration of gas species i (mol/cm^3)
D	Outer diameter (m)
D_i	Diffusion coefficient of species i (m^2/s)
D_{H_2}	Diffusion coefficient of hydrogen (m^2/s)
D_{O_2}	Diffusion coefficient of oxygen (m^2/s)
f_i	Flow of species i (mol/cm^2 s)
f_{H_2}	Flux of hydrogen produced at the cathode (mol/cm^2 s)
f_{O_2}	Flux of oxygen produced at the anode (mol/cm^2 s)
F	Faraday constant (A s/mol)
$\Delta_R g$	Gibbs enthalpy of reaction (J/mol)
G^j	Total molar flow crossing boundary j (mol/s)
$G_{\text{H}_2}^{\text{out}}$	Hydrogen flow rate leaving the electrolyzer ($\text{mol}_{\text{H}_2}/\text{s}$)
$G_{\text{O}_2}^{\text{out}}$	Oxygen flow rate leaving the electrolyzer ($\text{mol}_{\text{O}_2}/\text{s}$)
$G_{\text{H}_2}^{\text{cross}}$	Hydrogen crossover flow ($\text{mol}_{\text{H}_2}/\text{s}$)
$G_{\text{O}_2}^{\text{cross}}$	Oxygen crossover flow ($\text{mol}_{\text{O}_2}/\text{s}$)
h	Specific enthalpy (J/mol)
h_α	Specific enthalpy of species α (J/mol)
$h_{\text{H}_2\text{O}}^V$	Specific enthalpy of water vapour (J/mol)
$h_{\text{H}_2\text{O}}^L$	Specific enthalpy of liquid water (J/mol)
H_i	Solubility coefficient (Henry's constant) of species i (Pa m^3/mol)
H_{H_2}	Hydrogen solubility (Pa m^3/mol)
i	Cell current density (A/cm^2)
i_0	Exchange current density (A/cm^2)
I	Cell current (A)
j	Operating current density (A/cm^2)
k_e	Electrolyte conductivity (S/cm^2)
k_0	Gas-free electrolyte conductivity (S/cm^2)
K	Material-specific permissible stress (Pa)
L	Thickness of solid polymer electrolyte (m)
n	Number of electrons participating in reaction (1)

n_{H_2} Molar fraction of hydrogen in oxygen (1)
p Pressure (Pa)
p^j Pressure of stream crossing boundary j (Pa)
p^θ Standard pressure (101.325 kPa) (Pa)
p^A Pressure at electrolyzer anode (Pa)
p^C Pressure at electrolyzer cathode (Pa)
$p^{sat}_{H_2O}$ Saturation pressure of water (Pa)
p_0 Initial pressure (Pa)
p_i Partial pressure of gas species i (Pa)
P_{el} Electric power (W)
ΔP Difference in pressure set across membrane (Pa)
P^m_i Permeability of species i (m^2/s Pa)
q_{H_2} Specific heat demand per mole hydrogen (J/mol_{H_2})
$q^{rev}_{H_2}$ Specific reversible heat demand per mole hydrogen (J/mol_{H_2})
$q^{rev}_{O_2}$ Specific reversible heat demand per mole oxygen (J/mol_{O_2})
$q^*_{H_2}$ Heat demand for splitting of extra water to make up hydrogen crossover (J/mol_{H_2})
Q Thermal power (W)
R Ideal gas constant (J/mol K)
R_r Bubble detachment radius (m)
$\Delta_R s$ Entropy of reaction (J/mol K)
s Specific entropy (J/mol K)
$\dot{S}_{irr}$ Entropy production rate (J/K)
t Thickness (m)
t_r Bubble residence time (s)
T Temperature (K)
T^j Temperature of stream crossing boundary j (K)
T^θ Standard temperature (298.15 K) (K)
u_i Rate of permeation of species i (Nm^3/s)
v Electrolyte velocity (m/s)
V Single cell voltage (V)
V^{rev} Reversible single cell voltage (V)
ΔV Single cell polarization (V)
V_g Gas volume in electrolyzer compartment (m^3)
V_l Liquid volume in electrolyzer compartment (m^3)
V_r Bubble volume (m^3)
$\dot{V}_G/A$ Volumetric flux density of produced gas (m^3)
V Single cell voltage (V)
V^{rev} Reversible single cell voltage (V)
ΔV Single cell polarization (V)
V_g Gas volume in electrolyzer compartment (m^3)
V_l Liquid volume in electrolyzer compartment (m^3)
V_r Bubble volume (m^3)
$\dot{V}_G/A$ Volumetric flux density of produced gas (m^3)

Greek symbols

α Charge transfer coefficient (1)
ε Gas void fraction of liquid alkaline electrolyte (1)
ε_p Gas void fraction of liquid alkaline electrolyte (at p) (1)

ε_{p0}	Initial void fraction of liquid alkaline electrolyte (at p_0) (1)
ε_{H2}	Current (faradic) efficiency of hydrogen production (1)
ε_{O2}	Current (faradic) efficiency of oxygen production (1)
ζ_{rec}^{C}	Extent of recombination reaction at cathode (1)
ζ_{rec}^{A}	Extent of recombination reaction at anode (1)
θ	Gas coverage of electrode (1)
θ_0	Gas coverage of electrode without external circulation (1)
φ_{ohm}	Ohmic voltage drop of electrolyzer cell (V)
φ_{act}	Activation over-potential (V)
$\varphi_{\mathrm{act}}^{\theta}$	Influence of coverage on over-potential (V)

References

Allebrod, F., Chatzichristodoulou, C., & Mogensen, M. B. (2013). Alkaline electrolysis cell at high temperature and pressure of 250 degrees C and 42 bar. *Journal of Power Sources, 229*, 22−31.

Bensmann, B., Hanke-Rauschenbach, R., Pena Arias, I. K., & Sundmacher, K. (2013). Energetic evaluation of high pressure PEM electrolyzer systems for intermediate storage of renewable energies. *Electrochimica Acta, 110*, 570−580.

Bensmann, B., Hanke-Rauschenbach, R., & Sundmacher, K. (2014). In-situ measurement of hydrogen crossover in polymer electrolyte membrane water electrolysis. *International Journal of Hydrogen Energy, 39*, 49−53.

Bockris, J. O. M. (1956). Kinetics theory of adsorption intermediates in electrochemical catalysis. *Journal of Chemical Physics, 24*, 817.

Caspersen, M., & Kirkegaard, J. B. (2012). Modelling electrolyte conductivity in a water electrolyzer cell. *International Journal of Hydrogen Energy, 37*, 7436−7441.

Degiorgis, L., Santarelli, M., & Cali, M. (2007). Hydrogen from renewable energy: a pilot plant for thermal production and mobility. *Journal of Power Sources, 171*, 237−246.

DENA. Strategieplattform power to gas [Online]. Available http://www.powertogas.info/power-to-gas/interaktive-projektkarte.html.

Eigeldinger, J., & Vogt, H. (2000). The bubble coverage of gas-evolving electrodes in a flowing electrolyte. *Electrochimica Acta, 45*, 4449−4456.

ELYGRID. Improvements to integrate high pressure alkaline electrolyzers for Electricity/H_2 production from renewable energies to balance the grid [Online]. 2011−2014, FCH-JU 278824. Available www.elygrid.com.

FCH-JU. (February 2014). *Development of water electrolysis in the European Union*. FCH-JU, European Commission.

Fischer, J., Hofmann, H., Luft, G., & Wendt, H. (1980). Fundamental investigations and electrochemical engineering aspects concerning an advanced concept for alkaline water electrolysis. *AIChE Journal, 26*, 794−802.

Gahleitner, G. (2013). Hydrogen from renewable electricity: an international review of power-to-gas pilot plants for stationary applications. *International Journal of Hydrogen Energy, 38*, 2039−2061.

Ganley, J. C. (2009). High temperature and pressure alkaline electrolysis. *International Journal of Hydrogen Energy, 34*, 3604−3611.

Gierke, T. D., Munn, G. E., & Wilson, F. C. (1981). The morphology in Nafion perfluorinated membrane products, as determined by wide- and small-angle X-ray studies. *Journal of Polymer Science B: Polymers Physics, 19*, 1687−1704.

Grigoriev, S. A., Millet, P., Korobtsev, S. V., Porembskiy, V. I., Pepic, M., & Etievant, C. (2009). Hydrogen safety aspects related to high pressure polymer electrolyte membrane water electrolysis. *International Journal of Hydrogen Energy, 34*, 5986−5991.

Grigoriev, S. A., Porembskiy, V., Korobtsev, S., Fateev, V., Auprêtre, F., & Millet, P. (2011). High-pressure PEM water electrolysis and corresponding safety issues. *International Journal of Hydrogen Energy, 36*, 2721−2728.

Häussinger, P., Lohmüller, R., & Watson, A. M. (2000). Hydrogen, 2. Production. In *Ullmann's encyclopedia of industrial chemistry*.

IACS. (2012). *Requirements concerning pipes and pressure vessels international*. International Association of Classification Societies.

Ito, H., Maeda, T., Nakano, A., & Takenaka, H. (2011). Properties of Nafion membranes under PEM water electrolysis conditions. *International Journal of Hydrogen Energy, 36*, 10527−10540.

Janssen, L. J. J. (1978). Mass transfer at gas evolving electrodes. *Electrochimica Acta, 23*, 81−86.

Janssen, H., Bringmann, J. C., Emonts, B., & Schroeder, V. (2004). Safety-related studies on hydrogen production in high-pressure electrolysers. *International Journal of Hydrogen Energy, 29*, 759−770.

Janssen, H., Emonts, B., & Stolten, D. (2008). Alkalische Hochdruck-Elektrolyse − Status am Forschungszentrum Jülich. In *NOW-Workshop 2008: Regenrativer Wasserstoff aus Elektrolyse, 2008 Ulm*.

Janssen, L. J. J., Geraets, J. J. M., Barendrecht, E., & Stralen, S. D. J. V. (1982). Ohmic potential drop during alkaline water electrolysis. *Electrochimica Acta, 27*, 1207−1218.

Janssen, L. J. J., Sillen, C. W. M. P., Barendrecht, E., & Van Stralen, S. J. D. (1984). Bubble behaviour during oxygen and hydrogen evolution at transparent electrodes in KOH solution. *Electrochimica Acta, 29*, 633−642.

Krasil'shchikov, A. I. (1963). *Zhurnal Fizicheskoi Khimii, 37*, 273.

Kunz, O., Klimeck, R., Wagner, W., & Jaeschke, M. (2007). The GERG-2004 wide-range equation of state for natural gases and other mixtures. In *GERG technical monograph* (Vol. 15).

Laoun, B. (2007). Thermodynamics aspect of high pressure hydrogen production by water electrolysis. *Revue des Energies Renouvelables, 10*, 435−444.

Mandin, P., Derhoumi, Z., Roustan, H., & Rolf, W. (2014). Bubble over-potential during two-phase alkaline water electrolysis. *Electrochimica Acta, 128*, 248−258.

Mann, R. E., Amphlett, J. C., Peppley, B. A., & Thurgood, C. P. (2006). Henry's law and the solubilities of reactant gases in the modeling of PEM fuel cells. *Journal of Power Sources, 161*, 768−774.

Marangio, F., Santarelli, M., & Cali, M. (2009). Theoretical model and experimental analysis of a high pressure PEM water electrolyser for hydrogen production. *International Journal of Hydrogen Energy, 34*, 1143−1158.

Marini, S., Salvi, P., Nelli, P., Pesenti, R., Villa, M., Berrettoni, M., et al. (2012). Advanced alkaline water electrolysis. *Electrochimica Acta, 82*, 384−391.

Millet, P., Dragoe, D., Grigoriev, S. A., Fateev, V., & Etievant, C. (2009). GenHyPEM: a research program on PEM water electrolysis supported by the European Commission. *International Journal of Hydrogen Energy, 34*, 4974−4982.

Millet, P., & Grigoriev, S. (2013). Chapter 2 − Water electrolysis technologies. In L. M. Gandía, G. Arzamendi, & P. M. Diéguez (Eds.), *Renewable hydrogen technologies*. Amsterdam: Elsevier.

Millet, P., Grigoriev, S. A., & Porembskiy, V. I. (2013). Development and characterisation of a pressurized PEM Bi-stack electrolyzer. *International Journal of Energy Research, 37*, 449−456.

Millet, P., de Guglielmo, F., Grigoriev, S. A., & Porembskiy, V. I. (2012). Cell failure mechanisms in PEM water electrolyzers. *International Journal of Hydrogen Energy, 37*, 17478−17487.

Millet, P., Mbemba, N., Grigoriev, S. A., Fateev, V., Aukauloo, A., & Etiévant, C. (2011). Electrochemical performances of PEM water electrolysis cells and perspectives. *International Journal of Hydrogen Energy, 36*, 4134−4142.

Millet, P., & Ngameni, R. (2011). Non-harmonic electro-chemical and pneumato-chemical impedance spectroscopies for analyzing the hydriding kinetics of palladium. *Electrochimica Acta, 56*, 7907−7915.

Myles, T. D., Nelson, G. J., Peracchio, A. A., Roy, R. J., Murach, B. L., Adamson, G. A., et al. (2012). Species transport in a high-pressure oxygen-generating proton-exchange membrane electrolyzer. *International Journal of Hydrogen Energy, 37*, 12451−12463.

NOW. (2011). *Studie Wasserelektrolyse- Stand und Entwicklungspotenzial der Wasserelektrolyse zur Herstellung von Wasserstoff aus regenerativen Energien*. Nationale Organisation Wasserstoff- und Brennstoffzellentechnologie.

NSPTG. North sea power to gas platform [Online]. Available http://www.northseapowertogas.com/demonstrations.

Ogumi, Z., Takehara, Z., & Yoshizawa, S. (1984). Gas permeation in SPE method. *Journal of the Electrochemical Society, 131*, 769−773.

Onda, K., Kyakuno, T., Hattori, K., & Ito, K. (2004). Prediction of production power for high-pressure hydrogen by high-pressure water electrolysis. *Journal of Power Sources, 132*, 64−70.

Pletcher, D., & Li, X. H. (2011). Prospects for alkaline zero gap water electrolysers for hydrogen production. *International Journal of Hydrogen Energy, 36*, 15089−15104.

Pray, H. A., Schweickert, C. E., & Minnich, B. H. (1952). Solubility of hydrogen, oxygen, nitrogen, and helium in water at elevated temperatures. *Industrial & Engineering Chemistry, 44*, 1146−1151.

RESLYSER. Hydrogen from regenerative energy power sources: Pressurised alkaline electrolyser with high efficiency and wide operating range 2011−2014, European Union's 7th framework programme (FP7/2007−2013) [Online]. http://reselyser.eu/index.html.

Roy, A., Watson, S., & Infield, D. (2006). Comparison of electrical energy efficiency of atmospheric and high-pressure electrolysers. *International Journal of Hydrogen Energy, 31*, 1964−1979.

Rozain, C., & Millet, P. (2014). Electrochemical characterization of polymer electrolyte membrane water electrolysis cells. *Electrochimica Acta, 131*, 160−167.

Sakai, T., Takenaka, H., & Torikai, E. (1986). Gas diffusion in the dry and hydrated Nafion. *Journal of the Electrochemical Society, 133*, 88−92.

Sakai, T., Takenaka, H., Wakabayashi, N., Kawami, Y., & Torikai, E. (1985). Gas permeation properties of solid polymer electrolyte (SPE) membranes. *Journal of the Electrochemical Society, 132*, 1328−1332.

Schalenbach, M., Carmo, M., Fritz, D. L., Mergel, J., & Stolten, D. (2013). Pressurized PEM water electrolysis: efficiency and gas crossover. *International Journal of Hydrogen Energy, 38*, 14921−14933.

Sequeira, C. A. C., Santos, D. M. F., Sljukic, B., & Amaral, L. (2013). Physics of electrolytic gas evolution. *Brazilian Journal of Physics, 43*, 199−208.

Smolinka, T. (2009). Fuels − hydrogen production/water electrolysis. In J. Garche (Ed.), *Encyclopedia of electrochemical power sources*. Amsterdam: Elsevier.

Tham, M. J., Walker, R. D., & Gubbins, K. E. (1970). Diffusion of oxygen and hydrogen in aqueous potassium hydroxide solutions. *The Journal of Physical Chemistry, 74*, 1747−1751.

Tzimas, E., & Filiou, C. (2003). In European Commission (Ed.), *Hydrogen storage: State-of-the-art and future perspective*. Directorate General Joint Research Centre (DG JRC).

Ursua, A., Gandia, L. M., & Sanchis, P. (2012). Hydrogen production from water electrolysis: current status and future trends. *Proceedings of the IEEE, 100*, 410−426.

Ursua, A., Martin, I. S., Barrios, E. L., & Sanchis, P. (2013). Stand-alone operation of an alkaline water electrolyser fed by wind and photovoltaic systems. *International Journal of Hydrogen Energy, 38*, 14952−14967.

VDI-GVC. (2010). *VDI heat atlas*. Berlin Heidelberg: Springer-Verlag. http://dx.doi.org/10.1007/978-3-540-77877-6_12.

Vogt, H. (2012). The actual current density of gas-evolving electrodes-Notes on the bubble coverage. *Electrochimica Acta, 78*, 183−187.

Vogt, H., & Balzer, R. J. (2005). The bubble coverage of gas-evolving electrodes in stagnant electrolytes. *Electrochimica Acta, 50*, 2073−2079.

Wendt, H. (1984). Neue konstruktive und prozeßtechnische Konzepte für die Wasserstoff-Gewinnung durch Elektrolyse. *Chemie Ingenieur Technik, 56*, 265−272.

Yeager, H. L., & Steck, A. (1981). Cation and water diffusion in Nafion ion-exchange membranes: influence of polymer structure. *Journal of the Electrochemical Society, 128*, 1880−1884.

Yeo, R. S., & McBreen, J. (1979). Transport properties of Nafion membranes in electrochemically regenerative hydrogen/halogen cells. *Journal of the Electrochemical Society, 126*, 1682−1687.

Zeng, K., & Zhang, D. K. (2010). Recent progress in alkaline water electrolysis for hydrogen production and applications. *Progress in Energy and Combustion Science, 36*, 307−326.

Ziems, C., Tannert, D., & Krautz, H. J. (2012). Project presentation: design and installation of advanced high pressure alkaline electrolyzer-prototypes. *Energy Procedia, 29*, 744−753.

Hydrogen production by high-temperature steam electrolysis

8

J. Mougin
CEA-Liten, Grenoble, France

8.1 Introduction: what are high-temperature steam electrolyzers?

Electrolysis of water to produce hydrogen and oxygen can be performed at a low temperature using liquid water or a high temperature using steam. In this chapter, the latter process is presented, so-called high-temperature steam electrolysis (HTSE).

The global reaction remains the same:

$$H_2O \rightarrow H_2 + \frac{1}{2}O_2 \tag{8.1}$$

However, the main advantage of this technology is that the dissociation of steam ($H_2O(g)$) requires less energy compared with liquid water ($H_2O(l)$), as presented in Figure 8.1. In addition, when the temperature increases, part of the electrical energy needed to dissociate the water molecule can be replaced by heat. When heat sources are available at a low price, which is often the case compared with electricity, the

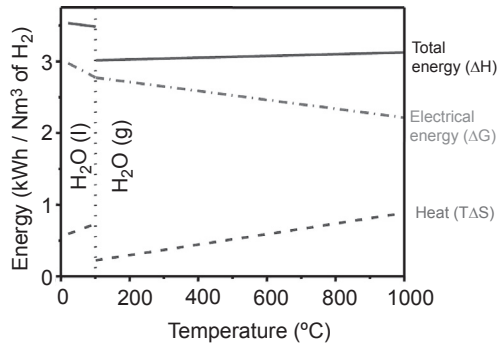

Figure 8.1 Energy need for the electrolysis reaction as a function of temperature; enthalpy (ΔH), corresponding to total energy, Gibbs enthalpy (ΔG), corresponding to electrical energy, entropy (TΔS), corresponding to heat.
Figure after Atkins (2002).

Compendium of Hydrogen Energy. http://dx.doi.org/10.1016/B978-1-78242-361-4.00008-X

replacement of electricity demand by heat results in high efficiency and contributes to decreasing the cost of the hydrogen produced.

However, there is an optimum in the temperature range to be used for HTSE, mainly owing to materials limitations, because a high temperature can be detrimental in terms of durability and requires the use of special expensive alloys. For those reasons, the HTSE operating temperature range is around 700−900 °C.

Section 8.2 provides details about the HTSE process, including the electrochemical reactions, constituting materials and components, and status of the technology in terms of performance and durability. Section 8.3 summarizes advantages and disadvantages of this technology compared with other electrolysis technologies. Section 8.4 gives an overview of future development trends for HTSE.

8.2 Process of producing hydrogen using HTSE

This section presents the global electrochemical reaction and the materials constituting the cells and other stack components. Performances curves, as well as the status of the technology, are also presented.

8.2.1 Global electrochemical reaction

As mentioned above, the global electrochemical reaction is:

$$H_2O \rightarrow H_2 + \frac{1}{2}O_2 \tag{8.1}$$

It corresponds to the two half-reactions:

$$H_2O + 2e^- \rightarrow H_2 + O^{2-} \text{ at the cathode} \tag{8.2}$$

$$O^{2-} \rightarrow \frac{1}{2}O_2 + 2e^- \text{ at the anode} \tag{8.3}$$

One can see from these reactions that the charge carrier is the O^{2-}ion; that is to say, the electrolyte is an anionic conductor.

8.2.2 Description of the technology

An HTSE involves a stack of several single repeat units (SRUs) (Figure 8.2). The electrochemical cell, the so-called solid oxide electrolysis cell (SOEC), the main electrolyzer's component in which the electrochemical reaction takes place, is composed of three ceramic layers: a dense electrolyte and two porous electrodes (cathode and anode, where hydrogen and oxygen are respectively produced) placed on both sides of the electrolyte. Taking into account the operating temperature range, the electrochemical cell is made of ceramics.

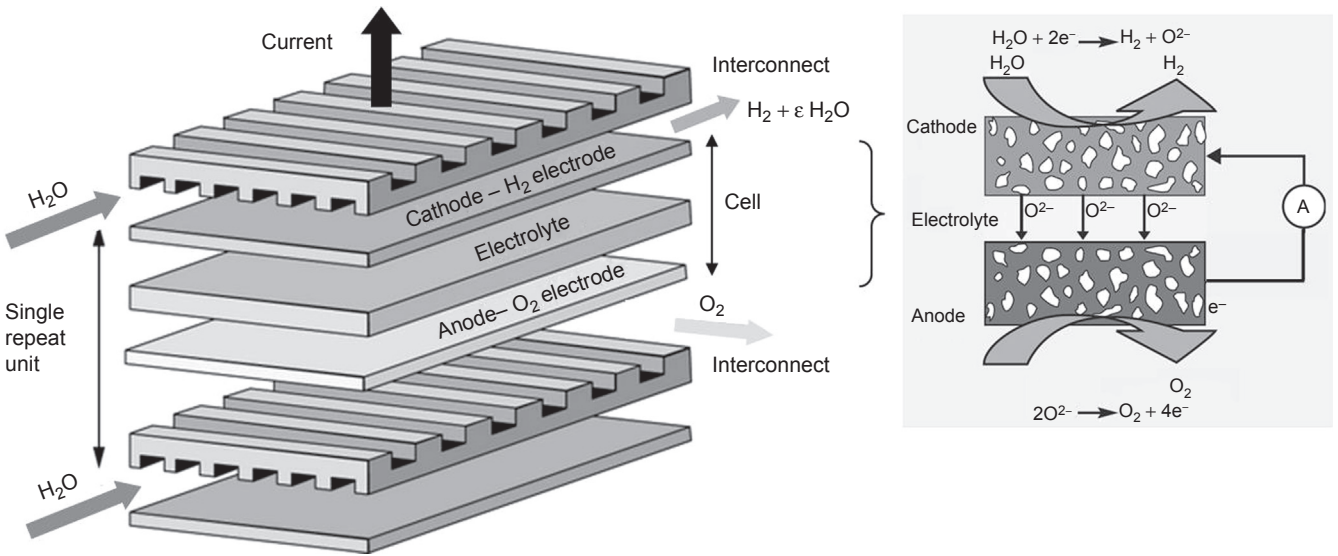

Figure 8.2 Schematic representation of an SRU including the three-layer cell (cathode/electrolyte/anode) and two half-interconnects; highlight of the anodic and cathodic half-reactions occurring in the cell.

The stack is also composed of interconnects with the purpose of carrying the electric current, ensuring fluid distribution for every cell, and acting as separators between the anode of a cell and the cathode of the adjacent one.

In addition, a stack is composed of sealings to ensure the gas-tightness of the stack toward the outside and also the anodic and the cathodic compartments of each cell.

The gaseous atmospheres consist of a water−hydrogen (H_2O/H_2) mixture on the cathode side and oxygen (O_2) on the anode side. Consequently, the stresses acting on the constituent materials of such an HTSE electrolyzer are not so different from those involved in solid oxide fuel cells (SOFCs), which correspond to the reverse mode, producing electricity from H_2 and O_2. For these reasons, and also because SOFCs have been developed for some decades and are currently reaching a maturity compatible for market commercialization, as can be seen in some countries such as Japan or the United States, for example, HTSE components and materials are currently similar to those considered for SOFCs.

8.2.3 Description of materials constituting solid oxide cells and other stack components

As mentioned, SOEC cells are similar to SOFC cells and several cell designs are considered. Most work on SOEC reported in the literature considers planar cells because they afford higher performance. In particular, we can quote electrolyte supported cells (ESC) and cathode supported cells (CSC).

For so-called ESC, the electrolyte (zirconia-based) has the role of mechanically supporting the cell (thickness 0.1−0.2 mm). In this design, electrodes with a thickness around 50 μm are deposited on both sides of the mechanical supporting electrolyte (Figure 8.3). The high electrolyte thickness requires an operating temperature between 850 °C and 1000 °C to reach appropriate ionic conductivity of the zirconia. The high operating temperature consequently requires special materials for the stack interconnects, made of expensive and difficult to manufacture ceramics or costly special alloys.

In the second type of planar cells developed, the electrolyte thickness is decreased to 5−20 μm to decrease electrolyte resistivity and allow reduced operating temperatures. However, the thin electrolyte is not able to support the cell mechanically; therefore, the thickness of one electrode (the hydrogen electrode) is increased in the range 0.2−1.5 mm (Figure 8.3). This geometry is named the anode supported cell for SOFC and has to be renamed the CSC for SOEC or, more generally, the electrode supported cell. Because of the thin electrolyte, the operating temperature can be decreased to 700−800 °C. High current densities can be obtained and cheaper stainless steel can be used for interconnects. These elements lead to an improvement in lifetime and cost, a further reduction in the operating temperature being pursued to obtain an additional lifetime improvement and an additional cost decrease with an operating temperature below 650 °C.

In these “self-supported cells”, one ceramic layer has the role of mechanical support, which is not the primary electrochemical function of that component. A third and more recent generation of SOFC uses an “external” electrochemically inactive

Figure 8.3 Schematic representation of the three types of cells: electrolyte supported cell, cathode supported cell, and metal supported cell.

metallic support on which the ceramic components of the cell are deposited as thin layers (Figure 8.3). This type of cell is the metal supported cell (MSC). This cell geometry is still in development for SOFC, and only a few tests in the SOEC mode have been performed (Schiller, Ansar, Lang, & Patz, 2009).

The electrolyte has to exhibit adequate gas tightness (density $> 95\%$, no open porosity), good ionic conductivity (10^{-2} S/cm at operating temperatures), a thermal expansion coefficient (TEC) close to that of the electrodes (to limit mechanical stresses), stability in both oxidizing and reducing environments, mechanical stability in HTSE operating conditions, and finally, no chemical reactivity with the electrode materials, as much as possible. In most cases, the electrolyte material is yttria-stabilized zirconia (YSZ), which is zirconium oxide stabilized with yttrium oxide (yttria), generally with 8 mol% of yttria owing to its higher conductivity compared with other rates. Other zirconia-based electrolytes such scandia-stabilized zirconia are considered for the lowest operating temperatures, but researchers are still verifying its stability and aging resistance because this is a relatively costly compound.

The electrodes must exhibit high electronic conductivity (>100 S/cm) with ionic conductivity to limit ohmic losses and delocalize the electrochemical reaction across the bulk of the electrode.

These electrodes are porous for gas diffusion to allow the distribution of steam to active sites and remove hydrogen and oxygen produced at the cathode and anode, respectively. This porosity must be optimized to achieve good electrochemical performance and avoid local overpressure, which could delaminate the electrodes' layers.

The hydrogen electrode requires good catalytic properties for water reduction and the ability to remain stable in a reducing environment. The reference material is a cermet, generally a nickel/yttria-stabilized zirconia (Ni/YSZ) cermet. Nickel is the most effective electro-catalyst discovered to date. Materials of the nickel/gadolinia-doped ceria (Ni/GDC) or nickel/samaria-doped ceria (Ni/SDC) cermets are also under investigation as substitutes for conventional Ni/YSZ cermets to achieve higher conductivity at low temperature. Some teams are also looking into all-oxide materials for the hydrogen electrode to act as mixed conductors; however, performance is still far from that of conventional cermets.

The oxygen electrode must exhibit suitable catalytic properties for the oxidation of O^{2-} ions while remaining stable in an oxidizing environment. A material belonging to the perovskite family is generally considered, with a structure ABO_3. Strontium-doped lanthanum manganite ($La_{1-x}Sr_xMnO_{3-\delta}$) (LSM) is considered to be the reference and is often found in ESCs because it is particularly suitable above 800 °C. However, because it is a purely electronic conductor, it is generally mixed with YSZ, the electrolyte material, to form an LSM-YSZ composite thus exhibiting mixed electronic and ionic conductivity, which allows the electrochemically active reaction site area to be extended. For CSCs operating at lower temperatures (below 800 °C), mixed ionic and electronic conductor materials are preferred, among which is $La_{1-x}Sr_xCo_{1-y}Fe_yO_{3-\delta}$ (LSCF), another perovskite. For the lowest temperatures (below 700 °C), $La_{1-x}Sr_xCoO_{3-\delta}$ (LSC) is considered owing to higher conductivity. Intermediate layers between the oxygen electrode and the electrolyte might be inserted in the case of LSCF or LSC, with the aim of minimizing reactivity between the

electrolyte and the electrode materials and promoting adhesion of the electrode, which has a TEC mismatch with the electrolyte. This layer generally consists of gadolinia- or yttria-doped ceria, which are compatible with the zirconia-based electrolyte and the electrode material. Thus, many CSCs developed to operate at temperatures around 700−750 °C feature an LSCF anode and a ceria-based barrier layer. Materials from the nickelate family ($A_2NiO_{4+\delta}$, A: Nd, La, or Pr) are currently undergoing development and qualification for the purposes of HTSE operation (Chauveau, Mougin, Bassat, Mauvy, & Grenier, 2010).

In mechanical terms, the cell must also have adequate strength.

Regarding interconnects, the material must first exhibit good electrical conductivity and high oxidation resistance under specific HTSE operating conditions (temperature and atmosphere), and also must not affect the electrochemical cells' proper operation because of mechanical or chemical issues. Thus, interconnect materials have to have a TEC as close as possible to that of the cell to avoid a mismatch and subsequent cell mechanical fracture, and they must avoid or minimize the formation of compounds that would be detrimental to the electrodes. To these technical issues an economic requirement is added: The HTSE system must remain inexpensive. For that purpose, the material used for the interconnect must be easily "workable", i.e. lend itself to cutting, machining and/or stamping. For operating temperatures below 900 °C, metallic interconnects are considered, made of alloys affording oxidation resistance at a high temperature because of the formation of chromium-rich oxide layers. Among alloys currently under consideration are ferritic stainless steels. Inexpensive as they are, these steels have further advantageous properties: They prove particularly suitable for shaping and welding purposes, exhibit expansion behaviors compatible with those found for the cell and are resistant to prolonged exposure to high temperatures. However, their surface properties are not altogether satisfactory: Their oxidation resistance for long-term operation is poor and the protective chromium oxide formed is a poor electrical conductor and emits volatile chromium compounds liable to contaminate the cell through the phenomenon of chromium poisoning, because such vapors are condensed at the electrochemically active sites of the cell. Research organizations and manufacturers are currently striving to optimize the composition of such steels, in particular by seeking to control the nature of naturally forming oxide layers. For instance, the Crofer 22 APU grade (an iron−chromium alloy containing 22 wt% chromium) was developed by ThyssenKrupp VDM. Because of the addition of manganese to the alloy it promotes the formation, at the very surface, of a mixed manganese−chromium oxide that emits lower quantities of chromium-compound vapors and is a far better conductor than chromium oxide by itself − even though the latter oxide still forms beneath this mixed oxide. Hence, rare earths (lanthanum, for instance) is added to decrease the oxide growth rate. Finally, titanium is added to increase the oxide's conductivity. This grade specifically developed for SOFC is suitable for HTSE. Sandvik also developed a specific grade called Sanergy HT, another 22 wt% Cr ferritic stainless-steel grade containing Mn, but with Mo and Nb rather than Ti.

Unfortunately, the effectiveness of such solutions is limited with regard to ensuring SOFC and HTSE operation over extended time scales. Thus, efforts have been made to

obtain improved properties by means of coatings. Investigations are focused more particularly on chromium-free oxides, with the target of increasing oxidation resistance of the underlying metal and increasing electrical resistivity. The reference compound investigated is a mixed manganese−cobalt oxide, exhibiting a spinel structure, with the composition $(Co, Mn)_3O_4$, with high conductivity: about 1000 times higher than that exhibited by chromium oxide at 800 °C. A commercial solution is available, commercialized by Sandvik as pre-coated strips covered by a thin Co coating (a few hundreds of nanometres) deposited by a vacuum process. As high-temperature oxidation takes place, the protective $(Co, Mn)_3O_4$ is formed from the Co coating, with the Mn coming from the steel.

Other compounds, e.g. lanthanum perovskites, derived from electrode compositions are proving equally interesting. Numerous deposition techniques are being considered. Most of these involve combining the coating operation itself with a post-treatment for the purposes of achieving the proper stoichiometry and/or its densification.

Concerning sealings, SOFC solutions can be considered. However, specifications in terms of gas-tightness are more severe in HTSE. Indeed, whereas an SOFC can be operated even if not fully gas-tight, SOEC cannot because each molecule of hydrogen produced but not recovered at the outlet leads to a decrease in process efficiency. Glass and glass-ceramic sealants are the most used solutions. They exhibit strong bonding to the interface; their adherence to the cell provides tight sealing and thus most requirements for SOEC are fulfilled. Although glass has the faculty of self-healing, which can be beneficial in the case of cracking, its excessive devitrification at operating temperatures leads to drastic changes in physicochemical properties. Thus, glass-ceramic sealants whose crystallization can be controlled are often preferred. However, for such materials the self-healing faculty is partially or even completely lost; therefore, glass-ceramic properties have to be completely determined, starting from their vitreous state, to be perfectly adapted to adjacent cell components. Their performance depends on their components, compositions and arrangement in the network structure, which is complex and not yet fully understood. The formulation process of a glass-ceramic is highly complex especially owing to the large number of elements that can be included (Khedim, Nonnet, & Méar, 2012). Glass-ceramics from several systems have been investigated and their suitability for sealing applications within SOECs has been checked. It was concluded that glass-ceramics based on the $CaO-Al_2O_3-SiO_2$ (CAS) system meet most requirements for efficient sealing, especially in terms of chemical durability.

8.2.4 Presentation of i-V curves

Performance of HTSE cells or stacks are generally represented in the form of an i-V curve. Figure 8.4 shows an example of such a curve. On the x axis the current (in A), or current density (in A/cm^2) is represented, whereas the y axis gives the voltage (in V). By convention, the current or current density is generally negative in electrolysis mode because a current has to be provided to the cell, and because i-V curves

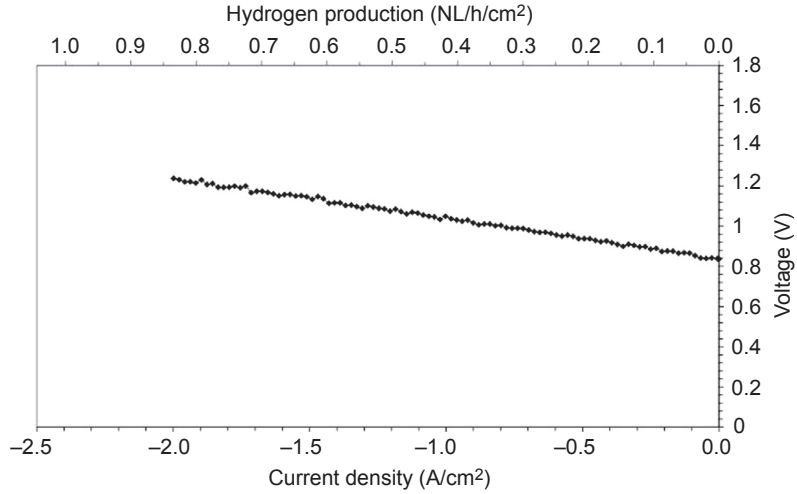

Figure 8.4 Presentation of i-V curve of an electrode-supported cell obtained at 800 °C. For this curve, the cathodic gas is a mixture of 90% H_2O/10% H_2, whereas the anodic gas is air; steam conversion is 43% at -2 A/cm^2.

obtained in fuel cell mode are represented with positive values. Hydrogen production is directly linked to the current or current density through Faraday's law:

$$Q = I/2\mathrm{F} \tag{8.4}$$

where Q is the hydrogen flow rate produced, I the current and F the Faraday constant equal to 96,485 C/mol.

This is why in Figure 8.4 a secondary x axis is superimposed, showing the hydrogen flow rate produced.

Improving the cell or stack performance means increasing the current densities and decreasing the voltage. Increasing current densities greatly influences the compacity of the electrolyzers, because fewer cell surfaces are required to produce the same amount of hydrogen and thus the investment cost is reduced. Decreasing the voltage is also profitable because it directly influences process efficiency, which can be expressed as kWh/Nm^3 and thus is inversely proportional to the voltage.

When no current is applied to the cell, the cell potential is open circuit voltage (OCV). It is calculated with the Nernst equation, assuming that there are no side reactions, gas leakage and so forth. The Nernst equation takes into account the Gibbs free energy of reaction and the partial pressures of the gas species present at the electrodes.

In the experimental conditions in Figure 8.4, the calculations give a Nernst potential of 0.87 V, which is close to the OCV value obtained on the i-V curve in Figure 8.4.

When a current is applied to the cell, cell polarizations or "over-potentials" η are added to the OCV. In electrolysis mode, it increases the voltage in operation according to:

$$U(i) = \mathrm{OCV} + |\eta| \tag{8.5}$$

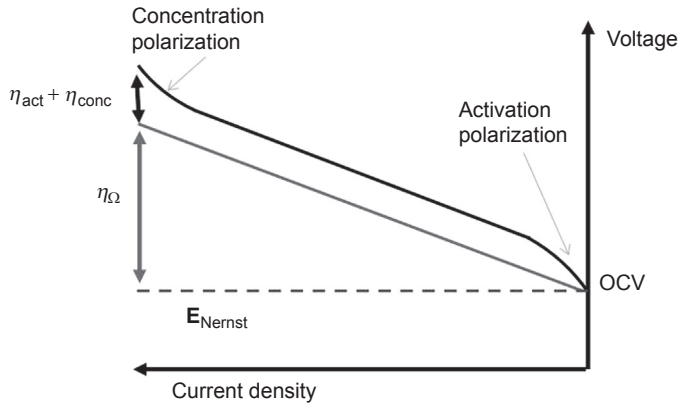

Figure 8.5 Schematic representation of i-V curve showing different types of polarization.

The global over-potential η depends on the current density and originates from the irreversible character of the electrolysis process leading to different polarization losses, which can be described as (see Figure 8.5):

η_{Ω}: the ohmic polarization, representing "ohmic losses." It is mainly caused by the ionic resistivity of the electrolyte, to which electronic resistivity in the electrodes and contact resistances are added. With the materials presented above, the electronic resistivity in the electrodes is often neglected, whereas the contact resistances can have a certain influence depending on the cell/stack assembly. Its expression is $R_{\Omega} \times I$, directly linked to the current I through an ohmic resistance R_{Ω}.
η_{conc}: the concentration polarization, which appears when electrode reactions are hindered by gas transport limitations within the electrodes. It strongly depends on the electrode microstructures and is accentuated at high current densities.
η_{act}: the activation polarization. It corresponds to the over-potential needed to overcome the energy barrier corresponding to the rate determining step in the electrochemical reaction. It depends on the material properties, the electrode microstructure, and the operating conditions (atmosphere, temperature and current density).

8.2.5 Presentation of different thermal regimes (endothermic, thermoneutral or exothermic)

Besides the Nernst potential, there is another specific voltage value for HTSE operation, the thermoneutral voltage.

Electrolysis is an endothermic reaction. However, heat is generated by Joule effect within the cell. Thermoneutral voltage corresponds to the voltage at which Joule heating exactly balances the reaction thermal energy needs. At 800 °C, the thermoneutral voltage equals 1.286 V. When the operating conditions lead to a voltage below this value, the operating thermal mode is endothermic and heat has to be provided to the electrolyzer.

On the contrary, when operating conditions lead to a voltage above this value, the operating thermal mode is exothermic and heat is generated in the electrolyzer.

In general, stacks are not operated in the exothermic mode for several reasons: first, to maximize electrical efficiency; second, to avoid strong heating (see Figure 8.6) and third, to minimize degradation, expected to be higher in this operating mode. Operating the electrolyzer close to the thermoneutral voltage is attractive from a heat management point of view, which is simplified. However, even if it decreases electrical efficiency, a slightly exothermic mode takes advantage of the heat in the exhaust gases that can be recovered in a heat exchanger to preheat the steam before entering the electrolyzer.

Because of a model of HTSE developed by Laurencin et al., it is possible to calculate the temperature within a stack over an i-V curve, highlighting the three thermal modes (Laurencin et al., 2011) (Figure 8.6). The thermoneutral mode is found at 1.3 V for the thermoneutral voltage.

Also because of this modeling tool, the electrical efficiency is plotted, taken as the ratio between the energy content of the hydrogen and the electric power used to produce it (Usseglio-Viretta, Laurencin, Loisy, Delette, & Leguillon, submitted for publication) (Figure 8.7).

8.2.6 Presentation of status of technology: size of stacks tested, results in terms of performance and durability, and impact of some operating parameters on performance and durability

As mentioned previously, the maturity of HTSE is less than that of SOFC. However, several teams around the world are performing experiments to evaluate the potentialities of this technology in terms of performance and durability. Several scales are considered. First, experiments are performed at the single cell level, where the cell is either a button cell (a few square centimeters of active area) or a larger one (around 100 cm^2 of active area). This type of test, generally carried out on a test bench with ceramic housing and grid current collectors, allows the intrinsic characteristics of the cell to be determined. Second, tests are carried out at the SRU level, with a cell size around 100 cm^2 but in a stack representative environment, with the interconnects and sealings. Finally, tests at the stack level are carried out generally with a few cells (three to five cells), but more recently with a larger amount of cells (above 10, with some tests up to 60 cell stacks). This last type of test allows scaling up of the technology to be validated. For larger powers, the size of the stack does not increase indefinitely but an arrangement of modules with multiple stacks is considered. Finally, only a few tests at the system level have been carried out.

In this section, results in terms of performance and durability at different testing scales are presented.

Cell or stack performance depends on the cell design considered. As mentioned in Section 8.2, ESCs and CSCs are two main designs considered and differ by electrolyte thickness, which is responsible for the main ohmic losses.

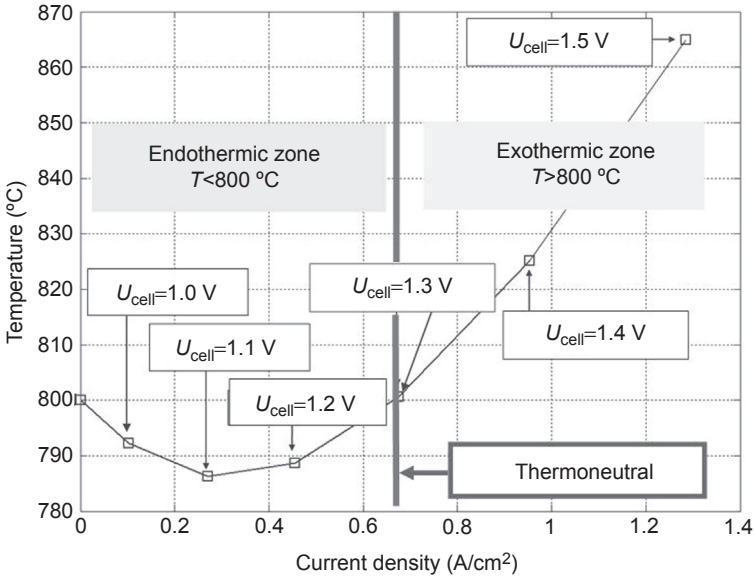

Figure 8.6 Cell temperature versus current density, highlighting the three thermal modes: exothermic mode above 800 °C, endothermic mode below 800 °C, and thermoneutral at 800°C. Figure after Laurencin, Kane, Delette, Deseure, and Lefebvre-Joud (2011).

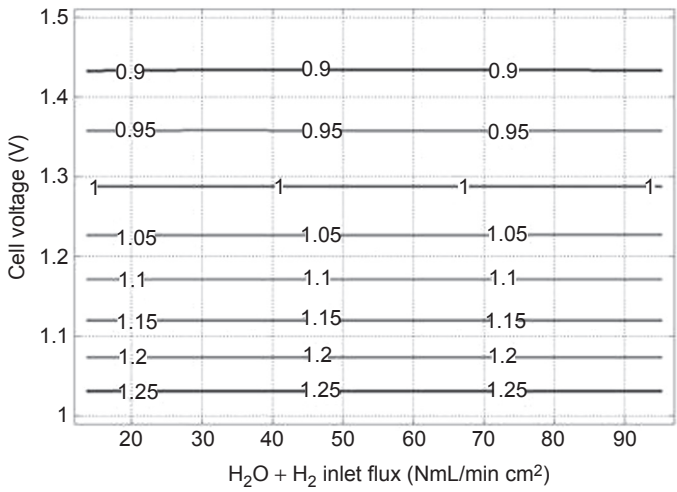

Figure 8.7 Simulated maps of electrical efficiency; simulation conditions: 90% H_2O + 10% H_2 on H_2 electrode, air on oxygen electrode, same gas flow rate on both electrodes, gas inlet and temperature fixed at 800 °C.

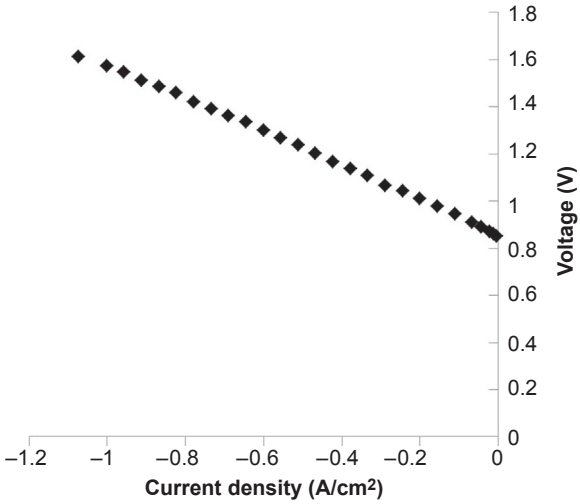

Figure 8.8 i-V curve of an ESC cell operated at 800 °C in 90% H_2O−10% H_2 on the hydrogen side, air on the oxygen side, in an SRU environment; advanced electrolyte supported cell, designed for low-temperature operation: Ni-GDC/YSZ/YDC/LSCF.

Thus, performance of ESCs is expected to be much lower than for CSCs at the same temperature, which is why in general ESCs are operated at a higher temperature. Generally, standard ESC cells reach a current density of −0.5 A/cm^2 and a maximum at 1.3 V at 800 °C, and can reach −0.6 A/cm^2 at 1.3 V at 850 °C (O'Brien, Stoots, Herring, Condie, & Housley, 2009). Only advanced ESC cells a targeting low-temperature operation can reach higher performance, such as the one presented in Figure 8.8. Indeed, because of materials tailored for low-temperature operation such as LSCF oxygen electrodes, a current density of −0.6 A/cm^2 at 1.3 V at 800 °C is achieved (Mougin et al., 2012).

On the contrary, CSC cells have improved performance. Values of −1 A/cm^2 at 1.3 V at 850 °C were reported by Hauch et al. in 2008 with LSM oxygen electrodes (Hauch, Ebbesen, Jensen, & Mogensen, 2008). The same current density can be achieved at 800 °C owing to the use of LSCF oxygen electrodes (Brisse, Schefold, & Zahid, 2008; Mougin et al., 2013). Current densities as high as −2.0 A/cm^2 or even higher can be achieved at thermoneutral voltage at 800 °C with advanced CSC cells; the major difference is the use of an LSC oxygen electrode (Figure 8.9).

In addition direct comparison between different published results is difficult because experimental conditions vary a lot; the test benches are different, as are the operating parameters: mainly temperature, gas composition and gas flow rate. Those parameters are expected to have a major role in performance.

Performance at the stack level is less numerous.

Most published results concern stacks in the range of three to six cells. O'Brien reported performance at the 10-cell stack level in the range of −0.4 A/cm^2 below thermoneutral voltage at 800 °C (O'Brien, Zhang, Houseley, Moore-McAteer, & Tao, 2012). Diethelm reported current densities between −0.32 and −0.52 A/cm^2 at

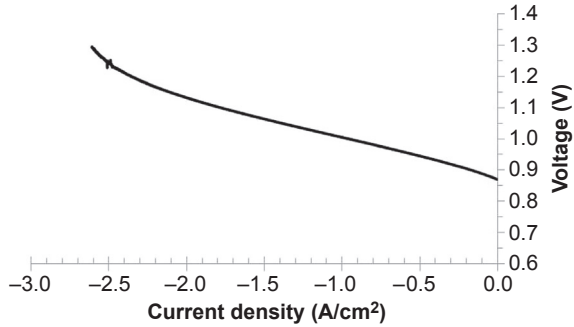

Figure 8.9 i-V curve of an advanced CSC cell made of Ni-YSZ/YSZ/GDC/LSC tested at 800 °C in 90% H_2O/10% H_2; steam conversion rate SC = 71% at −2.5 A/cm^2.

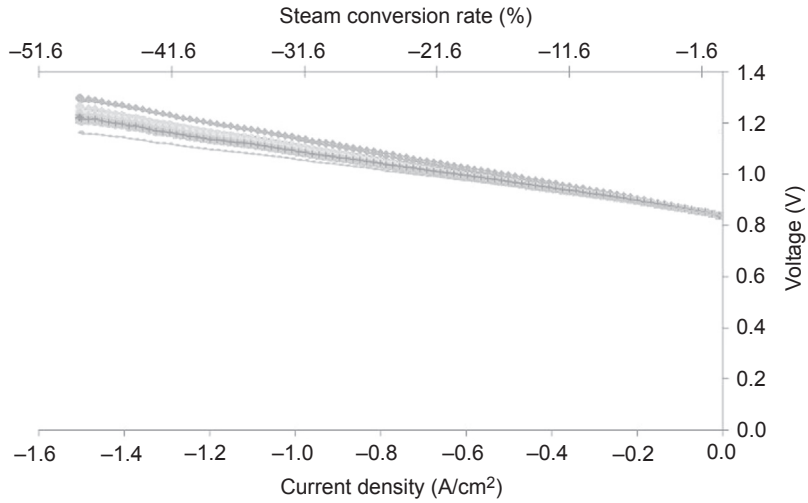

Figure 8.10 i-V curves at 800 °C of a 25-cell stack, fed with 90 vol% H_2O + 10 vol% H_2, flow rate = 24 NmL/min cm^2 on the hydrogen side.

thermoneutral voltage at 700 °C on a six-cell stack (Diethelm, Van Herle, Montinaro, & Bucheli, 2012). Petitjean highlighted performance above −1 A/cm^2 at thermoneutral voltage at 800 °C for a five-cell stack (Petitjean et al., 2011). Ebbesen reported performance results at the six-cell stack scale. At 850 °C, this stack containing six Ni-YSZ/YSZ/LSM-YSZ CSC cells had a current density from −0.25 A/cm^2 for the worst cells to above −0.6 A/cm^2 for the best cells at 1.3 V (Ebbesen, Høgh, Nielsen, Nielsen, & Mogensen, 2011).

In most of these results, scattering among different cells in the stacks was observed.

Test of larger stacks are far less numerous. We can quote works performed at Idaho National Laboratory (INL) in the United States, which tested several stacks including large ones of 60 cells and modules of several stacks leading to a total of 720 cells for a power of 15 kW (Stoots et al., 2009). As far as published results are concerned, that

test was the largest known. Performance results were not reported, but hydrogen production, which was 5.7 Nm^3/h for the whole system, suggests that performance was low. In 2012, the same team reported results at the scale of a 4-kW stack composed of two stacks of 40 cells, with a current density of -0.4 A/cm^2 at thermoneutral voltage (O'Brien et al., 2012).

Li et al. reported results at the scale of a 30-cell stack (Li et al., 2014). An average current density slightly above -0.2 A/cm^2 was achieved at thermoneutral voltage at 800 °C with CSC cells made of Ni-YSZ/YSZ/LSM.

Reytier reported the performance of a 10-cell stack (Reytier et al., 2013) with performance above -1.2 A/cm^2 at thermoneutral voltage at 800 °C, and other results on the scale of 10- and 25-cell stacks (Figure 8.10) (Reytier, Di Iorio, Petit, et al., 2014). One can see that performance above -1.6 A/cm^2 at thermoneutral voltage at 800 °C has been achieved with low scattering between cells.

Finally, in the literature, performance is often qualified in terms of current densities through i-V curves. However, another important parameter is the hydrogen outlet flow rate. Indeed, if the gas-tightness of the stack is imperfect, the hydrogen (and oxygen) produced from the current passing through the stack is not recovered in the exhaust tubes, and thus the efficiency of the electrolyzer decreases. Therefore, measurement of the hydrogen (and oxygen) outlet flow rates is of primary importance. Only by a few number of articles mention this parameter. As an example, results reported by Mougin et al. showed that when the stack is fully gas-tight, the hydrogen flow rate measured at the outlet is equal to that calculated from the Faraday law (Mougin et al., 2012; Reytier, Di Iorio, Chatroux, et al., 2014).

The same teams as those performing performance measurements mentioned above often conduct durability tests. Measurements from a few hundred hours up to 9000 h are reported on different scales (single cell, SRU, or stack). As for performance results, direct comparison among all data available is difficult because operating parameters might be different from one test to another. In addition, degradation rates taken from durability tests can be expressed differently, either from the durability curve representing the evolution of one parameter (voltage or current) versus time or from i-V curves taken before and after the durability tests. Thus, the unit can be mV/h or mV/1000 h if the test is performed at a fixed current, or mA/h or mA/1000 h if the test is performed at a fixed voltage, or $m\Omega cm^2/h$ or 1000 h if taken from the i-V curves. All of these degradation rates can be converted into %/h or 1000 h of degradation when divided by the initial value. Expressed as %/1000 h, they all can be compared, but this comparison might be unreliable because evolution of the different parameters over time is intrinsically dissimilar. In addition, in most cases degradation over time is not linear, and an expression in %/1000 h represents a strong approximation.

Nevertheless, some trends can be stated.

In the first part of this section, we will consider stationary durability tests in which operating parameters are fixed for the duration of the test, even if in some cases some uncontrolled incidents in the test rig or in the lab lead to unintentional transient operation (load cycling, shutdown, etc.).

First, degradation rates in HTSE are higher than in SOFC. Indeed, whereas degradation rates below 1%/1000 h are reported in SOFCs even at the stack level,

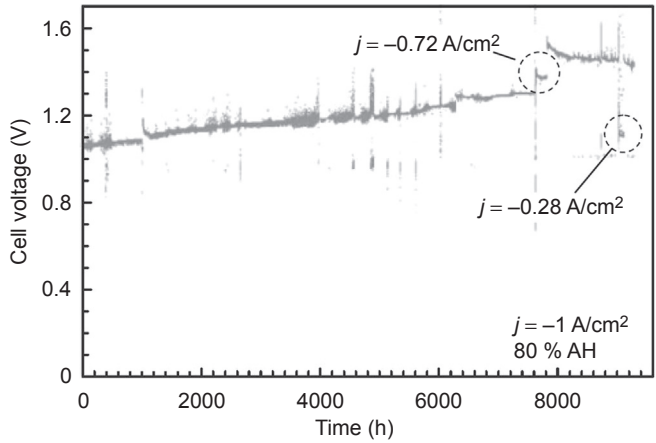

Figure 8.11 Evolution of voltage versus time for a CSC cell tested at 780 °C at −1 A/cm^2 over the first 5600 h; the corresponding steam conversion rate is 36%, before a decrease in the current density.
Schefold, Brisse, and Tietz (2012) reproduced by permission of ECS − The Electrochemical Society.

HTSE studies report degradation rates above 2%/1000 h (Brisse & Schefold, 2012; Moçoteguy & Brisse, 2013).

As an illustration, Figure 8.11 shows the durability curve obtained by Schefold on a CSC cell over 9000 h (Schefold, Brisse, and Tietz, 2012). The corresponding degradation rate over the first stationary durability period of 5600 h lies between 2.4%/1000 h and 1.7%/1000 h, with a tendency to decrease over time.

More recently, some degradation rates below 1%/1000 h have been reported, but they often correspond to the best cell within a stack and/or were obtained under mild testing conditions (mainly low current densities). For example, Fu et al. reported a degradation rate of 0.4%/1000 h for the best cell within a five-cell stack, whereas the other cells had rates around 2%/1000 h for a test performed at −0.6 A/cm^2 at 700 °C. In addition, some strong instabilities of cell voltage were observed several times in the stack, which makes degradation rate calculations difficult (Fu, Schefold, Brisse, & Nielsen, 2014). Nguyen et al. reported durability tests on a two-cell short stack operated between −0.3 and −0.875 A/cm^2 in SOEC mode after an initial period of 4000 h in SOFC mode. An average degradation rate of around 1.5%/1000 h was reported for the whole part of the test in SOEC mode (approximately 1000 h) (Nguyen, Fang, Packbier, & Blum, 2013).

Table 8.1 summarizes some durability results taken from the literature, non-exhaustively; some durability results are not expressed by authors in terms of the percentage of degradation per 1000 h. This highlights that testing conditions might be different from one test to another; perhaps because of this, no clear trend regarding the impact of the type of test (cell or stack) or of the different operating parameters (temperature, current density, or steam conversion ratio (SC)) can be easily stated. Only a few parametric studies are available that varied one parameter (*T*, *I*, or SC)

Table 8.1 Summary of some of the results of durability tests reported in literature

Type of test	Temperature (°C)	Test duration (h)	Operating point (i in A/cm^2 or U in V)	Steam conversion ratio, SC (%)	Degradation rate (%/1000 h)	References
CSC Cell	850	1316	−0.5 A/cm^2	28	2	Hauch (2007)
CSC Cell	850	800	−0.5 A/cm^2	70	5	Ouweltjes, van Tuel, van Berkel, and Rietveld (2009)
CSC cell	780	9000	−1 A/cm^2	36	3.8	Schefold et al. (2012)
CSC cell	800	1000	−0.5 A/cm^2	17, 34, 69, 83	6.0−14.4, increasing with SC	Mougin et al. (2013)
ESC SRU	800	4000	−0.4, −0.6 −0.8 A/cm^2	25, 37.5 50	1.6 2.4 2.7	Mougin et al. (2012)
MSC cell	800	2000	−0.3 A/cm^2	43	3.3	Schiller et al. (2009)
CSC cell and SRU	800	1000	−0.5 A/cm^2	25	6	Mougin et al. (2012)
CSC SRU	700	700	−0.5 A/cm^2	32	1.8	Chatroux et al. (2012)
6-CSC stack	650	1160	−0.26 A/cm^2	50	0.4−5.1	Diethelm et al. (2012)

Continued

Table 8.1 Continued

Type of test	Temperature (°C)	Test duration (h)	Operating point (i in A/cm^2 or U in V)	Steam conversion ratio, SC (%)	Degradation rate (%/1000 h)	References
5-CSC stack	800	2700	−0.5 A/cm^2	25	7−13	Petitjean et al. (2011)
3-CSC stack	700	700	−1 A/cm^2	40	1.9−3.6	Reytier et al. (2013)
10-ESC Stack	800	2500	1.29 V/cell		8.15	O'Brien et al. (2009)
5-CSC stack	850	2651	−0.4−0.6 A/cm^2	39−58	~3	Brisse and Schefold (2012)
5-ESC stack	850	4050	−0.4 A/cm^2	39	~5	Brisse and Schefold (2012)
5-CSC stack	850	3250	−0.8−1 A/cm^2	52	~4−5	Brisse and Schefold (2012)
2-CSC stack	750−810 °C	1000 h in SOEC mode	−0.3−0.875 A/cm^2	15−44	1.5	Nguyen et al. (2013)
5-CSC stack	700	2000	−0.6 A/cm^2	50	0.4−2	Fu et al. (2014)

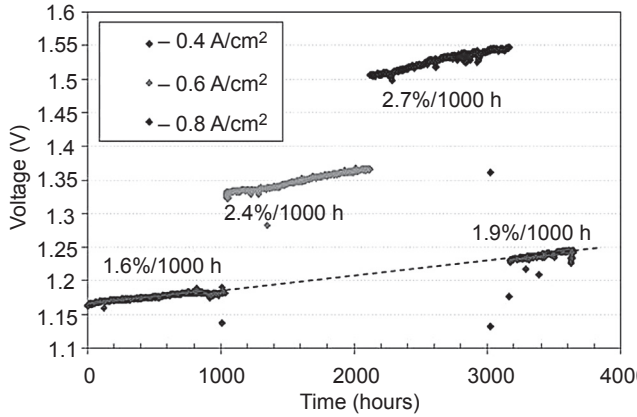

Figure 8.12 Evolution of cell voltage versus time for a CSC tested in an SRU at 800 °C and constant flow rate for three values of current densities, and thus three values of steam conversion rate: −0.4 A/cm^2 and SC = 25%, −0.6 A/cm^2 and SC = 37.5%, and −0.8 A/cm^2 and SC = 50%. Mougin et al. (2012).

with the other constant, and they tended to show that an increase in temperature, current density and SC is detrimental (Figure 8.12 to the effect of current density and SC). However, more systematic studies such as those done in SOFC over past years would be necessary to clarify the impact of operating parameters on durability and to understand the associated degradation mechanisms.

8.3 Advantages and disadvantages of hydrogen production using HTSE

In this section, the advantages and disadvantages (or issues remaining to be solved) of HTSE are discussed compared with other low-temperature electrolysis technologies, with both technical and economical considerations.

8.3.1 Advantages

As mentioned above and as is clearly visible in Figure 8.1, energy needs for HTSE are lower compared with low temperature water electrolyses. Thus, i-V curves in HTSE mode are in a more favorable current and voltage range, as shown in Figure 8.13, which presents the typical range of i-V curves achieved with HTSE technology compared with other water electrolysis technologies (alkaline and proton exchange membrane (PEM) water electrolysis). Figure 8.13 demonstrates that HTSE typical voltages are lower than for other technologies, which is directly linked to the fact that the energy required to split the steam molecule is lower than the energy required to split a water molecule, with lower over-potentials. Thus, power consumption, which is the product of voltage V by current I, is lower for HTSE, leading to better efficiency.

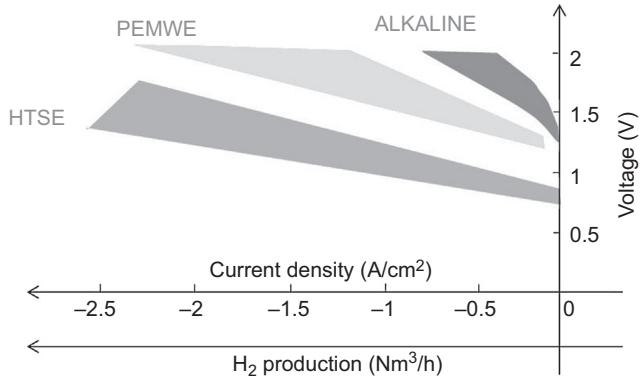

Figure 8.13 Typical range of performance represented by i-V curves achieved with HTSE technology compared with other water electrolysis technologies (alkaline and PEM water electrolysis).
Figure after Graves, Ebbesen, and Mogensen (2011).

In addition, current, represented in Figure 8.13 in terms of current density (current divided by the active area), is directly linked to hydrogen production through the Faraday law mentioned in Section 8.2.4. Thus, the higher the current (or current density) is, the higher will be the hydrogen production. Figure 8.13 shows that HTSE is an efficient process with which to increase the hydrogen production rate. For both reasons, high hydrogen production rate and lower voltage, both the capital expenditure and operational expenditure are promising.

At this point, and in agreement with HTSE experimental results at the stack level presented in Section 8.2, with a current density around -1.5 A/cm^2 at 1.3 V, an electrical efficiency of 96% (lower heating value) can be calculated (considering a "free" source of heat). For comparison, efficiencies for alkaline and PEM water electrolysis are 62% and 68%, respectively.

At the system level, some loss is expected in electrical converters and thermal auxiliaries. Taking into account a loss of 8% in all cases, efficiencies are equal to 89% for HTSE, 58% for alkaline electrolysis, and 63% for PEMWE. These values are consistent with those claimed by alkaline and PEM electrolyzer manufacturers, and with calculations performed by Ni et al. (Ni, 2008). For HTSE, due to the lower maturity of the technology only few system developments have been done so far. Very recently, French Alternative Energies and Atomic Energy Commission (CEA) developed a small integrated system able to produce up to 2.5 Nm3/h of hydrogen with a global efficiency above 90% at the system level.

Economical considerations are also a key point. Indeed, HTSE technology has to compete with low-temperature alkaline or PEM electrolysis in terms of the cost of the hydrogen produced. No commercial systems are available and the cost of laboratory demonstration units does not represent the potential cost of this technology when it will be produced massively. That is why techno-economical assessment has been carried out based on real performance and durability data, but extrapolating the stack and system design to larger units, including an estimate of the cost of mass production of these units, to be more representative.

An American study considered the coupling of an HTSE hydrogen production plant with a very high-temperature nuclear reactor (VHTR), which provides both electrical and heat energy (heat for the steam production and overheating, and for the electrolysis reaction) to the HTSE (Sohal, O'Brien, Stoots, McKellar, Harvego, & Herring, 2008). This economic analysis demonstrated that HTSE can deliver hydrogen at a cost of $3.23/kg of hydrogen, assuming an internal rate of return of 10%. This hydrogen cost is lower than that obtained with low-temperature electrolyses. It is even not far from the cost of hydrogen produced by widely used steam methane reforming technology, which produces hydrogen at around $2.50/kg (Manage, Hodgson, Milligan, Simons, & Brett, 2011).

However, finding such high temperature heat sources is not easy because VHTR reactors do not yet exist and the possibility of operating HTSE systems with heat sources at lower temperature would be necessary for earlier market penetration. Thus, Rivera-Tinoco et al. investigated options with heat sources at lower temperatures (Rivera-Tinoco, Mansilla, & Bouallou, 2010). They demonstrated that medium-temperature thermal energy sources could be coupled with high-temperature electrolysis without resulting in strong over-costs.

Finally, because HTSE plants reaching multi-megawatt power will not soon be available, and because there might be interest in smaller units for decentralized hydrogen production on sites presenting a heat source at intermediate temperatures, cost analyses have been performed by Reytier et al. for smaller units including a low-weight and performing stack design experimentally validated (Reytier et al., 2013). Based on these data, an SOEC system coupled with a low-temperature heat source (for steam generation) is modeled for a production capacity of 100 kg H_2/day. Electrolysis is considered to be achieved at a pressure of 13 bars at 700 °C with a steam conversion of 60%.

To compare the HTSE system with conventional water electrolysis technologies based on equivalent market maturity, a cost analysis was conducted considering a manufacturing scale of 100 system/year, 30% margin on the manufacturing cost and 20% contingencies. The calculations give a selling price for the system of €11.2/Nm^3/h for the HTSE system, compared with €6.5/Nm^3/h for alkaline and €11/Nm^3/h for PEM according to the suppliers' sources. It is worth noting that PEM is currently produced only in small volumes and the announced price should correspond to a lower production scale. Despite the higher price, the HTSE system has a reasonable competitive position compared with conventional technologies. Considering the achievement of developments in progress on the durability, performance and design of the stack as well as the mass production effect, this selling price could drop to €5/Nm^3/h (Reytier, Di Iorio, Petit, et al., 2014).

Figure 8.14 shows the levelized cost of hydrogen versus the electricity for HTSE compared with alkaline and PEM electrolyses. Figure 8.14 shows that the energetic efficiency of HTSE prevails over its higher investment and becomes competitive with alkaline electrolysis, for a high operating rate, allowing better amortization, and for an electricity price above €100/MWh, which concerns many European countries. Moreover, the advanced HTSE shows the promising potential of developments in progress. Whatever the electricity price, HTSE produces cheaper hydrogen compared with PEMWE.

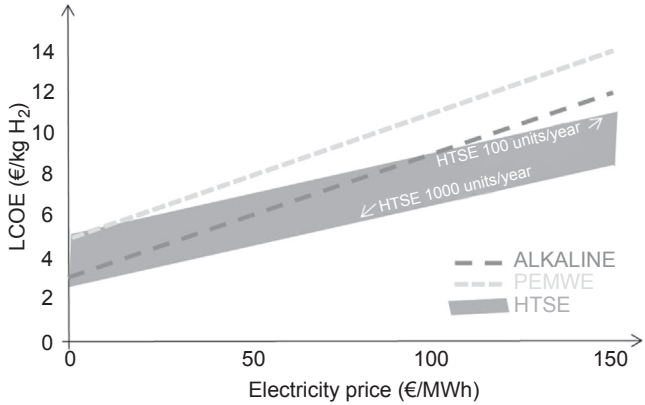

Figure 8.14 Levelized cost of hydrogen versus electricity price; comparison of HTSE with alkaline and PEM electrolyses.

8.3.2 Disadvantages

The previous sections showed that HTSE has improved performance and efficiency compared with low temperature electrolyses. However, it clearly appears that degradation rates are still an issue in reaching long-duration operations above 25,000 h, such those targeted for this technology.

Degradation issues encountered during HTSE operation can be divided into two categories: phenomena occurring during steady-state operation and those occurring during cycling. Both will be briefly described in this section.

Cell and other stack components are subject to degradation phenomena during steady-state operation in HTSE mode. Compared with SOFC, studies on SOEC degradation are less numerous. Generally, degradation phenomena in SOEC mode are close to those in SOFC mode. Even if some specificity exists, degradation rates are still higher in SOEC compared with SOFC, as mentioned in Section 8.2.6.

Different degradation phenomena that can be encountered at the cell and stack component levels are reported in review articles (Laguna-Bercero, 2012; Moçoteguy & Brisse, 2013; Sohal, 2009; Sohal et al., 2009). Most degradation issues are related to chemical, physico-chemical or electrochemical phenomena that are thermally activated. Others are related to mechanical phenomena, potentially partly linked to previous chemical/physico-chemical phenomena.

Only major mechanisms specific to HTSE operations will be briefly given below.

Regarding the hydrogen electrode (Ni-YSZ cermet), changes in its microstructure, such as Ni coarsening are observed. Compared with an SOFC operation, the high steam content in an SOEC operation is considered an accelerating factor, which might explain at least partly the higher degradation rates in SOEC mode (Moçoteguy & Brisse, 2013). On the oxygen electrode side, decomposition of the LSCF perovskite is often reported, as well as delamination. In the SOEC mode, this latter phenomenon is linked to the formation of oxygen at this electrode, which does not exist in SOFC. Electrolyte instability is also a key issue.

Regarding interconnects, because of oxygen formation, the more oxidant atmosphere in SOEC mode compared with SOFC mode makes oxidation more severe and the request for efficient protection more crucial.

Finally, degradation phenomena occurring on one component can affect others, such as chromium evaporation from the interconnects that provoke chromium poisoning of the oxygen electrode, or components of the sealing that can enhance corrosion of the interconnect or poison the cell, or a change in the Ni-YSZ microstructure and even its creep that can lead to electrolyte cracking.

Some degradation mechanisms also have an origin in extrinsic causes such as pollution of the inlet gas or pollution from the balance of plant components. For example, Ebbesen reported that impurities in cathodic gas led to cermet poisoning and that efficient gas cleaning can strongly decrease the degradation rate (Ebbesen, & Mogensen, 2010).

Therefore, degradation issues need to be considered globally at the stack and even the system level, to take into account interactions between various components. Further studies of degradation mechanisms are needed to understand what happens and to decrease the degradation rates reported in Section 8.2.6, which are still too high for application.

The cycling operation is also a potential cause of degradation. As for SOFC, thermal cycling of SOEC stacks is a weak point. Even if the operating mode forecasted will not consider frequent startup and shutdown, some thermal cycles will be needed over the lifetime of the system, some of which are programmed for periodic maintenance, to which unexpected ones can be added, for example, owing to building or grid shutdown. Degradation phenomena associated with these cycles have been much less studied than the steady-state operation. Indeed, transients from 700 to 800 °C to room temperature are severe due to the stack assembly made of rigid metallic interconnect plates and brittle ceramic cells, linked together with glass-ceramic sealants, all the more because TECs, even when selected as closely as possible, are not exactly similar. Thus thermo-mechanical issues at the stack level can be expected, as well as within the cell, because the cathode/electrolyte/anode also has different values of TEC. For SOFC stacks, some optimizations of the design have been performed to allow thermal cycling. Similar improvements are expected to be beneficial for SOEC. Few thermal cycling results are reported in SOEC mode, but we can cite the work of Mougin et al., who reported three thermal cycles on a one-cell stack and one thermal cycle on a three-cell stack, with no impact on the performances of wither or on gas-tightness (Mougin et al., 2012). Thermal cycling can affect cell microstructure − in particular, the electrode's microstructures − as well as the TEC, which can evolve over cycles. Further studies are required to understand its impact on the degradation rate.

The degradation phenomena mentioned occur at different scales, some of which are local and not easy to detect. Thus, in most cases, a combination of classical techniques and advanced characterization is required.

During operation, in situ diagnostics are often useful in addition to classical i-V curve measurements or monitoring of the voltage or current evolution over time, especially to understand slow and gradual degradation phenomena. Electrochemical

impedance spectroscopy is one of the most commonly used, extensively in SOFC and in an associated way in SOEC, even though studies in the latter mode are less numerous. In addition, modeling and description in equivalent circuits in SOEC mode can differ from SOFC mode and need specific studies. We can cite the work of Jensen et al., who described degradation phenomena in cells operated in SOEC mode owing to impedance spectra (Jensen, Hauch, Knibbe, Jacobsen, & Mogensen, 2013).

As reported above in Section 8.2.6, numerous studies have been performed at the cell and short stack level, only a couple at the stack level with 5 to 25 cells, and very few for larger stacks, whereas system development has just started. Thus, the maturity of the technology is much less than that of alkaline and PEM water electrolyses, and further extensive work is needed for system integration.

In addition, contrary to SOFC presenting a market for small units (around 1 kW for domestic micro-cogeneration), the HTSE market requires larger units. Therefore, challenges to building a complete system at such a large scale are higher. We can only reference work at the INL in the United States, where a 15-kW system made of three electrolysis modules, each consisting of four stacks of 60 cells, yielding 240 cells per module and 720 cells in total, has been tested, including heat exchangers. Peak hydrogen production with this facility was 5.7 Nm^3/h. The 15-kW system was operated for 1080 h but significant performance degradation was observed (Stoots, O'Brien, Condie, & Hartvigsen, 2010). The recent development of a small integrated HTSE system at CEA in France, evidencing a high global efficiency above 90% as reported above can also be reported.

Some demonstration projects are ongoing in Germany and Denmark, at the scale of a few tens of kilowatts, targeting coupling with synthetic gas or fuel production units for the power-to-gas market.

Finally, Section 8.3.1 presents the cost of investment, which is higher than for alkaline and only slightly higher than for PEMWE. This is logical because of more complex systems linked to the high temperature. However, as presented in Section 8.3.1, it does not necessarily lead to higher cost of the hydrogen produced, which means that this disadvantage is of second order; the benefit of the operation at better efficiency is larger than the investment over-cost.

8.4 Future trends

This section presents trends for upcoming developments in the field of HTSE.

Compared with other electrolysis technologies, HTSE has some specificities, which are highlighted here because they represent future potential applications for development.

8.4.1 Pressurized operation

Whichever electrolysis technology is considered, the hydrogen produced always need to be stored before being used. Because of its low volumetric density, it needs to be

stored pressurized, between 10 and a few tens of bars for injection into the natural gas grid, up to 350 or 700 bars for transportation. Hydrogen compression consumes part of the energy contained in the hydrogen, decreasing its overall process efficiency. On the contrary, compression of liquid water is much easier, which is why alkaline and PEMWE electrolyses consider a pressurized operation to be a few bars to a few tens of bars, with some attempts above 100 bars. To compete with these technologies and gain some points in global efficiency, operating HTSE under pressure is interesting and some studies have been carried out, although not numerous ones. Work at INL has been reported with a testing station able to operate up to 50 bars at stack level. Experimental results on a 10-cell stack have been published up to 15 bars, highlighting the possibility of operating HTSE stacks under pressure (O'Brien et al., 2012). Despite the higher OCV, the slope of i-V curves decreases with increasing pressure, indicating better performance associated with higher-pressure operation because of improved gas diffusion in the porous electrodes at high pressure. Thus, there is a double beneficial effect of pressure, with improved cell/stack performance and better global process efficiency. Work has also been performed in this field at the Technical University of Denmark and at the French Alternative Energies and Atomic Energy Commission.

8.4.2 Reversible operation

As mentioned in Section 8.2, SOEC cells are similar to SOFC cells, and thus by nature can be operated in both modes, which is not the case for the two other highly developed electrolysis technologies: alkaline and PEMWE, both of which require different catalysts or active materials in the fuel cell and electrolysis modes. This specificity is particularly interesting for application in the market of renewable energy storage. Indeed, intermittent renewable energy needs to be stored and hydrogen is one of the storage options, because it is produced by electrolysis when an excess of electricity is available and is consumed in a fuel cell to produce electricity when needed. Thus, an electrolyzer and a fuel cell are required, both of which are operated only part-time. A reversible system would be advantageous because only one system has to be purchased, which minimizes the investment cost, and is operated full-time, which maximizes the return on investment.

Some works have started to investigate transient operation and reversible operation. It has been demonstrated that transient operation (cycles of current from zero to defined values leading to voltages below, at, or above thermoneutral voltage) is possible (Mougin et al., 2012; Petipas, Brisse, & Bouallou, 2013; Petipas, Fu, Brisse, & Bouallou, 2013).

Although reversible performance curves (i-V curves) plotted in both SOEC and SOFC modes are common, either using the same gas mixture (generally 50% H_2O/50% H_2) or different mixtures (richer in steam in SOEC and in hydrogen in SOFC), long-term tests with several numbers of SOEC−SOFC cycles are less numerous. Nguyen reported a few long cycles (Nguyen et al., 2013); in 2013, Borglum presented much shorter cycles, which were more representative of such a reversible operation

(Borglum & Ghezel-Ayagh, 2013). These results, obtained at the scale of a 28-cell stack for a test duration of 900 h, proved feasibility at the scale of a large stack and showed that degradation is not accelerated with this type of cycle.

8.4.3 Co-electrolysis of steam and CO_2

Because of the high operating temperature, this HTSE technology is also liable to electrolyze different compounds, not only steam. For instance, CO_2 can also be electrolyzed, as well as a mixture of H_2O and CO_2 to produce syngas, or $H_2 + CO$ (Graves et al., 2011). Depending on the H_2O−CO_2 ratio at the inlet, several ratios of H_2−CO at the outlet can be obtained, which can be further transformed into synthetic gaseous (such as methane) or liquid synfuels (methanol, dimethyl ether, etc.) through catalytic reactors. Synfuels complement hydrogen for the storage of intermittent renewable energies through the "power-to-gas or power-to-chemicals" concept, and currently there is growing interest.

As an example, Figure 8.15 shows performance curves obtained at the scale of a 25-cell stack in co-electrolysis for two different H_2O−CO_2 ratios. Performance in co-electrolysis mode is close to that in pure steam electrolysis, which validates this operation mode. Gas composition at the outlet has been measured by gas microchromatography and was found to be as expected (Aicart, Laurencin, Petitjean, & Dessemond, 2014). Thus, the composition of the gas produced can be tailored to be exactly what is requested for a catalytic reactor that produces synfuel (Reytier, Di Iorio, Chatroux, et al., 2014; Reytier, Di Iorio, Petit, et al., 2014).

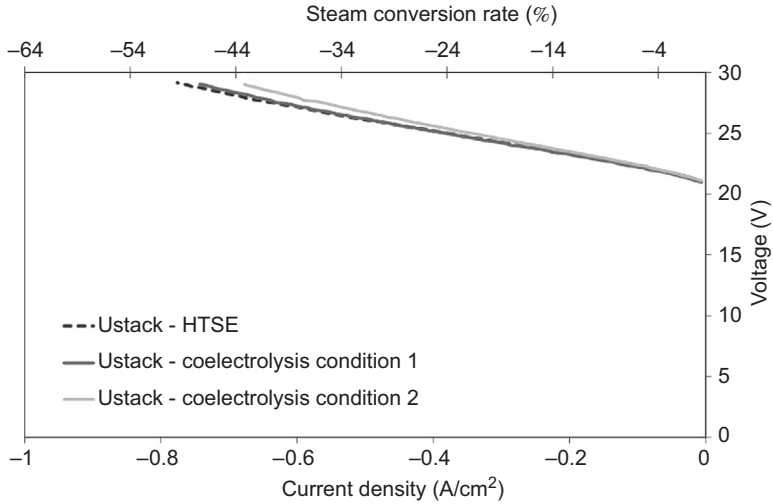

Figure 8.15 i-V curves of a 25-cell stack operated at 800 °C in pure steam electrolysis and in co-electrolysis for two H_2O−CO_2 ratios: condition 1 = 65% H_2O/25% CO_2/10% H_2; condition 2 = 50% H_2O/40% CO_2/10% H_2.
Figure after Reytier, Di Iorio, Chatroux, et al. (2014).

List of acronyms

CSC	Cathode supported cell
ESC	Electrolyte supported cell
HTSE	High-temperature steam electrolysis
MSC	Metal supported cell
OCV	Open circuit voltage
PEMWE	Proton exchange membrane water electrolysis
SOEC	Solid oxide electrolysis cell
SOFC	Solid oxide fuel cell
SC	Steam conversion ratio
SRU	Single repeat unit
TEC	Thermal expansion coefficient

References

Aicart, J., Laurencin, J., Petitjean, M., & Dessemond, L. (2014). *Fuel Cells, 14*(3), 430−447.

Atkins, P. W. (2002). *Physical chemistry* (Vol. 5). Oxford: Oxford University Press. p. 331.

Borglum, B., & Ghezel-Ayagh, H. (2013). *ECS Transactions, 57*(1), 61−66 (during oral presentation but not in proceedings).

Brisse, A., & Schefold, J. (2012). *Energy Procedia, 29*, 53−63.

Brisse, A., Schefold, J., & Zahid, M. (2008). *International Journal of Hydrogen Energy, 33*, 5375−5382.

Chatroux, A., Couturier, K., Petitjean, M., Reytier, M., Gousseau, G., Mougin, J., et al. (26−29 June 2012). Enhanced performance and durability of a high temperature steam electrolysis stack. In *10th European fuel cell forum*. Lucerne Switzerland, A1103.

Chauveau, F., Mougin, J., Bassat, J. M., Mauvy, F., & Grenier, J. C. (2010). *Journal of Power Sources, 195*, 744−749.

Diethelm, S., Van Herle, J., Montinaro, D., & Bucheli, O. (26−29 June 2012). In *10th European fuel cell forum*. Lucerne Switzerland, A1104.

Ebbesen, S., Høgh, J., Nielsen, K. A., Nielsen, J. U., & Mogensen, M. (2011). *International Journal of Hydrogen Energy, 36*, 7363−7373.

Ebbesen, S. D., & Mogensen, M. (2010). *Electrochemical and Solid-State Letters, 13*(9), B106−B108.

Fu, Q., Schefold, J., Brisse, A., & Nielsen, J. U. (2014). *Fuel Cells, 14*(3), 395−402.

Graves, C., Ebbesen, S. D., & Mogensen, M. (2011). *Solid State Ionics, 192*, 398−403.

Hauch. A. (2007). *Solid oxide electrolysis cells, performance and durability* (Ph.D. thesis). Denmark: Risoe National Laboratory.

Hauch, A., Ebbesen, S., Jensen, S., & Mogensen, M. (2008). *Journal of Material Chemistry, 18*, 2331−2340.

Jensen, S. H., Hauch, A., Knibbe, R., Jacobsen, T., & Mogensen, M. (2013). *Journal of the Electrochemical Society, 160*(3), F244−F250.

Khedim, H., Nonnet, H., & Méar, F. O. (2012). *Journal of Power Sources, 216*, 227−236.

Laguna-Bercero, M. A. (2012). *Journal of Power Sources, 203*, 4−16.

Laurencin, J., Kane, D., Delette, G., Deseure, J., & Lefebvre-Joud, F. (2011). *Journal of Power Sources, 196*, 2080−2093.

Li, Q., Zheng, Y., Guan, W., Jin, Le, Xu, C., & Wang, W. G. (2014). *International Journal of Hydrogen Energy, 39*, 10833−10842.

Manage, M. N., Hodgson, D., Milligan, N., Simons, S. J. R., & Brett, D. J. L. (2011). *International Journal of Hydrogen Energy, 36*, 5782−5796.

Mougin, J., Chatroux, A., Couturier, K., Petitjean, M., Reytier, M., Gousseau, G., et al. (2012). *Energy Procedia, 29*, 445−454.

Mougin, J., Mansuy, A., Chatroux, A., Gousseau, G., Petitjean, M., Reytier, M., et al. (2013). *Fuel Cells, 13*(4), 623−630.

Moçoteguy, P., & Brisse, A. (2013). *International Journal of Hydrogen Energy, 38*, 15887−15902.

Ni, M., Leung, M. K. H., & Leung, D. Y. C. (2008). Technological development of hydrogen production by solid oxide elecrolyzer cell (SOEC). *International Journal Hydrogen Energy, 33*, 2337−2354.

Nguyen, V. N., Fang, Q., Packbier, U., & Blum, L. (2013). *International Journal of Hydrogen Energy, 38*, 4281−4290.

Ouweltjes, J. P., van Tuel, M., van Berkel, F. S., & Rietveld, B. (2009). In *European fuel cell forum Lucern Switzerland*. B0904.

O'Brien, J. E., Stoots, C. M., Herring, J. S., Condie, K. G., & Housley, G. K. (2009). *The high-temperature electrolysis program at the Idaho national laboratory: Observations on performance degradation, international workshop on high temperature water electrolysis limiting factors*. INL/CON-09−15564.

O'Brien, J. E., Zhang, X., Housley, G. K., DeWall, K., Moore-McAteer, L., & Tao, G. (2012). *High temperature electrolysis pressurized experiment design, operation, and results*. INL/EXT-12−26891.

O'Brien, J. E., Zhang, X., Housley, G. K., Moore-McAteer, L., & Tao, G. (2012). *High temperature electrolysis 4 kW experiment design, operation, and results*. INL/EXT-12−27082.

Petipas, F., Brisse, A., & Bouallou, C. (2013). *Journal of Power Sources, 239*, 584−595.

Petipas, F., Fu, Q., Brisse, A., & Bouallou, C. (2013). *International Journal of Hydrogen Energy, 38*, 2957−2964.

Petitjean, M., Reytier, M., Chatroux, A., Bruguière, L., Mansuy, A., Sassoulas, H., et al. (2011). *ECS Transactions, 35*(1), 2905−2913.

Reytier, M., Cren, J., Petitjean, M., Chatroux, A., Gousseau, G., Di iorio, S., et al. (2013). *ECS Transactions, 57*(1), 3151−3160.

Reytier, M., Di Iorio, S., Chatroux, A., Petitjean, M., Cren, J., & Mougin, J. (2014). Stack performances in high temperature steam electrolysis and co-electrolysis. In *WHEC2014, June 15th−20th 2014, Gwangju, Korea*.

Reytier, M., Di Iorio, S., Petit, J., Chatroux, A., Gousseau, G., Aicart, J., et al. (1−4 July 2014). In *11th European fuel cell forum*. Lucerne, Switzerland, B1307.

Rivera-Tinoco, R., Mansilla, C., & Bouallou, C. (2010). Competitiveness of hydrogen production by high temperature electrolysis: impact of the heat source and identification of key parameters to achieve low production costs. *Energy Conversion and Management, 51*, 2623−2634.

Schefold, J., Brisse, A., & Tietz, F. (2012). *Journal of Electrochemical Society, 159*(2), A137−A144.

Schiller, G., Ansar, A., Lang, M., & Patz, O. (2009). *Journal of Applied Electrochemistry, 39*, 293−301.

Sohal, M. S., O'Brien, J. E., Stoots, C. M., McKellar, M. G., Harvego, E. A., & Herring, J. S. (2008). *Challenges in generating hydrogen by high temperature electrolysis using solid oxide cells*. INL/CON-08-14038. Idaho National Laboratory.

Sohal, M. S. (2009). *Degradation in solid oxide cells during high temperature electrolysis*. INL/EXT-09−15617.

Sohal, M. S., O'Brien, J. E., Stoots, C. M., Herring, J. S., Hartvigsen, J. J., Larsen, D., et al. (2009). *Critical causes of degradation in integrated laboratory scale cells during high-temperature electrolysis*. INL/EXT-09−16004.

Stoots, C. M., Condie, K. G., Moore-McAteer, L., O'Brien, J. E., Housley, G. K., & Herring, J. S. (2009). *Integrated laboratory scale test report*. INL/EXT-09−15283.

Stoots, C. M., O'Brien, J. E., Condie, K. G., & Hartvigsen, J. J. (2010). *International Journal of Hydrogen Energy, 35*, 4861−4870.

Usseglio-Viretta, F., Laurencin, J., Loisy, F., Delette, G., & Leguillon, D. International Journal of Hydrogen Energy, submitted for publication.

This page intentionally left blank

Hydrogen production by polymer electrolyte membrane water electrolysis

9

P. Millet
University of Paris-Sud, Orsay Cedex, France

9.1 Introduction

Among many others, typical applications of industrial hydrogen (obtained by steam methane reforming) are that it can be chemically consumed in the petroleum and chemical industries, mainly in the processing of fossil fuels and in the synthesis of ammonia. Alternatively, hydrogen can be produced by water electrolysis when cheap electricity is available or when hydrogen (or oxygen) of electrolytic grade (carbon-free) is required for various downstream processes. For example, it can be used in the food industry for the saturation of fats and can be consumed in the semiconductor industry; it can also be used as a coolant for generators in power stations.

Since the industrial revolution in the eighteenth century, the technological development of humankind has relied on natural hydrocarbon feedstocks, the combustion of which, with oxygen from air, releases heat that can be used as such or converted into electricity. Concerns about the sustainability of this fossil fuel economy based on natural hydrocarbons have risen over past decades because of the global energy situation (shortage of natural resources and climate change induced by increasing carbon dioxide atmospheric concentrations). Increasing shares of renewable energy sources in the energy mix is generally considered the most appropriate alternative strategy but new energy storage technologies are also needed. In this general context, hydrogen is now considered a potentially universal energy carrier that can be used for energy storage purposes in addition to its industrial application in the chemical industry (McCay, 2014). Although the energy required to extract 1 mol of hydrogen from water is about four times larger than that required to extract 1 mol of hydrogen from hydrocarbons (for example, methane), water is increasingly seen as the natural source of molecular hydrogen and water electrolysis as a convenient water-splitting process that can be operated efficiently at close to ambient temperatures. The water−hydrogen−oxygen system is an interesting chemical basis for carbon-free energy cycles because of its intrinsic high gravimetric density. (Other energy cycles involving carbon dioxide are also being investigated but most require hydrogen as a reducing agent.)

The next sections introduce the basic principles of water splitting by electrolysis. In this chapter, the emphasis is on low-temperature water electrolysis in acidic media, the polymer electrolyte membrane or proton exchange membrane (PEM) water electrolysis process.

Compendium of Hydrogen Energy. http://dx.doi.org/10.1016/B978-1-78242-361-4.00009-1

9.2 Water-splitting reaction as a source of molecular hydrogen

9.2.1 Thermodynamics of water-splitting reaction

Liquid (9.1) or vapor (9.2) water can be split and used as a source of pure oxygen and carbon-free molecular hydrogen:

$$H_2O(\text{liq}) \rightarrow H_2(g) + \frac{1}{2}O_2(g) \tag{9.1}$$

$$H_2O(\text{vap}) \rightarrow H_2(g) + \frac{1}{2}O_2(g) \tag{9.2}$$

Main thermodynamic functions associated with these two reactions (under atmospheric pressure) are plotted as a function of operating temperature in Figure 9.1, over the temperature range (0−1000 °C) of practical interest in the industry sector. At a temperature less than 100 °C, water is liquid; above it, water is vapor. Enthalpy change $\Delta H(T)$, which is a measure of the total energy required for the dissociation of the water molecule at constant pressure, is almost constant over the entire temperature range. The reaction is strongly endothermic. $\Delta H^{\circ}(298\text{K}) = +2856$ kJ/mol and

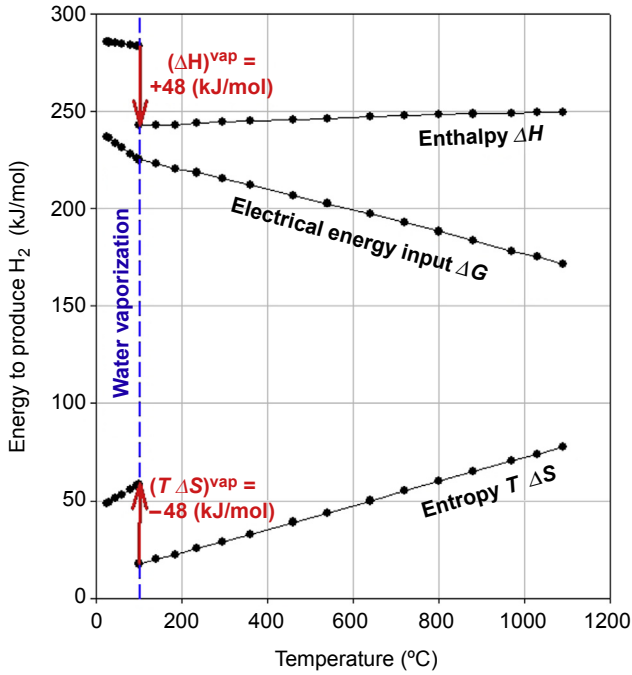

Figure 9.1 $\Delta G(T)$, $\Delta H(T)$, and $T\,\Delta S(T)$ plots associated with the water-splitting reaction.

$\Delta H(T > 100\,^{\circ}\text{C}) \sim +245$ kJ/mol. Discontinuity at 100 °C results from water vaporization. The enthalpy change of vaporization is $\Delta^{\text{vap}}H(100\,^{\circ}\text{C}) = 40.7$ kJ/mol. The energy required to split water vapor is therefore approximately 41 kJ/mol less than the energy required to split liquid water. The standard entropy change associated with reaction (1) is positive: $\Delta S_d^{\circ}(298\text{ K}) = +163.15$ J/mol K. The standard entropy change associated with reaction (2) (fictive state of water) is positive: $\Delta S_d^{\circ}(298\text{ K}) \sim +44$ J/mol K. The discontinuity at 100 °C also results from water vaporization. At 100 °C, liquid water is in equilibrium with water vapor and $\Delta G = 0$. Hence, $\Delta^{\text{vap}}H = T{\cdot}\Delta^{\text{vap}}S$ and $\Delta^{\text{vap}}S(373\text{ K}) \sim 109$ J/mol K. At temperatures >100 °C, the entropy change occurring as a result of the splitting of water vapor tends to increase slightly with temperature, from approximately $\Delta S_d^{\circ}(373\text{ K}) \sim +45$ J/mol K to $\Delta S_d^{\circ}(1465\text{ K}) \sim +55$ J/mol K. At 100 °C, magnitudes of enthalpy and entropy changes are identical and of opposed sign. As a result, there is a discontinuous change in the slope of $\Delta G(T)$ at 100 °C. Although the entropy contribution is favorable to the spontaneous dissociation of both liquid and vapor water, the enthalpy contribution of larger absolute magnitude is not favorable; as a result, the Gibbs free energy change is positive (the reaction is endergonic). The water-splitting reaction is a non-spontaneous process over the temperature range considered here. Extrapolation of $\Delta G(T)$ down to zero indicates that the direct thermo-dissociation of water molecules into H_2 and O_2 can take place at a very high temperature, close to 2500 K. Few if any solid materials can sustain such temperatures, and therefore the direct thermo-dissociation of water is not a viable technological option for hydrogen production. When water is split by electrolysis at a high temperature, more heat and less electricity are required compared with room temperature needs. For example, at 1000 °C, ~177 kJ/mol of electricity and ~71 kJ/mol of heat are required to satisfy the ~248 kJ/mol ΔH requirement at that temperature. This is why high-temperature water splitting is considered an interesting approach compared with low-temperature processes: When high-temperature heat is available—for example, in next-generation nuclear plants or solar towers—the cost of kilowatt-hours of heat is less than that of electricity.

9.2.2 Water splitting by electrolysis

9.2.2.1 Maximum work and cell voltage

In a water electrolysis cell, electricity is used to split water molecules into gaseous hydrogen and oxygen. According to the theorem of maximum work, at equilibrium the amount of electricity ($n{\cdot}F{\cdot}E$) required to split 1 mol of water is equal to the change of Gibbs free energy, ΔG_d, of the water dissociation reaction (9.3):

$$\Delta G_d - nFE = 0 \quad \text{where} \quad \Delta G_d > 0 \tag{9.3}$$

- $n = 2$ (number of electrons exchanged during the electrochemical splitting of water)
- $F = \sim 96{,}485$ C/mol (Faraday)
- $E =$ free energy voltage (volts) associated with reaction (9.1) or (9.2)
- $\Delta G_d =$ free energy change in J/mol associated with reaction (9.1) or (9.2)

ΔG_d is a function of both operating temperature and pressure:

$$\Delta G_d(T,P) = \Delta H_d(T,P) - T\Delta S_d(T,P) > 0 \tag{9.4}$$

$\Delta H_d(T,P)$ and $\Delta S_d(T,P)$ are, respectively, the enthalpy change (J/mol) and entropy change (J/mol K) associated with reaction (9.1) or (9.2). To split 1 mol of water, ΔG_d (J/mol) of electricity and $T\cdot\Delta S_d$ (J/mol) of heat are required. As can be seen in Figure 9.1, the higher the operating temperature is, the less electricity and the more heat are required to perform the reaction. Because the kilowatt-hours of electricity may be more expensive than those of heat, there is economic interest in performing water electrolysis at elevated temperatures (in the 800−1000 °C range) to reduce the cost of energy when heat sources are available at such temperatures (solar or nuclear).

The free energy voltage, E, in volts is defined as:

$$E(T,P) = \frac{\Delta G_d(T,P)}{nF} \tag{9.5}$$

The thermo-neutral or enthalpy voltage, V, in volt is defined as:

$$V(T,P) = \frac{\Delta H_d(T,P)}{nF} \tag{9.6}$$

Under standard conditions of temperature and pressure ($T^\circ = 298$ K; $P^\circ = 1$ atm), water is liquid and H_2 and O_2 are gaseous. Standard free energy, enthalpy, and entropy changes for reaction (9.1) are:

$$\Delta G_d^\circ(H_2O) = 237.22 \text{ kJ/mol} \rightarrow E^\circ = \Delta G_d^\circ(H_2O)/2F = 1.2293 \text{ V} \sim 1.23 \text{ V}$$

$$\Delta H_d^\circ(H_2O) = 285.840 \text{ kJ/mol} \rightarrow V^\circ = \Delta H_d^\circ(H_2O)/2F = 1.4813 \text{ V} \sim 1.48 \text{ V}$$

$$\Delta S_d^\circ(H_2O) = 163.15 \text{ J/mol K}$$

A voltage term, $T\cdot\Delta S_d^\circ/(2F) = 0.25$ V must be added to the free energy voltage, E, to provide the heat required by reaction (9.1). The temperature dependence of E and V is plotted in Figure 9.2. The enthalpy voltage required to split water vapor is almost constant and is close to 1.3 V. Free energy voltage E decreases continuously to less than 1 V for temperatures above 800 °C. As mentioned above, increasingly less electricity is required as the temperature increases owing to the increase in entropy. As a consequence, the electromotive force of H_2/O_2 fuel cells (the reverse reaction) also decreases with temperature.

Both enthalpy and free energy voltages are independent of electrolyte pH. A different pH only changes the potentials of anodic (O_2/H_2O in acidic media and HO^-/O_2 in alkaline media) and cathodic (H^+/H_2 in acidic media and H_2O/H_2 in alkaline media) redox couples, but the cell voltage (the difference between anode and

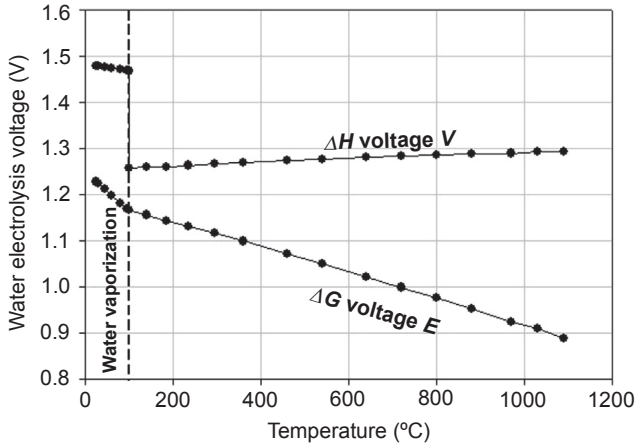

Figure 9.2 $E(T)$ and $V(T)$ plots associated with the water-splitting reaction.

cathode redox potentials) remains the same. Individual electrode potentials satisfy the Nernst equations. At 298 K, under standard conditions:

$$E^{+} = E^{\circ}_{H_2O/O_2} + \frac{R_{PG}T}{nF}\mathrm{Ln}\frac{\left(a^2_{H^+}\right)\left(f^{1/2}_{O_2}\right)}{a_{H_2O}} \sim 1.23 - 0.06\ \mathrm{pH} \tag{9.7}$$

$$E^{-} = E^{\circ}_{H_2/H^+} + \frac{R_{PG}T}{nF}\mathrm{Ln}\frac{a^2_{H^+}}{f_{H_2}} \sim -0.06\ \mathrm{pH} \tag{9.8}$$

Therefore, the free energy cell voltage is pH independent: $E_{cell} = E^{+} - E^{-} = 1.23$ V.

9.2.2.2 Kinetics of water splitting by electrolysis and cell efficiency

The free energy change (ΔG_d) of the water-splitting reaction is the minimum amount of electricity required to split 1 mol of water, assuming that the transformation takes place under isothermal conditions. The enthalpy change (ΔH_d) of the water-splitting reaction is the minimum amount of total energy required to split 1 mol of water. From a practical viewpoint, there is no interest in performing electrolysis close to equilibrium (reversible) conditions. To reduce capital expenses and hydrogen (and/or oxygen) production cost to market requirements, it is necessary to design electrolyzers as compact as possible and to significantly increase the operating current density. In conventional electrolyzers, current densities ranging from a few hundred mA/cm^2 (alkaline technology) up to several A/cm^2 (PEM and solid oxide technologies) are achieved. Part of what is gained on by reducing capital expenses is lost because higher current densities also means less efficient processes with higher operational (energy)

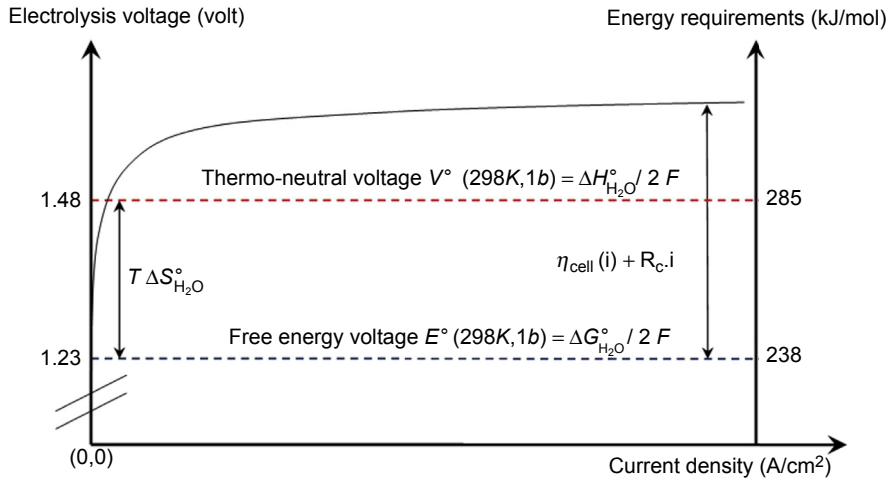

Figure 9.3 Schematic diagram of a voltage–current density polarization curve during water electrolysis.

costs. Capital expenditures (Capex) and operational expenditures (Opex) must be appropriately balanced, depending on the application.

The situation can be easily understood by considering the voltage–current diagram in Figure 9.3. Increasing cell voltages are required to overcome cell resistance. The cell resistance is the sum of a constant term (the resistance R_e of the electrolyte) and exponentially decreasing charge transfer resistance owing to interface over-voltages (η in volts) at both the anode and cathode. As a result, the voltage–current polarization curve is exponential in shape ($\eta(i)$ relationships follow the exponential Butler–Volmer laws of charge transfer kinetics (Hamann, Hamnett, & Vielstich, 1998)), at least at low current density values. As the current density increases, the ohmic resistance of the cell (electrolyte and other ohmic cell components) becomes predominant and the polarization curve tends to become linear in shape. At even higher current densities, limitations owing to mass transport effects (for example, transport of gaseous hydrogen and/or oxygen away from interfaces) may appear.

The energy efficiency ε of the electrolysis cell can be defined as follows: ε for an electrolysis cell relates the theoretical amount of energy W_t required to split 1 mol of reactant to the real amount of energy W_r required by the process. Because of the sources of irreversibility mentioned previously, $W_r > W_t$. The cell efficiency is defined as:

$$\varepsilon = \frac{W_t}{W_r} \tag{9.9}$$

where:

- W_r is $(U_{cell} \cdot I \cdot t)$, U_{cell} is the actual cell voltage in volts, I is current in A, and t is the duration in seconds
- W_t can be defined from the thermodynamic voltage E: $W_{t,\Delta G} = (E \cdot I \cdot t)$
- W_t can also be defined from thermo-neutral voltage V: $W_{t,\Delta H} = (V \cdot I \cdot t)$

Therefore, two different definitions can be used to express the efficiency of the electrolysis cell. Because E and V are both function of operating temperature (T) and operating pressure (P), and because U_{cell} is also a function of operating current density j, the two different cell efficiencies can be expressed as a function of T, P, j:

$$\varepsilon_{\Delta G}(T,P,j) = \frac{E(T,P)}{U_{\text{cell}}(T,P,j)} \quad \varepsilon_{\Delta H}(T,P,j) = \frac{V(T,P)}{U_{\text{cell}}(T,P,j)} \tag{9.10}$$

At low current densities, cell efficiencies close to 100% are obtained. In conventional water electrolyzers, $\varepsilon_{\Delta H} \sim 70\%$ at 1 A/cm^2, $T = 90\ ^\circ$C, and $P = 1$ bar. The efficiency of the electrolysis cell is a critical parameter responsible for the energy cost of the process. Operation at high current density is necessary to reduce investment costs, but because efficiency decreases when current density increases, a compromise has to be found between energy Capex and Opex.

9.2.2.3 Design of water electrolysis cells

Basically, an electrochemical cell is a galvanic chain formed by the series connection of an ionic conductor (the electrolytic solution made of ions dissolved in an appropriate solvent) clamped between electronic conductors (metallic electrodes). Usually, planar geometry is preferred over cylindrical geometry (more generally found in electrochemical generators) because it is more appropriate for the design of large systems. Such galvanic chains are used to perform electricity-driven non-spontaneous chemical transformations by applying a sufficient voltage between the two end electrodes. To prevent the spontaneous recombination of reaction products (H_2 and O_2) that form in the interpolar domain, a membrane separator is immerged in the electrolytic solution between the two electrodes. Based on these general constraints, different cell designs can be used. The simplest is the gap cell in which two electrodes are placed face-to-face a few millimeters away from the membrane separator. However, when gas bubbles are formed at metal−electrolyte interfaces (which happens during water electrolysis), a highly resistive and continuous gaseous film tends to form over electrode surfaces. The situation can be improved by using porous metallic electrodes and pressing them against the membrane separator. This is the zero-gap design. In this case, the interpolar distance is reduced to a minimum (ohmic losses across the electrolyte layer are minimized) and gases evolve through the porous electrodes at the rear of the cell. This design is used in advanced alkaline water electrolysis cells. The situation can be further improved using thin and highly conductive polymer electrolytes. Mobile ionic species remain confined inside the membrane, which acts simultaneously as an electrolyte and a cell separator. This is the solid polymer electrolyte (SPE) or PEM design. In such cells, no liquid electrolyte is in circulation in the electrolyzer. This concept was first proposed for application in H_2−O_2 fuel cells in the 1950s, at the dawn of the United States space program, to solve the problems associated with operation in a low-gravity environment and those caused by the corrosion of metals in acidic media. The idea was used the latter to develop water electrolyzers. In a PEM water electrolysis cell, porous electrodes are deposited on the surface of the membrane to form the

membrane–electrode assembly (MEA) and porous current collectors electrically connected to the external power supply are pressed on each side of the MEA. There is no liquid electrolyte. Only deionized water is circulated in the anodic chamber to feed the electrochemical reaction. Details are provided in the next section.

9.3 Polymer electrolyte membrane water electrolysis

9.3.1 Principles

In a PEM water electrolysis cell, electricity is used to split water molecules into gaseous hydrogen and oxygen (at close to ambient temperatures) according to the following half-cell reactions:

$$\text{Anode:}\quad H_2O(\text{liq}) \rightarrow \frac{1}{2}O_2(g) + 2H^+ + 2e^- \tag{9.11}$$

$$\text{Cathode:}\quad 2H^+ + 2e^- \rightarrow H_2(g) \tag{9.12}$$

$$\text{Full reaction:}\quad H_2O(\text{liq}) \rightarrow H_2(g) + \frac{1}{2}O_2(g) \tag{9.13}$$

A PEM water electrolysis cell is shown in Figure 9.4. Water-solvated protons formed at the oxygen-evolving anode of the PEM cell respond to the electric field set across the cell by the external direct current power supply and migrate through the SPE membrane down to the cathode, where they are reduced into molecular hydrogen. Liquid water is consumed at the anode for oxygen generation but is also transferred across the membrane and released at the cathode when solvated protons are de-solvated and reduced into hydrogen. This is electro-osmosis drag. The number of water molecules that solvate migrating protons depends on water loading or the hydration level (which can go up to 15 H_2O/SO_3^-) but is usually close to 1 H_2O/H^+ (Fuller & Newman, 1992; Vishnyakov & Neimark, 2000).

9.3.2 Polymer electrolyte

Ion-conducting polymer materials are used in electrolyzers for the double purpose of carrying electric charges (hydrated protons in the PEM water electrolysis cell) between the anode and cathode and separating the products formed at each electrode (H_2 and O_2) that would otherwise spontaneously recombine. For application in water electrolysis cells, polymeric membranes must satisfy a number of physical criteria, including (1) good ionic conductivity (which determines the internal ohmic resistance of the membrane) and good thermal conductivity (to favor heat dissipation to the surroundings, which results from the Joule effect during operation); (2) poor electronic conductivity (which would otherwise short-circuit the cell); (3) good chemical and mechanical stability (in particular, to sustain the strongly oxidizing conditions

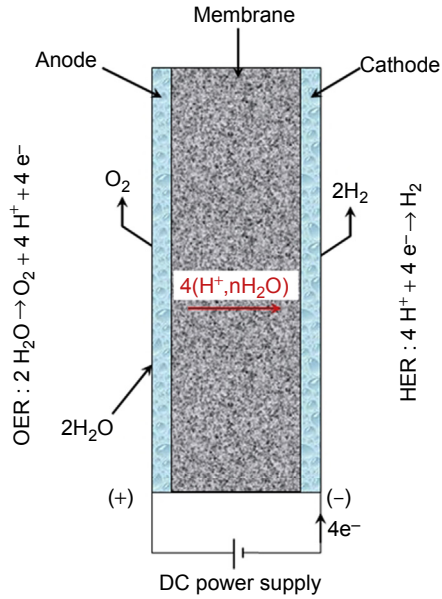

Figure 9.4 Cross-section diagram of a PEM water electrolysis cell.

encountered in the anodic compartment of the cell); (4) good thermal stability (for operation close to 100 °C); (5) ease of manufacture and production in the form of large surface membranes of homogeneous thickness; and (6) low gas solubility (to prevent gas cross-permeation effects as much as possible, which tend to increase when the operating pressure is raised). Some quantitative figures are discussed in this section (Millet, 2011).

9.3.2.1 Polymer membrane materials

The most suitable polymeric material that can be used in PEM water electrolysis cells is a chemically stable sulfonated tetrafluoroethylene-based fluoropolymer-copolymer (Figure 9.5), developed in the 1960s by W. Grot at E.I. DuPont Co. (Nafion® materials). Nafion® products are characterized by their equivalent weight (EW), i.e., the number of grams of dry Nafion® per mole of sulfonic acid groups when the material is in the acid form. The EW, which can be ascertained by acid−base titration, is usually in the range of 1100−1200 for commercial products (Mauritz & Moore, 2004). Several micro-structural models (for example, those of Yeager and Steck (1981) and Gierke, Munn, and Wilson (1981)) have been developed to account for the unexpected microstructure of these materials. Both evoke the concept of ionic cluster to design percolating hydrophilic micro-domains where ending sulfonic chains tend to gather. From a practical viewpoint, Nafion® can be considered a homogeneous two-phase medium, a mixture of hydrophobic regions concentrating fluorocarbon backbones and hydrophilic regions containing water, in which transport of hydrated protons takes place through a hopping mechanism. From a historical perspective, the cluster-network

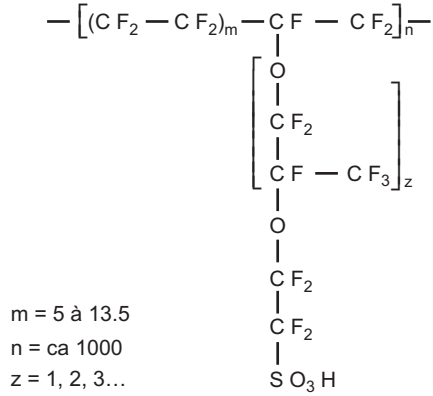

Figure 9.5 The structure unit of Nafion®.

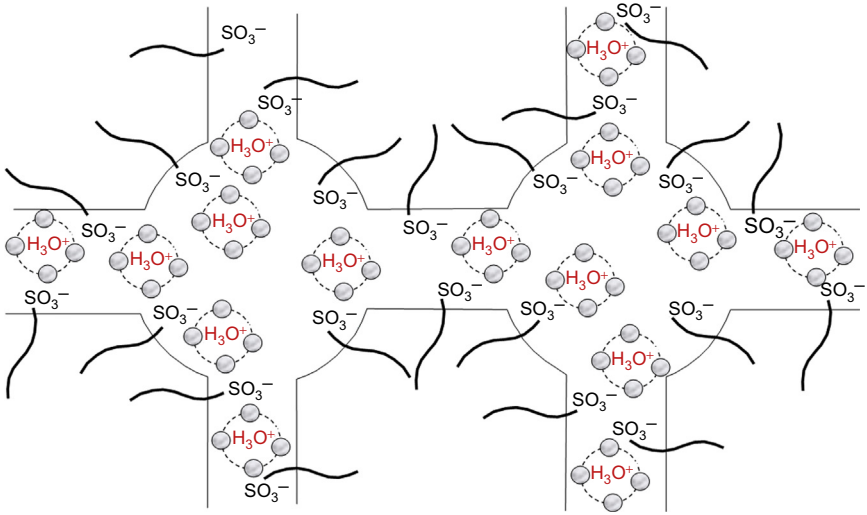

Figure 9.6 Model of nanoclusters in perfluorosulfonic acid materials.

model of Gierke et al. has been used for many years to interpret the properties of Nafion® membranes (especially ion and water transport and ion permselectivity). In this model (Figure 9.6), it is assumed that there are ∼40-Å-diameter clusters of sulfonate-ended perfluoroalkyl ether groups that are organized as inverted micelles and arranged on a lattice. These micelles are connected by pores or channels that are ∼10 Å in size. These $-SO_3^-$-coated channels were invoked to account for inter-cluster transfer of cations and ion conductivity. Ionic clusters that were initially believed to have a well-defined shape, morphology, and spatial distribution were later found to be more randomly distributed. Most important, Nafion® materials are now

described with intermediate interphase domains located between hydrophobic and hydrophilic regions, where ionic transport takes place.

9.3.2.2 Key properties of perfluorosulfonated membrane materials

Ionic conductivity

The first role of the membrane in the PEM water electrolysis cell is to convey electric charges (ions) between electrodes. Therefore, ionic conductivity is a key physical property of membrane materials. In conventional water electrolyzers, the operating current density ranges from a few hundred mA/cm^2 to several A/cm^2. A maximum ohmic drop of 100 mV at 1 A/cm^2 is a good performance target for electrolyzers. Therefore, the surface resistance of the membrane should be less than 0.1 Ω cm^2. In PEM water electrolysis, the typical membrane thickness is ∼200 μm (this is the case for commercial Nafion® products). At room temperature, the resistivity of 1100 EW Nafion® in H^+ form is $\rho < 5.0\ \Omega$ cm and the corresponding conductivity is $\sigma > 0.2$ S/cm (Tsampas, Pikos, Brosda, Katsaounis, & Vayenas, 2006). The surface resistance of the membrane is therefore 0.1 Ω cm^2. The conductivity of Nafion is assumed to come from both proton migration in the aqueous phase and proton tunneling between adjacent sulfonate groups in narrow pores.

Permselectivity

Permselectivity is the term used to define the preferential permeation of certain ionic species through ion-exchange membranes (IUPAC, 1993). When the membrane is used in a gap cell or in a zero-gap cell configuration with a liquid electrolyte, both cations and anions participate in the transport of electric charges according to their charge and individual mobility (Donnan exclusion effects must also be considered to differentiate between cationic and anionic transport). However, when the membrane is used in a PEM cell without liquid electrolyte, the only mobile species (charge carriers) are solvated protons. Sulfonate end groups of pendent chains (Figure 9.5) are covalently bound to side fluorocarbon chains and cannot participate in ionic mobility. In this case, the permselectivity of the membrane is unity.

Gas permeability

The second main role of the polymeric membrane in the PEM water electrolysis cell is to prevent recombination of reaction products (hydrogen at cathode and oxygen at the anode) formed during electrolysis at the electrode−electrolyte interfaces. When the electrochemical reaction produces gases at high pressure (as is the case in a pressurized PEM water electrolysis cell), the gas permeability (P^m) of the membrane becomes a critical physical property. Hydrogen and oxygen cross-permeation phenomena tend to increase hydrogen concentration in the oxygen production flow and oxygen concentration in the hydrogen production flow to values larger than the lower flammability thresholds. To prevent the risk of explosive recombination, it is therefore necessary to reduce these undesirable effects as much as possible. Gas permeability varies markedly with both the temperature and water content of the polymer membrane, bracketing

values measured on poly(tetrafluoroethylene) (PTFE) and liquid water. Gas permeability is defined as:

$$P^m = \frac{u}{\Delta P}\frac{\delta}{A} \text{ in } \mathrm{cm}^2/\mathrm{Pa\ s} \tag{9.14}$$

where u is the rate of gas permeation in Nm^3/s; ΔP is the difference in gas pressure across the membrane in Pa; δ is the thickness of the membrane in meters; and A is the section of the membrane in square meters. Data indicate that the transport of dissolved gases across Nafion® takes place mainly through ionic (hydrated) clusters. In a PEM water electrolyzer, liquid water is electrolyzed. The membrane is fully hydrated, and therefore H_2 and O_2 permeabilities are both significant. To estimate gas permeation flow, it is necessary to determine the value of diffusion coefficients. The P^m of species i is related to the diffusion coefficient D_i in cm^2/s through the following relationship:

$$D_i = P_i^m R_{\mathrm{PG}} T C_i \tag{9.15}$$

where R is the constant of perfect gas: 82×10^5 Pa·cm^3/K mol; T is the temperature in Kelvin; and C_i is the concentration of species i in $\mathrm{mol/cm}^3$. The hydrogen diffusion coefficient in Nafion® 117 varies from 3.9×10^{-7} cm^2/s at 10 °C to 2.6×10^{-6} cm^2/s at 100 °C. The oxygen diffusion coefficient is usually two times lower (see Section 9.5.2).

Thermal conductivity

During operation, a flow of solvated protons is conveyed from the anode (where they form during water oxidation) to the cathode (where they are reduced into molecular hydrogen). Because of membrane internal resistance, electrical energy is dissipated as heat by the Joule effect. The amount of heat generated inside the membrane is directly proportional to the operating current density (Millet, 1990). The thermal conductivity of the membrane must be sufficiently high to transfer this heat to the surroundings (for example, to the backing current collectors) and avoid the formation of unacceptable heat peaks that could provoke irreversible damage. This is particularly significant when the cell is operated at high current density (in the multi-$\mathrm{A/cm}^2$ range, which can commonly be reached in modern PEM water electrolyzers). Heterogeneous internal temperatures can provoke heterogeneous membrane swelling or shrinking, generate heterogeneous mechanical constraints, and lead to membrane perforation. The thermal conductivity λ of dry Nafion® is known to vary slightly with operating temperatures, from 160 ± 30 mW/m K at room temperature to 130 ± 20 mW/m K at 65 °C. The thermal conductivity of hydrated Nafion® is a function of water content: $\lambda = 180$ mW/m K (RH = 10%) and $\lambda = 300$ mW/m K (RH = 100%) (Khandelwal & Mench, 2006). Over the usual 0−100 °C temperature range of operation of these materials in water electrolysis cells, the thermal conductivity of Nafion® is closer to the thermal conductivity of PTFE ($\lambda = 210$−270 mW/m K) (Price & Jarratt, 2000) than the thermal conductivity of water ($\lambda = 600$−653 mW/m K).

9.3.3 Electrocatalysts

In conventional PEM water electrolyzers, unsupported platinum particles or carbon-supported platinum nanoparticles (Figure 9.7) are used as electrocatalysts at the cathode to promote a hydrogen evolution reaction (HER). At the anode, unsupported Ir° or IrO_2 particles (Figure 9.8) are used at the anode for the oxygen evolution reaction (OER). These catalyst particles are usually sprayed over the membrane surface and coated using an alcohol solution of perfluorinated ionomer that tends to polymerize upon thermal/pressure treatment and provides adequate adherence to the catalytic layer. Micrometer-thick porous catalytic layers are thus typically obtained.

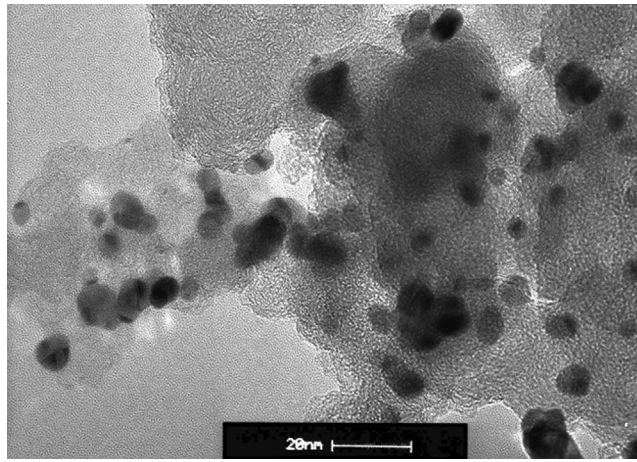

Figure 9.7 Transmission electron micrograph of Pt nanoparticles on Vulcan XC-72.

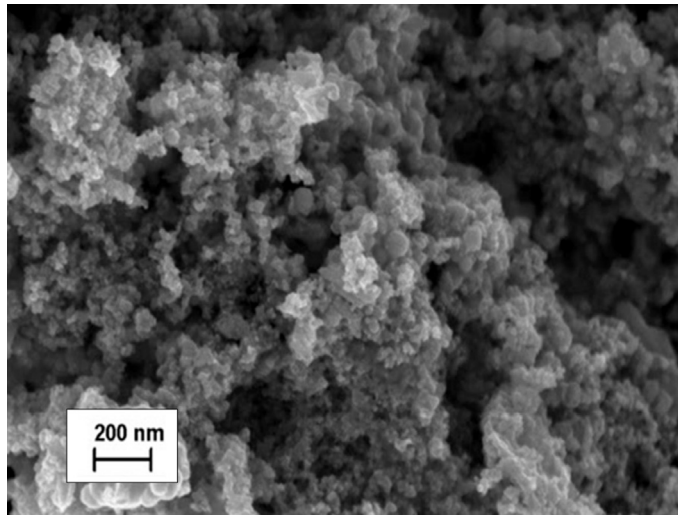

Figure 9.8 Scanning electron micrograph of IrO_2 particles.

9.3.4 Membrane-electrode assemblies

A large variety of processes can be used to synthesize MEAs. For example, catalytic inks containing an alcohol suspension of catalyst particles and a solution of perfluorosulfonated ionomers can be sprayed at ambient temperature over the membrane surface using an ink printer (Figure 9.9). Membrane-electrode assemblies of different sizes (up to 1000 cm^2 in industrial electrolyzers) and shapes can thus be prepared within minutes (Figure 9.10).

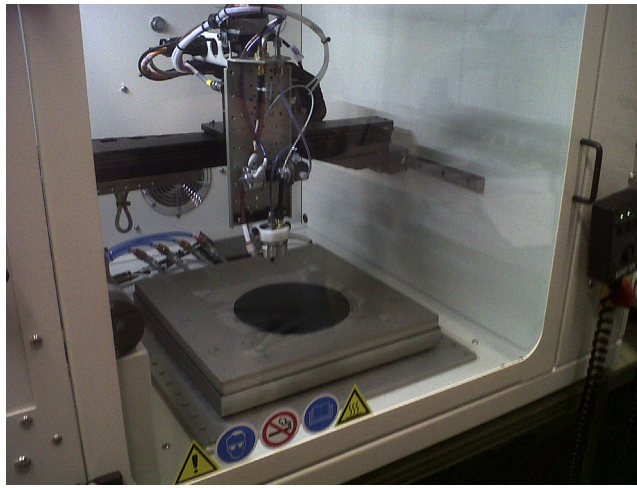

Figure 9.9 Photograph of an ink printer used to manufacture MEAs (SonoTek Co.).

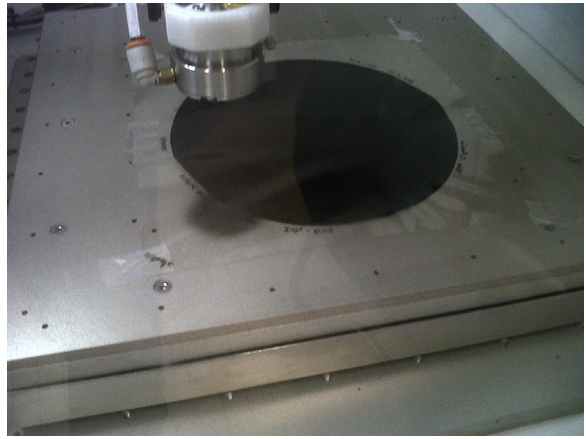

Figure 9.10 Photograph of a circular 250-cm^2 MEA obtained by pulverizing catalytic inks using the printer in Figure 9.9.

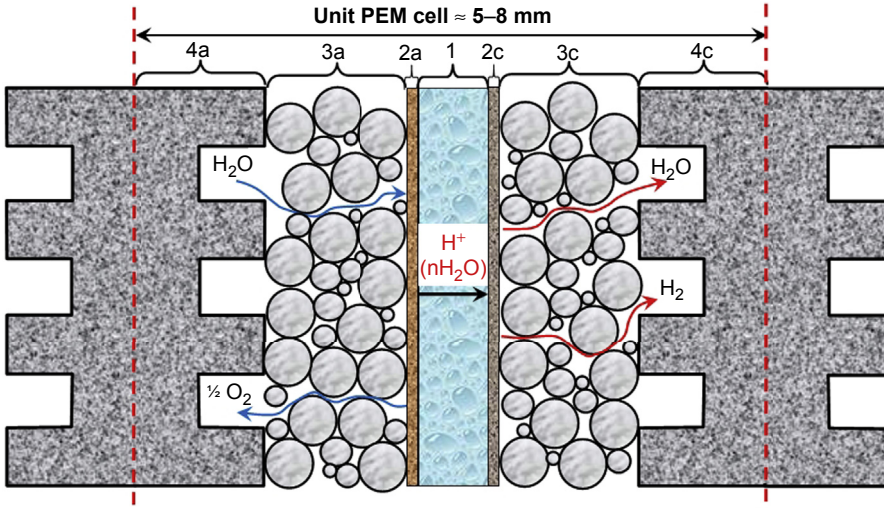

Figure 9.11 Cross-section of a PEM water electrolysis cell showing internal cell components. (1, membrane; 2a and 2c, two catalytic layers; 3a and 3c, two porous current collectors; 4a and 4c, two end plates).

9.3.5 Other cell components

A PEM water electrolysis cell contains several internal components. Details are provided in Figure 9.11. Several designs can be used, but in the simplest cases (for laboratory experiments), the cell contains the membrane (1) and its two catalytic layers (2a and 2c), two porous current collectors (3a and 3c), and two end plates (4a and 4c). Mass flow channels are machined at the surface of the titanium end plates that delimit the PEM cell. Liquid water is pumped across the channels of appropriate geometry and liquid−gas mixtures (H_2O−O_2 in the anodic compartment and H_2O−H_2 in the cathodic compartment) are collected at the exhausts.

The MEA is clamped between 2-mm-thick porous current collectors usually made of sintered titanium particles. Titanium is used as a standard material because it tends to passivate in contact with deionized liquid water. From a process viewpoint, the purpose of these porous plates is double. First, they convey electricity from end plates up to catalytic layers on each side of the MEA. Titanium particles must be small enough to increase the number of contact point with the catalytic layers and thus ensure the homogeneous distribution of current lines. Second, their porosity must be sufficiently open to let liquid water and gases flow across. At the anode, the plate must let liquid water come through and reach the anodic catalytic layer, where it is oxidized; at the same time, it must let gaseous oxygen formed at the anode during electrolysis come through, back to the end plate. In the cathodic compartment, the situation is simpler because both flows (electro-osmotic liquid water and gaseous hydrogen flow) are co-directional, from the cathodic catalytic layer to the end plate. Porous current collectors therefore have a critical role in these SPE cells and their porosity and structure

Figure 9.12 Photograph of a four-stack PEM water electrolyzer (courtesy of CETH Co.).

need to be optimized. In particular, the open porosity must be adapted to the gas production rate and therefore to the maximum current density during operation. If these plates are not sufficiently porous, gaseous films may form at their interfaces with catalytic layers and mass transport limitations may occur. More details can be found in Grigoriev, Millet, Volobuev, and Fateev (2009).

9.3.6 Balance of plant and technology developments

A photograph of a four-stack PEM water electrolyzer is provided in Figure 9.12. The corresponding process flow sheet is detailed in Figure 9.13. Although liquid water is required only on the anodic side to feed the electrochemical reaction, two high-pressure pumps are used to circulate water (one for the oxygen circuit and one for the hydrogen circuit), which can cool the process down and facilitate gas transport away from the electrolyzer. Biphasic water-gas mixtures formed inside the electrolyzer are separated by gravitation in two different separation units. Gases are then purified (traces of hydrogen in the oxygen main stream and traces of oxygen in the hydrogen main stream are removed by catalytic recombination into water) and dried, according to downstream process requirements. Gas purity on each line is monitored continuously for safety purposes. Gas exhaust pressures (O_2 and H_2) are continuously monitored. Compressed feed water is injected into the oxygen−water separator. The electro-osmotic flow of water collected on the cathodic loop is recycled. Pressurized nitrogen is used when the production starts to pressurize the stack, and for dilution purposes in case of an emergency shutdown (Millet et al., 2010).

According to the literature, several manufacturers are active in the market of PEM water electrolyzers. Table 9.1 lists some of these suppliers with details about their product lines. It is not an easy task to make detailed comparisons in terms of process maturity and efficiency because details are usually lacking in the literature, but several

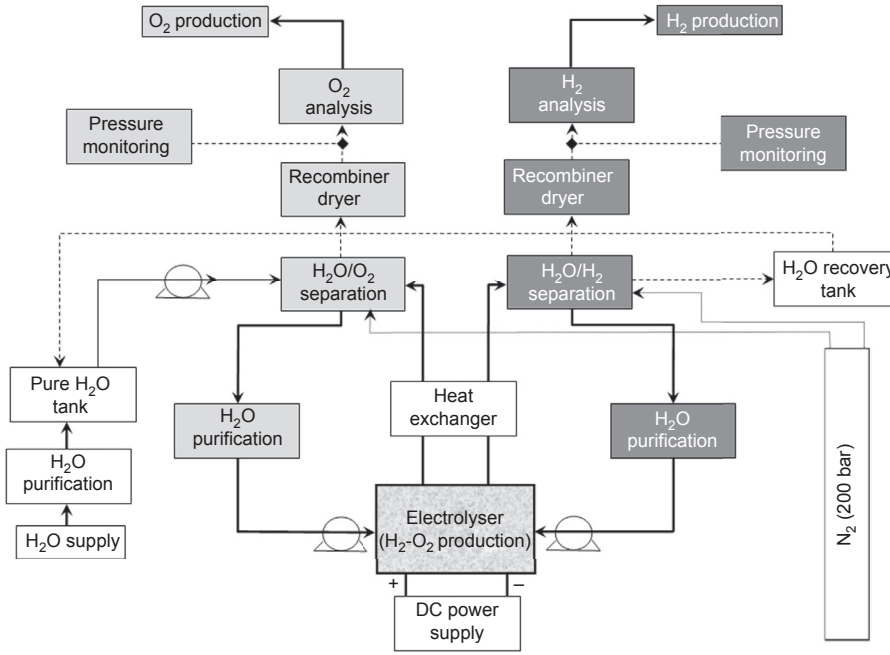

Figure 9.13 Polymer electrolyte membrane water electrolysis process flow sheet.

conclusions can be reached concerning the status of PEM water electrolysis technology at an industrial level:

- PEM water electrolyzers are becoming competitive with alkaline systems
- The range of production capacity is still limited to less than 100 Nm^3 H_2/h but research and development efforts are being made to develop larger systems
- Energy consumption (at approximately 1 A/cm^2) is close to 70% (high heating value (HHV))
- The operating pressure of commercially available units is limited to approximately 50 bars but prototype systems operating at much higher pressures have been developed and successfully tested
- In terms of durability, little technical information is available, but PEM technology has demonstrated an ability to operate in the 10^4- to 10^5-h range, at least for military applications

9.3.7 Electrochemical performances and efficiency

Typical polarization curves measured during PEM water electrolysis using membranes of two different thicknesses (Nafion® 115, dry thickness = 125 μm and Nafion® 117, dry thickness = 175 μm) are plotted in Figure 9.14. The gray rectangle shows state-of-the-art performance, at least at the laboratory scale. Cell efficiency $\varepsilon_{\Delta H}$ HHV (corresponding to the electrolysis of liquid water) is usually ~70% at 1 A/cm^2, $T = 90\ ^\circ C$, and $P = 1$ bar. As discussed, the polarization curve is exponential in shape in the low current density region and ends up in a linear current−voltage relationship at

Table 9.1 **Some manufacturers of PEM water electrolyzers and system characteristics**

Manufacturer	Country	Product name	Capacity range (Nm^3/h)	Pressure bar g	Energy consumption kWh/Nm^3 (ΔH efficiency)
Siemens	Germany	–	60	30	~4.9 (~60%)
Aréva H2Gen	France	E60	60	30	~4.9 (~60%)
Proton on-site	United States	Hogen C30	30	30	~5.8 (~50%)
ITM	United Kingdom	HPac 40	2.4	15	~4.8 (~60%)

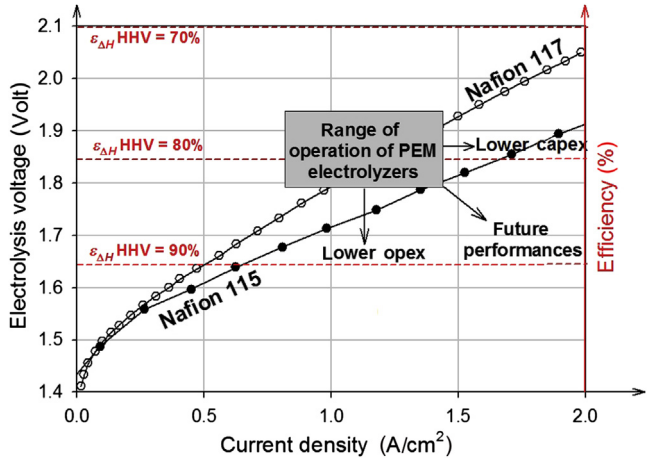

Figure 9.14 Typical polarization curves measured on a PEM water electrolysis cell. The gray rectangular area shows the state-of-the-art range of operation in conventional systems.

higher current density values, owing to internal cell resistance. Increasing current density at constant cell voltage would result in a lower Capex at constant efficiency; reducing cell voltage at constant current density would result in higher efficiency (lower Opex) at constant capital expenses. The role of the engineer is to design cheaper and more efficient systems, to reduce both Capex and Opex. The next generations of PEM water electrolyzers should operate in the multi-Amp/cm^2 current density range at cell voltages inferior to 2.0 V and possibly lower.

Figure 9.15 shows that the thermodynamic voltage is the most significant term of cell voltage. The anodic overvoltage required for OER is the main source of irreversibility at any current density. This is because the exchange current density on iridium is low (approximately 10^{-6} A/cm^2 at ambient temperature (Damjanovic & Bockris, 1966)). The overvoltage associated with the HER is small because the kinetics of the H^+/H_2 system is high (the exchange current density on platinum is approximately 10^{-3} A/cm^2 at ambient temperature (Bockris & Reddy, 1982)). The last source of irreversibility results from cell resistance (which is the sum of the ionic resistance of the electrolyte and the electronic resistance of metallic cell components).

9.4 Advantages and limitations of PEM water electrolysis

9.4.1 Main competing technologies

Water electrolysis is a clean (carbon-free) source of molecular hydrogen. In terms of cost, it cannot compete with processes that use hydrocarbons (mainly methane from natural gas in the industry sector) as a hydrogen source because of significantly different energy requirements (~238 kJ is required to extract 1 mol of hydrogen

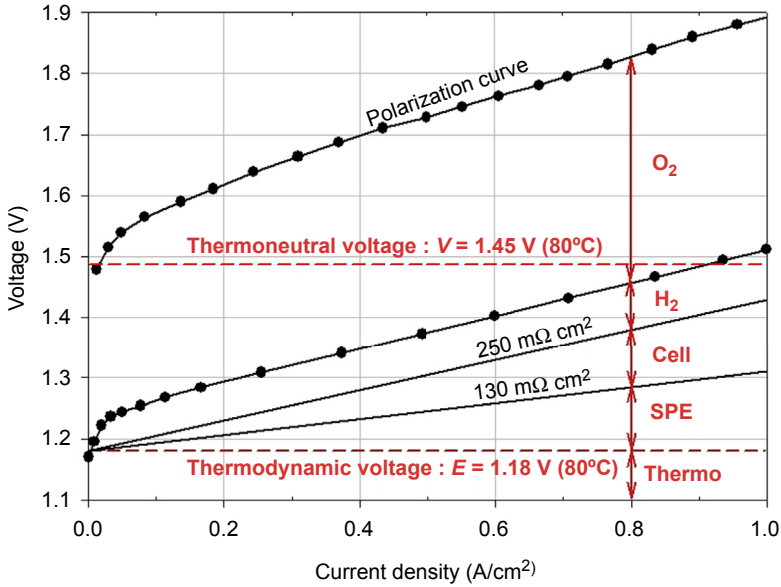

Figure 9.15 Main voltage terms of a PEM water electrolysis cell as a function of operating current density.

from water and ~41 kJ is required to extract 1 mol of hydrogen from methane by steam reforming under standard conditions). Nevertheless, water electrolyzers have some advantages in view of future large-scale deployments: They are compact and modular and can be powered by fluctuating power sources. There are three main competing water electrolysis technologies. The most mature one from an industrial viewpoint is the alkaline process, operating over the 60–140 °C temperature range and up to 30–40 bars. Despite some specific disadvantages (the need for chemically aggressive hot aqueous solutions of potassium hydroxide as liquid electrolyte and operation at moderate current densities), success is attributable to system simplicity, durability, and the use of cheap electrode materials. Technical maturity was gained over the twentieth century by continuous technical improvement in both material science and system engineering, which gradually allowed researchers to stop using dangerous cell materials (asbestos was used until recently as a cell diaphragm) and improved efficiency. Polymer electrolyte membrane water electrolysis, which is specifically considered in this chapter, is more recent (after developments in fuel cell technology in the 1960s) and operates at temperatures less than 100 °C. Solid polymer electrolyte technology was developed at the dawn of the United States space program for energy management in zero-gravity environments. Earlier developments led to H_2–O_2 fuel cells, and later to water electrolyzers when appropriate membrane materials were put on the market at the end of the 1960s. Solid oxide water electrolysis operating above 800 °C has been the focus of even more recent development, in the footprints of research and development in solid oxide fuel cell technology.

9.4.2 Main advantages of PEM water electrolysis

Polymer electrolyte membrane water electrolysis provides some well-established advantages over other water electrolysis technologies. First, PEM electrolyzers are more compact. Membrane-electrode assemblies are thin (anode−cathode interpolar distances are typically in the 100- to 200-μm range), flexible (this is not the case for oxide ions conducting ceramics used in solid oxide technology), and easily handled. They can be operated at significantly elevated current densities (in the multi-A/cm^2 range) with good energy efficiencies ($\sim$70% at 1 A/cm^2 using 200-μm-thick membranes). They are safe because ionic charge carriers remain confined inside the membrane and there is no need to use a corrosive and toxic electrolyte, as in the alkaline process. Operation of pressurized PEM electrolyzers is safer in the sense that potential leakage of hot water is more manageable than leakage of hot alkaline solutions. These are the main reasons why the technology has been and still is used to generate oxygen in confined atmospheres (for underwater or space applications). In view of application in the hydrogen economy to produce hydrogen as an energy carrier, PEM water electrolyzers can be operated in a flexible way: They accept highly transient power loads (such as those resulting from the use of intermittent energy sources of electricity via PV panels or wind turbines) and can operate over the quasi-entire power load range (10−100%) within seconds with no significant operational constraints. This is not the case for the alkaline process. Polymer electrolyte membrane water electrolyzers can also be operated under pressure (50 bars is available in some commercial products; operation under several 100 bars has been reported in the literature) and under pressure differences between the anode and cathode (more details are provided in Chapter 10). Finally, PEM water electrolysis cells are not prone to fast aging resulting from thermal cycling, as is the case in the high-temperature process.

9.4.3 Main limitations of PEM water electrolysis

Cost issues always come to mind when discussing PEM water electrolysis technology. This is probably because platinum group metals (PGM) are used as electrocatalysts. A closer look at the situation reveals that PGM materials used in these electrolyzers account for only a few percent of the total cost at system levels. At stack levels, perfluorosulfonated polymer materials and titanium current collectors are much more expensive and significant cost reduction in view of large-scale deployment will require appropriate innovative developments in material science in the future. In addition, gas cross-permeation phenomena that take place during operation under pressure or under differential pressures call for less permeable materials to maintain sufficiently high faradic efficiencies and reduce operation risks.

Another limitation compared with the alkaline process is that so far, the technology still needs to demonstrate that larger production capacities can be reached. Whereas commercial systems that can deliver approximately 50 Nm^3 H_2/h are available on the market, application in the industry sector requires larger systems and therefore the development of cell components up to the square meter size.

Also, PEM water electrolysis requires highly deionized water for operation. This is because mineral (metallic) impurities tend to penetrate into the PEM via ion-exchange processes. This, in turn, can increase the internal resistance of the membrane and HER overvoltage by depositing inactive metallic monolayers by under-potential deposition at platinum catalytic particles (Millet, Alleau, & Durand, 1993). Water deionization and online purification are expensive and inadequately purified water may require costly maintenance operations.

Solid oxide water electrolysis can be operated more efficiently at similar elevated current densities, but its deployment will probably remain limited until cell components become available that can sustain high temperatures and severe thermal cycling conditions.

9.5 Future trends

Most research and development activities launched today are aimed at developing new materials for operation over extended temperature ranges and designing cells that can operate at more elevated current densities.

9.5.1 Operation at elevated current densities

Industrial PEM water electrolyzers usually operate in the 0.8- to 1.2-A/cm^2 range. Laboratory tests reveal that much higher current densities can be achieved (in the multi-A/cm^2 range) when appropriate cell design is used. A typical example is provided in Figure 9.16.

As discussed, the ohmic shape of the polarization curve at high current densities indicates that ohmic losses resulting from cell internal resistance (the sum of electrolyte and other cell component resistances) are responsible for the increasing cell voltage. Cell internal resistance is obtained by taking the first-order derivative of the polarization curve. At high current density (larger than 500−1000 mA/cm^2, depending on polarization efficiency), cell resistance becomes almost constant and equal to ohmic cell resistance because charge transfer resistances tend toward zero (Butler−Volmer behavior). In a properly designed cell, the resistance of the polymer membrane should be the most significant term and the resistance of other cell components (current collectors, spacers, and end plates) should remain low owing to their higher electronic conductivity.

From the material science viewpoint, cell voltages should remain inferior to 2.0 V. At higher values, oxidative conditions become difficult to sustain and corrosion of anodic cell components (catalyst and current collectors) become unacceptable and reduce cell lifetimes.

9.5.2 Pressurized PEM water electrolysis

In PEM water electrolyzers, as discussed, ion-conducting polymer materials are used for the double purpose of carrying electric charge and separating reaction products. Hydrogen and oxygen solubility and diffusivity in perfluorinated ion-exchange

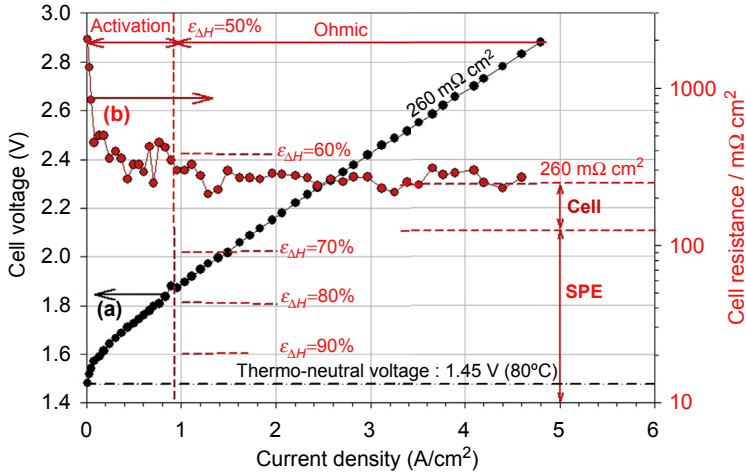

Figure 9.16 Polarization curve measured during PEM water electrolysis in the multi-A/cm^2 current density range and associated cell resistance.

polymers used as SPE in state-of-art PEM water electrolyzers are adequately low and gas cross-permeation during operation (hydrogen diffusion across the membrane from cathode to anode and oxygen diffusion from anode to cathode) can be neglected. This is true only when PEM water electrolysis cells are operated in near-atmospheric pressure conditions. In such cases, gaseous cross-permeation is negligible; as a result, faradic efficiency is close to unity and the hydrogen concentration in evolving oxygen (in the anodic compartment) and the oxygen concentration in evolving hydrogen (in the cathodic compartment) are negligible. The situation differs when the operating pressure is increased (Ogumi, Takehara, & Yoshizawa, 1984). Pressurized PEM water electrolysis is an interesting operating option because it creates the possibility of direct storage of pressurized gases with no need for external compressors. The PEM cell acts as an electrochemical compressor (more details are provided in Chapter 10). Most commercial electrolyzers can be operated at low to medium pressures (up to 50 bars). Reports in the literature indicate that the technology can be operated at much higher pressures (above 100 bars). Keeping in mind that hydrogen used in the automotive industry (H_2—air fuel cell powered cars) is usually stored at 350 or 700 bars, the interest in high-pressure PEM water electrolysis can easily be understood.

From a physical viewpoint, the driving force for gas cross-permeation through the polymer electrolyte is caused by the gradient of hydrogen and oxygen chemical potentials set across the membrane as a result of the desirable separation of evolving gases. Thermodynamics of gases teaches us that the chemical potential of a gaseous species is proportional to its partial pressure (at low pressure values) and to its fugacity at higher pressure. Because pure gases are evolving in each cell compartment during electrolysis, the gradient set across the membrane is proportional to the gradient of pressure. Nafion® can be seen as a two-phase medium, a combination of hydrophobic fluorinated organic backbone impregnated by a percolating aqueous phase in which pending

sulfonic groups and their hydrated proton counter-ions tend to cluster. Gas cross-permeation takes place because both hydrogen and oxygen solubility in Nafion® materials is non-zero. Solubility is water content dependent but gases also dissolve in the organic phase (Sakai, Takenaka, & Torikai, 1986). As a result of this solubility, two concentration gradients of dissolved gases and of opposite directions are set across the membrane, and dissolved gaseous species flow across the membrane according to Fick's laws of diffusion. H_2 and O_2 permeability (Eqn (9.14)) and their diffusion coefficients (Eqn (9.15)) are compiled in Table 9.2 (Mann, Amphlett, Peppley, & Thurgood, 2006; Sakai, Takenaka, Wakabayashi, Kawami, & Torikai, 1985).

A fraction of the two gaseous flows across the membrane is consumed at the opposite electrode: Hydrogen is re-oxidized into protons at the anode and oxygen is reduced as water at the cathode. As the result, the faradic efficiency of the cell decreases. However, part of these flows can come across the surface-bounded porous electrodes and be released into gaseous gas production. As a result, oxygen is contaminated by hydrogen. The level of contamination depends on both operating current density and operating pressure (Figure 9.17). Experimentally, it is observed that the hydrogen concentration in oxygen is inversely proportional to the current density. This is because the hydrogen crossover flow that comes across the membrane to contaminate oxygen production is proportional to the constant difference in pressure set across the membrane. At low current densities, the oxygen production is small; therefore, hydrogen contamination is more elevated (Fateev et al., 2011). Figure 9.17 provides model curves obtained using a simple permeation model. The significant disagreement observed at low current densities occurs because during operation, the faradaic efficiency is not constant. Chapter 11 provides more details about the different mass transport phenomena involved and the process and details about a model that can be used to analyze experimental results.

9.5.3 Research on innovative solid polymer electrolytes

9.5.3.1 High-temperature polymeric proton conductors

Concerning solid polymer electrolyte technology, research is driven by potential applications in H_2−O_2 fuel cell technology for the automotive industry. Because about half of the energy delivered by such fuel cells is released as heat, operation at conventional (80−90 °C) temperatures requires a larger heat exchanger compared with that used in internal combustion engine−driven cars. Operating temperatures close to 150 °C would be more appropriate. Much research and development is currently under way in the European Community and other developed countries to find alternative and less expensive materials. For example, different perfluorinated polymers (Hyflon® from Solvay Plastics Co.), stable at such temperatures, offer interesting new perspectives.

9.5.3.2 Low water content polymeric proton conductors

An additional problem in fuel cell technology comes from water management issues. Feed gases must be appropriately hydrated and the water produced at the cathode from the reduction of oxygen must be removed to avoid condensation and loss of

Table 9.2 H_2 **and** O_2 **permeability and diffusion coefficient in hydrated Nafion® 117 at different temperatures**

T (°C)	10	20	40	60	85
$P^m{}_{O_2}$ (cm^2/Pa s)	2.1×10^{-12}	2.3×10^{-12}	3.7×10^{-12}	5.3×10^{-12}	8.4×10^{-11}
D_{O_2} (cm^2/s)	2.1×10^{-7}	2.5×10^{-7}	4.2×10^{-7}	6.5×10^{-7}	1.1×10^{-6}
$P^m{}_{H_2}$ (cm^2/Pa s)	3.8×10^{-12}	4.6×10^{-12}	7.6×10^{-12}	1.2×10^{-11}	2.0×10^{-11}
D_{H_2} (cm^2/s)	3.9×10^{-7}	4.9×10^{-7}	8.7×10^{-7}	1.5×10^{-6}	2.6×10^{-6}
D_{H_2}/D_{O_2}	1.9	2.0	2.1	2.3	2.4

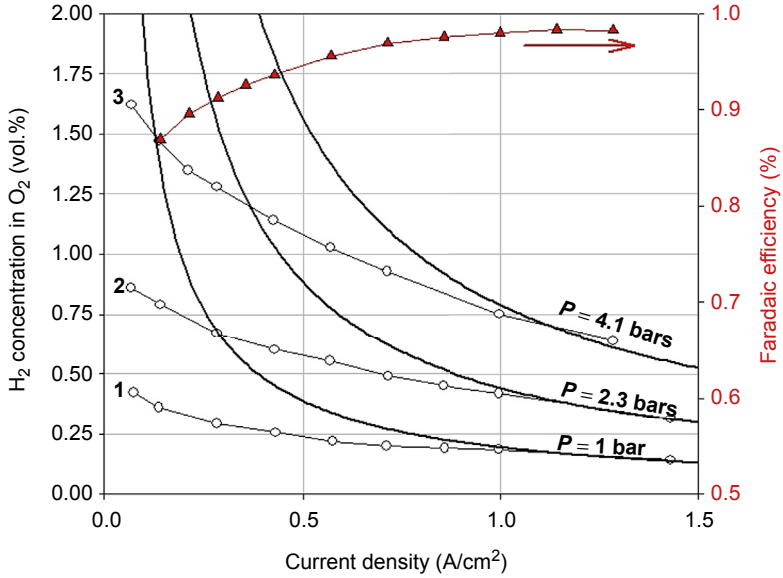

Figure 9.17 (Left) Hydrogen concentration (vol.%) in the anodic oxygen−water vapor mixture, measured by gas chromatography at $T = 85$ °C on a 250-cm^2 mono-cell at different pressures as a function of operating current density. Catalysts: Pt for the HER, Ir for the OER, and Nafion® 117 as SPE. (1) $P = 1.0$ bar; (2) $P = 2.3$ bars; (3) $P = 4.1$ bars. (Right) Current efficiency at the cathode at $P = 4.1$ bars as a function of operating current density. Open symbols: experimental data points. (—): model results.

performance. Such problems are critical and a trend in research is to develop new polymers involving proton conduction mechanisms and operating under quasi-dry conditions. It is expected that the results of these research efforts will also benefit PEM water electrolysis, bringing to the market new polymer materials for operation at higher temperature.

9.5.4 Research on innovative electrocatalysts

In a conventional PEM water electrolyzer, PGM are used as electrocatalysts (see Section 9.3.3). Two strategies can be followed to reduce PGM loading: (1) use of PGM nanoparticles supported by electronic carriers of appropriate chemical stability and large surface area; and (2) development of alternative non-PGM catalysts.

9.5.4.1 Reducing PGM loading

Noble metal content can be significantly reduced compared with that used in conventional MEAs. Following developments in the fuel cell industry, carbon-supported Pt nanoparticles can be used at the cathode of PEM water electrolysis cells and noble metal loading in the range of 0.2−0.8 mg/cm^2 is now common good practice. IrO_2 loading at anodes is usually larger (1.0−2.0 mg/cm^2). Reducing loading requires the

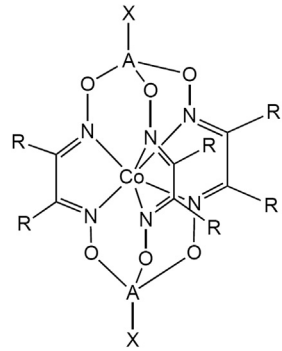

Figure 9.18 General structure of cobalt clathrochelate complexes. The *di*-phenyl compound is obtained for the X = R = phenyl group A = boron.

use of appropriate electronic carriers that are not as common. Most effort reported in the literature has been devoted to reducing IrO_2 loading by forming binary or ternary mix-oxide solid solutions with non-PGM oxides of sufficiently high electronic conductivity. A compromise is usually found between lower anodic loading and reduced lifetime or higher loading and long-term performance.

9.5.4.2 Alternative non-PGM catalysts

In the quest for non-PGM catalysts that could operate efficiently in strongly acidic polymer electrolyte environments, some significant progress has been made over the past years, at least to replace platinum at the cathode of PEM cells for the hydrogen evolution reaction. Analyzing why PGM catalysts are required (and usually used), it appears that this is not just a matter of electrochemical activity (with regard to the HER and OER) but is mainly because non-noble metals are corroded (oxidized) in strongly acidic environments, such as those encountered in PEM water electrolysis cells. In alkaline media, nickel and cobalt are chemically stable (owing to surface passivation) and their oxides offer significantly high electro-activity. A new idea has been to synthesize and use nickel- and cobalt-based molecular compounds to replace platinum. In such chemical compounds, the metallic active center is covalently bonded to organic ligands. Metals usually retain electrochemical activity and ligands have a double role: (1) setting the redox potential of the metallic active center (electronic donors/acceptors covalently linked to the ligand's structure can have long distance electronic effects of a molecular size that can shift the redox potential of the metallic active center along the potential axis, close to the reaction to catalyze); and (2) providing chemical ways to surface graft onto appropriate electronic carriers of a large surface area in view of practical applications. Ligands are used to firmly and irreversibly link (possibly covalently) the molecules to the surface of large surface area electronic conductors (for example, carbonaceous species), and the mixture can be used in place of Pt-nanoparticle—coated carbon powders at the cathode of PEM water electrolysis cells.

A typical example using a *di*-phenyl cobalt clathrochelate is provided in Figure 9.18 (Dinh Nguyen et al., 2012; Pantani et al., 2008). The oxidation state of the cobalt active

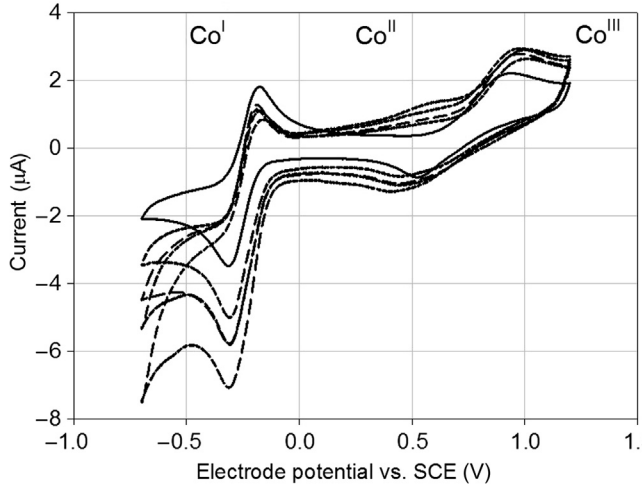

Figure 9.19 Cyclic voltammogram of a 0.87-mm acetonitrile solution of $Co(dpgBF_2)_2$ at a glassy carbon electrode (bold), and evolution upon addition of successive aliquots of 2 equivalents of $HClO_4$.

center is usually +II. In solution, it can be oxidized reversibly up to +III or reduced reversible down to +I (Figure 9.19). The +II → +I reduction takes place at potential values more negative than the redox potential of the H^+-H_2 couple. Once the Co^{+I} species is formed in the solution, it can trigger proton reduction into molecular hydrogen. This can be seen in Figure 9.19, where increasing proton concentrations are introduced into the cell, showing an increasing reduction current as a result of the HER.

Similar behavior is observed once molecular compounds are bound at the surface of carbonaceous species. Using appropriate coating techniques, it is thus possible to prepare efficient MEAs. Some typical polarization curves measured during PEM water electrolysis are provided in Figure 9.20 using a 250-cm^2 cell. The polarization curve measured on a conventional IrO_2/Nafion®/Pt-C MEA is plotted for comparison (the large ohmic resistance of the cell is caused by oxidized titanium cell components). The main difference with a conventional MEA is that the cobalt electrode needs to be activated under constant potential polarization before use. Once the activation step is completed, electrochemical performance becomes close to that obtained with platinum.

Some attempts have been made to develop a similar approach for the anodes of PEM water electrolysis cells, but the situation is more challenging. So far, no credible alternative to IrO_2 has been reported in the literature.

9.6 Conclusions

Commercial PEM water electrolyzers are competitive with their alkaline counterparts. Polymer electrolyte membrane water electrolysis is more efficient at higher current densities and more mature than solid oxide technology. The potential of the technology

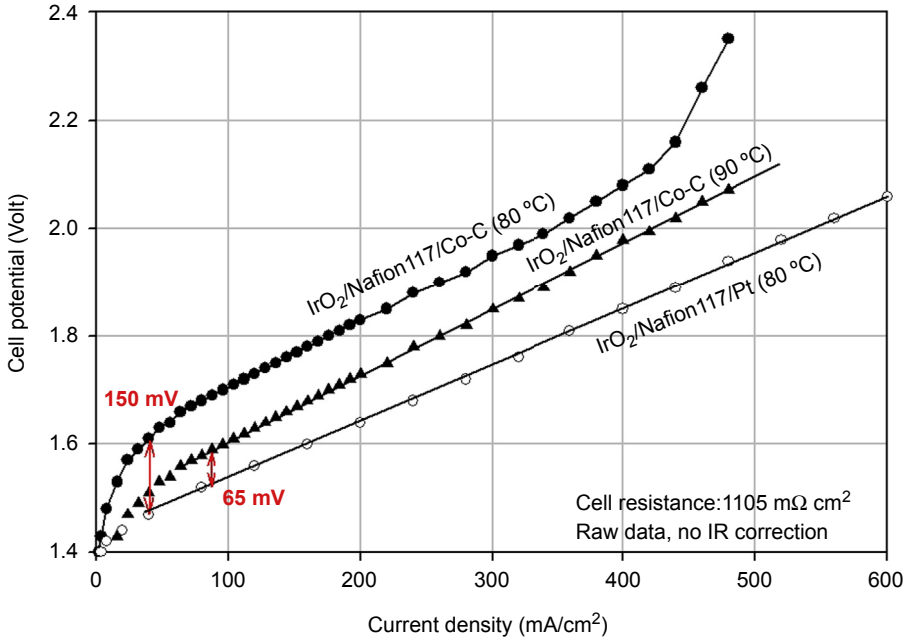

Figure 9.20 Polarization curve measured on a 25-cm^2 cell during water electrolysis at different temperatures. All anodes = 2 mg/cm^2 IrO_2; cathode: (•, ▲) 0.5 mg/cm^2 Co complex on carbon; (o) 0.5 mg/cm^2 Pt/C.

to operate at much higher current densities (in the multi-A/cm^2 range) is still largely unexplored, but laboratory results indicate that it is achievable and largely desirable for reducing Capex. However, to develop systems that will meet market requirements, new generations of polymer electrolytes capable of operating at temperatures significantly higher than 100 °C will be required, as well as efficient and stable electrocatalysts. It is also necessary to demonstrate that large-capacity (>100-Nm^3 H_2/h) PEM water electrolyzers can be designed and operated efficiently and flexibly over the 10^4−10^5 range of hours of operation. Because even larger production capacities will be required if hydrogen is to have a role as an energy carrier in the future, it is clear that substantial research and development efforts will be needed to contribute to the expansion of renewable energy sources.

9.7 Sources of further information and advice

Bockris, J. O'M., & Reddy, A. A. K. (1982). *Comprehensive treatise of electrochemistry.* Plenum Press *E.*

Hamann, C. H., Hamnett, A., & Vielstich, W. (1998). *Electrochemistry*. Wiley-VCH.

Carmo, M., Fritz, D. L., Merel, J., & Stolten, D. (2013). Comprehensive review on PEM water Electrolysis. *International Journal of Hydrogen Energy*, 38, 4901−4934.

Nomenclature

A	Membrane area (m^2)
a	Activity
C_i	Concentration of species i (mol/m^3)
D_i	Diffusion coefficient of species i (m^2/s)
E	Thermodynamic voltage (V)
F	Faraday constant (96,485 C/mol)
f	Gas fugacity
G	Gibbs free energy (J/mol)
H	Enthalpy (J/mol)
I	Current (A)
j	Current density (A/cm^2)
n	Number of electron exchanged in a chemical reaction
P	Pressure (Pa)
P^m	Membrane permselectivity (m^2/Pa s)
R	Resistance (Ω)
r	Specific resistance (Ω m^2)
R_{PG}	Constant of perfect gas (0.082 J/K mol)
S	Entropy (J/mol K)
t	Time (s)
T	Absolute temperature (K)
U_{cell}	Cell voltage (V)
V	Thermo-neutral electrolysis voltage (V)
W	Electrical work (J)

Greek symbols

δ	Membrane thickness (m)
Δ	Difference
ε	Cell efficiency (%)
η	Overvoltage (volt)
λ	Thermal conductivity (W/m K)
ρ	Electrical resistivity (Ω m)
σ	Electrical conductivity (S/m)

Subscripts or superscripts

°	Standard conditions (298 K, 1 bar)
Cell	Electrolysis cell
d	Dissociation
e	Electrolyte
i	Species i
r	Real
t	Theoretical

List of acronyms

Capex	Capital expenses or expenditures
EW	Equivalent weight of membrane (eq. g^{-1})
HER	Hydrogen evolution reaction
ICE	Internal combustion engine
OER	Oxygen evolution reaction
Opex	Operational expenses or expenditures
PEM	Proton exchange membrane
PEMFC	Polymer electrolyte membrane fuel cell
PGM	Platinum group metals
pH	Potential in hydrogen ions
SCE	Saturated calomel electrode
SPE	Solid polymer electrolyte

References

Bockris, J. O.'M., & Reddy, A. K. N. (1982). In *Comprehensive treatise of electrochemistry*. Plenum Press.

Damjanovic, A., & Bockris, J. O.'M. (1966). *Journal of the Electrochemical Society, 113*, 739.

Dinh Nguyen, M.-T., Ranjbari, A., Catala, L., Brisset, F., Millet, P., & Aukauloo, A. (2012). Implementing molecular catalysts for hydrogen production in proton exchange membrane water electrolysers. *Coordination Chemistry Reviews, 256*, 2435.

Fateev, V., Grigoriev, S. A., Millet, P., Korobtsev, S., Porembskiy, V., & Auprêtre, F. (2011). High pressure PEM water electrolysis and corresponding safety issues. *International Journal of Hydrogen Energy, 36*, 2721.

Fuller, T., & Newman, J. (1992). *Journal of the Electrochemical Society, 139*, 1332.

Gierke, T. D., Munn, G. E., & Wilson, F. C. (1981). The morphology in Nafion perfluorinated membrane products, as determined by wide and small-angle X-ray studies. *Journal of Polymer Science B: Polymers Physics, 19*(11), 1687.

Grigoriev, S. A., Millet, P., Volobuev, S. A., & Fateev, V. N. (2009). Optimization of porous current collectors for PEM water electrolysers. *International Journal of Hydrogen Energy, 34*, 4968.

Hamann, C. H., Hamnett, A., & Vielstich, W. (Eds.). (1998). *Electrochemistry*. Wiley-VCH.

IUPAC. (1993). *Compendium of chemical terminology* (vol. 65). p. 856.

Khandelwal, M., & Mench, M. M. (2006). Direct measurement of through-plane thermal conductivity and contact resistance in fuel cell materials. *Journal of Power Sources, 161*, 1106.

Mann, R. E., Amphlett, J. C., Peppley, B. A., & Thurgood, C. P. (2006). Henry's law and the solubilities of reactant gases in the modeling of PEM fuel cells. *Journal of Power Sources, 161*, 768.

Mauritz, K. A., & Moore, R. B. (2004). State of understanding of Nafion. *Chemical Reviews, 104*, 4535−4585.

McCay, M. H. (Ed.). (2014). *Future energy, chapter 23, hydrogen: An energy carrier*. Elsevier.

Millet, P. (1990). Water electrolysis using EME technology : temperature profile inside a Nafion membrane during electrolysis. *Electrochimica Acta, 36*, 263.

Millet, P. (2011). Advanced membrane science and technology for sustainable energy and environmental applications. In Angelo Basile, & S. Pereira Nunes (Eds.), *Membrane electrolysers*. WoodHead Science Editions.

Millet, P., Alleau, T., & Durand, R. (1993). Characterization of membrane-electrodes assemblies for solid polymer electrolyte water electrolysis. *Journal of Applied Electrochemistry, 23*, 322.

Millet, P., Ngameni, R., Grigoriev, S. A., Mbemba, N., Brisset, F., Ranjbari, A., et al. (2010). PEM water electrolysers: from electrocatalysis to stack development. *International Journal of Hydrogen Energy, 35*, 5043.

Ogumi, Z., Takehara, Z., & Yoshizawa, S. (1984). Gas permeation in SPE method. *Journal of the Electrochemical Society, 131*, 769.

Pantani, O., Naskar, S., Guillot, R., Millet, P., Anxolabéhère, E., & Aukauloo, A. (2008). Cobalt clathrochelate complexes as hydrogen-producing catalysts. *Angewandte Chemie International Edition, 120*, 10096.

Price, D. C., & Jarratt, M. (2000). Thermal conductivity of PTFE and PTFE composites. In *Proceedings of the twenty-eight conference of the North-American thermal analysis society, october 4–6, Orlando, Florida*.

Sakai, T., Takenaka, H., & Torikai, E. (1986). Gas diffusion in the dry and hydrated Nafion. *Journal of the Electrochemical Society, 133*, 88.

Sakai, T., Takenaka, H., Wakabayashi, N., Kawami, Y., & Torikai, E. (1985). Gas permeation properties of solid polymer electrolyte (SPE) membranes. *Journal of the Electrochemical Society, 132*, 1328.

Tsampas, M. N., Pikos, A., Brosda, S., Katsaounis, A., & Vayenas, C. G. (2006). The effect of membrane thickness on the conductivity of Nafion. *Electrochimica Acta, 51*(13), 2743.

Vishnyakov, A., & Neimark, A. V. (2000). Molecular simulation study of Nafion membrane solvation in water and methanol. *The Journal of Physical Chemistry B, 104*, 4471.

Yeager, H. L., & Steck, A. (1981). Cation and water diffusion in Nafion ion exchange membranes: influence of polymer structure. *Journal of the Electrochemical Society, 128*, 1880.

Part Four

Emerging methods for the production of hydrogen

This page intentionally left blank

Hydrogen production using photobiological methods

10

R.S. Poudyal[1,2,#], I. Tiwari[1,#], A.R. Koirala[3], H. Masukawa[4], K. Inoue[4], T. Tomo[5], M.M. Najafpour[6], S.I. Allakhverdiev[7,8,9], T.N. Veziroğlu[10]
[1]Pusan National University, Busan, Republic of Korea; [2]Tribhuvan University, Kirtipur, Kathmandu, Nepal; [3]Sogang University, Shinsu-dong, Seoul, Republic of Korea; [4]Research Institute for Photobiological Hydrogen Production, Kanagawa University, Tsuchiya, Hiratsuka, Kanagawa, Japan; [5]Tokyo University of Science, Kagurazaka, Shinjuku-ku, Tokyo, Japan; [6]Institute for Advanced Studies in Basic Sciences (IASBS), Zanjan, Iran; [7]Institute of Plant Physiology, Russian Academy of Sciences, Moscow, Russia; [8]Institute of Basic Biological Problems, Russian Academy of Sciences, Moscow Region, Russia; [9]M.V. Lomonosov Moscow State University, Moscow, Russia; [10]International Association for Hydrogen Energy, Miami, FL, USA

10.1 Introduction

Hydrogen is a versatile energy carrier that can release energy through a number of different processes such as direct combustion, catalytic combustion, steam production, and fuel cell operations. In terms of environmental impact, hydrogen may be the best alternative to fossil fuels because it drastically reduces the release of climate-changing gases and compounds harmful to human health (Zattel et al., 2008). Photobiological hydrogen production is an attractive option to generating hydrogen by photoautotrophic organisms from sunlight and water. This process is most effective and important for avoiding using fossil fuel (Ghirardi, Dubini, Yu, & Maness, 2009; Kruse, Rupprecht, Mussgnug, Dismukes, & Hankamer, 2005; Prince & Kheshgi, 2005). Photobiological hydrogen production consumes naturally occurring carbon dioxide gas to produce oxygen and biomass; hence, it is renewable and sustainable. Microorganisms such as green algae, cyanobacteria, purple nonsulfur bacteria, and dark fermentative bacteria are used to generate biohydrogen. In the light, solar energy is converted into adenosine triphosphate (ATP) and nicotinamide adenine dinucleotide phosphate (NADPH) as a source of energy and reductants, respectively. In the dark, organic compound is synthesized from CO_2 and H_2O. There are two different methods for photobiological hydrogen production: (1) direct photobiological hydrogen production, in which hydrogen gas is produced directly by the activity of hydrogenase without intermediate molecules such as carbohydrates; and (2) indirect photobiological hydrogen production, in which hydrogen

[#] These authors contributed equally to this work.

Compendium of Hydrogen Energy. http://dx.doi.org/10.1016/B978-1-78242-361-4.00010-8

gas is produced after the storage of carbohydrates or glycogen (Dasgupta et al., 2010; Eroglu & Melis, 2011). For photobiological H_2 production, microalgae require sunlight to donate e^- from electron-donating substances. This process can be categorized as oxygenic and non-oxygenic photobiological H_2 production, depending on oxygen generation during the process.

Oxygenic photobiological H_2 production is carried out during photoautotrophic growth of eukaryotic microalgae and cyanobacteria in water. The former organisms possess [FeFe] hydrogenases whereas the latter ones possess [NiFe] hydrogenases, with ferredoxin and NAD(P)H, respectively, as a direct electron donor (Ghirardi et al., 2009).

Although non-oxygenic photobiological H_2 production is carried out by purple non-sulfur bacteria (PNSB), these bacteria convert organic acids to produce H_2 by using sunlight as a source of energy, in a reaction catalyzed by nitrogenase. In a non-oxygenic or photofermentation process by PNSB, O_2 is not produced, so there is no debate about the repression of nitrogenase by oxygen.

Currently, several researchers are trying to achieve renewable hydrogen production with environmentally safe resources by using molecular biology, biotechnology, genetic engineering, and organometallic chemistry. Apart from this, artificial photosynthesis by biomimetic systems is a good candidate for generating hydrogen, and knowledge of the biochemical or biophysical study of hydrogenase and nitrogenase enzymes is exploited by organometallic chemists to synthesize biomimetic compounds for artificial photosynthesis.

Biohydrogen is a potentially useful gas to fulfill energy consumption with a high demand for hydrogen energy. Currently, around 80% of global energy is generated by fossil fuels (Kim, Jo, Jo, & Cha, 2012; Quintana, der Kooy, de Rhee, Voshol, & Verpoorte, 2011). However, the use of fossil fuels is comparatively costly and requires more energy consumption to generate hydrogen gas. Owing to the high demand for energy in the world, biohydrogen using microorganisms can be considered an alternative renewable source of energy, because it is estimated that energy consumption will increase at the rate of 44% by 2030 (Nel & Cooper, 2009; Rout et al., 2008).

10.2 Methods to generate photobiological hydrogen production

Previously, biological hydrogen production was categorized into five different groups; (1) direct biophotolysis of water, (2) indirect biophotolysis of water, (3) biophotofermentation, (4) hydrogen production by water gas reaction, and (5) dark fermentation (Das & Veziroğlu, 2001; Hallenbeck & Benemann, 2002; Nandi & Sengupta, 1998). The main available pathways to improved photosynthetic H_2 production have been summarized elsewhere (Allakhverdiev et al., 2009, 2010). Similarly, available methods to generate biohydrogen by using microorganisms have been summarized (Poudyal et al., in press). Although biohydrogen production is mediated by the

activity of two different enzymes, i.e., hydrogenase and nitrogenase, the activities of these enzymes depend on the availability of molecular oxygen (Bothe, Schmitz, Yates, & Newton, 2010; Ghirardi et al., 2007; Tsygankov, 2007). Hence, enhanced activation of these two enzymes will be more interesting in the future. As we know, the production of biohydrogen by microorganisms is inhibited by the presence of molecular oxygen generated by photosynthesis. Therefore, researchers are trying to overcome the inhibitory effect of molecular oxygen and enhance hydrogen production, which has been considered a major focus of photobiological hydrogen production. The enzymes are inactivated by molecular oxygen that diffuses into the catalytic center of the enzymes (Sundaram, Tripathi, & Gupta, 2010) to overcome this problem, some hypotheses have been applied in cyanobacteria.

Cyanobacteria (or blue-green algae) have characteristic features of both algae and bacteria. The algal character shows photosynthesis producing hydrogen; these cyanobacteria have [NiFe] hydrogenase but not an [FeFe] hydrogenase enzyme. NiFe enzyme is less sensitive to molecular oxygen, and hence it is favorable for hydrogen production. Based on this finding, an organism i.e., *Rubrivivax gelatinosus* CBS, has been identified that has the capacity for oxygen-tolerant hydrogenase during non-oxygenic photosynthesis (Ghirardi et al., 2005; Maness, Smolinski, Dillon, Heben, & Weaver, 2002). Some cyanobacteria may yield more hydrogen by a genetically engineered, optimized metabolic network (Quintana et al., 2011). Photobiological hydrogen production uses sunlight, which algae and cyanobacteria use to produce hydrogen as their metabolic processes. As these organisms grow in water, they can easily split water into hydrogen and oxygen. Some technology has been developed to increase the conversion efficiency of sunlight. According to the current status, the following photobiological methods are significantly applied to generate biohydrogen.

10.2.1 Direct and indirect biophotolysis

Direct biophotolysis means the production of H_2 gas under the illumination of light in biological organisms. In the chloroplast of algae and cyanobacteria, the thylakoid membranes consist of chlorophyll pigments in both photosystems, i.e., photosystem I (PSI) and photosystem II (PSII). The light energy absorbed by these pigments raises the energy level of electrons from water oxidation to PSII to PSI to ferredoxin, where a portion of the light energy is directly stored in hydrogen gas. Direct photobiological H_2 production from water using solar energy is a good example of massive (large-scale) production of hydrogen gas by photosynthesis, in which solar energy is used to split water into H_2 gas. Microorganisms include single-cell cyanobacteria (*Synechocystis*), multicellular cyanobacteria (*Nostoc* sp.), and green algae (*Chlamydomonas* sp.). Overall, the reaction of direct biophotolysis can be described as (Shaishav, Singh, & Tripathi, 2013):

$$2H_2O + \text{light} \rightarrow 2H_2 + O_2 \tag{10.1}$$

However, indirect biophotolysis refers to the production of H_2 from intracellular energy reserves including carbohydrates such as starch and glycogen in microalgae and cyanobacteria (Antal & Lindblad, 2005; Dauvillée et al., 2006; Miura et al., 1995). Hence, this process is composed of two stages: carbohydrates synthesis in the light and dark fermentation of carbohydrates for H_2 production (Lee, Klaus, Maness, & Spear, 2007; Melis & Melnicki, 2006; Miura et al., 1995; Skjånes, Rebours, & Lindblad, 2013). Hence, indirect biophotolysis can be described as the following reactions:

$$6H_2O + 6CO_2 + \text{light} \rightarrow C_6H_{12}O_6 + 6O_2 \tag{10.2}$$

$$C_6H_{12}O_6 + 2H_2O \rightarrow 4H_2 + 2CH_3COOH + 2CO_2 \tag{10.3}$$

$$2CH_3COOH + 4H_2O + \text{light} \rightarrow 8H_2 + 4CO_2 \tag{10.4}$$

In overall, (Shaishav et al., 2013):

$$12H_2O + \text{light} = 12H_2 + 6O_2 \tag{10.5}$$

10.2.2 Photobiological H_2 production by hydrogenase and nitrogenase

Photobiological H_2 production in algae and cyanobacteria is mediated by the activity of two enzymes: hydrogenase and nitrogenase (Bothe et al., 2010; Ghirardi et al., 2007; Tsygankov, 2007), both of which are sensitive to oxygen (Poudyal et al., in press). Generation of hydrogen by algae and cyanobacteria employs the activity of two distinct hydrogenases, i.e., [FeFe], also known as algal hydrogenase, and [NiFe], also known as cyanobacterial bidirectional hydrogenase enzyme, which that can consume and produce hydrogen (i.e., $2H^+ + 2e^- \leftrightarrow H_2$).

The exact mechanism of algal [FeFe] hydrogenase for H_2 production is not clear. It is theorized that electrons from ferredoxin are delivered to the metallocluster, making reduced iron atoms (Fe_2). This reduced iron atom is stabilized by the presence of CO and CN ligands and the proton pathway from the protein surface to the catalytic site is deconvoluted, which acts as the final binding site for one proton. Simultaneously, the second proton binds to Fe_2, where is doubly reduced to a hydride anion. Finally, the reaction involved in the process producing hydride anion recombines with the bound proton to release H_2 gas (Ghirardi et al., 2009).

In cyanobacteria, [NiFe] bidirectional hydrogenase has four different metal centers in which an NiFe active site for the catalytic domain and three Fe-S clusters for electron transfer have been identified. The NiFe active site is composed of bimetallic nickel and iron atoms; the nickel atom has four conserved cysteine residues, two of which bridge to the iron ion (Shima et al., 2008). However, it has been reported that [NiFe] hydrogenase is reversibly inactivated by molecular oxygen (Ogata et al., 2009). The [NiFe] enzyme catalyzes both the uptake and evolution of H_2. When the bridge ligand of [NiFe] is removed, the enzyme is activated and molecular hydrogen is produced. [NiFe] hydrogenases are bidirectional because they couple the reversible

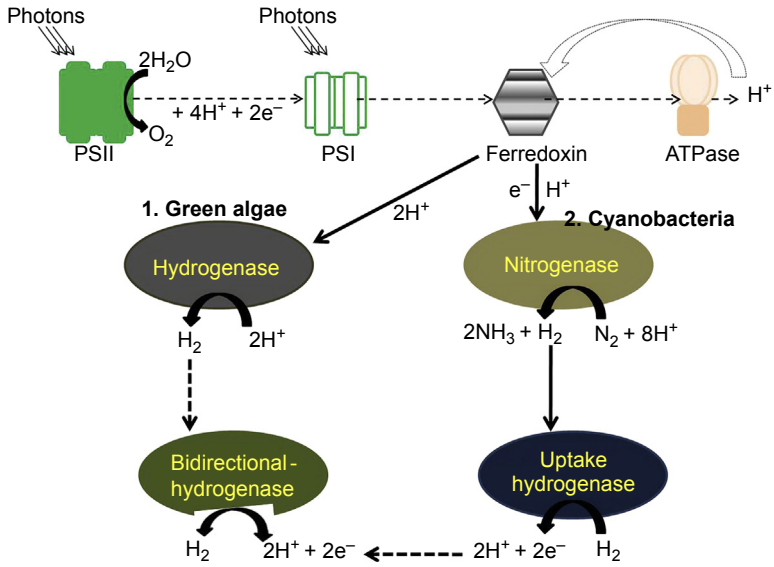

Figure 10.1 Summary of mechanism of photobiological H_2 production by algae. Light-dependent electron transport pathway for hydrogen production is shown in green algae and cyanobacteria with the involvement of their respective catalytic enzymes.
The figure is modified from Mathews and Wang (2009).

cleavage of hydrogen to the redox conversion of NAD(P)H (Horch, Lauterbach, Lenz, Hildebrandt, & Zebger, 2012). In green algae, only hydrogenase is present whereas in cyanobacteria two enzymes (hydrogenase and nitrogenase) work separately to catalyze H_2 production. A detailed scheme for two types of hydrogenases, uptake enzyme and bidirectional one, and nitrogenase in the respective microalgae, is given in Figure 10.1.

Similarly, nitrogenase enzyme is present in both unicellular and heterocystous nitrogen-fixing cyanobacteria and has a potential application for producing hydrogen. However, because of the higher energetic reaction, hydrogen production by nitrogenase is not efficient during nitrogen fixation, because most of the energy consumed by nitrogenase is used to produce ammonia (Tamagnini et al., 2002). The overall reaction under conditions optimal for nitrogen fixation can be written as:

$$N_2 + 8H^+ + 8e^- + 16ATP \rightarrow 2NH_3 + H_2 + 16ADP + 16P_i \quad (10.6)$$

However, in the absence of N_2, all electrons and ATP are used for H_2 production:

$$2e^- + 2H^+ + 4ATP \rightarrow H_2 + 4(ADP + P_i) \quad (10.7)$$

10.2.3 Mechanism of photobiological H_2 production

Two phases of photobiological hydrogen production in microalgae have been reported previously: aerobic and anaerobic (Melis, Zhang, Forestier, Ghirardi, & Seibert, 2000).

These two phases have different reactions to the contribution of hydrogen. The overall reactions are described as (Nguyen et al., 2008):

$$H_2O \rightarrow 2H^+ + 2e^- + \frac{1}{2}O_2 \text{ (Aerobic phase)} \tag{10.8}$$

$$2H^+ + 2e^- \rightarrow H_2 \text{ (Anaerobic phase)} \tag{10.9}$$

During the aerobic phase in microalgae, the H_2O is split into protons (H^+), electrons (e^-), and oxygen (O_2). Hence, the H^+ and e^- generated by water in PSII are stored as different metabolic products, such as proteins and carbohydrates, and these H^+ and e^- are essential precursors for H_2 production (Melis et al., 2000). During the anaerobic phase, H_2 is produced by hydrogenase. Mostly [FeFe] hydrogenase is rapidly activated under anaerobic conditions that catalyze the reduction of H^+ to H_2 using ferredoxin as an e^- donor. There, PSII contributes direct and indirect pathways for the source of e^-. In a direct pathway, e^- driven from the water-splitting activity of PSII (Najafpour & Allakhverdiev, 2012) is delivered into the electron transport chain (ETC) during state transition (Lemeille, Turkina, Vener, & Rochaix, 2010) and finally reaches [FeFe] hydrogenase, which reduces H^+ to H_2. However, in an indirect pathway, proteins, carbohydrates, or starches that are stored during the aerobic phase are subsequently fermented and enter into an ETC (Posewitz, Dubini, Meuser, Seibert, & Ghirardi, 2009).

The basic mechanism and biochemical pathway for photobiological H_2 production are shown in (Figure 10.1). The thylakoid membrane of algae and cyanobacteria contains a photosystem with a light-harvesting protein complex, reaction center, and chlorophyll. It has the ability to capture light energy, which facilitates water oxidation to release protons (H^+) and electrons (e^-). These electrons are transported via the ETC, and iron-sulfur protein ferredoxin (PetF) or NAD(P)H via FNR (ferredoxin/NAD(P)H oxidoreductase) acts as an e^- donor to [FeFe] or [NiFe] hydrogenase, respectively. In algae, ferredoxin directly linked to synthesize H_2 via the ETC and in cyanobacteria NAD(P)H donates e^- to [NiFe] bidirectional hydrogenase to synthesize H_2 (Kufryk et al., 2013). Adenosine triphosphate and NADPH generated by light reaction are used to fix CO_2 during a dark reaction. Based on current progress, three pathways have been employed for biohydrogen production in cyanobacteria: (1) The first is light-driven ETC from water via PSII to PSI, ferredoxin (Fd) to ferredoxin: $NADP^+$ oxidoreduction (FNR). Finally, H_2 is produced by [NiFe] bidirectional hydrogenase from the electrons supplied by reduced NADP. (2) Hydrogen is produced by the degradation of lipids, starches, and carbohydrates. In this pathway, NAD(P)H is oxidized and electrons are transported through plastoquinone (PQ) for H_2 production. (3) The last is cyanobacterial nitrogen fixation by nitrogenase, in which H_2 is produced as a byproduct under anaerobic conditions or in heterocysts that provide a microaerobic environment.

10.2.4 Hydrogen production by photofermentation

Hydrogen gas can also be produced by photofermentation. Some organic compounds such as acetic acids, lactic acids, and butyric acids are converted into H_2 and CO_2 by

photosynthetic bacteria in the presence of sunlight. However, this process also requires anaerobic conditions. During photofermentation, both hydrogenase and nitrogenase enzymes are involved in H_2 production depending on the physiological conditions of microorganisms. Five factors limit nitrogenase-mediated photofermentation in PNSB: (1) the occurrence of an H_2 uptake enzyme; (2) low photofermentation efficiency for H_2 production; (3) the low turnover rate of nitrogenase; (4) a low rate of carbon conversion; and (5) the availability of organic acids (Akkerman, Janssen, Rocha, & Wijffels, 2002). The overall reaction in photofermentation by PNSB for the reduction of organic compounds can be summarized as:

$$C_6H_{12}O_6 + 12H_2O + \text{Light energy} \rightarrow 12H_2 + 6CO_2 \tag{10.10}$$

The overall pathway is (Das, Khanna, & Veziroğlu, 2008):

$$(CH_2O)_2 + \text{NADPH} \rightarrow \text{Ferredoxin} + \text{ATP} \rightarrow \text{Nitrogenase} \rightarrow H_2 \tag{10.11}$$

These PNSB has some advantages owing to the lack of PSII, which creates difficulties for H_2 generation because of the presence of O_2 (Das et al., 2008). Purple non-sulfur bacteria have the action of nitrogenase and hydrogenase enzymes. Nitrogenase produces H_2 under nitrogen-deficient conditions in PNS bacteria (Figure 10.2). Thus, the question arises regarding the role of hydrogenase in PNS bacteria. Hence, hydrogenase produces H_2 under anaerobic conditions and hydrogenase oxidizes H_2 to recycle e^-, H^+, and ATP for energy metabolism (Koku, Eroğlu, Günfüz, Yücel, & Türker, 2002; Mathews & Wang, 2009; Oh, Raj, Jung, & Park, 2011). Some hydrogenases consume H_2 if a suitable e^- acceptor is present, or produce H_2 if anaerobic conditions are favorable (Vignais, Magnin, & Willison, 2006).

Several factors such as light intensity, duration of light, temperature, and age of inoculums are important for photofermentative H_2 production by photosynthetic bacteria. For example, 31 °C and 36 °C are the optimum temperatures for Rhodobacter sp. (Hey et al., 2013). These bacteria are able to convert organic acids into H_2 and CO_2

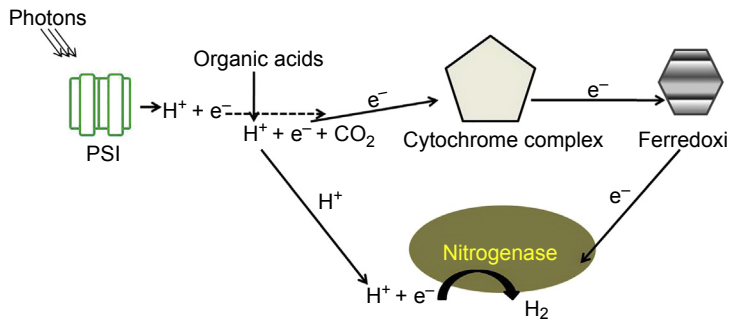

Figure 10.2 Mechanism of photofermentative H_2 production by PNSB by nitrogenase. Hydrogen gas is generated by the activity of nitrogenase after the breakdown of organic acids. The figure is modified from Androga, Özgür, Eroglu, Gündüz, and Yücel (2012).

under anaerobic conditions by using nitrogenase enzyme (Koku et al., 2002). It has been reported that supplementing micronutrients such as iron (Fe) and molybdenum (Mo) in a growth medium of some Rhodobacter increased photofermentative H_2 production (Kars, Gündüz, Yücel, Türker, & Eroğlu, 2006; Özgür et al., 2010; Uyar, Schumacher, Gebicki, & Modigell, 2009). Apart from this, the role of other nutrients such as iron (Fe), nickel (Ni), and magnesium (Mg) has been observed in *Rhodopseudomonas* sp (Liu, Ren, Ding, Xie, & Guo, 2009). Some strategies for the combination of dark and photofermentation have been applied to enhance H_2 production, because dark fermentation can produce lower amounts (2−4 mol H_2) from 1 mol of hexose. In addition, this process produced acetate and butyrate, which are environmental pollutants (Su, Cheng, Zhou, Song, & Cen, 2009a). To solve this problem, a combination of dark and photofermentation processes has been applied to *Rhodopseudomonas palustris* and greatly improved the production of H_2 from 240 to 402 ml H_2 per gram of starch (Su, Cheng, Zhou, Song, & Cen, 2009b). It was also revealed that H_2 production by mixed bacteria through dark and photofermentation increased the productivity of H_2. Dark fermentation by mixed anaerobic bacteria (*Clostridium* species) produced 351 ml H_2 per gram of starch, and during photofermentation by mixed photosynthetic bacteria (*Rhodopseudomonas palustris* species) produced 489 ml H_2 per gram of starch. These data clearly demonstrate that mixed bacteria can be used to improve dark and photofermentation (Cheng, Su, Zhou, Song, & Cen, 2011).

10.2.5 Hydrogen production by metabolic and genetic engineering of green algae

Both metalloprotein hydrogenase and nitrogenase enzymes are capable of reducing H^+ to H_2. However, O_2 molecules generated during photosynthesis inhibit the activity of these enzymes. To overcome this problem, some researchers studied the different biochemical mechanisms of algae and cyanobacteria. Genetic engineering of green algae is considered as pioneering research to enhance H_2 gas; genetic and other biochemical modifications as well as the generation of new strains of cyanobacteria to enhance H_2 production have been applied (Bonenthe et al., 2011; Ghysels & Franck, 2010; Nguyen et al., 2011; Papazi, Andronis, Loannidis, Chaniotakis, & Kotzabasis, 2012; Philipps, Happe, & Hemschemeier, 2012; Tiwari & Pandey, 2012; Winkler, Kuhlgert, Hippler, & Happe, 2009).

Some genetically modified cyanobacterial strains such as *Synechococcus* PCC 6301 and PCC 7942 and *Synechocystis* PCC 6803 have been considered good model organisms to enhance H_2 production (Thiel, 1994). Similarly, genetic transformation has been conducted in filamentous algae such as *Nostoc* and *Anabaena* to enhance photobiological H_2 production (Hansel & Lindblad, 1998). In addition, structural gene-encoding FeFe hydrogenase from *Clostridium pasteurianum* has been transformed into cyanobacterium strain, *Synechococcus* elongatus PCC 7942 for better H_2 production (Asada et al., 2000; Miyake, Schnackenberg, Nakamura, Asada, & Miyake, 2001). Genetic engineering was employed to obtain transformed strains to generate renewable biofuel in some cyanobacterial strains such as *Synechocystis* sp PCC6803 (Lindberg, Park, & Melis, 2010).

Genetic engineering has been conducted not only in cyanobacteria but also in some photosynthetic bacteria such as Rhodobacter *sphaeroides*. For example, the mutation of *pucBA* depleting B800−850 light-harvesting complex in *R. sphaeroides* RV increased H_2 production (Kondo et al., 2002, Kim, Kim, Kim, & Lee, 2006a), and mutation of *cyt cbb3* oxidase in Rhodobacter species enhanced hydrogen production because the deletion of *cyt cbb3* oxidase induced nitrogenase activity and inhibited uptake hydrogenase (Öztürk et al., 2006). Deletion of light-harvesting antenna complexes in *R. sphaeroides* and of uptake hydrogenase showed higher H_2 production (Eltsova, Vasilieva, & Tsygankov, 2010; Liang et al., 2009). Similarly, the composition of gene-encoding pathways involved in pyruvate catabolism and end-product synthesis pathways and genetic biomarkers were studied to identify potential methods for optimizing hydrogen production and metabolic engineering for biofuel production in bacteria (Carere et al., 2012; Cha, Chung, Elkins, Guss, & Westpheling, 2013).

10.2.6 Enhancement of photobiological H_2 production by repression of hydrogen uptake system in microorganisms

As mentioned elsewhere, hydrogenases are key enzymes for biohydrogen production and can be classified as H_2 uptake hydrogenase and H_2 production hydrogenase. Thus, an uptake hydrogenase mostly consumes molecular H_2 and gives protons (H^+), resulting in the inhibition of H_2 production. It is known that both aerobic and anaerobic microorganisms possess uptake hydrogenase to use H_2 as a source of energy (Richau, Kudahettige, Pujic, Kudahettige, & Sellstedt, 2013). Uptake hydrogenase oxidizes H_2 produced during nitrogen fixation by the activity of nitrogenase (Tamagnini et al., 2007). When uptake hydrogenase is repressed, the activity of H_2 production is enhanced in several species of *Nostoc* and *Anabaena* (Happe, Schütz, & Böhme, 2000; Lindberg, Schütz, Happe, & Lindblad, 2002; Masukawa, Mochimaru, & Sakurai, 2002; Yoshino, Ikeda, Masukawa, & Sakurai, 2007).

Many photosynthetic microorganisms including cyanobacteria have nitrogenase [FeFe], and/or [NiFe] bidirectional hydrogenases (Ghirardi et al., 2007; Prince & Kheshgi, 2005; Rupprecht et al., 2006; Tamagnini et al., 2002, 2007; Vignais & Billoud, 2007). Nitrogenase reduces H^+ to H_2 as a side reaction of nitrogen fixation and H_2 produced by nitrogenase is consumed by uptake hydrogenase to yield protons (H^+). Although bidirectional hydrogenase catalyzes both uptake and evolution of H_2, it cannot replace the function of uptake hydrogenase (Masukawa et al., 2002). Therefore, mutation of uptake hydrogenase is a good example for protecting generated H_2 molecules by nitrogen-fixing microorganisms (Cournac, Guedeney, Peltier, & Vignais, 2004; Tamagnini et al., 2007, Vignais & Billoud, 2007).

This uptake hydrogenase is a heterodimeric enzyme containing two functional subunits, i.e., HupS (small subunit) and HupL (large subunit). HupS, encoded by *hupS*, contains three FeS clusters that have the role of transfering electrons from the active site of HupL to ETC, whereas HupL, encoded by *hupL*, contains a bimetallic active site composed of four conserved cysteine residues (Khetkorn, Lindbald, & Incharoensakdi, 2012). In this way, uptake hydrogenase inhibits biohydrogen production by

consuming molecular H_2 (Figure 10.1). To overcome this problem, research has been carried out to knock out uptake hydrogenase for better bihydrogen production. Liang et al. (2009) knocked out membrane-bound [NiFe] hydrogenase (MBH) in photosynthetic bacterium *Allochromatium vinosum* to improve the H_2 production rate. Similarly, H_2 evolution activities were increased by the mutation of *hupW*, which encodes putative hydrogenase-specific protease in *Nostoc* strain PCC 7120 of cyanobacterium (Lindberg, Devine, Stensjö, & Lindblad, 2011), inactivation of functional uptake hydrogenase (*hupS*) in nitrogen-fixing cyanobacterium *Anabaena siamensis* TISTR 8012 (Khetkorn et al., 2012), and substitution of amino acid, which alters the ligation of Fe-S clusters of [NiFe] uptake hydrogenase even in marine bacterium *Alteromonas macleodii* (Yonemoto, Matteri, Nguyen, Smith, & Weyman, 2013).

10.2.7 Strategies for cultivation and growth of cyanobacteria and green algae to enhance H_2 production

In algae and cyanobacteria, physiological, biochemical, and environmental conditions have an important role for biological H_2 production. In addition, growth conditions, light intensity, carbon source, nitrogen source, sulfur, salinity, oxygen, and temperature are also essential for improving biohydrogen production by microorganisms (Poudyal et al., in press). Cyanobacteria are good sources for photobiological H_2 production and may be considered the most important microorganisms for a renewable source of H_2 gas (Dutta, De, Chaudhuri, & Bhattacharya, 2005). Among many microorganisms, cyanobacteria can grow with less nutrition and can use sunlight as a source of energy. The autotrophic nature of cyanobacteria produces H_2 as the final product of photosynthesis. Therefore, it is urgent to conduct research on photobiological H_2 production using cyanobacteria, because some species of *Chlamydomonas* such as *Chlamydomonas reinhardtii* and *Chlamydomonas noctigama* produce more H_2 under sulfur-deprived photoheterotrophic conditions (Skjånes, Knutsen, Källqvist, & Lindblad, 2008). According to Kosourov, Tsygankov, Seibert, and Ghirardi (2002), sulfur-deprived algal cultures have five phases: aerobic, anaerobic, O_2 anaerobic consumption, H_2 production, and 5) end of H_2 production. Research has been conducted in these five phases in *C. reinhardtii*, including light intensity and the effect of pH on the culture medium (Kosourov, Seibert, & Ghirardi, 2003), optimization of culture medium (Jo, Lee, & Park, 2006), and the addition of a small amount of sulfate in sulfur-deprived culture medium (Kosourov et al., 2005). Sulfur-deprived *C. reinhardtii* was able to produce photobiological H_2 production under photoautotrophic, photoheterotrophic, and photomixotrophic growth conditions (Kosourov et al., 2005). The remodeling of photosystem II light-harvesting complex, *LHCBM9* in *C. reinhardtii* for photobiological H_2 production under sulfur starvation conditions was also identified (Nguyen et al., 2008). Different strategies have been applied for photobiological H_2 production by adding iron to the growth medium of *Anabaena* (Prabina & Kumar, 2010), depriving culture medium of nitrogen to enhance H_2 production (Philipps et al., 2012), and mechanistically modeling sulfur-deprived photobiological H_2 production by including dense *C. reinhardtii* in culture medium, as well as changing light intensity and delaying the growth of cyanobacteria (Williams & Bees, 2013).

In addition, the intensity of light is important for photobiological H_2 production in cyanobacteria; Kim, Kang, Park, Kim, and Sim (2006b) observed maximum H_2 production by *C. reinhardtii* at 200 μmol/m^2 s. Oxygen molecules are thought to inhibit H_2 evolution by hydrogenase. To examine this phenomenon, Markov, Eivazova, and Greenwood (2006) used high-intensity light to suppress oxygen evolution in *C. reinhardtii* to evaluate H_2 generation. When 2000 μmol/m^2 s light intensity was applied for 30 s, and then 15 μmol/m^2 s, H_2 production increased, demonstrating that the photoinhibition of photosynthetic O_2 evolution leads to anaerobiosis favorable for H_2 production (Markov et al., 2006).

Hence, light intensity is required for better H_2 evolution in cyanobacteria; however, the effect of light intensity depends on the species of different cyanobacteria (Dutta et al., 2005). For example, *Arthrospira platensis* produces H_2 by day and night under anaerobic conditions. However, *Spirulina platensis* and *Synechococcus elongatus* PCC 7942 produce H_2 only in the dark under anaerobic conditions (Asada & Miyake, 1999) some species (*Azospirillum brasilense and A. lipoferum)* produce H_2 only in the presence of light (Stal & Krumbein, 1985). Therefore, we need to focus on the role of photoperiod and light intensity for H_2 production in cyanobacteria. Generally, 30−40 °C is the optimal temperature for cyanobacterial H_2 production. However, it has been also demonstrated that species of cyanobacteria produce more H_2 at 22 °C and others at 30 °C or 40 °C (Datta, Nikki, & Shah, 2000; Ernst, Kerfin, Spiller, & Böger, 1979; Serebryakova, Shremetieva, & Lindbald, 2000). The nutrient present in culture medium is also important for generating H_2 from cyanobacteria. For example, 8 mM NH_4^+, 1.11 mM PO_4^{3-}, and 0.69 mM SO_4^{2-} in Tris-acetate phosphate medium was the optimal condition for H_2 evolution in *C. reinhardtii* (Jo et al., 2006).

10.2.8 Designing bioreactors to harvesting green algae

After the identification of suitable strains of algae and cyanobacteria, various bioreactors can be used for photobiological H_2 production by microorganisms in which light energy is converted into biochemical energy. Some factors such as area−volume ratio, temperature, agitation, and gas exchange also influence the performance of bioreactors (Dasgupta et al., 2010). Bioreactors can be used to harvest light energy more easily and minimize energy loss. A few decades ago, Sathiyamoorthy and Shanmugasundaran (1994) developed a polypropylene bag that was a simple and inexpensive culture vessel on which to grow cyanobacteria. Later, tubular, flat panel, and bubble column types of major bioreactors had been designed for photobiological H_2 production (Akkerman et al., 2002). Several types of photobioreactors have been designed; a typical dual photobioreactor that uses sunlight to generate electricity and produce H_2 is depicted in Figure 10.3.

Based on the growth conditions of microorganisms, bioreactors are classified as two types: one-phase and two-phase. In a one-phase bioreactor, H_2 is produced by PSII turnover and the activity of HydA enzyme (chloroplast hydrogenase enzyme) under microoxic condition. The microoxic condition does not inhibit hydrogenase for H_2 production. Similarly, the two-phase bioreactor consists of both aerobic and anaerobic conditions for H_2 production. In the two-phase type, cells are grown under aerobic

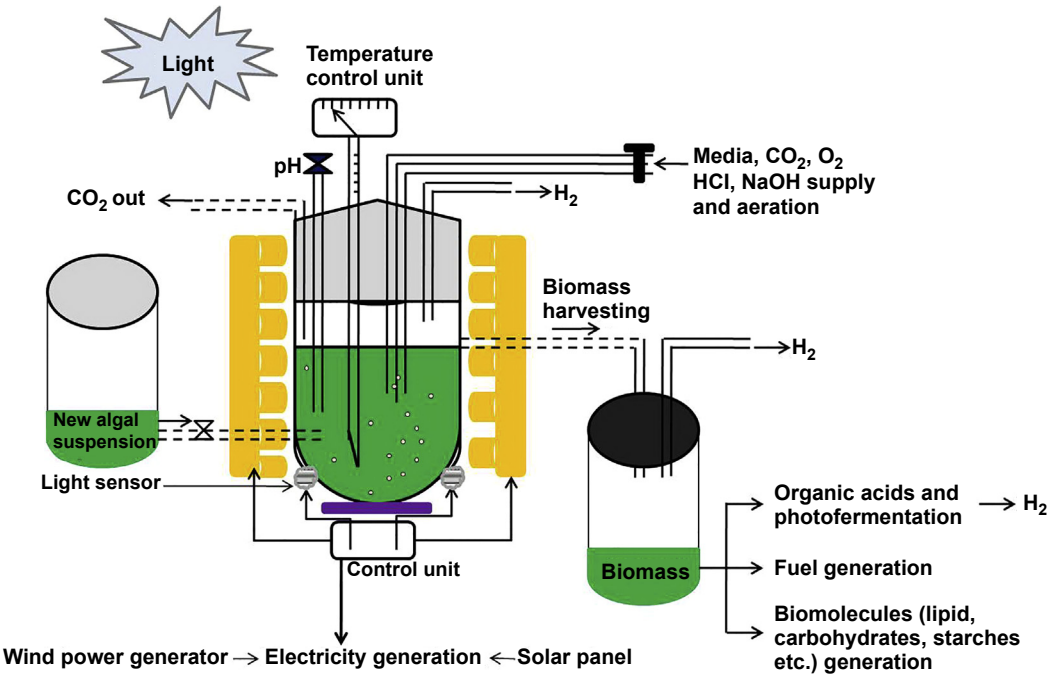

Figure 10.3 Schematic description of dual photobioreactor system for solar energy conversion by microorganisms. A photobioreactor with sunlight and light-emitting diode light sources with a solar panel and wind power generator is shown in the middle panel. Similarly, cultivation of microalgae for biomass and H_2 gas generation is shown.
The figure is modified from Chen, Yeh, Aisyah, Lee, and Chang (2011); Show, Lee, and Chang (2011); Kwon, Rögner, and Rexroth (2012); Rosner and Wagner (2012).

conditions to accumulate more biomass, and then cells are transferred into sulfur-deprived medium to induce H_2 production (Hankamer et al., 2007). The quality and quantity of light are also important for growing phototrophic microorganisms within the bioreactor. To achieve this goal, a tank bioreactor and high surface area−volume ratio bioreactor were developed. Owing to the shading effects of light, tank bioreactors have been considered less effective (Hankamer et al., 2007).

In addition, based on the effective production of biomass and H_2 by microorganisms, bioreactors are classified into two types: open system and closed system (Dasgupta et al., 2010). The open system bioreactor is a simple and traditional system in which algae and cyanobacteria can grow under natural conditions such as small ponds, lakes, or artificial containers for biomass production. However, the efficiency and collection of H_2 are inconvenient. Hence, closed-system bioreactors are considered safe reactors for improving the biomass and H_2 production efficiency of microorganisms in a modern way, because photobioreactors have been designed to multiply rapidly with a high density of microalgae biomass production (Evens, Chapman, Robbins, & D'Asaro, 2000). Some important points for designing bioreactors for photobiological H_2 production are summarized by (Dasgupta et al., 2010):

1. Temperature control and an agitation system in photobioreactors
2. Use of mixed microorganisms for better employment of solar energy
3. More research on genetic and metabolic engineering of microorganisms to improve better yield for overall performance of photobioreactors
4. Bioreactor performance with the same volume but different area−volume ratio for a given microorganism for H_2 production

In addition, the genetic study of microorganisms and the design of an effective photobioreactor for the long-term cultivation of microorganisms are essential because to date, photobioreactors have been developed only for laboratory purposes (Rosner & Wagner, 2012). Apart from this, two-stage culture strategies have been developed to induce the productivity of microalgae such as *Chlorophyta* and *Scenedesmaceae*. These processes consist of fast growth induction in stage 1 followed by lipid induction in stage 2. With this strategy, overall productivity was improved and a better quality of biodiesel was obtained (Xia, Ge, Zhou, Zhang, & Hu, 2013). Comparatively, two-stage culture strategies were more effective than biomass production by microalgae in open ponds (Lin & Lin, 2011) or vertical tank bioreactors (Chinnasamy, Bhatnagar, Claxton, & Das, 2010).

10.2.9 Feedstocks for photobiological H_2 production

Hydrogen is the most abundant element in the universe but it does not exist alone in nature. Therefore, H_2 can by produced from hydrogen-containing substances or feedstocks such as water (H_2O), natural gas by CH_4, biomass (cellulose, hemicellulose, or lignin), and hydrocarbons such as coal. Because of inadequate research on the mass production of H_2 by photobiological methods, H_2 has been produced from different varieties of feedstocks, from fossils to coal and natural gases. It has been predicted that H_2 will have a major role in the energy supply by 2100. Therefore, feedstock

for biohydrogen production has significant value for future generations (Saratale, Chen, Lo, Saratale, & Chang, 2008).

In the fermentative process, carbohydrates such as cellulose, hemicellulose, and starch are popular feedstocks that are freely available in plant biomass and agricultural waste (Nowak et al., 2005). Normally, organic acids are transferred from dark fermentation to photofermentation, and thus the feedstock must contain low nitrogen compound for nitrogenase-mediated H_2 production (Chen, Yang, Yeh, Liu, & Chang, 2008; Özgür et al., 2010).

Hydrogen production by lignocellulosic fermentation uses the feedstock of corn stover and microbial electrolysis cells (MEC) use fermentation waste as a feedstock; thus, integration of lignocellulosic fermentation and MEC consume the fermentative waste of fermentation as the MEC feedstock. Three main systems have been examined for a fermentative system (James, Baum, Perez, & Baum, 2009):

- H_2 production using dark fermentation of algal waste
- H_2 production using dark fermentation of lignocellulosic feedstock (corn stover)
- H_2 production from MEC using fermentation waste as a feedstock

Biogas is generated by anaerobic digestion of algal waste combined with several feedstocks (Weiss, Patyk, & Schebek, 2011). Research has been conducted into optimizing feedstock for photobiological H_2 production; to produce H_2, photosynthetic bacteria *Rhodopseudomonas* used sewage and wastewater (Sunita & Mitra, 1993), *Rhodopseudomonas* and *Cyanobacterium anacystis* used dairy and sugarcane wastewater (Thangaraj & Kulandaivelu, 1994), Rhodobacter *sphaeroides* used feedstock tofu wastewater (Zhu, Suzuki, Tsygankov, Asada, & Miyake, 1999), *R. sphaeroides* O.U. 001 used sugar refinery wastewater (Yetis et al., 2000), and *R. sphaeroides* O.U. 001 used brewery wastewater (Seifert, Waligorska, & Laniecki, 2010). Because several different feedstocks such as organic waste and algal biomass are used, both photofermentation and dark fermentation are considered to have potential advantages (Ferreira, Ribau, & Silva, 2011; Yang, Guo, Xu, Fan, & Luo, 2011). Similarly, the highest production of H_2 was produced using pretreated biomass of microalgae *Nannochloropsis* sp. as substrates for fermentation by immobilized *Clostridium acetobutylicum* cells among pretreated biomass of various microalgae such as Arthrospira platensis, *Nannochloropsis* sp., Dunaliella tertiolecta, Galdieria partita, Chlorella vulgaris, *Cosmarium* sp., and *Nostoc* sp. (Efremenko et al., 2012). Nobre et al. (2013) found the *Nannochloropsis* sp. to be a potential feedstock for dark and photofermentative H_2 production.

10.2.10 Hydrogen production by artificial photosynthetic systems

Artificial photosynthesis as a chemical process replicates natural photosynthesis to reduce anthropogenic carbon dioxide (CO_2), increase fuel security, and provide a sustainable global economy (Faunce et al., 2013). Because of the development of some suitable technologies, we can develop artificial photosynthesis using artificial leaves for the efficient conversion of solar energy into H_2 and other fuels (Centi & Perathoner,

2010, 2011). This method may be a potential technology for H_2 production by mimicking natural photosynthesis by green leaves. Therefore, research has been carried out to harvest solar energy to produce H_2 by artificial photosynthesis (Lewis & Nocera, 2006; Nocera, 2009). In artificial photosynthesis, the artificial leaf must be able to use sunlight and water to reduce CO_2 and water into H_2 (Centi & Perathoner, 2010, 2011; Roy, Varghese, Paulose, & Grimes, 2010). Hence, artificial photosynthesis has created great interest owing to the employment of photoelectrochemical cells (PEC) to use sunlight to produce solar fuel (Bensaid, Centi, Garrone, Perathoner, & Saracco, 2012; Listorti, Durrant, & Barber, 2009; Walter et al., 2010). In practice, solar-driven electrochemical fuel generation needs the integration of light-absorbing and electrochemical components able to separate product fuels (Modestino et al., 2013). Natural photosynthesis synthesizes glucose and oxygen in the presence of sunlight. In the presence of sunlight, the excitation of chlorophyll molecules in PSII and PSI generates ATP and NADPH along the ETC with the involvement of different protein complexes. Similarly, in artificial photosynthesis, the use of solar energy to produce NADPH as an electron donor by PSI must be achieved (Amao, Hamano, & Shimizu, 2012). Thus, we have to know all biochemical pathways before constructing an artificial photosynthetic system, because natural photosynthesis consists of the involvement of several pigments, proteins, and enzymes. The main barrier is producing artificial leaves for artificial photosynthesis to mimic the overall reactions of natural photosynthesis (Cogdel et al., 2010).

In artificial photosynthesis, model molecular systems, electron donor and acceptor assemblies, solar energy conversion by photo-induced charge separation, examination of photoelectrochemical cells to convert solar energy into fuels, light-harvesting component, charge separation, and catalysis in photosynthesis have been compared with natural photosynthesis. The three key components for solar energy conversion in artificial photosynthesis are light harvesting, charge separation, and catalysis (McConnell, Li, & Brudvig, 2010). According to Nocera (2012), a light-dependent reaction is required to mimic photosynthesis. Hence, artificial leaves were constructed by adding catalysts (Co-OEC and NiMoZn) to a light-harvesting silicon-based semiconductor to split water. Those silicon semiconductors in artificial leaves may be considered photosynthetic membranes in natural photosynthesis. The silicon junction harvests sunlight and converts it into a wireless current through Si. Then, Co-OEC is integrated with Si that functionalizes single-junction PEC. Several photochemical reactions that occur in this solar cell generate the photovoltage used for the water-splitting reaction to generate H_2 (Figure 10.4). In addition, electrocatalysts have been designed for a light-driven charge separation system for solar fuel production (Tran, Wong, Barber, & Loo, 2012). Based on the current situation, the concept of an artificial leaf has been developed as a source of clean fuel. An artificial leaf can be developed using a silicon-coated sheet that splits water into hydrogen and oxygen. Silicon has become an attractive material with which to design an artificial leaf because silicone is cheap and abundant and such cells can capture and store energy. Although the development of an artificial leaf is still a scientific challenge, some concepts have been developed to overcome technical difficulties. To overcome those difficulties, some researchers have focused on artificial leaves for artificial photosynthesis to

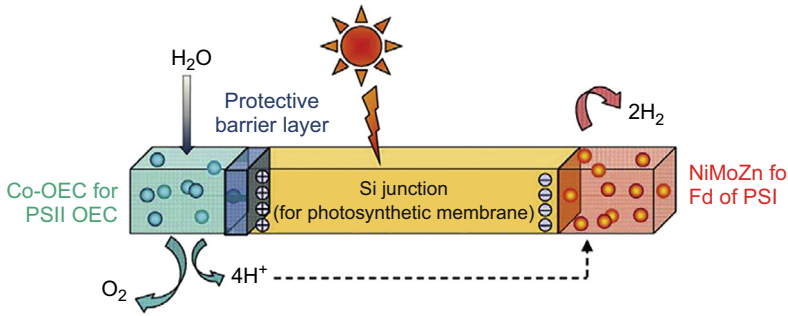

Figure 10.4 Construction of an artificial leaf. The photosynthetic membrane is replaced by an Si junction that performs light capture and conversion to a wireless current. The oxygen-evolving complex and ferredoxin reductase of the photosynthetic membrane are replaced by Co-OEC and NiMoZn OER and HER catalysts, respectively, to perform water splitting.
Figure and legend adopted from Nocera (2012).

generate clean hydrogen. Hybrid strategies for solar water splitting based on dye-sensitized photoelectrosynthetic cells (Alibabaei et al., 2013), by proposing natural to artificial photosynthesis with artificial photocatalysts, hybrid photocatalysts for water oxidation/proton reduction and hydrogen evolution, as well as construction of complete photocatalytic system for hydrogen and oxygen evolution from water (Barber and Tang, 2013), used a photovoltaic reactor for artificial photosynthesis, based on water electrolysis to produce high-energy hydrogen atoms (Nong et al., 2014). An artificial photosynthetic system using TiO_2 was developed that has the features of photosynthesis to overcome the challenge of solar-driven water splitting and CO_2 reduction. In addition, the photoreduction of CO_2 into hydrocarbon fuels (CO and CH_4) has been demonstrated, which solves the architectural model of artificial photosynthesis to produce solar cells, fuel cells, or battery electrodes (Zhou et al., 2013).

The Joint Center for Artificial Photosynthesis developed an idea for artificial photosynthesis using a water-splitting photoconversion system that produces H_2 directly from water. As in plants, water oxidation takes place in PSII with the help of visible light and electrons are transferred to the PSI with the help of electron transport mediators in which carbon dioxide is reduced to carbohydrates during a dark reaction. Plants prepare food (carbohydrates) with the help of water and carbon dioxide in the presence of visible light (Figure 10.5(a)). Scientists are trying to mimic the wonderful work carried out by green leaves. In this regard, different concepts have been proposed to prepare artificial leaves. The Joint Center for Artificial Photosynthesis proposed a model to design artificial leaves, is illustrated in Figure 10.5(b).

According to this model, water oxidation and reduction half-reaction take place separately in two different systems, as in natural photosynthesis. Semiconductor nanowires are used for water oxidation as well as the reduction half-reaction after modification with water oxidation and reduction catalyst, respectively. Upon irradiation of visible light, the nanowires absorb visible light and water is oxidized to produce oxygen, electrons, and protons. Electrons travel through semiconductor wires to the reduction side whereas protons are transferred to the reduction side with the help of

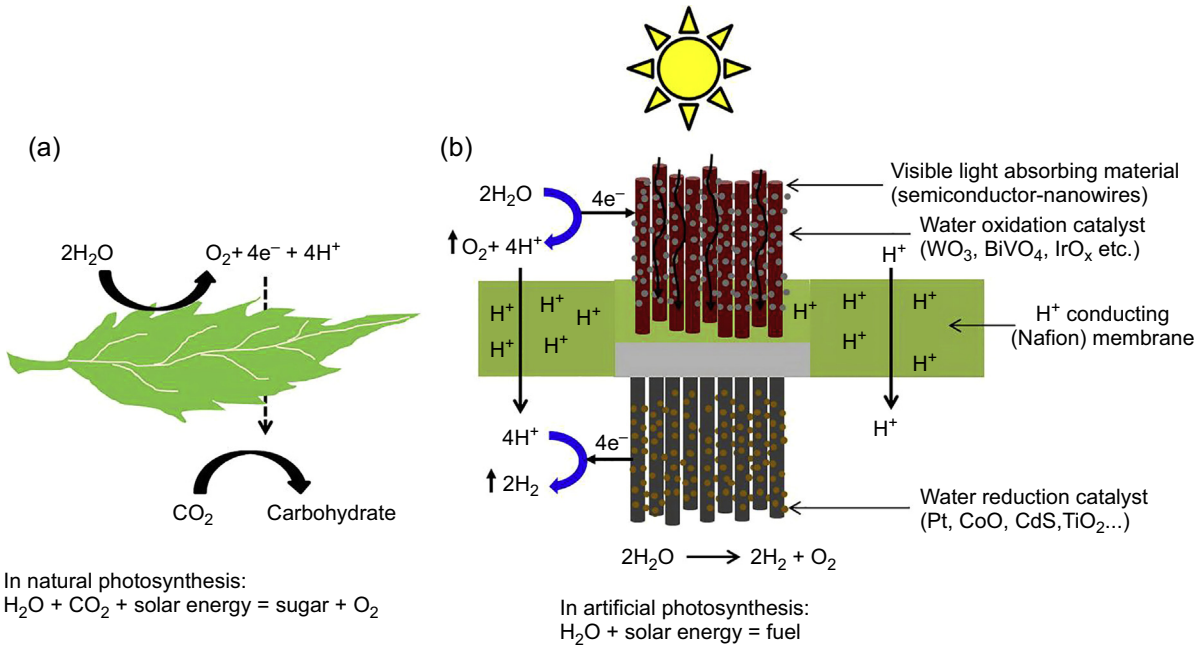

Figure 10.5 Schematic illustration of natural photosynthetic system (NPS) and artificial photosynthetic system (APS). (a) Basic process of photosynthesis in NPS. (b) Structural design of artificial photosynthesis in APS. In APS, electrons and protons are liberated by the water-splitting reaction and are passed through a proton-conducting membrane (Nafion), where protons are reduced to H_2.
Figure (b) is adopted and modified from the concept of Warren, Atwater, and Lewis (2014).

proton-conducting membrane (Nafion), in which protons are reduced to hydrogen gas. In this way, water splitting (generation of H_2 and O_2) can be achieved with high efficiency separately in two different systems. The development of an efficient catalyst for water oxidation to evolve O_2 is a key task for yielding breakthrough water splitting. Ruthenium- and iridium-based catalysts show better performance but they are scarce and expensive (Liu & Wang, 2012; Singh & Spiccia, 2013). Thus, earth-abundant elements are more promising (Hocking et al., 2011).

10.3 Advantages and disadvantages of hydrogen production using photobiological methods

Photobiological H_2 production has several advantages as compared with other methods such as petroleum refining, coal gasification, fossil fuel, and thermochemical techniques because those processes are hazardous. Hence, photobiological H_2 production can be considered as an effective method for producing pure and clean H_2 gas, although it has some disadvantages; therefore, the advantages and disadvantages of photobiological production are given below.

10.3.1 Advantages of hydrogen production using photobiological methods

- Photobiological H_2 production uses microorganisms to convert solar energy into hydrogen gas.
- Photobiological H_2 production, especially by photosynthetic microorganisms, has several advantages because it requires simple techniques and low-cost energy (natural sunlight) compared with electrochemical H_2 production based on water splitting. Hence, these methods only use sunlight and water as renewable sources of energy.
- Photobiological H_2 production does not emit environmentally polluting gases and toxic compounds.
- Pure and clean H_2 can be produced by photobiological methods.
- Green algae, cyanobacteria, and photosynthetic bacteria are abundant everywhere and we can easily grow them under suitable artificial conditions. Most of these microorganisms are not environmentally harmful. Hence, we can easily grow such microorganisms to fulfill our goal.
- During photobiological H_2 production, many photosynthetic bacteria can use wide-spectrum light energy and organic waste (Hussy, Hawkes, Dinsdale, & Hawkes, 2003).
- Photobiological H_2 production by microorganisms under anaerobic conditions produces valuable metabolites such as lactic acid, butyric acid, and acetic acid as byproducts (Lay, 2000; Lin & Chang, 1999).
- The photon conversion efficiency to produce H_2 from sunlight is high: $\sim$10–16% (Kruse et al., 2005, Prince & Kheshgi, 2005).
- This method is useful for carbon sequestration. Solar-powered H_2 production by microorganisms has a unique process for CO_2 sequester. In the aerobic phase, CO_2 is converted into biomass; in the anaerobic phase H_2 is subsequently produced (Hankamer et al., 2007).
- Biohydrogen production by photosynthetic microorganisms requires the use of a simple solar reactor such as a transparent closed box with a low energy requirement (Parmar, Singh, Pandey, Gnansounou, & Madamwar, 2011).

- Hydrogen production by sunlight is cheap compared with the current fossil fuel system and the synthetic fossil fuel system for H_2 production.

10.3.2 Disadvantages of hydrogen production using photobiological methods

- Hydrogenase is inactivated in the presence of molecular oxygen in microorganisms.
- In green algae the simultaneous production of O_2 and H_2 inhibits hydrogenase activity by O_2. The presence of uptake hydrogenase in cyanobacteria and photosynthetic bacteria also decreases H_2 production (Dasgupta et al., 2010).
- Production of H_2 by photofermentation is low (Hussy et al., 2003).
- The exact metabolic pathway for H_2 production by microorganisms is not clear. In addition, there is no clear contender for a robust, industrially capable microorganism that can be metabolically engineered to produce more H_2. Several engineering issues need to be addressed, including an appropriate bioreactor design for H_2 production (Bhutto et al., 2011).
- Photosynthetic bacteria do not produce more H_2 that will fulfill public demands (Bhutto et al., 2011).
- The development of a new strain of microorganisms is required to enhance high solar conversion efficiency for H_2 production.
- Mass cultivation of green algae and cyanobacteria is difficult because it may require a large surface area. Also, the yield of H_2 production by these microorganisms is not high, which may not fulfill demand.
- Scaling-up and materials for construction of several photobioreactors are costly, and there are many disadvantages (Dasgupta et al., 2010).
- Storing hydrogen is expensive because it needs to be compressed.
- Construction of artificial leaves for artificial photosynthesis is an expensive method for generating H_2.

10.4 Future trends to improve photobiological H_2 production

Photobiological H_2 production using photosynthetic microorganisms such as bacteria, algae, and cyanobacteria is an exciting topic for research. Currently, H_2 is considered a fuel for the future as a renewable source of energy that does not create greenhouse gases. In addition, the method of photobiological H_2 production using photosynthetic microorganisms shows promise and great interest for generating carbon-free, clean, and pure H_2 from abundant natural resources such as water and sunlight. However, feasible and commercial exploration for better yield of H_2 is required. Further exploration is needed to improve photosynthetic microorganisms by either metabolic or genetic engineering. There are some ideas for improving photobiological H_2 production: (1) identifying the most suitable microorganisms and incorporating hydrogenase and nitrogenase into selected microorganisms, (2) optimizing culture conditions, (3) stabilizing photobioreactors, (4) improving feedstocks, (5) performing comparative analyses of photobiological H_2 production, (6) improving H_2 yield using cheap or cost-effective raw materials, (7) exploring novel species of photosynthetic microorganisms that use better solar energy to improve H_2 production, and (8) improving photobioreactors for better propagation of microalgae for effective H_2 production.

List of acronyms

ATP	Adenosine triphosphate
NADPH	Nicotinamide adenine dinucleotide phosphate
NADH	Nicotinamide adenine dinucleotide
CO_2	Carbon dioxide
H_2O	Water
H_2	Hydrogen
O_2	Oxygen
PNSB	Purple non-sulfur bacteria
e^-	Electron
H^+	Proton
PSII	Photosystem II
PSI	Photosystem I
Fd	Ferredoxin
FNR	Ferredoxin-$NADP^+$-reductase
PQ	Plastoquinone
LED	Light-emitting diode
MEC	Microbial electrolysis cell
PEC	Photoelectrochemical cell
Si	Silicon
JCAP	Joint Center for Artificial Photosynthesis

Acknowledgments

This work was supported by grants from the Russian Science Foundation (No: 14-14-00039) to SIA. MMN is grateful to the Institute for Advanced Studies in Basic Sciences and the National Elite Foundation for financial support. KI was supported in part by grant-in-aid for Scientific Research on Innovative Areas (No. 24107004) and Strategic Research Base Development Program for Private Universities from MEXT, Japan. TT and HM were supported by a grant from JST PRESTO.

References

Akkerman, I., Janssen, M., Rocha, J., & Wijffels, R. H. (2002). Photobiological hydrogen production: photochemical efficiency and bioreactor design. *International Journal of Hydrogen Energy, 27*(11−12), 1195−1208.

Alibabaei, L., Brennaman, M. K., Norris, M. R., Kalanyan, B., Song, W., Losego, M. D., et al. (2013). Solar water splitting in a molecular photoelectrochemical cell. *Proceedings of the National Academy of Sciences of the United States of America, 110*(50), 20008−20013.

Allakhverdiev, S. I., Kreslavski, V. D., Thavasi, V., Zharmukhamedov, S. K., Klimov, V. V., Nagata, T., et al. (2009). Hydrogen photoproduction by use of photosynthetic organisms and biomimetic systems. *Photochemical and Photobiological Sciences, 08*(2), 148−156.

Allakhverdiev, S. I., Thavasi, V., Kreslavski, V. D., Zharmukhamedov, S. K., Klimov, V. V., Ramakrishna, S., et al. (2010). Photosynthetic hydrogen production. *Journal of Photochemistry and Photobiology C: Photochemistry Reviews, 11*(2−3), 101−113.

Amao, Y., Hamano, A., & Shimizu, K. (2012). Development of artificial leaf for solar hydrogen production. *Energy Procedia, 29*, 21−25.

Androga, D. D., Özgür, E., Eroglu, I., Gündüz, U., & Yücel, M. (2012). Photofermentative hydrogen production in outdoor conditions. In D. Minic (Ed.), *Hydrogen Energy−Challenges and Perspectives*, ISBN 978-953-51-0812-2. http://dx.doi.org/10.5772/50390.

Antal, T. K., & Lindblad, P. (2005). Production of H_2 by sulphur-deprived cells of the unicellular cyanobacteria *Gloeocapsa alpicola* and *Synechocystis* sp. PCC 6803 during dark incubation with methane or at various extracellular pH. *Journal of Applied Microbiology, 98*(01), 114−120.

Asada, Y., Koike, Y., Schnackenberg, J., Miyake, M., Uemura, I., & Miyake, J. (2000). Heterologous expression of clostridial hydrogenase in the cyanobacterium expression of clostridial hydrogenase in the cyanobacterium Synechococcus PCC7942. *Biochimica et Biophysica Acta (BBA)−Gene Structure and Expression, 1490*(3), 269−278.

Asada, Y., & Miyake, J. (1999). Photobiological hydrogen production. *Journal of Bioscience and Bioengineering, 88*(1), 1−6.

Barber, J., & Tran, P. D. (2013). From natural to artificial photosynthesis. *Journal of The Royal Society Interface, 10*(81), 20120984. http://dx.doi.org/10.1098/rsif.2012.0984

Bensaid, S., Centi, G., Garrone, E., Perathoner, S., & Saracco, G. (2012). Towards artificial leaves for solar hydrogen and fuels from carbon dioxide. *ChemSusChem, 05*(3), 500−521.

Bhutto, A. W., Bazmi, A. A., Kardar, M. N., Yaseen, M., Zahedi, G., & Karim, K. (2011). Developments in hydrogen production through microbial processes; Pakistan's prospective. *International Journal of Chemical and Environmental Engineering, 02*(3), 189−205.

Bonente, G., Formighieri, C., Mantelli, M., Catalanotti, C., Giuliano, G., Morosinotto, T., et al. (2011). Mutagenesis and phenotypic selection as a strategy toward domestication of *Chlamydomonas reinhardtii* strains for improved performance in photobioreactors. *Photosynthesis Research, 108*(2−3), 107−120.

Bothe, H., Schmitz, O., Yates, M. G., & Newton, W. E. (2010). Nitrogen fixation and hydrogen metabolism in cyanobacteria. *Microbiology and Molecular Biology Reviews, 74*(4), 529−551.

Carere, C. R., Rydzak, T., Verbeke, T. J., Cicek, N., Levin, D. B., & Sparling, R. (2012). Linking genome content to biofuel production yields: a meta-analysis a major catabolic pathways among select H_2 and ethanol-producing bacteria. *BMC Microbiology, 12*, 295.

Centi, G., & Perathoner, S. (2010). Towards solar fuels from water and CO_2. *ChemSusChem, 03*(2), 195−208.

Centi, G., & Perathoner, S. (2011). CO_2-based energy vectors for the storage of solar energy. *Greenhouse Gases: Science and Technology, 01*(1), 21−35.

Cha, M., Chung, D., Elkins, J. G., Guss, A. M., & Westpheling, J. (2013). Metabolic engineering of *Caldicellulosiruptor bescii* yields increased hydrogen production from lignocellulosic biomass. *Biotechnology for Biofuels, 6*, 85.

Cheng, J., Su, H., Zhou, J., Song, W., & Cen, K. (2011). Hydrogen production by mixed bacteria through dark and photo fermentation. *International Journal of Hydrogen Energy, 36*(1), 450−457.

Chen, C.-Y., Yang, M.-H., Yeh, K.-L., Liu, C.-H., & Chang, J.-S. (2008). Biohydrogen production using sequential two-stage dark and photo fermentation processes. *International Journal of Hydrogen Energy, 33*(18), 4755−4762.

Chen, C.-Y., Yeh, K.-L., Aisyah, R., Lee, D.-J., & Chang, J.-S. (2011). Cultivation, photobioreactor design and harvesting of microalgae for biodiesel production: a critical review. *Bioresource Technology, 102*(1), 71−81.

Chinnasamy, S., Bhatnagar, A., Claxton, R., & Das, K. C. (2010). Biomass and bioenergy production potential of microalgae consortium in open and closed bioreactors using untreated carpet industry effluent as growth medium. *Bioresource Technology, 101*(17), 6751−6760.

Cogdell, R. J., Brotosudarmo, T. H. P., Gardiner, A. T., Sanchez, P. M., & Cronin, L. (2010). Artificial photosynthesis−solar fuels: current status and future prospects. *Biofuels, 01*(6), 861−876.

Cournac, L., Guedeney, G., Peltier, G., & Vignais, P. M. (2004). Sustained photoevolution of molecular hydrogen in a mutant of *Synechocystis* sp. strain PCC 6803 deficient in the type I NADPH-dehydrogenase complex. *Journal of Bacteriology, 186*(6), 1737−1746.

Dasgupta, C. N., Gilbert, J. J., Lindbald, P., Heidorn, T., Borgvang, S. A., Skjånes, K., et al. (2010). Recent trends on the development of photobiological processes and photobioreactors for the improvements of hydrogen production. *International Journal of Hydrogen Energy, 35*(19), 10218−10238.

Das, D., Khanna, N., & Veziroğlu, T. N. (2008). Recent developments in biological hydrogen production processes. *Chemical Industry and Chemical Engineering Quarterly, 14*(2), 57−67.

Das, D., & Veziroğlu, T. N. (2001). Hydrogen production by biological processes: a survey of literature. *International Journal of Hydrogen Energy, 26*(1), 13−28.

Datta, M., Nikki, G., & Shah, V. (2000). Cyanobacterial hydrogen production. *World Journal of Microbiology and Biotechnology, 16*(8−9), 757−767.

Dauvillée, D., Chochois, V., Steup, M., Haebel, S., Eckermann, N., Ritte, G., et al. (2006). Plastidial phosphorylase is required for normal starch synthesis in *Chlamydomonas reinhardtii*. *The Plant Journal, 48*(2), 274−285.

Dutta, D., De, D., Chaudhuri, S., & Bhattacharya, S. K. (2005). Hydrogen production by Cyanobacteria. *Microbial Cell Factories, 4*, 36. http://dx.doi.org/10.1186/1475-2859-4-36.

Efremenko, E. N., Nikolskaya, A. B., Lyagin, I. V., Senko, O. V., Makhlis, T. A., Stepanov, N. A., et al. (2012). Production of biofuels from pretreated microalgae biomass by anaerobic fermentation with immobilized *Clostridium acetobutylicum* cells. *Bioresource Technology, 114*, 342−348.

Eltsova, Z. A., Vasilieva, L. G., & Tsygankov, A. A. (2010). Hydrogen production by recombinant strains of Rhodobacter *sphaeroids* using a modified photosynthetic apparatus. *Applied Biochemistry and Microbiology, 46*(5), 487−491.

Ernst, A., Kerfin, W., Spiller, H., & Böger, P. (1979). External factors influencing light-induced H_2 evolution by the blue-green algae, *Nostoc muscorum*. *Zeitschrift für Naturforschung, 34*, 820−825.

Eroglu, E., & Melis, A. (2011). Photobiological hydrogen production: recent advances and state of art. *Bioresource Technology, 102*(18), 8403−8413.

Evens, T. J., Chapman, D. J., Robbins, R. A., & D'Asaro, E. A. (2000). An analytical flat-plate photobioreactor with a spectrally attenuated light source for the incubation of phytoplankton under dynamic light regimes. *Hydrobiologia, 434*(1−3), 55−62.

Faunce, T., Styring, S., Wasielewski, M. R., Brudvig, G. W., Rutherford, W., Messinger, J., et al. (2013). Artificial photosynthesis as a frontier technology for energy sustainability. *Energy and Environmental Science*, (6), 1074−1076.

Ferreira, A. F., Ribau, J. P., & Silva, C. M. (2011). Energy consumption and CO_2 emissions of potato peel and sugarcane biohydrogen production pathways, applied to Portuguese road transportation. *International Journal of Hydrogen Energy, 36*(21), 13547−13558.

Ghirardi, M. L., Dubini, A., Yu, J., & Maness, P.-C. (2009). Photobiological hydrogen-producing systems. *Chemical Society Reviews, 38*(12), 3505.

Ghirardi, M. L., King, P. W., Posewitz, M. C., Maness, P. C., Fedorov, A., Kim, K., et al. (2005). Approaches to developing biological H_2-producing organisms and processes. *Biochemical Society Transactions, 33*, 70−72.

Ghirardi, M. L., Posewitz, M. C., Maness, P. C., Dubini, A., Yu, J., & Seibert, M. (2007). Hydrogenases and hydrogen photoproduction in oxygenic photosynthetic organisms. *Annual Review of Plant Biology, 58*, 71−91.

Ghysels, B., & Franck, F. (2010). Hydrogen photo-evolution upon S deprivation stepwise: an illustration of microalgal photosynthetic and metabolic flexibility and a step stone for future biotechnological methods of renewable H_2 production. *Photosynthesis Research, 106*(1−2), 145−154.

Hallenbeck, P. C., & Benemann, J. R. (2002). Biological hydrogen production; fundamentals and limiting processes. *International Journal of Hydrogen Energy, 27*(11−12), 1186−1194.

Hankamer, B., Lehr, F., Rupprecht, J., Mussgnug, J. H., Posten, C., & Kruse, O. (2007). Photosynthetic biomass and H_2 production by green algae: from bioengineering to bioreactor scale-up. *Physiologia Plantarum, 131*(1), 10−21.

Hansel, A., & Lindblad, P. (1998). Towards optimization of cyanobacteria as biotechnologically relevant producers of molecular hydrogen, a clean and renewable energy source. *Applied Microbiology and Biotechnology, 50*(2), 153−160.

Happe, T., Schütz, K., & Böhme, H. (2000). Transcriptional and mutational analysis of the uptake hydrogenase of the filamentous cyanobacterium *Anabaena variabilis* ATCC 29413. *Journal of Bacteriology, 182*(6), 1624−1631.

Hay, J. X. W., Wu, T. Y., Juan, J. C., & Jahim, J. M. (2013). Biohydrogen production through photo fermentation or dark fermentation using waste as a substrate: overview, economics, and future prospects of hydrogen usage. *Biofuels Bioproducts and Biorefining, 07*(3), 334−352.

Hocking, R. K., Brimblecombe, R., Chang, L., Singh, A., Cheah, M. H., Glover, C., et al. (2011). Water-oxidation catalysis by manganese in a geochemical-like cycle. *Nature Chemistry, 3*, 461−466.

Horch, M., Lauterbach, L., Lenz, O., Hildebrandt, P., & Zebger, I. (2012). NAD(H)-coupled hydrogen cycling-structure-function relationships of bidirectional [NiFe] hydrogenase. *FEBS Letters, 586*(5), 545−556.

Hussy, I., Hawkes, F. R., Dinsdale, R., & Hawkes, D. L. (2003). Continuous fermentative hydrogen production from a wheat starch co-product by mixed microflora. *Biotechnology and Bioengineering, 84*(6), 619−626.

James, B. D., Baum, G. N., Perez, J., & Baum, K. N. (2009). Technoeconomic Boundary analysis of biological pathways to hydrogen production. In *National Renewable Energy Laboratory, Subcontract Report NREL/SR-560-46674* (pp. 1−193). Arlington, Virginia: Directed Technologies, Inc.

Jo, J. H., Lee, D. S., & Park, J. M. (2006). Modeling and optimization of photosynthetic hydrogen gas production by green alga *Chlamydomonas reinhardtii* in sulfur-deprived circumstance. *Biotechnology Progress, 22*(2), 431−437.

Kars, G., Gündüz, U., Yücel, M., Türker, L., & Eroğlu, I. (2006). Hydrogenproduction and transcriptional analysis of *nifD*, *nifK* and *hupS* genes in *Rhodobacter sphaeroides* O.U.001 grown in media with different concentrations of molybdenum and iron. *International Journal of Hydrogen Energy, 31*(11), 1536−1544.

Khetkorn, W., Lindbald, P., & Incharoensakdi, A. (2012). Inactivation of uptake hydrogenase leads to enhanced and sustained hydrogen production with high nitrogenase activity under high light exposure in the cyanobacterium *Anabaena siamensis* TISTR 8012. *Journal of Biological Engineering, 06*, 19.

Kim, J. Y. H., Jo, B. H., Jo, Y., & Cha, H. J. (2012). Improved production of biohydrogen in light-powered *Escherichia coli* by co-expression of proteorhodopsin and heterologous hydrogenase. *Microbial Cell Factories, 11*, 2.

Kim, J. P., Kang, C. D., Park, T. H., Kim, M. S., & Sim, S. J. (2006). Enhanced hydrogen production by controlling light intensity in sulfur-deprived *Chlamydomonas reinhardtii* culture. *International Journal of Hydrogen Energy, 31*(11), 1585−1590.

Kim, E.-J., Kim, J.-S., Kim, M.-S., & Lee, J. K. (2006). Effect of changes in the level of light harvesting complexes of Rhodobacter *sphaeroides* on the photoheterotrophic production of hydrogen. *International Journal of Hydrogen Energy, 31*(4), 531−538.

Koku, H., Eroğlu, I., Günfüz, U., Yücel, M., & Türker, L. (2002). Aspects of the metabolism of hydrogen production by *Rhodobacter sphaeroides*. *International Journal of Hydrogen Energy, 27*(11−12), 1315−1329.

Kondo, T., Arakawa, M., Hirai, T., Wakayama, T., Hara, M., & Miyake, J. (2002). Enhancement of hydrogen production by a photosynthetic bacterium mutant with reduced pigment. *Journal of Bioscience and Bioengineering, 93*(2), 145−150.

Kosourov, S., Makarova, V., Fedorov, A. S., Tsygankov, A., Seibert, M., & Ghirardi, M. L. (2005). The effect of sulfur re-addition on H_2 photoproduction by sulfur-deprived green algae. *Photosynthesis Research, 85*(3), 295−305.

Kosourov, S., Seibert, M., & Ghirardi, M. L. (2003). Effects of extracellular pH on the metabolic pathways in sulfur-deprived, H_2-producing *Chlamydomonas reinhardtii* cultures. *Plant and Cell Physiology, 44*(2), 146−155.

Kosourov, S., Tsygankov, A., Seibert, M., & Ghirardi, M. L. (2002). Sustained hydrogen photoproduction by *Chlamydomonas reinhardtii*: effects of culture parameters. *Biotechnology and Bioengineering, 78*(7), 731−740.

Kruse, O., Rupprecht, J., Mussgnug, J. H., Dismukes, G. C., & Hankamer, B. (2005). Photosynthesis: a blueprint for solar energy capture and biohydrogen production technologies. *Photochemical and Photobiological Sciences, 04*(12), 957−970.

Kufryk, G. (2013). Advances in utilizing cyanobacteria for hydrogen production. *Advances in Microbiology, 03*(6A), 60−68.

Kwon, J.-H., Rögner, M., & Rexroth, S. (2012). Direct approach for bioprocess optimization in a continuous flat-bed photobioreactor system. *Journal of Biotechnology, 162*(1), 156−162.

Lay, J. J. (2000). Modeling and optimization of anaerobic digested sludge converting starch to hydrogen. *Biotechnology and Bioengineering, 68*(3), 269−278.

Lee, J. Z., Klaus, D. M., Maness, P.-C., & Spear, J. R. (2007). The effect of butyrate concentration on hydrogen production via photofermentation for use in a Martian habitat resource recovery process. *International Journal of Hydrogen Energy, 32*(15), 3301−3307.

Lemeille, S., Turkina, M. V., Vener, A. V., & Rochaix, J.-D. (2010). Stt7-dependent phosphorylation during state transitions in the green alga *Chlamydomonas reinhardtii*. *Molecular and Cellular Proteomics, 09*(6), 1281−1295.

Lewis, N. S., & Nocera, D. G. (2006). Powering the planet: chemical challenges in solar energy utilization. *Proceedings of the National Academy of Sciences of the United States of America, 103*(43), 15729−15735.

Liang, Y., Wu, X., Gan, L., Xu, H., Hu, Z., & Long, M. (2009). Increased biological hydrogen production by deletion of hydrogen-uptake system in photosynthetic bacteria. *Microbiological Research, 164*(6), 674−679.

Lin, C.-Y., & Chang, R.-C. (1999). Hydrogen production during the anaerobic acidogenic conversion of glucose. *Journal of Chemical Technology and Biotechnology, 74*(6), 498−500.

Lindberg, P., Devine, E., Stensjö, K., & Lindblad, P. (2011). HupW Protease specifically required for processing of the catalytic subunit of the uptake hydrogenase in the cyanobacterium *Nostoc* sp. strain PCC 7120. *Applied and Environmental Microbiology, 78*(1), 273−276.

Lindberg, P., Park, S., & Melis, A. (2010). Engineering a platform for photosynthetic isoprene production in cyanobacteria, using *Synechocystis* as the model organism. *Metabolic Engineering, 12*(1), 70−79.

Lindberg, P., Schütz, K., Happe, T., & Lindblad, P. (2002). A hydrogen producing, hydrogenase-free mutant strain of *Nostoc punctiforme* ATCC 29133. *International Journal of Hydrogen Energy, 27*(11−12), 1291−1296.

Lin, Q., & Lin, J. (2011). Effects of nitrogen source and concentration on biomass and oil production of a *Scenedesmus rubescens* like microalga. *Bioresource Technology, 102*(2), 1615−1621.

Listorti, A., Durrant, J., & Barber, J. (2009). Artificial photosynthesis: solar to fuel. *Nature Materials, 08*(12), 929−930.

Liu, B.-F., Ren, N.-Q., Ding, J., Xie, G.-J., & Guo, W.-Q. (2009). The effect of Ni^{2+}, Fe^{2+} and Mg^{2+} concentration on photo-hydrogen production by *Rhodopseudomonas faecalis* RLD-53. *International Journal of Hydrogen Energy, 34*(2), 721−726.

Liu, X., & Wang, F. (2012). Transition metal complexes that catalyze oxygen formation from water: 1979−2010. *Coordination Chemistry Reviews, 256*, 1115−1136.

Maness, P.-C., Smolinski, S., Dillon, A. C., Heben, M. J., & Weaver, P. F. (2002). Characterization of the oxygen tolerance of a hydrogenase linked to a carbon monoxide oxidation pathway in *Rubrivivax gelatinosus*. *Applied and Environmental Microbiology, 68*(6), 2633−2636.

Markov, S. A., Eivazova, E. R., & Greenwood, J. (2006). Photostimulation of H_2 production in the green alga *Chlamydomonas reinhardtii* upon photoinhibition of its O_2-evolving system. *International Journal of Hydrogen Energy, 31*(10), 1314−1317.

Masukawa, H., Mochimaru, M., & Sakurai, H. (2002). Disruption of the uptake hydrogenase gene, but not of the bidirectional hydrogenase gene, leads to enhanced photobiological hydrogen production by the nitrogen-fixing cyanobacterium *Anabaena* sp PCC 7120. *Applied Microbiology and Biotechnology, 58*(5), 618−624.

Mathews, J., & Wang, G. (2009). Metabolic pathway engineering for enhanced biohydrogen production. *International Journal of Hydrogen Energy, 34*(17), 7404−7416.

McConnell, I., Li, G., & Brudvig, G. W. (2010). Energy conversion in natural and artificial photosynthesis. *Chemistry and Biology, 17*(5), 434−447.

Melis, A., & Melnicki, M. R. (2006). Integrated biological hydrogen production. *International Journal of Hydrogen Energy, 31*(11), 1563−1573.

Melis, A., Zhang, L., Forestier, M., Ghirardi, M. L., & Seibert, M. (2000). Sustained photobiological hydrogen gas production upon reversible inactivation of oxygen evolution in the green alga *Chlamydomonas reinhardtii*. *Plant Physiology, 122*(1), 127−136.

Miura, Y., Akano, T., Fukatsu, K., Miyasaka, H., Mizoguchi, T., Yagi, K., et al. (1995). Hydrogen production by photosynthetic microorganisms. *Energy Conversion and Management, 36*(6−9), 903−906.

Miyake, M., Schnackenberg, J., Nakamura, C., Asada, Y., & Miyake, J. (2001). Molecular handling of hydrogenase. In J. Miyake, T. Matsunaga, & A. San Pietro (Eds.), *Biohydrogen II* (pp. 205−219). Oxford, United Kingdom: Elsevier Science Ltd.

Modestino, M. A., Walczak, K. A., Berger, A., Evans, C. M., Haussener, S., Koval, C., et al. (2013). Robust production of purified H_2 in a stable, self-regulating, and continuously operating solar fuel generator. *Energy and Environmental Science, 07*(1), 297−301.

Najafpour, M. M., & Allakhverdiev, S. I. (2012). Manganese compounds as water oxidizing catalysts for hydrogen production via water splitting: from manganese complexes to nano-sized manganese oxides. *International Journal of Hydrogen energy, 37*(10), 8753−8764.

Nandi, R., & Sengupta, S. (1998). Microbial production of hydrogen: an overview. *Critical Reviews in Microbiology, 24*(1), 61−84.

Nel, W. P., & Cooper, C. J. (2009). Implications of fossil fuel constraints on economic growth and global warming. *Energy Policy, 37*(1), 166−180.

Nguyen, A. V., Thomas-Hall, S. R., Malnoë, A., Timmins, M., Mussgnug, J. H., Rupprecht, J., et al. (2008). Transcriptome for photobiological hydrogen production induced by sulfur deprivation in the green alga *Chlamydomonas reinhardtii*. *Eukaryotic Cell, 07*(11), 1965−1979.

Nguyen, A. V., Toepel, J., Burgess, S., Uhmeyer, A., Blifernez, O., Doebbe, A., et al. (2011). Time-course global expression profiles of *Chlamydomonas reinhardtii* during photobiological H_2 production. *PLoS ONE, 06*(12), e29364.

Nobre, B. P., Villalobos, F., Barragán, B. E., Oliveira, A. C., Batista, A. P., Marques, P. A. S. S., et al. (2013). A biorefinery from *Nannochloropsis* sp. microalga−extraction of oils and pigments. Production of biohydrogen from the leftover biomass. *Bioresource Technology, 135*, 128−136.

Nocera, D. G. (2009). Personalized energy: the home as a solar power station. *ChemSusChem, 02*(5), 387−390.

Nocera, D. G. (2012). The artificial leaf. *Accounts of Chemical Research, 45*(5), 767−776.

Nong, G., Chen, S., Xu, Y., Huang, L., Zou, Q., Li, S., et al. (2014). Artificial photosynthesis of oxalate and oxalate-based polymer by a photovoltaic reactor. *Scientific Reports, 04*, 3572. http://dx.doi.org/10.1038/srep03572.

Nowak, J., Florek, M., Kwiatek, W., Lekki, J., Chevallier, P., Zieba, E., et al. (2005). Composite structure of wood cells in petrified wood. *Materials Science and Engineering: C, 25*(2), 119−130.

Ogata, H., Lubitza, W., & Higuch, Y. (2009). [NiFe] hydrogenases: structural and spectroscopic studies of the reaction mechanism. *Dalton Transactions Issue, 37*, 7577−7587.

Oh, Y.-K., Raj, S. M., Jung, G. Y., & Park, S. (2011). Current status of the metabolic engineering of microorganisms for biohydrogen production. *Bioresource Technology, 102*(18), 8357−8367.

Özgür, E., Mars, A. E., Peksel, B., Louwerse, A., Yücel, M., Gündüz, U., et al. (2010). Biohydrogen production from beet molasses by sequential dark and photofermentation. *International Journal of Hydrogen Energy, 35*(2), 511−517.

Öztürk, Y., Yücel, M., Daldal, F., Mandac, S., Gündüz, U., Türker, L., et al. (2006). Hydrogen production by using Rhodobacter *capsulatus* mutants with genetically modified electron transfer chains. *International Journal of Hydrogen Energy, 31*(11), 1545−1552.

Papazi, A., Andronis, E., Loannidis, N. E., Chaniotakis, N., & Kotzabasis, K. (2012). High yields of hydrogen production induced by meta-substituted dichlorophenols biodegradation from the green alga *Scenedesmus obliquus*. *PLoS ONE, 7*(11), e49037. http://dx.doi.org/10.1371/journal.pone.0049037.

Parmar, A., Singh, N. K., Pandey, A., Gnansounou, E., & Madamwar, D. (2011). Cyanobacteria and microalgae: a positive prospect for biofuels. *Bioresource Technology, 102*(22), 10163−10172.

Philipps, G., Happe, T., & Hemschemeier, A. (2012). Nitrogen deprivation results in photosynthetic hydrogen production in *Chlamydomonas reinhardtii*. *Planta, 235*(04), 729−745.

Posewitz, M. C., Dubini, A., Meuser, J. E., Seibert, M., & Ghirardi, M. L. (2009). Hydrogenases, hydrogen production, and anoxia. In D. B. Stern (Ed.), *The Chlamydomonas sourcebook: Organellar and metabolic processes* (2nd ed.), (Vol. 02, pp. 217−246). Academic Press.

Poudyal, R.S., Tiwari, I., Najafpour, M.M., Los, D.A., Carpentier, R., Shen, J-R., Allakhverdev, S.I. Current insights to enhance hydrogen production by photosynthetic organisms. In D. Stolten & B. Emonts (Eds.), *Hydrogen science and engineering*, Wiley-VCH Books, in press.

Prabina, B. J., & Kumar, K. (2010). Studies on the optimization of cultural conditions for maximum hydrogen production by selected cyanobacteria. *ARPN Journal of Agricultural Science and Biological Science, 05*(5), 22−31.

Prince, R. C., & Kheshgi, H. S. (2005). The photobiological production of hydrogen: potential efficiency and effectiveness as a renewable fuel. *Critical Reviews in Microbiology, 31*(1), 19−31.

Quintana, N., der Kooy, F. V., de Rhee, M. D. V., Voshol, G. P., & Verpoorte, R. (2011). Renewable energy from cyanobacteria: energy production optimization by metabolic pathway engineering. *Applied Microbiology and Biotechnology, 91*(3), 471−490.

Richau, K. H., Kudahettige, R. L., Pujic, P., Kudahettige, N. P., & Sellstedt, A. (2013). Structural and gene expression analyses of uptake hydrogenases and other proteins involved in nitrogenase protection in Frankia. *Journal of Bioscience, 38*(4), 703−712.

Rosner, V., & Wagner, H.-J. (2012). Life cycle assessment and process development of photobiological hydrogen production−from laboratory to large scale applications. *Energy Procedia, 29*, 532−540.

Rout, U. K., Akimoto, K., Sano, F., Oda, J., Homma, T., & Tomoda, T. (2008). Impact assessment of the increase in fossil fuel prices on the global energy system, with and without CO_2 concentration stabilization. *Energy Policy, 36*(9), 3477−3484.

Roy, S. C., Varghese, O. K., Paulose, M., & Grimes, C. A. (2010). Toward solar fuels: photocatalytic conversion of carbon dioxide to hydrocarbons. *ACS Nano, 04*(3), 1259−1278.

Rupprecht, J., Hankamer, B., Mussgnug, J. H., Ananyev, G., Dismukes, C., & Kruse, O. (2006). Perspectives and advances of biological H_2 production in microorganisms. *Applied Microbiology and Biotechnology, 72*(3), 442−449.

Saratale, G. D., Chen, S.-D., Lo, Y.-C., Saratale, R. G., & Chang, J.-S. (2008). Outlook of biohydrogen production from lignocellulosic feedstock using dark fermentation−a review. *Journal of Scientific and Industrial Research, 67*(11), 962−979.

Sathiyamoorthy, P., & Shanmugasundaran, S. (1994). A low-cost bioreactor for cyanobacterial biomass production. *Bioresource Technology, 49*(3), 279−280.

Seifert, K., Waligorska, M., & Laniecki, M. (2010). Brewery wastewaters in photobiological hydrogen generation in presence of *Rhodobacter sphaeroides* O.U. 001. *International Journal of Hydrogen Energy, 35*(9), 4085−4091.

Serebryakova, L. T., Shremetieva, M. E., & Lindbald, P. (2000). H_2-uptake and evolution in the unicellular cyanobacterium *Chroococcidiopsis thermalis* CALU 758. *Plant Physiology and Biochemistry, 38*(6), 525−530.

Shaishav, S., Singh, R. N., & Tripathi, S. (2013). Biohydrogen from algae: fuel of the future. *International Research Journal of Environment Sciences, 02*(4), 44−47.

Shima, S., Pilak, O., Vogt, S., Schick, M., Stagni, M. S., Meyer-Klaucke, W., et al. (2008). The crystal structure of [Fe]-hydrogenase reveals the geometry of the active site. *Science, 321*(5888), 572−575.

Show, K.-Y., Lee, D.-J., & Chang, J.-S. (2011). Bioreactor and process design for biohydrogen production. *Bioresource Technology, 102*(18), 8524−8533.

Singh, A., & Spiccia, L. (2013). Water oxidation catalysts based on abundant 1st row transition metals. *Coordination Chemistry Reviews, 257*, 2607−2622.

Skjånes, K., Knutsen, G., Källqvist, T., & Lindblad, P. (2008). H_2 production from marine and fresh water species of green algae during sulfur deprivation and considerations for bioreactor design. *International Journal of Hydrogen Energy, 33*(2), 511−521.

Skjånes, K., Rebours, C., & Lindblad, P. (2013). Potential for green microalgae to produce hydrogen, pharmaceuticals and other high value products in a combined process. *Critical Reviews in Biotechnology, 33*(2), 172−215.

Stal, L. J., & Krumbein, W. E. (1985). Oxygen protection of nitrogenase the aerobically nitrogen fixing, non-heterocystous cyanobacterium *Oscillatoria* sp. *Archives of Microbiology, 143*(1), 72−76.

Su, H., Cheng, J., Zhou, J., Song, W., & Cen, K. (2009a). Combination of dark- and photofermentation to enhance hydrogen production and energy conversion efficiency. *International Journal of Hydrogen Energy, 34*(21), 8846−8853.

Su, H., Cheng, J., Zhou, J., Song, W., & Cen, K. (2009b). Improving hydrogen production from cassava starch by combination of dark and photo fermentation. *International Journal of Hydrogen Energy, 34*(4), 1780−1786.

Sundaram, S., Tripathi, A., & Gupta, V. (2010). Structure prediction and molecular simulation of gases diffusion pathways in hydrogenase. *Bioinformation, 05*(4), 177−183.

Sunita, M., & Mitra, C. K. (1993). Photoproduction of hydrogen by photosynthetic bacteria from sewage and waste water. *Journal of Biosciences, 18*(1), 155−160.

Tamagnini, P., Axelsson, R., Lindberg, P., Oxelfelt, F., Wünschiers, R., & Lindbland, P. (2002). Hydrogenases and hydrogen metabolism of cyanobacteria. *Microbiology and Molecular Biology Reviews, 66*(01), 1−20.

Tamagnini, P., Leitão, E., Oliveira, P., Ferreira, D., Pinto, F., Harris, D. J., et al. (2007). Cyanobacterial hydrogenases: diversity, regulation and applications. *FEMS Microbiology Review, 31*(6), 692−720.

Thangaraj, A., & Kulandaivelu, G. (1994). Biological hydrogen photoproduction using dairy and sugarcane waste waters. *Bioresource Technology, 48*(1), 9−12.

Thiel, T. (1994). Genetic analysis of cyanobacteria. In D. A. Bryant (Ed.), *The molecular biology of cyanobacteria. Advances in photosynthesis and respiration* (pp. 581−611). Dordrecht, The Netherlands: Kluwer Academic Publishers.

Tiwari, A., & Pandey, A. (2012). Cyanobacterial hydrogen production−a step towards clean environment. *International Journal of Hydrogen Energy, 37*(1), 139−150.

Tran, P. D., Wong, L. H., Barber, J., & Loo, J. S. C. (2012). Recent advances in hybrid photocatalysts for solar fuel production. *Energy and Environmental Science, 05*(3), 5902−5918.

Tsygankov, A. A. (2007). Nitrogen-fixing cyanobacteria. A review. *Applied Biochemistry and Microbiology, 43*(3), 250−259.

Uyar, B., Schumacher, M., Gebicki, J., & Modigell, M. (2009). Photoproduction of hydrogen by *Rhodobacter* capsulatus from thermophilic fermentation effluent. *Bioprocess and Biosystems Engineering, 32*(5), 603−606.

Vignais, P. M., & Billoud, B. (2007). Occurrence, classification, and biological function of hydrogenases: an overview. *Chemical Reviews, 107*(10), 4206−4272.

Vignais, P. M., Magnin, J.-P., & Willison, J. C. (2006). Increasing biohydrogen production by metabolic engineering. *International Journal of Hydrogen Energy, 31*(11), 1478−1483.

Walter, M. G., Warren, E. L., McKone, J. R., Boettcher, S. W., Mi, Q., Santori, E. A., et al. (2010). Solar water splitting cells. *Chemical Reviews, 110*(11), 6446−6473.

Warren, E. L., Atwater, H. A., & Lewis, N. S. (2014). Silicon microwire arrays for solar energy-conversion applications. *The Journal of Physical Chemistry, 118*(2), 747−759.

Weiss, A., Patyk, A., & Schebek, L. (2011). Nutrient recycling and energy production with microalgae from a life cycle perspective. In Gesellschaftzur Förderung des Instituts für Siedlungswasserwirtschaft der Technischen Universität Braunschweig e.V (Ed.), *Tagungsband 3. Internationales Symposium "Re-Water Braunschweig" 21. und 22. November 2011. Braunschweig: Institut für Siedlungswasserwirtschaft* (Vol. 81).

Williams, C. R., & Bees, M. A. (2013). Mechanistic modeling of sulfur-deprived photosynthesis and hydrogen production in suspensions of *Chlamydomonas reinhardtii*. *Biotechnology and Bioengineering, 111*(2), 320−335.

Winkler, M., Kuhlgert, S., Hippler, M., & Happe, T. (2009). Characterization of key step for light-driven hydrogen evolution in green algae. *The Journal of Biological Chemistry, 284*(52), 36620−36627.

Xia, L., Ge, H., Zhou, X., Zhang, D., & Hu, C. (2013). Photoautotrophic outdoor two-stage cultivation for oleaginous microalgae *Scenedesmus obtusus* XJ-15. *Bioresource Technology, 144*, 261−267.

Yang, Z., Guo, R., Xu, X., Fan, X., & Luo, S. (2011). Fermentative hydrogen production from lipid-extracted micro algal biomass residues. *Applied Energy, 88*(10), 3468−3472.

Yetiş, M., Gündüz, U., Eroğlu, I., Yücel, M., & Türker, L. (2000). Photoproduction of hydrogen from sugar refinery wastewater by *Rhodobacter sphaeroides* O.U. 001. *International Journal of Hydrogen Energy, 25*(11), 1035−1041.

Yonemoto, I. Y., Matteri, C. W., Nguyen, T. A., Smith, H. O., & Weyman, P. D. (2013). Dual organism design cycle reveals small subunit substitutions that improve [NiFe] hydrogenase hydrogen evolution. *Journal of Biological Engineering, 07*, 17.

Yoshino, F., Ikeda, H., Masukawa, H., & Sakurai, H. (2007). High photobiological hydrogen production activity of a *Nostoc* sp. PCC 7422 uptake hydrogenase-deficient mutant with high nitrogenase activity. *Marine Biotechnology, 09*(1), 101−112.

Zhou, H., Guo, J., Li, P., Fan, T., Zhang, D., & Ye, J. (2013). Leaf-architectured 3D hierarchical artificial photosynthetic system of perovskite titanates towards CO_2 photoreduction into hydrocarbon fuels. *Scientific Report, 3*, 1667. http://dx.doi.org/10.1038/srep01667.

Zhu, H., Suzuki, T., Tsygankov, A. A., Asada, Y., & Miyake, J. (1999). Hydrogen production from tofu wastewater by *Rhodobacter sphaeroides* immobilized in agar gels. *International Journal of Hydrogen Energy, 24*(4), 305−310.

Zuttel, A., Borgschulte, A., & Schlapbach, L. (Eds.). (2008). *Hydrogen as a future energy carrier* (Vol. 427). Weinheim: John Wiley & VCH, ISBN 978-3-527-30817-0.

This page intentionally left blank

Hydrogen production via thermochemical water splitting

11

M. Roeb, C. Agrafiotis, C. Sattler
German Aerospace Center (DLR), Köln, Germany

11.1 Introduction

The currently most used energy sources, fossil fuels, are limited and their combustion causes high amounts of carbon dioxide, resulting in global warming. For a sustainable energy economy and to reduce global warming, other energy sources are needed. Solar energy is a suitable candidate owing to its broad availability in many regions of the world. Main problems to overcome are intermittent availability and storage in transportable energy carriers, or solar fuels.

Hydrogen is a favorite option for such a solar fuel. In the near term, fossil fuels are the easiest and most economic resource for hydrogen production by either steam reforming of natural gas or decarbonization of materials such as coal or natural gas. However, in the long term, a sustainable energy economy will need other options to generate hydrogen. Simultaneous use of renewable energy and water as raw materials is a promising alternative.

The single-step thermal dissociation of water is, at a first glance, the simplest reaction to split water. However, because of its unfavorable thermodynamics, the process is one of the most challenging with respect to practical realization. Although water thermolysis is conceptually simple, the need for a high-temperature heat source above 2500 K to achieve a reasonable degree of dissociation and the need for an effective technique to separate H_2 and O_2 at high temperatures to avoid an explosive mixture of these two gases are major barriers to technical success. Water-splitting thermochemical cycles avoid the separation problem and allow operation at moderately high temperatures. Thermochemical cycles are a series of consecutive chemical reactions (two or more) their net sum is the splitting of H_2O to H_2 and O_2, in which the maximum temperature (endothermic) step takes place at a temperature lower than that of the single water decomposition chemical reaction. Examples of reaction cycles are provided in subsequent sections. Typical temperatures required for the high-temperature step of these cycles to reach full conversion range from 1100 to 2300 K. The necessary solar heat can be generated by concentrating optics that direct solar radiation into a single point in solar towers or central receiver systems.

The screening of and search for appropriate thermochemical cycles started in the 1960s; the number of theoretical candidates was immense (Funk & Reinstrom, 1966). Therefore, in the 1970s and early 1980s, many studies and comparisons were

Compendium of Hydrogen Energy. http://dx.doi.org/10.1016/B978-1-78242-361-4.00011-X

carried out to identify the most promising cycles based on different criteria such as thermodynamics, theoretical efficiency, and projected cost (Beghi, 1981, 1986; Funk, 1976; Pretzel & Funk, 1987). In general, most development effort applied during those years was promoted by research institutions and industries from the nuclear energy sector, with the intention of diversifying the use of thermal energy supplied by nuclear reactors. To this end, programs developed by the Joint Research Center (JRC) of the European Union in Ispra, Italy (Beghi, 1986); by General Atomics (Norman et al., 1982) and Westinghouse in the United States (Farbman, 1979), and by the Japanese Atomic Energy Research Institute (Shimizu, Onuki, & Nakajima, 1991) are particularly worth mentioning. In the late 1980s, interest in thermochemical cycles decreased drastically. Until the late 1990s only marginal progress was reported, mainly on the UT-3 cycle developed by and named after the University of Tokyo (Sakurai, Bilgen, Tsutsumi, & Yoshida, 1996) and on the sulfur−iodine cycle originally proposed and named after the company General Atomics (Brown et al., 2003).

Revival of research in and development of thermochemical cycles has taken place in the past few years. The driving force is the production of hydrogen as a greenhouse gas-free energy carrier to fulfill the requirements of the Kyoto Protocol. The goal of the Protocol is to lower overall emissions of six greenhouse gases − carbon dioxide, methane, nitrous oxide, sulfur hexafluoride, hydrofluorocarbons, and perfluorocarbons − averaged over the period of 2008−2012. National limitations range from 8% reductions for the European Union and some other regions to 7% for the United States (the United States signed but declined ratification of the treaty), 6% for Japan, and 0% for Russia, and permitted increases of 8% for Australia and 10% for Iceland.

As in the 1970s, prospective studies and comparative analyses of cycles have been frequent, but in addition, hardware has been developed and tested. In contrast to the work conducted 30−40 years ago, concentrated solar radiation has become more important as a heat source than nuclear heat. The first step of a solar-powered process requires the reflection and concentration of direct insolation using collectors or heliostats. Primarily four types of solar concentrating systems have been developed: parabolic trough, linear Fresnel, solar power tower, and dish, which provide in the listed order increasingly higher solar concentrations and increasingly higher process temperatures. Because process temperatures of several hundred up to more than 1300 K are required to drive thermochemical cycles, only solar towers and dishes remain the technologies of choice. Considering that hydrogen production plants require a certain size, most research and development work in this field concentrated on implementing thermochemical cycles with solar towers. Concentrating solar radiation is an important aspect of solar thermochemical water splitting. Another requirement is suitable materials for substrates and containments stable against the reaction system and environmental influences, in particular considering the harsh thermal conditions and chemical atmospheres they have to face. In this context, solar absorbance and resistance against thermal shock and fatigue also must be considered. Those aspects will be highlighted and analyzed for the most prominent thermochemical cycles in the following chapters. The analysis concentrates on the two currently most common families of cycles: sulfur and redox pair. The relevant receiver, reactor, and receiver reactor technologies developed for the different thermochemical processes will be presented as well.

11.2 Redox cycles based on metal oxide pairs and metal–metal oxide pairs

Redox-pair-based thermochemical cycles are composed of two reactions: water splitting and thermal reduction (regeneration), which occur at different temperatures. During the first, higher-temperature step (thermal reduction/TR), the oxidized form of the redox material – usually the higher-valence oxide of a metal exhibiting multiple oxidation states – releases a quantity of oxygen and transforms to its reduced (lower-valence) state; during the second (water-splitting/WS) step, the reduced and therefore activated material is oxidized back to the higher-valence one by taking oxygen from water and producing hydrogen, thus establishing a cyclic process. These reactions are generally described as follows:

$$MO_{oxidized} \rightarrow MO_{reduced} + {}^{1}\!/_{2}\,O_2(g) \tag{11.1}$$

$$H_2O(g) + MO_{reduced} \rightarrow MO_{oxidized} + H_2(g) \tag{11.2}$$

The same thermochemical principle can be exploited for carbon dioxide (CO_2) splitting (CDS) as well, for the production of CO, according to the following reaction scheme:

$$MO_{oxidized} \rightarrow MO_{reduced} + {}^{1}\!/_{2}\,O_2(g) \tag{11.3}$$

$$CO_2(g) + MO_{reduced} \rightarrow MO_{oxidized} + CO(g) \tag{11.4}$$

Hydrogen produced via reaction (11.2) and CO produced via reaction (11.4) can then be combined, leading to synthesis gas (syngas), which can be further used via the established Fischer–Tropsch (FT) technology to create any of a number of different product streams including diesel-like fuel, alcohols, and other chemicals. This has led various researchers (Chueh et al., 2010) to propose a solar syngas production scheme in solar reactors. The approach is conceptually simple because the thermal reduction step is common for both WS and CDS (reactions (11.2) and (11.4), respectively). Therefore, a particular redox material can be used for both water and CO_2 splitting either separately, i.e., to produce a stream of H_2 and a separate stream of CO, or simultaneously – when steam and CO_2 are co-fed above the redox material – to produce syngas in one step. In fact, because the experimental test rig for CDS is simpler, many materials are currently tested for CDS first rather than for WS.

Obviously, the oxygen yield during the first step depends on the extent of dissociation: The oxidized form of the redox material with the metal cation at its highest valence can dissociate either to a lower-metal-valence oxide or all the way to the respective metal (of zero valence). In this respect, highest possible dissociations are sought in principle because full replenishment of the oxygen released during dissociation by oxygen taken from H_2O/CO_2 during oxidation results in higher H_2/CO product yields per gram of redox material and thus higher cycle efficiencies. It is

unsurprising, therefore, that both kinds of system have been explored for hydrogen generation via the cycle above: either metal oxide−metal systems (e.g., ZnO/Zn) or metal oxide−metal oxide pairs. The latter category can be further distinguished into two subcategories: the first involves oxides of a single multivalent metal such as Fe_3O_4/FeO, Mn_3O_4/MnO, and the more recently tested CeO_2/Ce_2O_3. In these cases, starting from a higher-metal-valence oxide and assuming that all metal cations change valence from the higher to the lower number during reduction, and vice versa during oxidation, reactions (11.1) and (11.2) can be written with the following exemplary specific stoichiometry for example, the Fe_3O_4/FeO and CeO_2/Ce_2O_3 systems:

$$Fe_3O_4 \rightarrow 3FeO + {}^1/_2\,O_2(g) \tag{11.5}$$

$$H_2O(g) + 3FeO \rightarrow Fe_3O_4 + H_2(g) \tag{11.6}$$

$$2CeO_2 \rightarrow Ce_2O_3 + {}^1/_2\,O_2(g) \tag{11.7}$$

$$H_2O(g) + Ce_2O_3 \rightarrow 2CeO_2 + H_2(g) \tag{11.8}$$

The second subcategory involves oxides containing multiple metal cations that can demonstrate various valence states, such as spinels and perovskites. Spinels and perovskites are of the general formulas AB_2O_4 and ABO_3, respectively; however, more than one cation of the same valence can occupy the A or B sites: for instance, $(A_x,B_{1-x})^{+2}(C_y,D_{2-y})^{+3}O_4$ and $(A_x,B_{1-x})^{+2}(C_y,D_{2-y})^{+4}O_3$ are typical formulas with two metal cations at each site.

Both single- and multi-metal multivalent metal oxides such as Fe_3O_4, CeO_2, ferrites, and perovskites form a wide range of nonstoichiometric compounds denoted as $Fe_3O_{4\pm\delta}$, $CeO_{2\pm\delta}$, $AB_2O_{4\pm\delta}$, and $ABO_{3\pm\delta}$, respectively. On the other hand, the TR step takes place at much higher temperature levels (1600−1900 K, depending on the redox material used) than the splitting reaction (1000−1300 K). This TR is actually a step that needs to be solar-aided but reactor operation conditions are challenging, resulting in complex situations in relation to reactor construction and oxide material handling between the two stages. High TR temperatures may cause evaporation of volatile compounds present in the redox material, reactant loss or composition changes, activity reduction, or side reactions with the reactor materials. Therefore, when lower TR temperatures are selected to avoid such phenomena, the reduction reactions do not proceed as the theoretical schemes as shown in Eqns (11.5), (11.6), (11.7), and (11.8), but rather under the following schemes represented in Eqns (11.9)−(11.12) for a mixed ferrite and ceria, respectively:

$$(A_xB_{1-x})Fe_2O_4 \rightarrow (A_xB_{1-x})Fe_2O_{4-\delta} + \delta/2\ O_2(g) \tag{11.9}$$

$$\delta\ H_2O(g) + (A_xB_{1-x})Fe_2O_{4-\delta} \rightarrow (A_xB_{1-x})Fe_2O_4 + \delta\ H_2(g) \tag{11.10}$$

$$CeO_2 \rightarrow 1/\delta\ CeO_{2-\delta} + \delta/2\ O_2(g) \tag{11.11}$$

$$\delta\ H_2O(g) + CeO_{2-\delta} \rightarrow CeO_2 + \delta\ H_2(g) \tag{11.12}$$

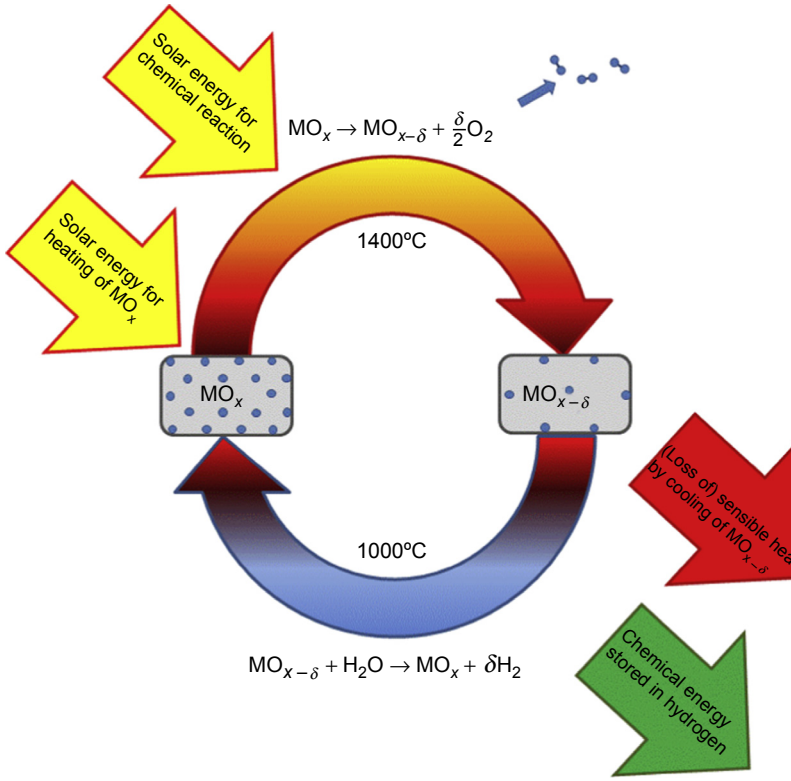

Figure 11.1 General scheme of a two-step redox-pair-based thermochemical cycle.

In other words, the reduction product does not contain all reducible metal cations at their lower-valence state but only a smaller percentage of them because δ is much smaller than 1. As a result, this end up with much less oxygen during the TR step and the consequent generation of less H_2 at the subsequent WS step, and thus overall lower cycle efficiency. An advantage of this is that one can make use of the percentage of the divalent metal(s) present in the single/mixed oxide phase and oscillate during the redox cycle between the activated and nonactivated structure without undergoing phase transformations (such as to the lower-valence metal oxide or to the respective metal), which can cause structure disruption. This generic scheme is depicted in Figure 11.1. The various redox pair categories used so far are also described in detail in Figure 11.1.

11.2.1 The Zn/ZnO cycle

One well-known candidate redox pair for a 2-step cycle is ZnO/Zn. Several chemical aspects of the thermal dissociation of ZnO have been investigated (Palumbo et al., 1998). Work originally focused mostly on the application of this cycle for WS and

hydrogen generation, but investigations into CDS have come into play (Galvez, Frei, Albisetti, Lunardi, & Steinfeld, 2008; Loutzenhiser, Elena Galvez, Hischier, Graf, & Steinfeld, 2010; Steinfeld, 2002).

For the water-splitting cycle, exergy efficiency reaches 29% with no heat recovery (Steinfeld, 2002). The theoretical upper limit in exergy efficiency, with complete heat recovery during quenching and hydrolysis, is 82%. An examination (Loutzenhiser & Steinfeld, 2011) used with a second-law of thermodynamic analysis to assess the potential of the cycle for syngas production. At 2235 K and 1 bar, where $\Delta G = 0$, and for a desired syngas with a molar ratio H_2:CO equal to 2, which is optimal for Fischer–Tropsch and methanol syntheses, the cycle efficiency reaches 31.5% when heat recuperation is not employed. At 2030 K, cycle efficiencies of up to 52.1% are attainable with a molar ratio of H_2:CO of 2 by recuperating the sensible and latent heat of the hot products exiting the solar reactor and the heat rejected by the reaction of Zn with H_2O/CO_2. The most challenging part of this process is the reduction of ZnO via solar decomposition into Zn and $^1/_2O_2$. The reaction rate law and Arrhenius parameters for this reaction were derived for the case of directly solar irradiated ZnO pellets (Möller & Palumbo, 2001b). The condensation of zinc vapor in the presence of O_2 by fractional crystallization in a temperature-gradient tube furnace has also been studied (Weidenkaff et al., 1999). The oxidation of Zn is a heterogeneous process, and in the absence of nucleation sites, Zn(g) and O_2 can coexist in a metastable state. Otherwise, the product mixture needs to be quenched to avoid recombination. In particular, the quenching efficiency is sensitive to the dilution ratio of Zn(g) in an inert gas flow and to the temperature of the surface on which the products are quenched. Separation at high temperatures would enable recovery of the sensible and latent heat of the products.

Several experimental tests on the dissociation of ZnO were carried out in solar furnaces (Bilgen, Ducarroir, Foex, Sibieude, & Trombe, 1977; Möller & Palumbo, 2001a; Palumbo et al., 1998). A solar chemical reactor concept was developed and tested by Eidgenössische Technische Hochschule Zurich (ETH) in cooperation with Paul-Scherer-Institute (PSI) (Haueter, Moeller, Palumbo, & Steinfeld, 1999). It is a windowed rotating cavity-receiver lined with ZnO particles held by centrifugal force. In this reactor, ZnO is directly exposed to high-flux solar irradiation and simultaneously serves the functions of radiant absorber, thermal insulator, and chemical reactant. Solar tests carried out with a 10-kW prototype (Figure 11.2) at temperatures above 2000 K subjected to peak solar concentration ratios exceeding 4000 suns proved the low thermal inertia of the reactor system, its resistance to thermal shock, and the functionality of the overall engineering design (Loutzenhiser, Meier, & Steinfeld, 2010).

Nonsolar exothermic oxidation of Zn by H_2O and/or CO_2 to form fuel (H_2 and/or CO) has been investigated (Stamatiou, Steinfeld, & Jovanovic, 2013). The presence of inert ZnO affects both the oxidation kinetics and the final asymptotic conversion of Zn. The effect of dilution with inert particles on the Zn oxidation was analyzed. The presence of Al_2O_3 diluent had no positive effect on asymptotic conversion of Zn, whereas the presence of solid ZnO diluent generally increased asymptotic conversion of Zn and made it less affected by CO_2 concentration in the gas phase. At 400 °C, about 95% of Zn was converted into the product after being diluted with 50 wt% ZnO, resembling the composition of a typical product mixture generated in a solar reactor.

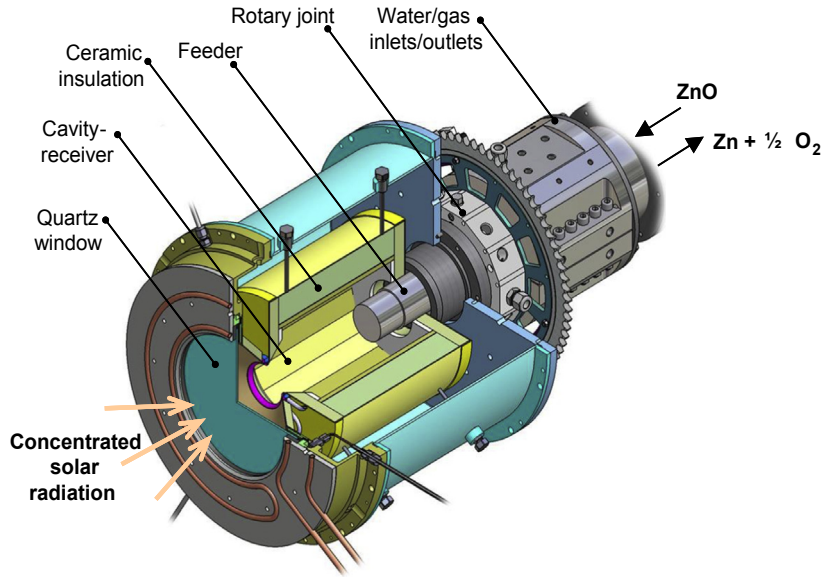

Figure 11.2 Ten-kilowatt solar rotary reactor prototype for ZnO reduction tested at PSI. (Loutzenhiser, Meier, et al., 2010).

This process is currently being demonstrated at the Megawatt Solar Furnace (MWSF) at the Laboratoire Procédés, Matériaux et Energie Solaire research facility in Odeillo, France (CNRS-PROMES, 2010). In this context, a 100-kW solar pilot reactor for the thermal dissociation of ZnO was designed (Gstoehl, Cooper, Villasmil, & Meier, 2010). The reactor features a rotating cavity-receiver lined with ZnO particles. With this arrangement, ZnO is directly exposed to concentrated solar radiation and simultaneously functions as a radiant absorber, chemical reactant, and thermal insulator. Testing campaigns were carried out in 2012 and 2013 (Meier, 2013). During those campaigns the solar reactor was operated at temperatures up to 1936 K, yielding a Zn molar fraction of the condensed products in the range 12–49% that largely depended on the flow rate of Ar injected to quench evolving gaseous products (Villasmil, Brkic, Wuillemin, Meier, & Steinfeld, 2014).

Owing to the extreme conditions regarding temperature and the separation of zinc and oxygen, another process was developed using additional carbon-containing raw materials to promote the reduction of ZnO. This constitutes an open thermochemical cycle, which is not free of CO_2 emissions and therefore is thought of as a process option for a transition period leading from fossil fuel-based hydrogen to hydrogen produced only by renewable resources. In the reduction process, a mixture of ZnO and carbon is converted into Zn and CO at temperatures above 1500 K. The Zn is condensed from the flow of waste gas. The stored energy and produced CO can be used for H_2 production by zinc hydrolysis and the Water–gas shift reaction. The zinc can also be used in zinc–air fuel cells for direct power generation. In both

cases, ZnO is formed, which can be returned to the reactor. After laboratory-scale experiments and the construction and testing of a small-scale solar chemical reactor (Kräupl, Frommherz, & Wieckert, 2006), a pilot plant was successfully tested. The setup is shown in Figure 11.3. With the use of biomass as a carbon source, the technology becomes CO_2 neutral, as demonstrated in test series (Wieckert et al., 2007).

11.2.2 The ferrite cycle

The concept of using oxide pairs of multivalent metals for thermochemical production of hydrogen first appeared in the literature in 1997, when cycling between Fe_3O_4/FeO (magnetite−wüstite) under the pair of reactions (11.5) and (11.6) above was proposed (Nakamura, 1977). This approach introduced the notion of metal oxides as thermochemical reaction media and a new strategy for thermochemical fuel production (Chueh & Haile, 2010). The first such systems studied for solar-aided WS were oxide pairs of multivalent metals such as iron oxides Fe_3O_4/FeO (Charvin, Abanades, Flamant, & Lemort, 2007; Steinfeld, Sanders, & Palumbo, 1999) or Mn_3O_4/MnO (Sibieude et al., 1982; Sturzenegger & Nüesch, 1999), with which the proof-of-concept of the particular process was demonstrated. However, although such reaction schemes led to high theoretical efficiencies, practical problems occurred during their actual implementation. For instance, the thermochemistry

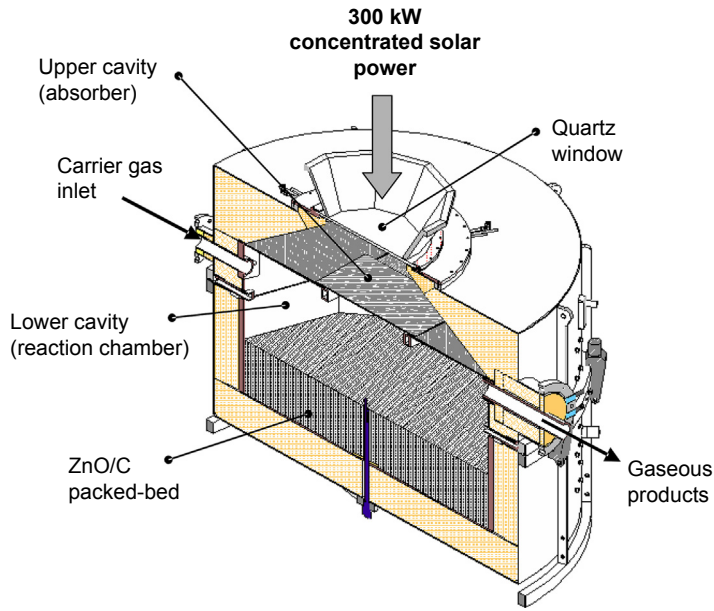

Figure 11.3 SolZinc reactor, featuring two cavities in series, with the upper one functioning as the solar absorber and the lower one as the reaction chamber containing a ZnO/C packed-bed (Wieckert, Frommherz, et al., 2007).

of the Fe_3O_4/FeO pair of reactions is such that (under standard pressures) the first is favored at temperatures above 3100 K and the latter at temperatures around 1000−1200 K. The extremely high temperatures required for the reduction step, which exceed the melting temperatures of both FeO and Fe_3O_4, render this specific cycle impracticable.

To lower the temperature of the reduction step, substitution of Fe by more easily reducible metals has been pursued. It has been reported that partial substitution of iron in the magnetite phase by Mn, Ni, or Zn forms mixed-metal oxides of the type MFe_2O_4 (mixed ferrites) that are more reducible and require moderate, upper (thermal reduction) operating temperatures. A whole series of such ferrites has been tested experimentally and studied thermodynamically, including either only one divalent metal cation in the M site, such as $MnFe_2O_4$ (Tamaura et al., 1999), $ZnFe_2O_4$ (Aoki, Kaneko, et al., 2004; Kaneko et al., 2004), $NiFe_2O_4$ (Agrafiotis, Zygogianni, Pagkoura, Kostoglou, & Konstandopoulos, 2013; Fresno, Yoshida, Gokon, Fernandez-Saavedra, & Kodama, 2010; Gokon, Takahashi, Yamamoto, & Kodama, 2008; Gokon, Mataga, Kondo, & Kodama, 2011), or $CoFe_2O_4$ (Miller et al., 2008), or two such cations—i.e., of the type $(C_xD_{1-x})^{+2}Fe_2^{+3}O_4$—including $Ni_{0.5}Mn_{0.5}Fe_2O_4$ (Tamaura et al., 1998; Tamaura, Steinfeld, Kuhn, & Ehrensberger, 1995), $Mn_{0.5}Zn_{0.5}Fe_2O_4$ (Inoue et al., 2004), and other cation stoichiometries (Allendorf, 2008; Kodama & Gokon, 2007; Kojima et al., 1996; Miller et al., 2006). However, their thermal reduction temperatures are still high ($\approx$1600−1700 K), which is an important drawback because it can cause significant sintering of the metal oxide. Attempts to tackle this problem have been realized by supporting the redox reagent on high-temperature-stable ZrO_2 fine particles or supports (Gokon, Mizuno, Nakamuro, & Kodama, 2008; Kodama, Nakamuro, & Mizuno, 2006; Scheffe et al., 2013).

With respect to materials composition, the current consensus seems to be that among the many ferrite materials tested for the targeted application, Zn-containing ones exhibit Zn-volatilization problems and Mn-containing ones have phase stability problems under air atmosphere at high temperatures (Agrafiotis et al., 2012; Fresno et al., 2009; Rosmaninho et al., 2011; Tsuji, Togawa, Wada, Sano, & Tamaura, 1995). These facts leave only $NiFe_2O_4$ and $CoFe_2O_4$ as the most robust ferrites capable of operating reliably at the real conditions of a solar-aided process.

11.2.3 The ceria cycle

In the quest for metal oxide redox pairs with satisfactory behavior, the CeO_2/Ce_2O_3 system, known for its extensive use in automotive emission exhaust after-treatment as an oxygen storage system, has gained attention. Results from studies of Sandia National Laboratories in the United States that compared the thermodynamics of the WS and CDS processes and considered CeO_2 to be a redox material (Miller, 2007) indicated that at any temperature below about 1800 K, reduction of CO_2 to CO by Ce_2O_3 (the reduced form of CeO_2 according to reaction (11.7)) is thermodynamically favored, and furthermore, at temperatures greater than 1100 K, CO_2 reduction is more favored than H_2O reduction. Similar efforts were extended to ferrites (Miller et al., 2009). Researchers from ETH, Switzerland, modeled oxygen non-stoichiometry of

several doped cerium oxide-based materials as a function of temperature and oxygen partial pressure (Scheffe & Steinfeld, 2012). Above 1200 K, ceria was found to react more efficiently with H_2O and CO_2 as the dopant concentration increased.

The group of CNRS-Odeillo, France also investigated ceria as a redox pair material for WS. Dissociation of CeO_2 to Ce_2O_3 was achieved via a solar reactor at pressures of 100−200 mbar and temperatures higher than 2220 K, in which CeO_2 was already in the molten state (Abanades & Flamant, 2006). Subsequently, thermal reduction of CeO_2 was studied by TGA in an N_2 stream at 1773 K, whereas WS was performed in a separate packed-bed reactor in the temperature range 973−1318 K (Abanades et al., 2010). The addition of a cationic element M^{y+} into the ceria structure was considered to favor oxygen ion mobility during reduction. The elements considered were Al, Mn, Fe, Co, Cu, Zn, Zr, and yttria-stabilized zirconia (YSZ); ceria reduction yielding Ce(III) species was obtained only in the case of Zr and YSZ, whereas addition of zirconium (up to 50 mol.%) improved reduction yield and suppressed sublimation of the solid-oxide solution.

The ETH researchers in collaboration with researchers from Caltech, United States employed CeO_2 and $Sm_{0.15}Ce_{0.85}O_{1.925}$ annealed for 3 h at 1773 K to perform WS and CDS separately (Chueh & Haile, 2010). In the former case, the materials were shaped in the form of 65% porous pellet monoliths loaded into a tubular reactor inside an infrared furnace and operated for 400 cycles. With respect to the TR step, upon heating to 1773 K under an inert atmosphere ($p_{O_2} = 10^{-5}$ atm), release of oxygen was observed, whereas ceria reduction at 1873 K resulted in higher oxygen yield. Hydrogen production was observed by introducing steam at 1073 K, with the total amount of hydrogen produced implying complete reoxidation of the reduced ceria. The first solar campaign was reported by the same group (Chueh et al., 2010) employing a cavity-receiver containing a porous monolithic ceria cylinder directly exposed to concentrated solar radiation impinging on its inner walls for the (separate) two-step, solar-driven thermochemical WS and CDS. Thermal reduction of ceria was performed at $\approx$1873 K and CDS at $\approx$1173 K. An analogous set of experiments was performed for H_2O dissociation for 500 WS cycles, in which the most obvious feature was the much faster rate of fuel production than that of O_2 release. In a subsequent work, Furler et al. (2012) employed a solar cavity-receiver containing porous ceria felt directly exposed to concentrated thermal radiation provided by a solar simulator. Thermal reduction of ceria was performed at 1800 K and reoxidation with a gas mixture of H_2O and CO_2 (varying concentrations of the two compounds) at 1100 K, producing syngas with H_2/CO molar ratios from 0.25 to 2.34. Although CeO_2 sublimation was observed, 10 consecutive H_2O/CO_2 gas-splitting cycles were performed. Based on this, the researchers prepared and tested at a laboratory-scale solar-thermal high-temperature chemistry configuration (1873 K) reticulated porous ceramic foams manufactured entirely from cerium oxide (CeO_2) to split CO_2 via thermochemical redox cycles (Furler, Scheffe, & Steinfeld, 2012).

Ceria offers several benefits for thermochemical cycling over alternative metal oxide systems: Oxygen-deficient ceria shows good reactivity with water and satisfactory H_2 production yield. However, it has its own set of challenges, the most significant of which is the requirement of high thermal reduction temperatures—higher than those of

the ferrites—to attain significant reduction efficiency. At such high temperatures (higher than 1800 K), partial sublimation of ceria occurs, which gradually decreases the reduction yield (Abanades et al., 2010).

11.2.4 The hercynite cycle

As mentioned, (doped) ferrites belong to the family of spinel materials, AB_2O_4, which are known for high thermal stability. In this respect, ferrospinels (ferrites) of the general formula $(A_x,B_{1-x})^{+2}Fe_2^{+3}O_4$, with elements A and B being bivalent metal cations such as Mn, Ni, or Zn, are considered state-of-the-art materials for performing such solar-aided water-splitting thermochemical cycles. However, another spinel material family, (doped) aluminum spinels of the formula $(A_x,B_{1-x})^{+2}Al_2^{+3}O_4$, with cations A and B being iron and/or copper, were proposed in the literature as thermochemical water splitters. The rationale is to exploit the redox effect of iron oxides in conjunction with the thermal stability of aluminum oxides. For instance, Al-Cu ferrites with various Cu/Al/Fe cation ratios have been synthesized and tested (Kaneko et al., 2006); such systems exhibited lower thermal reduction temperatures than $NiFe_2O_4$ and $ZnFe_2O_4$. A mixed cobalt ferrite−hercynite system ($CoFe_2O_4/FeAl_2O_4$) was proposed by researchers from the University of Colorado, United States as an effective water-splitting−thermal reduction system (Scheffe, Li, & Weimer, 2010); in fact, the hercynite occurred as a result of the reaction between $CoFe_2O_4$ and Al_2O_3 (the ferrite was deposited on an Al_2O_3 support) at the elevated temperatures employed during testing of the ferrite in cyclic experiments. In this case, the redox pair reactions are as follows:

$$CoFe_2O_4 + 3Al_2O_3 \rightarrow CoAl_2O_4 + 2FeAl_2O_4 + {}^1/_2O_2(g) \quad (11.13)$$

$$CoAl_2O_4 + 2FeAl_2O_4 + H_2O(g) \rightarrow CoFe_2O_4 + 3Al_2O_3 + H_2(g) \quad (11.14)$$

Very low thermal reduction temperatures (reaction (11.13), 1213 K, ~ 200 K lower than that of $CoFe_2O_4$) have been attributed to a reaction between the ferrite and Al_2O_3, resulting in the formation of the stable aluminates such as $FeAl_2O_4$ and $CoAl_2O_4$, which are thermodynamically more favorable than the formation of solid solutions or vacancies. In addition, $CoFe_2O_4/Al_2O_3$ was capable of being cycled between 1473 (TR) and 1273 K (WS) and produced significant amounts of H_2 with no obvious changes in H_2 conversion.

11.2.5 The perovskite cycle

Other mixed oxides such as perovskites have been explored. Interestingly, although perovskites are also nonstoichiometric compounds and can operate in a reaction pair scheme similar to that of Eqns (11.1) and (11.2) above, they were not employed at first in such a thermal reduction−water-splitting scheme. Instead, a chemical reduction was employed in combination with a mixed oxygen-ion and electron-conducting (MIEC) membrane reactor concept proposed almost simultaneously and independently by one Greek group (Evdou, Nalbandian, et al., 2008; Evdou, Zaspalis, & Nalbandian, 2008)

and one German research group (Jiang, Wang, Werth, Schiestel, & Caro, 2008). This concept is based on continuously extracting oxygen from the reaction products and thus shifting the equilibrium of the TR reaction. This efficient removal of oxygen at high temperatures can be achieved by MIEC membranes with high oxygen permeability, such as dense perovskite membranes that can act as oxygen transfer materials when a difference in oxygen concentration is established along their sides. Figures 11.4 and 11.5, extracted from the relevant publications, show the operating principle of this concept. In compartment 1 (Figure 11.4) an oxygen-vacancy-containing material reacts with water vapor to fill the vacancies with oxygen. This leads to the simultaneous production of hydrogen. The lattice oxygen ions are transported through the membrane to the opposite side, at compartment 2, which is kept at low or zero partial pressure of oxygen, where they desorb to produce gaseous oxygen and oxygen vacancies. Alternatively, an oxidizable compound (CX, e.g., methane CH_4) can be fed in compartment 2, acting as an oxygen sink to facilitate the membrane regeneration and vacancy creation process. In this respect, the two reactions, H_2O/CO_2 splitting and methane reforming, can be combined in a single reactor, producing simultaneously hydrogen and syngas, respectively. This concept has been further elaborated in a series of publications (Evdou, Zaspalis, & Nalbandian, 2010; Nalbandian, Evdou, Zaspalis, et al., 2009, 2011). This route has the inherent advantage of being isothermal and continuous; however, it also requires elevated temperatures (in the order of 1023−1273 K, depending on the perovskite's composition), and thus external heating, which can be also accomplished via

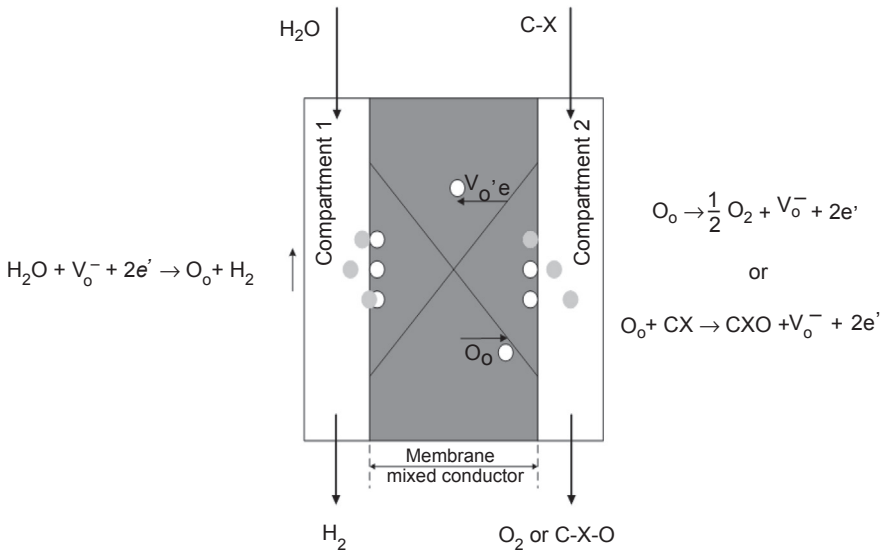

Figure 11.4 Schematics of the membrane reactor operating principle for simultaneous production of hydrogen and syngas in a perovskite oxygen-permeable membrane, in which $V_o^{\bullet\bullet}$ denotes a positively charged oxygen vacancy, e^- a negatively charged electron, and O_o lattice oxygen, according to the Kröger−Vinck notation
Adapted from Evdou, Nalbandian, et al. (2008).

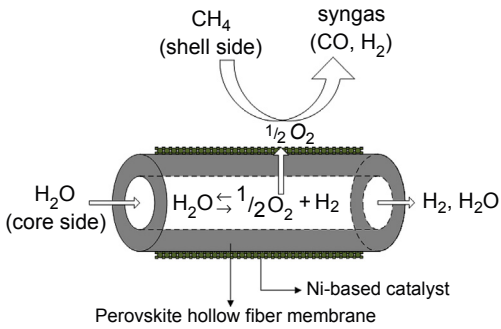

Figure 11.5 Schematics of the membrane reactor operating principle for simultaneous production of hydrogen and syngas.
Adapted from Jiang et al. (2008).

solar energy. On the other hand, these temperatures are significantly lower than the thermal reduction temperatures of state-of-the art redox oxide materials currently employed in CSP-aided water splitting, such as mixed ferrites (TR ≈ 1623−1723 K) or ceria (TR ≈ 1723−1873 K). The two groups performed water-splitting experiments with laboratory-scale cylindrical or disc-shaped, single-membrane modules employing different perovskite formulations: the Greek group used ironate compositions of the type $La_{1-x}Sr_xM_yFe_{1-y}O_{3-\delta}$(M = Ni, Co, Cu, Cr) and the German group used compositions of the type $Ba_{1-x}Sr_xCo_yFe_{1-y}O_{3-\delta}$ (BSCF/BSFZ, respectively). In both cases, an Ni-based reforming catalyst is coated on the fuel side wall to convert the methane to syngas.

Thermal dissociation studies of perovskites from some of the research groups mentioned previously appeared in the literature. Researchers from ETH thermodynamically and experimentally investigated lanthanum−strontium−manganate/$La_{1-x}Sr_xMnO_{3-\delta}$ perovskites for both WS and CDS (Scheffe et al., 2013). Thermal reduction results at 1273 K corroborated the higher O_2 yield of perovskites compared with that of ceria; however, the perovskites were characterized by incomplete reoxidation from CO_2 at 1073, 1173, and 1273 K. A subsequent study from Sandia (McDaniel et al., 2013) on lanthanum−strontium−aluminates ($La_{1-x}Sr_xMn_yAl_{1-y}O_{3-\delta}$) tested on WS as well as on CDS reported much higher reduction than for ceria, and was also achieved at about 300 K lower temperature as well as with multicyclic capability between 1623 (TR) and 1273 K (WS or CDS).

11.2.6 Technical issues and reactor concepts

Although it has been demonstrated experimentally up to a pilot solar-plant level, CSP-aided WS still has to resolve several technical barriers to reach full technical maturity for large-scale implementation. A major one toward commercialization of the process is that the thermal reduction step takes place at much higher temperature levels (1600−1900 K, depending on the redox material used) than the splitting reaction (1000−1300 K). This is a common problem for all single- and mixed-oxide redox systems mentioned. This TR is actually the step that needs to be solar-aided, but reactor operation conditions are challenging and result in complex situations in relation to reactor construction and oxide material handling between the two stages. The high

TR temperatures may cause evaporation of volatile compounds present in the redox material, reactant loss or composition changes, activity reduction, or side reactions with the reactor materials.

Despite early basic research with respect to active redox pairs, relevant solar reactor concepts were reported in the literature much later. The HYDROSOL research group (including, among others, the current authors) introduced the concept of monolithic, honeycomb solar reactors for performing redox pair cycles for the production of hydrogen from splitting steam using solar energy (Agrafiotis, Roeb, et al., 2005; Roeb et al., 2006). The reactor, inspired from well-known automobile catalytic converters, has no moving parts and is based on the incorporation of active redox pair powders as coatings on multichanneled monolithic honeycomb structures capable of achieving and sustaining high temperatures when irradiated with concentrated solar irradiation (Agrafiotis et al., 2007). When steam passes through the solar reactor, the coating material splits water vapor by trapping its oxygen and leaving in the effluent gas stream pure hydrogen. In a subsequent step, the oxygen-trapping coating is thermally reduced by increasing the amount of solar heat absorbed by the reactor. A modular, dual-chamber, ferrite-based, redox-material-coated-honeycomb HYDROSOL reactor was scaled up to the 100-kW level, coupled with a solar tower facility (Plataforma Solar de Almeria, Spain) (Figure 11.6), and achieved continuous, solar-operated, water-splitting–thermal reduction cycles, demonstrating the "proof-of-concept" of the proposed design (Roeb et al., 2011).

Several other solar reactor types were subsequently proposed and reviewed (Agrafiotis, Pagkoura, Lorentzou, Kostoglou, & Konstandopoulos, 2007). Researchers from the University of Tokyo, Japan, introduced a rotary-type reactor in which a cylindrical rotor coated with redox pair of materials such as CeO_2 and mixed ferrites ($Ni_{0.5}Mn_{0.5}Fe_2O_4$) rotates between two chambers, one in which the water-splitting reaction is performed and one where thermal regeneration is performed (Kaneko, Fuse, Miura, Ishihara, & Tamaura, 2006). The research group at Niigata University in Japan proposed a spouted bed-type reactor in which redox powders of $NiFe_2O_4/ZrO_2$ are irradiated by concentrating solar irradiation (Gokon et al., 2008, 2011; Gokon, Yamamoto, Kondo, & Kodama, 2010). In the United States, the research group at Sandia National Laboratories developed

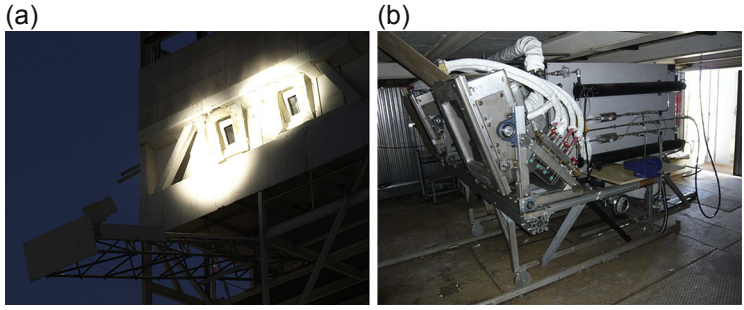

Figure 11.6 Actual dual-chamber, HYDROSOL reactor, and concept demonstration at the Plataforma Solar de Almería, Spain.

a counter-rotating-ring receiver/reactor/recuperator consisting of a stack of counter-rotating disks with fins constructed from a reactive cobalt ferrite material, situated along the perimeter of each disk. Concentrated solar flux illuminates the stack of disks/fins, heating the fins to temperatures in excess of 1373 K. This results in thermal reduction of a portion of the iron in the ferrite from Fe(III) to Fe(II), and the evolution of O_2. On the opposite side of the stack, the reduced ferrite is exposed to steam at a lower temperature, resulting in reoxidation of the ferrite and evolution of H_2 (Diver, Miller, Allendorf, Siegel, & Hogan, 2006; Miller et al., 2006). In another design (Ermanoski, Siegel, & Stechel, 2013), oxidized particles are elevated by a vertical screw elevator with a rotating casing toward the reduction chamber where concentrated solar radiation enters through a window-covered aperture, as a moving packed-bed in a counter-flow arrangement with respect to the reduced particles moving downward toward the fuel production chamber, inducing a heat recuperation effect. Finally, the particles in the fuel production chamber are exposed to reactant gases (H_2O or CO_2), reducing them to fuel products (H_2 or CO); the mix of reactants and products (H_2O/H_2 or CO_2/CO) is removed from the chamber and the reoxidized particles empty into a return elevator that brings them to the inlet of the recuperator/elevator. However, none of these reactors that include moving parts has been successfully scaled up so far.

Thermal reduction requires high temperatures and low oxygen partial pressures, whereas oxidation is favored by lower temperatures and high partial pressures of steam. However, the reaction kinetics needs to be considered, which imposes restrictions on the temperature of water oxidation: If the temperature of this step is too low, the reaction becomes too slow and thus is inapplicable. Therefore, all categories of solar reactors mentioned above, irrespective of their operating principle—except the (nonsolar) membrane reactor mentioned in Section (e)—operate under a temperature swing. In such an operation, associated heat losses, if heat recovery (Figure 11.1) is not performed sufficiently, can be detrimental for the efficiency and economics of the process (Roeb & Sattler, 2013).

To overcome the problems of cyclic WS-TR mentioned, the hercynite reaction scheme was also proposed by the research group at the University of Colorado (Muhich et al., 2013) in conjunction with an isothermal two-step process, because the forward and reverse reactions can take place at the same temperature (Shah, Kim, Zhou, Fornasiero, & Gorte, 2006). By performing both reactions (11.9) and (11.10) at 1623 K, the researchers demonstrated that hercynite can split water into a two-step isothermal cycle with much higher H_2 yield than a ceria redox cycle performed between 1623 K (TR) and 1273 K (WS), thus avoiding the need for temperature swings and reduced efficiency. However, isothermal cycles in a real-scale solar reactor will face the problem of spatial competition between oxidation and reduction. It seems unavoidable that at some regions of the reactor at least local oxygen evolution will coexist with hydrogen evolution. In the best case, this can reduce the efficiency/product yield of the process owing to recombination; in the worst case it could lead to explosive mixtures. It seems that the only way to perform isothermal cycles is by physically separating in the process oxygen from hydrogen in situ, e.g., by an oxygen-conducting membrane.

11.3 Sulfur and sulfuric acid-based cycles

11.3.1 The hybrid sulfur cycles

The hybrid sulfur cycle, also known as the Westinghouse cycle or ISPRA Mark 11 cycle, is a hybrid electrochemical–thermochemical cycle (Bilgen, 1988). It was originally proposed in 1975 (Brecher & Wu, 1975) and developed by Westinghouse Electric Corporation. It is a two-step cycle consisting of the splitting of sulfuric acid, which is divided into two substeps (the vaporization and the dissociation of sulfuric acid (15)) and the decomposition of the resulting SO_2 (16):

$$H_2SO_4 \rightarrow H_2O(g) + SO_3(g) > 723\ K \tag{11.15}$$

$$SO_3(g) \rightarrow SO_2(g) + \tfrac{1}{2}O_2(g) > 1123\ K \text{ with catalyst (1423 K without catalysts)} \tag{11.16}$$

$$2H_2O + SO_2 \rightarrow H_2SO_4 + H_2(g)\ 353\ K, \text{ electrolysis} \tag{11.17}$$

This process is called a hybrid cycle because of the combination of the thermal decomposition of sulfuric acid with the electrochemical oxidation of SO_2. This requires electrical power but it is more efficient than the electrolytic splitting of water. The voltage needed for the electrolysis is 0.17 V and therefore is much lower than the 1.23 V needed for water electrolysis, which reduces electrical power consumption. Sulfuric acid is vaporized to produce steam and sulfur trioxide, which is decomposed at a high temperature in the presence of a catalyst into sulfur dioxide and oxygen. This reaction is better performed at higher temperatures that can be reached with concentrated solar energy. The overall thermal efficiency of the process is calculated to be about 40% (Bilgen, 1988). Savannah River National Laboratory (SRNL) conducted a lot of work on electrolyzer and component development as well as on flow sheet modeling (Gorensek & Summers, 2009; Summers & Gorensek, 2006). Carbon-supported platinum electrodes are used for SO_2 oxidation. Cells made from ceramics such as silicon carbide, silicon nitride, and cermets have excellent resistance to corrosion by sulfuric acid at ambient temperature and at a low acid concentration. Catalysts principally based on iron oxide are available for accelerating the reaction rate of the SO_3 reduction at temperatures of 1123 K. The kinetics of the reaction is much faster if higher temperatures are available. Therefore, the use of a catalyst might be reduced or even unnecessary if sulfuric acid splitting is coupled to concentrated solar radiation at temperatures above 1123 K. Process design and economic analysis were performed for this coupling by SRNL and CSIRO (Corgnale & Summers, 2011; Hinkley, O'Brien, Fell, & Lindquist, 2011; Steimke & Steeper, 2005). Hydrogen production costs with such a process were calculated to be between US$3.19/kg and US$5.57/kg. In the frame of the European Union projects, HycycleS and HYTHEC, the reliability and potential hybridization of the hybrid sulfur cycle with solar energy (Monnerie et al., 2011) were analyzed and qualified materials were identified for technical realization of the solar thermal decomposition of sulfuric acid (Thomey et al., 2010). For this step, a test reactor was developed and tested in the solar furnace of

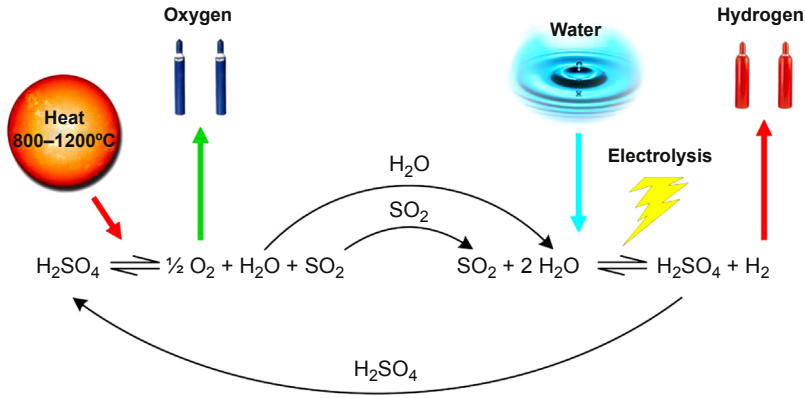

Figure 11.7 Scheme of hybrid sulfur cycle.

DLR in Cologne at temperatures up to 1223 K. A thermal efficiency of up to 28% was found whereas reradiation of the solar absorbers was identified as the main heat loss. This can be reduced by using smaller windows and better insulation in the housing. Results indicate that the efficiency can also be increased at sulfuric acid flow rates higher than those actually employed until now because of the limitations of the equipment used. The multichamber concept of the reactor is scalable and mainly uses commercial materials such as steel and mass-produced silicon carbide structures; only a few components are made of quartz, especially for the reactor. Thus, this development is an important step in the direction of the industrial realization of solar hydrogen production by the sulfur-based thermochemical cycle. A project to scale up the technology into the several hundred kilowatts scale has begun (SOL2HY2, 2013) (Figure 11.7).

11.3.2 The sulfur–iodine cycle

One of the best known sulfur-based thermochemical cycles is the sulfur–iodine cycle, also known as ISPRA Mark 16 cycle or General Atomics Cycle. It was originally proposed and developed in the United States by General Atomics in the mid-1970s (Norman, 1978).

$$2H_2O + SO_2 + I_2 \rightarrow H_2SO_4 + 2HI \quad 300-400\ K \tag{11.18}$$

$$2HI \rightarrow I_2(g) + H_2(g) \quad 400-1000\ K \tag{11.19}$$

$$H_2SO_4 \rightarrow H_2O(g) + SO_2(g) + \tfrac{1}{2}O_2(g) \quad 1120-1200\ K \tag{11.20}$$

Reaction (11.20) proceeds actually in two stages:

$$H_2SO_4 \rightarrow H_2O(g) + SO_3(g) \tag{11.21a}$$

$$SO_3(g) \rightarrow SO_2(g) + \tfrac{1}{2}O_2(g) \tag{11.21b}$$

The Bunsen reaction (11.18) proceeds exothermically, producing two immiscible aqueous concentrated acid phases. A lot of water and iodine is necessary for the Bunsen reaction to proceed and to obtain the two acids, HI and H_2SO_4. Removal of the two acids by distillation requires a lot of energy. Major challenges of the sulfur−iodine cycle are to reduce the surplus of water and iodine and find separation processes consuming less energy than distillation (Figure 11.8).

Hydrogen iodide is then decomposed according to reaction (11.19) with a small amount of endothermic heat and H_2SO_4 is decomposed according to reaction (11.20), which is the major endothermic reaction of the cycle and takes place in the vapor phase in a catalytic reactor at about 1200 K.

The three sections of the process were built to demonstrate its feasibility in a glass, quartz, and Teflon laboratory-scale facility by JRC in ISPRA, Italy (International Atomic Energy Agency, 1999). Coupling to a solar thermal plant had been designed in the 1980s. The process was improved at various locations such as the Technical University of Aachen in Germany (Roth & Knoche, 1989) and in Japan, where JAEA operated closed-loop continuous hydrogen production at the rate of 32 l/h for 20 h in an experimental apparatus made of glass and fluorine resin (Kubo et al., 2004).

After being abandoned because of experimental problems, since the past decade the S-I cycle has again become the focus of intensive research owing to challenging reaction conditions. Thus, the process was demonstrated on the solar power tower of the Georgia Institute of Technology (General Atomics, 1985; Schultz, 2003) and in the solar furnace of DLR in Cologne, Germany (Roeb et al., 2005), where the effective potential for massive hydrogen production of the S-I cycle was also investigated in the framework of the European project HYTHEC (Le Duigou et al., 2007). Further laboratory- to bench-scale demonstration studies were carried out by JAEA in Japan (Kubo et al., 2004), ENEA in Italy (Parisi et al., 2011) and CEA, Sandia NL, and General Atomics in a common project in San Diego, United States (Russ, 2009). Researchers at ENEA, Italy suggested a modified S-I process based on the use of SO_2 from other sources, forming a so-called open S-I cycle (Liberatore et al., 2012). Sulfur dioxide-containing flue gases stemming from the combustion of sulfur-containing fuels represent the sulfur source of this cycle. Such a process could be suitable to treat exhaust flue gases produced by combusting sulfur-containing fuels. It results in significant cost savings compared with conventional sulfur recovery

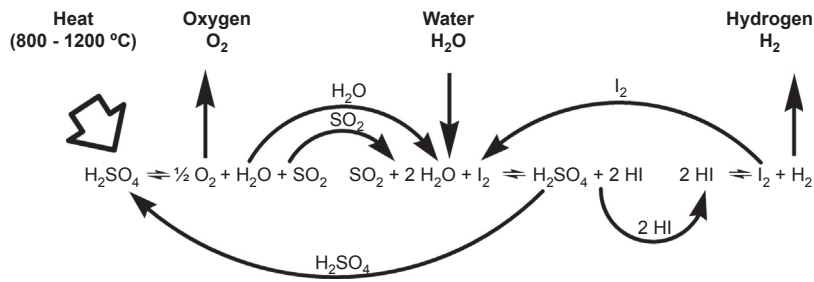

Figure 11.8 Scheme of S−I cycle.

methods. In addition, the production of concentrated sulfuric acid and hydrogen, which are the process outputs, can lead to significant revenue. Most recently, groups from Tsinghua University–INET, Beijing, China (Guo, Zhang, Chen, Wang, & Xu, 2011) and from the Korean Atomic Energy Research Institute (Song, Hong, Lee, & Park, 2011) have intensified work on different aspects of the S-I process. Both groups are operating closed-loop bench-scale experiments on the S-I cycle at their facilities (Chang et al., 2007; Zhang, Chen, Wang, Yao, & Xu, 2010).

11.3.3 Other sulfur-based cycles

The JRC in ISPRA, Italy suggested the so-called Mark 13 V2 process, a hybrid cycle to be coupled with a concentrating solar power plant.

$$SO_2 + Br_2 + 2H_2O \rightarrow 2HBr(g) + H_2SO_4 \quad 373-413\ K \tag{11.22}$$

$$2HBr(g) \rightarrow H_2(g) + Br_2(g) \quad \text{electrochemical step} \tag{11.23}$$

$$H_2SO_4 \rightarrow H_2O(g) + SO_2(g) + \tfrac{1}{2}O_2(g) \quad 723-1393\ K \tag{11.24}$$

The use of bromine creates a process in which decomposition of the hydrobromic acid formed can be performed in an electrolytic cell. A solar plant with a capacity of 1.4×10^6 GJ/year was simulated. The calculated process efficiency of this cycle is 37% (Engels, Funk, Hesselmann, & Knoche, 1987).

The JRC also suggested and evaluated the Mark 13A sulfur dioxide cycle. It is a modification of the Mark 13 cycle and represents an open thermochemical cycle for flue-gas desulfurization. Sulfur dioxide from flue gases is one of the raw materials. The absorbent is a dilute solution of sulfuric acid and hydrobromic acid also containing elemental bromine.

$$SO_2(g) + Br_2 + 2H_2O \rightarrow 2HBr(g) + H_2SO_4 \quad 373-413\ K \tag{11.25}$$

$$2HBr(g) \rightarrow H_2 + Br_2 \quad \text{electrochemical step} \tag{11.26}$$

A complete bench-scale, continuous process was successfully built and operated at JRC's facilities in ISPRA (Langenkamp & Velzen, 1988), followed by the construction of a pilot plant. This plant was erected and operated at the SARAS oil refinery in Sardinia, Italy in 1989 (Velzen, 1991).

Neither the Mark 13 V2 nor the Mark 13 A process has been studied in recent years. Compared with the other known sulfur-based thermochemical processes, the use of bromine and bromine-containing compounds causes too many challenges.

More recent is JAEA's ongoing work on developing the thermochemical and electrolytic hybrid hydrogen process at a lower temperature range (HHLT). It can be regarded as a modification of the hybrid sulfur cycle, allowing operation at lower process temperatures. The HHLT process is made up of the same reactions as the hybrid sulfur process. However, whereas the hybrid sulfur process needs a maximum

temperature of 1173−1273 K for reaction (11.16), the HHLT process only needs 773−823 K. To achieve this, it employs two electrolyzers, one of which is an innovative gaseous sulfur trioxide electrolyzer for the sulfuric acid decomposition reaction (Takai, Kubo, Nakagiri, & Inagaki, 2011):

$$SO_3 + 2e^- \rightarrow SO_2 + \tfrac{1}{2}O_2^{2-} \quad \text{(Cathode)} \tag{11.27}$$

$$\tfrac{1}{2}O_2^{2-} \rightarrow \tfrac{1}{2}O_2(g) + 2e^- \quad \text{(Anode)} \tag{11.28}$$

The process was demonstrated in a small laboratory-scale apparatus achieving hydrogen production rates up to 5 cm^3/h for 60 h (Takai, Kubo, et al., 2011). The experimentally achieved thermal efficiency was only 0.5%, but calculations suggested that the potential is much higher and can exceed 28% by optimizing operating conditions and improving equipment performance, optimizing the flow rate of sulfuric acid vaporization, concentrating sulfuric acid with a multiple-effect evaporator, and reducing overpotential and thereby the cell voltages required for the electrolyzers. Detailed flow sheet evaluation is ongoing to determine more accurate predictions on more realistic thermal efficiencies.

A process to coproduce hydrogen and concentrated sulfuric acid from sulfur dioxide and water has been proposed by the Finnish company Outotec (Rauser, Gasik, Peltola, & Taskinen, 2010). The process represents a combination of the generation of sulfuric acid from sulfur or from sulfide-based ore via the double contact process and the generation of hydrogen via hybrid sulfur. In the Outotec process, the sulfur dioxide stream is divided into two substreams. The first—at least 40% of the mass flow—is mixed with water to enable the electrochemical production of hydrogen and sulfuric acid. The second is oxidized over a V_2O_5 catalyst to sulfur trioxide applying the double contact process. Sulfur trioxide is absorbed by the diluted sulfuric acid provided by the first substream to yield additional sulfuric acid and achieve further concentration (Lokkiluoto & Gasik, 2012). The hydrogen-producing process step is preferably the electrolysis of sulfurous acid according to the hybrid sulfur cycle. Alternatively, the Bunsen reaction and HI decomposition according to the S−I cycle are possibly useful to close the cycles. In any case, the coproduction of concentrated sulfuric acid and hydrogen introduces flexibility into the process and offers enormous economic advantages.

11.4 Summary

Thermochemical cycles are a feasible way to produce storable and transportable fuels from solar energy. This route of hydrogen and syngas production uses solar heat at high temperatures for an endothermic thermochemical process. It offers some intriguing thermodynamic advantages with direct economic implications. A number of interesting and potentially viable techniques for the production of hydrogen from renewable resources using solar thermal energy have been shown to be successful

by bench-scale and pilot-scale demonstrations. Direct thermal water splitting is not likely to be feasible because of material issues, but thermochemical cycles present a number of choices and opportunities. The efficiencies of those cycles make it likely that at least one of the cycles will be chosen to prove the capability to provide large amounts of hydrogen, e.g., in a demonstration plant.

Metal−metal oxide pairs and multivalent metal oxides are the basic materials for redox cycles. The most promising material families are based on rare earth metals, ferrites, or perovskites. A number of process concepts have been introduced to integrate such cycles in a solar plant. Some are based on fixed or moving particle technologies such as fixed beds, fluidized beds, and rotary kilns; others use monolithic bodies such as honeycomb structures or foams made of or coated by the active redox material. Besides the required high process temperatures and separation issues, the main challenge of those processes is the availability of sufficiently active and stable redox materials. Recent developments reveal promise and significant improvement of the process if the high temperature reduction is performed under vacuum and if the two process steps involved are carried at the same temperature level or at least at temperature levels that are close.

Sulfur-based cycles represent processes that comprise as one central step the industrially widely established decomposition of sulfuric acid. That process step can be solarized by coupling in concentrated solar energy at temperatures below 1200 K. As the most prominent examples of sulfur-based cycles, the S-I cycle and the two-step hybrid sulfur cycle are particularly promising because they exhibit low specific hydrogen costs at high efficiencies. All reaction steps have been successfully demonstrated and reached a level of maturity sufficient for the development of a pilot plant. Further improvements in catalyst and construction materials need to be addressed for industrial realization. This is in particular true for a key step that all of the sulfur-based processes have in common: the high-temperature decomposition of sulfuric acid. Sulfuric acid-based thermochemical cycles can profit a lot in terms of economics and flexibility if they are operated as open cycles, e.g., in combination with sulfuric acid production or with flue-gas desulfurization. In those cases, besides solar energy a part of the required energy is introduced by the raw material sulfur, sulfur-containing ores, or sulfur dioxide.

Generally, two main research tasks for the development of thermochemical cycles are an improvement in solar interfaces and integrated heat recovery schemes and a solution to the main materials-related issues, providing the right functional materials at reasonable costs. Solutions to those tasks will decisively help solar thermal processes to achieve the role of contributing significantly to carbon-free and sustainable hydrogen and syngas production on a large scale, using only solar energy, carbon dioxide, and water as clean and abundant sources for those fuels.

Even though no thermochemical cycle is currently operating at an industrial scale, the political will to establish an alternative energy economy based on hydrogen supports the implementation of thermochemical cycles. Technologically, the market introduction of solar−thermal power plants makes a heat source available to power thermochemical cycles. This paves the way for the successful future of these challenging technologies.

Nomenclature

H_2	Hydrogen
O_2	Oxygen
H_2O	Water
CO_2	Carbon dioxide
CO	Carbon monoxide
$MO_{reduced}$	Metal oxide (reduced form)
$MO_{oxidized}$	Metal oxide (oxidized form)
FeO; Fe_3O_4	Wüstite; magnetite
MnO; Mn_3O_4	Manganese(II) oxide; Manganese(II−III) oxide
Zn; ZnO	Zinc; zinc oxide
CeO; Ce_2O_3	Cerium(II) oxide; Cerium(III) oxide
Al_2O_3	Aluminum oxide
$NiFe_2O_4$; $ZnFe_2O_4$; $CoFe_2O_4$	Nickel ferrite; zinc ferrite; cobalt ferrite
H_2SO_4	Sulfuric acid
SO_3	Sulfur trioxide
SO_2	Sulfur dioxide
Br_2	Bromine
HBr	Hydrobromic acid
V_2O_5	Vanadium pentoxide
e^-	Electron
(g)	Gaseous
ΔG	Free enthalpy
TR	Thermal reduction
WS	Water splitting
CSP	Concentrated solar power
CDS	Carbon dioxide splitting
FT	Fischer−Tropsch process
YSZ	Yttria-stabilized zirconia
DLR	Deutsches Zentrum für Luft- und Raumfahrt e.V. (German Aerospace Center)
CSIRO	Commonwealth Scientific and Industrial Research Organization
ETH	Eidgenössische Technische Hochschule Zurich
PSI	Paul-Scherer Institute
MWSF	Megawatt solar furnace
MIEC	Mixed oxygen-ion and electron-conducting
TGA	Thermogravimetric analysis
JRC	Joint Research Center
JAEA	Japanese Atomic Energy Agency
SRNL	Savannah River National Laboratory

Acknowledgments

Part of this work was co-funded by the Initiative and Networking Fund of the Helmholtz Association of German Research Centers in the frame of the Virtual Institute SolarSyngas.

Dr Agrafiotis would like to thank the European Commission for funding his stay at DLR during the time of this work, within the Project "FP7-PEOPLE-2011-IEF, 300194" under the Intra-European Fellowship Marie Curie Actions of the Seventh Framework Programme.

References

Abanades, S., & Flamant, G. (2006). Thermochemical hydrogen production from a two-step solar-driven water splitting cycle based on cerium oxides. *Solar Energy, 80*, 1611−1623.

Abanades, S., Legal, A., Cordier, A., Peraudeau, G., Flamant, G., & Julbe, A. (2010). Investigation of reactive cerium-based oxides for H_2 production by thermochemical two-step water-splitting. *Journal of Materials Science, 45*(15), 4163−4173.

International Atomic Energy Agency. (1999). *Hydrogen as an energy carrier and its production by nuclear power International, Atomic Energy Agency Report IAEA-TECDOC-1085*.

Agrafiotis, C. C., Mavroidis, I., Konstandopoulos, A. G., Hoffschmidt, B., Stobbe, P., Romero, M., et al. (2007). Evaluation of porous silicon carbide monolithic honeycombs as volumetric receivers/collectors of concentrated solar radiation. *Solar Energy Materials and Solar Cells, 91*(6), 474−488.

Agrafiotis, C. C., Pagkoura, C., Lorentzou, S., Kostoglou, M., & Konstandopoulos, A. G. (2007). Hydrogen production in solar reactors. *Catalysis Today, 127*(1−4), 265−277.

Agrafiotis, C. C., Pagkoura, C., Zygogianni, A., Karagiannakis, G., Kostoglou, M., & Konstandopoulos, A. G. (2012). Hydrogen production via solar-aided water splitting thermochemical cycles: combustion synthesis and preliminary evaluation of spinel redox pair materials. *International Journal of Hydrogen Energy, 37*(11), 8964−8980.

Agrafiotis, C., Roeb, M., Konstandopoulos, A. G., Nalbandian, L., Zaspalis, V. T., Sattler, C., et al. (2005). Solar water splitting for hydrogen production with monolithic reactors. *Solar Energy, 79*(4), 409−421.

Agrafiotis, C., Zygogianni, A., Pagkoura, C., Kostoglou, M., & Konstandopoulos, A. G. (2013). Hydrogen production via solar-aided water splitting thermochemical cycles with nickel ferrite: experiments and modeling. *AIChE Journal, 59*(4), 1213−1225.

Allendorf, M. D. (2008). Two-step water splitting using mixed-metal ferrites: thermodynamic analysis and characterization of synthesized materials. *Energy & Fuels, 22*, 4115−4124.

Aoki, H., Kaneko, H., Hasegawa, N., Ishihara, H., Suzuki, A., & Tamaura, Y. (2004). The $ZnFe_2O_4/(ZnO + Fe_3O_4)$ system for H_2 production using concentrated solar energy. *Solid State Ionics, 172*, 113−116.

Beghi, G. E. (1981). Review of thermochemical hydrogen production. *International Journal of Hydrogen Energy, 6*(6), 555−566.

Beghi, G. E. (1986). A decade of research on thermochemical hydrogen at the joint research centre, ISPRA. *International Journal of Hydrogen Energy, 11*, 761−771.

Bilgen, E. (1988). Solar hydrogen production by hybrid thermochemical processes. *Solar Energy, 41*(2), 199−206.

Bilgen, E., Ducarroir, M., Foex, M., Sibieude, F., & Trombe, F. (1977). Use of solar energy for direct and two-step water decomposition cycles. *International Journal of Hydrogen Energy, 2*, 251−257.

Brecher, L. E., & Wu, C. K. (1975). *Electrolytic decomposition of water*. United States. Pittsburgh, PA: Westinghouse Electric Corporation.

Brown, L. C., Besenbruch, G. E., Lentsch, R. D., Schultz, K. R., Funk, J. F., Pickard, P. S., et al. (2003). *High efficiency generation of hydrogen fuels using nuclear power*. General Atomics.

Chang, J., Kim, Y.-W., Lee, K.-Y., Lee, Y.-W., Lee, W.-J., Noh, J.-M., et al. (2007). A study of a nuclear hydrogen production demonstration plant. *Nuclear Engineering and Technology, 39*(2).

Charvin, P., Abanades, S., Flamant, G., & Lemort, F. (2007). Two-step water splitting thermochemical cycle based on iron oxide redox pair for solar hydrogen production. *Energy, 32*, 1124−1133.

Chueh, W. C., Falter, C., Abbott, M., Scipio, D., Furler, P., Haile, S. M., et al. (2010). High-flux solar-driven thermochemical dissociation of CO_2 and H_2O using nonstoichiometric ceria. *Science, 330*, 1797−1801.

Chueh, W. C., & Haile, S. M. (2010). A thermochemical study of ceria: exploiting an old material for new modes of energy conversion and CO_2 mitigation. *Philosophical Transactions of the Royal Society A: Mathematical, Physical and Engineering Sciences, 368*(1923), 3269−3294.

CNRS-PROMES. (2010). *CNRS 1000 kW solar furnace, Centre National de la Recherche Scientifique (CNRS)*. http://www.promes.cnrs.fr/TOUT-PUBLIC/Les-fours/englesfours1.htm.

Corgnale, C., & Summers, W. A. (2011). Solar hydrogen production by the hybrid sulfur process. *International Journal of Hydrogen Energy, 36*(18), 11604−11619.

Diver, R. B., Miller, J. E., Allendorf, M. D., Siegel, N. P., & Hogan, R. E. (2006). Solar thermochemical water-splitting ferrite-cycle heat engines. In *Proceedings of ISEC2006 ASME international solar energy conference, Denver, Colorado, USA*.

Engels, H., Funk, J. E., et al. (1987). Thermochemical hydrogen production. *International Journal of Hydrogen energy, 12*(5), 291−295.

Ermanoski, I., Siegel, N. P., & Stechel, E. (2013). A new reactor concept for efficient solar-thermochemical fuel production. *Journal of Solar Energy Engineering, 135*(3), 031002.

Evdou, A., Nalbandian, L., & Zaspalis, V. T. (2008). Perovskite membrane reactor for continuous and isothermal redox hydrogen production from the dissociation of water. *Journal of Membrane Science, 325*(2), 704−711.

Evdou, A., Zaspalis, V. T., & Nalbandian, L. (2008). La_{(1-x)}Sr_xMnO_{3-δ} perovskites as redox materials for the production of high purity hydrogen. *International Journal of Hydrogen Energy, 33*(20), 5554−5562.

Evdou, A., Zaspalis, V. T., & Nalbandian, L. (2010). La1−xSrxFeO3−δ perovskites as redox materials for application in a membrane reactor for simultaneous production of pure hydrogen and synthesis gas. *Fuel, 89*(6), 1265−1273.

Farbman, G. H. (1979). Hydrogen production by the Westinghouse sulfur cycle process: program status. *International Journal of Hydrogen Energy, 4*(2), 111−122.

Fresno, F., Fernandez-Saavedra, R., Gomez-Mancebo, M. B., Vidal, A., Sanchez, M., Rucandio, M. I., et al. (2009). Solar hydrogen production by two-step thermochemical cycles: evaluation of the activity of commercial ferrites. *International Journal of Hydrogen Energy, 34*(7), 2918−2924.

Fresno, F., Yoshida, T., Gokon, N., Fernandez-Saavedra, R., & Kodama, T. (2010). Comparative study of the activity of nickel ferrites for solar hydrogen production by two-step thermochemical cycles. *International Journal of Hydrogen Energy, 35*(16), 8503−8510.

Funk, J. E. (1976). Thermochemical production of hydrogen via multistage water splitting processes. *International Journal of Hydrogen Energy, 1*, 33−43.

Funk, J. E., & Reinstrom, R. M. (1966). Energy requirements in the production of hydrogen from water. *I & EC Process Design and Development, 5*(3), 336−342.

Furler, P., Scheffe, J., Gorbar, M., Moes, L., Vogt, U., & Steinfeld, A. (2012). Solar thermochemical CO_2 splitting utilizing a reticulated porous ceria redox system: Energy & fuels. *Energy Fuels, 16*, 7051−7059.

Furler, P., Scheffe, J., & Steinfeld, A. (2012). Syngas production by simultaneous splitting of H_2O and CO_2 via ceria redox reactions in a high-temperature solar reactor. *Energy & Environmental Science, 5*(3), 6098−6103.

Galvez, M., Frei, A., Albisetti, G., Lunardi, G., & Steinfeld, A. (2008). Solar hydrogen production via a two-step thermochemical process based on MgO/Mg redox reactions − thermodynamic and kinetic analyses. *International Journal of Hydrogen Energy, 33*(12), 2880−2890.

General Atomics. (1985). *DOE Report GA-A17573: Decomposition of sulfuric acid using solar thermal energy*.

Gokon, N., Mataga, T., Kondo, N., & Kodama, T. (2011). Thermochemical two-step water splitting by internally circulating fluidized bed of $NiFe_2O_4$ particles: successive reaction of thermal-reduction and water-decomposition steps. *International Journal of Hydrogen Energy, 36*(8), 4757−4767.

Gokon, N., Mizuno, T., Nakamuro, Y., & Kodama, T. (2008). Iron-containing yttria-stabilized zirconia system for two-step thermochemical water splitting. *Journal of Solar Energy Engineering, 130*(1), 11016−11018.

Gokon, N., Takahashi, S., Yamamoto, H., & Kodama, T. (2008). Thermochemical two-step water-splitting reactor with internally circulating fluidized bed for thermal reduction of ferrite particles. *International Journal of Hydrogen Energy, 33*(9), 2189−2199.

Gokon, N., Yamamoto, H., Kondo, N., & Kodama, T. (2010). Internally circulating fluidized bed reactor using m-ZrO_2 supported $NiFe_2O_4$ particles for thermochemical two-step water splitting. *Journal of Solar Energy Engineering, 132*(2), 021102−021110.

Gorensek, M. B., & Summers, W. A. (2009). Hybrid sulfur flowsheets using PEM electrolysis and a bayonet decomposition reactor. *International Journal of Hydrogen Energy, 34*(9), 4097−4114.

Gstoehl, D., Cooper, T., Villasmil, W., & Meier, A. (2010). Towards industrial solar production of zinc and hydrogen modeling and design of a 100 kW Solar pilot reactor for ZnO dissociation. In *18th world hydrogen energy conference 2010-WHEC 2010*. T. g. e. Detlef Stolten. Essen, Germany.

Guo, H., Zhang, P., Chen, S., Wang, L., & Xu, J. (2011). Review of thermodynamic properties of the components in HI decomposition section of the iodine−sulfur process. *International Journal of Hydrogen Energy, 36*(16), 9505−9513.

Haueter, P., Moeller, S., Palumbo, R., & Steinfeld, A. (1999). The production of zinc by thermal dissociation of zinc oxide—solar chemical reactor design. *Solar Energy, 67*(1−3), 161−167.

Hinkley, J. T., O'Brien, J. A., Fell, C. J., & Lindquist, S.-E. (2011). Prospects for solar only operation of the hybrid sulphur cycle for hydrogen production. *International Journal of Hydrogen Energy, 36*(18), 11596−11603.

Inoue, M., Hasegawa, N., Uehara, R., Gokon, N., Kaneko, H., & Tamaura, Y. (2004). Solar hydrogen generation with $H_2O/ZnO/MnFe_2O_4$ system. *Solar Energy, 76*, 309−315.

Jiang, H., Wang, H., Werth, S., Schiestel, T., & Caro, J. (2008). Simultaneous production of hydrogen and synthesis gas by combining water splitting with partial oxidation of methane in a hollow-fiber membrane reactor. *Angewandte Chemie International Edition, 47*(48), 9341−9344.

Kaneko, H., Fuse, A., Miura, T., Ishihara, H., & Tamaura, Y. (2006). Two-step water splitting with concentrated solar heat using rotary-type reactor. In *13th solar PACES international symposium, Seville, Spain*.

Kaneko, H., Kodama, T., Gokon, N., Tamaura, Y., Lovegrove, K., & Luzzi, A. (2004). Decomposition of Zn-ferrite for O_2 generation by concentrated solar radiation. *Solar Energy, 76*, 317−322.

Kaneko, H., Yokoyama, T., Fuse, A., Ishihara, H., Hasegawa, N., & Tamaura, Y. (2006). Synthesis of new ferrite, Al-Cu ferrite, and its oxygen deficiency for solar H_2 generation from H_2O. *International Journal of Hydrogen Energy, 31*, 2256−2265.

Kodama, T., & Gokon, N. (2007). Thermochemical cycles for high-temperature solar hydrogen production. *Chemical Reviews, 107*(10), 4048−4077.

Kodama, T., Nakamuro, Y., & Mizuno, T. (2006). A two-step thermochemical water splitting by iron-oxide on stabilized zirconia. *Journal of Solar Energy Engineering, 128*, 3−7.

Kojima, M., Sano, T., Wada, Y., Yamamoto, T., Tsuji, M., & Tamaura, Y. (1996). Thermochemical decomposition of H_2O to H_2 on cation-excess ferrite. *Journal of Physics and Chemistry of Solids, 57*(11), 1757−1763.

Kräupl, S., Frommherz, U., & Wieckert, C. (2006). Solar carbothermic reduction of ZnO in a two-cavity reactor: laboratory experiments for a reactor scale-up. *Journal of Solar Energy Engineering, 128*(1), 8−15.

Kubo, S., Nakajima, H., Kasahara, S., Higashi, S., Masaki, T., Abe, H., et al. (2004). A demonstration study on a closed-cycle hydrogen production by the thermochemical water-splitting iodine−sulfur process. *Nuclear Engineering and Design, 233*(1−3), 347−354.

Langenkamp, H., & Velzen, D. V. (1988). *The European commission − Flue-gas desulphurization by the Ispra mark 13 process. (Ispra, Italy).*

Le Duigou, A., Borgard, J. M., Larouss, B., Doizi, D., Allen, R., Ewan, B. C., et al. (2007). HYTHEC: an EC funded search for a long term massive hydrogen production route using solar and nuclear technologies. *International Journal of Hydrogen Energy, 32*(10−11), 1516−1529.

Liberatore, R., Lanchi, M., Caputo, G., Felici, C., Giaconia, A., Sau, S., et al. (2012). Hydrogen production by flue gas through sulfur−iodine thermochemical process: economic and energy evaluation. *International Journal of Hydrogen Energy, 37*(11), 8939−8953.

Lokkiluoto, A. K. K., & Gasik, M. M. (2012). Activities and free energy of mixing of sulfuric acid solutions by Gibbs−Duhem equation integration. *Journal of Chemical & Engineering Data, 57*(6), 1665−1671.

Loutzenhiser, P. G., Elena Galvez, M., Hischier, I., Graf, A., & Steinfeld, A. (2010). CO_2 splitting in an aerosol flow reactor via the two-step Zn/ZnO solar thermochemical cycle. *Chemical Engineering Science, 65*(5), 1855−1864.

Loutzenhiser, P. G., Meier, A., & Steinfeld, A. (2010). Review of the two-step H_2O/CO_2-splitting solar thermochemical cycle based on Zn/ZnO redox reactions. *Materials, 3*(11), 4922−4938.

Loutzenhiser, P. G., & Steinfeld, A. (2011). Solar syngas production from CO_2 and H_2O in a two-step thermochemical cycle via Zn/ZnO redox reactions: thermodynamic cycle analysis. *International Journal of Hydrogen Energy, 36*(19), 12141−12147.

McDaniel, A. H., Miller, E. C., Arifin, D., Ambrosini, A., Coker, E., O'Hayre, R., et al. (2013). Sr- and Mn-doped $LaAlO_3$-δ for solar chemical H_2 and CO production. *Energy and Environmental Science, 6*, 2424−2428.

Meier, A. (2013). *Project Status Report for Switzerland*. Las Vegas, USA: SolarPACES Task II Meeting Las Vegas.

Miller, J. E. (2007). *Initial case for splitting carbon dioxide to carbon monoxide and oxygen*. Sandia Report SAND2007−8012.

Miller, J. E., Allendorf, M. D., Diver, R. B., Evans, L. R., Siegel, N. P., & Stuecker, J. N. (2008). Metal oxide composites and structures for ultra-high temperature solar thermochemical cycles. *Journal of Materials Science, 43*(14), 4714−4728.

Miller, J. E., Evans, L. R., Stuecker, J. N., Allendorf, M. D., Siegel, N. P., & Diver, R. B. (2006). Materials development for the CR5 solar thermochemical heat engine. In *Proceedings of ISEC2006 ASME international solar energy conference, Denver, Colorado, USA*.

Miller, J. E., Evans, L. R., Siegel, N. P., Diver, R. B., Gelbard, F., Ambrosini, A., et al. (2009). *Sandia summary report: Direct approaches for recycling carbon dioxide into synthetic fuel*.

Möller, S., & Palumbo, R. (2001a). The development of a solar chemical reactor for the direct Thermal dissociation of zinc oxide. *Journal of Solar Energy Engineering, 123*, 83−90.

Möller, S., & Palumbo, R. (2001b). Solar thermal decomposition kinetics of ZnO in the temperature range 1950−2400 K. *Chemical Engineering Science, 56*, 4505−4515.

Monnerie, N., Schmitz, M., Roeb, M., Quantius, D., Graf, D., Sattler, C., et al. (2011). Potential of hybridisation of the thermochemical hybrid-sulphur cycle for the production of hydrogen by using nuclear and solar energy in the same plant. *International Journal of Nuclear Hydrogen Production and Applications, 2*(3), 178−201.

Muhich, C. L., Evanko, B. W., Weston, K. C., Lichty, P., Liang, X., Martinek, J., et al. (2013). Efficient generation of H_2 by Splitting water with an isothermal redox cycle. *Science, 341*(6145), 540−542.

Nakamura, T. (1977). Hydrogen production from water utilizing solar heat at high temperatures. *Solar Energy, 19*, 467−475.

Nalbandian, L., Evdou, A., & Zaspalis, V. T. (2009). La1−xSrxMO3 (M = Mn, Fe) perovskites as materials for thermochemical hydrogen production in conventional and membrane reactors. *International Journal of Hydrogen Energy, 34*(17), 7162−7172.

Nalbandian, L., Evdou, A., & Zaspalis, V. T. (2011). La1−xSrxMyFe1−yO3−δ perovskites as oxygen-carrier materials for chemical-looping reforming. *International Journal of Hydrogen Energy, 36*(11), 6657−6670.

Norman, J. H. (1978). *Process for the thermochemical production of hydrogen*. U.S., General Atomic company.

Norman, J. H., Besenbruch, G. E., Besenbruch, G. E., Brown, L. C., O'Keefe, D. R., & Allen, C. L. (1982). *Thermochemical water-splitting cycle, bench-scale investigations, and process engineering*. General Atomics.

Palumbo, R., Lede, J., Boutin, O., Elorza Ricart, E., Steinfeld, A., Möller, S., et al. (1998). The production of Zn from ZnO in a high-temperature solar decomposition quench process-I. The scientific framework for the process. *Chemical Engineering Science, 53*(14), 2503−2517.

Parisi, M., Giaconia, A., Sau, S., Spadoni, A., Caputo, G., & Tarquini, P. (2011). Bunsen reaction and hydriodic phase purification in the sulfur−iodine process: an experimental investigation. *International Journal of Hydrogen Energy, 36*(3), 2007−2013.

Pretzel, C. W., & Funk, J. E. (1987). *The development status of solar thermochemical hydrogen production*. Sandia Report. Albuquerque, NM and Livermore, CA: Sandia National Laboratories.

Rauser, W.-C., Gasik, M., Peltola, H., & Taskinen, P. (2010). *Method for producing hydrogen and sulphuric acid*. Outotec Oyj.

Roeb, M., Noglik, A., Rietbrock, P. M., Mohr, S., de Oliveira, L., Sattler, C., et al. (2005). HYTHEC: development of a dedicated solar receiver-reactor for the decomposition of sulphuric acid. In *European hydrogen energy conference EHEC 2005, Zaragoza, Spain*.

Roeb, M., Säck, J. P., Rietbrock, P., Prahl, C., Schreiber, H., Neises, M., et al. (2011). Test operation of a 100 kW pilot plant for solar hydrogen production from water on a solar tower. *Solar Energy, 85*(4), 634−644.

Roeb, M., & Sattler, C. (2013). Isothermal water splitting. *Science, 341*(6145), 470−471.

Roeb, M., Sattler, C., Klüser, R., Monnerie, N., de Oliveira, L., Konstandopoulos, A. G., et al. (2006). Solar hydrogen production by a two-step cycle based on mixed iron oxides. *Journal of Solar Energy Engineering, 128*(2), 125−133.

Rosmaninho, M., Herreras, S., Lago, R. M., Araujo, M. H., Navarro, R. M., & Fierro, J. L. G. (2011). Effect of the partial substitution of Fe by Ni on the structure and activity of nanocrystalline NixFe3xO4 ferrites for hydrogen production by two-step water-splitting. *Nanoscience and Nanotechnology Letters, 3*(5), 705−716.

Roth, M., & Knoche, K. F. (1989). Thermochemical water splitting through direct HI-decomposition from $H_2O/HI/I_2$ solutions. *International Journal of Hydrogen Energy, 14*(8), 545−549.

Russ, B. (2009). *Sulfur iodine process summary for the hydrogen technology down-selection*. from https://inlportal.inl.gov Accessed 30.08.12.

Sakurai, M., Bilgen, E., Tsutsumi, A., & Yoshida, K. (1996). Adiabatic UT-3 thermochemical process for hydrogen production. *International Journal of Hydrogen Energy, 21*(10), 865−870.

Scheffe, J. R., Li, J., & Weimer, A. W. (2010). A spinel ferrite/hercynite water-splitting redox cycle. *International Journal of Hydrogen Energy, 35*(8), 3333−3340.

Scheffe, J. R., McDaniel, A. H., Allendorf, M. D., & Weimer, A. W. (2013). Kinetics and mechanism of solar-thermochemical H_2 production by oxidation of a cobalt ferrite−zirconia composite. *Energy & Environmental Science, 6*, 963−973.

Scheffe, J. R., & Steinfeld, A. (2012). Thermodynamic analysis of cerium-based oxides for solar thermochemical fuel production. *Energy & Fuels, 26*(3), 1928−1936.

Scheffe, J. R., Weibel, D., & Steinfeld, A. (2013). Lanthanum−Strontium−Manganese perovskites as redox materials for solar thermochemical splitting of H_2O and CO_2. *Energy & Fuels, 27*, 4250−4257.

Schultz, K. R. (2003). Use of the modular helium reactor. In *World nuclear association annual symposium, London*. World Nuclear Association.

Shah, P. R., Kim, T., Zhou, G., Fornasiero, P., & Gorte, R. J. (2006). Evidence for entropy effects in the reduction of Ceria−Zirconia solutions. *Chemistry of Materials, 18*(22), 5363−5369.

Shimizu, S., Onuki, K., & Nakajima, H. (1991). *Japan atomic energy research institute − JAERI report: Bench-scale studies of the iodine-sulfur process*.

Sibieude, F., Ducarroir, M., Tofighi, A., & Ambriz, J. (1982). High temperature experiments with a solar furnace: the decomposition of Fe_3O_4, Mn_3O_4, CdO. *International Journal of Hydrogen Energy, 7*(1), 79−88.

SOL2HY2. (2013). From https://sol2hy2.eucoord.com/.

Song, K.-N., Hong, S.-D., Lee, H.-Y., & Park, H.-Y. (2011). Macroscopic structural analysis on a 10 kW Class lab-scale process heat exchanger prototype under a high-temperature gas loop condition. *Engineering, 5*, 117−124.

Stamatiou, A., Steinfeld, A., & Jovanovic, Z. R. (2013). On the effect of the presence of solid diluents during Zn oxidation by CO_2. *Industrial & Engineering Chemistry Research, 52*(5), 1859−1869.

Steimke, J. L., & Steeper, T. J. (2005). *WSRC-TR-2005−00310: Characterization testing of H_2O − SO_2 electrolyzer at ambient pressure* (Aiken, SC, USA).

Steinfeld, A. (2002). Solar hydrogen production via a two-step water-splitting thermochemical cycle based on Zn/ZnO redox reactions. *International Journal of Hydrogen Energy, 27*(6), 611−619.

Steinfeld, A., Sanders, S., & Palumbo, R. (1999). Design aspects of solar thermochemical engineering − a case study: two-step water-splitting cycle using the Fe_3O_4/FeO redox system. *Solar Energy, 65*(1), 43−53.

Sturzenegger, M., & Nüesch, P. (1999). Efficiency analysis for a manganese-oxide-based thermochemical cycle. *Energy, 4*, 959−970.

Summers, W. A., & Gorensek, M. B. (2006). *Nuclear hydrogen production based on the hybrid sulfur thermochemical process*. Reno, NV, USA: International Congress on Advances in Nuclear Power Plants (ICAPP).

Takai, T., Kubo, S., Nakagiri, T., & Inagaki, Y. (2011). Lab-scale water-splitting hydrogen production test of modified hybrid sulfur process working at around 550 °C. *International Journal of Hydrogen Energy, 36*(8), 4689−4701.

Tamaura, Y., Kojima, M., Sano, T., Ueda, Y., Hasegawa, N., & Tsuji, M. (1998). Thermodynamic evaluation of water splitting by a cation-excessive (Ni, Mn) ferrite. *International Journal of Hydrogen Energy, 23*(12), 1185−1191.

Tamaura, Y., Steinfeld, A., Kuhn, P., & Ehrensberger, K. (1995). Production of solar hydrogen by a novel, 2-step, water-splitting thermochemical cycle. *Energy, 20*, 325−330.

Tamaura, Y., Ueda, Y., Matsunami, J., Hasegawa, N., Nezuka, M., Sano, T., et al. (1999). Solar hydrogen production by using ferrites. *Solar Energy, 65*(1), 55−57.

Thomey, D., Roeb, M., de Oliveira, L., Gumpinger, T., Schmücker, M., Sattler, C., et al. (2010). Characterisation of construction and catalyst materials for solar thermochemical hydrogen production. In *Conference on materials for energy, Karlsruhe, Germany*.

Tsuji, M., Togawa, T., Wada, Y., Sano, T., & Tamaura, Y. (1995). Kinetic study of the formation of cation-excess magnetite. *Journal of the Chemical Society, Faraday Transactions, 91*(10), 1533−1538.

Velzen, D. V. (1991). *Desulphurization and denoxing of waste gases producing hydrogen as a by-product*.

Villasmil, W., Brkic, M., Wuillemin, D., Meier, A., & Steinfeld, A. (2014). Pilot scale demonstration of a 100-kWth solar thermochemical plant for the thermal dissociation of ZnO. *Journal of Solar Energy Engineering, 137*, 011017-1/11.

Weidenkaff, A., Steinfeld, A., Wokaun, A., Auer, P. O., Eichler, B., & Reller, A. (1999). Direct solar thermal dissociation of zinc oxide: condensation and crystallization of zinc in the presence of oxygen. *Solar Energy, 65*(1), 59−69.

Wieckert, C., Frommherz, U., Kraupl, S., Guillot, E., Olalde, G., Epstein, M., et al. (2007). A 300 kW solar chemical pilot plant for the carbothermic production of zinc. *Journal of Solar Energy Engineering, 129*, 190−196 (May).

Zhang, P., Chen, S. Z., Wang, L. J., Yao, T. Y., & Xu, J. M. (2010). Study on a lab-scale hydrogen production by closed cycle thermo-chemical iodine−sulfur process. *International Journal of Hydrogen Energy, 35*, 10166−10172.

This page intentionally left blank

Hydrogen production via the Kværner process and plasma reforming

12

D.H. Lee
Korea Institute of Machinery and Materials, Yuseong-Gu, Daejeon, Republic of Korea

12.1 Introduction: what is plasma

12.1.1 Plasma and discharge phenomena

Plasma is the ionized state of gas. Material in the solid, liquid, and gas phases is generally electrically neutral, although on occasion it can be electrically charged after the loss or acquisition of electrons under an external force. For this reason, plasma is often called the fourth state of material, in addition to the states of solid, liquid, and gas. The name "plasma" was first used by Irving Langmuir (Langmuir, 1928). There are many different plasmas around us in nature, including lightning, the sun, and aurora. Plasma can also be produced artificially by causing neutral atoms or molecules to lose or acquire electrons. This requires an energy sufficiently higher than the amount that binds an electron to an atom or molecule. A possible way of providing the necessary energy is by heating and imposing a high electric field on an atom or molecule.

In principle, plasma is expected to be electrically neutral. However, because of the difference in mass between electrons, which are the major carriers of charge, and positive ions, which are much heavier than electrons, a typical ionized gas is electrically conductive and interacts with an external electric field. For the same reason, charge can be distributed nonuniformly within a discharge region, and this nonuniformity causes the chemical reactivity to vary with the method of plasma generation.

Regardless of the exact definition of electrical neutrality, various industrial discharges are now designated as plasma. These discharges are typically generated by the following procedure.

Once a high voltage (electric field) above a certain threshold level is applied to a gas system that is electrically nonconductive, the gas loses its characteristic of being a nonconducting material and behaves as a conducting medium, resulting in current flow. That is the basic nature of discharge. Figure 12.1 shows the typical voltage–current behavior during discharge. The parameters that determine the discharge conditions include the gas species, electrode configuration (e.g., shape and arrangement), and characteristics of the imposed voltage.

The theories that explain the discharge process are the Townsend discharge theory (Townsend & Gill, 1938) and the streamer theory (Meek, 1940). The Townsend theory is known to be more appropriate for low-pressure discharge phenomena.

Compendium of Hydrogen Energy. http://dx.doi.org/10.1016/B978-1-78242-361-4.00012-1

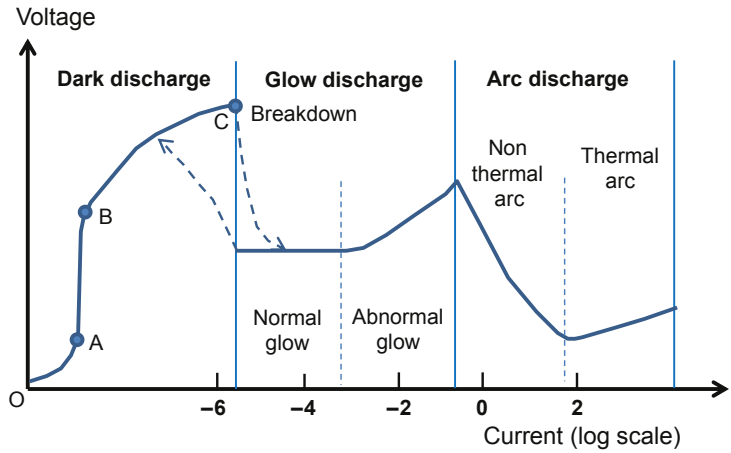

Figure 12.1 Typical voltage−current behavior in the discharge process.

The gas discharge process can be explained as follows. In the gas phase, electrons produced by ultraviolet and other photons via natural processes generally disappear through attachment to neutral particles or adsorption to the opposite electrode. However, as the applied voltage increases, ions and electrons are accelerated, and the number of electrons adsorbed by the opposite electrode, which can produce a current flow, begins to outnumber that of electrons removed by diffusion, attachment, and recombination. Therefore, the current increases at this stage (O to A in Figure 12.1). However, once the current approaches a certain value, it stops increasing because the ionization process is limited; this results in a continuous increase in voltage without an increase in current (A to B in Figure 12.1). In this state, with the electric field above the threshold value, electrons can be accelerated above the velocity of ionization and produce additional electrons by colliding with neutral molecules or atoms. This process induces an abrupt increase in the number of electrons and positive ions (B to C in Figure 12.1). A continuous increase in the applied voltage causes electrons to proliferate, and the so-called electron avalanche begins. The current increases steeply at this moment, resulting in breakdown of the gas medium. Next, the discharge proceeds to the glow stage and the subsequent arc stage.

An electron avalanche is induced by collisions of electrons and positive ions. The probability of electron production is called the ionization coefficient and is determined by the voltage and pressure between the electrodes. It can be expressed by Paschen's law (Fridman, 2008):

$$V_s = f(Pd) \tag{12.1}$$

V_s: breakdown voltage, P: pressure, d: distance between electrodes.

This equation shows that the breakdown voltage is a function of the pressure times the distance. A typical Paschen curve shows parabolic behavior according to the product Pd, as shown in Figure 12.2.

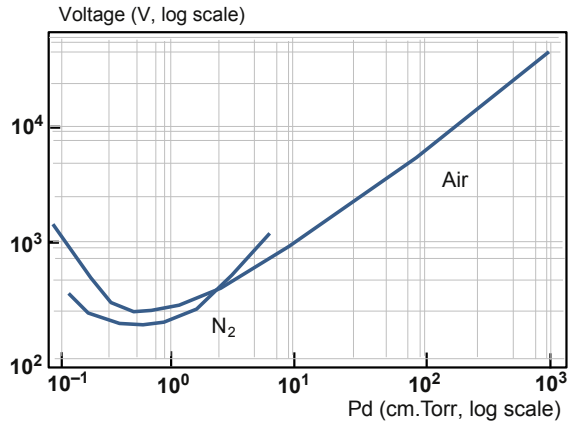

Figure 12.2 Paschen curves for air and nitrogen.

Here, we can understand that the gas properties and the arrangement of and distance between the electrodes determine whether plasma can be generated under a given condition.

12.1.2 Definition and classification of plasma

The energy state of a particle can be expressed in terms of the temperature. The plasma energy state can also be expressed in terms of the temperature. However, plasma differs from a typical gas system in that, in plasma, it is possible for various particles in a system to have different temperatures or energy states. As explained previously, during the discharge process, an electron is accelerated by an applied electric field. Defining the mean free path l between collisions, the energy obtained by the electron from the electric field can be expressed as (Griffiths, 1999):

$$E_e = e \cdot E \cdot l \tag{12.2}$$

E_e: energy, e: electron charge, E: electric field, l: mean free path.

An electron that has gained that energy collides with gas molecules as it moves. Here, the mean free path is determined by the pressure of the gas system. In the collision process, the electron loses part of its energy. However, because the mass of the electron is too small compared with that of a typical gas molecule, the amount of energy lost in the collision is small. In contrast to the electron, a heavy molecule gains energy. Because of the different processes for obtaining energy, the temperatures of electrons and heavy particles can differ. The difference in the energy is controlled by the applied electric field and pressure. The reduced electric field, E/n, is defined to parameterize both the electric field and pressure and is useful in explaining their behavior. The temperature of electrons usually differs from that of heavy particles except at low E/n, where the degree of acceleration is not great (i.e., the numerator

is small), or the mean free path is too short and the collision frequency is too high (i.e., the denominator is large). On the basis of this fact, plasma can be classified into equilibrium plasma and nonequilibrium plasma depending on the relative equilibrium state between electrons and heavy particles (Grill, 1993).

During plasma generation, local thermodynamic equilibrium can be generated locally; however, except for that condition, most of the plasmas around us in industrial applications and chemical processes are nonequilibrium plasmas.

In nonequilibrium plasma in local thermodynamic equilibrium, the gas temperature determines the ionization and chemical processes; this is called a thermal plasma. When the electron energy, not the temperature, determines the ionization and chemical processes, it is called a nonthermal plasma.

The ionization and chemical processes in nonthermal plasma are initiated by high-energy electrons and do not depend on the gas temperature. Therefore, controlling the electron temperature and density is a major issue in plasma chemistry.

On the other hand, "nonequilibrium" means that the temperatures of the particles are different. In addition, it means that the degrees of freedom of particles also have different states. In a nonthermal plasma, the temperature for each degree of freedom is generally on the order of the following.

$$T_e > T_v > T_r \sim T_i \sim T_o \tag{12.3}$$

where the subscripts v, r, i, and o indicate the vibrational mode, rotational mode, ions, and heavy molecules, respectively.

Thermal and nonthermal plasmas exhibit different mechanisms for the initiation and maintenance of chemical processes, and the characteristics of the process also produce different results. In thermal plasma, chemical processes are driven by the high-temperature environment and governed mostly by the equilibrium condition. For this reason, the activation energy for all possible reaction paths can be provided, resulting in a less selective reaction process. In contrast, in nonthermal plasma, the reaction system has a relatively low gas temperature and a low density of high-energy electrons. Further, although the overall degree of activation is not very high because of collisions with electrons in specific energy states, relatively selective reactions can be obtained compared with those driven by thermal plasma.

These characteristics are clearly visible in the process of methane activation by different plasma sources, as shown in Figure 12.3 (Lee, Song, et al., 2013).

As mentioned previously, as the thermal environment changes to approach that of a thermal plasma, the selectivity of the product is also changed. Thus, in the design of plasma processes, it is essential to understand these characteristics of thermal and nonthermal plasma to optimize the process.

12.1.3 Plasma kinetics in chemical processes

The plasma chemistry or electron-impact-induced process produces various types of reactions that are induced by electrons, positive ions, and excited species. Representative reactions are listed as follows.

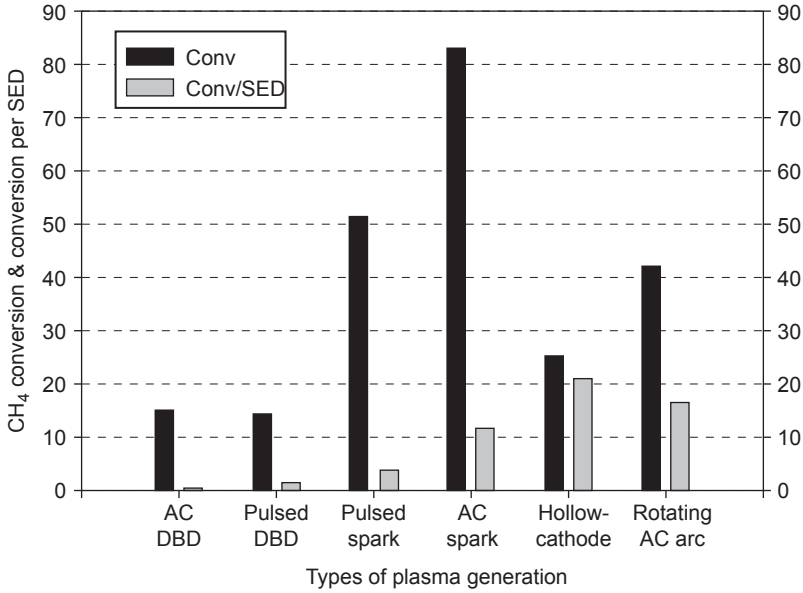

Figure 12.3 Comparison of methane activation by different plasma sources (Lee, Song, Kim & Jo, 2013). SED: specific energy density.
With permission by Springer.

1. Ionization:

$$e + AB \rightarrow AB^+ + e + e \tag{12.4}$$

$$e + AB \rightarrow A + B^+ + e + e \tag{12.5}$$

$$A^* + B \rightarrow A + B^+ + e \tag{12.6}$$

Ionization is a process in which an atom or molecule loses an electron in an electron impact. Ionization occurs through direct collision of heavy particle with electrons, collision between heavy particles, and collisions between excited species and heavy particles.

2. Attachment

$$e + A + B \rightarrow A^- + B \tag{12.7}$$

$$e + AB \rightarrow A^- + B \tag{12.8}$$

In attachment, a high-energy electron is lost via a collision with an atom or molecule that results in attachment.

3. Detachment

$$e + A^- \rightarrow A + e + e \tag{12.9}$$

$$A^- + B \rightarrow (AB^-)^* \rightarrow AB + e \tag{12.10}$$

$$A^- + B^* \rightarrow A + B + e \tag{12.11}$$

Detachment is the process in which negative ions lose an electron during a collision with an electron or excited species.

4. Electron exchange

$$A^+ + B \rightarrow A + B^+ \tag{12.12}$$

In addition, electron exchange between ions and molecules can occur in the collision process.

5. Excitation

During the collision process, if an atom or molecule does not gain enough energy for ionization, the energy state of each degree of freedom changes. Excitation is also an important process because the excited species can provide sufficient energy for ionization during collisions with other molecules if the excitation level is high enough for ionization in successive collisions.

The processes listed previously for the plasma chemistry provide different reaction steps that are not observable in typical chemistry. During activation of methane by plasma, in addition to the typical three-body activation reaction expressed in Eqn (12.13), which produces primarily CH_3, radicals such as CH_2, CH, methane ions (CH_4^+), and excited species such as $CH_4(v_{13})$ and $CH_4(v_{24})$ can be produced. Further, all of these chemically active species contribute to the chemical activation of methane. Table 12.1 summarizes the species that can be produced during methane activation (Nozaki, Muto, Kado, & Okazaki, 2004).

$$CH_4 + M \rightarrow CH_3 + H + M \tag{12.13}$$

As shown in Table 12.1, ionization and radical formation require a rather high activation energy, but excited species such as CH_4v show lower energies of activation. Considering that the bond dissociation energy of CH_4 to produce methyl radicals or the bond dissociation energy of $H_3C{-}H$ is 105 kcal/mol, or 4.55 eV, efficient energy use in plasma can be assumed.

12.2 Plasma sources used in hydrogen production

Plasma has various appearances depending on the generation method. Plasma generation methods can be classified according to the shape and arrangement of the electrodes and the type of electric field applied. Depending on the electrode shape,

Table 12.1 Electrical processes and energy branching in methane activation (Nozaki et al., 2004)

Reaction (CH_4 + e)	Threshold energy	Energy branch (%)
→ $CH_4(v24) + e$	0.162	11.9
→ $CH_4(v13) + e$	0.361	24.5
→ $CH_3 + H + e$	9.0	17.0
→ $CH_2 + H_2 + e$	10.0	13.2
→ $CH + H_2 + H + e$	11.0	10.8
→ $C + 2H_2 + e$	12.0	9.3
→ $CH_4^+ + e + e$	12.6	9.4
→ $CH_4^+ + H + e + e$	14.3	4.0

plasma can be classified as corona discharge, dielectric barrier discharge (DBD), hollow cathode plasma, spark plasma, and so on. Depending on the type of electric field, plasma can be classified as direct current (DC) plasma, alternating current plasma, microwave plasma, and radiofrequency (RF) plasma.

The electron temperature and density in each type of plasma are different. Further, different types of plasma naturally exhibit different visibilities, chemical reactivities, thermal degrees of activation, and so on. Representative types of plasma are briefly explained below.

12.2.1 Corona discharge

The term "corona" originates from the Latin word for crown because the discharge is observed at a sharp edge of the electrode, resulting in a crown shape. Corona discharge refers to that from a sharp (high-curvature) electrode to a rather planar (smaller curvature) opposite electrode. Typical configurations are the pin-to-plate and wire-to-cylinder configurations, as shown in Figure 12.4. Depending on how the electric

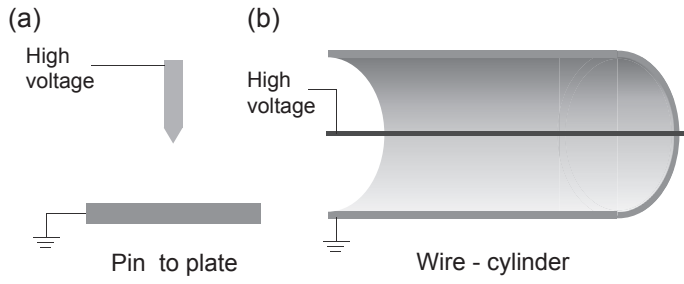

Figure 12.4 Typical electrode configurations for corona discharge. (a) Pin to plate type and (b) Wire-cylinder type configuration.

field is applied, a pulsed, alternating current, or DC (positive/negative) corona can be generated. Compared with a DBD, the corona discharge produces a relatively high electron energy and is spatially nonuniform. Compared with a thermal plasma such as an arc plasma, the electron temperature is higher but the electron density is lower.

12.2.2 Dielectric barrier discharge

DBD is generated using a configuration of single or multiple dielectric barriers between electrodes, as shown in Figure 12.5.

The dielectric layer suppresses charge buildup on the electrode surface, which prevents the transition to an arc. Under atmospheric pressure, DBD generally produces a filamentary microdischarge between the electrodes. It produces electron energies that are a few electronvolts lower than those of a corona discharge. During the discharge, dielectric heating of the dielectric layer occurs, deteriorating the energy cost. The DBD configuration has been used to generate ozone.

12.2.3 Gliding arc

The gliding arc method is the most traditional way of generating an arc. It uses electrodes that are opposite each other with an increasing distance between them, as shown schematically in Figure 12.6. The discharging gas flow follows the path toward increasing distance between the electrodes. An arc is ignited at the point where the gap between the electrodes is smallest and is convected outward with the gas flow.

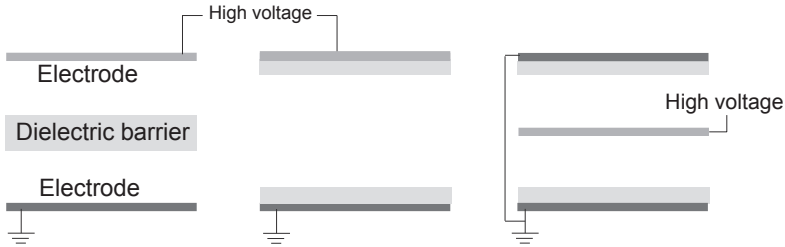

Figure 12.5 Typical configuration of dielectric barrier discharge (DBD) reactor.

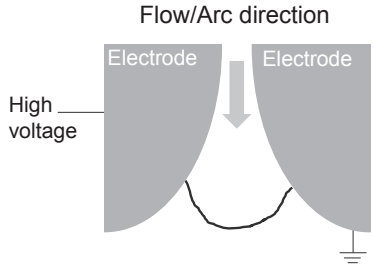

Figure 12.6 Typical configuration and arc development in a gliding arc.

At some point downstream, the arc is detached and reignites at the ignition point, repeating the procedure. As the arc develops, it is expanded lengthwise, producing arc instabilities; during expansion, increased heat transfer alters the characteristics of the arc.

In terms of chemical reactions, the gliding arc has limited reactivity because of the two-dimensional structure and relative velocity of the flow and arc expansion. The coverage of the reactant by the plasma volume is not very high. However, to compensate for the low volume coverage and reaction efficiency, a multistep gliding arc has also been studied.

A gliding arc generally produces relatively low-energy electrons compared with a corona discharge or DBD, but the electron density is much higher (by one or two orders of magnitude).

12.2.4 Rotating arc

The rotating arc was proposed to overcome the limitations of the two-dimensional geometry of the gliding arc. The rotating arc uses a conical electrode and a cylindrical electrode, as shown in Figure 12.7. The discharge gas is supplied to the reaction volume with a tangential flow to generate a swirling flow inside the reactor.

The arc is ignited at the point of the smallest gap between the electrodes. However, in the rotating arc, unlike the gliding arc, the ignition point is not fixed. It can be distributed around the circumference of the electrode, which is highly useful to prevent damage to the electrode.

The most important difference between the rotating arc and the gliding arc is that there are several different modes of arc generation (Lee, Kim, Kang, Jo, & Song, 2014). By applying arc control, the length of the arc column can be fixed without expansion. Under certain conditions, the arc reignites at the tip of the electrode, not at the smallest gap, and the arc column can be sustained in an elongated state. The fixed arc column length enables a highly thermal environment that covers all of the flow, resulting in a much higher reaction thermal efficiency for the rotating arc.

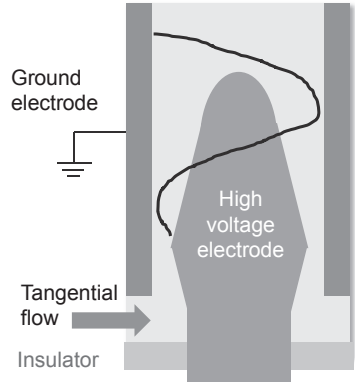

Figure 12.7 Configuration and arc development in rotating arc.

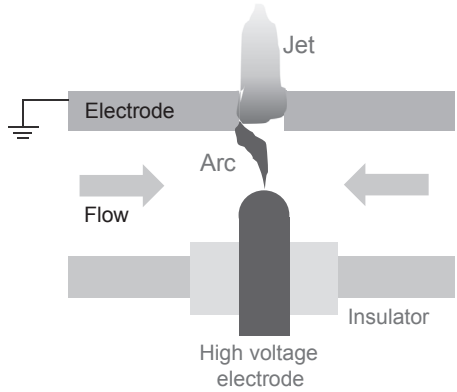

Figure 12.8 Schematic of reactor configuration and arc/jet development in hollow cathode plasma.

12.2.5 Hollow cathode plasma

In most plasma reactors, it is difficult to fill the reaction volume with plasma. However, a hollow cathode plasma can provide high-volume coverage of the plasma for a reaction. By placing a small hole that functions as an exit nozzle, an arc and the following jet can fill the hole, as shown in Figure 12.8. A hollow cathode plasma consists of two different regimes. One is the arc regime, in which a typical arc is generated. However, the arc length and location are fixed by the reactor geometry. The arc touches the ground electrode, and much of its heat is transferred. The other is the jet regime, in which species with somewhat longer lifetimes and excited species are abundant. The temperature of the jet regime is much lower than that of the arc regime, but somewhat nonthermal characteristics are stronger in the jet regime. Thus, the hollow cathode plasma can provide two different conditions simultaneously, thermal but less selective reactions in the arc regime and nonthermal conditions but higher selectivity in the jet regime.

When plasma is applied for a chemical process, it is necessary to determine which plasma characteristics are favorable for the specific reaction, a highly thermal environment or nonequilibrium chemistry. It is necessary to understand the generation and configuration of each plasma source and the characteristics of the reaction.

12.3 Plasma processes for hydrogen production

For precise understanding and design of the hydrogen production process using plasma, the various processes should be classified. The plasma processes for hydrogen production can be classified according to the following features:

1. what type of process is applied,
2. what type of feed stock is chosen as the hydrogen source, and
3. what type of plasma source is applied.

The processes can be further classified according to the reactant that is added to the hydrogen feedstock. If no reactant is added to the feedstock, the product will be hydrogen, hydrocarbon species, and carbon. (In the case of alcohol, CO is included in the product.) The most important representative of this type of process is the Kværner process, which is described in Section 12.3.1.

Except for processes with no additives, H_2O, CO_2, and O_2 (air) generally are used, and the characteristics of the reaction, such as the heat of the reaction, H_2/CO ratio of the product, reaction temperature, and thermal efficiency, vary depending on which species is added.

The subcategories and the associated additives are as follows.

1. Steam reforming: H_2O
2. Partial oxidation: O_2 (air)
3. Steam reforming with oxygen (SRO): H_2O and O_2
4. Dry reforming: CO_2
5. Tri-reforming: H_2O, O_2, and CO_2

Table 12.2 compares the advantages and disadvantages of each process without plasma (Holladay, Hu, King, & Wang, 2009).

On the other hand, in the typical reforming process, to reduce the CO production and catalyst poisoning (if a catalyst is used), carbon generation should be suppressed. Coke formation in the reforming condition depends on the water usage, but in general, a rather high reaction temperature is required to avoid coke formation, as shown in Table 12.3 (Holladay et al., 2009).

In the application of plasma for the reforming process, except for some plasma sources that generate much higher gas temperatures, such as a microwave plasma or thermal arc, there is actually a wide range of temperature inside the reaction volume. Especially for nonthermal plasma, a locally low temperature can be produced within the reaction volume, and it is hard to avoid coke formation.

Another important issue in the design of plasma reforming is the thermal efficiency. A widely accepted definition of the thermal efficiency of the reforming process is the

Table 12.2 Comparison of reforming technologies

Technology	Advantages	Disadvantages
Steam reforming	Highest H_2/CO ratio Commercialized technology O_2 is not required	Highest air emissions
Partial oxidation	Catalyst is not necessary Low methane slip	Low H_2/CO ratio High process temperature Soot formation
Autothermal reforming	Possible thermal control Low methane slip	Need for oxygen (air)

Table 12.3 Temperature that avoids coke formation in iso-octane reforming processes

Reactions	Minimum temperature to avoid coke formation (°C)
Partial oxidation (O/C = 1)	1180
Autothermal reforming (O/C = 1)	1030
Steam reforming (O/C = 1)	950
Autothermal reforming (O/C = 2)	575
Steam reforming (O/C = 2)	225

ratio of the heating value of the produced hydrogen and that of the reactant. For an endothermic reaction, the heat provided to the reaction system is also included as another term in the denominator as in Eqn (12.14). In some cases, the CO in the product is included in the amount of hydrogen, considering that an additional water gas shift reaction (Eqn (12.15)) can produce the same amount of hydrogen with CO in the product.

$$\eta = \frac{\text{heating value of produced hydrogen}}{\text{heating value of the fuel used} + \text{external heating}} = \frac{(n_{H_2} + n_{co})\Delta H_{H_2}}{n_{fuel}\Delta H_{fuel} + Q} \tag{12.14}$$

$$CO + H_2O \rightarrow CO_2 + H_2 \quad \Delta H = -41.1 \text{ kJ/mol} \quad (0.43 \text{ eV}) \tag{12.15}$$

In the plasma reforming process, the electric power used to generate the plasma should be considered in the thermal efficiency. Further, the definition of the reforming thermal efficiency should be revised as in Eqn (12.16).

$$\eta = \frac{(n_{H_2} + n_{co})\Delta H_{H_2}}{n_{fuel}\Delta H_{fuel} + Q + P_e} \tag{12.16}$$

Essentially, as can be understood from Eqn (12.16), because the denominator has an additional term P_e, the use of plasma lowers the thermal efficiency. Thus, plasma should be used in applications in which it can provide a particular function, such as enabling a low-temperature reaction where a catalyst cannot be used or under conditions with an abruptly changing reactant flow such as mobile applications.

In a reaction involving plasma activation of hydrocarbon species, the reaction is initiated by the collision of gas molecules with high-energy electrons. Further, during the collisions, the dissociation cross section is also a function of the reaction conditions. The dissociation cross section for typical species in the reforming process is

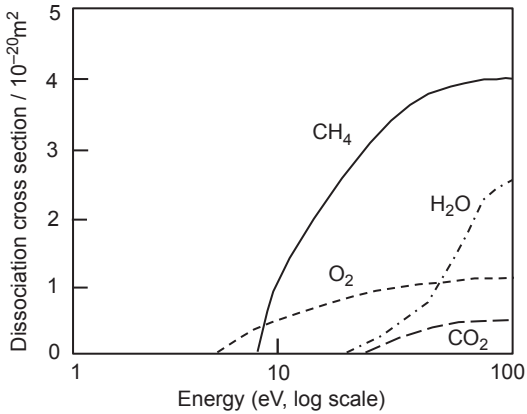

Figure 12.9 Electron collision cross section of species in the reforming process. Reconstructed from Kappes, Hammer, and Ulrich (2003).

given in Figure 12.9 (Kappes et al., 2003). The information on the cross section of the reactant can be considered in choosing the plasma source because each plasma source produces different electron states.

12.3.1 Kværner process

Thermal pyrolysis without added oxygen produces hydrogen and carbon from a hydrocarbon feedstock, as shown in Eqn (12.17).

$$C_nH_m \rightarrow nC + \frac{m}{2}H_2 \tag{12.17}$$

Essentially, a pyrolysis process depends on thermal energy for the cleavage of the C−H bond. For this reason, the process has a disadvantage in terms of decomposition of the feedstock itself compared with the process that has a reactant that contains O and OH.

In the equilibrium condition, the highest selectivity of hydrogen and carbon can be obtained in the range of 1300−2200 K (1027−1927 °C), as shown in Figure 12.10 (Anderson, Fincke, & Taylor, 2002).

Hydrogen production via thermal pyrolysis requires high-temperature conditions, and it is expensive to use thermal plasma to generate a thermal environment for the reaction. However, in a plasma process, unlike a typical combustion process, the heating of nitrogen or water can be omitted, which can reduce the enthalpy for heating up the reactant. Further, in the typical combustion process, high temperatures (above about 1500 K (1227 °C)) can be obtained only by oxy combustion, which also lowers the thermal efficiency and cost-effectiveness. Considering these factors, thermal plasma can be applied in high-temperature thermal pyrolysis.

In the application of plasma to methane decomposition, the reaction characteristics vary according to the plasma source and whether it is a nonthermal or thermal plasma.

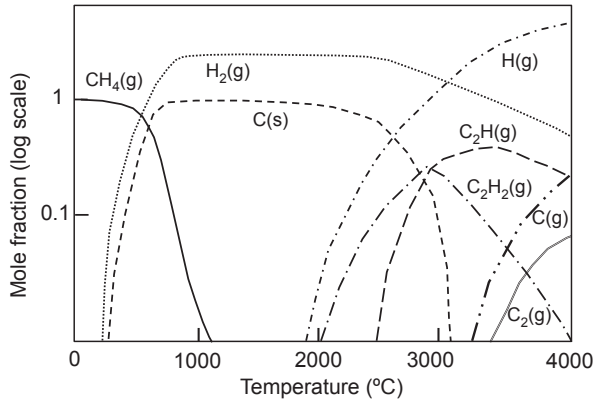

Figure 12.10 Equilibrium composition of methane.

A nonthermal plasma contains high-energy electrons under conditions in which the temperature of heavy particles is low enough that a thermal reaction is not initiated. Further, it naturally enables the activation reaction under relatively low-temperature conditions. It differs from typical thermal activation in that, because the reaction relies mainly on the electron impact, the probability of complete cleavage of C−H bonds decreases. Instead, radicals produced from incomplete cleavage of C−H bonds in the reactant are abundant. The relative proportion of the radicals is a function of the electron temperature of the plasma.

Another point of difference is that the successive reaction steps following incomplete cleavage of the C−H bond also occur under low-temperature conditions, so the products tend to form hydrocarbon species such as C_2H_x rather than hydrogen and carbon (Kado, Urasaki, et al., 2003). Reactions at lower electron energies tend to produce C_2H_6, and those under higher electron energies tend to produce C_2H_2 (Lee, Kim, Song, Kang, & Jo, 2013).

Methane activation by nonthermal plasma sources such as DBD, spark plasma, and corona discharge, is easily realized. Among these nonthermal sources, the spark plasma exhibits the lowest gas temperature, which ranges from 420 to 460 K, and results in higher C_2H_2 selectivity (Kado, Sekine, Muto, Nozaki, & Okazaki, 2003).

The multi-knife gliding arc plasma, the characteristics of which are intermediate between those of a nonthermal plasma and a thermal plasma, yields a somewhat higher temperature than a typical nonthermal plasma and produces acetylene, hydrogen, and soot from methane (Czernichowski & Czernichowski, 2000).

On the other hand, thermal plasma can generate high-temperature conditions in which thermal activation is possible, and the process is influenced by the thermal equilibrium condition. Thermal plasma provides a temperature that is higher than that of typical combustion processes and results in high hydrogen selectivity.

The processing cost for hydrogen production using thermal plasma is actually higher than that of the steam reforming process. According to a report, if only hydrogen is considered, the Kværner process, which decomposes methane using

thermal plasma, costs 73% more than typical steam reforming and also requires 82% more primary energy (Wagner, Geiger, & Shaefer, 1998). However, it produces only hydrogen and carbon, without CO and CO_2, and if the purity of the carbon black can be guaranteed, the process using thermal plasma can become economically feasible. The process that produces hydrogen and carbon black from a hydrocarbon feedstock is called the Kværner process or the Kværner carbon black and hydrogen process. The name comes from the developer (Aker Kværner Solutions of Norway), which first used the process in the 1980s.

Once the carbon black is included as a product, the Kværner process is found to have the same process cost as steam reforming (Wagner et al., 1998).

The Kværner process adopts a coaxial graphite electrode for the generation of thermal plasma (Figure 12.11) (Bakken, Jensen, Monsen, Raaness, & Waernes, 1998).

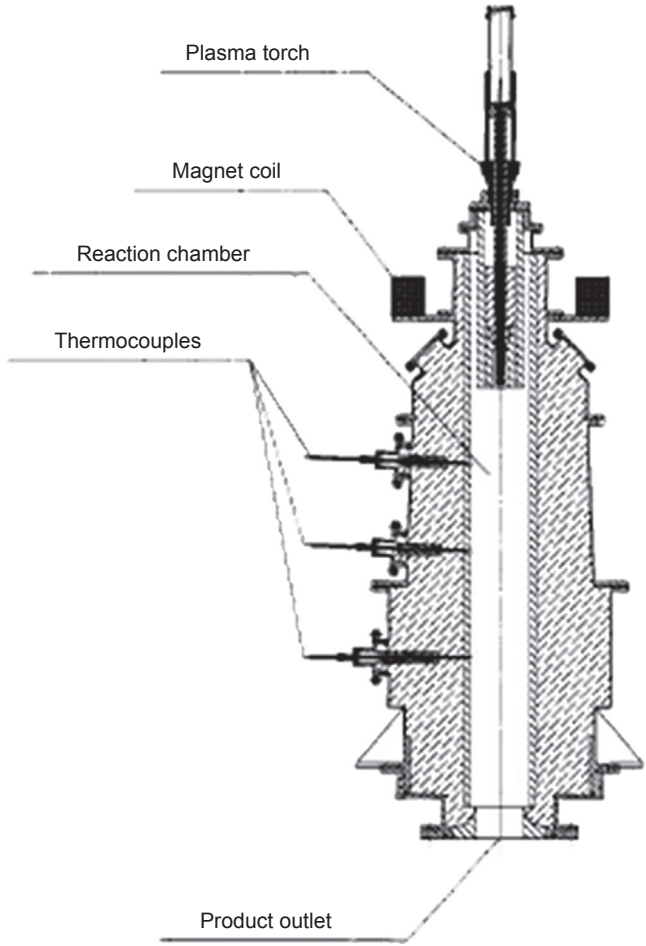

Figure 12.11 Schematic of reactor for Kværner process.
With permission from IUPAC.

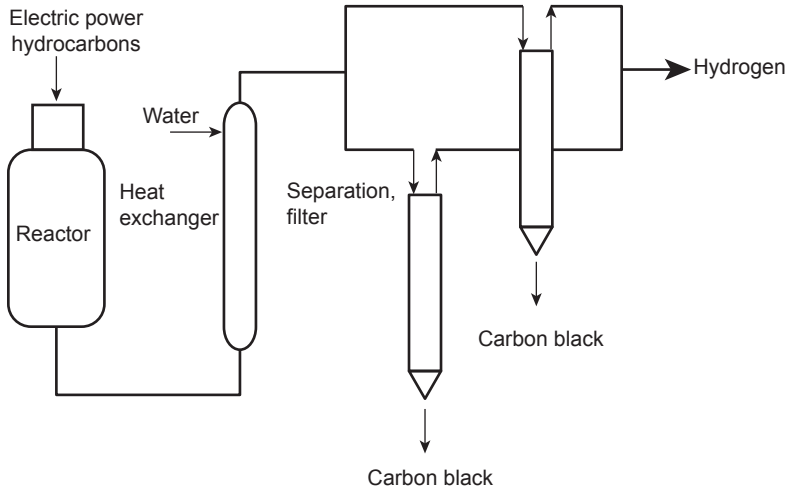

Figure 12.12 Schematic of flow in Kværner process.
With permission from IUPAC.

The arc can become focused spatially during arc generation; to prevent this, a magnet coil is used. The magnet coil induces rotation of the arc, which contributes to uniform feedstock heating and pyrolysis. The rotation of the arc also minimizes the electrode erosion. The reported electrode erosion rate is around 0.1 g/kWh (Bakken et al., 1998).

The parameters of the process are the flow rate and temperature of the feedstock and method of feedstock feeding (e.g., location and number of ports). Because the electrode itself is graphite, other by-products that are not contained in the feedstock are not produced.

Figure 12.12 shows a flowchart for the Kværner process (Bakken et al., 1998).

Processes at scales of a few megawatts to tens of megawatts are in commercial operation, and the uses for carbon black include toners, tires, and paints. The quality of the carbon black can be controlled by adjusting the process parameters.

12.3.2 Reforming process

The reforming process produces a synthesis gas composed of hydrogen and carbon monoxide from the hydrocarbon fuel. Depending on how the oxygen is supplied, the processes are classified as steam reforming, partial oxidation, and dry reforming, as well as SRO (autothermal reforming) and tri-reforming, which are combinations of these processes (Dicks, 1996; Kothari, Buddhi, & Sawhney, 2008; Song & Pan, 2004).

The H_2/CO ratio in the product of the reforming process depends on the reactant used in the process, and the reactant species should be determined considering successive reforming processes such as the Fischer−Tropsch (F−T) process. If hydrogen and not syngas is the goal of the process, the water gas shift reaction (Eqn (12.15)) can be applied for the production of additional hydrogen.

12.3.2.1 Steam reforming

Steam reforming uses H_2O as a source of oxygen. The reaction proceeds as in Eqns (12.18) and (12.19) (including a shift reaction).

$$CH_4 + H_2O \rightarrow 3H_2 + CO \quad \Delta H = 206.2 \text{ kJ/mol} \quad (2.14 \text{ eV}) \tag{12.18}$$

$$CH_4 + 2H_2O \rightarrow 4H_2 + CO_2 \quad \Delta H = 165.1 \text{ kJ/mol} \quad (1.71 \text{ eV}) \tag{12.19}$$

Steam reforming is the only reforming process that is commercialized in bulk chemistry. The steam reforming reaction is essentially endothermic, and the reaction temperature ranges above 800 °C to prevent coke formation. Because of the relatively low gas hourly space velocity (GHSV, S/V), a rather large reaction volume is required, with an S/V of less than 10,000 h^{-1} (Rostrup-Nielsen & Sehested, 2003; http://www.topsoecom/business_areas/ammonia/~/media/PDF%20files/Steam_reforming/Topsoe_steam_reforming_cat.ashx).

Because of the use of external heating, the need for pretreatments such as desulfurization, and the low S/V, the process requires relatively large-scale facilities. Steam reforming is generally based on a catalytic reaction. And Ni, and a Ni-based catalyst, is commonly used (Matsumura & Nakamori, 2004; Rakass, Oudghiri-Hassani, Rowntree, & Abatzoglou, 2006; Sehested, 2006).

Many studies have reported the application of plasma in the steam reforming process. Using steam as a reactant in the plasma process has the advantage of using radicals such as H, O, and OH. The plasma generates these reactive radicals in the gas phase; thus, the reactions described by Eqns (12.20)–(12.25) can be hosted (Patiño, Pérez, & Caetano, 2005).

$$H_2O + e \rightarrow H + OH + e \tag{12.20}$$

$$H_2O + e \rightarrow H_2O^* + e \tag{12.21}$$

$$H_2O^* \rightarrow H + OH \tag{12.22}$$

$$OH + e \rightarrow H + O + e \tag{12.23}$$

$$OH + e \rightarrow OH^* + e \tag{12.24}$$

$$OH^* \rightarrow H + O \tag{12.25}$$

The plasma processes for steam reforming can be classified as those that use plasma alone and those that use plasma with a catalyst. Steam reforming itself is actually a strong endothermic reaction; in addition, the dissociation cross section of H_2O is effective for high-energy electrons, and H_2O is an electronegative species. Because of these characteristics of the reaction, a plasma source that provides a thermal environment is better than a nonthermal plasma that relies mainly on high-energy electrons for the initiation and sustenance of the reaction. This is why most of the

steam reforming processes in which plasma is applied adopt RF and microwave plasma sources (Jasinski, Dors, Nowakowska, & Mizeraczyk, 2008; Patiño et al., 2005; Sekiguchi & Mori, 2003; Wang, Tsai, Chang, & Kuo, 2010).

On the other hand, there have been attempts to apply nonthermal plasma sources such as DBD, which produce a less thermal environment than a microwave plasma (Nozaki et al., 2004). In these cases, thermal activation cannot be expected because of the low gas temperature, and the reaction is expected to be driven mostly by high-energy electrons. However, considering that the typical electron density is 10^8–10^{13} cm^{-3} in nonthermal plasma, the conversion of the hydrocarbon reactant obviously cannot be high, so the process is more expensive than one in which a thermal plasma is applied.

That is why nonthermal plasma is typically combined with a catalyst. When a nonthermal plasma is combined with a catalyst in the reforming process, the energy cost for hydrogen production is typically an order of magnitude lower than that of a process using a nonthermal plasma alone, as shown in Table 12.4 (Nozaki et al., 2004).

The most common DBD configuration for a plasma–catalyst reaction is a packed-bed type reactor. In this configuration, the discharge space can be located close to the catalyst surface for the reaction. Figure 12.13 shows a schematic illustration of the packed-bed type DBD reactor.

Table 12.4 Comparison of energy costs

Reaction type	Condition (°C, kHz)	Energy cost (MJ/kg-H_2)
DBD	200/10	5974
DBD	400/76	8080
DBD + Ni/SiO_2	400/10	1330
DBD + Ni/SiO_2	400/76	1004
DBD + Ni/SiO_2	600/10	136

Data from Nozaki et al. (2004).

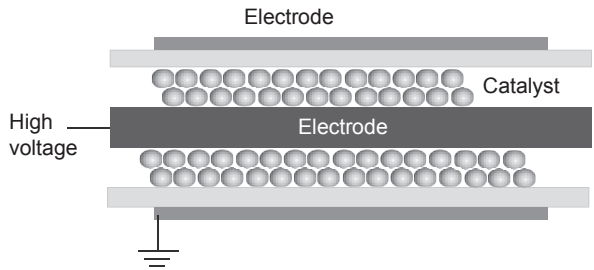

Figure 12.13 Schematic configuration of a typical packed-bed type dielectric barrier discharge (DBD) reactor.

The combination of the plasma and catalyst could possibly lower the light-off temperature of the catalyst because of the interaction between the plasma and catalyst (Kim, Jo, Song, & Lee, 2014). However, because the catalyst cannot be activated at room temperature, a certain level of thermal activation of the catalyst is required. In other words, the cost of the plasma–catalyst reaction includes the electrical energy consumed in plasma generation and the thermal energy needed to provide the minimum level of thermal activation. Thus, a plasma–catalyst reaction system is cost-effective for special applications in which typical catalytic reactions are not available or for a specific by-product that cannot be obtained through typical catalytic reactions.

The cost is the main reason that the concept of steam reforming with oxygen was proposed. The addition of oxygen results in oxidation of the fuel, which produces heat and reduces the need for external heating.

12.3.2.2 Steam reforming with oxygen

Using an oxygen source inevitably results in the production of CO and CO_2. However, supplying steam and oxygen has the advantages of providing process control and reducing the cost, as mentioned previously. The main reaction of the SRO process consists of steam reforming (Eqn (12.26)) and partial oxidation (Eqn (12.27)). Once the restriction condition (Eqn (12.28)) is provided, Eqns (12.26) and (12.27) are combined as in Eqn (12.29).

$$CH_4 + xH_2O \rightarrow xCO + xH_2 + (1 - x)CH_4 \tag{12.26}$$

$$CH_4 + \frac{y}{2}O_2 \rightarrow \frac{y}{2}CO + yH_2 + (1 - y)CH_4 \tag{12.27}$$

$$x + y = 2 \tag{12.28}$$

$$CH_4 + \left(1 - \frac{x}{2}\right)(O_2 + 3.76N_2) + xH_2O \rightarrow CO_2 + (x + 2)H_2 + 3.76\left(1 - \frac{x}{2}\right)N_2 \tag{12.29}$$

According to Eqn (12.29), the heat of the reaction can be calculated as in Eqn (12.30).

$$\Delta H = \Delta H_{f,CO_2} - x\Delta H_{f,H_2O} - \Delta H_{f,\text{fuel}} \tag{12.30}$$

If the amount of heat required by Eqn (12.26) and that released by Eqn (12.27) are the same, external heating is not required; this is the so-called condition of autothermal reaction. The x and y values for the autothermal reaction can be calculated by Eqn (12.31).

$$x = \frac{\Delta H - \Delta H_{f,CO_2} - \Delta H_{f,\text{fuel}}}{\Delta H_{f,H_2O}} \tag{12.31}$$

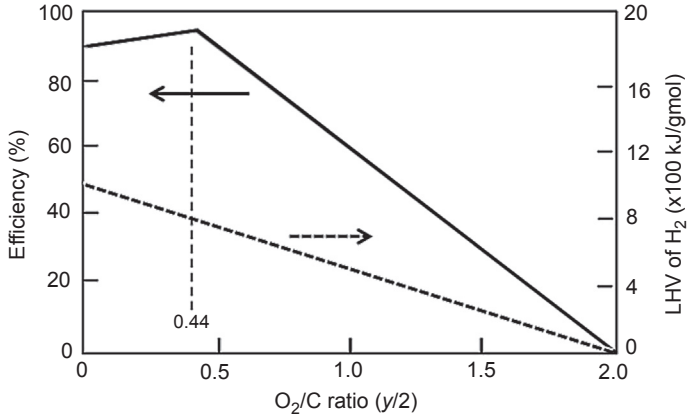

Figure 12.14 Efficiency and lower heating value (LHV) of produced hydrogen according to the O_2/C ratio.

For methane, $x = 1.12$ ($y = 0.88$) for the autothermal reaction. The autothermal reaction is also used to represent a generic SRO reaction regardless of the heat balance. However, strictly speaking, heat balance is a prerequisite of the autothermal condition.

The thermal efficiency of the SRO reaction is greatest in the autothermal condition, as shown in Figure 12.14, and the supply of additional oxygen decreases the thermal efficiency to 0 under the condition of combustion (Ahmed & Krumpelt, 2001).

In the evaluation of the thermal efficiency of a plasma process, as noted previously, an electric power term in included. This is also true of the evaluation of thermal balance because a large portion of the electric power used to generate plasma tends to be converted to thermal energy during plasma generation. This reduces the amount of oxygen required for thermal balance. Here, if we define the portion of electric power that is converted to thermal energy as η, the heat of the reaction is modified as shown in Eqn (12.32). Further, the values of x (and y) for the autothermal condition are also modified, as shown in Eqn (12.33), and the resulting O_2/C ratio for the autothermal reaction is given by Eqn (12.34) (assuming the conditions in Eqn (12.35)).

$$\Delta H = \Delta H_{f,\mathrm{CO_2}} - x\,\Delta H_{f,\mathrm{H_2O}} - \Delta H_{f,\mathrm{fuel}} + \eta \cdot P_\mathrm{e} \tag{12.32}$$

$$x = \frac{\Delta H - \Delta H_{f,\mathrm{CO_2}} - \Delta H_{f,\mathrm{fuel}} - \eta \cdot P_\mathrm{e}}{\Delta H_{f,\mathrm{H_2O}}} \tag{12.33}$$

$$\frac{\mathrm{O_2}}{\mathrm{C}}\, ratio_{\mathrm{auto}} = 1 - \frac{x}{2} = 1 - \frac{1}{2} \cdot \frac{\Delta H - \Delta H_{f,\mathrm{CO_2}} - \Delta H_{f,\mathrm{fuel}} - \eta \cdot P_\mathrm{e}}{\Delta H_{f,\mathrm{H_2O}}} \tag{12.34}$$

$$\eta \cdot P_\mathrm{e} < \Delta H - \Delta H_{f,\mathrm{CO_2}} - \Delta H_{f,\mathrm{fuel}} \tag{12.35}$$

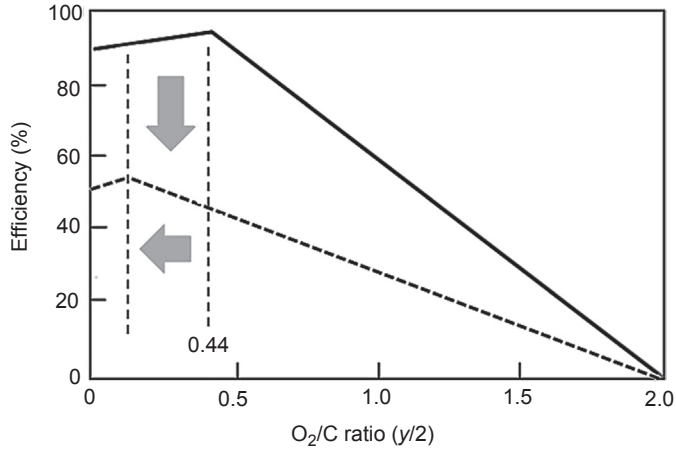

Figure 12.15 Changes in balancing point of heat balance and reduction of thermal efficiency with the application of plasma in the SRO process.

The modification expressed in Eqns (12.32)−(12.35) lowers the thermal efficiency and changes the conditions for autothermal balance, as illustrated in Figure 12.15.

A combination of plasma and a catalyst can be effectively used in the SRO process, as in the steam reforming process. However, in the typical catalytic SRO reaction, the temperature for coke formation is lowered and does not actually fall within the typical range of reaction temperatures that allow the existence of steam. However, once plasma is included in the reaction, carbon can be produced directly by the collision of highly energetic electrons with methane molecules. Further, the relative proportion of steam determines the possible coking of the catalyst.

A cost issue also emerges in the plasma SRO process. However, in the SRO process, the reaction can be sustained without the help of plasma-generated radicals, and the application of plasma should be minimized to eliminate coking and reduce the process cost. The role of the plasma can be to lower the reaction temperature by generating the minimum amount of radicals needed to initiate the reaction with a minimal use of electric power.

Studies on the role of excited species have also been reported. Unlike radical generation, which requires a somewhat higher energy (ranging from a few electronvolts to tens of electronvolts), vibrational excitation of gas molecules does not require much energy (typically less than 1 eV). Considering that much of the energy distribution can be used to excite the molecules, methods of using excited species are attracting attention as a way to maximize the synergetic effect of plasma and a catalyst. The challenge is that the lifetimes of these excited species are typically very short, ranging from nanoseconds to microseconds. The delivery of excited species to the catalytic surface within an effective time scale is an important issue, and debate is ongoing on the effectiveness of these excited species.

Cormier and Rusu (Cormier & Rusu, 2001) compared the typical chemical SRO and plasma SRO processes. Their review introduced plasma sources for the SRO

process such as the plasmatron, glidarc, and microwaves (Bromberg, Cohn, Rabinovich, O'Brien, & Hochgreb, 1998; Fridman, Nester, Kennedy, Saveliev, & Yardimci, 1999; Potapkin, Rusanov, & Jivotov, 2000; Reveau, Nikravech, Martinie, Lefaucheux, & Cormier, 2000). The important factor in the comparison of plasma sources is the process cost, which varies widely according to the plasma source. For the SRO process, sustenance without plasma is possible, and a plasma source that elevates the gas temperature too much inevitably has a high process cost. However, the glidarc, which has a somewhat shorter residence time and lower gas temperature heat-up, yields a better hydrogen generation cost in the range of a few tens of MJ/kg-H_2.

Other cases of plasma SRO include gasoline reforming by a multistep gliding arc (Paulmier & Fulcheri, 2005). However, for automobile applications, the important points in selecting the process are, first, that the use of H_2O should be carefully considered because water storage in automobile systems is not feasible. Second, the electric power available in an automobile is limited by the capacity of the onboard battery. Installation of an additional battery may be not possible in that application. A low-pressure RF process for methane SRO has been reported, but as is known, low-pressure processes have weak feasibility because of the expected low throughput, which might increase the cost of hydrogen production by several orders of magnitude (Patiño et al., 2005).

12.3.2.3 Partial oxidation

Partial oxidation uses oxygen (air) to activate hydrocarbon species; the reaction can be expressed as in Eqn (12.36).

$$CH_4 + \frac{1}{2}O_2 \rightarrow 2H_2 + CO \quad \Delta H = -43.6 \text{ kJ/mol} \quad (0.45 \text{ eV}) \tag{12.36}$$

The advantage of the partial oxidation process is that external heating is not required, which increases the compactness of the reaction system. Further, the H_2/CO ratio in the product is closer to that required by the F–T process than that in the steam reforming process. Its disadvantages are possible overheating and the need for an additional gas separation process to remove nitrogen (if air is used), which also affects the cost of the process. Nitrogen and carbon dioxide, which occupy considerable space in the product, are actually a type of heat sink that degrades the thermal efficiency of the process. Therefore, partial oxidation is not yet applied in bulk commercial processes. Further, unlike steam reforming, which is used mainly to produce feedstock hydrogen for chemical processes, other applications have been used (Ahmed et al., 1998; Ogden, 2001). However, most current applications focus on conditions under which steam reforming is not applicable, such as valorization of heavy oil residue. However, the partial oxidation process has recently attracted attention for application to onboard reforming. The reason is that mobile systems cannot provide sufficient water for steam reforming and do not have room for a slow reaction and external heating facility, and, most importantly, there is no need for gas separation.

Compared with other types of process, more attempts to apply plasma have been reported. Partial oxidation is an exothermic reaction and does not depend much on the plasma characteristics. The use of plasma can reduce the need to provide a thermal environment. However, for this reason, there has been debate on the relative contributions of chemical reactions and plasma reactions. Benilov and Naidis reported that simple thermal kinetics can express the partial oxidation of octane by an arc plasma (Benilov & Naidis, 2006). Further, Lee et al. studied the relative contributions of plasma chemistry and thermally activated processes and found that plasma cannot provide high methane conversion because of its nonthermal characteristics. In addition, the highly thermal environment produced by heat transfer from an arc can accelerate the partial oxidation process (Lee, Kim, Cha, & Song, 2010a). In particular, he reported that, as Benilov and Naidis stated, the major products such as hydrogen and carbon monoxide can be predicted to some degree by the thermal kinetics; however, the minor products such as hydrocarbon species cannot be predicted or explained by the thermal kinetics. There are two reasons for this. First, the products of reactions steered by high-energy electrons and excited species have low densities and cannot be a kinetic path for a major product. Second, the products of reactions steered by high-energy electrons and excited species experience successive reaction steps of oxidation steered by the thermally activated environment and cannot be distinguished (Lee, Kim, et al., 2013). The current understanding is that the relative contribution of the plasma chemistry varies depending on the temperature of the reaction volume (Lee et al., 2010a).

For a rotating arc, the arc column rotates to produce the reaction volume. By proper control of the plasma generation, the arc column can be expanded lengthwise. The expansion of the arc column and subsequent increase in heat transfer produces a highly thermal reaction volume encompassed by the trajectory of the arc column. In that case, a reaction volume at about 2000 K, which is not available in a typical nonthermal plasma, can be produced that abruptly accelerates the decomposition of methane. On the basis of this phenomenon, Lee et al. provided theoretical and experimental tools for controlling the relative contribution of the plasma chemistry in the overall partial oxidation process (Lee, Kim, Cha, & Song, 2007; Lee et al., 2014).

The application of plasma-induced partial oxidation in a mobile system was first attempted by a research group at Massachusetts Institute of Technology. The plasmatron proposed by that group has been applied in various plasma partial oxidation processes with different types of fuel (Bromberg, Cohn, Rabinovich, & Alexeev, 1999; Bromberg et al., 2000; Bromberg, Cohn, Rabinovich, & Heywood, 2001).

Other plasma sources, such as a corona discharge that uses a pin-to-disc type configuration and is operated at a relatively low frequency, have been reported (Supat, Kruapong, & Chavadej, 2003). A low-temperature partial oxidation process using DBD was also reported. In that case, because of the low temperature of the reaction, the oxygenate pathways are increased; consequently, oxygenated species such as formaldehyde and formic acid survived with the hydrogen in the final product (Larkin, Zhou, Lobban, & Mallinson, 2001). With the same reactor configuration and gap control, once the reduced electric field is controlled to a lower value, the rate of oxygen dissociation decreases, which increases the excitation rate. Excitation rather than

Figure 12.16 Plasma burner (reformer) commercially installed in heavy-duty diesel truck and railway machine.

dissociation of oxygen tends to induce a lower selectivity of oxygenated species and a higher selectivity of C_2 hydrocarbon species. All of these characteristics can be realized by suppressing the heat release and enhancing the plasma chemistry during the partial oxidation process.

A pulse corona obtained from a cylinder-to-wire type reactor configuration has been reported (Sobacchi et al., 2002). The reactor was serially connected to a catalytic reactor, and two process orders (plasma → catalyst vs catalyst → plasma) were compared. In the comparison, preprocessing (plasma → catalyst) showed a very slightly higher hydrogen yield than postprocessing (catalyst → plasma). However, the power consumption exhibited a meaningful difference. That is why, when preprocessing is used, incomplete methane activation by low-temperature plasma is effective in successive catalytic reactions, whereas the catalytic reaction tends to complete the partial oxidation before the product enters the plasma region.

Diesel reforming by a rotating arc has been extensively studied. As mentioned previously, a rotating arc can control the degree to which the plasma is nonthermal and the gas temperature (Lee et al., 2010a, 2007). The partial oxidation process has been applied in a mobile application. An onboard plasma reformer for diesel fuels was adopted in a de-nitric oxide (NO_x) system. Partial oxidation of diesel fuel produces hydrogen, which acts as a reductant in the selective catalytic reduction (SCR) system (Lee et al., 2011; Park et al., 2010), and the configuration can also be applied in plasma-assisted combustion. Partial oxidation of diesel fuel produces hydrogen, which contributes to flame stabilization in the harsh combustion conditions inside a tailpipe. A plasma burner tool for elevating the exhaust gas temperature (Lee et al., 2009; Lee, Kim, Song & Kim, 2014). Figure 12.16 shows the world's first commercialized plasma burner for mobile application in rail machines and heavy-duty trucks.

12.3.2.4 Dry reforming

CO_2 reforming, or dry reforming, refers to the reaction (Eqn (12.37)) of a hydrocarbon (usually methane) and CO_2 to produce a synthesis gas.

$$CH_4 + CO_2 \rightarrow 2CO + 2H_2 \quad \Delta H = 247\ \text{kJ/mol} \tag{12.37}$$

Dry reforming produces synthesis gas with an H_2/CO ratio of 1, which is optimal for the F−T process. Dry reforming has the advantage of using the greenhouse gas CO_2 as a reactant. Considering the attempts to reduce CO_2 emissions, dry reforming can be an attractive choice for hydrogen production. However, dry reforming is a strongly endothermic reaction and has a relatively low process efficiency. In addition, it may generate considerable carbon, which is a challenging problem for a catalytic reaction. Because of these characteristics, dry reforming has attracted less attention than the steam reforming and partial oxidation processes.

However, direct collision of electrons can cause bond dissociation and possibly lower the reaction temperature. Dissociation from collisions of energetic electrons has a threshold value depending on the reacting species, and the threshold value and energy distribution of the generated electrons determine the characteristics of the reaction.

The threshold value for CO−O bond dissociation is 5.52 eV (BO, Yan, Li, Chi, & Cen, 2008b), and that of CH_3−H in the collision of methane gas molecules and electrons is 4.55 eV, which is lower than the dissociation threshold of CO_2 (Darwent, 1970; Dobis & Benson, 1987). Thus, methane dissociation is more likely than CO_2 dissociation under the same plasma source. In fact, all of the plasma sources exhibit a higher conversion of CH_4 than of CO_2 in their dry reforming processes (after the ratio of CH_4 to CO_2 is 1:1) (Bo, Yan, Li, Chi, & Cen, 2008a; Li et al., 2009; Wei, Huang, & Wu, 2001).

In the presence of high-energy electrons, collisions induce both dissociation and excitation. Although the dissociation energy threshold is 5.25 eV, the excitation of CO_2 has a large cross section over about 1 eV of energy (Takekawa & Itikawa, 1998). Considering the typical energy distribution (Maxwellian or Druyvesteyn) (Capriati, Colonna, Gorse, & Capitelli, 1992), the contribution of high-energy electrons is limited and a higher density of excited species is expected. That is an important point when considering the energy efficiency and cost of the process. More importantly, the vibrational excitation state of CO_2 has a relatively low relaxation rate and may contribute to the overall reforming process (Ghorbanzadeh & Modarresi, 2007). In particular, excited species are known to have higher adsorption coefficients in catalysts; this is why plasma−catalyst reactions are promising.

The most common type of plasma source applied to reforming is DBD. Both plate- and coaxial-type configurations have been attempted (Kraus, Eliasson, Kogelschatz, & Wokaum, 2001; Tu, Gallon, Twigg, Gorry, & Whitehead, 2011; Tu & Whitehead, 2012; Wang, Yan, Jin, & Cheng, 2009). An important reason for the use of the DBD configuration is that it is easy to construct a packed-bed type plasma-catalyst reaction system. The environment in a packed-bed type reactor provides the closest interaction between the catalyst surface and discharge volume (Jo, Kim, Lee, & Kang, 2014; Lee, Jo, et al., 2013). Distortion of the discharge volume by the catalyst and the electrical conductivity of the catalyst surface, which is also the discharge surface, change the filamentary structure of the discharge, which affects the conversion of methane and carbon dioxide (Jo et al., 2014; Tu & Whitehead, 2012).

A strong filamentary microdischarge generates electrons with relatively high energies, which increases the conversion of fuels but also tends to increase the coke formation.

In dry reforming, the CH_4/CO_2 ratio is generally an important parameter of the reaction. Because CO_2 is an oxygen source, increasing the amount of CO_2 from a 1:1 ratio of CH_4 to CO_2 helps enhance the methane conversion. Likewise, in the plasma dry reforming process, increasing the amount of CO_2 causes increased methane conversion. In addition, increasing the amount of CO_2 positively affects the conversion of CO_2 itself by increasing the multistage ionization (Wang et al., 2009).

Plasma dry reforming using a plasma source that is somewhat close to a thermal plasma, rather than typical nonthermal plasma sources such as a DBD, has also been reported. Bo et al. (Bo et al., 2008b) reported that in dry reforming using a gliding arc plasma, the process cost is lower than that of other nonthermal plasma sources; this is why a thermal environment is used in the conversion of CH_4/CO_2.

Yan et al. compared dry reforming by DC arc and pulsed DC arc plasmas (Yan, Wang, Jin, & Cheng, 2010). They concluded that a DC arc is better than a pulsed DC arc in terms of conversion and selectivity. The difference originates from the use of thermal energy in the conversion of CH_4/CO_2 because the pulsed state of discharge is negative for production of thermal energy. In the reported case, DC power showed a cost of 120 kJ/L for hydrogen production, which corresponds to the typical cost of nonthermal plasma sources for hydrogen production. Considering that the thermal characteristics might have a useful function, the reported cost seems to be too high and requires further optimization.

To avoid the expense of a nonthermal plasma and excessive heating by thermal plasma sources, plasma sources having characteristics between those of nonthermal and thermal sources have been investigated. Daihong et al. (Li et al., 2009) adopted a pin-type electrode to generate plasma with a jet configuration, which produced a glow-type plasma.

Only the current increases in the proposed plasma source, with no increase in the voltage, which is typical of a normal glow discharge. In this case, the increased spatial uniformity of the discharge distributes the thermal energy around the reaction volume and results in efficient energy usage.

12.4 Feedstocks of hydrogen

To produce hydrogen by a plasma process, different types of hydrocarbon species are used as the feedstock. The following are the most commonly used feedstocks.

1. Light paraffins such as methane and propane are most commonly used (Czernichowski, Czernichowski, & Czernichowski, 2003; Czernikowski, Czernikowski, & Wesolowska, 2003a).
2. Commercial liquid fuels or gasoline, diesel, and kerosene (Gallagher et al., 2010; Lee, Kim, Cha, & Song, 2010b; Rollier et al., 2008).
3. Heavy hydrocarbon species to simulate or replace liquid fuel (Czernichowski, Czernichowski, & Czernichowski, 2002; Sekiguchi & Mori, 2003).

4. Gas-phase biomass such as landfill gas (Chun, Yang, & Yoshikawa, 2009; Goujard, Tatibouët, & Batiot-Dupeyrat, 2009).
5. Liquid-phase biomass such as soybean and rapeseed oil (Czernikowski, Czernikowski, & Wesolowska, 2003b; Rafiq & Hustad, 2011; Wemlinger et al., 2009).
6. Oxygenated hydrocarbon species such as methanol, ethanol, and dimethyl ether (Sarmiento et al., 2007; Yanguas-Gil, Hueso, Cotrino, Caballero, & Gonzalez-Elipe, 2004; Zou, Zhang, & Liu, 2007).

The following points should be considered when choosing the hydrogen source.

1. Feedstock supply

Any special conditions or environment for the application should be considered. For instance, mobile applications should be based on commercial fuel from a gas station. Electricity generation at landfill sites should be based on landfill gas.

2. H/C ratios in reactant and product

The hydrogen yield from a process is determined primarily by the number of hydrogen atoms in the fuel. The H/C ratio of hydrocarbon fuel is generally higher at lower carbon numbers; thus, methane has the largest value, 4. If the F–T process using the product is included in the design, the H_2/CO ratio should be close to 1, which is also based on the consideration of the fuel H/C ratio.

3. Whether the reactant contains oxygen

In a typical reforming process, H_2O, oxygen (air), and CO_2 supply the oxygen necessary for the process. However, an oxygenated hydrocarbon feedstock such as methanol can produce a synthesis gas without a supply of oxygen in the reactant.

4. The phase of the fuel

For a liquid- or solid-phase fuel, an additional facility for gasification/vaporization is required. In most of the research that adopts a liquid-phase fuel, the evaluation of the process cost does not include the cost of this pretreatment step. Further, for a more accurate evaluation of the process, all of these pretreatment costs should be included. What is especially important in the plasma process is that the phase of the reactant affects the discharge instability. The liquid phase can affect the dielectric constant and conductivity of the reaction field; furthermore, an electronegative reactant causes further instability in the discharge. Therefore, thermal plasma that can provide heat for gasification/vaporization is beneficial.

5. Reactivity and cost

A plasma process inevitably incurs a cost for electricity; the overall cost of hydrogen production is more sensitive to the feedstock cost.

The thermal efficiency is another important factor for evaluating the process cost. As mentioned previously, among the reforming processes, autothermal processes have the highest thermal efficiency. In addition to the type of process itself, different fuels have different heating values thus different inherent thermal efficiencies. The highest possible thermal efficiencies of selected fuels are presented in Table 12.5.

Table 12.5 Maximum theoretical thermal efficiency of selected fuels in autothermal reforming

Fuel	$\Delta H_{f,fuel}$ (kcal/gmol)	Efficiency (%)
Methanol (CH_3OH (I))	−57.1	96.3
Methane (CH_4)	−17.9	93.9
Ethane (C_2H_6)	−20.2	92.4
Ethanol (C_2H_6O (I))	−108.6	93.7
Pentane (C_5H_{12} (g))	−35.0	91.5
Benzene (C_6H_6 (I))	11.7	88.2
Iso-octane (C_8H_{18} (I))	−62	91.2
Gasoline ($C_{7.3}H_{14.8}O_{0.1}$ (I))	−53	90.8

Data from Ahmed and Krumpelt (2001).

The recent development of shale gas production significantly lowered the price of natural gas (Kennedy, Knecht, & Georgi, 2012; Paltsev et al., 2011). On the basis of this trend, various attempts to synthesize olefin, a base material in the chemical industry, from natural gas instead of naphtha have been reported. Considering the shift from petrochemicals to natural gas chemicals, natural gas is the most attractive hydrogen feedstock.

12.5 Advantages and disadvantages of hydrogen production via the Kværner process and plasma reforming

12.5.1 Advantages of plasma process

Most previous hydrogen production processes were based on the catalytic process. Therefore, the advantages of the plasma process should be estimated in terms of their differences from the catalytic process. The plasma and catalytic processes can be compared using parameters such as the possible poisoning, durability, required facilities, and reaction velocity, as listed briefly in Table 12.6.

The advantages of the plasma process are described in detail as follows.

1. The most important benefit of the plasma process over the catalytic process is that the reaction is initiated without thermal activation. A catalytic reaction, which is governed by thermal equilibrium, requires thermal energy to elevate the temperature of the entire reactant to the designed value. In a plasma process, however, because of the nonthermal nature of the process, high-energy electrons can be produced, and the reaction for the desired product can be initiated using these electrons, without raising the bulk gas temperature to an equilibrium value. Heating the reactant is certainly also beneficial for the plasma process, but what is important is that the chemically active species generated by the plasma can initiate a reaction.

Table 12.6 Comparison of catalyst and plasma processes

	Catalyst process	Plasma process
Poisoning	Possible coking	Coke-free
Pretreatment (including heating)	Heating (if necessary)	Simple (heating is not necessary)
Reaction volume	Large (low S/V)	Small
Lifetime	Depends on catalyst	Depends on electrode erosion
Start-up time	Slow	Fast

2. The plasma process is a coking-insensitive process. At any temperature, coking cannot be a severe problem of deactivation. Rather, as in the Kværner process, carbon species generated during the plasma process can be used as another product.
3. There is no need for pretreatment of the reactant. In a catalytic process, depending on the process, the reactant may require a pretreatment such as desulfurization. However, low concentrations of sulfur or other additives in the reactant do not affect the electrode or the discharge process, and pretreatment is not necessary. The reduction or removal of any step in the entire process is important in terms of the installation cost and system volume.
4. Next, the advantage of durability and reliability can be addressed. In nonthermal plasma, material durability is not a concern. In thermal plasma, electrode erosion is possible. However, cooling and optimization of the material can guarantee long-term operation of the system. Highly thermal plasma sources such as the thermal torch are inappropriate for the reforming process. The thermal plasma sources used in reforming are exposed to a much less thermal environment than the thermal torch and are actually close to a nonthermal plasma.
5. The next advantage is that the plasma process provides quick reaction start-up. Thermal pyrolysis and catalytic systems that require a high temperature for a reaction inevitably require a long time to heat the reaction system in the start-up procedure. In contrast, the plasma process does not rely on thermal activation, and time for heating the reactant is not necessary. The point is important in applications that involve frequent on/off operation. Figure 12.17 shows the time to reach de-NO_x performance in a hydrocarbon- (HC-) SCR system in which a plasma reformer supplies the reducing agent. The production of hydrogen and light hydrocarbon species from diesel fuel begins when the plasma reactor is switched on. The observed time delays are mainly those caused by the flow path between the SCR catalyst and reformer and the distance between the SCR catalyst and NO_x measurement system.
6. Finally, a reaction in plasma does not occupy the reacting volume. In a typical catalytic reforming reaction, except for the oxidation process, the reforming process itself exhibits a rather slow reaction, with a GHSV of less than 10,000 h^{-1}. For plasma, however, although a direct comparison is not available, GHSV values of hundreds of thousands per hour are obtainable. This is an important advantage of the system design.

Among these advantages of using plasma, considering the small reaction volume, possible quick start-up, and simple reaction system (without the need for other

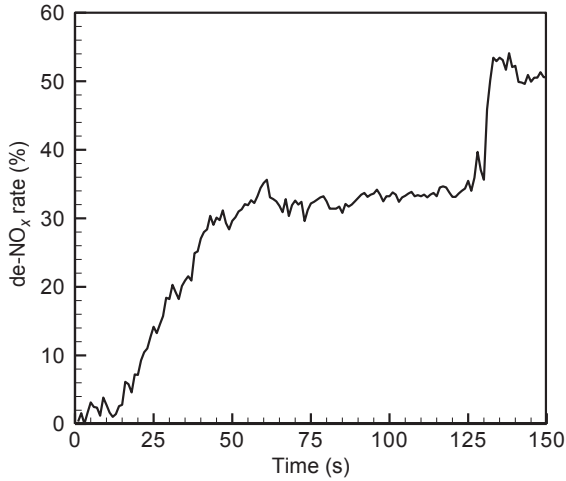

Figure 12.17 Time history of de-NO_x performance in HC-SCR system in which a plasma diesel reformer supplies the reducing agent.

facilities), the most appropriate applications of plasma are mobile applications. In fact, the concept of onboard reforming first brought attention to plasma reforming, and many researchers have developed plasma processes for transport systems. Further, the first commercial plasma reformer was also an onboard diesel reformer.

12.5.2 Disadvantages of plasma process

In applications of the plasma process, the most important drawback of the process is that it consumes electrical energy, which is an expensive energy source. The characteristic of "nonequilibrium" function is an important benefit of plasma, but it is one side of a coin, the other side of which is inefficient energy usage. Most reactions steered by high-energy species are initiated by electrons with energies of a few electronvolts, but these high-energy species have low number densities. Depending on the method of generation, electrons with densities of 10^8–10^{13} cm^{-3} have less impact in terms of the product yield, which reduces the efficiency of the process.

If the process conditions for a specific product require a low-temperature environment with a high-threshold energy for initiation, which is typical in ozone generation, regardless of the absolute value of the yield, the benefits of the "nonthermal" nature of the plasma can be fully exploited (Kogelschatz, Eliasson, & Hirth, 1988). However, in hydrogen production, which requires some method of thermal activation, the nonequilibrium nature of plasma has both advantages and disadvantages. The definition of the thermal efficiency in Eqn (12.16), in which the electrical power term is in the denominator, clearly shows that optimization of the process to reduce the electrical power consumption is essential. The sensitivity of the thermal efficiency to the electrical power can be obtained from Eqn (12.16), as shown in Eqn (12.38).

$$\frac{d\eta}{dP_e} = \frac{-(n_{H_2} + n_{co})\Delta H_{H_2}}{(n_{fuel}\Delta H_{fuel} + Q + P_e)^2} \tag{12.38}$$

Here the electrical power term in the denominator is squared and is critical for optimizing the efficiency.

The process cost of plasma can be evaluated from two different viewpoints. One is based on the total volume of a reactant or the specific energy density (SED, J/L); the other is based on the hydrogen produced or the specific input energy density (J/L). Typical SED values for nonthermal plasma sources used in reforming range from tens to hundreds of kJ/L, and in thermal plasma they are a few kJ/L to tens of kJ/L.

Considering that 1 J/L of energy is roughly equivalent to the energy required to heat 1 L of air by 1 °C, tens to hundreds of kJ/L is too much energy compared with the simple thermal energy used to heat the entire reactant. Instead, the value of the plasma process lies in the simplicity of the facility, the reactor volume, and so on.

The most obvious benefit of the catalytic process is that selective production under thermal equilibrium is possible. In contrast, in the plasma process, only the threshold level of reaction initiation is determined, but owing to the statistical properties of the electrons (Figure 12.18) (Capriati et al., 1992), a selective reaction is harder to obtain. The electron generation itself means the generation of a distribution of electrons with various energy states.

The statistical properties of electrons place an inherent limit on selective reactions. An exception is acetylene production, where further dehydrogenation and decomposition are hard to obtain; the use of thermal plasma can provide somewhat highly selective production of acetylene with an optional quenching step (Onoe, Fujie, Yamaguchi, & Hatano, 1997; Shakourzadeh Bolouri & Amouroux, 1986). However, this capacity weakens as the plasma source more closely resembles nonthermal plasma.

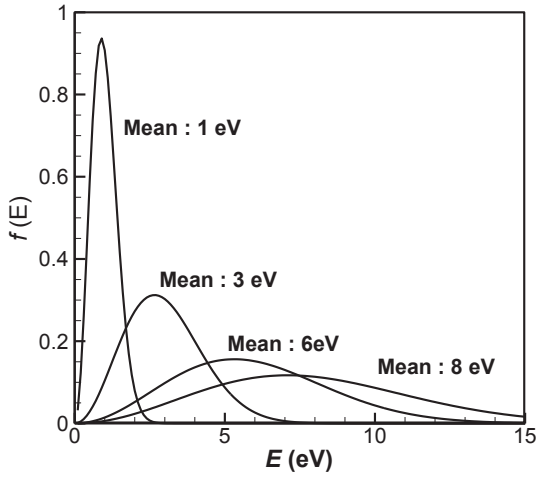

Figure 12.18 Maxwell–Boltzmann electron energy distribution according to mean electron energy.

In the case of hydrogen production, increasing the thermal environment can elevate the hydrogen selectivity to about 100%, but the shortage of thermal energy results in the production of a considerable amount of other hydrocarbon species (Lee et al., 2010a, 2007).

The application of plasma should be based on the consideration of these advantages and disadvantages of the plasma process.

12.6 Conclusion

Diverse technological aspects of hydrogen generation by plasma are introduced. For the understanding of the plasma process, principles of plasma generation and application are briefly introduced. After that, detailed explanations of each process are introduced with the discussion of advantage and disadvantage of using plasma as a tool of hydrogen generation.

The Kvaerner process and reforming process have been tried to achieve economic feasibility of industrially applicable hydrogen generation. However, the advancement of the technology should be steered by the insights and information on the fast changing market. Important trends in the future applications of plasma for the production of hydrogen can be considered in terms of the process itself and of changes in the market and environment.

12.6.1 Environmental and market changes

Recent changes in energy and environmental issues affect the potential of hydrogen production. Hydrogen usage in industry to date is confined to use in a chemical process for ammonia synthesis and refining by upgrading heavy crude oil into refined fuels (Holladay et al., 2009; Ramachandran & Menon, 1998). In other words, the use of hydrogen is limited to the field of material processing. Despite various recent attempts to use hydrogen in the field of energy and the environment, there is still no meaningful market for applications. Fuel cells are one of the major markets for hydrogen, and much research on hydrogen production is motivated by interest in fuel cell systems. However, recent advances in hybrid and electric vehicles make it more difficult to expect any expansion of the fuel cell vehicle and hydrogen market.

Direct combustion of hydrogen also has not found a place yet in mobile applications. Instead, hybridized combustion of hydrogen and fuel by onboard reforming to reduce emissions seems more realistic and immediately likely than direct combustion of hydrogen.

Energy carrier does not currently seem to occupy the role of hydrogen and additives for existing combustion systems, and chemical processes are more realistic and feasible for the near future. Hydrogen-assisted combustion and hydrogen-assisted posttreatment are representative examples of these processes. First, hydrogen-assisted combustion can be applied to low NO_x combustion. Flue gas recirculation is a typical way of reducing NO_x in combustion devices, but an increase of the amount of flue gas in reactant inevitably cause abrupt increase in CO content in the product.

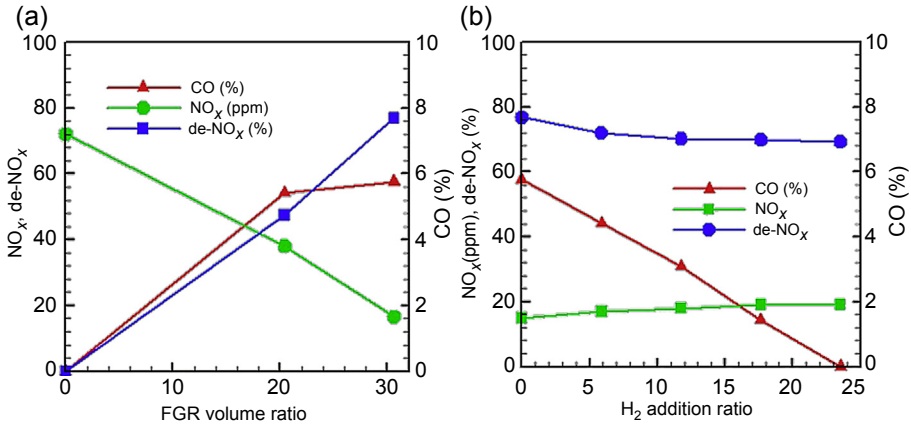

Figure 12.19 NO_x reduction by FGR in industrial boiler (a) and suppression of CO in the course of FGR by addition of on-site hydrogen (b).

Here, the addition of hydrogen in the flue gas recirculation effectively suppresses increase of CO without increase of NO_x, as shown in Figure 12.19. The concept has been further developed as an HCNG or dual-fuel internal combustion engine (Boehman & Corre, 2008; Ma et al., 2008; Shirk, McGuire, Neal, & Haworth, 2008; Verhelst & Wallner, 2009).

This concept can lessen the burden of CO_2 reduction. Table 12.7 compares the CO_2 emissions of various types of onboard reforming technology and the existing internal combustion engine (Dunn, 2002; Pembina Institute, 2000).

Representative emissions from diesel fuel are NO_x, CO, and particulate material. NO_x is typically removed by an SCR process that reduces NO_x into N_2 by a reaction between NO_x and a reducing agent in the SCR catalyst (Johnson, 2010). The reducing agents used in the SCR process are NH_3 (urea) or hydrocarbon species. The reducing agent itself is a parameter for classifying SCR processes. In NH_3- (urea-) SCR, NH_3 (urea) is adopted as a reducing agent, and in HC-SCR hydrocarbon (fuel) is adopted.

The HC-SCR system is simpler and less expensive to install than the NH_3-SCR system but exhibits a lower de-NO_x rate. Recent studies have reported that the addition of hydrogen in HC-SCR greatly enhances the de-NO_x performance of the

Table 12.7 CO_2 reduction by using onboard reforming technology

Method	g-CO_2/km-traveled
Gasoline ICE	247
Onboard gasoline fuel processing	194
Onboard methanol fuel processing	163
Centralized natural gas reforming	70
Decentralized natural gas reforming	80

HC-SCR catalyst. The reason is that hydrogen induces fast oxidation of hydrocarbon species, resulting in the formation of amine and light hydrocarbon species (Breen & Burch, 2006; Lee et al., 2012). Especially for an Ag catalyst, aromatic hydrocarbon species, which are a major cause of catalyst deactivation, are oxidized with local heating of the catalyst active site by hydrogen combustion (Arve, Backman, Klingstedt, Eränen, & Murzin, 2007).

Considering this information, in addition to the existing applications of hydrogen in chemical processes, it seems that combustion and emission control will be the next major application. In particular, onboard reforming by plasma partial oxidation is the candidate most likely to satisfy continuously strengthened environmental regulations.

Two recently emerging trends in power generation are the active exploitation of new and renewable energy sources and distributed power generation. What is remarkable is that for most new and renewable energy sources, the final product is in the form of electrical energy. Increased degrees of freedom in on-site electricity usage for plasma generation by distributed power generation and continuous reductions in the cost of power generation will be advantageous for possible commercialization of the plasma process.

12.6.2 Development of new plasma processes

12.6.2.1 Plasma-catalyst fusion process

In terms of the process itself, plasma catalysis in plasma catalytic processes is emerging as a possible method of overcoming the existing limitations of the plasma process. Plasma catalysis can provide a synergistic effect due to the high selectivity of the catalyst and low-temperature activation of the plasma. In addition, by combining the two, concerns about the cost of the plasma process can be resolved to some degree. However, discharge phenomena interact closely with the catalyst material, and the plasma-induced kinetics can strongly affect heterogeneous reactions on the catalyst surface. Therefore, without a clear understanding of the interactive phenomena, a simple spatial combination of the two may result in a simple summing or even a negative effect on the process. A few fine reviews on plasma catalysis are available that will be helpful for understanding the physics underlying the interaction (Boutonnet Kizling & Jaras, 1996; Chen, Lee, Chen, Chao, & Chang, 2008; Van Durme, Dewulf, Leys, & Van Langenhove, 2008).

Plasma catalysis can be classified into two different types. One acts by a simple serial connection between the plasma and the catalyst; the other acts by discharge on the catalytic surface. In the serial type, the interactions of the plasma's and catalyst's reaction and properties are not very strong, but in the other case, the interactive aspects become an important parameter in the process. The catalysts are generally metallic or electrically conductive components that may alter the electric field and surface charge of the catalyst (Jo et al., 2014). The conductive catalyst surface alters the structure of the microdischarge, decreasing the electron energy. In addition, radicals produced by the discharge process are produced in a very short time scale from the onset of the discharge, and the radical-induced reaction path alters the kinetics of

the catalyst (Kim et al., 2014). What is important in these interactions is the role of excited species. In methane reforming, vibrationally excited methane may affect the reaction kinetics because of the short lifetime of these excited species, which ranges from a few nanoseconds to tens of nanoseconds. The use of these excited species is an important concern in determining the synergetic effect in plasma catalysis.

12.6.2.2 Atmospheric pressure glow discharge

A recent increase in the possible applications of atmospheric pressure plasma is driving the development of entirely new plasma sources. Glow plasma at low pressure, which can typically be observed in semiconductor processing, has high spatial uniformity. Under atmospheric pressure, however, it is hard to generate a uniform plasma. DBD and corona discharge produce a filamentary microdischarge, and a uniform discharge is not obtainable. Many researchers have nonetheless tried to develop a glow plasma under atmospheric pressure (Francoise et al., 1998; Trunec, Brablec, & Buchta, 2001). The necessary conditions for this are (1) a very narrow spatial gap in the discharge volume, (2) discharge driven by very short (ranging from a few nanoseconds to tens of nanoseconds) pulses or nanopulses, and (3) the use of an inert gas such as He or Ar. These conditions suppress the development of streamers, induce motion only in light particles or electrons without the transfer of ions to the electrode, and produce a discharge in a rather low electric field. Various methods of realizing these conditions are the key to the development of atmospheric pressure glow discharge.

12.7 Sources of further information and advice

12.7.1 Related conferences

Followings are list of conferences related to a plasma process and plasma physics.

- *ISPC: International Symposium on Plasma Chemistry*

ISPC is a biannual conference and deals the topics of plasma process, plasma sources. ISPC is the biggest conference in this topic. Its latest conference was held in Cairn, Australia, in 2013; the next one is to be held in Antwerp, Belgium, July 5−10, 2015.

- *ICOPS: International Conference on Plasma Science*

ICOPS is an annual conference steered by IEEE. The conference covers traditional plasma physics and engineering topics. The latest conference was held in Washington, DC, on May 25−29, 2014; the next meeting will be held in Antalya, Turkey, May 24−28, 2015.

- *ISNTP: International Symposium on Nonthermal/Thermal Plasma Pollution Control Technology & Sustainable Energy*

ISNTP is a biannual conference especially focused on nonthermal plasma process. ISNTP is rather a small conference but has specialty in nonthermal plasma process. The latest one was held in Dalian, China, June 16−20, 2014.

- *ESCAMPIC: Europhysics Conference on Atomic and Molecular Physics of Ionized Gases*

ESCAMPIC is a biannual conference steered by the European Physical Society. The conference deals topics about basics of plasma physics and application. The most recent meeting was held in Greifswald, Germany, July 15−19, 2014; the next meeting will be in Bratislava, Slovakia, in 2016.

- *GEC: Gaseous Electronics Conference*

GEC is annual conference that covers diverse phenomena in discharge system. The latest conference was held in in Raleigh, NC, during November 2−7, 2014; the next (68th) will be held in Honolulu, HI, October 12−16, 2015.

- *EPS: European Physical Society Conference on Plasma Physics*

The EPS conference covers the wide field from nuclear fusion research to the low-temperature plasmas as well as space and astrophysical plasmas. The last meeting was in Berlin, June 23−27, 2014; the next meeting will be held in Lisbon, Portugal, June 22−26, 2015.

12.7.2 Related journals

Journals where articles regarding the topics of plasma process, plasma chemistry, hydrogen production, and recent plasma catalysis can be found are listed below.

Plasma Chemistry and Plasma Processing
International Journal of Hydrogen Energy
Journal of Physics D: Applied Physics
Physics of Plasma
Plasma and Polymers
Applied Catalysis A: General
Applied Catalysis B: Environmental
IEEE Transactions of Plasma Science
Chemical Engineering Journal
Fuels
Energy & Fuels
Catalysis Today

12.7.3 Recommended review articles

Recommended review articles about the topic of hydrogen generation by plasma process are listed.

Petipas, G., et al. (2007). A comparative study of non-thermal plasma-assisted reforming technologies. *International Journal of Hydrogen Energy*, *32*, 2848−2867.
Lee, D. H., et al. (2013). Mapping plasma chemistry in hydrocarbon fuel processing process. Plasma Chemistry and Plasma Processing, *33*, 249−269.
Chen, H. L., et al. (2008). Review of plasma catalysis on hydrocarbon reforming for hydrogen production-Interaction, integration and prospects. *Applied Catalysis B: Environmental*, *85*, 1−9.

Samukawa, S., et al. (2012). The 2012 Plasma Roadmap. *Journal of Physics D: Applied Physics*, *45*, 253001.
Holladay, J.D., Hu, J., King, D. L., & Wang, Y. (2009). An overview of hydrogen production technologies. *Catalysis Today*, *139*, 244−260.

Nomenclature

d	Distance between electrodes
$\mathbf{e}$	Electron charge
$E_\mathbf{e}$	Energy gained by electron
E	Electric field
l	Mean free path
n	Concentration of neutral particles
P	Pressure
$P_\mathbf{e}$	Electric power for discharge
Q	Heat (across the reaction system)
$T_\mathbf{e}$	Electron temperature
$T_\mathbf{i}$	Ion temperature
$T_\mathbf{o}$	Gas temperature (heavy molecule)
$T_\mathbf{r}$	Rotational temperature
$T_\mathbf{v}$	Vibrational temperature
$V_\mathbf{s}$	Breakdown voltage
η	Thermal efficiency
ΔH	Heat of reaction
ΔH_f	Enthalpy of formation

List of acronyms

AC	Alternating current
DC	Direct current
DBD	Dielectric barrier discharge
GHSV	Gas hourly space velocity (S/V)
ICE	Internal combustion engine
NO_x	Nitric oxides (NO, NO_2)
O/C	Oxygen to carbon ratio (in fuel)
PO_x	Partial oxidation
SCR	Selective catalytic reduction
HC-SCR	Selective catalytic reduction using HC as reductant
NH_3 SCR	Selective catalytic reduction using NH_3 as reductant
SED	Specific energy density (energy required for the unit volume of reactant)
SRO	Steam reforming with oxygen
RF	Radiofrequency

References

Ahmed, S., & Krumpelt, M. (2001). Hydrogen from hydrocarbon fuels for fuel cell. *International Journal of Hydrogen Energy, 26*, 291−301.

Ahmed S., Krumpelt, M., Kumar, R., Lee S. H. D., Carter J. D., Vlilkenhoener R., et al. (1998). Catalytic partial oxidation reforming of hydrocarbon fuels. In *Proceeding of 1998 fuel cell seminar, November 16−19*. CA: Palm Springs.

Anderson, R. P., Fincke, J. R., & Taylor, C. E. (2002). Conversion of natural gas to liquids via acetylene as an intermediate. *Fuel, 81*, 909−925.

Arve, K., Backman, H., Klingstedt, F., Eränen, K., & Murzin, D. Yu. (January 31, 2007). Hydrogen as a remedy for the detrimental effect of aromatic and cyclic compounds on the HC-SCR over Ag/alumina. *Applied Catalysis B: Environmental, 70*(1−4), 65−72.

Bakken, J. A., Jensen, R., Monsen, B., Raaness, O., & Waernes, A. N. (1998). Thermal plasma process development in Norway. *Pure and Applied Chemistry, 70*(6), 1223−1228.

Benilov, M. S., & Naidis, G. V. (2006). Modeling of hydrogen-rich gas production by plasma reforming of hydrocarbon fuels. *International Journal of Hydrogen Energy, 31*, 769−774.

Bo, Z., Yan, J., Li, X., Chi, Y., & Cen, K. (2008a). Plasma assisted dry reforming using gliding arc gas discharge: effect of feed gases proportion. *International Journal of Hydrogen Energy, 33*, 5545−5553.

Bo, Z., Yan, J., Li, X., Chi, Y., & Cen, K. (October 2008b). Plasma assisted dry methane reforming using gliding arc gas discharge: effect of feed gases proportion. *International Journal of Hydrogen Energy, 33*(20), 5545−5553.

Boehmana, A. L., & Corre, O. Le. (2008). Combustion of syngas in internal combustion engines. *Combustion Science and Technology, 180*(6), 1193−1206.

Boutonnet Kizling, M., & Jaras, S. G. (1996). A review of the use of plasma techniques in catalyst preparation and catalytic reactions. *Applied Catalysis A: General, 147*, 1−21.

Breen, J. P., & Burch, R. (September 2006). A review of the effect of the addition of hydrogen in the selective catalytic reduction of NO_x with hydrocarbons on silver catalysts. *Topics in Catalysis, 39*(1−2), 53−58.

Bromberg, L., Cohn, D. R., Rabinovich, A., & Alexeev, N. (December 1999). Plasma catalytic reforming of methane. *International Journal of Hydrogen Energy, 24*(12), 1131−1137.

Bromberg, L., Cohn, D. R., Rabinovich, A., Alexeev, N., Samokhin, A., Ramprasad, R., et al. (December 2000). System optimization and cost analysis of plasma catalytic reforming of natural gas. *International Journal of Hydrogen Energy, 25*(12), 1157−1161.

Bromberg, L., Cohn, D. R., Rabinovich, A., & Heywood, J. (October 2001). Emissions reductions using hydrogen from plasmatron fuel converters. *International Journal of Hydrogen Energy, 26*(10), 1115−1121.

Bromberg, L., Cohn, D. R., Rabinovich, A., O'Brien, C., & Hochgreb, S. (1998). Plasma reforming of methane. *Energy & Fuels, 12*, 11−18.

Capriati, G., Colonna, G., Gorse, C., & Capitelli, M. (September 1992). A parametric study of electron energy distribution functions and rate and transport coefficients in nonequilibrium helium plasmas. *Plasma Chemistry and Plasma Processing, 12*(3), 237−260.

Chen, H. L., Lee, H. M., Chen, S. H., Chao, Y., & Chang, M. B. (December 17, 2008). Review of plasma catalysis on hydrocarbon reforming for hydrogen production—Interaction, integration, and prospects. *Applied Catalysis B: Environmental, 85*(1−2), 1−9.

Chun, Y. N., Yang, Y. C., & Yoshikawa, K. (2009). Hydrogen generation from biogas reforming using a gliding arc plasma-catalyst reformer. *Catalysis Today, 148*, 283−289.

Cormier, J. M., & Rusu, I. (2001). Syngas production via methane steam reforming with oxygen : plasma reactors versus chemical reactors. *Journal of Physics D: Applied Physics, 34*, 2798−2803.

Czernichowski, A., & Czernichowski, P. (2000). Pyrolysis of natural gas in the gliding electric discharges. In *Proceeding of 10th Canadian hydrogen conference* (Quebec, Canada).

Czernichowski, M., Czernichowski, P., & Czernichowski, A. (2002). Non-catalytical reforming of various fuels into syngas. In *France Deutschland fuel cell conference on "material, engineering, systems, applications", October 7−10*.

Czernichowski, M., Czernichowski, P., & Czernichowski, A. (2003). Glidarc assisted reforming of carbonaceous feedstocks into synthesis gas. In *Detailed study of propane. 16th international symposium on plasma chemistry, Taormina* (symposium proceedings).

Czernikowski, A., Czernikowski, M., & Wesolowska, K. (2003). Glidarc-assisted reforming of propane into synthesis gas. In *First European hydrogen energy conference, Grenoble, France, September 2−5*.

Czernikowski, A., Czernikowski, M., & Wesolowska, K. (2003). Glidarc-assisted production of synthesis gas from rapeseed oil. In *1st European hydrogen energy conference, Grenoble, France* (symposium proceedings).

Darwent, D. B. (1970). *Bond dissociation energies in simple molecules* (vol. 31). Washington, DC: NBSDS-NBS.

Dicks, A. L. (1996). Hydrogen generation from natural gas for the fuel cell systems of tomorrow. *Journal of Power Sources, 61*, 113−124.

Dobis, O., & Benson, S. W. (1987). Analysis of flow dynamics in a new, very low-pressure reactors. Application to the reaction $Cl + CH_4 = HCl + CH_3$. *International Journal of Chemical Kinetics, 19*, 691−708.

Dunn, S. (March 2002). Hydrogen futures: toward a sustainable energy system. *International Journal of Hydrogen Energy, 27*(3), 235−264.

Francoise, M., Ahmed, R., Philippe, D., Rami Ben, G., Pierre, S., & Christian, M. (1998). Experimental and theoretical study of a glow discharge at atmospheric pressure controlled by dielectric barrier. *Journal of Applied Physics, 83*(6), 2950−2957.

Fridman, A. (2008). *Plasma chemistry*. Cambridge University press.

Fridman, A., Nester, S., Kennedy, L. A., Saveliev, A., & Yardimci, O. M. (1999). Gliding arc gas discharge. *Progress in Energy and Combustion Science, 25*, 211−231.

Gallagher, M. J., Geiger, R., Polevich, A., Rabinovich, A., Gutsol, A., & Fridman, A. (June 2010). On-board plasma-assisted conversion of heavy hydrocarbons into synthesis gas. *Fuel, 89*(6), 1187−1192.

Ghorbanzadeh, A. M., & Modarresi, H. (2007). Carbon dioxide reforming of methane by pulsed glow discharge at atmospheric pressure: the effect of pulse compression. *Journal of Applied Physics, 101*, 123303.

Goujard, V., Tatibouët, J.-M., & Batiot-Dupeyrat, C. (February 1, 2009). Use of a non-thermal plasma for the production of synthesis gas from biogas. *Applied Catalysis A: General, 353*(2), 228−235.

Griffiths, D. J. (1999). *Introduction to electrodynamics*. Prentice-Hall.

Grill, A. (1993). *Cold plasma in material fabrication*. IEEE Press.

Holladay, J. D., Hu, J., King, D. L., & Wang, Y. (2009). An overview of hydrogen production technologies. *Catalysis Today, 139*, 244−260.

Lee, D. H., Lee, J.-O., Kim, K.-T., Song, Y.-H., Kim, E., & Han, H.-S. (2011). Characteristics of plasma-assisted hydrocarbon SCR system. *International Journal of Hydrogen Energy, 36*, 11718−11726.

Lee, D. H., Kim, K.-T., Suk Cha, M., Ok Lee, J., Song, Y.-H., Cho, H., et al. (2009). Active regenerative DPF using a plasma assisted burner. In *Proceeding of SAE international powertrains, fuels and lubricants meeting*. SAE 09SFL-0065.

Jasinski, M., Dors, M., Nowakowska, H., & Mizeraczyk, J. (2008). Hydrogen production via methane reforming using various microwave plasma sources. *Chemicke Listy, 102*, s1332−s1337.

Jo, S., Kim, T., Lee, D. H., & Kang, W. S. (2014). Effect of the electric conductivity of a catalyst on methane activation in a dielectric barrier discharge reactor. *Plasma Chemistry and Plasma Processing, 34*, 175−186.

Johnson, T. V. (August 2010). Review of diesel emissions and control. *SAE International Journal of Fuels and Lubricants, 3*(1), 16−29.

Kado, S., Sekine, Y., Muto, N., Nozaki, T., & Okazaki, K. (2003). Application of non-thermal plasmas to natural gas utilization. In *Proceeding of 16th ISPC, international symposium on plasma chemistry* (Taorima, Italy).

Kado, S., Urasaki, K., Sekine, Y., Fujimoto, K., Nozaki, T., & Okazaki, K. (2003). *Fuel, 8*, 2291−2297.

Kappes, T., Hammer, T., & Ulrich, A. (2003). Methane reforming with low energy electron beans. In *Proceeding of 16th ISPC, international symposium on plasma chemistry*.

Kennedy, R. L., Knecht, W. N., & Georgi, D. T. (2012). Comparisons and contrasts of shale gas and tight gas developments, North American experience and trends. *SPE Saudi Arabia section technical symposium and Exhibition, 11 April, Al-Khobar, Saudi Arabia, SPE-160855-MS*.

Kim, T., Jo, S., Song, Y.-H., & Lee, D. H. (2014). Synergetic mechanism of methanol−steam reforming reaction in a catalytic reactor with electric discharges. *Applied Energy, 113*, 1692−1699.

Kogelschatz, U., Eliasson, B., & Hirth, M. (1988). Ozone generation from oxygen and air: discharge physics and reaction mechanisms. *Ozone: Science & Engineering: The Journal of the International Ozone Association, 10*(4), 367−377.

Kothari, R., Buddhi, D., & Sawhney, R. L. (2008). Comparison of environmental and economic aspects of various hydrogen production methods. *Renewable and Sustainable Energy Reviews, 12*, 553−563.

Kraus, M., Eliasson, B., Kogelschatz, U., & Wokaum, A. (2001). CO_2 reforming of methane by the combination of dielectric barrier discharge and catalysis. *Physical Chemistry Chemical Physics, 3*, 294−300.

Langmuir, I. (1928). Oscillations in ionized gases. *Proceedings of the National Academy of Sciences of the United States of America, 14*, 627−637.

Larkin, D. V., Zhou, L., Lobban, L. L., & Mallinson, R. G. (2001). Product selectivity control and organic oxygenate pathways from oxidation of methane in a silent electric discharge reactor. *Industrial & Engineering Chemistry, 40*, 5496−5506.

Lee, D. H., Jo, S., & Song, Y.-H. (2013). Interactive aspects of plasma-catalyst hybrid reaction. *International Journal of Environmental Science and Technology, 7*(2), 115−120.

Lee, D. H., Kim, K.-T., Cha, M. S., & Song, Y.-H. (2007). Optimization scheme of a rotating gliding arc reactor for partial oxidation of methane. *Proceedings of the Combustion Institute, 31*, 3343−3351.

Lee, D. H., Kim, K.-T., Cha, M. S., & Song, Y.-H. (2010). Plasma-controlled chemistry in plasma reforming of methane. *International Journal of Hydrogen energy, 35*, 10967−10976.

Lee, D. H., Kim, K.-T., Cha, M. S., & Song, Y.-H. (May 2010b). Effect of excess oxygen in plasma reforming of diesel fuel. *International Journal of Hydrogen Energy, 35*(10), 4668−4675.

Lee, D. H., Kim, K.-T., Song, Y.-H., Kang, W. S., & Jo, S. (2013). Mapping plasma chemistry in hydrocarbon fuel processing processes. *Plasma Chemistry and Plasma Processing, 33*, 249−269.

Lee, D. H., Kim, K.-T., Kang, H. S., Jo, S., & Song, Y.-H. (2014). Optimization of NH3 decomposition by control of discharge mode in a rotating arc. *Plasma Chemistry and Plasma Processing, 34*, 111−124.

Lee, D. H., Lee, J.-O., Kim, K.-T., Song, Y.-H., Kim, E., & Han, H.-S. (2012). Hydrogen in plasma-assisted hydrocarbon selective catalytic reduction. *International Journal of Hydrogen Energy, 37*, 3225−3233.

Lee, D. H., Kim, H., Song, Y.-H., & Kim, K.-T. (2014). Plasma burner for active regeneration of diesel particulate filter. *Plasma Chemistry and Plasma Processing, 34*, 159−173.

Lee, D. H., Song, Y.-H., Kim, K.-T., & Lee, J.-O. (2013). Comparative study of methane activation process by different plasma sources. *Plasma Chemistry and Plasma Processing, 33*, 647−661.

Li, D., Li, X., Bai, M., Tao, X., Shang, S., Dai, X., et al. (2009). CO_2 reforming of CH_4 by atmospheric pressure glow discharge plasma: a high conversion ability. *International Journal of Hydrogen Energy, 34*, 308−313.

Ma, F., Liu, H., Wang, Y., Li, Y., Wang, J., & Zhao, S. (January 2008). Combustion and emission characteristics of a port-injection HCNG engine under various ignition timings. *International Journal of Hydrogen Energy, 33*(2), 816−822.

Matsumura, Y., & Nakamori, T. (February 10, 2004). Steam reforming of methane over nickel catalysts at low reaction temperature. *Applied Catalysis A: General, 258*(1), 107−114.

Meek, J. M. (1940). A theory of spark discharge. *Physical Review, 57*, 722−728.

Nozaki, T., Muto, N., Kado, S., & Okazaki, K. (2004). Dissociation of vibrationally excited methane on Ni catalyst Part.1 application to methane steam reforming. *Catalysis Today, 89*, 57−65.

Ogden, J. M. (March 9, 2001). Review of small stationary reformers for hydrogen production. In *Report to the international energy agency*.

Onoe, K., Fujie, A., Yamaguchi, T., & Hatano, Y. (1997). Selective synthesis of acetylene from methane by microwave plasma reactions. *Fuel, 76*(3), 281−282.

Paltsev, S., Jacoby, H. D., Reilly, J. M., Ejaz, Q. J., Morris, J., O'Sullivan, F., et al. (2011). The future of U.S. natural gas production, use, and trade. *Energy Policy, 39*, 5309−5321.

Park, C., Kim, C., Kim, K. T., Lee, D. H., Song, Y.-H., & Moriyoshi, Y. (2010). The influence of hydrogen-enriched gas on the performance of lean NO_x trap catalyst for a light-duty diesel engine. *International Journal of Hydrogen Energy, 35*, 1789−1796.

Patiño, P., Pérez, Y., & Caetano, M. (November 2005). Coupling and reforming of methane by means of low pressure radio-frequency plasmas. *Fuel, 84*(16), 2008−2014.

Paulmier, T., & Fulcheri, L. (2005). Use of non-thermal plasma for hydrocarbon reforming. *Chemical Engineering Journal, 106*, 59−71.

Pembina Institute. (March 2000). *Climate-friendly hydrogen fuel: A comparison of the life-cycle greenhouse gas emissions for selected fuel cell vehicle hydrogen production systems* (Drayton Valley, Alberta).

Potapkin, B., Rusanov, V., & Jivotov, V. K. (2000). Microwave discharge for the environment protection. In E. M. Van Veldhuizen (Ed.), *Electrical discharges for environmental purpose. Fundamentals and applications*. Nova: Huntington.

Rafiq, M. H., & Hustad, J. E. (July 2011). Biosyngas production by autothermal reforming of waste cooking oil with propane using a plasma-assisted gliding arc reactor. *International Journal of Hydrogen Energy, 36*(14), 8221−8233.

Rakass, S., Oudghiri-Hassani, H., Rowntree, P., & Abatzoglou, N. (July 14, 2006). Steam reforming of methane over unsupported nickel catalysts. *Journal of Power Sources, 158*(1), 485−496.

Ramachandran, R., & Menon, R. K. (July 1998). An overview of industrial uses of hydrogen. *International Journal of Hydrogen Energy, 23*(7), 593−598.

Reveau, N., Nikravech, M., Martinie, O., Lefaucheux, P., & Cormier, J.-M. (2000). In H. E. Wagner, J. F. Behnke, & G. Babucke (Eds.), *Proceedings of the seventh international symposium on high pressure, low temperature plasma chemistry (HAKONE VII), Greifswald, Germany* (pp. 252−256).

Rollier, J.-D., Gonzalez-Aguilar, J., Petitpas, G., Darmon, A., Fulcheri, L., & Metkemeijer, R. (2008). Experimental study on gasoline reforming assisted by nonthermal arc discharge. *Energy Fuels, 22*(1), 556−560.

Rostrup-Nielsen, J. R., & Sehested, J. (2003). Steam reforming for hydrogen. The process and the mechanism. *Fuel Chemistry Division Preprints, 48*(1), 218.

Sarmiento, B., Brey, J. J., Viera, I. G., González-Elipe, A. R., Cotrino, J., & Rico, V. J. (June 10, 2007). Hydrogen production by reforming of hydrocarbons and alcohols in a dielectric barrier discharge. *Journal of Power Sources, 169*(1), 140−143.

Sehested, J. (January 15, 2006). Four challenges for nickel steam-reforming catalysts. *Catalysis Today, 111*(1−2), 103−110.

Sekiguchi, H., & Mori, Y. (2003). Steam plasma reforming using microwave discharge. *Thin Solid Films, 435*, 44−48.

Shakourzadeh Bolouri, K., & Amouroux, J. (December 1986). Reactor design and energy concepts for a plasma process of acetylene black production. *Plasma Chemistry and Plasma Processing, 6*(4), 335−348 (희석 참조).

Shirk, M. G., McGuire, T. P., Neal, G. L., & Haworth, D. C. (December 2008). Investigation of a hydrogen-assisted combustion system for a light-duty diesel vehicle. *International Journal of Hydrogen Energy, 33*(23), 7237−7244.

Sobacchi, M. B., Saveliev, A. V., Fridman, A. A., Kennedy, L. A., Ahmed, S., & Krause, T. (2002). Experimental assessment of a combined plasma/catalytic system for hydrogen production via partial oxidation of hydrocarbon fuels. *International Journal of Hydrogen Energy, 27*, 635−642.

Song, C., & Pan, W. (2004). Tri-reforming of methane: a novel concept for catalytic production of industrially useful synthesis gas with desired H_2/CO ratios. *Catalysis Today, 98*, 463−484.

Supat, K., Kruapong, A., & Chavadej, S. (2003). Synthesis gas production from partial oxidation of methane with air in AC electric gas discharge. *Energy & Fuels, 17*, 474−481.

Takekawa, M., & Itikawa, Y. (1998). Vibrational excitation of carbon dioxide by electron impact: symmetric and antisymmetric stretching modes. *Journal of Physics B: Atomic, Molecular and Optical Physics, 31*, 3245−3261.

Townsend, J. S., & Gill, E. W. B. (1938). *Philosophical Magazine Series 7, 26*(174), 290−311.

Trunec, D., Brablec, A., & Buchta, J. (2001). Atmospheric pressure glow discharge in neon. *Journal of Physics D: Applied Physics, 34*, 1697−1699.

Tu, X., Gallon, H. J., Twigg, M. V., Gorry, P. A., & Whitehead, J. C. (2011). Dry reforming of methane over a Ni/Al_2O_3 catalyst in a coaxial dielectric barrier discharge reactor. *Journal of Physics D: Applied Physics, 44*, 274007.

Tu, X., & Whitehead, J. C. (August 2012). Plasma-catalytic dry reforming of methane in an atmospheric dielectric barrier discharge: understanding the synergistic effect at low temperature. *Applied Catalysis B: Environmental, 125*(21), 439−448.

Van Durme, J., Dewulf, J., Leys, C., & Van Langenhove, H. (February 7, 2008). Combining non-thermal plasma with heterogeneous catalysis in waste gas treatment: a review. *Applied Catalysis B: Environmental, 78*(3−4), 324−333.

Verhelst, S., & Wallner, T. (December 2009). Hydrogen-fueled internal combustion engines. *Progress in Energy and Combustion Science, 35*(6), 490−527.

Wagner, U., Geiger, B., & Shaefer, H. (1998). Energy life cycle analysis of hydrogen system. *International Journal of Hydrogen Energy, 23*, 1−6.

Wang, Ya-F., Tsai, C.-H., Chang, W.-Y., & Kuo, Yi-M. (2010). Methane steam reforming for producing hydrogen in an atmospheric-pressure microwave plasma reactor. *International Journal of Hydrogen Energy, 35*, 135−140.

Wang, Q., Yan, B.-H., Jin, Y., & Cheng, Y. (2009). Investigation of dry reforming of methane in a dielectric barrier discharge reactor. *Plasma Chemistry and Plasma Processing, 29*, 217−228.

Wei, Ta-C., Huang, H.-F., & Wu, C.-C. (2001). Modeling study on plasma reforming of greenhouse gases in a silent discharge. In *Proceeding 3rd int. Symp. Non-thermal plasma technology for pollution control, Nakyung Hwang, Min* (pp. 45−49) (Cheju, Korea).

Wemlinger, E., Pedrow, P., Garcia-Perez, M., Su, H., Marin-Flores, O., & Pitts, M. (2009). Atmospheric pressure cold plasma applied to steam reforming of small oxygenated molecules from bio-oil. In *ICOPS 2009. IEEE international conference on plasma science*.

Yanguas-Gil, A., Hueso, J. L., Cotrino, J., Caballero, A., & Gonzalez-Elipe, A. R. (2004). Reforming of ethanol in a microwave surface-wave plasma discharge. *Applied Physics Letters, 85*, 4004.

Yan, B. H., Wang, Q., Jin, Y., & Cheng, Y. (April 2010). Dry reforming of methane with carbon dioxide using pulsed DC arc plasma at atmospheric pressure. *Plasma Chemistry and Plasma Processing, 30*(2), 257−266.

Zou, Ji-J., Zhang, Y.-P., & Liu, C.-J. (June 2007). Hydrogen production from partial oxidation of dimethyl ether using corona discharge plasma. *International Journal of Hydrogen Energy, 32*(8), 958−964.

This page intentionally left blank

Part Five

Hydrogen purification and low-carbon hydrogen production

This page intentionally left blank

Hydrogen purification methods: iron-based redox processes, adsorption, and metal hydrides

13

E. Acha, J.M. Requies, J.F. Cambra
Department of Chemical and Environmental Engineering, University of the Basque Country (UPV/EHU), Bilbao, Spain

13.1 Introduction

Hydrogen can be directly converted from chemical energy into electricity via fuel cells, which are environmentally friendly. High-purity hydrogen is also required in different industrial processes, as for example the steel manufacturing. However, nowadays there are some difficulties for hydrogen economy implantation. One of them is the lack of efficient and low-cost storage systems suitable for stationary or mobile applications (Otsuka, Kaburagi, Yamada, & Takenaka, 2003). Second, high-purity hydrogen is required to operate efficient fuel cells. Hydrogen can be produced from hydrogen-containing compounds, nowadays mainly done from hydrocarbons. It can be produced from steam reforming, partial oxidation, or auto-thermal reforming reactions. In all those processes, hydrogen is produced as a part of a mixture together with other compounds such as CO, CO_2, H_2O, and N_2 (in case air is fed) or the unconverted hydrocarbon.

If the produced hydrogen is not pure enough, there can be some inconveniences when using it, and the impurities can poison the following steps in the process. Together with the hydrogen production, the purification is critical if hydrogen economy wants to be implemented in the future. As an example CO molecules can be irreversibly and strongly adsorbed over the surface of the proton exchange membrane fuel cells electrode reducing their lifetime, or the presence of CO_2 molecules can reduce the lifetime of the alkaline fuel cells.

Currently, the main processes employed for hydrogen purification are: pressure swing adsorption and its variants, as for example temperature swing adsorption, cryogenic processes, membrane-based separation, and catalytic processes for compounds elimination or to enhance hydrogen production (Alijani & Irankhah, 2013; Atsonios, Panopoulos, Doukelis, Koumanakos, & Kakaras, 2013; Grande, 2012; Piemonte, Di Paola, De Falco, Iulianelli, & Basile, 2014; Yang, Feng, Chu, & Liu, 2014; Zornoza, Casado, & Navajas, 2013). In the current chapter, a deep review of the most recent advances on redox, metal hydrides, and adsorption processes for hydrogen purification are discussed.

Compendium of Hydrogen Energy. http://dx.doi.org/10.1016/B978-1-78242-361-4.00013-3

13.2 Principles and processes

In the past few years, the research on hydrogen purification and storage in porous materials has grown significantly (Mueller et al., 2006). There are some solids in which H_2 can be stored and, therefore, where hydrogen can be purified as for example complex hydrides, iron sponges, and porous carbon materials (Lozano-Castelló, Suárez-García, Linares-Solano & Cazorla-Amorós, 2013; Ragheb, 2011; Varin & Zbroniec, 2012).

13.2.1 Iron-based redox processes

When employing metals with the purpose of purifying hydrogen, such as iron oxides, oxygen is removed from the oxide during the metal reduction step, and thus hydrogen is in some way collected, being released during an oxidation step with water. Several metals or alloys can be employed to separate and store hydrogen (Kusada, Yamauchi, Kobayashi, & Kubota, 2010). During the metal reduction, hydrogen is stored and then it can be released during an oxidation step. Among the options, and taking into account the thermodynamics and price, iron seems to be one of the most suitable metals (Thaler & Hacker, 2012). The reduction of iron oxides can be done in different steps, but overall. Fe_3O_4 is reduced with hydrogen into metallic iron (Eqn (13.1)), where potential hydrogen is stored, and then, when hydrogen supply is required, steam is used to oxidize the metallic iron (Eqn (13.2)), generating pure hydrogen and regenerating the iron oxides. The theoretical maximum amount of hydrogen that can be chemically stored is 4.8 wt% of Fe weight. This corresponds to 537 L of hydrogen gas (standard temperature and pressure) that can be stored per kilogram of iron (Acha et al., 2014). An advantage of the process is that iron and iron oxides are nontoxic and very inexpensive materials that are easy to handle because they are stable at ambient conditions.

$$Fe_3O_4 + 4H_2 \rightarrow 3Fe + 4H_2O \tag{13.1}$$

$$3Fe + 4H_2O \rightarrow Fe_3O_4 + 4H_2 \tag{13.2}$$

The oxidation and reduction steps of the iron oxides have been widely studied. Pineau, Kanari, and Gaballah (2006) postulated that the reduction of hematite by hydrogen proceeds in two or three steps, lower than and higher than 570 °C, respectively, via magnetite (Fe_3O_4) and wüstite ($Fe_{(1-x)}O$) according to the Bell's diagram (Figure 13.1) and the following equations:

$$3Fe_2O_3 + H_2 \rightarrow 2Fe_3O_4 + H_2O \tag{13.3}$$

$$Fe_3O_4 + 4H_2 \rightarrow 3Fe + 4H_2O \tag{13.4}$$

$$(1 - x)Fe_3O_4 + (1 - 4x)H_2 \rightarrow 3Fe_{(1-x)}O + (1 - 4x)H_2O \tag{13.5}$$

$$Fe_{(1-x)}O + H_2 \rightarrow (1 - x)Fe + H_2O \tag{13.6}$$

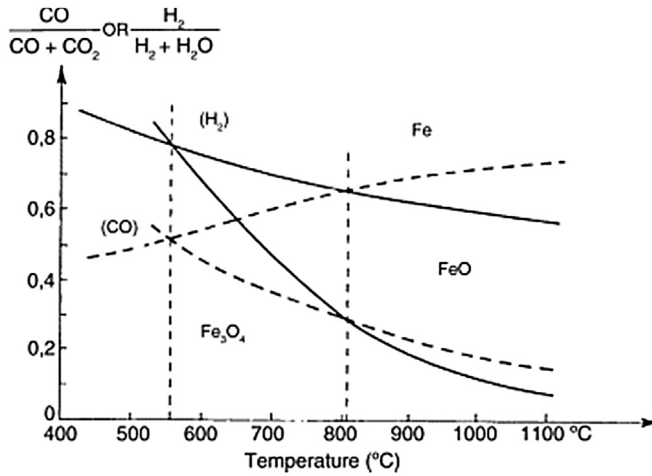

Figure 13.1 Bell's diagram for the Fe−C−O and Fe−H−O equilibrium at 1 atm. Pineau et al. (2006).

Jozwiak, Kaczmarek, Maniecki, Ignaczak, and Maniukiewicz (2007) postulated a three-stage mechanism: $3Fe_2O_3 \rightarrow 2Fe_3O_4 \rightarrow 6FeO \rightarrow 6Fe$, especially when reduction temperature overlaps 570 °C. They also observed that the reduction temperatures were strongly dependent on the employed heating rates, which makes difficult the comparison of the literature data. In the study by Lin, Chen, and Li (2003), only two reduction steps were detected $Fe_2O_3 \rightarrow Fe_3O_4 \rightarrow Fe$ and FeO was not detected as intermediate. Datta, Rihko-Struckmann, and Sundmacher (2014) observed that the steps varied along the reduction cycles, in the first reduction cycle the steps were $Fe_2O_3 \rightarrow Fe_3O_4 \rightarrow FeO \rightarrow Fe$, whereas the second cycle on the reduction was from Fe_3O_4 to Fe. This meant that during the oxidation step it, was not possible to reoxidize the iron to Fe_2O_3, which is not thermodynamically feasible (Bleeker, Veringa, & Kersten, 2009).

One of the most important parameters of the hematite reduction is the apparent activation energy because it defines the reactor dimensions and the energy consumption. This activation energy varies from 18 to 246 kJ/mol, according to the literature, and depends on factors such as the starting raw material, nature of reducing gas, temperature range, reaction step, presence of water vapor in the gas mixture, impurities, and physical shape, etc. (Pineau et al., 2006). According to Pineau, Kanari, and Gaballah (2007), mathematical modeling of experimental data suggests that the controlling mechanism of the reaction rate is nucleation at temperatures lower than 650 °C and diffusion at higher temperatures.

Pure iron oxides cannot be used repeatedly for this process. The redox cycle at relative high temperatures causes structural changes, such as agglomeration, sintering, and finally the deactivation of the iron oxides (David, 2005; Huang et al., 2006; Kock, Fortuin, & Geus, 1985; Requies et al., 2013). For the economy of this process, it is crucial to improve conventional iron systems, developing iron oxide systems that

can be used in as many redox cycles as possible with small losses of hydrogen storage capacity. The addition of some metal cations such as Al, Cr, Ga, Zr, Rh, Pt, and Mo could improve the iron oxide behavior in these redox cycles. A comparison of data found in the literature regarding iron oxide systems with different additives and at different conditions is shown in Table 13.1. As can be concluded from the table, it is difficult to compare the data because of different units when indicating the hydrogen storage capacity.

The particles size will affect the iron systems. Preliminary experiments with iron nanoparticles were performed by Gangwal et al. (2006), together with a review of some previous steam-iron results. The particle size of the additive metals will also affect their influence in the iron systems. Some investigations indicate that metals such as Fe, Ru, Pt, Pd, and Ir show a strong affinity toward hydrogen molecules when they are as nanosized particles, whereas bulk materials do not adsorb hydrogen (Kobayashi, Yamauchi, & Kitagawa, 2011, 2012; Lebon, Garcia-Fuente, Vega, & Aguilera-Granja, 2011, 2012).

The influence of 26 metal additives on the redox property of the iron oxide was studied by Otsuka et al. (2003). Among the investigated materials, Al, Mo, and Ce were reported to stabilize iron oxide. Molybdenum has been further studied as in the work by Datta et al. (2011). They observed that the incorporation of Mo mitigated the metallic iron formation and increased the active phase stability. They repeated the redox cycles 100 times at 750 °C and the samples retained more than the 90% of their initial activity. The measured amount of hydrogen purified was between 4200 and 4700 $\mu mol/g_{material}$, which is about 30% of the maximum that can be produced. In the comparison between Mo, Cu, or Mg, Galvita et al. (2007) found that the Mo inclusion improved the material stability. A clear decrease in the activation energy of the steam oxidation of iron oxide samples containing Mo was reported by Wang, Wang, Wang, and Bai (2008), Wang et al. (2013). They concluded that the positive effect of Mo was because of the change in the composition and the microstructure of the doped samples, which led to the improved stability. The initial +6 oxidation number was not reached later in the subsequent cycles and it varied between +4, +3, and 0.

The positive influence of Cr on the material stability above 750 °C was observed by Takenaka et al. (2004), Takenaka, Nomura, Hanaizumi, and Otsuka (2005). This was corroborated by Requies et al. (2013): they observed that adding 10−20% of chromium to some iron oxides increased the storage capacity and also their stability. The chromium addition improved the resistance to sinterization and it directly reduced Fe_3O_4 to Fe, improving the H_2 storage. Acha et al. (2014) compared natural and synthetic iron oxides and it was observed that the solid structure was strongly affecting the coke formation and the presence of some elements, such as chromium, in the natural oxides decreased its reduction capacity, but increased the stability.

Other metals, such as Pd, enhanced both the reduction and the reoxidation of the metallic iron (Urasaki et al., 2005) and Rh has been found to promote sintering (Takenaka, Kaburagi, Yamada, Nomura, & Otsuka, 2004), whereas Mo inclusion prevented sintering of iron species of samples containing Rh.

Table 13.1 Iron oxide systems reported in the literature

Iron system	T (K)	Cycles	H_2 produced	References
Fe_2O_3−$Ce_{0.5}Zr_{0.5}O_2$−Mo (1−5 wt%)	750	200	4.2−4.7 mmol/$G_{material}$	Datta et al. (2014)
Fe_2O_3	550	44 h	20% of the fed amount	Herguido, Peña, and Carazo (2014)
$Fe_{50}Al_{50}$ $Fe_{45}Al_{45}Cr_{10}$	700 700	8 cycles 8 cycles	1.2 $mmol_{H2}/g_{Fe}$ 3.5 $mmol_{H2}/g_{Fe}$	Acha et al. (2014)
$Fe_{30}Al_{70}$ $Fe_{10}Al^{80}$	700 700	8 cycles 8 cycles	0.5 $mmol_{H2}/g_{Fe}$ 5.2 $mmol_{H2}/g_{Fe}$	Acha et al. (2014)
Fe_2O_3−8%Mo	300−400	4 cycles	900−1000 μmol/min g_{Fe}	Wang, Zhang, Wen, and Bai (2013)
98 wt%Fe_2O_3−1.75 wt%Al_2O_3−0.25 wt%MoO_3	500	17 cycles	8.1 g_{H2}/(h kg solid)	Romero, Soto, Duran, Herguido, and Pena (2012)
Fe-10%Cr	700	8 cycles	12−14 $mmol_{H2}/g_{Fe}$	Requies et al. (2013)
Ni (5 mol%)−Cr (5 mol%)−FeO_x	823−1023 K	4 cycles	8 $mmol_{H2}$/min g_{Fe}	Takenaka, Hanaizumi, Son, and Otsuka (2004)
Fe_2O_3 (85 wt%) SiO_2 (0−10 wt%) CaO (0−10 wt%) Al_2O_3 (5 wt%)	1073 K	20 cycles	Structural analysis	Thaler et al. (2006)
Mo (2 wt%)−Fe_2O_3 (80 wt%)−$Ce_{0.5}Zr_{0.5}O_2$	873 K	100 cycles	850 μmol/g_{sample}	Galvita, Hempel, Lorenz, Rihko-Struckmann, and Sundmacher (2007)
Mo (3 wt%)−Fe_2O_3 (80 wt%)−$Ce_{0.5}Zr_{0.5}O_2$	923−1023 K	100 cycles	Structural analysis	Datta, Rihko-Struckmann, and Sundmacher (2011)
Fe_2O_3 3 mol% of Mg, Al, Ca, Sc, Ti, V, Cr, Mn, Co, Ni, Cu, Zn, Ga, Y, Zr, Nb, Mo, Ru, Rh, Pd, Ag, Ce, W, Re, Ir, and Pt	373−873 K	5 cycles	Stability analysis	Otsuka et al. (2003)

More complex iron oxide systems have also been researched: Fe_2O_3−$Ce_{0.5}$−$Zr_{0.5}O_2$ showed stable behavior during 30−40 cycles when impregnating it with 1−5 wt% of Mo (Datta et al., 2014). The inclusion of 7.5 wt% SiO_2, 5 wt% Al_2O_3, and less than 2.5 wt% of CaO has been found to prevent the sintering of the iron oxides to a large extent (Thaler et al., 2006). Romero et al. (2012) found out that a mixed oxide with composition 98 wt% Fe_2O_3−1.75 wt% Al_2O_3 and with a minor doping of 0.25 wt% MoO_3, maintained a slightly better hydrogen production rate than the corresponding cerium sample (98 wt% Fe_2O_3−1.75 wt% Al_2O_3−0.25 wt% CeO_2).

Iron oxides (Fe_2O_3) have been also researched to perform hydrogen separation from H_2/CH_4 mixtures in an interconnected circulating fluidized bed reactor (Herguido et al., 2014) and they are already employed in quite some patents (Akira, 2006; Anton, 1910; Hitoshi & Masakatsu, 2007; Shoji, 2009; Tadashi, 1995; Xiang Wenguo, Zhipeng, & Xin, 2010).

13.2.2 Metal hydrides

Metal hydrides have been widely studied as storage systems (Basile and Iulianelli, 2014), but they can also be employed to purify hydrogen from a mixture. Nowadays they are mainly applied in the automotive sector, with strict operating restrictions. In the case of applying hydrides for hydrogen purification, after a reactor for example, the operating temperature and pressure range will be higher and less restricted.

In this section, a review of the latest research regarding hydrides is shown. Initially, an introduction to hydration process is presented, followed by a summary of the main hydride groups tested. During this analysis, special attention will be paid to high storage capacities because this is an important aspect to obtain high purification yields of hydrogen. After this, the hydrogen purification issues are described with a deeper analysis of the works that have analyzed the polluting effect of gases other than hydrogen and the concentration polarization effect of diluting the hydrogen. Finally, some works and comments about the process design characteristics when purifying hydrogen with hydrides are included.

Hydrogen forms hydrides and solid solutions with a lot of metals or alloys. Metal hydrides are composed of metal and hydrogen atoms in interstitial sites. The metal hydrides can be formed in two ways: direct dissociative chemisorptions (Eqn (13.7)) and electrochemical splitting of water (Eqn (13.8)) (David, 2005).

$$M + \frac{x}{2}H_2 \leftrightarrow MH_x \tag{13.7}$$

$$M + \frac{x}{2}H_2O + \frac{x}{2}e^- \leftrightarrow MH_x + \frac{x}{2}OH^- \tag{13.8}$$

Hydrides can be divided into high- and low-temperature hydrides depending on the temperature of adsorption/desorption process (David, 2005). In the low-temperature hydrides, the hydrogen is normally bound through covalent bonding and the metal

hydride consists of high-molecular-weight material. In the high-temperature hydrides, the hydrogen is normally ionically bound, and the metal hydride consists of low-molecular-weight material. The hydrogen storage capacities are higher for the high-temperature hydrides. The variation of attractive surface forces as a function of distance from the surface decides whether van der Waals−type weak physisorption of molecular hydrogen or dissociation and chemisorption of atomic hydrogen takes place (Schlapbach & Züttel, 2001).

Depending on the hydrogen concentration and temperature, the reaction shown in Eqn (13.7) proceeds to the right or to the left. If the hydrogen pressure is higher than the equilibrium pressure, it proceeds to the right to form the hydride. The operating temperature of a metal hydride system is fixed by the plateau pressure in thermodynamic equilibrium and by the overall reaction kinetics. The thermodynamic aspects of hydride formation from gaseous hydrogen are described by a $P-c-T$ diagram in which the hydrogen pressure (P) is plotted as a function of atomic ratio of hydrogen (c) at a given temperature (T). In this diagram, there is a plateau where the solid solution is continuously transformed in the hydride. In Figure 13.2, the $P-c-T$ curves for $LmNi_{4.91}Sn_{0.15}$ alloy is shown as an example.

The thermodynamic $P-c-T$ or pressure-composition-isotherm properties of metal hydrides are related in direct relationship to the van't Hoff equation (Ragheb, 2011):

Where:

LnP: natural logarithm of pressure in absolute atmospheres
T: temperature in Kelvins
ΔH: enthalpy change of hydriding,
ΔS: entropy change of hydriding,
R: gas constant = 0.008,314 kJ/mol K

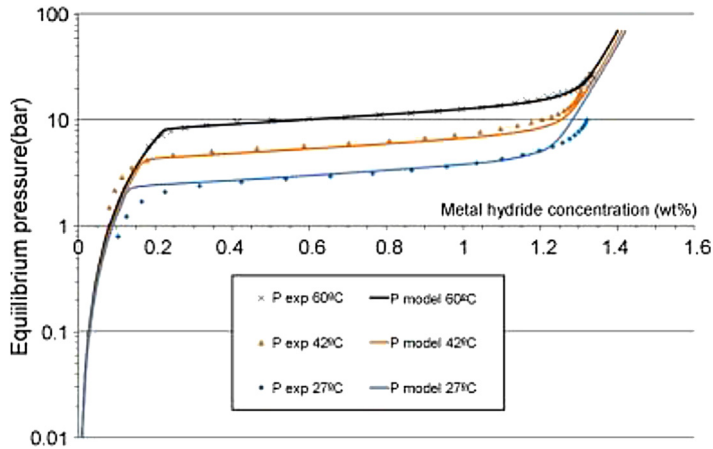

Figure 13.2 The experimental and simulated $P-c-T$ curves for the $LmNi_{4.91}Sn_{0.15}$ alloy. Payá, Linder, Laurien, and Corberán (2009).

The isotherm shape will determine the pressure range over which the majority of the reversible uptake will occur, but the kinetics are also important because they define the production and storage rates. The reversible storage capacity is determined by the width of the plateau pressure-composition isotherm. The temperature affects the sorption process, increasing the absorption plateau pressure when increasing the temperature. As the temperature increases, the phase diagram reaches a critical point above which there is no phase transition between the α and β phases that coexist in the plateau region. The $P{-}c{-}T$ data are obtained by keeping an alloy sample at a constant temperature while precisely measuring the quantity of sorbed hydrogen and the pressure at which sorption occurs. Modifying the alloy composition and the production techniques allows operating at different temperatures and pressures.

Most of the solids used for hydrogen purification/storage need to be previously activated in one way or another. Depending on the preparation method, some need the removal of extra elements present in the synthesis steps, or just the "cleaning" of adsorbates present in the environment, so that they can adsorb and react with hydrogen. This can be done operating at high temperature under vacuum, or with an inert gas, or in the case of hydrides they need to be activated with hydrogen before being able to reversibly adsorb/desorb it. During activation, the material will not only adsorb hydrogen on its surface, but it will also typically undergo significant changes in its physical properties.

In most of the hydrides, the activation mechanism has not been yet well analyzed. Thermodynamic properties of the hydrides are critical, in addition to kinetics, because they define the optimum operation temperature and pressures and they also indicate the produced or consumed heat (which can be critical for the engineering design). The enthalpy of adsorption provides a measure of the strength of the interaction between a molecule and the adsorbent surface (increasing the contact surface the density of the adsorbed hydrogen can be higher).

The kinetics determine the practical rate at which the solids can operate. The kinetics of hydrogen sorption and desorption are characterized by hydrogen adsorption and hydrogen absorption. The kinetics of hydrogen adsorption includes: diffusion through porous media, which can occur in different ways, and the dominant mechanism depends on the pore dimension and mean free path of the diffusing molecules. (1) Poiseuille flow, in which the diffusion is driven by the pressure gradient. (2) Molecular diffusion. (3) Knudsen diffusion, which is induced by the collision of the gas molecules in the walls of the pore. (4) Surface diffusion, in which adsorbed molecules diffuse between different surface adsorption sites. Surface diffusion is more significant when the pore diameter decreases, so it is a critical mechanism in microporous materials. Another process that must occur before diffusion through the pore network can proceed is the entry of the hydrogen molecules into the pores. However, in practice, the entire hydrogen adsorption process is very rapid. Neither entry into the pores nor surface diffusion effects limit the overall kinetic hydrogen adsorption process within timescales readily observable.

It is a common approach to assume that in the processes the kinetics is limited by the slowest step. In the case of hydrogen adsorption in hydrides, it is complex to

describe, understand, and quantify the different steps, doing difficult to identify the limiting one. The steps can be summarized as: (1) The transport of the molecular hydrogen through the gas phase to the surface region. (2) Physisorption of molecular hydrogen onto the surface. (3) Dissociation of hydrogen into atomic hydrogen and chemisorption. (4) Penetration of the chemisorbed atomic hydrogen through the surface of the material, followed by diffusion between interstitial sites in the lattice, which initially takes place through a disordered solid solution (alpha) phase. With further hydrogen absorption, an ordered hydride (beta) phase will form, or nucleate. The final step is the formation of the hydride. A deep knowledge of the exact formation and growth of the hydride phase is not clear and is challenging. There are three parameters that can be applied to kinetic hydrogen adsorption and desorption processes: apparent activation energy, hydrogen diffusion coefficient, and apparent hydride formation rate.

Among the different studied materials to be employed as hydrides are some problems that can occur in the hydride formation process, in the case of magnesium (a light material), are the following: (1) Hydrogen slowly diffuses through its hydride. To improve this rate, small Mg crystals can be formed, thus increasing the surface area, or another element can be added. (2) Hydrogen molecules do not readily dissociate at the surface of Mg. (3) Hydrogen atoms bind too strongly with the Mg atoms. To avoid this issue, other elements can be added to the samples. The desorption temperature of Mg_2Ni, for example, is lower than that of pure Mg. But the storage capacity is decreased and the weight of the sample is increased, thus other lighter metals should be alloyed with Mg. A deeper analysis of the Mg hydrides advances have been published by Zhao and Zhang (2014).

Some of the lightest elements in the periodic table, for example lithium, boron, sodium, and aluminum, form stable ionic compounds with hydrogen. There are several works related to this group of elements (Ares-Fernandez et al., 2007; Bogdanovic, Brand, Marjanovic, Schwickardi, & Tölle, 2000; Gross, Sandrock, & Thomas, 2002; Ismail, Zhao, Yu, & Dou, 2010; Varin, Czujko, & Wronski, 2009; Varin & Zbroniec, 2012; Wang, Ebner, Zidan, & Ritter, 2005; Xiao et al., 2008). The hydrogen content reaches values of up to 18 wt% for $LiBH_4$. However, desorption occurs at temperatures from 80 °C up to 600 °C. This temperature may be high because of kinetics (which could be improved by adding some elements to act as a catalyst, or milling the material or adding defects) or from thermodynamics. A deep review of complex hydrides advances through 2008 was made by Varin et al. in "Nanomaterials for Solid State Hydrogen Storage" (Varin et al., 2009) and from 2008 to 2013 in Varin and Wronski (2013).

Metal borohydrides are very interesting because they have high theoretical hydrogen capacities. For example, $LiBH_4$ and $NaBH_4$ both have high hydrogen storage capacity. But because of a relatively high enthalpy change for dehydrogenation, the operating temperature is higher than 400 °C. To try to overcome the unfavorable thermodynamics, several works have been published focused on converting them to other borohydrides with more favorable thermodynamics (Cerný, Penin, Hagemann, & Filinchuk, 2009; Choudhury et al., 2009; Liu, Reed, & Book, 2012; Nakamori et al., 2007).

A single phase lithium amide, $LiNH_2$, can also be attractive, but it releases NH_3, which can be poisonous for proton exchange membrane fuel cells. With the addition of LiH, NH_3 formation can be decreased but depending on the method some NH_3 release is still observed (Varin, Jang, & Polanski, 2010). There are several studies with the system $LiNH_2$-MgH_2 as an alternative to the $LiNH_2$-LiH system. But there are critical differences among the experimental conditions employed, which makes difficult to reach general conclusions about it (Varin & Wronski, 2013).

Rare earth intermetallic compounds have been widely researched because they created great hopes for storing hydrogen for some applications (as for example rechargeable batteries). The precursor alloys that are used for hydrides can be classified into six categories, based on A-B component systems (Chandra, Chien, & Talekar, 2011).

1. AF (HfNi, FeTi)
2. AB_2 (Mn_2Zn, $TiFe_2$)
3. A_2B (Hf_2Fe, Mg_2Ni)
4. A_2B_7 (Pr_2Ni_7, Ce_2Co_7)
5. AB_3 ($NdCo_3$, $GdFe_3$)
6. AB_5 ($LaNi_5$, $CeNi_5$)

An adequate substitution of A or B determines the properties of the solid, and enhances life cycle, corrosion resistance, and electrochemical properties. In the studies by Lambert, Chandra, Cathey, Lynch, and Bowman (1922) they observed that the hydrogen adsorption properties of $La_{0.9}Gd_{0.1}Ni_5$ were seriously degraded in both prolonged thermal cycling and aging tests (after 10,000 cycles) but the $LaNi_{4.8}Sn_{0.2}$ and $LaNi_{4.27}Sn_{0.24}$ hydrides were virtually unaffected. Toyota Prius (II−V models) use sealed NiMH batteries. Many NiMH batteries are AB_5-type structured materials, as for example $LaNi_5$ and $MnNi_5$ (Chandra et al., 2011).

An additional problem is metal surface passivation resulting from the formation of metal oxides, hydroxides, carbon compounds, or water. This passivated layer is a diffusion barrier that decreases the hydrogen adsorption rate. Poisoning effects can also occur in the surface, decreasing or inhibiting the hydrogen adsorption. Some of the metallic hydrides systems have also been analyzed as hydrogen purification systems. It is difficult to reach general conclusions in this because the compounds can have a different effect as a function of compound type, concentration, and contact time. Furthermore, the effect of each compound will be different if changing the hydride, its composition, its preparation method, operating variables, and type of process.

Hydrides do not only have to present a high hydrogen adsorption/desorption capacity but also long-term cycling stability. In the case of applying hydrates for hydrogen storage, the 2015 US Department of Energy storage targets specify an ability to undergo 1500 hydrogenation/dehydrogenation cycles. The problem of low cycling stability is more significant for hydrides than it is for porous adsorbents, because metal hydrides invariably undergo physical and chemical degradation during prolonged hydrogen cycling. The degradation mechanisms can be classified as either intrinsic or extrinsic (Broom, 2011). One of the main intrinsic problems is the

disproportionation, the process by which a ternary or higher hydride decomposes into more thermodynamically stable products. For example, in the $LaNi_5 - H$ system, $LaH_2 + Ni$ system is thermodynamically more stable than $LaNi_5H_x$. Therefore, if the atoms have enough mobility (which is directly influenced by the operation temperature), segregation into pure Ni and La hydride will tend to occur. There will be at least some separation into Ni-rich and La-rich regions. The mobility of the host metals can be reduced by the addition of substituent atoms in the lattice, as for example Al ($LaNi_5 - xAl_x$).

The extrinsic mechanisms are those induced by impurities in the gas phase, and can include poisoning and corrosion of the surface. Hydrogen mixtures can contain different compounds, depending on the employed production process, as for example: CO, CO_2, H_2O, O_2, H_2S, NH_3, hydrocarbons, etc. When analyzing the effect of these compounds in hydrides performance, it is important to first analyze the behavior of the hydride in pure hydrogen and then go adding them one by one with a controlled concentration. It is important to be aware that the different adsorbents or hydrides have different affinities to compounds, so the conclusions reached with one compound could not be always generalized. Sandrock and Goodell (1980) proposed four types of interaction: (1) Poisoning, which results in quick loss of hydrogen storage capacity without a decrease in the kinetics of the unaffected portion of the sample, as for example H_2S. (2) Retardation, which reduces the kinetics of hydrogen adsorption but does not reduce the storage capacity, as NH_3. (3) Reaction in which the capacity is reduced by bulk corrosion of the alloy, as O_2. (4) Innocuous, does not damage the surface but decreases the sorption kinetics because of inert gas blanketing or concentration polarization effect, such as CH_4, or N_2.

The effect of oxygen and nitrogen on hydration was analyzed by Zhang et al. (2012). Samples were exposed to O_2 and N_2 for 30, 60, and 180 s and room temperature. The hydrogen absorption capacity of a $Zr_{0.9}Ti_{0.1}V_2$ alloy was entirely degraded by the oxygen poisoning. After the regeneration, the O_2 poisoned sample could hardly adsorb hydrogen, whereas the nitrogen poisoned sample reobtained the hydrogen adsorption capacity; at the regeneration conditions, the O_2 poisoned sample needed more time because the oxide layer on the surface was thicker than that of the fresh-prepared sample. The thick oxide film and hydrocarbons on the surface inevitably block the hydrogen diffusion to the inside of the alloy.

Sun et al. (2014) analyzed a complex system ($2LiNH_2 + MgH_2$) with a mixture fed containing 1% CO. With 1% CO, the sample desorption capacity decreased from the first to the sixth cycle, whereas it was stable in pure hydrogen. They also observed that the CO damage was irreversible, or at least it was not corrected applying a pure hydrogen flow. The CO effect was also analyzed with X-ray diffraction. When working in pure hydrogen, $Mg(NH_2)_2$ and LiH were the compounds observed, whereas in a mixture with 1% of CO, Li_2CN_2 and MgO appeared. These two components were still detected in the sample after the recovery test. In the Fourier transform infrared spectroscopy analysis, the conclusions were in accordance with those obtained in X-ray diffraction. Therefore, in presence of CO, the bond between C and O breaks and the carbon reacts with the Li^{2+} and N^{3-}, whereas the O reacts with the Mg^{2+}. Not only the hydrogen adsorption capacity declined, but so did the desorption rate.

The calculated dehydrogenation activation energy increased after being in contact with CO, and the main reason for this could be that the formed new compounds prevent the adsorption of compounds.

Similar irreversible effect of CO was also observed by Wan et al. (2014) with a $LaNi_{4.7}Al_{0.3}$ alloy. The sample was completely deactivated after three hydriding/dehydriding cycles in hydrogen containing 300 ppm CO at 30 °C, but hydrogen storage capacity did not degrade when tested at 80 °C. The poisoning mechanism for CO is suggested to be that it deactivates the alloy surface and thus hinders hydriding and dehydriding processes. X-ray photoelectron spectroscopy results confirmed that the bond between Ni and CO was formed by a simple chemisorptions process, rather than forming nickel carbonyl.

Modibane et al. (2013) studied the deterioration of AB_5 type hydride in hydrogen purification from gases containing carbon dioxide (up to 30%) and monoxide (up to 100 ppm). The substrate La(Ni, Co Mn, Al)$_5$ was surface-modified by fluorination followed by electroless deposition of palladium. The fluorination increased the specific surface area of the material and the deposition of Pd enhanced the activation kinetics, forming materials with exquisite hydrogen sorption properties. They tested with mixtures containing 25% $H_2 + (0 - 30\%)$ $CO_2 + 0 - 100$ ppm CO + N_2 until balanced. The hydrogen adsorption was strongly retarded with 10% CO_2 and the H_2 adsorption capacity during cycling operation decreased, whereas the surface-modified material just showed a slight deterioration of the hydrogenation rate and negligible deterioration during cycles. Similar results were observed when adding 100 ppm of CO. They concluded that the hydrogen purification was limited by mass transfer in the gas phase, which can be due to employing quite low concentration of hydrogen.

Carbon monoxide and dioxide effect was further analyzed by Lototskyy et al. (2013). They worked with an alloy AB_5 type, $LaNi_{3.55}Co_{0.75}Al_{0.4}Mn_{0.3}$, with a surface modification carried out through fluorination followed by aminosilane functionalization and electroless deposition of Pd. The mixture employed as feed gas was H_2 with up to 30% CO_2, 0.33% CO, and balanced with N_2. They focused on the scaling up of the surface modification step, and they observed that the hydrogen adsorption kinetics of samples prepared in big batches were lower. This was mainly because of mixing problems, but this can also be a problem when comparing the data of different hydrides from literature. They again observed no significant deterioration of the adsorption rate with mixtures up to 10% CO_2 and up to 100 ppm CO and the samples were quite stable at those conditions during 460 cycles of 30 min.

The correlation between surface coverage of the sample, because of the presence of CO, O_2, H_2S, N_2, and CO_2, and the reaction rate reduction was analyzed by Schweppe, Martin, and Fromm (1997). They first exposed the samples to the gases and then the hydrogen adsorption rate was measured with pure hydrogen. They indicate that N_2, CO_2, H_2S, and CO are known to form only one or not much more than one monolayer of adsorbate onto metal surfaces. The effect of CO and H_2S in the initial reaction rate was a big decrease, whereas CO_2 affected but much less. The effect of oxygen was more complex, there was an initial decrease of the rate, then a plateau under certain oxygen amount, and then a further decrease. They also concluded that the reaction was controlled by both diffusion and surface processes.

The negative effect of CO and H_2S was confirmed in the work by Lin, Lin, Sung, and Wu (2007). They studied $LmNi_{4.8}Al_{0.2}$ alloy in the presence of 300 and 1000 ppm of H_2S and CO at 40 and 80 °C. In the presence of CO not only adsorption was decreased, but desorption was also negatively affected. At 80 °C the operation was almost not affected by 1000 pm CO. According to their results the poisoning effect of H_2S was less than that of CO, because of the weak van der Waals bonding with which they adhere to the surface, whereas the C-metal bond was strong. They reactivated the adsorbing capacities with pure hydrogen cycles at high pressures (45 atm).

Another compound that can be part of the hydrogen mixture is the sulfur dioxide. Myhra, Kisi, and Gray (1995) studied its effect in a $LaNi_5$ sample. They suggested that SO_2 is a reversible poison, so if the SO_2 concentration in the surrounding decreases, it is desorbed from the surface. In the surface film, the species were mainly oxides, whereas the sulfur is present as tetravalent sulfate-like specie. In the decomposition layer, a mixture of oxides, hydroxide, and metallic species as well as some carbonate were found.

According to the obtained results, it can be suggested that the negative effect of CO_2, O_2, and N_2 is mainly due to a concentration polarization effect (low hydrogen driving force), whereas CO, H_2S, and SO_2 are also adsorbed and affect the activity of the adsorption centers. Therefore, special engineering solutions (fluid-dynamics) or flowing-circulation modes are needed to allow having high space velocities that decrease the mass transfer limitation.

The process design improvement is another critical step for the implementation of hydrides in real processes. To avoid the negative effect of CO on hydrogen adsorption, Miura et al. (2013) performed a system where CO was first removed by a selective adsorber (adsorbent based on porous alumina supporting Cu(I) mixed with activated alumina so that humidity was also removed in this step) and then, hydrogen was purified by an AB_5 type hydride that was resistant to start and stop and load changes. When designing the hydrides system to purify, the system has to be also redesigned. The conventional hydrides system for hydrogen storage is horizontal, with free space in the top to allow the hydride expansion during the adsorption and contraction during the desorption steps. But if applying the same design when purifying hydrogen, hydrogen mixture gas will go to the top, decreasing the purification efficiency. Therefore, Miura et al. (2013) designed a vertical device that initially presented problems, because the hydride was solidified from repeated expansion and contractions. They solved those problems blending the MH with iron powder and improving the properties of MH. They produced the hydrogen containing mixture from methanol reforming with three towers operated in continuous flow at an adsorption pressure of 0.8 MPa. The produced and consumed heat in hydrogenation/dehydrogenation cycles was controlled with cold and hot water to keep the towers' temperature constant. In the first tower (MH-1), they employed $MmNi_{3.99}Co_{0.6}Mn_{0.36}Al_{0.05}$, an adjusted composition to obtain hydrogen equilibrium pressure of 0.2 MPa at 20 °C. In the second tower (MH-2), they employed $MmNi_{4.025}Co_{0.4}Mn_{0.275}Al_{0.3}$, being the hydrogen equilibrium pressure 0.1 MPa at 25 °C. The apparatus operated in daily start and stop mode during 100 cycles with MH-1 and 1000 cycles with MH-2. The hydrogen recovery rate with MH-2 was 94% with a purity of 99−99.9%. They scaled

up the system to 3 Nm^3/h hydrogen production and observed similar hydrogen recovery and purity results. The hydrogen concentration at the entrance of the system is not specified in the work.

Talagañis, Meyer, Oliva, Fuentes, and Aguirre (2014) described the use of hydrides to purify hydrogen as pressure swing absorption (PSA) system. They obtained 98% of hydrogen recovery in large systems with large cycle times (the order of hours) and around 60% of hydrogen recovery when cycles were of a few seconds. In this process, gases other than hydrogen remained in the gas phase. To recover the purified hydrogen, the hydride has to be depressurized. They performed a theoretical analysis to model the purification of hydrogen when it is part of a gas mixture operating batch wise (not in continuous flow as with typical PSA).

Because adsorption reaction is exothermic and reaction heat is high, the reactor must be continuously refrigerated during this stage to keep equilibrium pressure below hydrogen partial pressure (the equilibrium pressure increases exponentially with temperature, van't Hoff). Minko, Artemov, and Yan'kov (2014a,b) performed a mathematical modeling of pressure drop, interfacial convective heat, and mass transfer coefficients in packed beds saturated with gaseous mixtures containing hydrogen. The strong dependence of equilibrium pressure on temperature makes the optimization of the heat of reaction critical in the sorption/desorption steps. The low effective heat conductivity and the permeability of the accumulating medium are the major factors that negatively influence the beds. They performed numerical simulations with gas mixtures in beds of spherical particles to simulate the purification of hydrogen. Effective thermal conductivity of the beds was obtained experimentally.

In the work by Fujisawa, Miura, Mitsutake, and Monde (2013), the behavior of a hydrogen purification system with metal hydrides was simulated. In the hydride's container design, it is important to take into account the heat transfer. When it is designed to purify hydrogen, the process has to be a flow-through type to constantly discharge the impurities that have not been adsorbed. They worked with 75% H_2 and 25% N_2, employing an adjusted hydride ($MmNi_{4.025}Co_{0.4}Mn_{0.275}Al_{0.3}$) to have a hydrogen equilibrium pressure of 0.1 MPaG at 25 °C. To avoid volume expansion issues from adsorption and desorption, the hydride was mixed with 60% (in weight) of iron powder. The space velocity was 330 h^{-1} (gas flow/packed bed (hydride + Fe) volume). They clearly observed the saturation curve of the hydride and it was reproducible with the simulation. The pressure drop simulation also correlated well with the experimental data: in 6000 s the pressure increased from 0.7 MPaG to 1.0 in the test with the bigger container 5.8 kg hydride. The pressure drop is a critical factor when scaling up the process, as it is in all the heterogeneous processes where gas and particles are involved.

13.2.3 Adsorption

Adsorption is a spontaneous phenomenon of attraction between a molecule and the adsorbent. Generally adsorbents have high surface area, allowing a quicker adsorption. When the adsorbent is put in contact with the molecules an adsorption equilibrium will be reached after a time, which thermodynamically limits the adsorption process.

Therefore, modifying the operating parameters the adsorption process can be inversed, allowing the adsorbent regeneration. As a conclusion, to design an adsorption process, the equilibrium data of the species are critical, but so is the engineering process design. When the regeneration of the adsorbent is performed by modifying the system pressure, the process is named PSA, the total pressure of the system swings between high pressure in the feed and low pressure in regeneration. Another possibility to regenerate the adsorbents is to modify the temperature (temperature swing adsorption). In both cases, the beds operate in batch mode; therefore, to operate in a continuous and economic way, the process design is critical. The design parameters, such as the adsorbents used, the relative length and position of the different adsorbent layers, and the composition of the mixture have an important effect on the separation performance.

PSA technology has been widely applied for hydrogen purification, especially for high-throughput plants. Nowadays, the process is being adapted to medium-/small-sized plants for distributed hydrogen production. As a general rule, pressure swing adsorption is preferred to other processes when the concentration of the components to be removed is quite important (more than a few percent) (Grande, 2012). There have been a lot of advances in the adsorbents as well as in engineering designs. Porous solids such as zeolites and activated carbon are widely used now, but a new class of adsorbents named metal organic frameworks (MOFs) can present better selectivity, productivity, and lower energy costs.

The PSA industrial process for hydrogen purification usually includes several beds. Each bed is made of different adsorbents layers (normally three), with different affinities to each impurity. One common structure can be the first layer to remove water vapor, the second layer for other impurities with high adsorption affinity (as carbon dioxide), and a third layer for the lighter impurities (methane and carbon monoxide).

There is a lot of research work aimed at obtaining adsorbents with better characteristics. Cellulose acetate and zeolite, for example, were tested by Lively, Bessho, Bhandari, Kawajiri, and Koros (2012) to be packed in modules to purify H_2 from CO_2 in rapidly cycled pressure swing adsorption. In a recent publication by Delgado et al. (2014), fundamental information about adsorption and diffusion of the components of steam methane reforming−off gas are obtained for an activated carbon and a zeolite to be able to improve a PSA process through the simulation with the data obtained experimentally for the two adsorbents.

Hydrogen adsorption on porous materials can be also done in MOFs, zeolites, or covalent organic frameworks. Among carbon materials, single-walled carbon nanotubes and carbon nanofibers also created high expectations because of their hydrogen storage capacity. If an appropriate MOF is prepared, the MOF has much higher adsorption of CH_4, CO, and CO_2 than H_2; for example, allowing a separation (Broom, 2011). In the work by Meng et al. (2013), they propose a MOF for hydrogen purification and storage that could allow separating hydrogen at ambient temperatures and low pressures. Further review of carbon materials for storing is done in Seung, Haesol, Taehoon, and Chong (2012), Lozano-Castelló et al. (2013), Broom and Book (2014), and Oriňáková and Oriňák (2011). Mueller et al. (2006) reviewed the different types of MOF and their possible applications. Carbonaceous materials are more complex and still are more appropriate for storing than for purifying hydrogen.

The adsorption process redesign and optimization are also the main objective of a large number of works. Silva et al. (2013) designed a hydrogen purification system using a type of MOF, CuBTC, which has already commercial availability. They designed a four-step PSA cycle and performed a mathematical model of multicomponent adsorption in fixed bed that allowed the optimization of PSA. They validated the model with experiments purifying hydrogen from CO_2, CH_4, and CO. Another kinetic model to predict the CO_2 adsorption capacity and kinetics was published by Zheng, Shi, Li, Yang, and Cai (2014). They experimentally tested the separation of CO_2 and H_2, and then modeled the purification at elevated temperature using multibed pressure swing adsorption. In the work by Moon, Kim, Ahn, and Lee (2014), the effects of operating variables in a two-bed PSA packed with activated carbon were analyzed, with the objective of being able to produce different quality of recovered hydrogen from the effluent gas of a melting incinerator to adapt the produced hydrogen to the needs of industries that can be near the installation. Another industrial application was performed by Luberti, Friedrich, Brandani, and Ahn (2014). They designed a PSA system for hydrogen purification integrated in an advanced gasification combined cycle plant for cogenerating power and ultrapure hydrogen.

The hydrogen adsorption process has been also integrated in more complex processes to enhance hydrogen production through sorption enhanced water gas shift (Najmi, Bolland, & Westman, 2013). This process involves the CO_2 adsorption (based on PSA system) that enables a higher hydrogen production in more compact and economic processes.

The adsorption process is well-established industrially and is getting more mature; there are two research works published in recent years about how to further employ the adsorption/PSA concept. Angers et al. (2014) analyzed, with computational fluid-dynamic simulations, the engineering safety issues from working with hydrogen under pressure in the PSA. And Papadias, Lee, and Ahmed (2012), based on the PSA process, developed a method to be able to measure the impurities in a hydrogen sample. It can be employed for less expensive and simpler analytical instruments for hydrogen quality monitoring and certification.

13.3 Advantages and disadvantages of the methods

Depending on the required purity of hydrogen the previously described processes show some advantages and/or disadvantages. For ultra-high pure hydrogen production, PSA adsorption, membranes, methanation, or selective oxidation in the presence of various catalysts could be not adequate techniques. Cryogenic techniques and CO preferential oxidation are suitable to decrease residual contents of CO in the hydrogen. The cryogenic techniques require huge amounts of energy to reach low temperatures and high pressures; therefore, this process is only adequate for high hydrogen flows.

The PSA technology can be considered a mature technology for air separation, but there is plenty of work to do to apply this technique in other fields. It can take 2 h to start up and, during that time, the purification efficiency decreases. To compensate for

this disadvantage, there are a few experiments that have combined it with metal hydrides, which can store hydrogen just after the start up.

13.4 Conclusion

There is a lot of experimental work done on adsorbents, hydrides, and iron-based redox cycles for hydrogen storage. This is also an important step for hydrogen purification application. To purify hydrogen from a mixture, the higher the capacity of removing hydrogen from the mixture, the higher the hydrogen amount purified. This first step is still under development, but there are already some commercial metal hydrides and adsorbents. Now the main issue to focus on can be to further improve the systems that have shown better experimental results, to increase their stability on time, and to develop theoretical studies. With these studies, it is possible to model the systems, which allows the development of engineering design and the implementation on the industry.

On the other hand, there is a second step in employing these solids for hydrogen purification. The effect that compounds, other than hydrogen, have in these solids still needs a great deal of experimental work. It is important to experiment in different conditions and with different compounds with the adsorbents, metal hydrides, and iron materials. There is a lot of work still to be done in this area before developing the simulation tools.

List of acronyms

CNF	Carbon nanofibers
COF	Covalent organic frameworks
DOE	Department of Energy
FTIR	Fourier transform infrared spectroscopy
MH	Metal hydride
MOF	Metal organic frameworks
PEM	Proton exchange membrane
PSA	Pressure swing adsorption
SMR	Steam methane reforming
STP	Standard temperature and pressure
SWCN	Single-walled carbon nanotubes
XPS	X-ray photoelectron spectroscopy
XRD	X-ray diffraction

References

Acha, E., Requies, J., Güemez, M. B., Barrio, V. L., Cambra, J. F., & Arias, P. L. (2014). Process integration for hydrogen production, purification and storage using iron oxides. *International Journal of Hydrogen Energy, 39*, 5257−5266.

Akira, N. (2006). *Iron-microparticles composite hydrogen-generating agent, its manufacture, and hydrogen production by steam-iron process with the agent*. JP 2006298659.

Alijani, A., & Irankhah, A. (2013). Medium-temperature shift catalysts for hydrogen purification in a single-stage reactor. *Chemical Engineering & Technology, 36*(2), 209−219.

Angers, B., Hourri, A., Benard, P., Demaël, E., Ruban, S., & Jallais, S. (2014). Modelling of hydrogen explosion on a pressure swing adsorption facility. *International Journal of Hydrogen Energy, 39*, 6210−6221.

Anton, M. (1910). *Making hydrogen*. US 971206.

Ares-Fernandez, J. R., Aguey-Zinsou, K. F., Elsaesser, M., Ma, X. Z., Dornheim, M., Klassen, T., et al. (2007). Mechanical and thermal decomposition of $LiAlH_4$ with metal halides. *International Journal of Hydrogen Energy, 32*, 1033−1040.

Atsonios, K., Panopoulos, K. D., Doukelis, A., Koumanakos, A., & Kakaras, E. (2013). Cryogenic method for H_2 and CH_4 recovery from a rich CO_2 stream in pre-combustion carbon capture and storage schemes. *Energy, 53*, 106−113.

Basile, A., & Iulianelli, A. (Eds.). (2014). *Advances in hydrogen production, storage and distribution*. Woodhead Publishing.

Bleeker, M. F., Veringa, H. J., & Kersten, S. R. A. (2009). Deactivation of iron oxide used in the steam-iron process to produce hydrogen. *Applied Catalysis A, 357*(1), 5−17.

Bogdanovic, B., Brand, R. A., Marjanovic, A., Schwickardi, M., & Tölle, J. (2000). Metal-doped sodium aluminium hydrides as potential new hydrogen storage materials. *Journal of Alloys and Compounds, 302*, 36−58.

Broom, D. P. (2011). Hydrogen storage materials. *Green energy technology*. London: Springer-Verlag.

Broom, D. P., & Book, D. (2014). 15-Hydrogen storage in nanoporous materials. *Advances in hydrogen production, storage and distribution* (pp. 410−450).

Cerný, R., Penin, N., Hagemann, H., & Filinchuk, Y. (2009). The first crystallographic and spectroscopic characterization of a 3d-metal borohydride: $Mn(BH_4)_2$. *Journal of Physical Chemistry C, 113*, 9003−9007.

Chandra, D., Chien, W., & Talekar, A. (2011). Metal hydrides for NiMH battery applications. *Mat Mat*, 6. article 2.

Choudhury, P., Srinivasan, S. S., Bhethanabotla, V. R., Goswami, Y., McGrath, K., & Stefanakos, E. K. (2009). Nano-ni doped Li-Mn-b-h system as a new hydrogen storage candidate. *International Journal of Hydrogen Energy, 34*, 6325−6334.

Datta, P., Rihko-Struckmann, L. K., & Sundmacher, K. (2011). Influence of molybdenum on the stability of iron oxide materials for hydrogen production with cyclic water gas shift process. *Materials Chemistry & Physics, 129*, 1089−1095.

Datta, P., Rihko-Struckmann, L. K., & Sundmacher, K. (2014). Quantification of produced hydrogen in a cyclic water gas shift process with Mo stabilized iron oxide. *Full Processing Technology, 128*, 36−42.

David, E. (2005). An overview of advanced materials for hydrogen storage. *Journal of Materials Processing Technology, 169*, 162−163.

Delgado, J. A., Águeda, V. I., Uguina, M. A., Sotelo, J. L., Brea, P., & Grande, C. A. (2014). Adsorption and diffusion of H_2, CO, CH_4, and CO_2 in BPL activated carbon and 13X zeolite: evaluation of performance in pressure swing adsorption hydrogen purification by simulation. *Industrial & Engineering Chemistry Research, 53*(40), 15414−15426.

Fujisawa, A., Miura, S., Mitsutake, Y., & Monde, M. (2013). Simulation study of hydrogen purification using metal hydride. *Journal of Alloys and Compounds, 580*, 423−426.

Galvita, V., Hempel, T., Lorenz, H., Rihko-Struckmann, L. K., & Sundmacher, K. (2007). Deactivation of modified iron oxide materials in the cyclic water gas shift process for CO-free hydrogen production. *Industrial & Engineering Chemistry Research, 47*, 303−310.

Gangwal, S. K., Subramani, V., Li, W., Turk, B. S., Gupta, R. P., & Silverston, P. L. (2006). Production of pure hydrogen from syngas by steam-iron process using nanoparticle iron catalysts. *Preprints of Papers-American Chemical Society Division of Petroleum Chemistry, 51*(1), 78−80.

Grande, C. A. (2012). Advances in pressure swing adsorption for gas separation. article ID 982934 *ISRN Chemical Engineering*, 13.

Gross, K., Sandrock, G., & Thomas, G. J. (2002). Dynamic in situ X-Ray diffraction of catalyzed alanates. *Journal of Alloys and Compounds, 330-322*, 691−695.

Herguido, J., Peña, J. A., & Carazo, E. (2014). Experimental assessment of hydrogen separation from H_2/CH_4 mixtures by the "steam-iron process" in an interconnected circulating fluidized bed reactor. *International Journal of Hydrogen Energy, 39*(26), 14050−14060.

Hitoshi, N., & Masakatsu, M. (2007). *Economic production of hydrogen by employing redox reaction of metal oxides, and apparatus for it*. JP 2007112672.

Huang, Z. G., Guo, Z. P., Calka, A., Wexler, D., Lukey, C., & Liu, H. K. (2006). Effects of iron oxide (Fe_2O_3, Fe_3O_4) on hydrogen storage properties of Mg-based composites. *Journal of Alloys Compounds, 422*, 299−304.

Ismail, M., Zhao, Y., Yu, X. B., & Dou, S. X. (2010). Effects of NbF_5 addition on the hydrogen storage properties of $LiAlH_4$. *International Journal of Hydrogen Energy, 35*, 2361−2367.

Jozwiak, W. K., Kaczmarek, E., Maniecki, T. P., Ignaczak, W., & Maniukiewicz, W. (2007). Reduction behaviour of iron oxides in hydrogen and carbon monoxide atmospheres. *Applied Catalysis A-General, 326*(1), 17−27.

Kobayashi, H., Yamauchi, M., & Kitagawa, H. (2011). Nanosize-induced hydrogen storage and capacity control in a non-hydride-forming element: rhodium. *Journal of the American Chemical Society, 133*(29), 11034−11037.

Kobayashi, H., Yamauchi, M., & Kitagawa, H. (2012). Finding hydrogen-storage capability in iridium induced by the nanosize effect. *Journal of the American Chemical Society, 134*(16), 6893−6895.

Kock, A. J. H. M., Fortuin, H. M., & Geus, J. W. (1985). The reduction behaviour of supported iron catalysts in hydrogen or carbon monoxide atmospheres. *Journal of Catalysis, 96*(1), 261−275.

Kusada, K., Yamauchi, M., Kobayashi, H., & Kubota, Y. (2010). Hydrogen storage properties of solid-solution alloys of immiscible neighbouring elements with Pd. *Journal of American Chemical Society, 132*(45), 15896−15898.

Lambert, S. W., Chandra, D., Cathey, W. N., Lynch, F. E., & Bowman, R. C., Jr. (1992). Investigation of hydriding properties of $LaNi_{4.8}Sn_{0.2}$, $LaNi_{4.27}Sn_{0.24}$ and $La_{0.9}Gd_{0.1}Ni_5$ after thermal cycling and aging. *Journal of Alloys and Compounds, 187*, 113−135.

Lebon, A., Garcia-Fuente, A., Vega, A., & Aguilera-Granja, F. (2011). Hydrogen insertion in Pd core/Pt shell cubo−octahedral nanoparticles. *Physical Review B, 83*, 125427.

Lebon, A., Garcia-Fuente, A., Vega, A., & Aguilera-Granja, F. (2012). Hydrogen interaction in Pd−Pt alloy nanoparticles. *The Journal of Physical Chemistry, 116*, 126−133.

Lin, H. Y., Chen, Y.-W., & Li, C. (2003). The mechanism of reduction of iron oxide by hydrogen. *Thermochimica Acta, 400*(1−2), 61−67.

Lin, H. C., Lin, K. M., Sung, C. W., & Wu, K. C. (2007). Characteristics of activation and anti-poisoning in an $LmNi_{4.8}Al_{0.2}$ hydrogen storage alloy. *International Journal of Hydrogen Energy, 32*, 2494−2500.

Liu, R., Reed, D., & Book, D. (2012). Decomposition behaviour of $Mn(BH_4)_2$ formed by ball-milling $LiBH_4$ and $MnCl_2$. *Journal of Alloys and Compounds, 515*, 32−38.

Lively, R. P., Bessho, N., Bhandari, D. A., Kawajiri, Y., & Koros, W. J. (2012). Thermally moderated hollow fiber sorbent modules in rapidly cycled pressure swing adsorption mode for hydrogen purification. *International Journal of Hydrogen Energy, 37*, 15227−15240.

Lototskyy, M., Modibane, K. D., Williams, M., Klochko, Ye., Linkov, V., & Pollet, B. G. (2013). Application of surface-modified metal hydrides for hydrogen separation from gas mixtures containing carbon dioxide and monoxide. *Journal of Alloys and Compounds, 580*, 382−385.

Lozano-Castelló, D., Suárez-García, F., Linares-Solano, A., & Cazorla-Amorós, D. (2013). Chapter 12-advances in hydrogen storage in carbon materials. *Renewable hydrogen technologies* (pp. 269−291).

Luberti, M., Friedrich, D., Brandani, S., & Ahn, H. (2014). Design of a H_2 PSA for cogeneration of ultrapure hydrogen and power at an advanced integrated gasification combined cycle with pre-combustion capture. *Adsorption, 20*, 511−524.

Meng, Z., Lu, R., Rao, D., Kan, E., Xiao, C., & Deng, K. (2013). Catenated metal-organic frameworks: promising hydrogen purification materials and high hydrogen storage medium with further lithium doping. *International Journal of Hydrogen Energy, 28*, 9811−9818.

Minko, K. B., Artemov, V. I., & Yan'kov, G. G. (2014a). Numerical simulation of sorption/desorption processes in metal-hydride systems for hydrogen storage and purification. Part I: development of a mathematical model. *International Journal of Heat and Mass Transfer, 68*, 683−692.

Minko, K. B., Artemov, V. I., & Yan'kov, G. G. (2014b). Numerical simulation of sorption/desorption processes in metal-hydride systems for hydrogen storage and purification. Part II: verification of the mathematical model. *International Journal of Heat and Mass Transfer, 68*, 693−702.

Miura, S., Fujisawa, A., Tomekawa, S., Taniguchi, Y., Hanada, N., & Ishida, M. (2013). A hydrogen purification and storage system using CO adsorbent and metal hydride. *Journal of Alloys and Compounds, 580*, 414−417.

Modibane, K. D., Williams, M., Lototskyy, M., Davids, M. W., Klochko, Ye., & Pollet, B. G. (2013). Poisoning-tolerant metal hydride materials and their application for hydrogen separation from CO_2/CO containing gas mixtures. *International Journal of Hydrogen Energy, 38*(23), 9800−9810.

Moon, D. K., Kim, Y. H., Ahn, H., & Lee, C. H. (2014). Pressure swing adsorption process for reconverting H_2 from the effluent gas of a melting incinerator. *Industrial & Engineering Chemistry Research, 53*(40), 15447−15455.

Mueller, U., Schubert, M., Teich, F., Puetter, H., Schierle-Arndt, K., & Pastré, J. (2006). Metal-organic frameworks-prospective industrial applications. *Journal of Materials Chemistry, 16*, 626−636.

Myhra, S., Kisi, E. H., & Gray, E. M. (1995). A surface analytical study of SO_2 stabilisation of $LaNi_5H_x$ surfaces. *Journal of Alloys and Compounds, 224*, 305−315.

Najmi, B., Bolland, O., & Westman, S. F. (2013). Simulation of the cyclic operation of a PSA-based SEWGS process for hydrogen production with CO_2 capture. *Energy Procedia, 37*, 2293−2302.

Nakamori, Y., Li, H. W., Kikuchi, K., Aoki, M., Miwa, K., Towata, S., et al. (2007). Thermodynamical stabilities of metal-borohydrides. *Journal of Alloys & Compounds, 446−447*, 296−300.

Oriňáková, R., & Oriňák, A. (2011). Recent applications of carbon nanotubes in hydrogen production and storage. *Fuel, 90*(11), 3123−3140.

Otsuka, K., Kaburagi, T., Yamada, C., & Takenaka, S. (2003). Chemical storage of hydrogen by modified iron oxides. *Journal of Power Sources, 122*, 111−121.

Papadias, D. D., Lee, S. H. D., & Ahmed, S. (2012). Facilitating analysis of trace impurities in hydrogen: enrichment based on the principles of pressure swing adsorption. *International Journal of Hydrogen Energy, 37*, 14413−14426.

Payá, J., Linder, M., Laurien, E., & Corberán, J. M. (2009). Mathematical models for the *P*−*c*−*T* characterization of hydrogen absorbing alloys. *Journal of Alloys and Compounds, 484*(1−2), 190−195.

Piemonte, V., Di Paola, L., De Falco, M., Iulianelli, A., & Basile, A. (2014). Hydrogen production using inorganic membrane reactors. In A. Basile, & A. Iulianelli (Eds.), *Advances in hydrogen production, storage and distribution* (pp. 283−316). Woodhead Publishing.

Pineau, A., Kanari, N., & Gaballah, I. (2006). Kinetics of reduction of iron oxides by H_2: Part I: low temperature reduction of hematite. *Thermochimica Acta, 447*(1), 89−100.

Pineau, A., Kanari, N., & Gaballah, I. (2007). Kinetics of reduction of iron oxides by H_2: Part II. Low temperature reduction of magnetite. *Thermochimica Acta, 456*(2), 75−88.

Ragheb, M. (2011). *Hydrides alloys for hydrogen storage*. http://mragheb.com/NPRE%20498ES%20Energy%20Storage%20Systems/Metal%20Hydrides%20Alloys%20for%20Hydrogen%20Storage.pdf. Assessed September 2014.

Requies, J., Güemez, M. B., Perez, S., Barrio, V. L., Cambra, J. F., Izquierdo, U., et al. (2013). Natural and synthetic iron oxides for hydrogen storage and purification. *Journal of Materials Science, 48*, 4813−4822.

Romero, E., Soto, R., Duran, P., Herguido, J., & Pena, J. (2012). Molybdenum addition to modified iron oxides for improving hydrogen separation in fixed bed by redox processes. *International Journal of Hydrogen Energy, 37*, 6978−6984.

Sandrock, G. D., & Goodell, P. D. (1980). Surface poisoning of $LaNi_5$, FeTi and (Fe, Mn)Ti by O_2, CO and H_2O. *Journal of the Less Common Metals, 73*, 161−168.

Schlapbach, L., & Züttel, A. (2001). Hydrogen-storage materials for mobile applications. *Nature, 414*, 353−358.

Schweppe, F., Martin, M., & Fromm, E. (1997). Hydrogen absorption of $LaNi_5$ powders precovered with O_2, CO, H_2S, CO_2 or N_2. *Journal of Alloys and Compounds, 253*−*254*, 511−514.

Seung, J. Y., Haesol, J., Taehoon, K., & Chong, R. P. (2012). Recent advances in hydrogen storage technologies based on nanoporous carbon materials. *Progress in Natural Science, 22*(6), 631−638.

Shoji, H. (2009). *Materials for supplying hydrogen utilizing reversible redox reactions of iron oxide*. JP 2009040669.

Silva, B., Solomon, I., Ribeiro, A. M., Lee, U.-H., Hwang, Y. K., Chang, J. S., et al. (2013). H2 purification by pressure swing adsorption using CuBTC. *Separation & Purification Technology, 118*, 744−756.

Sun, F., Yan, M.-Y., Liu, X.-P., Ye, J.-H., Li, Z.-N., Wang, S. M., et al. (2014). Effect of CO on hydrogen storage performance of $2LiNH_2 + MgH_2$ system. *International Journal of Hydrogen Energy, 39*(17), 9288−9292.

Tadashi. (1995). *Power generation from hydrogen manufactured from iron oxide and steam*. JP 07144901.

Takenaka, S., Hanaizumi, N., Son, V. T. D., & Otsuka, K. (2004). Production of pure hydrogen from methane mediated by the redox of Ni- and Cr-added iron oxides. *Journal of Catalysis, 228*, 405−416.

Takenaka, S., Kaburagi, T., Yamada, C., Nomura, K., & Otsuka, K. (2004). Storage and supply of hydrogen by means of the redox of the iron oxides modified with Mo and Rh species. *Journal of Catal, 228*, 66−74.

Takenaka, S., Nomura, K., Hanaizumi, N., & Otsuka, K. (2005). Storage and formation of pure hydrogen mediated by the redox of modified iron oxides. *Applied Catalysis A-General, 282*, 333−341.

Talagañis, B. A., Meyer, G. O., Oliva, D. G., Fuentes, M., & Aguirre, P. A. (2014). Modeling and optimal design of cyclic processes for hydrogen purification using hydride-forming metals. *International Journal of Hydrogen Energy*. http://dx.doi.org/10.1016/j.ijhydene.2014.09.045.

Thaler, M., & Hacker, V. (2012). Storage and separation of hydrogen with the metal steam process. *International Journal of Hydrogen Energy, 37*, 2800−2806.

Thaler, M., Hacker, V., Anilkumar, M., Albering, J., Besenhard, J. O., Schröttner, H., et al. (2006). Investigations of cycle behaviour of the contact mass in the RESC process for hydrogen production. *International Journal of Hydrogen Energy, 31*, 2025−2031.

Urasaki, K., Tanimoto, N., Hayashi, T., Sekine, Y., Kikuchi, E., & Matsukata, M. (2005). Hydrogen production via steam -iron reaction using iron oxide modified with very small amounts of palladium and zirconia. *Applied Catalysis A-General, 288*, 143−148.

Varin, R. A., Czujko, T., & Wronski, Z. S. (2009). *Nanomaterials for solid state hydrogen storage*. New York, NY, USA: Springer Science & Business Media.

Varin, R. A., Jang, M., & Polanski, M. (2010). The effects of Ball milling and molar ratio of LiH on the hydrogen storage properties of nanocrystalline lithium amide and lithium hydride ($LiNH_2 + LiH$) system. *Journal of Alloys and Compounds, 491*, 658−667.

Varin, R. A., & Wronski, Z. S. (2013). Progress in hydrogen storage in complex hydrides. In *(Chapter 13) of renewable hydrogen technologies*. Elsevier.

Varin, R. A., & Zbroniec, L. (2012). Catalytic effects of nanometric Ni (*n*-Ni) on the dehydrogenation of ball milled sodium alanate ($NaAlH_4$). *Nanoscience & Nanotecnology Letters, 4*, 149−159.

Wan, Q., Li, P., Li, Y., Zhai, F., Zhang, W., Cui, L., et al. (2014). CO impurities effect on $LaNi_{4.7}Al_{0.3}$ hydrogen storage alloy hydrogenation/dehydrogenation properties. *Bulletin of Material Science, 37*(4), 837−842.

Wang, H., Wang, G., Wang, X., & Bai, J. (2008). Hydrogen production by redox of cation modified iron oxide. *Journal of Physical Chemistry C, 112*, 5679−5688.

Wang, H., Zhang, J., Wen, F., & Bai, J. (2013). Effect of Mo dopants on improving hydrogen production by redox of iron oxide: catalytic role of Mo cation and kinetic study. *RSC Advances, 3*, 10341−10348.

Wang, J., Ebner, A. D., Zidan, R., & Ritter, J. A. (2005). Synergistic effects of co-dopants on the dehydrogenation kinetics of sodium aluminum hydride. *Journal of Alloys and Compounds, 391*, 245−255.

Wenguo, X., Zhipeng, X., & Xin, W. (2010). *Method and device for preparing H_2 and separating CO_2 based on Fe or Fe oxide*. CN 101746721.

Xiao, X., Chen, L., Wang, X., Li, S., Chen, C., & Wang, Q. (2008). Reversible hydrogen storage properties and favorable co-doping mechanism of the metallic Ti and Zr co-doped sodium aluminum hydride. *International Journal of Hydrogen Energy, 33*, 64−73.

Yang, M., Feng, X., Chu, K. H., & Liu, G. (2014). Graphical method for identifying the optimal purification process of hydrogen systems. *Energy, 73*, 829−837.

Zhang, T. B., Yang, X. W., Li, J. S., Hu, R., Xue, X. Y., & Fu, H. Z. (2012). On the poisoning effect of O_2 and N_2 for the $Zr_{0.9}Ri_{0.1}V_2$ hydrogen storage alloy. *Journal of Power Sources, 202*, 217−224.

Zhao, D.-L., & Zhang, Y. H. (2014). Research progress in Mg-based hydrogen storage alloys. *Rare Metals, 33*, 499−510.

Zheng, Y., Shi, Y., Li, S., Yang, Y., & Cai, N. (2014). Elevated temperature hydrogen/carbon dioxide separation process simulation by integrating elementary reaction model of hydrotalcite adsorbent. *International Journal of Hydrogen Energy, 39*, 3771−3779.

Zornoza, B., Casado, C., & Navajas, A. (2013). Advances in hydrogen separation and purification with membrane technology. In *Renewable Hydrogen Technologies*. Elsevier.

This page intentionally left blank

Polymeric membranes for the purification of hydrogen

14

P. Bernardo, J.C. Jansen
Institute on Membrane Technology of the Italian National Research Council (ITM-CNR), Rende, Italy

14.1 Introduction

Hydrogen is an important industrial feedstock for the production of fuels and many chemicals (Bartels, Pate, & Olson, 2010). The demand for hydrogen has risen rapidly owing to increased use in refineries for hydrotreating (removing sulfur) and hydrocracking (converting heavy hydrocarbons to lighter, higher value fuels). This has stimulated the implementation of separation systems for hydrogen recovery in refineries instead of flaring, thus reducing emissions and costs. At the same time, increased demand for hydrogen for fuel cell applications combined with environmental concerns related to atmospheric pollution and greenhouse gas emissions, has spurred the development of new methods for hydrogen production involving renewable sources such as biomass (Fatsikostas, Kondarides, & Verykios, 2002). Whatever the adopted process, hydrogen production typically involves different separation and purification steps, depending on the final use for the produced hydrogen.

Membrane gas separation offers various advantages over conventional, more mature and commercially available technologies such as pressure swing adsorption (PSA) and cryogenic distillation (Adhikari & Fernando, 2006). Important benefits of membrane systems are related to their operational flexibility, ease of operation combined with low energy consumption, small footprint, and cost-effectiveness, even at low gas volumes (Spillman, 1989). Membrane gas separation could have a significant role in biohydrogen technology (Bakonyi, Nemestóthy, & Bélafi-Bakó, 2013).

A wide range of membrane types is available for hydrogen separation, based on organic polymers and inorganic materials or metals. Metallic membranes, mainly made with palladium and its alloys, are the most investigated owing to their extreme selectivity to hydrogen (Yan, Maeda, Kusakabe, & Morooka, 1994; Yun & Oyama, 2011). However, they have a high cost, are fragile, and require elevated operating temperatures that restrict their application and flexibility. Composite membranes allow reduction of the Pd layer thicknesses, thus increasing hydrogen permeability (Hu, Huang, Shu, Fan, & Xu, 2008; Jayaraman, Lin, Pakala, & Lin, 1995; Roa, Way, McCormick, & Paglieri, 2003; Tong et al., 2006). Amorphous alloy membranes (e.g., $Zr_{36}Ni_{64}$) were also considered substitutes for expensive palladium membranes (Ishitsukaa et al., 2008). Inorganic hydrogen-selective membranes were widely studied for use in membrane reactors for hydrogen-producing reactions that are often carried out under severe temperature and pressure conditions (Tong, Matsumura, Suda, & Haraya, 2005).

Compendium of Hydrogen Energy. http://dx.doi.org/10.1016/B978-1-78242-361-4.00014-5

They are also based on crystalline zeolites (Hong, Falconer, & Noble, 2005) and silica (Balachandran et al., 2006; Gu & Oyama, 2007; Khatib & Oyama, 2013). However, these membranes are expensive and it is difficult to produce modules with a high surface area to volume ratio. Current challenges of silica membranes include their stability (Balachandran et al., 2006). Recently, metal organic frameworks (MOF), a newly developed family of crystalline microporous materials, were considered for producing hydrogen-selective membranes (Huang et al., 2014; Huang, Wang, Kong, & Caro, 2012). Carbon membranes are prepared by the pyrolysis of polymeric precursors such as polyimide materials (Jones & Koros, 1994; Kita, 2006; Kusuki, Shimazaki, Tanihara, Nakanishi, & Yoshinaga, 1997). They have excellent gas separation performance but major drawbacks are brittleness and poor mechanical strength (Jones & Koros, 1994; Hosseini & Chung, 2009). A recent development is related to ultrathin graphene oxide membranes (Li et al., 2013). In these membranes permeation occurs through selective structural defects on graphene oxide, resulting in mixture selectivity as high as 3400 and 900 for H_2/CO_2 and H_2/N_2 separation, respectively.

Even if they are less selective than inorganic or metal membranes, polymeric membranes are widely applied because of relatively cheap and reproducible preparation methods and their processability. This chapter will present background information and an overview of their main properties and performance.

14.2 Hydrogen sources: syngas, petrochemical industry, biohydrogen

Most hydrogen is industrially obtained by catalytic steam reforming of hydrocarbons, such as natural gas, LPG or naphtha, to yield a gas mixture referred to as syngas (Ockwig & Nenoff, 2007a). The process is followed by a water gas shift reaction, producing a mixture mainly containing hydrogen and carbon dioxide, and other separation and purification steps.

Various process streams produce hydrogen as a product that can be recovered by suitable secondary purification steps. Refinery off-gas (ROG) is currently recognized as an attractive source for hydrogen recovery, instead of using only its heating value in the refinery fuel gas system. The choice of the separation process depends on the hydrogen content, which varies in a broad range, from 5−10% up to 90%. The largest source of easily recovered hydrogen in a refinery is the off-gas from catalytic reforming, which typically contains 70−90+ vol% hydrogen mixed with $C_1-C_6^+$ hydrocarbons.

Other sources for hydrogen recovery are high-pressure and low-pressure purge gases from high-pressure hydrocrackers and hydrotreaters. The high-pressure purge streams, available at 50−200 bar, contain 75−90 vol% hydrogen mixed with hydrocarbons, whereas low-pressure purge gases are available at 5−20 bar and have a reduced hydrogen concentration (50−75 vol%). Hydrogen recovery from these streams would reduce the makeup requirements.

Large amounts of hydrogen are produced in steam cracking plants for ethylene production. A series of cryogenic units is conventionally applied to separate the products

from the cracking furnace, producing a high-purity hydrogen stream. Typically, a small fraction of the hydrogen is used in the same plant (for acetylene hydrogenation); the balance is sent to fuel or exported. The hydrogen-rich ethylene off-gas normally contains 80−90 vol% of hydrogen, with CO, CH_4, ethylene, and nitrogen as the major impurities. This off-gas could be upgraded for refinery use if the ethylene plant is in close proximity to a refinery. This operation requires removal of CO to parts per million by volume levels to avoid catalyst poisoning.

Biohydrogen is biologically generated hydrogen (Bakonyi, Nemestóthy, & Bélafi-Bakó, 2013). Hydrogen can be produced in a renewable manner from lignocellulosic biomass by several methods, including pyrolysis, gasification, and steam reforming (Fatsikostas et al., 2002). The gas obtained during biohydrogen fermentation is a mixture of H_2, CO_2, and N_2 with several trace components (e.g., H_2S) saturated with water (Bakonyi, Nemestóthy, & Bélafi-Bakó, 2013).

14.3 Hydrogen separation methods

Separation and purification of hydrogen can be carried out by different methods. Conventional methods include PSA or cryogenic distillation, and membrane separation (Adhikari & Fernando, 2006).

14.3.1 Conventional hydrogen separation methods

PSA processes are used to produce high-purity hydrogen from steam, methane, and ROG (Sircar & Golden, 2000). PSA is carried out in multiple packed beds that produce constant product and tail gas streams. It can be operated at near-ambient temperatures, using the difference in adsorption properties of various molecules in a solid, which selectively adsorbs undesired gases at high pressure (e.g., carbons, zeolites, silica). This gas is then desorbed by reducing the pressure. Therefore, the process is not easy and is difficult to model accurately. PSA technology is generally considered to be low in energy consumption although it allows high H_2 purity (99.99%) (Yang, 1987). In hydrogen production by steam reforming, impurities are mainly CO, CO_2, and CH_4. The impurity partial pressure is lowered by swinging the adsorber pressure from the feed pressure to the tail gas pressure. An additional high-purity hydrogen purge stream can be used as a sweep gas to carry away the contaminants, resulting in a hydrogen loss of about 8−20% of the total throughput (Miller & Stöcker, 2003). The hydrogen rich-stream obtained from a PSA unit is available at essentially feed pressure, which is 15−30 bar in refinery applications. PSA with layered beds can be adopted to separate hydrogen from syngas (Yang, 1987), involving activated carbon (adsorbing carbon dioxide, and a part of methane and carbon monoxide) and zeolites (adsorbing methane and carbon monoxide).

Cryogenic distillation is a low-temperature process that operates at different boiling temperatures (relative volatilities) of the feed components. The feed stream is cooled in multipass heat exchangers, thus condensing feed impurities. Refrigeration duty is

obtained by Joule–Thomson refrigeration derived by throttling the condensed liquid hydrocarbons. Additional refrigeration, if required, can be obtained by external refrigeration systems or by turboexpansion of the hydrogen product. Therefore, the process is capital- and energy-intensive. One main advantage of the cryogenic process is the possibility of producing separate hydrocarbon streams rich in C_4^+, ethane, propane, and so forth.

14.3.2 Hydrogen separation by membrane systems

Membrane separation is an economical method applicable to several processes related to hydrogen separation, as summarized in Table 14.1.

14.3.2.1 Hydrogen recovery

Ammonia purge streams. Hydrogen recovery from ammonia purges was the first commercial application of membrane systems for gas separation (Bernardo, Drioli, & Golemme, 2009). The purge stream from the ammonia reactor contains hydrogen, nitrogen, methane, and argon and is almost clean and free of condensable vapors. These features are ideal for application to membrane technology, because hydrogen is highly permeable with respect to other gases in different membrane types and the stream to be treated is already at high pressure (ca 140 bar).

Refinery fuel/flare gas. Residual gas from refining processes contains a significant amount of unused hydrogen at elevated pressure. Hydrogen content in the various refinery purges and off-gases ranges between 30% and 80%, mixed with C_1–C_5 light hydrocarbons. A hydrogen purity of 90–95% is required to recycle it to a process unit. The demand for hydrogen recovery in refineries is rapidly increasing because of environmental regulations, as well.

Hydrodesulfurization purges. The primary purpose of hydrotreating, hydrocracking, or HDS operations is to saturate olefins and/or reduce the sulfur and/or nitrogen within a feedstock. Residual gas from these processes contains a significant amount

Table 14.1 Membrane separation of hydrogen-containing mixtures

Application area	Source/process
Hydrogen recovery	Ammonia purge streams
	Refinery fuel/flare gas
	Hydrodesulfurization purges
	Hydrocracker purges
	Catalytic reformer net gas
	Fluidized catalytically cracked overhead gas
	Pressure swing adsorption tail gas
H_2/CO ratio adjustment in syngas	Steam reforming

of unused hydrogen at pressure. The use of membranes for hydrogen separation provides additional recyclable hydrogen for these applications.

In a conventional HDS process, sulfur is removed from liquid hydrocarbons by reacting the sulfur with hydrogen to form H_2S. The sour hydrogen gas stream consisting of unreacted hydrogen, H_2S, and undesired light hydrocarbons is then separated from the liquid hydrocarbons, and the H_2S is removed to sweeten the hydrogen stream for recycling.

Hydrocracker and hydrotreater purges. The boiling range of the feed can be lowered in hydrocracking or remain constant in hydrotreating. A typical refinery operation is separation of hydrogen contained in the stream coming out from the hydrocracker. This process has the disadvantage of removing 4 moles of hydrogen for every mole of hydrocarbon removed. The membranes can be used alone or combined with an absorber system, at a reduced capital cost and better process efficiency (Zolandz & Fleming, 1992a). A membrane system can be integrated into the design of a hydroprocessing unit to optimize the use of hydrogen. The flash gas from these units is often sent to a PSA system for hydrogen recovery. High-pressure purge gas can be treated in a membrane system to recover hydrogen for reuse.

Catalytic reformer net gas. The reformer is a net hydrogen producer. Typically, the overhead vapor is split into at least two streams: one is recycled to the reactor and the other is purged from the recycle loop and is frequently sent for additional separation and treatment, such as adsorption of hydrocarbons. The net hydrogen stream is obtained at a high hydrogen concentration, 80% or more, for use elsewhere in the refinery, whereas the waste hydrocarbon stream is sent for light ends recovery or to the fuel header. The PSA process is normally used to upgrade large quantities of ROG, producing makeup hydrogen for a hydrocracker or hydrotreater.

Fluidized catalytically cracked (FCC) overhead gas. Depending on the flow rate, feed composition and variability, feed pressure, and required hydrogen product purity, either the cryogenic or the membrane process can be used for hydrogen recovery from FCC off-gas and other low-pressure refinery purge streams with a low hydrogen concentration (Miller and Stöcker, 2003). The upgrading process produces also a valuable tail gas. The cryogenic process is normally used if there are valuable hydrocarbons, particularly olefins, which can be recovered in addition to hydrogen, or if the required hydrogen purity is greater than 90 vol%. The membrane process can recover hydrogen efficiently from these streams at a hydrogen purity of 80–90 vol%. This low-purity hydrogen product can be used effectively in some applications, such as low-pressure hydrotreaters, and the tail gas can sometimes be sent to downstream hydrocarbon recovery units, because it is already compressed.

PSA tail gas. The overhead vapor from the reformer reactors is typically split into at least two portions. One is recycled in the reactor loop and the other is purged from the loop and is the source of the net hydrogen product. This purge stream is often sent to PSA for upgrading to obtain a high-purity hydrogen product (>99%). The hydrocarbon tail gas produced during the regeneration of the PSA beds is frequently sent to the plant fuel header. It can be treated in a membrane system for the recovery of valuable H_2 and hydrocarbon streams.

14.3.2.2 Syngas ratio (H_2/CO) adjustment

Several hundreds of membrane separation plants have been installed worldwide for treating syngas produced by reformers, stripping hydrogen out (H_2/CO ratio adjustment) (Ockwig & Nenoff, 2007b). In this case, the feed stream is clean and available at a high pressure, and thus is ideally suited for use in membrane modules.

14.3.3 Hybrid membrane/PSA systems

Membrane systems can also be operated in combination with other well-established unit operations in the chemical and petrochemical industries, such as PSA (Doshi, Werner, & Mitariten, 1989), which favorably combines their advantages. In these integrated systems, membranes perform the bulk separation, providing a moderately pure product at low cost that may be economically upgraded by a subsequent process. Typically, a combination of membranes and PSA is considered in H_2 separation, whereas hybrid membranes and amine absorption are applied to CO_2 separation. A hybrid membrane/PSA process should combine the high throughput and purity of a PSA process with a membrane separation process that has lower operating costs. PSA has moderate hydrogen recovery (65–90%), depending on the tail gas pressure. Indeed, the membrane–PSA hybrid process is expected to increase overall H_2 recovery without sacrificing purity. Furthermore, it coproduces a CO_2 stream ready for capture and sequestration.

14.3.4 Membrane separation versus other methods

The PSA process features high product purity (99%+) and moderate hydrogen recovery (65–90%), depending on the tail gas pressure, whereas polymeric membrane systems recover hydrogen at moderate purity (90–95%) and moderate recovery (85–90%). The cryogenic process has moderate purity (90–95%) with high recovery (90–95%) (Peramanu, Cox, & Pruden, 1999). Compared with the PSA process, a polymeric membrane system has no moving parts and is extremely reliable, although it is of lower purity. Additional modules can be added for expansion or increased recovery.

The membrane process is the most economical process for high-pressure purge gas upgrading. The product delivery pressure is chosen to allow the product to enter one of the stages of the makeup hydrogen compressors. Low-pressure purge gases are usually upgraded by the PSA process. The PSA process is preferred to the cryogenic process because the flow rates are relatively small and the stream composition can be highly variable. The combination of lower pressure and lower hydrogen content makes the PSA system less economical than the membrane system. The membrane process usually gives the highest rate of return on investment because of the tail gas at high pressure.

If the hydrogen content in the ROG is too low, the implementation of PSA or membrane systems becomes less economical compared with the direct use of ROG as steam reformer feedstock. Membrane systems are most suitable for upgrading ethylene off-gas containing 80–90 vol% hydrogen. Indeed, the pressure and high H_2 concentration results in high purity of the product (95–97 vol.% of H_2), although it is lower

than for a PSA process. Moreover, the residue gas stream is available at high pressure, whereas PSA systems require compression of tail gas from 0.1−0.3 bar to fuel system pressure. The cost of compressing the membrane hydrogen product compared with the cost of compressing PSA tail gas is one difference between the membrane and PSA processes.

In general, membrane systems using feed compression may be most economical for applications requiring less than about 1000 m^3/h of hydrogen product, owing to low capital costs. For larger flow rates, cryogenic upgrading has sometimes been used, requiring external refrigeration. Commercial polymeric membrane modules can operate at high pressure (up to 120 bar), with flow rates up to 330,000 Nm^3/h, reaching a hydrogen recovery up to 98 vol% and hydrogen purity as high as 99.9% (Bernardo et al., 2009).

Main problems that limit the application of membrane technology are membrane plasticization by strongly adsorbing components and condensation of light hydrocarbons on the membrane surface, which strongly affects membrane performance and stability. Aromatic removal in the pretreatment section is also an important design consideration. Unless recovered hydrocarbons are of high value, the cryogenic process is not normally used to process ROG alone. The development of new membrane materials more resistant to high hydrocarbon partial pressure, and the introduction of a more efficient pretreatment stage will allow this technology to expand rapidly.

14.4 Membrane types for hydrogen separation

14.4.1 Neat polymer membranes

Polymeric membranes are the most commonly used membranes in the field of gas separation because of their low price and easy processability. Depending on their glass transition temperature (T_g) and on the operating temperature, amorphous polymers can be distinguished as rubbery or glassy (Ebewele, 2000). A glassy polymer is in a nonequilibrium state. As the temperature increases and it approaches the T_g, the polymer chains become more flexible; above the T_g the polymer is referred to as rubbery.

14.4.1.1 Rubbery versus glassy polymers

Rubbery polymers have a much higher permeability than conventional glassy polymers. Their liquid-like flexible matrix has poor ability to sieve molecules based on their size. In rubbers, the diffusivity is only a weak function of penetrant size and overall selectivity is mainly governed by differences in penetrant solubility (Merkel, Bondar, Nagai, Freeman, & Pinnau, 2000). These materials have solubility-controlled permeation and preferentially allow the permeation of readily condensable large gas or vapor molecules in a gaseous mixture also containing smaller molecules (Grinevich, Starannikova, Yampolskii, Gringolts, & Finkelshtein, 2011; Matteucci, Yampolskii, Freeman, & Pinnau, 2006).

Instead, permeation in glassy polymers is diffusivity controlled, with preferential permeation of smaller and more mobile molecules. This results in an inverse permeability

order with respect to that of rubbery polymers, but also in higher separation factors. A variety of novel glassy polymers has been developed, some of which are shown in Figure 14.1 and discussed in the following sections.

14.4.1.2 Low free-volume glassy polymers

Membrane-based hydrogen separation has long been based on polymers with low selectivity, such as cellulose acetate. Commercial membranes based on polyimides and brominated polysulfone have improved permeability and selectivity. In particular, polyimides, which are low free-volume glassy polymers, are the most extensively used materials for hydrogen membrane separation (Rezac, Koros, & Miller, 1995; Yampolskii, 2012). Aromatic polyimides have high glass transition temperatures and thus are more suitable for use at high temperature than cellulose acetate or polysulfone (Zolandz & Fleming, 1992a). Polyimide membranes are currently successfully applied for H_2 recovery in refineries, owing to their good stability and interesting separation factors (e.g., H_2/N_2 of ca 100−200) (Hayes et al, 1992; Zolandz & Fleming, 1992b). Matrimid 5218 is a representative example, with H_2/CH_4 selectivity of about 100 (Shishatskiy, Nistor, Popa, Pereira Nunes, & Peinemann, 2006). Fluorinated polyimides usually possess higher H_2 permeability and lower selectivity over other gases compared with nonfluorinated polyimides. For instance, the 6FDA-DDBT polyimide exhibits H_2 permeability of 156 Barrer and H_2/CH_4 selectivity of 80 (Li, Zhu, Ratinac,

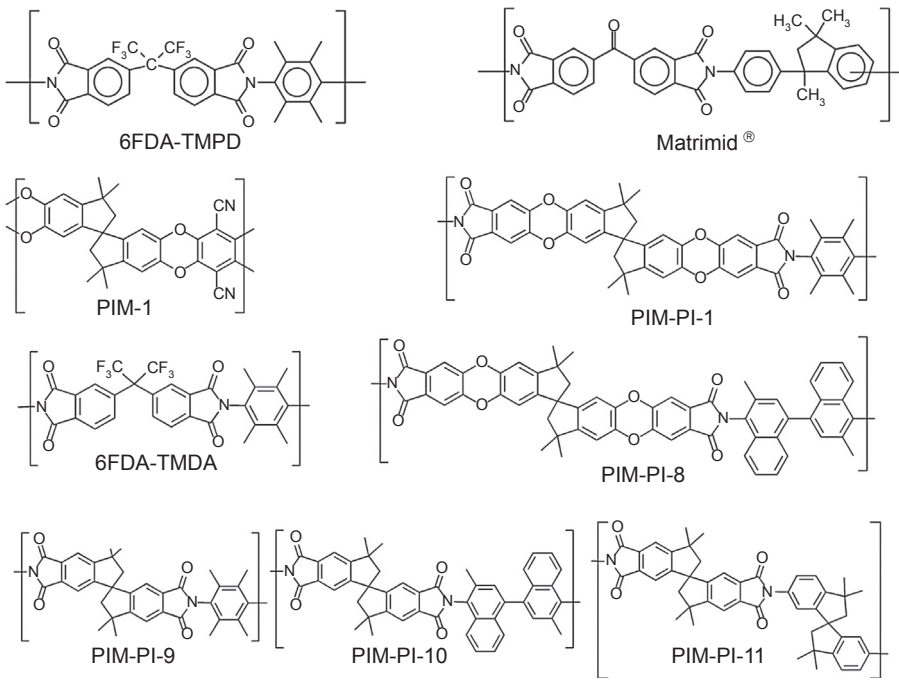

Figure 14.1 Structures of a selection of previously reported polyimides and polymers of intrinsic microporosity referred to in the text.

Ringer, & Wang, 2009), whereas the nonfluorinated BPDA-ODA polyimide has H_2 permeability of 1.33 Barrer and H_2/N_2 selectivity of 370 (Li, Wang, Ding, & Xu, 1996; Yampolskii, 2012). Diamino-modified polyimides have an ideal H_2/CO_2 selectivity of 101, which is far superior to other polymeric membranes and is well above the Robeson's upper-bound line (Chung, Shao, & Tin, 2006).

Polybenzimidazole (PBI) has emerged as a prime candidate for low-cost PEMs as a result of its intrinsic physicochemical properties, e.g., heat resistance and proton conductivity above 100 °C without humidification. Polybenzimidazole was identified as a unique polymeric material for H_2 separation, owing to superior thermal stability and good intrinsic H_2/CO_2 selectivity under high-temperature environments (Pesiri, Jorgensen, & Dye, 2003).

14.4.1.3 High free-volume glassy polymers

Interesting novel ladder-type polymers were synthesized and referred to as polymers with intrinsic microporosity (PIMs) (Budd et al., 2004). Their poor chain packing ability results in a large free-volume amount, and thus in exceptional permeability coupled with moderate selectivity (McKeown & Budd, 2010). A more shape-persistent PIM structure (PIM-EA-TB) was obtained via the Troger's base formation (Carta et al., 2013). This polymer shows a more pronounced size-sieving character and thus preferential permeation of H_2 with respect to CO_2, surpassing the Robeson's upper bound in the case of H_2/CH_4 separation.

Polyimides with intrinsic microporosity (PIM-PIs) were synthesized and showed high permeability with respect to conventional polyimides (Rogan et al., 2013, 2014). Novel polyimides with intrinsic microporosity were produced using the Troger's base (Zhuang et al., 2014) and trypticene unit as well (Swaidan, Al-Saeedi, Ghanem, Litwiller, & Pinnau, 2014). These high free-volume PIM-PIs demonstrated high permeability values with respect to low free-volume conventional polyimides, overcoming tradeoffs in permeability and selectivity embodied by the upper bounds to polymeric gas separation performance for sieving-based air and hydrogen separation (Swaidan et al., 2014).

14.4.2 Hybrid materials

Blending different polymers is an interesting approach to tailoring the properties of polymeric membranes. It was also considered for hydrogen separation (Hosseini, Teoh, & Chung, 2008; Weng, Tseng, & Wey, 2008; Yong et al., 2012).

Another strategy that in principle allows synergistic enhancement in the performance of polymeric materials involves the combination of well-dispersed filler nanoparticles in a polymeric matrix. The resulting membranes are referred to as mixed-matrix membranes (Chung, Jiang, Li, & Kulprathipanja, 2007; Mahajan & Koros, 2002). Different fillers (e.g., zeolites, carbon nanotubes, MOF, metal oxides) were investigated for this purpose to introduce other transport mechanisms or modify the polymer-free volume. The basic idea of the use of size selective filler particles is to facilitate the diffusion of hydrogen and to create additional resistance for larger

molecules (Figure 14.2). Critical issues are represented by the filler dispersion and compatibility with the polymer matrix, and thus by interfacial effects.

A decrease in permeability was frequently observed that can be attributed to increased rigidity of polymer chains in the presence of zeolite particles (Huang, Li, Wen, Teoh, & Kulprathipanja, 2006; Moore & Koros, 2005), partial blockage of zeolite pores by polymer chains (Li, Chung, Cao, & Kulprathipanja, 2005), and/or extended diffusion pathways of hydrogen molecules through the membrane (Li et al., 2005; Li, Guan, Chung, & Kulprathipanjana, 2006; Süer, Baç, & Yilmaz, 1994). Polycarbonate loaded with 30 wt% highly crystalline zeolite-4A particles of 3 μm reached an H_2/N_2 selectivity of 73, 30% higher than neat polycarbonate (Şen, KalipçIlar, & Yilmaz, 2007). However, reduced hydrogen permeability was observed. A similar trend was reported for polyethersulfone (PES) loaded with zeolite 5A (1−5 μm), exhibiting about 25% higher H_2/N_2 selectivity than PES, coupled with a decrease in gas permeability of at least 25% (Wang, Holmberg, & Yan, 2002).

The size of the filler particles is a key factor influencing membrane performance. Nano-sized fillers are required to fabricate mixed-matrix membranes, because for practical application polymeric membranes are usually shaped into asymmetric hollow fibers or flat sheets with a thin selective layer (e.g., <1 μm). The use of nanoparticles could limit the formation of bypasses, as shown by a comparison of zeolite A microparticles (1−5 μm) and nanoparticles (50−140 nm) in PES (Huang et al., 2006). The nano-zeolite produced a much lower drop in hydrogen permeability (from 8.96 to 8.3 Barrer) compared with the micro-zeolite (down to 4.94 Barrer). This was compensated for by much more pronounced enhancement of permselectivity using the zeolite nanocrystals. Interfacial voids formed between the zeolite crystals and the polymer matrix in the case of poor adhesion between the two phases (Mahajan & Koros, 2002b; Moore & Koros, 2005; Şen et al., 2007) could be responsible for reduced selectivity. Nanocrystals (80 nm) of silicalite-1 in Teflon AF1600 in a concentration up to 40 wt% yielded 15-fold higher H_2 permeability than that of the neat polymer, even with 50% lower H_2/N_2 selectivity than in pure Teflon (Golemme, Bruno, Manes, & Muoio, 2006).

Functionalization of the fillers causes an increase in compatibility with the polymeric matrix (Li et al., 2006). Silylation of the external zeolite surface was effective in improving compatibility with the rubbery PDMS (Vankelecom, Scheppers, Heus, & Uytterhoeven, 1994). A polyimide membrane containing 35 wt% of organic-functionalized sodalite nanocrystals had a hydrogen permeability of 8.0 Barrer and an ideal H_2/N_2 selectivity of 280 at 25 °C, respectively, 14% and 41% higher than corresponding values for the neat polyimide membrane (Li et al., 2009).

MOF are believed to have intrinsically better compatibility with polymers because of their metal organic structure. Polyimide was also loaded with MOFs and spun into hollow fibers. At 6 wt% loading of $Cu_3(BTC)_2$, H_2 permeance increased by 45% and ideal selectivity increased by a factor of 2−3 compared with corresponding values for pure polyimide (Hu et al., 2010). Although PBI has high intrinsic H_2/CO_2 selectivity in high-temperature environments (Pesiri et al., 2003), it has low permeability. To overcome this problem, PBI was loaded with ZIF-8 particles in a dual-layer hollow fiber configuration (Yang, Shi, & Chung,

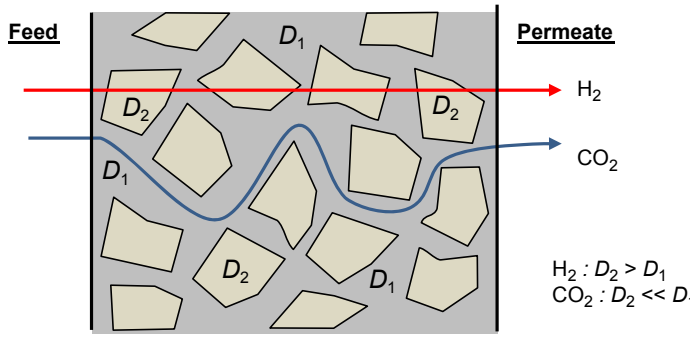

Figure 14.2 Schematic representation of a mixed-matrix membrane with a size-selective filler for H_2 separation.

2012). The same MOF in FDA-based polyimide yielded intrinsic H_2/CO_2 selectivity equal to 29 (Wijenayake et al., 2014).

Enhanced gas permeability in nanocomposite membranes can be ascribed to gas transport through the interface between the filler and the polymer matrix, as observed with poly (bisphenol A-*co*-4-nitrophthalic anhydride-*co*-1,3-phenylene diamine) loaded with multi-walled carbon nanotubes (MWCNTs) (Weng, Tseng, & Wey, 2009). At high MWCNT concentrations (>5%), permeability and selectivity of H_2, CO_2, and CH_4 improved significantly (e.g., by 200% in the case of H_2 at 15% loading).

14.4.3 Hydrogen-selective versus hydrogen-retaining membranes

Gas separation membranes can be distinguished in conventional membranes that operate on the basis of gas diffusivity selectivity, i.e., size selection, and reverse-selective membranes that have solubility selectivity (Lau et al., 2011). Table 14.2 lists hydrogen permeability and H_2/CO_2 ideal selectivity for different polymers.

In most polymers the solubility term favors the transport of CO_2 instead of H_2. However, diffusion of the smaller H_2 is much faster than for CO_2 and represents the most significant contribute to permeability. Conventional glassy polymer membranes are usually hydrogen selective (Lin & Freeman, 2004) and thus produce a hydrogen-rich stream at low pressure in the permeate side. The high cost of repressurizing purified hydrogen favors the use of more conventional processes such as liquid absorption to remove acid gases such as CO_2 from these streams.

Instead, reverse-selective membranes have sufficiently high solubility selectivity that overcomes adverse diffusivity selectivity, allowing larger gas molecules such as CO_2 to permeate while retaining smaller gas molecules such as H_2 in the residue stream at high pressure, thus reducing or completely eliminating the need for expensive recompression steps (Lin, Van Wanger, Freeman, Toy, & Gupta, 2006; Merkel et al., 2002; Shao & Chung, 2009). Polymers containing polar moieties, such as ether groups, have an affinity for CO_2 because of dipole−quadrupole interaction between

Table 14.2 Hydrogen permeability and H_2/CO_2 selectivity for selected polymer membranes

Polymer	H_2 permeability[a] (Barrer)	H_2/CO_2 selectivity(−)	References[b]
Cellulose acetate	2.63	0.4	Phair and Badwal (2006)
Polydimethyl siloxane	375	0.3	Phair and Badwal (2006)
Polyethylene low density	17.3	0.9	Phair and Badwal (2006)
Ethyl cellulose	87	3.3	Phair and Badwal (2006)
Poly (ethylene-*co*-vinyl alcohol) (Eval)	0.5	2.5	Phair and Badwal (2006)
Polybenzyl methacrylate	11.0	1.4	Phair and Badwal (2006)
Polyetherimide	7.8	5.9	Phair and Badwal (2006)
Polyimide (Matrimid)	28.1	2.6	Phair and Badwal (2006)
Polyimide (6-FDA-TMPD)	549	0.80	Phair and Badwal (2006)
Polymethyl methacrylate	2.4	4	Phair and Badwal (2006)
Polymethylpentene	125	1.5	Phair and Badwal (2006)
Polyphenyleneoxide	113	1.5	Phair and Badwal (2006)
Polystyrene MW 280K	23.8	2.3	Phair and Badwal (2006)
Polystyrene-*co*-butadiene	7.9	0.5	Phair and Badwal (2006)
Polysulfone	12.1	2.0	Phair and Badwal (2006)
Polyvinyl acetate	15.1	1.2	Phair and Badwal (2006)
Polyvinylidene fluoride (Kynar)	2.4	2.0	Phair and Badwal (2006)
PIM-1	3300	0.3	Budd et al. (2008)
PIM-PI-9	840	2.6	Rogan et al. (2013)
PIM-PI-10	670	3.2	Rogan et al. (2013)
PIM-PI-11	624	2.4	Rogan et al. (2013)
PIM-EA-TB	7140	1.1	Carta et al. (2013)
T-PIM1	2670	1.7	Ghanem et al. (2006)
PI-TB-2	134	2.45	Zhuang et al. (2014)

[a] 1 Barrer = 10^{-10} cm^3 (STP)cm/(cm^2 s cm Hg)
[b] Permeabilities reported in Phair and Badwal (2006) are determined at 30 °C and 30 psi feed pressure.

the acidic CO_2 and the polar ether oxygen (Ghosal, Chen, Freeman, Daly, & Negulescu, 1996). This affinity may be harnessed to prepare membranes able to remove CO_2 and other acid gases selectively from mixtures with H_2. A family of reverse-selective membrane materials based on highly branched, cross-linked PEO exhibited outstanding separation performance for H_2 purification by removing acid gases such as CO_2 and H_2S from feed streams of practical interest (Lin et al., 2006; Merkel et al., 2002). Moreover, the presence of moisture and high-pressure CO_2 in the feed actually improved permeability and selectivity, in contrast to the detrimental behavior associated with plasticizing agents in conventional membrane materials (Lin et al., 2006; Merkel et al., 2002).

PIM-1, the archetypal representative of the family of polymers of intrinsic microporosity, is a CO_2-selective polymer with the following unusual permeability order: $CO_2 > H_2 > He > O_2 > Ar > CH_4 > N_2 > Xe$, whereas in most glassy polymers the typical behavior is $H_2 > CO_2$. The H_2 and CO_2 permeability are of about 1300−4000 and 3000−8000 Barrer, respectively, with relatively low H_2/CO_2 selectivity of 0.4−0.8. However, H_2-selective membranes were obtained by blending PIM-1 with Matrimid and then cross-linking with diamines (Yong, Li, Chung, & Tong, 2013). Modified membranes with more than 1 order of magnitude increased ideal H_2/CO_2 selectivity (from 0.4 to 0.8−9.6) and H_2 permeability of 400 Barrer, surpass the current upper bound for different hydrogen-related separations (e.g., H_2/CO_2, H_2/N_2, and H_2/CH_4). Reduced permeability in the modified membrane with respect to the parent PIM-1 is the result of smaller *d*-spacing and a decrease in the diffusivity coefficient as proven by X-ray diffraction analysis and sorption data.

The type of membrane determines whether the hydrogen will be collected as the product in the permeate stream or retained in the retentate stream. Two representative systems are schematically displayed in Figure 14.3.

14.5 Polymeric membrane preparation and characterization

14.5.1 Neat polymer membranes by phase inversion

The most frequently used process for preparing commercial polymeric membranes is phase inversion. This method transforms the polymer in a controlled manner from the solution phase into the solid phase, creating the membrane as a flat film or a hollow fiber (Mulder, 1996). The polymer solution can be precipitated by different approaches including cooling, immersion in a nonsolvent bath, and evaporation (Ren & Wang, 2008). Main parameters determining membrane morphology are the polymer concentration in the initial solution, solvent/nonsolvent affinity, and the presence of additives in the polymer solution or in the coagulation bath. This technique enables the formation of different morphologies. Porous to dense membranes can be prepared, either in a symmetric or asymmetric form. Gas separation requires dense membranes in which the separation is normally based on the solution-diffusion mechanism.

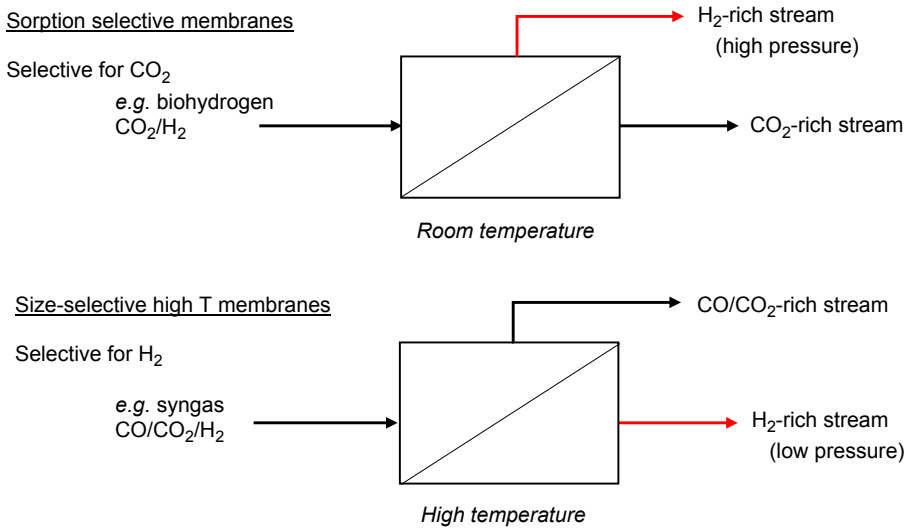

Figure 14.3 Scheme of membrane systems for low-temperature separation of condensable gases in sorption selective membranes (top) and high-temperature hydrogen separation in size-selective membranes.

The demand for higher productivity in industrial applications drove the development of asymmetric membranes (Loeb & Sourirajan, 1962), composite membranes (Henis & Tripodi, 1981) with a thin selective skin on a relatively open porous support, instead of thicker, flat, dense membranes. The selective layer of a membrane should be as thin as possible because the flux is inversely proportional to the membrane thickness.

Polymers can be easily shaped as flat sheets or hollow fibers. Asymmetric hollow fiber membranes with a dense skin layer are generally made by the dry−wet spinning method via the nonsolvent-induced phase inversion process. The preparation of hollow fiber membranes requires careful control of the spinning parameters, including the amount and type of polymers, solvents, additives to the spinning dope solution, the dope and bore fluid rate, the type of bore fluid, the fiber take-up velocity, the air−gap distance (unless wet spinning is used), the temperature and type of the coagulant bath (Feng, Khulbe, Matsuura, & Ismail, 2013), and others. Inline cross-linking can be used as an approach to increasing H_2/CO_2 selectivity of polyimide hollow fiber membranes (Choi, Jansen, Tasselli, Barbieri, & Drioli, 2010).

14.5.2 Thin film composite membranes

Membranes for industrial application frequently have a composite structure with a thin, selective, dense layer (0.5−5 μm) supported on a porous and mechanically stable layer (Pinnau, Wijmans, Blume, Kuroda, & Peinemann, 1988a). The support can be selected among organic (e.g., cellulose acetate, polysulfone, polytetrafluoroethylene, poly(vinylidene fluoride)) or inorganic (e.g., alumina, titania) materials. The role of

the support on the mass transport should be negligible, even if it may be predominant in some cases (Beuscher & Gooding, 1999). In the case of flat-sheet membranes the support is often backed by a highly porous nonwoven layer. Composite hollow-fiber membranes are typically prepared by a dip-coating process. A triple-nozzle (triple orifice) spinneret has been developed for preparing composite hollow-fiber membranes in one step (Feng et al., 2013).

Typically, a PDMS coating layer is added to composite gas separation membranes to seal possible pinholes and protect the thin selective layer (Chen, Miyano, Fouda, & Matsuura, 1990; Henis & Tripodi, 1981; Madaeni, Badieh, Vatanpour, & Ghaemi, 2012). Silicone is chosen for its low cost, combined with high permeability that does not affect the properties of the selective layer. It is generally applied as a dilute solution after drying the membrane (Mohammadi, Matsuura, & Sourirajan, 1995; Wang, Teo, & Li, 2002).

14.5.3 Characterization of polymeric membranes

Permeability and selectivity are key factors to evaluate the performance of a specific membrane material for gas separation. The time lag measured during the barometric determination of gas permeability provides an estimation of gas diffusion coefficients, and hence solubility coefficients indirectly (Paul & Koros, 1976). Instead, gravimetric sorption measurements are able to provide direct evaluation of the solubility coefficients in a membrane material.

Structural and morphological properties of polymeric membranes correlate with gas transport properties. Composition and properties of polymer materials such as glass transition and elastic modulus can be evaluated by different techniques such as Fourier transform infrared spectroscopy, differential scanning calorimetry, and scanning electron microscopy. These properties, as well as gas transport parameters, are related to the nature of the free-volume element within the polymer matrix (Higuchi, Jamieson, & Simha, 1996; Yampolskii & Shantarovich, 2006). Positron annihilation lifetime spectroscopy and 129Xe nuclear magnetic resonance techniques have been applied to probe the cavity space in microporous solids as well as in dense polymeric films. Positron annihilation lifetime spectroscopy correlates the *ortho*-positronium lifetime and formation probability with free-volume dimension and concentration, respectively (Eastmond, Daly, McKinnon, & Pethrick, 1999). Different probing methods may give quantitatively different results but they can be fundamental to an understanding of the transport properties of dense polymers (Jansen et al., 2009).

14.6 Transport phenomena through polymeric membranes

14.6.1 Pure gas transport

The driving force promoting selective permeation in membrane systems is a partial pressure difference between the two membrane sides. Gas permeation through

nonporous polymeric films is described by the solution-diffusion model (Wijmans & Baker, 1995), applying the following equation:

$$J = P\left(\frac{p_{\mathrm{H}} - p_{\mathrm{L}}}{l}\right) = D \times S\left(\frac{p_{\mathrm{H}} - p_{\mathrm{L}}}{l}\right) \tag{14.1}$$

where J is the flux of the gas through the membrane, P is the permeability of the penetrant species, p_{H} and p_{L} are the partial pressures of the penetrant on the upstream and downstream membrane sides, respectively, and l is the thickness of the membrane. The permeability is the product of the diffusivity D and solubility coefficient S of the gas species.

The ideal selectivity for a gas pair ($\alpha_{\mathrm{A/B}}$) is defined as the ratio of the individual gas permeabilities. It can be decoupled in two terms that account for differences in the diffusivity and solubility coefficients of the two gases:

$$\alpha_{A/B} = \frac{P_A}{P_B} = \frac{D_A}{D_B} \times \frac{S_A}{S_B} \tag{14.2}$$

Diffusion favors smaller molecules whereas sorption favors the more condensable and generally larger molecules. The diffusion coefficient is related to the polymer fractional free volume, which is a measure of the theoretical volume of the polymer divided by the actual volume of the polymer, whereas the penetrant solubility depends on its condensability (Matteucci et al., 2006). In real systems, the diffusion coefficient and the solubility coefficient may both be a function of the concentration.

Moreover, in the case of the sorption in glassy polymers there are considerable deviations from the simple Henry-type mechanism typically valid in rubbery materials (Paul & Koros, 1976; Wang, Corriou, Castel, & Favre, 2013). Therefore, the adsorbed concentration is obtained by considering two concurrent sorption mechanisms: ordinary dissolution described by Henry's law and a hole-filling process described by Langmuir adsorption. Selective permeation of hydrogen thus generally requires stiff size-selective glassy polymers, whereas selective permeation of the larger species with retention of hydrogen requires rubber-like materials. Some additives, such as ionic liquids, may enable tailoring of membrane properties from size-sieving to solubility selective (Jansen, Friess, Clarizia, Schauer, & Izák, 2011).

14.6.1.1 Robeson's diagrams

Polymeric materials have a tradeoff limitation between permeability and selectivity: As permeability increases, selectivity decreases, and vice versa, as shown empirically for different gas separations in 1991 (Robeson, 1991) and then updated in 2008 (Robeson, 2008). The Robeson's diagrams virtually summarized all existing membrane materials, indicating the best performance achievable by a polymeric membrane material for a specific gaseous separation. It was predicted that greater size selectivity could be obtained by increasing polymer chain rigidity, whereas high gas permeability

relies on large interchain separation (Freeman, 1999). A shift in the original 1991 upper bound was obtained for several separations, mainly owing to the development of perfluoro-polymers and the introduction of PIM polymers (Robeson, 2008).

14.6.2 Transport of gas mixtures and influence of operation conditions

Permeability and selectivity values reported in most scientific papers are often obtained in permeation experiments carried out with pure gases. However, the ideal and real separation factors, which are measured using single gases or their mixtures, can be significantly different. A diamino-modified polyimide showed ideal H_2/CO_2 selectivity of 101, which was reduced to 42 in mixed gas tests (Chung et al., 2006). The lower selectivity depends on the sorption competition between transport of H_2 and highly condensable CO_2 molecules. This phenomenon was shown in the purification of biohydrogen using a commercial polyimide membrane module (Bakonyi, Nemestóthy, Lin, & Bélafi-Bakó, 2013). Hydrogen permeability in polyimide (Matrimid 5218) membranes was unaffected by the presence of nitrogen and carbon monoxide; as a result, the mixed gas selectivity for the $H_2/N_2/CO$ mixtures is close to that calculated from pure gas-permeation data (David, Gorri, Urtiaga, & Ortiz, 2011). On the contrary, a strong dependency of the hydrogen permeability on CO_2 concentration was observed even at low concentrations of CO_2. A reduction of 42% of the hydrogen permeability coefficient was obtained when a mixture of 10/90 vol% H_2/CO_2 was fed, resulting in an H_2/CO_2 selectivity decayed from an ideal value of 4.2 to 2.7 in mixed gas experiments. This result was explained by considering dual-mode sorption for the glassy polyimide (Paul & Koros, 1976) and the preferential sorption of CO_2 on the Langmuir sites of the excess free-volume portion of the polymer (David et al., 2011). Moreover, gas composition, temperature, and stage-cut (ratio of permeate to feed flow rate) could significantly affect achievable selectivity (Bakonyi, Nemestóthy, Lin, et al., 2013).

14.6.3 Process technological aspects

Hollow-fiber and spiral-wound modules are commercially available for gas separation applications. The performance of the membrane module depends on the flow pattern: complete mixing, countercurrent flow, cocurrent flow, and cross-flow. For gas separation, countercurrent and cross-flow are generally used (Zolandz & Fleming, 1992a). The countercurrent flow pattern best describes flow in a hollow-fiber module. The latter is normally used in applications involving hydrogen separation (Baker, 2002; Zolandz & Fleming, 1992a). The polymeric membranes employed in gas separation modules are usually shaped as asymmetric hollow fibers or flat sheets with a thin selective layer ($<<1$ μm) to maximize the processed flow rate (Chung, Kafchinski, Foley, Kohn, & Straff, 1994; Pinnau, Wijmans, Blume, Kuroda, & Peinemann, 1988b). To achieve high H_2 purity, the modules are typically arranged in series. Results for single-stage separation show that only with glassy membranes can product gas specifications be reached in case of lower-quality requirements. Applying a two-stage gas-permeation process

enables higher quality requirements to be met with both glassy and rubbery membrane types (Wukovits, Chudzicki, Makaruk, & Friedl, 2012).

14.7 Advantages and disadvantages of the use of polymeric membranes for the purification of hydrogen

The application of membrane systems for upgrading hydrogen in refineries is rapidly evolving at the commercial level, owing to advantages related to low capital costs, low energy requirements, and modularity. Process flexibility, reliability, ease of response to variations, expansion capability, and versatility are the main parameters for choosing the best technology (Miller & Stöcker, 1989). In this sense, the application of membrane systems for hydrogen recovery has environmental benefits such as reduced waste and recovered/recycled valuable raw materials that are currently lost to fuel or flares.

A disadvantage of most membranes used today is that they are susceptible to contaminants commonly found in coal-derived syngas, such as sulfur, ammonia, mercury, and trace metals. Therefore, extensive gas cleanup is necessary and suitable technologies have to be carefully considered as membrane pretreatment. Furthermore, a limitation of polymeric membranes is modest thermal stability; only a few types are able to operate for long times at elevated temperatures. This required further studies on optimizing available membrane materials.

14.8 Future trends

The future of hydrogen separation by membranes depends first on available sources of hydrogen. Industrial-scale CO_2/H_2 separation for green hydrogen production by membranes should be carried out at relatively mild conditions in which CO_2 permeation might be favored. This would be more practical if the CO_2 permeability of current state-of-the-art PEO-based membranes is significantly increased, with similar or higher selectivity. Biohydrogen production is a relatively slow production process and is likely to remain a niche sector.

On the other hand, increased attention to hydrogen production via biomass gasification or gasification of other feedstocks necessitates the development of better membranes for use under high-temperature precombustion gas separation conditions (EU's FP7 project).

Both approaches require the development of novel membrane materials with increased performance and the proper combination of permeability and selectivity, as well as excellent long-term stability and stability under demanding operation conditions.

References

Adhikari, S., & Fernando, S. (2006). Hydrogen membrane separation techniques. *Industrial and Engineering Chemistry Research, 45*(3), 875−881.

Baker, R. W. (2002). Future directions of membrane gas separation technology. *Industrial and Engineering Chemistry Research, 41*, 1393−1411.

Bakonyi, P., Nemestóthy, N., & Bélafi-Bakó, K. (2013). Biohydrogen purification by membranes: an overview on the operational conditions affecting the performance of non-porous, polymeric and ionic liquid based gas separation membranes. *International Journal of Hydrogen Energy, 38*(23), 9673−9687.

Bakonyi, P., Nemestóthy, N., Lin, C. Y., & Bélafi-Bakó, K. (2013). Biohydrogen purification using a commercial polyimide membrane module: studying the effects of some process variables. *International Journal of Hydrogen Energy, 38*(35), 15092−15099.

Balachandran, U., Lee, T. H., Chen, L., Song, S. J., Picciolo, J. J., & Dorris, S. E. (2006). Hydrogen separation by 1dense cermet membranes. *Fuel, 85*, 150−155.

Bartels, J. R., Pate, M. B., & Olson, N. K. (2010). An economic survey of hydrogen production from conventional and alternative energy sources. *International Journal of Hydrogen Energy, 35*, 8371−8384.

Bernardo, P., Drioli, E., & Golemme, G. (2009). Membrane gas separation: a review/state of the art. *Industrial & Engineering Chemistry Research, 48*(10), 4638−4663.

Beuscher, U., & Gooding, C. H. (1999). The influence of the porous support layer of composite membranes on the separation of binary gas mixtures. *Journal of Membrane Science, 152*, 99−116.

Budd, P. M., Elabas, E. S., Ghanem, B. S., Makhseed, S., McKeown, N. B., Msayib, K. J., et al. (2004). Solution-processed, organophilic membrane derived from a polymer of intrinsic microporosity. *Advanced Materials, 16*, 456−459.

Budd, P. M., McKeown, N. B., Ghanem, B. S., Msayib, K. J., Fritsch, D., Starannikova, L., et al. (2008). Gas permeation parameters and other physicochemical properties of a polymer of intrinsic microporosity: polybenzodioxane PIM-1. *Journal of Membrane Science, 325*, 851−860.

Carta, M., Malpass-Evans, R., Croad, M., Rogan, Y., Jansen, J. C., Bernardo, P., et al. (2013). An Efficient polymer-based molecular sieve membranes for membrane gas separations. *Science, 339*, 303−307.

Chen, Y., Miyano, T., Fouda, A., & Matsuura, T. (1990). Preparation and gas permeation properties of silicone-coated dry polyethersulfone membranes. *Journal of Membrane Science, 48*, 203−219.

Choi, S.-H., Jansen, J. C., Tasselli, F., Barbieri, G., & Drioli, E. (2010). In-line formation of chemically cross-linked P84® co-polyimide hollow fibre membranes for H_2/CO_2 separation. *Separation and Purification Technology, 76*, 132−139.

Chung, T.-S., Jiang, L. Y., Li, Y., & Kulprathipanja, S. (2007). Mixed matrix membranes (MMMs) comprising organic polymers with dispersed inorganic fillers for gas separation. *Progress in Polymer Science, 32*, 483−507.

Chung, T. S., Kafchinski, E. R., Foley, P., Kohn, R. S., & Straff, R. S. (1994). Fabrication of composite hollow fibers for air separation. *Journal of Applied Polymer Science, 53*, 701−708.

Chung, T. S., Shao, L., & Tin, P. S. (2006). Surface modification of polyimide membranes by diamine for H_2 and CO_2 separation. *Macromolecular Rapid Communications, 27*, 998−1003.

David, O. C., Gorri, D., Urtiaga, A., & Ortiz, I. (2011). Mixed gas separation study for the hydrogen recovery from $H_2/CO/N_2/CO_2$ post combustion mixtures using a Matrimid membrane. *Journal of Membrane Science, 378*(1−2), 359−368.

Doshi, K. J., Werner, R. G., Mitariten, M. J. (1989). *Integrated membrane/PSA process and system*, U.S. Patent 4,863,492.

Eastmond, G. C., Daly, J. H., McKinnon, A. S., & Pethrick, R. A. (1999). Poly(ether imide)s: correlation of positron annihilation lifetime studies with polymer structure and gas permeability. *Polymer, 40*, 3605−3610.

EU's FP7 project M^4CO_2, web-site: www.m4co2.eu.

Fatsikostas, A. N., Kondarides, D. I., & Verykios, X. E. (2002). Production of hydrogen for fuel cells by reformation of biomass-derived ethanol. *Catalysis Today, 75*(1−4), 145−155.

Feng, C. Y., Khulbe, K. C., Matsuura, T., & Ismail, A. F. (2013). Recent progresses in polymeric hollow fiber membrane preparation, characterization and applications. *Separation and Purification Technology, 111*(25), 43−71.

Freeman, B. D. (1999). Basis of permeability/selectivity tradeoff relations in polymeric gas separation membranes. *Macromolecules, 32*, 375−380.

Ghanem, B. S., Swaidan, R., Ma, X., Litwiller, E., & Pinnau, I. (2006). Energy-efficient hydrogen separation by AB-type ladder-polymer molecular sieves. *Science and Technology of Advanced Materials, 7*, 792−805.

Ghosal, K., Chen, R. T., Freeman, B. D., Daly, W. H., & Negulescu, I. I. (1996). Effects of basic substituents on gas sorption and permeation in polysulfone. *Macromolecules, 29*, 4360−4369.

Golemme, G., Bruno, A., Manes, R., & Muoio, D. (2006). Preparation and properties of superglassy polymers − zeolite mixed matrix membranes. *Desalination, 200*, 440−442.

Grinevich, Y., Starannikova, L., Yampolskii, Y., Gringolts, M., & Finkelshtein, E. (2011). Solubility controlled permeation of hydrocarbons in novel highly permeable polymers. *Journal of Membrane Science, 378*, 250−256.

Gu, Y., & Oyama, S. T. (2007). High molecular permeance in a poreless ceramic membrane. *Advanced Materials, 19*, 1636−1640.

Hayes, R. A., et al. (1992). *Aromatic Polyimide double layered hollow filamentary membrane and process for producing same*, U.S. Patent 5,141,642.

Henis, J. M. S., & Tripodi, M. K. (1981). Composite hollow fibre membranes for gas separation: the resistance model approach. *Journal of Membrane Science, 8*, 233−246.

Higuchi, H., Jamieson, A. M., & Simha, R. (1996). Free volume quantities and viscoelasticity of polymer glasses. *Journal of Polymer Science: Part B, 34*, 1423−1426.

Hong, M., Falconer, J. L., & Noble, R. D. (2005). Modification of zeolite membranes for H_2 separation by catalytic cracking of methyldiethoxysilane. *Industrial & Engineering Chemistry Research, 44*, 4035−4041.

Hosseini, S. S., & Chung, T. S. (2009). Carbon membranes from blends of PBI and polyimides for N_2/CH_4 and CO_2/CH_4 separation and hydrogen purification. *Journal of Membrane Science, 328*, 174−185.

Hosseini, S. S., Teoh, M. M., & Chung, T. S. (2008). Hydrogen separation and purification in membranes of miscible polymer blends with interpenetration networks. *Polymer, 49*, 1594−1603.

Hu, J., Cai, H., Ren, H., Wei, Y., Xu, Z., Liu, H., et al. (2010). Mixed-matrix membrane hollow fibers of Cu_3(BTC) MOF and polyimide for gas separation and adsorption. *Industrial and Engineering Chemistry Research, 49*, 12605−12612.

Hu, X., Huang, Y., Shu, S., Fan, Y., & Xu, N. (2008). Toward effective membranes for hydrogen separation: multichannel composite palladium membranes. *Journal of Power Sources, 181*, 135−139.

Huang, A., Chen, Y., Liu, Q., Wang, N., Jiang, J., & Caro, J. (2014). Synthesis of highly hydrophobic and permselective metal−organic framework $Zn(BDC)(TED)_{0.5}$ membranes for H_2/CO_2 separation. *Journal of Membrane Science, 454*, 126−132.

Huang, Z., Li, Y., Wen, R., Teoh, M. M., & Kulprathipanja, S. (2006). Enhanced gas separation properties by using nanostructured PES-Zeolite 4A mixed matrix membranes. *Journal of Applied Polymer Science, 101*, 3800−3805.

Huang, A., Wang, N., Kong, K., & Caro, J. (2012). Organosilica-functionalized zeolitic imidazolate framework ZIF-90 membrane with high gas-separation performance. *Angewandte Chemie Internation Edition, 51*, 10551−10555.

Ishitsukaa, M., Hara, S., Mukaida, M., Haraya, K., Kita, K., & Kato, K. (2008). Hydrogen separation from dry gas mixtures using a membrane module consisting of palladium-coated amorphous-alloy. *Desalination, 234*, 293−299.

Jansen, J. C., Friess, K., Clarizia, G., Schauer, J., & Izák, P. (2011). High ionic liquid content polymeric gel membranes: preparation and performance. *Macromolecules, 44*, 39−45.

Jansen, J. C., Macchione, M., Tocci, E., De Lorenzo, L., Yampolskii, YuP., Sanfirova, O., et al. (2009). Comparative study of different probing techniques for the analysis of the free volume distribution in amorphous glassy perfluoropolymers. *Macromolecules, 42*, 7589−7604.

Jayaraman, V., Lin, Y. S., Pakala, M., & Lin, R. Y. (1995). Fabrication of ultrathin metallic membranes on ceramic supports by sputter deposition. *Journal of Membrane Science, 99*, 89−100.

Jones, C. W., & Koros, W. J. (1994). Carbon molecular sieve gas separation membranes-I. Preparation and characterization based on polyimide precursors. *Carbon, 32*(8), 1419−1425.

Khatib, S. J., & Oyama, S. T. (2013). Silica membranes for hydrogen separation prepared by chemical vapor deposition (CVD). *Separation and Purification Technology, 111*, 20−42.

Kita, H. (2006). Gas and vapour separation membranes based on carbon. In Y. Yampolskii, I. Pinnau, & B. Freeman (Eds.), *Materials science of membranes for gas and vapor separation* (pp. 337−354). Chichester, UK: John Wiley & Sons, Ltd.

Kusuki, Y., Shimazaki, H., Tanihara, N., Nakanishi, S., & Yoshinaga, T. (1997). Gas permeation properties and characterization of asymmetric carbon membranes prepared by pyrolyzing asymmetric polyimide hollow fiber membrane. *Journal of Membrane Science, 134*, 245−253.

Lau, C. H., Liu, S., Paul, D. R., Xia, J., Jean, Y.-C., Chen, H., et al. (2011). Silica nanohybrid membranes with high CO_2 affinity for green hydrogen purification. *Advanced Energy Materials, 1*, 634−642.

Li, Y., Chung, T.-S., Cao, C., & Kulprathipanja, S. (2005). The effects of polymer chain rigidification, zeolite pore size and pore blockage on polyethersulfone (PES)-zeolite A mixed matrix membranes. *Journal of Membrane Science, 260*, 45−55.

Li, Y., Guan, H., Chung, T., & Kulprathipanja, S. (2006). Effects of novel silane modification of zeolite surface on polymer chain rigidification and partial pore blockage in polyethersulfone (PES)−zeolite A mixed matrix membranes. *Journal of Membrane Science, 275*, 17−28.

Li, H., Song, Z., Zhang, X., Huang, Y., Li, S., Mao, Y., et al. (2013). Ultrathin, molecular-sieving graphene oxide membranes for selective hydrogen separation. *Science, 342*(6154), 95−98.

Li, Y., Wang, X., Ding, M., & Xu, J. (1996). Effect of molecular structure on the permeability and permselectivity of aromatic polyimides. *Journal of Applied Polymer Science, 61*, 741−748.

Li, D., Zhu, H. Y., Ratinac, K. R., Ringer, S. P., & Wang, H. (2009). Synthesis and characterization of sodalite−polyimide nanocomposite membranes. *Microporous and Mesoporous Materials, 126*(1−2), 14−19.

Lin, H., & Freeman, B. D. (2004). Gas solubility, diffusivity and permeability in poly(ethylene oxide). *Journal of Membrane Science, 239*(1), 105−117.

Lin, H., Van Wagner, E., Freeman, B. D., Toy, L. G., & Gupta, R. P. (2006). Plasticization-enhanced hydrogen purification using polymeric membranes. *Science, 311*, 639−642.

Loeb, S., & Sourirajan, S. (1962). Sea water demineralization by means of an osmotic membrane. *Advances in Chemistry Series, 38*, 117−132.

Madaeni, S. S., Badieh, M. M. S., Vatanpour, V., & Ghaemi, N. (2012). Effect of titanium dioxide nanoparticles on polydimethylsiloxane/polyethersulfone composite membranes for gas separation. *Polymer Engineering & Science, 52*(12), 2664−2674.

Mahajan, R., & Koros, W. J. (2002). Mixed matrix membrane materials with glassy polymers. Part 1. *Polymer Engineering & Science, 42*(7), 1420−1431.

Mahajan, R., & Koros, W. J. (2002). Mixed matrix membrane materials with glassy polymers. Part 1. *Polymer Engineering & Science, 42*, 1420−1431.

Matteucci, S., Yampolskii, Y., Freeman, B., & Pinnau, I. (2006). Transport of gases and vapors in glassy and rubbery polymers. In Y. Yampolskii, I. Pinnau, & B. Freeman (Eds.), *Material science of membranes for gas and vapor separation* (pp. 1−48). Chichester: John Wiley & Sons.

McKeown, N. B., & Budd, P. M. (2010). Exploitation of intrinsic microporosity in polymer-based materials. *Macromolecules, 43*(12), 5163−5176.

Merkel, T. C., Freeman, B. D., Spontak, R. J., He, Z., Pinnau, I., Meakin, P., et al. (2002). Ultrapermeable, reverse-selective nanocomposite membranes. *Science, 296*, 519−522.

Merkel, T., Bondar, V. I., Nagai, K., Freeman, B. D., & Pinnau, I. (2000). Gas sorption, diffusion, and permeation in poly(dimethylsiloxane). *Journal of Polymer Science, 38*(3), 415−434.

Miller, G. Q., & Stöcker, J. (1989). Selection of a hydrogen separation process. In *NPRA annual meeting held March 19−21, 1989, San Francisco, California (USA)*.

Miller, G. Q., & Stöcker, J. (October 2003). In *Selection of a hydrogen separation process, 4th European technical seminar on hydrogen plants, Lisbon, Portugal*.

Mohammadi, A. T., Matsuura, T., & Sourirajan, S. (1995). Gas separation by silicone-coated dry asymmetric aromatic polyamide membranes. *Gas Separation & Purification, 9*(3), 181−187.

Moore, T. T., & Koros, W. J. (2005). Non ideal effects in organic − inorganic materials for gas separation membranes. *Journal of Molecular Structure, 739*, 87−98.

Mulder, M. (1996). *Basic principles of membrane technology*. Kluwer Academic Publishers.

Ockwig, N. W., & Nenoff, T. M. (2007a). Membranes for hydrogen separation. *Chemical Reviews, 107*, 4078−4110.

Ockwig, N. W., & Nenoff, T. M. (2007b). Membranes for hydrogen separation. *Chemical Reviews, 107*, 4078−4093.

Paul, D. R., & Koros, W. J. (1976). Effect of partially immobilizating sorption on permeability and the diffusion time lag. *Journal of Polymer Science Part B: Polymer Physics, 14*, 675−685.

Peramanu, S., Cox, B. G., & Pruden, B. B. (1999). Economics of hydrogen recovery processes for the purification of hydroprocessor purge and off-gas. *International Journal of Hydrogen Energy, 24*, 405−424.

Pesiri, D. R., Jorgensen, B., & Dye, R. C. (2003). Thermal optimization of polybenzimidazole meniscus membranes for the separation of hydrogen, methane, and carbon dioxide. *Journal of Membrane Science, 218*, 11−18.

Phair, J. W., & Badwal, S. P. S. (2006). Materials for separation membranes in hydrogen and oxygen production and future power generation. *Science and Technology of Advanced Materials, 7*, 792−805.

Pinnau, I., Wijmans, J. G., Blume, I., Kuroda, T., & Peinemann, K.-V. (1988a). Gas permeation through composite membranes. *Journal of Membrane Science, 37*, 81−87.

Pinnau, I., Wijmans, J. G., Blume, I., Kuroda, T., & Peinemann, K.-V. (1988b). Gas permeation through composite membranes. *Journal of Membrane Science, 37*, 81−88.

Ren, J. Z., & Wang, R. (2008). Preparation of polymeric membranes. In L. K. Wang, J. P. Chen, Y.-T. Hung, & N. K. Shammas (Eds.), *Membrane and desalination technologies, handbook of environmental engineering* (Vol. 13, pp. 47−100).

Rezac, M. E., Koros, W. J., & Miller, S. J. (1995). Chemical stability of polyimide membranes at temperatures near *T*g. *Journal of Applied Polymer Science, 58*(1), 165−170.

Roa, F., Way, J. D., McCormick, R. L., & Paglieri, S. N. (2003). Preparation and characterization of Pd−Cu composite membranes for hydrogen separation. *Chemical Engineering Journal, 93*, 11−22.

Robeson, L. M. (1991). Correlation of separation factor versus permeability for polymeric membranes. *Journal of Membrane Science, 62*, 165−185.

Robeson, L. M. (2008). The upper bound revisited. *Journal of Membrane Science, 320*, 390−400.

Rogan, Y., Malpass-Evans, R., Carta, M., Lee, M., Jansen, J. C., Bernardo, P., et al. (2014). A highly permeable polyimide with enhanced selectivity for membrane gas separations. *Journal of Materials Chemistry A, 2*(14), 4874−4877.

Rogan, Y., Starannikova, L., Ryzhikh, V., Yampolskii, Y., Bernardo, P., Bazzarelli, F., et al. (2013). Synthesis and gas permeation properties of novel spirobisindane-based polyimides of intrinsic microporosity. *Polymer Chemistry, 4*, 3812−3820.

Şen, D., KalipçIlar, H., & Yilmaz, L. (2007). Development of polycarbonate based zeolite 4A filled mixed matrix gas separation membranes. *Journal of Membrane Science, 303*, 194−203.

Shao, L., & Chung, T. S. (2009). In situ fabrication of cross-linked PEO/silica reverse-selective membranes for hydrogen purification. *International Journal of Hydrogen Energy, 34*, 6492−6504.

Shishatskiy, S., Nistor, C., Popa, M., Pereira Nunes, S., & Peinemann, K. V. (2006). Polyimide asymmetric membranes for hydrogen separation: influence of formation conditions on gas transport properties. *Advanced Engineering Materials, 8*(5), 390−397.

Sircar, S., & Golden, T. C. (2000). Purification of hydrogen by pressure swing adsorption. *Separation Science and Technology, 35*, 667−687.

Spillman, R. W. (1989). Economics of gas separation membranes. *Chemical Engineering Progress, 85*, 41−62.

Süer, M. G., Baç, N., & Yilmaz, L. (1994). Gas permeation characteristics of polymer zeolite mixed matrix membranes. *Journal of Membrane Science, 91*, 77−86.

Swaidan, R., Al-Saeedi, M., Ghanem, B., Litwiller, E., & Pinnau, I. (2014). Rational design of intrinsically ultramicroporous polyimides containing bridgehead-substituted triptycene for highly selective and permeable gas separation membranes. *Macromolecules, 47*(15), 5104−5114.

Thermal transition in polymers. In R. O. Ebewele (Ed.), *Polymer science and technology* (2000) (pp. 95−115). Boca Raton: CRC Press.

Tong, J., Matsumura, Y., Suda, H., & Haraya, K. (2005). Experimental study of steam reforming of methane in a thin (6 micron) Pd-based membrane reactor. *Industrial & Engineering Chemistry Research, 44*, 1454−1465.

Tong, J., Su, L., Kashima, Y., Shirai, R., Suda, H., & Matsumura, Y. (2006). Simultaneously depositing Pd−Ag thin membrane on asymmetric porous stainless steel tube and application to produce hydrogen from steam reforming of methane. *Industrial & Engineering Chemistry Research, 45*, 648−655.

Vankelecom, I. F. J., Scheppers, E., Heus, R., & Uytterhoeven, J. B. (1994). Parameters influencing zeolite incorporation in PDMS membranes. *Journal of Physical Chemistry, 98*, 12390−12396.

Wang, L., Corriou, J.-P., Castel, C., & Favre, E. (2013). Transport of gases in glassy polymers under transient conditions: limit-behavior investigations of dual-mode sorption theory. *Industrial & Engineering Chemistry Research, 52*, 1089−1101.

Wang, H. T., Holmberg, B. A., & Yan, Y. S. (2002). Homogeneous polymer-zeolite nanocomposite membranes by incorporating dispersible template-removed zeolite nanocrystals. *Journal of Materials Chemistry, 12*, 3640−3643.

Wang, D., Teo, W. K., & Li, K. (2002). Preparation and characterization of high-flux polysulfone hollow fibre gas separation membranes. *Journal of Membrane Science, 204*, 247−256.

Weng, T.-H., Tseng, H.-H., & Wey, M.-Y. (2008). Preparation and characterization of PPSU/PBNPI blend membrane for hydrogen separation. *International Journal of Hydrogen Energy, 33*, 4178−4182.

Weng, T.-H., Tseng, H.-H., & Wey, M.-Y. (2009). Preparation and characterization of multi-walled carbon nanotube/PBNPI nanocomposite membrane for H_2/CH_4 separation. *International Journal of Hydrogen Energy, 34*(20), 8707−8715.

Wijenayake, S. N., Panapitiya, N. P., Nguyen, C. N., Huang, Y., Balkus, K. J., Jr., Musselman, I. H., et al. (2014). Composite membranes with a highly selective polymer skin for hydrogen separation. *Separation and Purification Technology, 135*, 190−198.

Wijmans, J. G., & Baker, R. W. (1995). The solution-diffusion model. A review. *Journal of Membrane Science, 107*, 1−21.

Wukovits, W., Chudzicki, M., Makaruk, A., & Friedl, A. (2012). Simulation study on the applicability and performance of conventional and reverse-selective membranes for upgrading of H_2 mixtures via gas-permeation. *Chemical Engineering Transactions, 29*, 1171−1176.

Yampolskii, Y. (2012). Polymeric gas separation membranes. *Macromolecules, 45*, 3298−3311.

Yampolskii, Y., & Shantarovich, V. (2006). Positron annihilation lifetime spectroscopy and other methods for free volume evaluation in polymers. In Yu Yampolskii, I. Pinnau, & B. D. Freeman (Eds.), *Materials science of membranes for gas and vapor separation* (pp. 191−210). Chichester, England: John Wiley & Sons.

Yang, R. T. (1987). *Gas separation by adsorption processes*. Boston: Buttenvorths.

Yang, T., Shi, G. M., & Chung, T.-S. (2012). Symmetric and asymmetric zeolitic imidazolate frameworks (ZIFs)/Polybenzimidazole (PBI) nanocomposite membranes for hydrogen purification at high temperatures. *Advanced Energy Materials, 2*, 1358−1367.

Yan, S., Maeda, H., Kusakabe, K., & Morooka, S. (1994). Thin palladium membrane formed in support pores by metal-organic chemical vapor deposition method and application to hydrogen separation. *Industrial & Engineering Chemistry Research, 33*, 616−622.

Yong, W. F., Li, F. Y., Chung, T.-S., & Tong, Y. W. (2013). Highly permeable chemically modified PIM-1/Matrimid membranes for green hydrogen purification. *Journal of Materials Chemistry A, 1*, 13914−13925.

Yong, W. F., Li, F. Y., Xiao, Y. C., Li, P., Pramoda, K. P., Tong, Y. W., et al. (2012). Molecular engineering of PIM-1/Matrimid blend membranes for gas separation. *Journal of Membrane Science* (Vol. 407−408), 47−57.

Yun, S., & Oyama, S. T. (2011). Correlations in palladium membranes for hydrogen separation: a review. *Journal of Membrane Science, 375*, 28−45.

Zhuang, Y., Lee, J., Seong, J. G., Lee, Y. M., Do, Y. S., Guiver, M. D., et al. (2014). Intrinsically microporous soluble polyimides incorporating Tröger's base for membrane gas separation. *Macromolecules, 47*, 3254−3262.

Zolandz, R. R., & Fleming, G. K. (1992). Design of gas permeation systems. In W. S. Ho, & K. Sirkar (Eds.), *Membrane handbook* (pp. 54−77). New York: Van Nostrand Reinhold.

Zolandz, R. R., & Fleming, G. K. (1992). Gas permeation applications. In W. S. W. Ho, & K. K. Sirkar (Eds.), *Membrane handbook* (pp. 78−94). New York: Chapman & Hall.

This page intentionally left blank

Single-stage hydrogen production and separation from fossil fuels using micro- and macromembrane reactors

15

A. Basile[1], *A. Iulianelli*[1], *J. Tong*[2]
[1]Institute on Membrane Technology of the Italian National Research Council (ITM-CNR), Rende, Italy; [2]Colorado School of Mines, Golden, CO, USA

15.1 Oil exploitation and the hydrogen economy

In past decades, the overconsumption of energy represented two critical issues to be solved. Indeed, during global industrialization, there has been a particular balance between the population level and the amount of energy consumed around the world. Therefore, this matter has negatively affected the consumption of worldwide energy, making it difficult to predict the global peak point of oil production and the ensuing decline (Campbell, 1997; Laherrere, 1999). Regarding the scenario of oil production and consumption, in the 1950s M. K. Hubbert was one of the first scientists to make a prediction about the world's petroleum resources (Iulianelli, Liguori, Longo, & Basile, 2012). He stated that the point of maximum production (known as the Hubbert peak) matches the midpoint of resource depletion under consideration. As a particular case, once the Hubbert peak is achieved, almost half of all estimated recoverable oil on Earth will be consumed. Today, although fossil fuels still have the role of the most important energy contributor, a future decline is foreseen owing to the depletion of oil, gas, and coal extraction. Furthermore, the exploitation of derived fossil fuels has a large impact on the global environment owing to greenhouse gas emissions. Therefore, in recent years different kinds of renewable energy have been taken into account, making lower carbon emissions possible and becoming more environmentally friendly. Among solar, wind power, geothermal power, hydroelectric energy, and biomass, the latter has been significantly considered for its potentiality as an exploitable renewable source. It is a biological material derived from wood, biodegradable waste, and alcohol fuels. Furthermore, biomass includes plant or animal matter used in the production of fibers or chemicals. In particular, biomass in the form of organic waste makes an economic and environmental friendly route possible for generating renewable hydrogen (Ni, Leung, Sumathy, & Leung, 2006). Indeed, with respect to fossil fuel exploitation, the production of hydrogen from biomass has some benefits such as a reduction in CO_2 emissions, increased conversion of the agricultural output value owing to the crop residue use, replacement of fossil fuels with renewable biomass fuel, and the cost of getting rid of municipal solid waste.

Compendium of Hydrogen Energy. http://dx.doi.org/10.1016/B978-1-78242-361-4.00015-7

In the 1970s, the concept of hydrogen economy began with the aim of describing a sustainable energy infrastructure based on the generation of hydrogen from nonfossil energy sources. Regarding the definition of hydrogen economy, even in the absence of general agreement, it is commonly viewed as an alternative to the large use of petroleum fuels, with hydrogen burned in internal combustion and external combustion engines and/or used in fuel cells (Basile, Iulianelli, & Liguori, 2013). This last aspect is important mainly for the economy of countries highly dependent on imported petroleum products. However, the most important reason for promoting hydrogen as an energy vector is its outstanding characteristics for environmental protection, particularly with the scope of solving climate change and air pollution issues caused by the exploitation of fossil fuels (Goltsov & Veziroğlu, 2001).

15.1.1 Hydrogen production in conventional systems

Industrially, hydrogen is produced by steam reforming natural gas, partially oxidizing heavy oil, and gasifying coal (Bartholomew & Farrauto, 2006, chap. 6; Kalamaras & Efstathiou, 2013). More than 95% of worldwide hydrogen production derives from the exploitation of fossil fuels, whereas only 4% is produced through water electrolysis. Unfortunately, these industrial processes are the main cause of the global pollution and therefore are not considered environmentally friendly. However, conventional hydrogen generation is based on the methane steam reforming (MSR) reaction (Eqn (15.1)) (because natural gas is mainly composed by methane) and partial oxidation of hydrocarbons:

$$CH_4 + H_2O = CO + 3H_2 \quad \Delta H^{\circ}_{298K} = +206\ \text{kJ/mol} \tag{15.1}$$

This reaction is endothermic and is commonly coupled with the water gas shift (WGS) reaction (Eqn (15.2)):

$$CO + H_2O = CO_2 + H_2 \quad \Delta H^{\circ}_{298K} = -41\ \text{kJ/mol} \tag{15.2}$$

Thus, the overall reaction (Eqn (15.3)) is:

$$CH_4 + 2H_2O = CO_2 + 4H_2 \quad \Delta H^{\circ}_{298K} = +165\ \text{kJ/mol} \tag{15.3}$$

On the contrary, during the partial oxidation reaction, natural gas (or other liquid/gaseous hydrocarbons) and oxygen are injected into a conventional reactor (CR) exercised at high pressure. In particular, the partial oxidation of methane (Eqn (15.4)) is less energy efficient than steam reforming.

$$CH_4 + \frac{1}{2}O_2 \Rightarrow CO + 2H_2 \quad \Delta H^{\circ}_{298K} = -36\ \text{kJ/mol} \tag{15.4}$$

Furthermore, autothermal reforming of natural gas or liquid hydrocarbons is developed by steam and oxygen reacting in a single vessel, where two zones are

individuated: a combustion zone and a reforming zone. The heat resulting from the partial oxidation reaction (exothermic) balances that necessary for the steam reforming reaction (endothermic).

Conventional hydrogen is also produced by coal gasification, which represents a practical option for hydrogen generation in large plants. However, taking into account the high carbon content of coal, CO_2 emissions are much larger than those resulting from other feedstock use.

Therefore, as reported above, conventional processes for producing hydrogen are unfavorable from an environmental point of view because they are responsible for a huge amount of CO_2 production.

15.1.2 Hydrogen production by MSR

As introduced previously, MSR represents a consolidated conventional process for hydrogen generation. Furthermore, when hydrogen needs to be high-grade, a multistep system is used consisting of a CR, WGS reactors (high- and low-temperature reactors), and hydrogen separation/purification devices (Figure 15.1). In the first stage, methane and steam react in the conventional reformer under harsh operating conditions such as 800−1000 °C and 14−20 bar over Ni-based catalysts. Because the CO content is relatively high in the outlet stream of the CR, it needs two stages of WGS reaction, realized in two reactors in series. The first reactor (high-temperature WGS) is packed with chromium-promoted iron oxide catalysts, operating between 350 and 400 °C; the second reactor (low-temperature WGS) is packed with copper-promoted zinc oxide, operating at around 200 °C.

Commonly, the outlet stream from the shift reactors contains 86% H_2, 12% CO_2, 0.4% CO, and 1.6% CH_4 on a dry basis (Kirk-Othmer, 1999). Therefore, further steps are mandatory for obtaining high-grade hydrogen. Further techniques can be adopted for separating/purifying the reformed hydrogen, each of which can be chosen

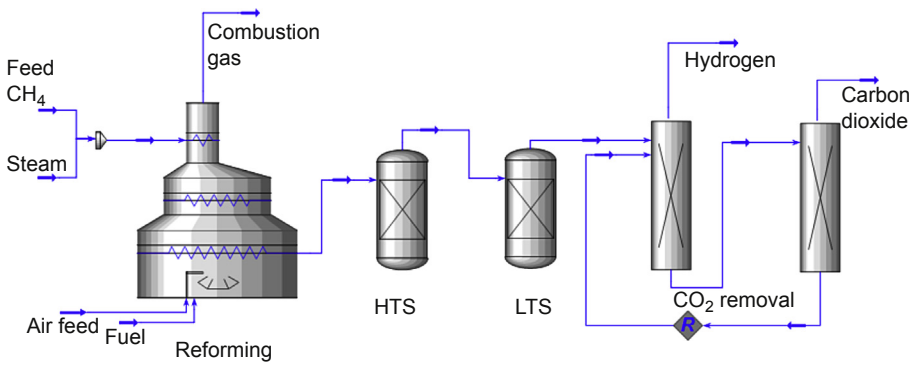

Figure 15.1 Conceptual scheme of a conventional system for high-grade hydrogen generation from methane steam reforming reaction (HTS = high-temperature WGS reactor; LTS = low-temperature WGS reactor).

according to hydrogen purity requirements. In particular, they are the cryogenic separation, pressure swing adsorption (PSA), dense palladium (Pd) membranes, metal hydride separation, reversible reaction of hydrogen with metals to form hydrides, and solid polymer electrolyte cells. Cryogenic distillation does not result in deep hydrogen separation but its advantage is a low operating temperature (Adhikari & Fernando, 2006). Pd membranes are able to achieve high hydrogen purity, even though sulfuric-based compounds and unsaturated hydrocarbon can have poisonous effects on the membrane, with consequent depletion of membrane permeation characteristics. Conventionally, the most commonly used technique for purifying hydrogen is the PSA, owing to the high hydrogen purity reached, although around 20% of hydrogen is lost under operation.

15.1.2.1 Open issues regarding conventional reforming

The MSR reaction needs to overcome various limitations such as thermodynamic equilibrium constraint, mass and heat transfer limitation, and coke formation. In particular, heat transfer is an important and open issue because the MSR reaction is strongly endothermic. Indeed, to achieve an adequate heat transfer rate from the outer zone of catalyst bed to the inner one, the catalyst has to be packed in long narrow tubes composed of expensive superalloys (Rostrup-Nielsen, Sehested, & Norskov, 2002).

Coke formation is another important issue for MSR reaction that is responsible for breakdown of the catalyst and the buildup of carbon deposits. Furthermore, degraded catalyst can make partial or total blockage of reformer tubes possible. Noble metal-based catalysts are less affected by coke influence, but their high cost limits their use, making it advantageous to use active and stable nickel-based catalysts, which are not as expensive. Therefore, in past years, Ni-based catalyst performance has been improved by modifying the type of support, by introducing promoters and additives to make the catalyst more durable.

15.2 Hydrogen generation via membrane reactor technology

To reduce atmospheric pollution and greenhouse gas emissions, proton-exchange membrane fuel cells (PEMFCs) may represent a reliable solution. It is well known that PEMFCs are supplied by high-grade hydrogen producing zero pollution. Proton-exchange membrane fuel cells are commonly operated at $T < 100\ ^{\circ}C$ and are top candidates as an alternative technology to conventional systems. The need to supply them with high-grade hydrogen is due to the low tolerance of the anodic Pt catalysts to CO, which should be lower than 10 ppm (Iulianelli & Basile, 2012). As an alternative solution to conventional systems, membrane reactor (MR) technology represents a valid option for combining the reforming reaction for producing hydrogen and its separation into only one system (Figure 15.2).

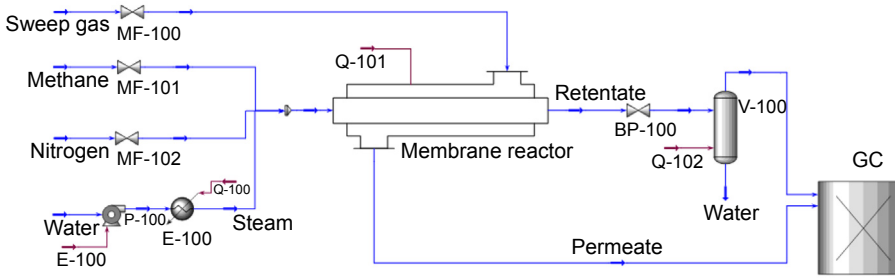

Figure 15.2 Scheme of a membrane reactor for producing hydrogen from MSR on a laboratory scale (from ITM-CNR Laboratories).

Several advantages account for the use of inorganic MRs over CRs:

1. Ability to perform the chemical reaction and hydrogen separation at the same time with a consequent reduction of capital costs owing to the lower number of devices
2. Enhancement of conversion equilibrium limited reactions
3. Higher conversion than CRs (performed under the same MRs conditions), or the same conversion but operating at milder conditions than CRs
4. Potential to directly produce a high-grade hydrogen stream

In past years, considerable scientific interest was related to use of dense Pd-based membranes because of their full hydrogen permselectivity to hydrogen permeation with respect to all other gases (Lu et al., 2007). In the case of Pd membranes exposed to a hydrogen flow at $T > 300\ ^{\circ}C$, embrittlement represents the most important drawback, taking place after a few cycles of $\alpha \leftrightarrows \beta$ transitions of pure Pd (Basile, Campanari, et al., 2011). This phenomenon of phase transition takes place in lattice dilatation instead of changing the lattice structure. If Pd is alloyed with silver, copper, or other metals, Pd−H phases have an improved reticular step and the ability to anticipate reticular expansion from hydrogen.

15.2.1 Pd-based membrane reactors

When a Pd-based membrane is housed inside an MR module (Figure 15.3) and a reaction process is under operation, the well-known shift effect overcomes the thermodynamic equilibrium restrictions of a correspondent CR. As a more general approach, depending on the type of inorganic MRs used for such a process, MR conversion strictly depends on parameter H, defined as the permeation rate to reaction rate ratio (Keizer, Zaspalis, De Lange, & Harold, 1994).

If $H = 0$, permeation does not take place, reporting the behavior of a CR. If the H parameter has relatively low values, a low permeation to reaction rate occurs. In this region, microporous, dense, and mesoporous MRs have the same behavior (Keizer et al., 1994). Membrane reactors with a finite separation factor (defined as the ratio between the permeability of a gas such as hydrogen with respect to that of referenced gas as a blank, such as He or Ar) are able to achieve an optimum in terms of H factor. Overcoming the optimum, reactant loss owing to permeation through the membrane

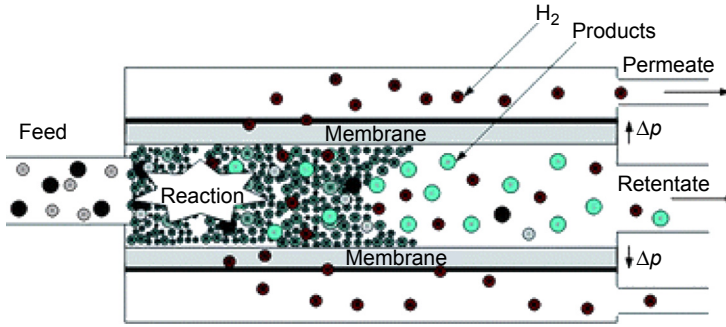

Figure 15.3 Scheme of a Pd-based membrane reactor module.

causes a detrimental effect on conversion. Otherwise, the higher the separation factor is, the higher is the conversion. In the case of MRs with infinite separation factors, this effect does not occur because of the absence of permeation.

In the scientific area of inorganic membranes, dense metallic ones have gained special interest (Adhikari & Fernando, 2006). In particular, dense Pd membranes have been more highly considered in the scientific community although their commercialization is limited owing to low hydrogen permeability and high costs. However, between 0 and 700 °C, various metals such as niobium, vanadium, and tantalum have higher hydrogen permeability than Pd, although they have stronger surface resistance to hydrogen transport than Pd.

Regarding dense Pd-based membranes, hydrogen molecular transport through them takes place via a solution/diffusion mechanism involving six stages: (1) dissociation of molecular hydrogen at the gas−metal interface, (2) adsorption of the atomic hydrogen on the membrane surface, (3) dissolution of atomic hydrogen into the Pd matrix, (4) diffusion of atomic hydrogen through the membrane, (5) recombination of atomic hydrogen to form hydrogen molecules at the gas−metal interface, and (6) desorption of hydrogen molecules.

As a result, the hydrogen flux permeating through the membrane can be expressed as:

$$J_{H_2} = Pe_{H_2}\left(p^n_{H_2,\text{retentate}} - p^n_{H_2,\text{permeate}}\right)/\delta \tag{15.5}$$

where J_{H_2} is the hydrogen flux permeating through the membrane, Pe_{H_2} the hydrogen permeability, δ the membrane thickness, $p_{H_2-\text{retentate}}$ and $p_{H_2-\text{permeate}}$ the hydrogen partial pressures in the retentate (reaction side) and permeate (side in which hydrogen permeating through the membrane is collected) zones, respectively, and n (variable in the range 0.5−1) the dependence factor of hydrogen flux to hydrogen partial pressure. At relatively low pressure and membrane thickness greater than 5 μm, the rate-limiting step of hydrogen permeation through the membrane is assumed to be the diffusion (Iulianelli et al., 2012). In this case, Eqn (15.5) becomes the Sieverts−Fick law (Eqn (15.6)):

$$J_{H_2,\ \text{Sieverts−Fick}} = Pe_{H_2}\cdot\left(p^{0.5}_{H_2,\text{retentate}} - p^{0.5}_{H_2,\text{permeate}}\right)/\delta \tag{15.6}$$

At high pressure, if hydrogen−hydrogen interactions in the Pd bulk are not negligible, n becomes equal to 1 (Eqn (15.7)):

$$J_{H_2} = Pe_{H_2} \cdot \left(p_{H_2,\text{retentate}} - p_{H_2,\text{permeate}}\right)/\delta \tag{15.7}$$

The dependence of hydrogen permeability on temperature can be expressed by an Arrhenius-like equation (Eqn (15.8)):

$$Pe_{H_2} = Pe^{\circ}_{H_2} \exp(-E_a/RT) \tag{15.8}$$

where Pe_0 is the preexponential factor, E_a the apparent activation energy, R the universal gas constant, and T the absolute temperature.

Therefore, when the Sieverts−Fick law is valid, hydrogen flux is expressed as indicated by the Richardson's equation:

$$J_{H_2} = Pe^{\circ}_{H_2}[\exp(-E_a/RT)] \cdot \left(p^{0.5}_{H_2,\text{retentate}} - p^{0.5}_{H_2,\text{permeate}}\right)/\delta \tag{15.9}$$

Although dense Pd-based membranes have great behavior in terms of hydrogen permselectivity, their commercialization has been limited by several factors:

- Embrittlement can take place if Pd-based membranes are exposed to pure hydrogen at temperatures below 300 °C
- Carbon deposition on Pd-based membranes can make a covering effect possible, with consequent depletion of permeation characteristics
- Pd-based membranes are subject to irreversible poisoning by sulfur compounds
- Pd is expensive

15.2.2 Hydrogen generation in MRs: a case study − methane steam reforming

As a renewable and alternative method, methane can be also produced from biogas (Martins das Neves, Converti, & Vessoni Penna, 2009). As reported earlier, MSR is performed in CRs and conversion can achieve 100% only at elevated temperature, even though the catalyst can show deactivation as a result of carbon formation. Regarding MSR in MRs, several articles are present in the scientific literature, most of them focused on Pd-based MRs (Basile, Liguori, & Iulianelli, 2015, Chap. 2).

In particular, Oertel, Schmitz, Weirich, Jendryssek-Neumann, and Schulten (1987) first performed MSR in an MR housing a Pd disk of 100 μm and achieved better conversion than an equivalent CR. Nevertheless, because of low hydrogen permeance through the membrane, this MR needed a high reaction temperature to obtain satisfactory methane conversion. With the intent of improving hydrogen permeance, Uemiya et al. (1991) used an MR housing a thin Pd membrane supported on porous glass, and reached 90% methane conversion at 500 °C (Table 15.1).

Table 15.1 Experimental data taken from open literature concerning MSR reaction in MRs

Membrane Reactor Configuration	Catalyst	Temp. (K)	Pressure (bar)	Feed ratio H_2O/CH_4	Hydrogen recovery (%)	CH_4-conversion (%)	References
Pd−Ag supported onto inconel FBMR	–	873	3.5	3/1	57	–	Roses, Gallucci, Manzolini, and Van Sint Annaland (2013)
Pd-supported onto cermic support PBMR	Ni-based	923	16	3/1	65	70	Dittmar et al. (2013)
Pd supported onto PSS PBMR	Ni/Al_2O_3	773	20.0	3/1	90	86	Lin, Liu, Chuang, and Chu (2003)
Pd supported onto Al_2O_3 PBMR	Ni-La/Mg-Al	823	9.0	3/1	95	99	Chen, Wang, Xu, and Xiong (2008)
Pd-supported onto Al_2O_3 PBMR	Ni-based	853	28	3/1	98	80	Saric, van Delft, Sumbharaju, Meyer, and de Groot (2012)
Dense self-supported Pd−Ag PBMR	Ni/ZrO	723	5.0	2/1	80	65	Basile, Campanari, et al. (2011)
Dense self-supported Pd-Ag PBMR	Ni/Al_2O_3	723	3.0	2/1	70	50	Iulianelli et al. (2010)
Pd supported onto inconel FBMR	–	923	4.0	4/1	–	97	Patil, Annaland, and Kuipers (2007)
Pd-Ag supported onto PSS PBMR	Ni/Al_2O_3	773	1.36	3/1	–	55	–

Pd supported onto PSS PBMR	Ni/Al_2O_3	800	3.0	3/1	–	100	Tong, Matsumura, Suda, and Haraya (2005)
Flat Pd–Ag PBMR	Ru/Al_2O_3	573	1.0	–	–	16.5	Basile et al. (2013)
Pd-based PBMR	Ni/Al_2O_3	773	1.0	3/1	–	100	Kikuchi et al. (2000)
Dense Pd-tube FBMR	–	913	10	2.4/1	43	–	Adris and Grace (1997)
Pd–Ag supported onto PSS PBMR	Cu/ZnO	773	6.0	2.9/1	–	50	Jorgensen, Nielsen, and Lehrmann (1995)
Pd–Ag supported onto inconel PBMR	Ni/Al_2O_3	773	2.0	3/1	–	80	Shu, Grandjean, and Kaliaguine (1994)
Pd supported on Vycor PBMR	–	773	9.1	–	–	90	Uemiya et al. (1991)

Shu et al. (1994) performed MSR in an MR, allocating Pd or Pd−Ag supported on porous stainless-steel membranes. At a higher reaction temperature, steam to carbon ratio, and sweep gas, these researchers observed improvement in methane conversion.

Jorgensen et al. (1995) studied MSR in a Pd−Ag MR, in which the membrane was 100 μm thick. At 500 °C and 6 bar, 51% of methane conversion was reached, increasing at more than 60% by operating at 10 bar. They also predicted possible coke-free working conditions for MSR.

Lin et al. (2003) pointed out benefits resulting from the use of a Pd-based MR, demonstrating that methane conversion can overcome 80% at 500 °C with respect to 850 °C necessary for the correspondent CR.

Tong et al. (2005) used an MR housing a supported Pd membrane. At 550 °C, they reached around 97% of methane conversion and hydrogen recovery higher than 90%.

Also, Chen et al. (2008) confirmed the benefit of using MR to carrying out MSR. In particular, the selective removal of hydrogen from MR to the permeate zone made higher performance possible in terms of methane conversion and hydrogen production than the correspondent CR. In their experiments, they used a thin Pd membrane supported on alumina substrate and reached almost 100% of methane conversion at 550 °C, whereas only 27% was obtained using a CR. Furthermore, 95% pure hydrogen recovery was achieved.

Iulianelli et al. (2010) achieved 50% methane conversion and 70% hydrogen recovery at 450 °C in a dense Pd-based MR. They observed that the low methane conversion is probably the result of the relatively low operating temperature and the low Ni concentration as a metallic phase (0.5 wt%) in the catalyst. Basile, Iulianelli, Longo, Liguori, and De Falco (2011) carried out MSR in an MR system using an Ni/ZrO_2 catalyst and achieved a best result of 80% methane conversion and 65% hydrogen recovery at 450 °C and 5 bar.

Saric et al. (2012) used a thin Pd-layer supported MR for MSR that was packed with an Ni-based catalyst, and achieved almost 100% methane conversion at 28 bar and 580 °C. Furthermore, the authors confirmed the constant performance of the membrane for more than 1000 h under operation.

An analogous study about the long lifetime of a Pd composite membrane was also published by Dittmar et al. (2013) at various temperatures. The researchers pointed out that membrane performance was stable at 650 °C for a long time under operation, which made it possible to achieve 60% methane conversion and 70% hydrogen recovery.

In all of these cases, the macro-MRs were packed-bed type. On the contrary, in the case of macrofluidized MRs, as pioneers from a modeling point of view, Adris and Grace (1997) proposed this kind of reactor configuration, stating that under MSR, 100% methane conversion could be attained using typical industrial operating temperatures. Obviously, various other researchers have been involved in demonstrating the validity of fluidized bed MRs to perform MSR. Only a few authors have experimentally performed MSR reaction with this kind of MR (Patil, Annaland, & Kuipers, 2006; Patil et al., 2007; Roses et al., 2013), probably because of the difficulty in constructing this kind of reactor, and because of membrane sealing and erosion.

15.3 Hydrogen production using membrane microreactors

Membrane microreactors or micromembrane reactors (MMRs) can be defined as microreactors reinforced by membrane separation/purification or membrane reactors miniaturized into characteristic dimensions of 1−1000 μm, which combine the advantages of both MRs and microreactors, leading to a greatly intensified operation unit. The advantages of MMRs include: (1) improvement of mass/heat transfer owing to reduction of the scale length; (2) removal of mass transfer limitations owing to the mitigation of concentration polarization; (3) intensification of process owing to the integration of different steps in a small-scale device; (4) enhancement of surface area to volume ratio owing to extremely high intensification; (5) high reactant conversion or low reaction temperature owing to thermodynamic equilibrium shifting resulting from the removal of specified products from reacted mixture; and (6) high selectivity of the achieved product owing to optimized reactant distribution resulting from the addition of specified reactants in a controllable way (Alfadhel & Kothare, 2005; Gallucci, Fernandez, Corengia, & Van Sint Annaland, 2013; Jensen, 1999; Kim, Kellogg, Livaich, & Wilhite, 2009; Kolb, 2013; Kothare, 2006; Tan & Li, 2013).

Among versatile MMRs, those with a hydrogen separation function are being investigated and have found a number of applications such as hydrogen production from WGS, hydrogen production from methanol steam reforming (MeOHSR), onboard fuel processing for portable PEMFCs, production of moisture-free formaldehyde by the dehydrogenation of methanol, and dehydrogenation of cyclohexane to benzene (Alfadhel & Kothare, 2005; Allen, Irving, & Thomson, 2000; Franz, Schmidt, & Jensen, 1999; Karnik, Hatalis, & Kothare, 2003; Mauer, Claivaz, Fichtner, Schubet, & Renken, 2000; Zheng, Jones, Fang, & Cui, 2000). In this section, hydrogen production in three types of MMRs (planar, hollow-fiber, and monolithic configurations) will be described using some specific examples. After that, the concept of MMRs used as the fuel processor for portable PEMFCs will be briefly discussed.

15.3.1 Hydrogen production in MMRs

15.3.1.1 Planar configuration

Although MMRs are promising devices for hydrogen production, the related research is still limited. Pioneering investigations on MMRs have focused on microchannels in a planar configuration based on microelectromechanical systems (MEMS).

In the work of Karnik et al. (2003), a Pd-based MMR was built on a silicon substrate and integrated with copper catalysts using a standard MEMS microfabrication method. The membrane is composed of four layers: Cu, Al, spin-on-glass (SOG), and Pd. Cu, Al, and SOG layers have a pattern of holes, serving as a structural support for the Pd membrane. A Cu layer also acts as a catalyst for WGS occurring in the channels. Hydrogen gas is separated through the Pd membrane, and thus WGS can be shifted into the direction of the product. Separated hydrogen then flows through corresponding channels. For example, an MMR with 66 nm Cu, 200 nm Al, 500 nm

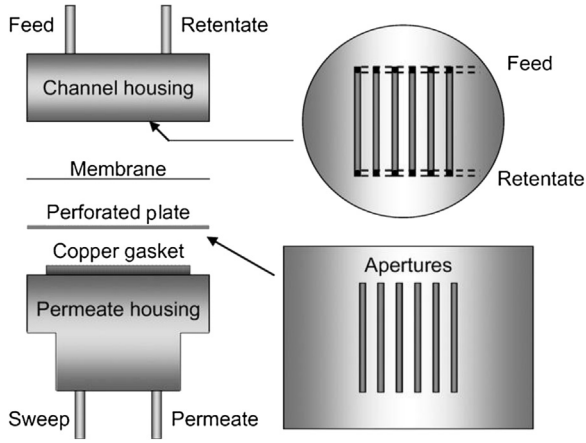

Figure 15.4 Sketch of microchannel MMRs configuration.
Reprinted from Mejdell, A. L., Jøndahl, M., Peters, T. A., Bredesen, R., Venvik, H. J. (2009a). Experimental investigational of microchannel membrane configuration with a 1.4 μm Pd/Ag 23 wt% membrane-effects of flow and pressure. *Journal of Membrane Science*, *327*, 6−10 permitted by Elsevier Ltd.

SOG, and 200 nm Pd was constructed. Hydrogen permeation behavior was tested using a mixture of 20 wt% H_2 and 80 wt% Ar. Hydrogen flux increased with temperature as well as the hydrogen partial pressure gradient across the membrane. Hydrogen flux at 100 °C under a hydrogen partial pressure gradient of 8.3 psi was as high as 5.2 mol/m^2 s. The activation energy for hydrogen permeation was calculated to be 1.0 kJ/mol, which is much smaller than reported values for Pd membranes, and was attributed to the microstructure of the sputtering deposited film.

Mejdell, Jøndahl, Peters, Bredesen, and Venvik (2009a, 2009b) and Mejdell, Peters, Stange, Venvik, and Bredesen (2009c) constructed a microchannel MMR in a planar configuration from thin defect-free Pd-23 wt% Ag membranes and tested hydrogen permeation behavior in detail.

The Pd-23 wt% Ag dense thin films were prepared by DC magnetron sputtering (CVC 601 magnetron sputtering apparatus) on polished silicon single crystal substrates (Si-Mat, Germany) from a Pd-23 wt% Ag target (FHR Anlagenbau GmbH, Germany) using argon as a sputtering gas (Mejdell, Jøndahl, et al., 2009a). After sputtering, Pd-Ag thin films were removed manually from the substrate and integrated into stainless-steel microchannels to produce a planar microchannel MMR. As shown in Figure 15.4, this microchannel MMR consisted of a stainless-steel feed channel plate with six parallel channels with the dimensions 1 × 1 × 13 mm. The Pd-23 wt% Ag membrane was placed between the channel housing and a stainless-steel plate with apertures corresponding to the channel geometry. The stainless-steel plate was employed for mechanical support. In total, the six channels created a 0.78 cm^2 active membrane area. Both the feed housing and the perforated steel plate were highly polished (to 3 μm) before mounting. On the permeate side, open housing was employed and a copper gasket was placed between the perforated steel plate and the permeate housing for sealing.

From measurements of pure hydrogen in a microchannel MMR integrated with 1.4 μm Pd/23 wt% Ag membrane (Mejdell, Jøndahl, et al., 2009a), a permeance of 1.7×10^{-2} mol/m^2 s Pa$^{0.5}$ was obtained. This MMR was tested for ~7 days at 300 °C while differential pressure greater than 470 kPa was applied. The H_2/N_2 separation factor decreased from ~5700 to ~390 at ~300 kPa differential pressure.

Furthermore, the effects of CO and CO_2 on hydrogen permeation behavior through a ~3-μm Pd/23 wt% Ag membrane employed in microchannel MMRs were investigated in detail (Mejdell, Jøndahl, et al., 2009b). Membrane permeance was 5.1×10^{-3} mol/m^2 s Pa$^{0.5}$ at 300 °C under pure hydrogen. After the last experiment, a small amount of leakage occurred that reduced H_2/N_2 separation factor to ~3300 at a pressure gradient of 200 kPa. Both CO and CO_2 showed an inhibitive effect on hydrogen permeation. The CO effect strongly depended on both temperature (275−300 °C) and CO concentration (0−5 mol%). The CO inhibition occurred so rapidly that a sharp drop in the hydrogen permeation flux was found when the CO concentration was between 0 and 0.25 mol%. The time required to restore the initial hydrogen permeation flux after CO exposure became longer when the exposure temperature was lowered. CO desorption was thought to be the main mechanism for hydrogen permeation flux restoration at the higher temperatures, whereas it was controlled by other, slower processes at lower temperatures. The inhibitive effect of CO_2 was milder, and long-time exposure was necessary to reach apparently stable hydrogen permeation values. Only a weak effect was observed at 350 °C, whereas at 300 °C a nearly linear decrease was observed over several days. The main inhibition mechanism was thought to be slow formation and the removal of some strongly adsorbed species rather than CO_2 competitive adsorption.

15.3.1.2 Hollow-fiber configuration

When the diameter of a membrane tube is reduced to a certain level, i.e., inner diameter less than 1000 μm, it becomes a hollow fiber and the fiber lumen may have the effect of a microchannel. Catalysts can be coated on the inner surface of hollow fibers or impregnated in the porous wall, whereas separation can be achieved via the porous hollow fibers themselves or through the membrane formed on the outer surface of the hollow fibers. This kind of hollow-fiber MR can also be attributed to MMRs, called hollow-fiber MMRs (Tan & Li, 2013). Hollow-fiber MMRs were investigated in detail for hydrogen production in Li's group (Garía-García & Li, 2013; García-García, Rahman, & González-Jiménez, 2011; García-García, Rahman, Kingsbury, & Li, 2010; Rahman, García-García, Irfan Hatim, Kingsbury, & Li, 2011; Rahman, García-García, & Li, 2012; Tan & Li, 2013).

A hollow-fiber MMR (Figure 15.5) consisting of a thin Pd membrane and a 30% CuO/CeO_2 catalyst on asymmetric Al_2O_3 hollow fibers was developed (García-García et al., 2010, 2011; Rahman et al., 2011).

The Pd membrane was deposited onto the outer surface of the hollow fiber by electroless plating. The 30% CuO/CeO_2 catalyst was introduced by sol-gel impregnation of the finger pores on the inner surface of the hollow fiber. Catalytic activity of the hollow-fiber MMR was tested using WGS and compared with that of a hollow-fiber

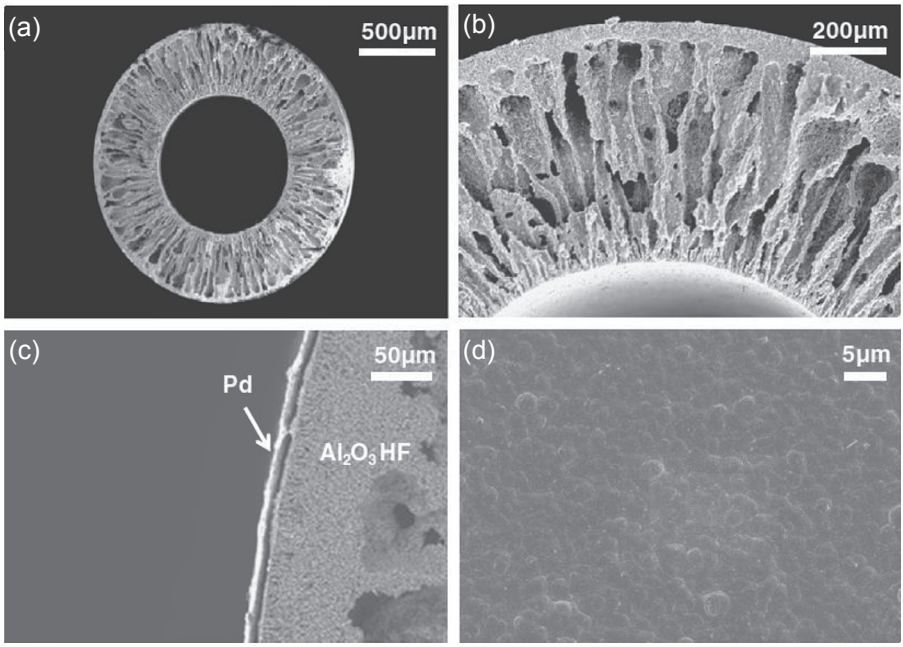

Figure 15.5 Scanning electron microscopy pictures of Al_2O_3 hollow-fiber MMR; (a−b) cross section at different magnifications before Pd deposition, (c) cross-section after Pd deposition, and (d) top of the Pd membrane surface.
Reprinted from García-García, F. R., Rahman, M. A., Kingsbury, B. F. K., Li, K. (2010). A novel catalytic membrane microreactor for Cox free H_2 production. *Catalysis Communications*, *12*, 161−164 permitted by Elsevier Ltd.

microreactor and a conventional fixed-bed reactor. Catalytic activity tests were performed at 1 atm from 200 to 500 °C using different flow rates of sweep gas (from 50 to 75 mL/min). The ratio between CO and H_2O in the feed was 1−0.5 with a space velocity of 80,000 mL/g h. Thermodynamic equilibrium conversions at different temperatures were used as references. In the fixed-bed reaction, the maximum conversion of 23% was obtained at 450 °C, which was much lower than the equilibrium value (∼41%). A small decrease was found when the temperature was increased to 500 °C. In the hollow-fiber microreactor, conversion of 43% was obtained at 500 °C, which was consistent with thermodynamic equilibrium conversion (43%). The highest conversion of 60% was obtained in hollow-fiber MMR at 500 °C and a sweep gas follow of 75 mL/min, which is 17% higher than the value in a hollow-fiber microreactor and the thermodynamic equilibrium value. In addition, high-purity H_2 was produced in the hollow-fiber MMR during WGS. That study showed that H_2 permeability through the Pd membrane increased with temperature and sweep gas flow rate under the operating conditions studied. Hollow-fiber MMR offered exclusive advantages over existing H_2 production systems and could be considered an extremely promising system to produce CO_x-free H_2 via the WGS reaction.

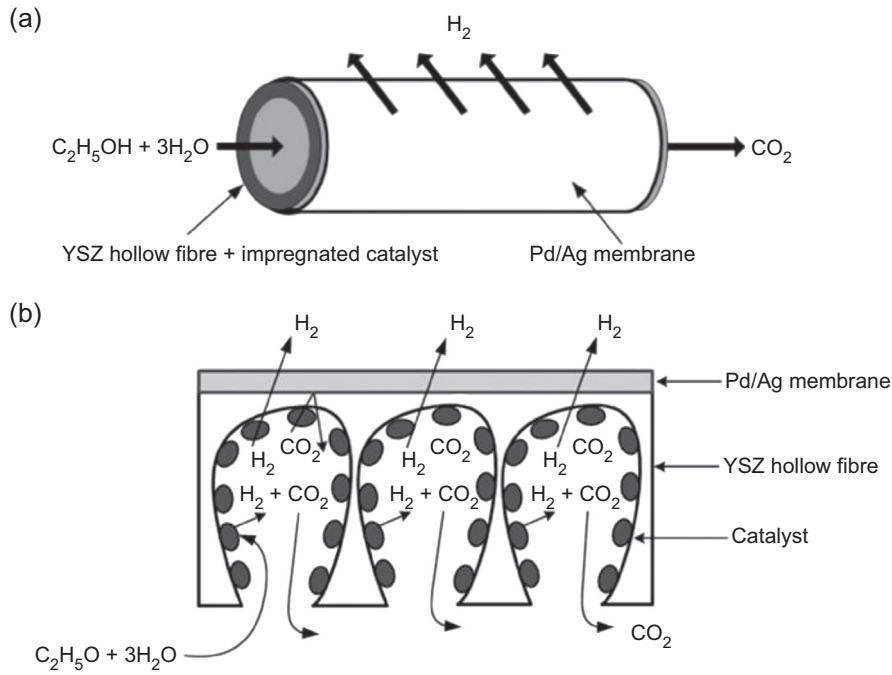

Figure 15.6 (a) Schematic representation of hollow-fiber MMR for high-purity hydrogen production using ESR. (b) The reactants enter the conical microchannels in which the ESR takes place. H_2 is separated using the Pd/Ag membrane whereas CO_2 stays in the lumen. Reprinted from Rahman, M. A., García-García, F. R., Li, K. (2012). Development of a catalytic hollow fiber membrane microreactor as a microreformer for automotive application. *Journal of Membrane Science*, *390–391*, 68–75 permitted by Elsevier Ltd.

Another hollow-fiber MMR (Figure 15.6) was constructed by using an yttria-stabilized zirconia hollow fiber as substrate for the deposition of Pd/Ag membrane on the outer shell of the hollow fiber and for 10 wt% NiO/MgO-CeO_2 catalyst inside the hollow fiber (Rahman et al., 2012).

Ethanol steam reforming (ESR) was carried out in this hollow-fiber MMR at temperatures ranging from 350 to 550 °C. Compared with ESR in a fixed-bed reactor and a hollow-fiber microreactor, performance occurred at the same temperature range. At 510 °C, the flow rate of hydrogen produced in the hollow-fiber MMR was three times higher than that in the fixed-bed reactor and two times higher than that in the hollow-fiber microreactor even though less catalyst was used in the hollow-fiber MMR. Moreover, during operation of the high-fiber MMR, high-purity hydrogen was obtained outside the shell and the yield was more than 53% of total hydrogen produced in the ESR.

15.3.1.3 Monolithic configuration

Honeycomb or straight-channel monoliths can provide an inexpensive and rapid means of constructing scalable two-dimensional arrays of identical square

microchannels with diameters of 500−5000 μm and wall thickness of 200−2000 μm (Kim et al., 2009). This kind of structure can be formed from a variety of porous ceramic materials such as cordierite, mullite, and alumina, which can create large networks of MMRs. Monolithic MMRs can provide much better mechanical stability than hollow-fiber MMRs and much higher intensification than planar microchannel MMRs.

In the research of Kim et al. (2009), dense thin Pd membranes were fabricated within cordierite microchannel networks cut from honeycomb-monolith support and hydrogen permeation behavior was evaluated. Cordierite extruded honeycomb monoliths (64 cpsi) were first wash-coated with a micropowder γ-Al_2O_3 layer to form cylindrical surfaces for subsequent deposition onto Pd films. After that, a nanopowder γ-Al_2O_3 layer was deposited to obtain a uniform surface for deposition of defect-free Pd films. Thin (8 μm) defect-free Pd films with crystallite sizes of ~2 μm were deposited onto a nanopowder γ-Al_2O_3 layer by conventional electroless plating under kinetic limited conditions. Analysis of the resulting two-channel membrane systems for hydrogen separation at 350 °C demonstrated hydrogen fluxes of $1.0-5.5 \times 10^{-3}$ mol/m^2 s and H_2/He separation factors of 40−360. The authors also detailed a novel MMR strategy to employ mini-channel membrane networks as part of a thermally integrated portable reformer for high-purity hydrogen production (Figure 15.7).

15.3.2 MMRs as a fuel processor for portable PEMFCs

The current energy demand for portable electronic devices has encouraged researchers to investigate miniaturized fuel cell systems based on PEMFCs (Ilinich et al., 2008; Karnik et al., 2003; Kawamura, Ogura, Yamamoto, & Igarashi, 2006; Kolb, 2013; Kothare, 2006). However, owing to the low energy density of compressed hydrogen, it is not an ideal option. Liquid fuel, and in particular methanol, has much higher energy density and is easier to transport and handle, which makes it attractive as an onboard fuel for portable PEMPCs. Two types of portable PEMPC systems were proposed: direct methanol fuel cells (DMFCs) have the advantage of room-temperature operation and the disadvantage of relatively low power density owing to methanol crossover and a low reaction rate of methanol oxidation. In contrast, the portable system of an onboard reformer combined with PEMFCs can generate electricity in the fuel cell from concentrated hydrogen produced by steam reforming from methanol, for example, which can achieve high power density. However, it is difficult to miniaturize an onboard reformer because of the complexity of the required structure, which includes not only a fuel reformer but also a hydrogen purifier. Hydrogen-permeable MMRs have begun to be used as onboard reformers for portable PEMPCs.

In the work of Kawamura et al. (2006), a miniaturized methanol reformer was developed to provide hydrogen for a small PEMFC. The microreformer (Figure 15.8(a)) consisted of a catalyst-coated microchannel in a serpentine arrangement, with a length of 333 mm and cross section of 0.6×0.4 mm^2.

The microreformer was fabricated from silicon and glass substrates using a number of microfabrication techniques. Selective deposition of the Cu/ZnO/Al_2O_3 catalyst in the microchannel was achieved by employing photolithography. The overall size of

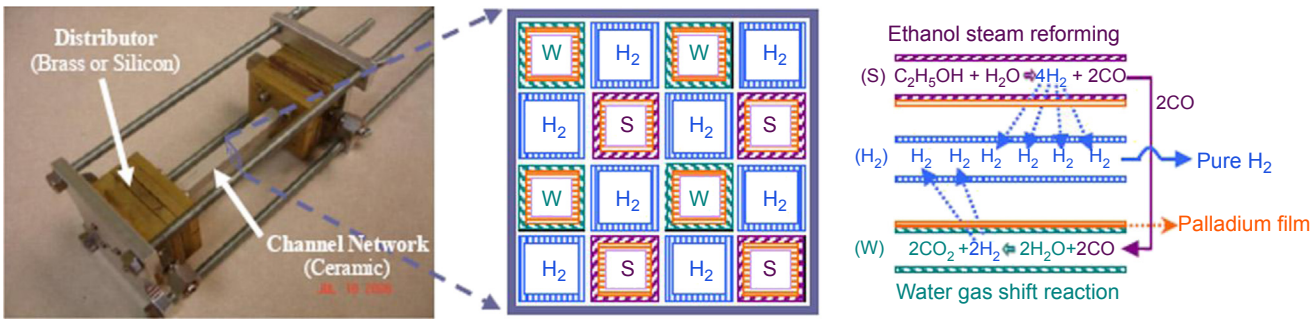

Figure 15.7 Picture of prototype of honeycomb-monolith MMRs, with inset showing schematic of integration schemes.
Reprinted from Kim, D., Kellogg, A., Livaich, E., Wilhite, B. A. (2009). Towards an integrated ceramic micro-membrane network: electroless plated palladium membranes in cordierite supports. *Journal of Membrane Science*, *340*, 109−116 permitted from Elsevier Ltd.

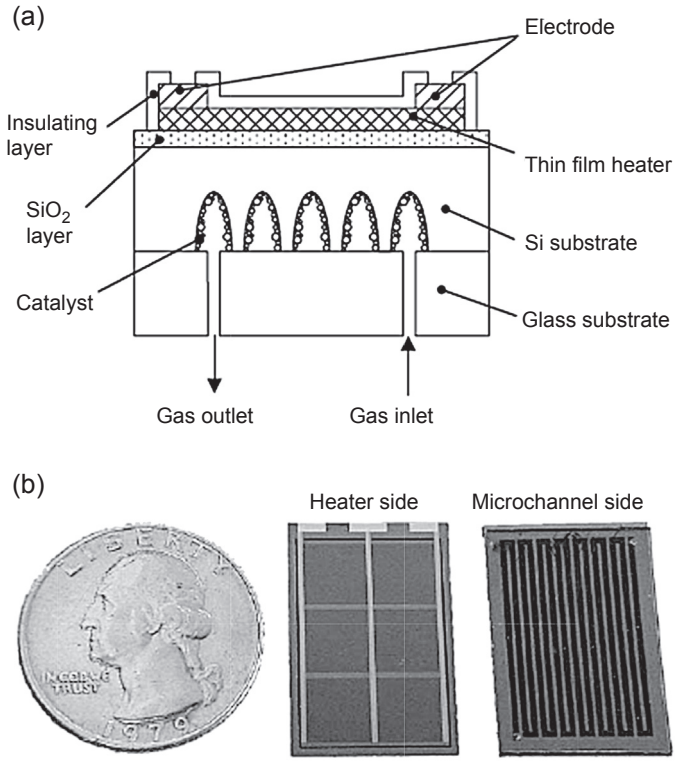

Figure 15.8 Schematic structure (a) and photograph (b) of microreformer.
Reprinted from Kawamura, Y., Ogura, N., Yamamoto, T., Igarashi, A. (2006). A miniaturized methanol reformer with Si-based microreactor for small PEMFC. *Chemical Engineering Science*, *61*, 1092−1101.

the microreformer ($25 \times 17 \times 1.3$ mm^3) (Figure 15.8(b)) makes the small fuel cells suitable for application as a power source for portable electronic devices. Methanol steam reforming was tested in this microreformer, and demonstrated that the microreformer was capable of hydrogen production rates exceeding 0.05 mol/h at reactant feed rate of 1.6 mL/h. Based on the lower hydrogen heating value of 241 kJ/mol, this hydrogen production rate corresponded to 3.3 W_{th} of hydrogen power, in which electrical power greater than 1 W was expected with assumed 45% fuel cell efficiency and 70% hydrogen use, making it potentially applicable as a power source for cell phones.

In the work of Ilinich et al. (2008), a Pd-based catalyst was developed for the ceramic microreformer in a miniaturized PEMFC for the catalytic reaction of MSR. In the microreformer, the catalyst was wash-coated directly onto the walls of the steam reforming section, and provided favorable conditions for efficient heat transfer between the heat-generating catalytic combustion section of the microreformer and its heat-consuming steam reforming section. The Pd-based catalyst showed activity and selectivity similar to those of Cu-Zn-Al catalysts, but was more durable and stable under the duty-cycle conditions of a portable power source.

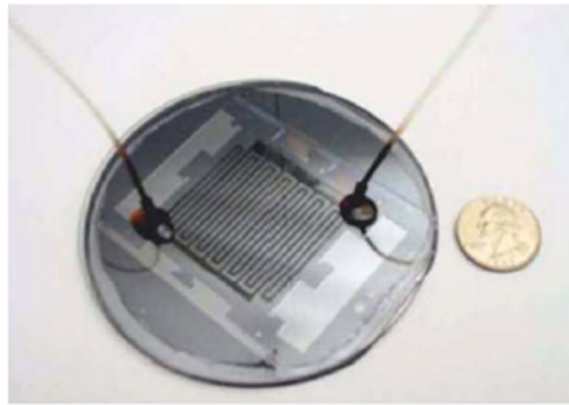

Figure 15.9 View of the final microreformer fabricated by Kothare et al.
Reprinted from Kothare, M. V. (2006). Dynamics and control of integrated microchemical systems with application to micro-scale fuel processing. *Computers & Chemical Engineering*, *30*, 1725−1734.

In the works of Kothare et al. (Kothare, 2006; Pattekar & Kothare, 2003, 2004, 2005), MEMS-based microreformers (Figure 15.9) on silicon chips were fabricated to supply pure hydrogen for small PEMFCs. The microreformers consisted of a network of Cu/ZnO catalyst-packed parallel microchannels 200−400 μm deep with a catalyst particle filter near the outlet. Issues have been addressed related to microchannel and filter capping, on-chip heating and temperature sensing, introduction and trapping of catalyst particles in the microchannels, flow distribution, microfluidic interfacing, and thermal insulation. The catalytic reaction of methanol steam reforming was carried in this microreformer. Experimental runs demonstrated methanol to hydrogen molar conversion over 85% at flow rates enough to supply hydrogen to an 8- to 10-W microfuel cell.

The authors also designed, fabricated, and tested a novel radial high-throughput microreformer (Pattekar & Kothare, 2003, 2004), which led to nearly an order of magnitude reduction in pressure drop with twice the throughput of methanol and conversions approaching 98%. The throughput from this single planar radial microreformer produced enough hydrogen for 20-W small PEMFCs.

The concept of using MMRs as fuel processors or fuel reformers for portable PEMFCs was proposed in the work of Karnik et al. (2003). Their MMR-based fuel processor included four components: (1) a mixer/vaporizer of methanol and water; (2) a catalytic steam reformer with an appropriate catalyst in which gaseous methanol and steam react at an elevated temperature to produce carbon dioxide, carbon monoxide, and hydrogen; (3) an WGS reactor consisting of a perforated copper catalyst, which in the presence of steam converts carbon monoxide into hydrogen and carbon dioxide, and a Pd-based membrane for hydrogen separation; and (4) integrated resistive heaters/sensors and control electronics. In their MMR reformer, high-purity hydrogen was produced directly and supplied hydrogen to PEMFCs without concerns of poisonous Pt catalysts because of carbon monoxide. Furthermore, hydrogen

removal can promote the conversion of carbon monoxide in the shift reaction and the total area required for the entire microreactor can be greatly decreased.

15.4 Conclusions

Membrane microreactors or MMRs are promising area from both scientific and technological points of view. Planar microchannel MMRs based on MEMS, hollow-fiber MMRs, and monolithic MMRs are three important configurations that have been integrated into Pd-based membranes. Hydrogen permeation behavior and hydrogen production reactions such as WGS and MSR were carried out. Monolithic configuration MMRs are thought to be more promising than the other two configurations. The application of MMRs as onboard liquid fuel reformers for miniaturized PEMFCs for portable electronic devices is the most promising compared with other applications. However, fabrication of MMRs and integration with miniaturized PEMFCs still has serious challenges.

Nomenclature

E_a	Apparent activation energy
H	Permeation rate
J_{H_2}	Hydrogen flux permeating through membrane
n	Dependence factor of hydrogen flux to hydrogen partial pressure
Pe_0	Preexponential factor
Pe_{H_2}	Hydrogen permeability
$p_{H_2\text{-permeate}}$	Hydrogen partial pressures in permeate side
$p_{H_2\text{-retentate}}$	Hydrogen partial pressures in retentate side
R	Universal gas constant
T	Absolute temperature
δ	Membrane thickness

List of acronyms

CR	Conventional reactor
DMFCs	Direct methanol fuel cells
ESR	Ethanol steam reforming
FBMR	Fluidized-bed membrane reactor
HTS	High-temperature shift (reactor for WGS carried out at high temperature)
ID	Internal diameter
LTS	Low temperature shift (reactor for WGS carried out at low temperature)
MEMS	Microelectromechanical systems
MeOHSR	Methanol steam reforming
MMRs	Membrane microreactors or micromembrane reactors
MR	Membrane reactor
MSR	Methane steam reforming

PBMR	Packed-bed membrane reactor
PEMFCs	Proton exchange membrane fuel cells
PSA	Pressure swing adsorption
SOG	Spin-on-glass
WGS	Water gas shift
YSZ	Yttria-stabilized zirconia

References

Adhikari, S., & Fernando, S. (2006). Hydrogen membrane separation techniques. *Industrial and Engineering Chemistry Research, 45*, 875−881.

Adris, A. M., & Grace, J. R. (1997). Characteristics of fluidized-bed membrane reactors: scale-up and practical issues. *Industrial and Engineering Chemistry Research, 36*, 4549−4556.

Alfadhel, K., & Kothare, M. V. (2005). Modeling of multicomponent concentration profiles in membrane microreactors. *Industrial and Engineering Chemistry Research, 44*, 9794−9804.

Allen, W. L., Irving, P. M., & Thomson, W. J. (2000). Microreactor systems for hydrogen generation and oxidative coupling of methane. In *IMRET 4: 4th international conference on microreaction technology, AIChE Spring National Meeting, Atlanta, GA, March 5−9, 2000* (pp. 351−357).

Bartholomew, C. H., & Farrauto, R. J. (2006). *Fundamentals of industrial catalytic processes*. Hoboken, New Jersey, USA: John Willey and Sons.

Basile, A., Campanari, S., Manzolini, G., Iulianelli, A., Longo, T., Liguori, S., et al. (2011). Methane steam reforming in a Pd−Ag membrane reformer: an experimental study on the reaction pressure influence at middle temperature. *International Journal of Hydrogen Energy, 36*, 1531−1539.

Basile, A., Iulianelli, A., & Liguori, S. (2013). Process intensification in the chemical and petrochemical industry. In V. Piemonte, M. De Falco, & A. Basile (Eds.), *Sustainable development in chemical engineering* (pp. 119−151). Chichester, West Sussex: Wiley, ISBN: 978-1-11995-352-4.

Basile, A., Iulianelli, A., Longo, T., Liguori, S., & De Falco, M. (2011). Pd-based selective membrane state-of-the-art. In L. Marrelli, M. De Falco, & G. Iaquaniello (Eds.), *Membrane reactors for hydrogen production processes* (pp. 21−55). Springer London Dordrecht Heidelberg New York, ISBN: 978-0-85729-150-9. http://dx.doi.org/10.1007/978-0-85729-151-6.

Basile, A., Liguori, S., & Iulianelli, A. (2015). Membrane reactors for steam reforming of methane. In A. Basile, F. Hai, L. Di Paola, & V. Piemonte (Eds.), *Membrane reactors for energy applications and basic chemical production*. Woodhead.

Campbell, C. J. (1997). The coming oil crisis. *Oil and Gas Journal, 95*, 33−37.

Chen, Y., Wang, Y., Xu, H., & Xiong, G. (2008). Efficient production of hydrogen from natural gas steam reforming in palladium membrane reactor. *Applied Catalysis B: Environmental, 80*, 283−294.

Dittmar, B., Behrens, A., Schodel, N., Ruttinger, M., Franco, Th., Straczewski, G., et al. (2013). Methane steam reforming operation and thermal stability of new porous metal supported tubular palladium composite membranes. *International Journal of Hydrogen Energy, 38*, 8759−8771.

Franz, A. J., Schmidt, M. A., & Jensen, K. F. (April 18−21, 1999). Palladium membrane micro-reactors. In *The 3rd international conference on microreaction technology*. DECHEMA.

Gallucci, F., Fernandez, E., Corengia, P., & Van Sint Annaland, M. (2013). Recent advances on membranes and membrane reactors for hydrogen. *Chemical Engineering Science, 92*, 40−66.

García-García, F. R., & Li, K. (2013). New catalytic reactors prepared from symmetric and asymmetric ceramic hollow fibers. *Applied Catalysis A: General, 456*, 1−10.

García-García, F. R., Rahman, M. A., González-Jiménez, I. D., & Li, K. (2011). Catalytic hollow fiber membrane microreactor: high purity H_2 production by WGS reaction. *Catalysis Today, 171*, 281−289.

García-García, F. R., Rahman, M. A., Kingsbury, B. F. K., & Li, K. (2010). A novel catalytic membrane microreactor for Cox free H_2 production. *Catalysis Communications, 12*, 161−164.

Goltsov, V., & Veziroğlu, N. (2001). From hydrogen economy to hydrogen civilization. *International Journal of Hydrogen Energy, 26*, 909−915.

Ilinich, O., Liu, Y., Castellano, C., Koermer, G., Moini, A., & Farrauto, R. (2008). A new palladium-based catalyst for methanol steam reforming in a miniature fuel cell power source. *Platinum Metals Review, 52*(3), 134−143.

Iulianelli, A., & Basile, A. (2012). Sulfonated PEEK-based polymers in PEMFC and DMFC applications: a review. *International Journal of Hydrogen Energy, 37*, 15241−15255.

Iulianelli, A., Liguori, S., Longo, T., & Basile, A. (2012). Inorganic membrane and membrane reactor technologies for hydrogen production. In Damon Robert Honery, & Patrick Moriarty (Eds.), *Series: Energy science, engineering and technology Hydrogen production: Prospects and processes* (pp. 377−398). Victoria, Australia: Nova Science Publishers, ISBN: 978-1-62100-246-8.

Iulianelli, A., Manzolini, G., De Falco, M., Campanari, S., Longo, T., Liguori, S., et al. (2010). H_2 production by low pressure methane steam reforming in a Pd−Ag membrane reactor over a Ni-based catalyst: experimental and modeling. *International Journal of Hydrogen Energy, 35*, 11514−11524.

Jensen, K. F. (1999). Microchemical systems: status, challenges and opportunities. *AIChE, 45*(10), 2051−2054.

Jorgensen, S., Nielsen, P. E. H., & Lehrmann, P. (1995). Steam reforming of methane in membrane reactor. *Catalysis Today, 25*, 303−307.

Kalamaras, C. M., & Efstathiou, A. M. (2013). *Hydrogen production technologies: Current state and future developments*. http://dx.doi.org/10.1155/2013/690627.

Karnik, S. V., Hatalis, M. K., & Kothare, M. V. (2003). Towards a palladium micro-membrane for the water gas shift reaction: microfabrication approach and hydrogen purification results. *Journal of Microelectromechanical System, 12*(1), 93−100.

Kawamura, Y., Ogura, N., Yamamoto, T., & Igarashi, A. (2006). A miniaturized methanol reformer with Si-based microreactor for small PEMFC. *Chemical Engineering Science, 61*, 1092−1101.

Keizer, K., Zaspalis, V. T., De Lange, R. S. A., & Harold, M. P. (1994). In J. G. Crespo, & K. W. Boddeker (Eds.), *Membrane processes in separation and purification* (pp. 415−429). Dordrecht, Netherlands (HB): Kluwer Academic Publishers, ISBN: 0-7923-2929-5.

Kikuchi, E., Nemoto, Y., Kajiwara, M., Uemiya, S., & Kojima, T. (2000). Steam reforming of methane in membrane reactors: comparison of electroless-plating and CVD membranes and catalyst packing modes, *Catalysis Today, 56*, 75−81.

Kim, D., Kellogg, A., Livaich, E., & Wilhite, B. A. (2009). Towards an integrated ceramic micro-membrane network: electroless plated palladium membranes in cordierite supports. *Journal of Membrane Science, 340*, 109−116.

Kirk-Othmer. (March 1999). *Concise encyclopedia of chemical technology* (Vol. 12). New York: Wiley. p. 950.

Kolb, G. (2013). Review: microstructured reactors for distributed and renewable production of fuels and electrical energy. *Chemical Engineering and Processing: Process Intensification, 65*, 1−44.

Kothare, M. V. (2006). Dynamics and control of integrated microchemical systems with application to micro-scale fuel processing. *Computers and Chemical Engineering, 30*, 1725−1734.

Laherrere, J. H. (1999). World oil supply—what goes up must come down—but when will it peak? *Oil and Gas Journal, 97*, 57−64.

Lin, Y. M., Liu, S. L., Chuang, C. H., & Chu, Y. T. (2003). Effect of incipient removal of hydrogen through palladium membrane on the conversion of methane steam reforming. Experimental and modeling. *Catalysis Today, 82*, 127−139.

Lu, G. Q., Diniz da, Costa J. C., Dukec, M., Giessler, S., Socolow, R., Williams, R. H., et al. (2007). Inorganic membranes for hydrogen production and purification: a critical review and perspective. *Journal of Colloid and Interface Science, 314*, 589−603.

Martins das Neves, L. C., Converti, A., & Vessoni Penna, T. C. (2009). Biogas production: new trends for alternative energy sources in rural and urban zones. *Chemical Engineering and Technology, 32*, 1147−1153.

Mauer, R., Claivaz, C., Fichtner, M., Schubet, K., & Renken, R. (2000). A microstructured reactor system for the methanol dehydrogenation to water free formaldehyde. In *IMRET 4: 4th international conference on microreaction technology, AIChE Spring National Meeting, Atlanta, GA, March 5−9, 2000* (pp. 100−105).

Mejdell, A. L., Jøndahl, M., Peters, T. A., Bredesen, R., & Venvik, H. J. (2009a). Experimental investigational of microchannel membrane configuration with a 1.4 μm Pd/Ag 23 wt% membrane-effects of flow and pressure. *Journal of Membrane Science, 327*, 6−10.

Mejdell, A. L., Jøndahl, M., Peters, T. A., Bredesen, R., & Venvik, H. J. (2009b). Effects of CO and CO_2 on hydrogen permeation through a ∼3 μm Pd/Ag 23 wt% membrane employed in a microchannel membrane configuration. *Separation and Purification Technology, 68*, 178−184.

Mejdell, A. L., Peters, T. A., Stange, M., Venvik, H. J., & Bredesen, R. (2009c). Performance and application of thin Pd-alloy hydrogen separation membranes in different configurations. *Journal of the Taiwan Institute of Chemical Engineers, 40*, 253−259.

Ni, M., Leung, M. K. H., Sumathy, K., & Leung, D. Y. C. (2006). Potential of Renewable hydrogen production for energy supply in Hong Kong. *International Journal of Hydrogen Energy, 31*, 1401−1412.

Oertel, M., Schmitz, J., Weirich, W., Jendryssek-Neumann, D., & Schulten, R. (1987). Steam reforming of natural gas with integrated hydrogen separation for hydrogen production. *Chemical Engineering and Technology, 10*, 248−255.

Patil, C. S., Annaland, M. V. S., & Kuipers, J. A. M. (2007). Fluidized bed membrane reactor for ultrapure hydrogen production via methane steam reforming: experimental demonstration and model validation. *Chemical Engineering Science, 62*, 2989−3007.

Patil, C. S., Annaland, M. Van Sint, & Kuipers, J. A. M. (2006). Experimental study of a membrane assisted fluidized bed reactor for H_2 production by steam reforming of CH_4. *Chemical Engineering Research and Design, 84*, 399−404.

Pattekar, A. V., & Kothare, M. V. (2003). Fuel processing microreactors for hydrogen production in micro fuel cell applications. In *7th international conference on microreaction technology (IMRET 7)*.

Pattekar, A. V., & Kothare, M. V. (2004). A microreactor for hydrogen production in micro-fuel cell applications. *Journal of Microelectromechanical System, 13*, 7−18.

Pattekar, A. V., & Kothare, M. V. (2005). A radial microfluidic fuel processor. *Journal of Power Sources, 147*, 116−127.

Rahman, M. A., García-García, F. R., Irfan Hatim, M. D., Kingsbury, B. F. K., & Li, K. (2011). Development of a catalytic hollow fiber membrane microreactor for high purity H_2 production. *Journal of Membrane Science, 368*, 116−123.

Rahman, M. A., García-García, F. R., & Li, K. (2012). Development of a catalytic hollow fiber membrane microreactor as a microreformer for automotive application. *Journal of Membrane Science, 390−391*, 68−75.

Roses, L., Gallucci, F., Manzolini, G., & Van Sint Annaland, M. (2013). Experimental study of steam methane reforming in a Pd-based fluidized bed membrane reactor. *Chemical Engineering Journal, 222*, 307−320.

Rostrup-Nielsen, J. R., Sehested, J., & Norskov, J. K. (2002). Hydrogen and synthesis gas by steam and CO_2 reforming. *Advances in Catalysis, 47*, 65−139.

Saric, M., van Delft, Y. C., Sumbharaju, R., Meyer, D. F., & de Groot, A. (2012). Steam reforming of methane in a bench-scale membrane reactor at realistic working conditions. *Catalysis Today, 193*, 74−80.

Shu, J., Grandjean, B. P. A., & Kaliaguine, S. (1994). Methane steam reforming in asymmetric Pd- and Pd-Ag/porous SS membrane reactors. *Applied Catalysis A: General, 119*, 305−325.

Tan, X. Y., & Li, K. (2013). Membrane microreactors for catalytic reactions. *Journal of Chemical Technology and Biotechnology, 88*, 1771−1779.

Tong, J., Matsumura, Y., Suda, H., & Haraya, K. (2005). Experimental study of steam reforming of methane in a thin (6 mm) Pd-based membrane reactor. *Industrial and Engineering Chemistry Research, 44*, 1454−1465.

Uemiya, S., Sato, N., Ando, H., Kude, Y., Matsuda, T., & Kikuchi, E. (1991). Separation of hydrogen through palladium thin film supported on a porous glass tube. *Journal of Membrane Science, 56*, 303−313.

Zheng, A., Jones, F., Fang, J., & Cui, T. (2000). Dehydrogenation of cyclohexane to benzene in a membrane microreactor. In *IMRET 4: 4th international conference on microreaction technology, AIChE Spring National Meeting, Atlanta, GA, March 5−9, 2000* (pp. 284−292).

Chemical and calcium looping reforming for hydrogen production and carbon dioxide capture

16

E.J. Anthony
Cranfield University, Cranfield, UK

16.1 Introduction

The production of hydrogen on an industrial scale has long been established using steam methane reforming; as such, it is extremely difficult for new technology to displace current established technology options. However, there is a desire to manufacture hydrogen in even larger quantities so that it might be used in a cost-effective manner in what is often called the hydrogen economy (Scott, 2008). There is also a drive in certain practical situations where the demand for hydrogen risks adversely affecting available reserves of natural gas, as for example, with the Canadian oil sands development, to be able to produce hydrogen from a wide range of existing feedstocks. However, possibly the most important reason for considering and developing new technology is concern regarding climate change/global warming and carbon dioxide (CO_2) emissions (IPCC, 2014).

In connection with this, two technologies appear to have significant potential to serve as game changers in this area: are calcium (Ca) looping, which can remove CO_2 from any gaseous environment, and chemical looping combustion (CLC), which can achieve inherent oxygen separation and bring oxygen to the environment in the form of a solid oxide. Both of these technologies also offer the potential to be deployed in strategies involving carbon capture and storage (CCS) or possibly use, which may be a key factor in encouraging their development for this application. This chapter gives an overview of Ca looping and CLC and their technology basics, and then discusses important variants and fuels, before finishing with a discussion of pilot plant demonstrations and issues for these technologies.

16.2 Historical development

16.2.1 Calcium looping

Most developments in this technology with Ca looping are no more than 10−15 years old (Blamey, Anthony, Wang, & Fennell, 2010). However, the idea of using lime to

Compendium of Hydrogen Energy. http://dx.doi.org/10.1016/B978-1-78242-361-4.00016-9

remove CO_2 and produce industrial hydrogen is not new. In 1868, Tessié du Motay and Maréchal wrote a short article on the subject of preparing industrial hydrogen. In it, they noted that lime heated to cherry red could be reacted with pyrolysis products from coal to yield calcium carbonate and hydrogen. Subsequently, the goal of producing either hydrogen or high calorific value gas was first explored in what was known as the CO_2 acceptor process (Curran, Fink, & Goran, 1967, Chapter 10). In 1976, this work culminated in the first large pilot plant demonstration of the Ca looping approach, which was carried out in Rapid City, South Dakota, using a high-pressure (1-MPa) dual fluidized-bed gasifier operating at up 10 t/h of coal (McCoy, Curran, & Sudbury, 1976). In this system coal was gasified in the presence of steam and heat for the gasification reaction was provided by a hot stream of lime (1000 °C), which also served as a CO_2 sorbent. This was a genuine looping approach, because the spent sorbent was then recycled back to a separate vessel, an air-fired regenerator, and the char from the gasifier was used to supply heat for the calcination step. However, because the main goal of this project was to produce synthetic natural gas, it went no further when economic conditions changed, which made this approach commercially unattractive.

In 1995, Silaban and Harrison (Silaban & Harrison, 1995) proposed the use of lime in a cyclic process for high-temperature CO_2 removal with the goal of storage and sequestration, and carried out a series of tests in a high-pressure electrobalance reactor system at pressures ranging from atmospheric to 1.5 MPa, to determine optimum performance conditions for such a cycle. Subsequently, a full CO_2 capture scheme was proposed by Shimizu et al. (1999), who carried out a concept study on an atmospheric pressure dual fluidized-bed reactor that could be used to remove CO_2 from flue gases, as a carbon capture and sequestration (CCS) technology.

Subsequently, most research focused on use of the technology for CCS (Blamey et al., 2010), and that work culminated in the production of several demonstration plants, the largest of which currently is a 1.7-MWth demonstration unit in Spain (Arias, Diego, Abanades, Lorenzo, & Diaz, 2013), In addition, a 1-MWth CLC reactor has been designed and demonstrated in Germany (Orth, Strohle, & Epple, 2012). The same unit can operate as a 1-MWth Ca looping rig (Stőhle, Junk, Kremer, Galloy, & Epple, 2014). There was also a 3-MWth demonstration of CLC technology supported by the United States (US) Department of Energy (DOE) (USDOE, 2013a).

16.2.2 Chemical looping combustion technology

Chemical looping combustion was first suggested by Lewis, Gilliland, and Reed (1949). In their initial work, the researchers carried out experimental investigation of the use of CuO to oxidize methane to CO and H_2, with a small fluidized-bed reactor operating at a temperature of 925 °C. Their intention was to avoid using oxygen and the high net heating requirements necessary in the reforming process. Subsequently, they proposed an approach to produce pure CO_2 from hydrocarbons (Lewis & Gilliland, 1954). Later, that idea was represented by Richter and Knoche (1983), who focused on the potential of this technology to offer "controlled combustion." This technology was then largely ignored again until it was explored by Japanese

scientists, most notably Ishida and Jin (1994a,b). Small pilot plant units were then built at Chalmers University (Lyngfelt, Leckner, & Mattisson, 2001) and research on the technology was taken up globally.

16.2.3 Technology basics and sorbent issues

Both technologies work by using a solid sorbent or carrier to transfer O_2 in the case of CLC, and CO_2 in the case of Ca looping from one chemical environment to another, or in the case of a batch reactor to accept either O_2 or CO_2 under one set of conditions (pressure and/or temperature) and release it under another.

The dominant reactions for Ca looping can be represented globally as follows:

Carbonation (16.1) is a reversible reaction

$$\mathrm{CaO(S) + CO_2(g) = CaCO_3(s)} \quad \Delta H^{\circ}_{298} = -178\ \mathrm{kJ/mol} \tag{16.1}$$

for which equilibrium is described by Eqn. (16.2) (Baker, 1962):

$$\log_{10} P_{\mathrm{CO_2}}[\mathrm{atm}] = 7.079 - \frac{8308}{T[\mathrm{K}]} \tag{16.2}$$

When used to capture CO_2 from flue gases it can be regarded as a hot post-combustion capture technology, similar to amine scrubbing (Figure 16.1). The primary difference is that, because the capture process must occur at elevated temperatures (>600 °C), and the regeneration step to release the CO_2 will likely occur at temperatures above 900 °C in the absence of high levels of steam, the entire cycle can be used as part of a steam cycle, thus reducing efficiency losses for the capture process by several percentage points. Because it depends on an equilibrium reaction, such a process cannot completely remove CO_2, and probably CO_2 removal of 90% is a reasonable goal for a cost-effective process for carbon capture and storage. For reforming processes there are no clear guidelines as to what is required, given that there is a much larger choice of temperature and pressure conditions than would be typical of back-end scrubbing.

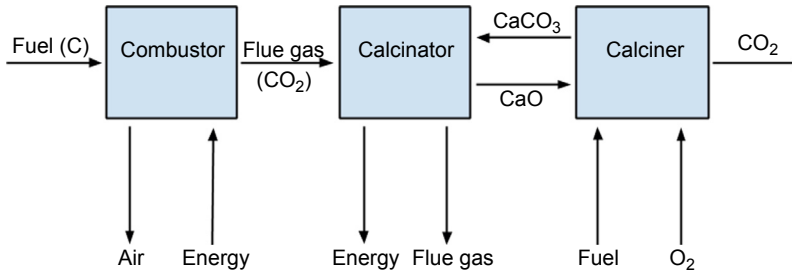

Figure 16.1 Schematic representation of CaO-based CO_2 looping cycles.

Whereas it is normal to assume that a Ca looping cycle is carried out in two vessels – a carbonator that removes CO_2 and a regenerator or calciner that produces a pure stream of CO_2 suitable for compression and subsequent sequestration along with the CaO-based sorbent to be returned to the carbonator – this arrangement is not necessarily the only possible one. Thus, in principle it might be possible to have a fixed arrangement, for instance, whereby flue gases were introduced for a carbonation cycle, and then a hot stream of gas (consisting of CO_2, and/or low quality steam) subsequently reintroduced for sorbent regeneration; the use of fixed beds is also extremely common in reforming applications. However, to date the vast bulk of the literature in this area has been devoted to the twin-bed approach, using fluidized-bed technology composed of a carbonator, and a calciner consisting of a small oxy-fired circulating bed (perhaps 40% of a full-scale oxy-fired plant, because its only duty is to provide heat for the calcination reaction); this approach will be discussed below. Here we will mainly focus on work in which CO_2 removal is done at atmospheric pressure, although high-pressure applications are not only possible but desirable.

For CLC, Figure 16.2 provides a typical schematic for such processes and the basic reactions are for gasification (16.3) and reforming (16.4):

$$(2n + m)M_yO_x + CnH_{2m} = (2n + m)M_yO_{x-1} + mH_2O + nCO_2 \quad (16.3)$$

$$nM_yO_x + C_nH_{2m} = nM_yO_{x-1} + mH_2 + nCO \quad (16.4)$$

Here a metal oxide (typically Ni, Cu, Fe, Mn or possibly Co) is reduced by a hydrocarbon to produce CO_2 and H_2O for a combustion reaction, or CO and H_2 for a gasification reaction, and the reduced metal oxide is then regenerated by reaction with air, in this way achieving inherent air separation. For combustion, H_2O can be removed by

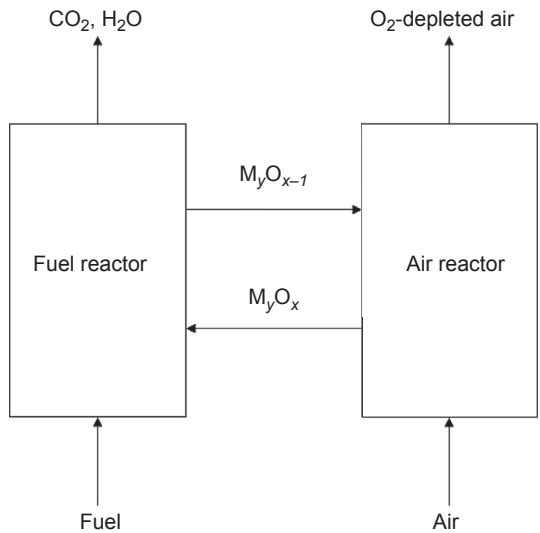

Figure 16.2 Typical schematic for a CLC system.

condensation resulting in a pure stream of CO_2. There is the possibility of using $CaSO_4$ as the oxidizing agent, and endeavouring to cycle between $CaSO_4$/CaS. This option, although attractive from the point of view of the extremely high oxygen-carrying capacity of $CaSO_4$, will not be considered further here, because of stability issues associated with the $CaSO_4$/CaS, which can also produce SO_2 and decay. However, this assessment is provisional, because there was a major USDOE project endeavouring to demonstrate CLC with this system, for which we await more detailed analysis (USDOE, 2013a).

For pure reforming processes involving CH_4 for instance, the water gas reaction can be employed allowing for reactions of the type:

$$C + H_2O = CO + 2H_2O \quad \Delta H^{\circ}_{298} = -131\ \text{kJ/mol} \tag{16.5}$$

$$CH_4 + H_2O = CO + 3H_2 \quad \Delta H^{\circ}_{298} = 206\ \text{kJ/mol} \tag{16.6}$$

$$CO + H_2O = CO_2 + H_2 \quad \Delta H^{\circ}_{298} = -41\ \text{kJ/mol} \tag{16.7}$$

followed, in the case of Ca looping, by removal of CO_2 by reaction (16.1), in what is known as sorbent enhanced reforming. Because reaction (16.6) is strongly endothermic, the exothermic carbonation step (Eqn. (16.8)) can supply the heat requirement for reforming:

$$CH_4 + 2H_2O + CaO = 4H_2 + CaCO_3 \quad \Delta H^{\circ}_{298} = -13\ \text{kJ/mol} \tag{16.8}$$

Finally, for the sake of completeness, a schematic is provided for a possible system combining the two technologies (Figure 16.3).

Both technologies have essential limits associated with them. First, any technology operating with particulate solids is likely to be limited by temperature, because of

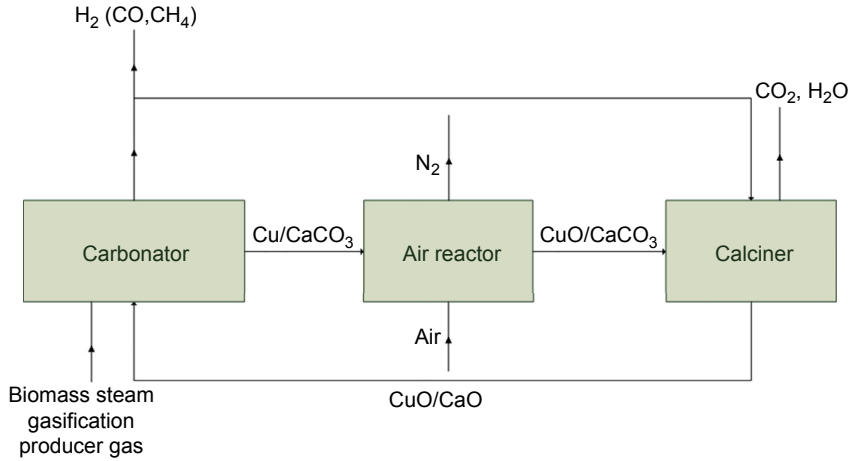

Figure 16.3 Combined CLC and Ca looping reactor.

either the melting point of the solids, or, if using a solid fuel, ash fusion issues, so that practically a limit of around 1200 °C applies to both CLC and Ca looping technologies, with a more typical range being 800−1000 °C for the regeneration step in the case of Ca looping and both the combustion and regeneration steps for CLC. Such temperatures ensure that the essential reactions occur at a sufficient rate to be compatible with a fluidized-bed system, and that sintering is minimized. Although both systems can be run at pressure, as noted above, the vast majority of the work done to date is at atmospheric pressure.

The second limit is the essential property of these materials. In the case of Ca looping the CO_2 carrying capacity of the CaO is exceptionally high (780 mg of CO_2/g of CaO). Because the reactivity decays massively to levels of 10−20% by 20 or 30 cycles (Blamey et al., 2010), carrying capacity of these materials is understandably a major issue.

In the case of CLC, the oxygen carrying capacity of all of the metals is relatively low, and because an inert carrier must be used to stabilize the material, the active oxygen carrying capacity is even lower. Any given oxide system will have a carrying capacity that can be defined as:

$$\mathrm{Rox} = (m_{\mathrm{ox}} - m_{\mathrm{red}})/m_{\mathrm{ox}} \tag{16.9}$$

where m_{ox} is the mass of the fully oxidized sample and m_{red} is the mass of the reduced sample. The value Rox for the common systems (Fe_2O_3/Fe_3O_4, Ni/NiO and Cu/CuO) is 0.03, 0.22 and 0.24, respectively, and the oxidation reactions are of the type shown below:

$$3Fe_2O_3 + CO/H_2 = 2Fe_3O_4 + CO_2/H_2O \tag{16.10}$$

$$CuO + CO/H_2 = Cu + CO_2/H_2O \tag{16.11}$$

$$NiO + CO/H_2 = Ni + CO_2/H_2O \tag{16.12}$$

Other systems exist, of course, such as the Mn_3O_4/MnO and CoO/Co systems:

$$Mn_3O_4 + CO/H_2 = 3MnO + CO_2/H_2O \tag{16.13}$$

$$CoO + CO/H_2 = Co + CO_2/H_2O \tag{16.14}$$

These have also received limited investigation (Johansson, Mattisson, & Lyngfelt, 2006a,b). There has also been some success in preparing oxygen carriers with mixed oxide systems, which together show better overall performance. For example, the addition of small amounts of Ni was shown to improve the performance of various oxygen carriers, and it is suggested that this arises because NiO catalyzes methane conversion by methane pyrolysis and steam reforming (Johansson et al., 2006a).

In practice, it is more usual and useful to consider the carrying capacity of the particles themselves, because they contain an inert substrate to support the active

component and the oxygen carrying capacity figures will be lower, depending on the formulation of the particle itself. Also, in some instances the carrier itself will form a compound with the support material which is itself inert, an example of which is Al_2O_3 with Ni, which forms a Ni spinel ($NiAl_2O_4$); in itself it is not active as an oxygen carrier and consumes some of the Ni that would otherwise be available for reaction (Gayán et al., 2009). Thus, for instance, Abad et al. (2007) gave figures for three oxygen carriers based on Fe, Ni and Cu, showing that actual carrying capacities are 0.013, 0.084 and 0.02.

Finally, any system must be cost-competitive with conventional technology. This means that exotic and expensive materials (such as rare earth metals, for example) must be able to last a large number of cycles, and must be in sufficient supply to make it feasible to use them on a large industrial scale, without causing significant price concerns (Abanades, Rubin, & Anthony, 2007). In addition, the formulation method to make these sorbents, if natural materials are not used, must also be cost-effective and capable of scale-up to industrial levels.

16.2.4 Chemical looping with oxygen uncoupling

The idea that certain oxides that can be used in CLC can also release oxygen was originally recognized by Lewis and Gilliland (1954). More specifically, the two potential candidates currently being considered are the Cu and Mn systems (although such a process is also possible with Co). The release of gaseous oxygen is important for gasification of solid fuels, because in principle they must first be gasified by H_2O or CO_2 before reaction with the oxygen carrier can take place, and this is an inherently slow step. Arguably, the most promising of these is CuO, which can release O_2 in the reaction (Eqn (16.15)), although the ability of Mn to perform in the presence of other metals such as iron makes it a potentially important candidate (Imtiaz, Hooseini, & Müller, 2013) and the area of doping less reactive systems such as the iron one to improve performance is receiving increasing attention, especially where coal combustion is considered (Fan & Siriwardane, 2014):

$$2CuO = Cu_2O + {}^1\!/_2\, O_2 \tag{16.15}$$

Unfortunately, the CuO/CuO system is close to its melting point at the most favourable temperatures for this process (>900 °C). Nonetheless, significant work is ongoing on this subject, offering as it does a potential to permit the use of solid fuels, and coal for CLC technology.

16.2.5 Pressurized Ca looping and pressurized CLC

Pressurized applications have been considered for Ca looping because of the possibility of using pressure swing instead of temperature swing to drive the calcination process. Moreover, when considering steam methane reforming it is relevant for this to be carried out typically around 16 bar, even though this is unfavourable in terms of the equilibrium yield of hydrogen (e.g. reactions 5, 6 and 8). Another argument in favour

of pressure swing applications is that as pressure increases, pressure vessels can become increasingly smaller with a potential decrease in costs. Another important argument is that pressure swing cycling could potentially eliminate the need for cooling the sorbent before carbonation, thus reducing the heating requirements for the calciner and potentially reducing the requirement for O_2 for oxy-fuel combustion in the calciner.

The use of pressure swing calcination/carbonation for Ca looping was first studied at the University of British Columbia for several hundred cycles in a thermogravimetric analyzer (TGA) (Butler, Lim, & Grace, 2011). Their experiments were carried out at 1000 °C, with carbonation performed at 6, 11 or 21 bar, followed by calcination at atmospheric pressure. In a situation somewhat analogous to the temperature swing situation, sorbent reactivity reached near asymptotic values ranging from about 12% to 28% after 250 cycles, but their work showed that pressure swing nonetheless led to better overall calcium use over several hundred cycles. Their work showed that sintering was greater for carbonation at 21 bar than 11 bar, suggesting that there is an optimized carbonation pressure. In a subsequent study (Butler, Lim, & Grace, 2014), on high-pressure carbonation of Strassburg limestone over 100 or more cycles with pressures varying from 2 to 20 bar and temperatures ranging from 975 °C to 1025 °C, results showed that increased residual sorbent use was achieved over 100 cycles. Researchers at Southeast University, China also examined pressurized Ca looping cycles (Chen & Zhao, 2011; Chen, Zhao, Chen, Li, & Chen, 2011) and found that they were able to achieve the best performance, in a pressurized cycle at 700 °C and 0.5 MPa carbonation over 10 cycles, of 88%. This work strongly suggests there may be an optimum carbonation pressure, but it needs to be extended over more cycles.

Finally, there is a £5.8 million project funded by the United Kingdom Department of Climate Change to demonstrate a 3-MWe high-pressure Ca looping pilot plant (10–40 bar for the carbonator) to produce hydrogen from natural gas. The purpose of this unit is to provide the basis for scale-up to 50 MWt units for industrial applications, or for multiple units to decarbonize natural gas combined cycle or integrated gasification combined cycle power stations. However, although the project dates were from September 2012 to April 2014 (UKCCS, 2014), there does not currently appear to be a major report available evaluating its performance.

Pressurized CLC has also been considered for a number of applications (Adanez, Abad, Garcia-Labiano, Gayan, & de Diego, 2012). However, a number of challenges are associated with this system. First for pressurized gas systems, it will be necessary to circulate higher amounts of oxygen carriers; second, higher values are probably necessary for Rx values (Abad et al., 2007). An early study by these same scientists using a pressurized TGA carried out with pressures up to 3 MPa using H_2/N_2 and $CO_2/CO_2/N_2$ mixtures showed that increasing total pressures reduces the reaction rate of the oxygen carriers examined, and it was suggested that increasing the pressure might affect the internal structure of the oxygen carrier (Garcia-Labiano, Adánez, de Diego, Gayán, & Abad, 2006). Siriwardane et al. (2007) looked at the behaviour of a nickel oxide (60 wt%) oxygen carrier supported on bentonite, using a high-pressure flow reactor operating from 101 to 690 kPa, and showed a more complicated picture for this system, with improved reaction at the highest pressure. These workers also examined a

copper oxide carrier using bentonite as a support on a tapered-element oscillating microbalance, at pressures up to 690 kPa, and concluded that reaction pressures have a negative effect on reaction rates (Tian et al., 2008), in agreement with the work of Garcia-Labiano et al. (2006).

Pressurized CLC systems seem to offer promise in power generation cycles; to that end Xiao, Song, Song, et al. (2010) and Xiao, Song, Zhang, et al. (2010) examined the performance of Chinese bituminous coal in a small fixed-bed reactor at pressures up to 0.6 MPa, with an iron ore-based oxygen carrier using a laboratory-scale fixed-bed reactor. In that work the cycle responsible for providing oxygen was assumed to be Fe_2O_3/Fe_3O_4. The primary focus of those studies was to determine what effect pressure had on performance rather than reactor design or scale-up, and therefore, issues such as the amount of carrier required per megawatt were not examined. In the initial study by Xiao, Song, Song, et al. (2010), they looked at three to five reaction cycles and found that increasing the pressure up to about 0.5 MPa enhanced the reduction of the oxygen carrier, but that a higher pressure (0.6 MPa, which was the highest pressure examined in this work) resulted in slightly lower conversions being obtained. In a subsequent study, experiments were carried out for up to 20 cycles (Xiao, Song, Zhang, et al., 2010). Interesting results from that study included no evidence of agglomeration or the formation of large grains; a high stable average of CO_2 production (96%); and no evidence of deterioration of the oxygen carrier. Zhang et al. studied the effect of pressure in both the fixed and fluidized modes in pressurized CLC of coal and found that increased pressure up to about 0.5 MPa improved performance but thereafter did not, which they attribute to the suppression of coal pyrolysis (Zhang, Xiao, & Zheng, 2014). At the time of this writing it would appear that the use of pressure in CLC is much less advanced than it is in atmospheric pressure studies.

16.3 Past developments and future directions

The production of H_2 is important for many reasons, some of which are longer-term, such as introducing the H_2 economy, possibly with the use of fuel cells and encompassing the transportation industry (McGlashan, 2010; Scott, 2008) rather than just stationary power sources or industrial processes as are the bulk of examples considered in this chapter. However, H_2 itself is an important chemical produced in large amounts (on the order of 50 Mt/a (USDOE, 2013b)) and is of profound interest to some national economies, such as in Canada for oil sands upgrading, where current needs are around 1 Mt/a but have been predicted to rise to 7.7 Mt/a by 2030 (Larsen et al., 2004; National Energy Board, 2014). Thus, cheap methods of producing H_2 are desired, especially if some source other than natural gas can be used. Currently around 96% of H_2 production is attributed to natural gas (48%), and oil and coal (48%) (USDOE, 2013b), which puts pressure on natural gas reserves in Canada.

The idea of using H_2 from CLC was considered early on in a scheme to simply make a syngas containing CO and H_2 directly (reaction (16.4), i.e. an autothermal scheme), in the first published article on chemical looping using the copper system (Lewis et al., 1949). Later, it was studied by Jin and Ishida (2001), and subsequently

received considerably more international attention (Chiesa, Lozza, Malandrino, Romano, & Piccolo, 2008; Go, Son, Kim, Kang, & Park, 2009; Xiang, Chen, Xue, & Sun, 2010; Zafar, Mattisson, & Gevert, 2005). For example, Zafar et al. looked at the possibility of integrated hydrogen and power production for the CuO, Mn_2O_3, NiO and Fe_2O_3 systems with SiO_2 as a support (Zafar et al., 2005). For their experimental work they used a small quartz fluidized-bed reactor and looked at system performance in a fuel-rich situation. The concept they proposed was that methane is first converted into CO_2 and H_2 and then is shifted in a separate reactor. In particular, the authors were interested in the potential performance of their oxygen carriers, which they ranked in the order of decreasing reactivity as:

$$NiO/SiO_2 > CuO/SiO_2 > Mn_2O_3/SiO_2 > Fe_2O_3/SiO_2.$$

An interesting study performed by Chiesa et al. (2008) envisaged the use of three reactors using the iron system, and natural gas. There, in the fuel reactor hematite (Fe_2O_3) is oxidized primarily to wustite (FeO, which should more properly be written as $Fe_{(1-y)}O$, where $0.05 < y < 0.17$ (Bohn et al., 2008)) by oxidizing the natural gas; in the steam reactor most of the reduced FeO reacts with steam to form magnetite (Fe_3O_4); and finally, in the third reactor, the Fe_3O_4 is reoxidized to Fe_2O_3. An interesting aspect of such a scheme is that, unlike most chemical looping schemes, it involves the metal in more than two oxidation states, and the result of the simulation performed suggested that it was economically preferable simply to produce H_2, rather than H_2 and electricity. This study suggested that the economics of such a scheme were comparable with other approaches, but that the environmental performance (100% CO_2 capture) was better given that the best alternative would achieve only 80% CO_2 capture.

A similar scheme, again with an iron-based carrier in three reactors, was explored by Xiang et al. (2010) using coal as the fuel source, for the simultaneous production of hydrogen and electricity, using an ASPEN plus simulation. For the system considered by the authors, they noted that the costs of such were high but the environmental benefits were significant. One limitation they saw in a scheme producing both H_2 and electricity is that it is not possible to greatly vary the ratio of hydrogen production to electricity because this depends on the circulation rates for the oxygen carrier and hence the heat balance for three reactors. The iron system with H_2 production from coal syngas, using an ASPEN simulation based on bench-scale results, was also explored by Fan, Li, and Ramkumar (2008), again with a positive evaluation.

This scheme was also explored experimentally, but using mixtures of CO plus CO_2 and N_2 as the fuel source, using a small packed-bed reactor (diameter of 103 mm) by workers at the University of Cambridge (Bohn et al., 2008), whose work supported the general feasibility of such a scheme for producing very pure H_2. In 2009, these researchers carried out simulations of the same scheme, looking at steam pressures of 1 and 10 bar, and showed that it was possible to achieve the necessary heat integration for such a scheme (Cleeton, Bohn, Dennis, & Scott, 2009).

This scheme was also explored experimentally using a lignitic coal and its chars (Yang, Cai, & Li, 2008) and a small fluidized-bed reactor using batches of haematite or Fe_2O_3. It demonstrated successful reduction of the haematite with potassium

carbonate-promoted chars; production of H_2 via the reaction of water with the FeO; Fe produced by reaction with char; and final oxidation of the resulting magnetite (Fe_3O_4) to haematite (Fe_2O_3) by reaction with air. Damen, van Troost, Faaij, and Turkenburg (2006) also made a detailed study of various schemes for electricity and hydrogen production with CO_2 capture, and suggested that CLC was promising and that net electric efficiencies might reach between 50% and 55% for CO_2 capture of between 85% and 100% for CLC systems.

Korean scientists have also explored the iron system using a bench-scale (300 Wth) reactor with 20% Fe_2O_3/ZrO_2 as the oxygen carrier and reported CH_4 conversions of 94%, and the production of nearly pure H_2 (99.95%) (Cho et al., 2014). Rydén and Armand (2012) also examined the Fe system in a bench-scale circulating fluidized reactor and carried out 12 h of operation with 9 h of H_2 production using CO and syngas; the researchers reported no defluidization or attrition, nor particular problems with the operation, over the period of the experiments. Providing such systems can be made to function at a large scale, it appears that studies such as the one on Fe analyzed by Zhang, Li, Hong, and Jin (2014), who claimed that it would be possible to obtain an overall net efficiency of 59.8% with CO_2 separation when the turbine inlet temperature was 1300 °C, are supportive of future developments of this system.

16.3.1 The use of coal and fuel issues

Despite the large-scale availability of natural gas, especially in countries such as the US (owing to hydraulic fracturing), coal conversion with CLC remains a major objective of many research groups, especially in Asia but also in Europe. Initial studies focused on using syngas, which must first be produced in a gasifier. However, coal direct chemical looping remains a major goal, and initial simulations, such as the one made by Gnanapragasam, Reddy, and Rosen (2009), suggested that it should have a higher H_2 to CO_2 ratio than systems using a first gasification step to produce syngas. The possibility of combining such an operation with a solid oxide fuel cell has also been examined, and one study estimated that such a system could achieve 43.53% efficiency with no CO_2 emissions (Chen, Xue, Wang, & Xiang, 2012). An inherent problem of such an approach, of course, is that it demands significant development in fuel cell technology in addition to the development of a large-scale CLC system.

Cormos, Cormos, and Petrescu (2014) performed research in the hydrogen and power cogeneration area and carried out further study of direct coal chemical looping (Cormos & Cormos, 2014). Without the fuel cell option, net electrical efficiencies ranged from 35% to 41% but with the benefit of high inherent CO_2 capture from such a system (>99%). In their work they considered the Fe-based system and concluded that efficiencies of 41−42% are possible for the direct coal-based CLC option. There are similar studies on biomass and CLC, such as a study by Gopaul, Dutta, and Clemmer (2014), but these will not receive further attention here because aside from small-scale applications it seems unlikely that biomass will be used in the near future with CLC technology, other than in the co-fired mode, in which case the challenges of using coal are the principal ones.

16.3.2 Combining Ca looping and CLC

Lyon and Cole (2000) proposed unmixed combustion to be used for steam reforming, in which the heat for the process was supplied by hot solids from the air reactor. They specifically considered the CuO/Cu and Fe_2O_3/Fe_3O_4 system, which they referred to as catalysts. The idea was then extended by Abanades et al. (2010), using the CuO/Cu system for sorbent enhanced combustion (reaction (16.8)). The copper system, which is exothermic in both oxidation and reduction reactions with methane, is used to supply the heat for lime calcination, and in this case a fixed bed was proposed for H_2 production. Martínez et al. (2014) produced a detailed design for such a process.

$$2Cu_{(s)} + O_{2(g)} = 2CuO_{(s)} \qquad \Delta H_r^\circ = -156 \text{ kJ/mol} \quad (16.15)$$

$$4CuO_{(s)} + CH_{4(g)} = 4Cu_{(s)} + CO_{2(g)} + 2H_2O_{(g)} \qquad \Delta H_r^\circ = -178 \text{ kJ/mol} \quad (16.16)$$

Subsequently, Manovic and others (Manovic & Anthony, 2011a,b and Manovic, Wu, He, & Anthony, 2011) prepared composite pellets of Cu oxygen carriers, lime (together with Ca alumina silicates as a binder) and Ni to demonstrate that such an approach might be feasible in a fluidized-bed system. They also explored the effect of an Ni catalyst in the production of H_2, and confirmed that this was a technically feasible process (Manovic & Anthony, 2011a). All of this work confirms that high-purity H_2 ($\geq$99%) can be produced from combined pellets. This work was further supported by joint work at ETH, Switzerland (Broda et al., 2013; Broda, Manovic, Anthony, & Mueller, 2014). Similar conclusions were reached by Rydén and Ramos (2012) using a small (22-mm-diameter) fluidized-bed reactor with Ni as the reforming catalyst. Similar combined sorbents/carriers were also prepared by Qin, Yin, Liu, An, and Feng (2012).

16.4 Scale-up issues and technology option

To date, both CLC and Ca looping are in the 1.7- to 3-MWth size range. Plans to develop the technology further have run into a lack of financial support. Large boiler companies such as Foster Wheeler and others are still developing concepts, but in the absence of substantial government or industrial support, further development can be expected to be slow. Hydrogen production, per se, is not a major objective for funding internationally, although this may change if projects such as the 3-MWth project supported by the USDOE and now completed are considered to be successful (USDOE, 2013a,c). In a 2012 review on progress in CLC and reforming technologies, Adanéz and colleagues (Adanéz et al., 2012) noted the potential of the technology in a wide range of areas, and pointed out that operation of a 1-MWth unit with coal is under way, which is presumably the University of Darmstadt plant (Orth et al., 2012); however, the researchers offered no other examples of larger-scale plants. This situation has not substantially changed at the time of writing although there is a conceptual study being carried out for USDOE by Babcock and Wilcox in collaboration with Ohio State University and Clear Skies Consulting

to develop an advanced, iron-based, 550-MWe plant (USDOE, 2013c). The situation with Ca looping technology is basically the same, and there a front-end engineering and design study is also under way at the University of Darmstadt for a 10-MWth plant (Epple, 2014).

For other than reactive fuels such as lignites or biomass (Saucedo, Lim, Dennis, & Scott, 2014), combustion efficiency with coal will remain an issue for the technology. Current solutions appear to be the use of burn-up cells or carbon strippers (Markstőm, Linderholm, & Lyngfelt, 2013), although if CO_2 emissions are not an issue, the unreacted char materials could be eliminated in the air reactor. There are also some issues with ash and sulphur interactions with oxygen carriers, but apart from the Ni/NiO system, these do not appear to represent a major problem for use of coal in CLC applications (Adanéz et al., 2012; Keller, Arjmand, Leion, & Mattisson, 2014).

16.5 Limits to sorbent developments

To date, a significant amount of sorbent development work has been focused on complicated and potentially expensive routes for producing oxygen carriers (sometimes involving the use of rare earths such as lanthanum, cerium and yttrium (Cao, Sit, & Pan, 2014; Chen, Galinsky, Wang, & Li, 2014)) or enhanced Ca looping materials. For steam reforming with natural gas and the use of fixed-bed technology, such approaches may be justifiable. What is less clear is whether such approaches could be justified with direct gasification of coal using CLC.

The use of spray-drying technology to produce oxygen carriers in bulk represents a promising method of avoiding the expense of multi-step procedures (Linderholm, Mattisson, & Lyngfelt, 2009). The use of natural ores also offers a considerable advantage in terms of cost and is currently being explored (Mendiara et al., 2014). Calcium looping has many of the same problems, although the drop in reactivity of such sorbents remains the largest weakness of the technology (Blamey et al., 2010). For coal, at least, it is probably difficult to justify modifying lime-based sorbents in hydrogen manufacture from coal. Also, given the milder conditions that are likely to be achieved in steam methane reforming, if CO_2 capture is not an issue, it seems sensible to use unmodified natural lime-based sorbents; however, such questions need further examination in pilot plant trials (Connell et al., 2013).

16.6 Sources of further information

There are many sources of information in the literature on CLC and Ca looping. The major review by (Adanéz et al. (2012)) provides an in-depth analysis of CLC technology worldwide. There are also many sources of information in the literature ranging from Elsevier journals such as *Fuel* and the *International Journal of Hydrogen Energy*

to American Chemical Society journals such as *Environment Science and Technology* and *Energy and Fuels*. Another valuable resource is the book on chemical looping by L. S. Fan (Fan, 2010). For Ca looping and CLC, a new book on the subject will also provide an up-to-date analysis of the technology (Fennell & Anthony, 2014), especially Ca looping, for which there is less material available. However, there are hundreds of articles produced yearly on the two technologies in a large number of journals, as indicated by the bibliography provided here.

In terms of organizations involved in the two technologies, there are easily hundreds, including Chalmers University, Sweden; the Spanish National Research Council (INCAR-CSIC and ICB-CSIC); IFK, Germany; Ohio State University, US; and CanmetENERGY, Canada (among others, Canada has had a pivotal role so far). In terms of conferences, two major ones at this point are the Chemical Looping Conferences and the High-Temperature Solid Looping Cycles Network series, organized by the International Energy Agency, both of which are easily found through a basic Internet search.

16.7 Conclusions

Both CLC and Ca looping have reached the stage of 1- to 3-MWth demonstration plants. Throughout the world there are also a substantial number of small pilot plants (typically of the 100-kW size). Active research is being carried out on improving sorbents and oxygen carriers, and the experimental and simulation studies that have been done leave no doubt that both technologies can be used in reforming and H_2 production schemes. For CLC, one of the major areas of challenge remains the development of technology for coal-based applications and, in particular, achieving high conversion efficiencies. For Ca looping, the possibility of using it in enhanced reforming is being explored in numerous laboratories worldwide. What are missing at this time are larger-scale demonstrations of the technology. With the advent of lower natural gas prices over the past few years, it does not seem that commercial considerations will drive these projects, so they must depend on other drivers such as concern about CO_2 emissions. There is also a considerable focus on sorbent and oxygen carrier development, but to date it seems clear that in the right economic environment, sorbent and oxygen carrier properties would not represent a major limiting step to hydrogen production from these technologies.

Nomenclature

m_{ox}	Mass of fully oxidized sample
m_{red}	Mass of reduced sample.
P	Pressure
Rox	Oxygen carrying capacity
T	Temperature

List of acronyms

Ca looping	Calcium looping
CLC	Chemical looping combustion
CLOU	Chemical looping with oxygen uncoupling
FBC	Fluidized-bed combustion
IFK	Institute of Combustion and Power Plant Technology
IGCC	Integrated gasification combined cycle
INCAR-CSIC	Instituto Nacional del Carbón Consejo Superior de Investigaciones Cientificas
ICB	CSIC Instituto de Carboquímica−Consejo Superior de Investigaciones Cientificas
PFBC	Pressurized fluidized-bed combustion
TGA	Thermogravimetric analyzer

References

Abad, A., Adánez, J., García-Labiano, F., de Diego, L. F., Gayán, P., & Celaya, J. (2007). Mapping of the range of operational conditions for Cu-, Fe-, and Ni-based oxygen carriers in chemical-looping combustion. *Chemical Engineering Science, 62*, 533−549.

Abanades, J. C., Murillo, R., Fernandez, J. R., Grasa, G., & Martinez, I. (2010). New CO_2 capture process for hydrogen production combining Ca and Cu chemical loops. *Environmental Science & Technology, 44*, 6901−6904.

Abanades, J. C., Rubin, E. S., & Anthony, E. J. (2007). Sorbent cost and performance in CO_2 capture systems. *Industrial and Engineering Chemistry Research, 43*, 3462−3466.

Adanéz, J., Abad, A., Garcia-Labiano, F., Gayan, P., & de Diego, L. (2012). Progress in chemical-looping combustion and reforming technology. *Progress in Energy and Combustion Science, 38*, 215−282.

Arias, B., Diego, M. E., Abanades, J. C., Lorenzo, M., & Diaz, L. (2013). In J. Martínez, & A. A. Sánchez-Biezma (Eds.), Demonstration of steady state CO_2 capture in a 1.7 MW_{th} calcium looping pilot. *International Journal of Greenhouse Gas Control, 18*, 237−245.

Baker, E. H. (1962). The calcium oxide-carbon dioxide system in the pressure range 1−300 atmospheres. *Journal of the Chemical Society, 70*, 464−470.

Blamey, J., Anthony, E. J., Wang, J., & Fennell, P. S. (2010). The calcium looping cycle for large-scale CO_2 capture. *Progress in Energy and Combustion Science, 36*, 260−279.

Bohn, C. D., Mueller, C. R., Cleeton, J. P., Hayhurst, A. N., Davidson, J. F., Scott, S. A., et al. (2008). Production of very pure hydrogen with simultaneous capture of carbon dioxide using the redox reactions of iron oxide in packed beds. *Industrial and Engineering Chemistry Research, 47*, 7623−7630.

Broda, M., Manovic, V., Anthony, E. J., & Mueller, C. (2014). The effect of pelletization and the addition of steam on the cyclic performance of carbon templated, CaO-based CO_2 sorbents. *Environmental Science & Technology, 48*, 5322−5328.

Broda, M., Manovic, V., Imtiaz, Q., Kierzkowska, A. M., Anthony, E. J., & Mueller, C. R. (2013). High-purity hydrogen via the sorption enhanced steam methane reforming reaction over a synthetic CaO-based sorbent and a Ni-catalyst. *Environmental Science & Technology, 47*, 6007−6014.

Butler, J. W., Lim, C. J., & Grace, J. R. (2011). CO_2 capture capacity of CaO in a long series of pressure swing sorption cycles. *Chemical Engineering Research Design, 89*, 1794−1804.

Butler, J. W., Lim, J., & Grace, J. R. (2014). Kinetics of CO_2 absorption by CaO through pressure swing cycling. *Fuel, 127*, 78−87.

Cao, Y., Sit, S. P., & Pan, W.-P. (2014). Preparation and characterization of lanthanum-promoted copper based oxygen carriers for chemical looping combustion processes. *Aerosol and Air Quality Research, 14*, 572−584.

Chen, Y., Galinsky, N., Wang, Z., & Li, F. (2014). Investigation of Perovskite supported composite oxides for chemical looping of syngas. *Fuel, 134*, 521−530.

Chen, S., Xue, Z., Wang, D., & Xiang, W. (2012). An integrated system combining chemical looping hydrogen generation process and solid oxide fuel cell/gas turbine cycle for power production with CO_2 capture. *Journal of Power Sources, 215*, 89−98.

Chen, H., & Zhao, G. (2011). Development of a CaO-based sorbent with improved cyclic stability for CO_2 capture in a pressurized carbonation. *Chemical Engineering Journal, 171*, 197−205.

Chen, H., Zhao, C., Chen, M., Li, Y., & Chen, X. (2011). CO_2 uptake of modified calcium-based sorbents in a pressurized carbonation-calcination looping. *Fuel Processing Technology, 92*, 1144−1151.

Chiesa, P., Lozza, G., Malandrino, A., Romano, M., & Piccolo, V. (2008). Three-reactor chemical looping process for hydrogen production. *International Journal of Hydrogen Energy, 33*, 2233−2245.

Cho, W. C., Lee, D. Y., Seo, M. W., Kim, S. D., Kang, K., Bae, K. K., et al. (2014). Continuous operation characteristics of chemical looping hydrogen production system. *Applied Energy, 113*, 1667−1674.

Cleeton, J. P. E., Bohn, C. D., Dennis, J. S., & Scott, S. A. (2009). Clean hydrogen production and electricity from coal via chemical looping: identifying a suitable operating regime. *International Journal of Hydrogen Energy, 34*, 1−12.

Connell, D. P., Lewandowski, D. A., Ramkumar, S., Phalak, N., Statnick, R., & Fan, L.-S. (2013). Process simulation and economic analysis of the calcium looping process (CLP) for hydrogen and electricity production from coal and natural gas. *Fuel, 105*, 383−396.

Cormos, A. M., & Cormos, C.-C. (2014). Investigation of hydrogen and power generation co-generation based on direct coal chemical looping systems. *International Journal of Hydrogen Energy, 39*, 2067−2077.

Cormos, C.-C., Cormos, A.-M., & Petrescu, L. (2014). Assessment of chemical looping-based conceptual design for high efficient hydrogen and power co-generation applied to gasification processes. *Chemical Engineering Research and Design, 92*, 741−751.

Curran, G. P., Fink, C. E., & Goran, E. (1967). CO_2 acceptor process: studies of acceptor process, fuel gasification. *Advances in Chemistry, 69*, 141−165.

Damen, K., van Troost, M., Faaij, A., & Turkenburg, W. (2006). A comparison of electricity and hydrogen systems with CO_2 capture and storage: part A: review and selection of promising conversions and capture systems. *Progress in Combustion and Science, 32*, 215−246.

Epple, B. (July 2014). *Personnel communication*. University of Damstadt.

Fan, L.-S. (2010). *Chemical looping systems for fossil energy conversion*. Published Wiley. ISBN: 978-0-470-87252-9.

Fan, L., Li, F., & Ramkumar, S. (2008). Utilization of chemical looping strategy in coal gasification processes. *Particuology, 6*, 131−142.

Fan, Y., & Siriwardane, R. (2014). Novel new oxygen carriers for chemical looping combustion of solid fuels. *Energy and Fuels, 28*, 2248−2257.

Fennell, P. S., & Anthony, E. J. (Eds.), Calcium and chemical looping technology for power generation and carbon dioxide (CO_2) capture, submitted for publication.

Garcia-Labiano, F., Adánez, J., de Diego, L. F., Gayán, P., & Abad, A. (2006). Effect of pressure on the behavior of copper-, iron-, and nickel-based oxygen carriers for chemical-looping combustion. *Energy and Fuels, 20*, 26−33.

Gayán, P., Dueso, C., Abad, A., Adanez, J., de Diego, L. F., & García-Labiano, F. (2009). NiO/Al_2O_3 oxygen carrier for chemical looping combustion prepared by impregnation and deposition-precipitation methods. *Fuel, 88*, 1016−1023.

Gnanapragasam, N. V., Reddy, B. V., & Rosen, M. A. (2009). Hydrogen production from coal using coal direct chemical looping and syngas chemical looping systems: assessment of systems operation and resource requirements. *International Journal of Hydrogen Energy, 34*, 2606−2615.

Gopaul, S. G., Dutta, A., & Clemmer, R. (2014). Chemical looping gasification for hydrogen production: a comparison of two unique processes simulated using ASPEN plus. *International Journal of Hydrogen Energy, 39*, 5804−5817.

Go, K. S., Son, S. R., Kim, S. D., Kang, K. S., & Park, C. S. (2009). Hydrogen production from two-step steam methane reforming in a fluidized bed reactor. *International Journal of Hydrogen Energy, 34*, 1301−1309.

Imtiaz, Q., Hooseini, D., & Müller, C. R. (2013). Review of oxygen carriers for chemical looping with oxygen uncoupling (CLOU): thermodynamics, material, development and synthesis. *Energy Technology, 1*, 633−647.

IPCC, (2014). Impacts, adaption and vulnerability: Summary for policy makers, http://ipcc-wg2.gov/AR5/images/uploads/WG2AR5_SPM_FINAL.pdf Accessed August 2014.

Ishida, M., & Jin, H. (1994). A novel combustor based on chemical looping reactions and its reaction conditions. *Chemical Engineering Research and Design, 84*, 795−806.

Ishida, M., & Jin, H. (1994). A new advanced power-generation system using chemical looping combustion. *Energy, 19*, 415−419.

Jin, H., & Ishida, M. (2001). Reactivity study on a novel hydrogen fueled chemical-looping combustion. *International Journal of Hydrogen Energy, 26*, 889−894.

Johansson, M., Mattisson, T., & Lyngfelt, A. (2006a). Creating a synergy effect by using mixed oxides of iron- and nickel oxides in the combustion of methane in a chemical-looping combustor reactor. *Energy and Fuels, 20*, 2399−2407.

Johansson, M., Mattisson, T., & Lyngfelt, A. (2006b). Investigation of Mn_3O_4 with stabilized ZrO_2 for chemical looping combustion. *Chemical Engineering Research and Design, 84*, 807−818.

Keller, M., Arjmand, M., Leion, H., & Mattisson, T. (2014). Interactions of mineral matter of coal with oxygen carriers in chemical-looping combustion (CLC). *Chemical Engineering Research and Design, 92*(9), 1753−1770.

Larsen, R., Wang, M., Santini, D., Mintz, M., Wu, Y., & Vyas, A. (20 April, 2004). *Might Canadian oil sands promote hydrogen production technology for transportation*. Argonne National Laboratory Presentation.

Lewis, W. K., Gilliland, E. R., & Reed, W. A. (1949). Reaction of methane with copper oxide in a fluidized bed. *Industrial and Engineering Research, 41*, 1227−1237.

Lewis, W. K., and Gilliland, E. R. (1954). Production of pure carbon dioxide, US Patent No. 2,665,972.

Linderholm, C., Mattisson, T., & Lyngfelt, A. (2009). Long-term integrity testing of spray-dried particles in a 10-kW chemical-looping combustor using natural gas as fuel. *Fuel, 88*, 2083−2096.

Lyngfelt, A., Leckner, B., & Mattisson, T. (2001). A fluidized-bed combustion process with inherent CO_2 separation: application of chemical looping combustion. *Chemical Engineering Science, 56*, 3101−3113.

Lyon, R. K., & Cole, J. A. (2000). Unmixed combustion. *Combustion and Flame, 121*, 249−261.

Manovic, V., & Anthony, E. J. (2011a). The use of CaO-based pellets with oxygen carriers and catalysts. *Energy and Fuels, 25*, 4846−4851.

Manovic, V., & Anthony, E. J. (2011b). Integration of calcium and chemical looping combustion using composite CaO/CuO-based materials. *Environmental Science & Technology, 45*, 10750−10756.

Manovic, V., Wu, Y., He, I., & Anthony, E. J. (2011). Core-in-shell CaO/CuO-based composite for CO_2 capture. *Industrial and Engineering Chemistry Research, 50*, 12384−12391.

Markstőm, P., Linderholm, C., & Lyngfelt, A. (2013). Chemical-looping of solid fuels − design and operation of a 100 kW unit with Bituminous coal. *International Journal of Greenhouse Gas Control, 15*, 150−162.

Martínez, I., Romano, M. C., Fernández, J. R., Chiesa, P., Murillo, R., & Abanades, J. C. (2014). Process design of a hydrogen production plant from natural gas with CO_2 capture based on a novel Ca/Cu chemical loop. *Applied Energy, 114*, 192−208.

McCoy, D. C., Curran, G., & Sudbury, J. D. (18−20 October, 1976). CO_2 acceptor process pilot plant. In *Proc. 8th synthetic pipeline gas symposium. Chicago IL.* American Gas Association Catalogue No. L 51176.

McGlashan, N. R. (2010). The thermodynamics of chemical looping combustion applied to the hydrogen economy. *International Journal of Hydrogen Energy, 35*, 6465−6474.

Mendiara, T., de Diego, L. F., García-Labiano, F., Gayán, P., Abad, A., & Adánez, J. (2014). *Fuel, 239−249*.

National Energy Board, http://www.neb.gc.ca/clf-nsi/rnrgynfmtn/nrgyrprt/lsnd/pprtntsndchllngs20152004/qapprtntsndchllngs20152004-eng.html Accessed August 2014.

Orth, M., Strohle, J., & Epple, B. (26−28 September, 2012). Design and operation of a 1 MWth chemical looping plant. In *2nd international conference on chemical looping* (Darmstadt, Germany).

Qin, C., Yin, J., Liu, W., An, H., & Feng, B. (2012). Behavior of CaO/CuO based composite in a combined calcium and copper chemical looping process. *Industrial & Engineering Chemistry Research, 51*, 2274−12281.

Richter, H. J., & Knoche, K. (1983). Reversibility of combustion processes. *ACS Symposium Series, 235*, 71−85.

Rydén, M., & Arjmand, M. (2012). Continuous hydrogen production via the steam-iron reaction by chemical looping in a circulating fluidized-bed reactor. *International Journal of Hydrogen Energy, 37*, 4843−4854.

Rydén, M., & Ramos, P. (April, 2012). H_2 production with CO_2 capture by sorption enhanced chemical-looping reforming using NiO as oxygen carrier and CaO as CO_2 sorbent. *Fuel Processing Technology, 96*, 27−36.

Saucedo, M. A., Lim, Y. Y., Dennis, J. S., & Scott, S. A. (2014). CO_2-Gasification of a Lignite coal in the presence of an iron-based oxygen carrier for chemical-looping combustion. *Fuel, 127*, 186−201.

Scott, D. S. (April 2008). *Smelling land: The hydrogen defense against climate change catastrophe*. Published Canadian Hydrogen Association.

Shimizu, T., Hirama, T., Hosoda, H., Kitano, K., Inagaki, M., & Tejima, K. (1999). A twin fluid-bed reactor for removal of CO_2 from combustion processes. *Transactions of IChemE, 77*, 62−67.

Silaban, A., & Harrison, D. P. (1995). High temperature capture of carbon dioxide characteristics of the reversible reaction between CaO(s) and CO_2(g). *Chemical Engineering Communications, 137*, 177−190.

Siriwardane, R., Poston, J., Chaudhari, K., Zinn, A., Simonyi, T., & Robinson, C. (2007). Chemical looping combustion of simulated synthesis gas using nickel oxide oxygen carrier supported on bentonite. *Energy and Fuels, 3*, 1582−1591.

Strőhle, J., Junk, M., Kremer, J., Galloy, A., & Epple, B. (2014). Carbonate looping experiments in a 1 MWth pilot plant and model validation. *Fuel, 127*, 13−22.

Tessié du Motay, M., & Maréchal, M. (1868). Industrial preparation of hydrogen (in French). *Bulletin Mensuel de La Société Chimique de Paris, 9*, 334.

Tian, H., Chaudhari, K., Simonyi, T., Poston, J., Liu, T., Sanders, T., et al. (2008). Chemical looping combustion of coal derived synthesis gas over copper oxide oxygen carriers. *Energy and Fuels, 22*, 3744−3755.

UKCCS. (2014). https://ukccsrc.ac.uk/resources/ccs-projects-directory/calix-endex-reactor-carbon-capture-technology-feasibility-study. Accessed August 2014.

USDOE. (2013a). http://www.netl.doe.gov/File%20Library/Research/Coal/carbon%20capture/handbook/CO2-Capture-Tech-Update-2013-Chemical-Looping.pdf. Accessed August 2014.

USDOE. (2013b). http://www.hydrogen.energy.gov/pdfs/hpep_report_2013.pdf. Accessed August 2014.

USDOE. (2013c). http://www.netl.doe.gov/File%20Library/Research/Coal/Combustion/Chemical-Looping-Summary−-2013_20131105.pdf. Accessed August 2014.

Xiang, W., Chen, S., Xue, Z., & Sun, X. (2010). Investigation of coal gasification hydrogen and electricity co-production with three-reactors chemical looping process. *International Journal of Hydrogen Energy, 37*, 16852−16863.

Xiao, R., Song, Q., Song, M., Lu, Z., Shange, S., & Shen, L. (2010). Pressurized chemical-looping combustion of coal with an iron ore-based oxygen carrier. *Combustion and Flame, 157*, 1140−1153.

Xiao, R., Song, S., Zhang, S., Zheng, W., & Yang, Y. (2010). Pressurized chemical-looping combustion of chinese bituminous coal: cyclic performance and characterization of iron-ore based oxygen carrier. *Energy and Fuels, 24*, 1449−1463.

Yang, J., Cai, N.-S., & Li, Z.-S. (2008). Hydrogen production from the steam-iron process with direct reduction of iron oxide by chemical looping combustion of coal char. *Energy and Fuels, 22*, 2530−2679.

Zafar, Q., Mattisson, T., & Gevert, B. (2005). Integrated hydrogen and power production with CO_2 capture using chemical-looping reforming-redox reactivity of particles of CuO, NiO and Fe_2O_3 using SiO_2 as a support. *Industrial and Engineering Chemistry Research, 44*, 3485−3496.

Zhang, X., Li, S., Hong, H., & Jin, H. (2014). A hydrogen and oxygen combined cycle with chemical looping combustion. *Energy Conversion and Management, 85*, 701−708.

Zhang, S., Xiao, R., & Zheng, W. (2014). Comparative study between fluidized-bed and fixed-bed operation modes in pressurized chemical looping combustion of coal. *Applied Energy, 130*, 181−189.

This page intentionally left blank

Low-carbon production of hydrogen from fossil fuels

17

N. Muradov
University of Central Florida, Orlando, FL, USA

17.1 Introduction

Currently, most industrial manufacturing of hydrogen in the world is based on fossil fuels: natural gas (NG) (48%), coal (18%), and refinery/chemical off-gases (30%) (International Energy Agency, 2007). The remaining 4% of H_2 is produced through water electrolysis; but if one takes into consideration that globally 80% of electricity generation is based on combustion of fossil fuels, it will be evident that the latter are responsible for about 99% of all industrial production of hydrogen.

Steam methane reforming (SMR) is the most widely used process for industrial hydrogen manufacturing, which produces significant amounts of CO_2 emissions (close to 10 kg CO_2 per kilogram of H_2 product). The fact that fossil-based production of hydrogen is associated with the emission of such enormous quantities of CO_2 may diminish the environmental appeal of hydrogen as an ecologically clean fuel.

The objective of this chapter is to analyze existing and emerging technological options and solutions for eliminating or drastically reducing the amount of CO_2 emissions from fossil-based manufacturing of hydrogen. In the following sections, the main approaches to low-to-zero CO_2 production of hydrogen from fossil fuels (primarily, NG and coal) are outlined, namely:

- Integration of hydrogen plants with CO_2 capture and storage
- Production of CO_2-free hydrogen via dissociation of methane
- Combination of fossil-based hydrogen production processes with non-carbon energy sources such as nuclear and solar.

17.2 Fossil fuel-based hydrogen production with carbon capture and storage

17.2.1 Overview of carbon capture and storage

The main objective of carbon capture and storage (CCS) is to prevent anthropogenic CO_2 from entering the atmosphere by capturing and permanently storing it in various carbon sinks. As long as fossil fuels continue to dominate the global economy, CCS will remain a critical component of the portfolio of carbon mitigation options. According to Global CCS Institute (2013), in 2012 there were eight large-scale

Compendium of Hydrogen Energy. http://dx.doi.org/10.1016/B978-1-78242-361-4.00017-0

CCS projects in operation around the world and nine projects under construction with the total CO_2 capture and storage capacity of 37 million tons per year. Cumulative spending on CCS large-scale demonstration projects (including component technologies in the CCS chain) between 2007 and 2012 has reached US$10.2 billion (International Energy Agency, 2013b). This is an indication of a growing confidence in CCS technology.

However, despite progress in the development and industrial deployment of CCS technology, it is not currently used in hydrogen production or power generation plants, mostly because of considerable energy penalties and associated additional large capital and operational costs. Today, all existing large-scale CCS projects relate to gas-processing facilities or enhanced oil recovery (EOR), where CO_2 capture is part of an already established industrial process.

Technologically, CCS is a complex set of the operations encompassing three major steps: CO_2 capture, transport, and storage. Within each of these major operations, there are multiple technological routes that best suit specific fuel types, geographical locations, climate conditions, and economic development level. Figure 17.1 provides a general outline of existing and emerging CCS technologies related to hydrogen production, power generation, and other technologies.

17.2.2 Steam methane reforming with CCS

SMR is by far the most important industrial process for hydrogen manufacturing, amounting to about 80% of hydrogen produced in the US and 40% in the world (US DOE, 2005). A detailed discussion of the SMR process is presented in Chapter 4 of this volume; in this chapter, only the CO_2 balance of the SMR process and the perspectives of its coupling with CCS technology are discussed.

According to Scholz (1993), CO_2 emission from SMR process amounts to 0.44 Nm^3 CO_2/Nm^3 H_2 (or 9.7 kg CO_2/kg H_2). Spath and Mann (2000) estimated that the global warming potential (GWP) of hydrogen production via SMR process reaches 13.7 kg CO_2 (equivalent) per kilogram of net hydrogen produced with CO_2

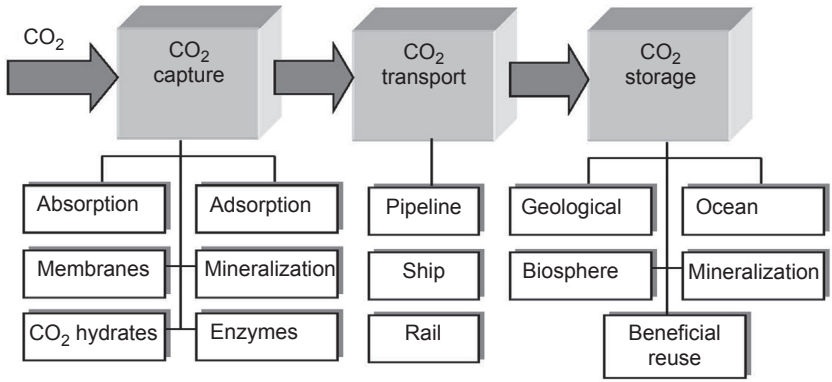

Figure 17.1 Outline of main CO_2 capture, transport, and storage systems.

accounting for 77.6% of the system's GWP. Thus, a typical SMR hydrogen plant with the capacity of 1 million m^3/day of hydrogen produces close to 0.4 million m^3/day of CO_2, which is typically vented into the atmosphere. Coupling of SMR with CCS was advocated by a number of research groups worldwide as a potentially viable approach to drastically diminishing CO_2 emissions from H_2 manufacturing processes (Audus, Kaarstad, & Kowal, 1996; IPCC, 2005).

Until about 2−3 decades ago, CO_2 was separated from raw hydrogen (after a CO-shift reactor) using chemical absorption methods (e.g., amine-based or hot potassium carbonate solvents) resulting in pure CO_2 stream released to the atmosphere. Modern SMR plants use physical adsorption technology: in particular, pressure swing adsorption (PSA) units (discussed in Section 17.2.4.1). Figure 17.2 depicts a simplified block diagram of a modern SMR plant.

In a typical modern SMR plant, about 60% of the total CO_2 produced is contained in the shifted gas (i.e., after a water gas shift (WGS) unit), with the remaining 40% of CO_2 being the product of NG fuel combustion that provides heat input to the steam reformer (Collodi, 2010). Although the PSA unit produces high-purity hydrogen gas (99.999%) it does not selectively separate CO_2 from other waste gases (CH_4 or CO). As a result, the off-gas (or tail gas) from the PSA unit contains CO_2, CH_4, CO, and small amounts of H_2, which is used as fuel in the reforming reactor with CO_2 is vented into the atmosphere (as flue gas). Average CO_2 concentrations in the shifted gas, PSA tail gas, and steam reformer flue gas are (in mol.%): 15.0, 45.1, and 19.0, respectively (Collodi, 2010). Typical CO_2 flow rates and CO_2 partial pressures in the shifted gas, PSA tail gas, and steam reformer flue gas of an SMR plant with the capacity of 100,000 Nm^3/h gas are shown in Table 17.1.

It is apparent from the data presented in Figure 17.2 and Table 17.1 that practically all CO_2 produced in the SMR process ends up in the flue gas of the steam reformer heater (i.e., about 9 tons of CO_2 is emitted per 1 ton of H_2 product).

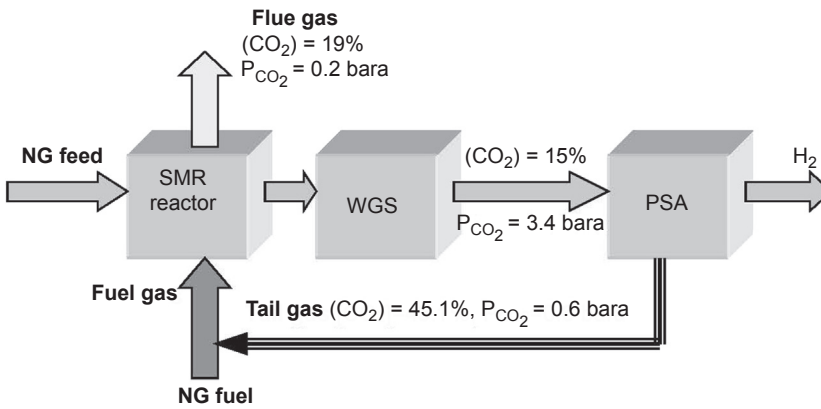

Figure 17.2 Simplified block diagram of a typical modern SMR plant. WGS is a water gas shift reactor. CO_2 concentrations are in mol.%.
Collodi (2010).

Table 17.1 Typical CO_2 flow rates and CO_2 partial pressures for different streams in an SMR plant with the capacity of 100,000 Nm^3/h

SMR streams	CO_2 flow rate (kmol/h)	CO_2 partial pressure (bara)
Shifted gas	1,000	3.40
PSA tail gas	1,000	0.60
Flue gas	1,850	0.20

Collodi (2010).

In principle, CO_2 could be captured from any of three CO_2-containing streams, as shown in Figure 17.3.

The CO_2 removal efficiency from SMR streams at different removal points could be as high as 99% for location 1 (shifted gas), and 90% for locations 2 (PSA tail gas) and 3 (flue gas) (Collodi, 2010). As shown in Figure 17.2, CO_2 concentration and partial pressure vary from one location to another in the SMR process chain; thus, different sets of technologies could be applied for CO_2 removal from these streams. The range of available and emerging technologies for CO_2 removal from different technological streams is discussed in detail in Section 17.2.4 of this chapter.

Recently, there have been new technological developments in the SMR process, in which a post-WGS section was modified to recover both pure H_2 and CO_2 by including an additional CO_2 removal stage before the H_2 separation step in the PSA stage. Air Products and Chemicals, Inc. (APC) with the support of US Department of Energy (DOE) is working on retrofitting its two steam methane reformers located within the

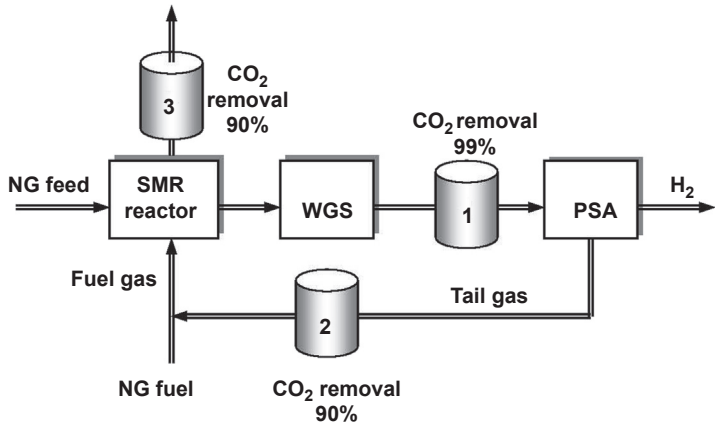

Figure 17.3 Carbon dioxide removal options from SMR CO_2-containing streams. Carbon dioxide removal locations: 1, after WGS reactor; 2, from PSA tail gas; 3, from flue gas. Collodi (2010).

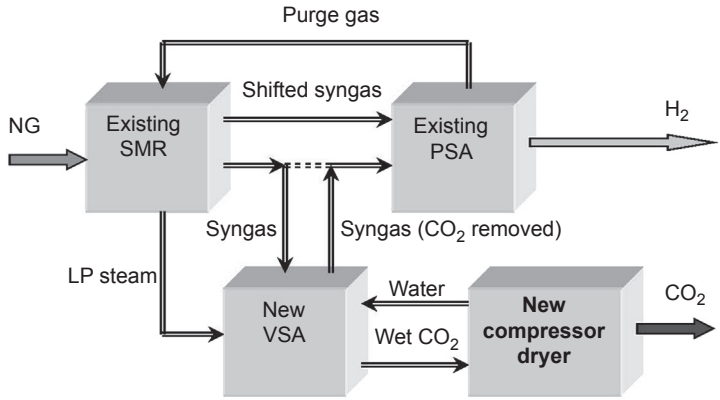

Figure 17.4 Simplified block diagram of Air Products and Chemicals' Port Arthur SMR plant integrated with CO_2 capture.
Baade et al. (2012).

Valero refinery in Port Arthur (Texas) to capture and sequester CO_2 (Baade, Farnand, Hutchinson, & Welch, 2012). Figure 17.4 depicts a simplified block diagram of one of the two reformers, which shows how the new CO_2 capture facility will be integrated within the existing facility. The retrofitted plant uses a proprietary vacuum swing adsorption (VSA) system on each of the two existing SMR trains. The VSA cyclic system is similar to the PSA cycle in that adsorbent-filled vessels are fed with gaseous mixture at high pressure resulting in the selective adsorption of the components onto the adsorbent beds.

Carbon dioxide-containing syngas from the steam methane reformer is routed to the VSA unit, which is composed of a series of vessels filled with adsorbent beds that selectively remove CO_2 from gas. The hydrogen-rich stream that is not adsorbed by the bed is sent to hydrogen PSA for further purification. Each vessel in the VSA unit undergoes a series of pressure equalizations resulting in CO_2 drawn off by a vacuum pump (an evacuation step). In the following "rinse" step, the blowdown gas is taken from a lower pressure bed, compressed, and fed to a higher pressure bed. The inclusion of both "evacuation" and "rinse" steps is critical for achieving high-purity CO_2. Raw CO_2 undergoes a series of cooling, dehydrating, and drying operations and enters a CO_2 pipeline at a pressure of 135 atm. The CO_2 produced at the APC plant is intended for EOR, and it will be transported to the oil fields in Texas and Louisiana via a system of pipelines (Baade et al., 2012).

US DOE National Energy Technology Laboratory (NETL) researchers analyzed an alternative scheme for SMR integration with CO_2 capture, as presented in Figure 17.5 (DOE/NETL, 2010).

Among the major differences using the NETL's scheme is the inclusion of monoethanolamine (MEA) and methyldiethanolamine (MDEA) CO_2 scrubbing units along with the PSA system. In this study, the SMR plant was reported to have an effective thermal efficiency of 69.7% (HHV) and a capacity of 617 t/day H_2. The amounts of CO_2 recovered and emitted were estimated at 8.84 and 0.98 t CO_2/t H_2, respectively.

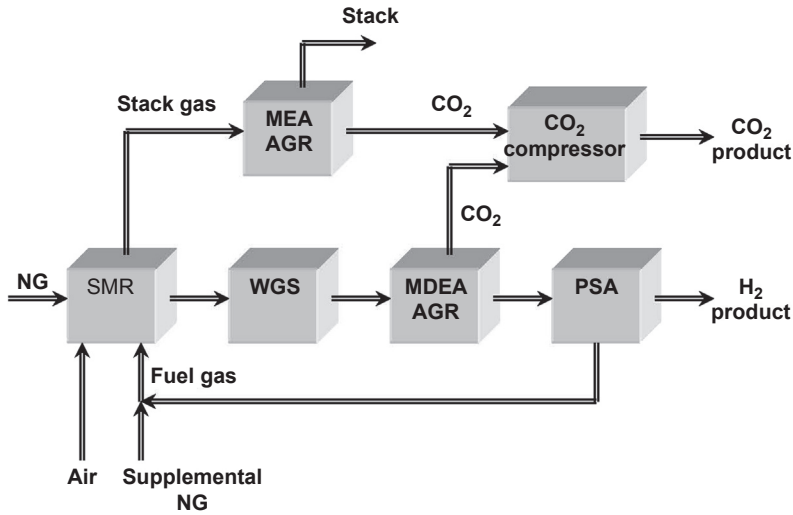

Figure 17.5 Block flow diagram of SMR with CO_2 capture by chemical absorption and PSA methods. AGR, acid gas removal; MEA, monoethanol amine; MDEA, methyldiethanol amine. NETL (2010).

The addition of CO_2 capture to an SMR plant inevitably affects its energy efficiency. According to a study analyzing different SMR plant designs, the overall efficiency of a modern SMR plant with a capacity of 720 t/day H_2 (at a pressure of 6 MPa) without CO_2 capture is estimated at 76% (on a lower heating value (LHV) a basis) with overall CO_2 emissions of 9.1 kg CO_2 per kg H_2 (International Energy Agency, 1996). However, if the SMR plant is modified to produce nearly pure CO_2 as a coproduct (e.g., via combination of amine solvent scrubbing with PSA), the efficiency would be decreased to 73%, with the CO_2 removal rate reduced to 8.0 kg CO_2 per kg H_2.

17.2.3 Hydrogen production from coal with CCS

Hydrogen production via coal gasification is well-developed technology: It has been practiced for more than a century in the chemical and fertilizer industries. In 2010, there were 128 gasification plants operating worldwide with 366 gasifiers producing 42,700 MW_{th} of syngas, with about 4000−5000 MW_{th} of syngas capacity added annually (NETL, 2010). Currently, large-scale commercial coal gasification processes mainly focus on the production of the following chemical products: hydrogen, ammonia (many plants are operated in China), substitute NG (e.g., North Dakota plant in the US), and liquid fuels via Fischer−Tropsch synthesis (e.g., Sasol technology in South Africa).

Integrated gasification combined cycle plants result in the combined production of hydrogen and electricity, because syngas produced in the coal gasification process can be used to produce both end products. This flexibility is made possible because of the

WGS reaction that converts CO contained in syngas to H_2 and CO_2. A coal gasification plant that can produce both hydrogen and power is called HYPOGEN (Garcia Cortes, Tzimas, & Peteves, 2009).

There are few studies dedicated to H_2 production from coal with CO_2 capture and storage: e.g., Kreutz, Williams, Chiesa, and Consonni (2005), Gray and Tomlinson (2003), DOE/NETL (2010), Garcia Cortes et al. (2009). For example, Kreutz et al. (2005) analyzed a hydrogen manufacturing plant with a capacity of 1,070 MW_{th} H_2 using high-sulfur bituminous coal (with sulfur content of 3.4%). An entrained flow coal gasifier operating at a pressure of 7 MPa was assumed as a base case design. The H_2S and CO_2 were removed from syngas using a physical solvent-based process (Selexol) in the first and second stages of the process, respectively, with H_2S converted to sulfur (via the Claus process) and CO_2 dried and compressed to 150 atm for pipeline transport and underground storage. In the PSA unit, high-purity H_2 (99.999%) was extracted from CO-shifted syngas, whereas PSA purge gas was combusted in a gas turbine to generate 39 MW_{el} of electricity. The efficiency of H_2 production process and associated CO_2 emissions was estimated to be 61% and 1.4 kg CO_2 per kilogram of H_2, respectively. For comparison, without CO_2 capture, the efficiency and CO_2 yield would increase to 64% and 16.9 kg CO_2 per kilogram of H_2, respectively.

NETL researchers analyzed coal-to-H_2 plant with CO_2 capture and storage with the capacity of 617 kg/day H_2 (DOE/NETL, 2010). The plant used a GE Energy radiant gasifier (with a coal feed rate of 5,302 t/day) and PSA. The study found that CO_2 recovery and emission rates were (in kilograms of CO_2 per kilogram of H_2) 17.8 and 1.9, respectively. Figure 17.6 provides a simplified block diagram of a coal-to-H_2 plant with CO_2 capture.

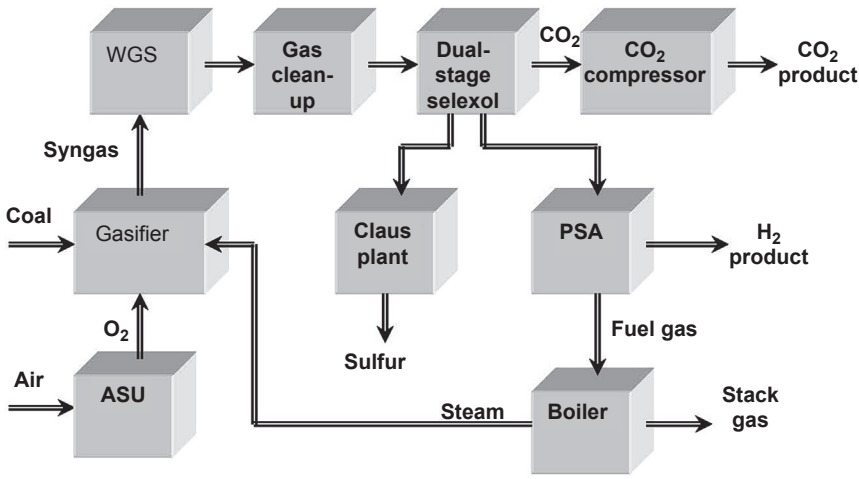

Figure 17.6 Block flow diagram of coal-to-hydrogen process with CO_2 capture. Only major process streams and equipment are shown. ASU, air separation unit.
NETL (2010).

In the gasifier, coal feedstock is gasified with an oxygen−steam mixture to hot syngas, which after the removal of particulates is further subjected to CO-shift in sulfur-tolerant shift reactors to produce an H_2−CO_2 mixture. A double-stage Selexol unit is typically used to remove H_2S and CO_2 from syngas (Wilson & Gerard, 2007). The H_2S-containing gas is treated in a Claus unit, where H_2S is oxidized to elemental sulfur. After the Selexol unit, the gas is sent to PSA for H_2 purification and delivery as a final product. The compressed CO_2 gas is ready for pipeline transport.

17.2.4 Carbon dioxide capture technologies: status and prospects

Carbon dioxide capture is a first step in the multistage CCS process. In general, CO_2 capture is an energy-intensive and costly process; in most cases, capturing CO_2 (especially from diluted streams), purifying it, and compressing it to a state that makes its transport economically feasible represents the largest components of the overall cost of the CCS chain. Intensive worldwide effort focuses on improving CO_2 capture process efficiency and reducing its cost; most effort targets CO_2 capture from coal-fired power plants because they are the largest stationary sources of CO_2 emissions. The existing CO_2 capture technologies are also applicable to hydrogen plants and other large industrial sources of CO_2 emissions.

The search for efficient CO_2 capture materials is of great commercial interest, and it has been a focus of intensive research and development (R&D) for many decades, which has recently intensified owing to the development of commercial CCS systems. A large variety of materials are suitable for CO_2 capture: zeolites, amines, activated carbons (AC), alkali and alkaline earth metal oxides, ionic liquids, polymeric membranes, microporous polymers, amine-modified mesoporous silica, metal-organic frameworks (MOF), and so forth (He et al., 2013; Brennecke and Gurkan, 2010). The most important characteristics determining the suitability of CO_2 capture materials are:

- CO_2 sorption capacity
- Sorption/desorption kinetics and operational parameters (temperature and pressure)
- Interference with potential contaminants (e.g., SO_x, NO_x, H_2S)
- Regenerability and long-term stability
- Economic feasibility (cost)

The selection of a particular technology for CO_2 capture is dictated by many parameters, most important of which are CO_2 concentration in the gaseous stream, required pressure, and the presence of contaminants. The following is a brief discussion of existing and emerging CO_2 capture technologies applicable to gaseous streams with different ranges of CO_2 concentration as applied to hydrogen production technologies.

17.2.4.1 Carbon dioxide capture from streams with relatively high CO_2 content

This section discusses CO_2 removal options from gaseous streams with relatively high CO_2 concentration, e.g., shifted syngas (i.e., post-WGS stream) and tail gas (after the

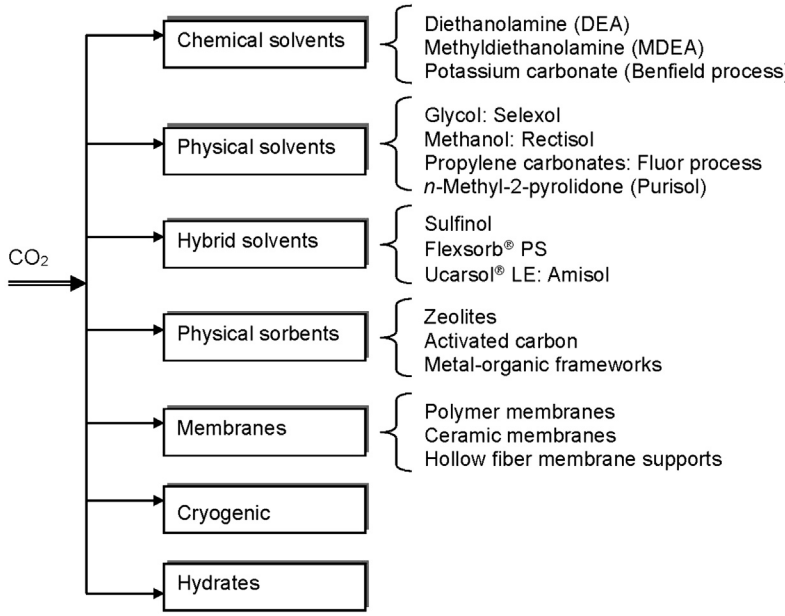

Figure17.7 CO_2 capture technologies from syngas and other gases with a relatively high CO_2 content.
Global CCS Institute (2009), US DOE (2007).

PSA unit). Major existing and emerging technological options for CO_2 capture from shifted syngas and other gaseous streams are summarized in Figure 17.7.

Current commercial CO_2 capture technologies are predominantly based on absorption processes that use selective solvents capable of separating and removing greater than 90% of CO_2. Absorption could be purely a physical process (e.g., dissolution of CO_2 in cold methanol), or a chemical process (e.g., reaction of CO_2 with amine compounds), depending on the nature of the interaction between CO_2 and the solvent.

Chemical Absorption. Because CO_2 is an acidic gas, most absorbing solvents used for its capture are of a basic nature. Chemical absorption systems most commonly used in industry include aqueous alkanolamines (e.g., MEA diethanolamine and MDEA), chilled ammonia (NH_4OH), and hot potassium carbonate (K_2CO_3) (Resnick, Yeh & Pennline, 2004). The use of existing alkanolamine-based solvents, however, incurs high energy penalties owing to their energy-intensive regeneration step (steam stripping). It was estimated that for MEA solvent, the energy penalty is equal to 1.9 MJ/kg CO_2 captured (Rochelle, 2009).

Physical Absorption. Physical absorption methods are governed by Henry's law (i.e., low temperature and high pressure favor CO_2 capture); therefore, this method is preferred for CO_2 capture from mixtures in which CO_2 partial pressure is relatively high (greater than 500 kPa). The regeneration of physical solvents is less energy intensive compared with chemical solvents. Commercial processes using physical absorption of CO_2 include glycol-based compounds (e.g., dimethyl ether of polyethylene

glycol), cold methanol, and propylene carbonate (Global CCS Institute, 2009). On the downside, glycols exhibit a relatively low carrying capacity, which necessitates circulation of significant volumes of the solvent (e.g., about 20 kg of the glycol solution per kilogram of CO_2 captured). Among commercial methanol-based absorption systems, the Rectisol process (Lurgi) is most commonly used in CO_2 capture applications. The process can capture more than 90% of CO_2 from gaseous streams, but at the high cost of refrigeration, which hurts the process economics (US DOE/NETL, 2003).

Adsorption. Processes for the physical adsorption of CO_2 are based on the preferential selective adsorption of CO_2 on high-surface area solids such as zeolites, AC, and nanostructured sorbents. In this category, PSA is the most widely used commercial technology. In particular, PSA is the process of choice for separating CO_2 from gaseous mixtures in which high purity of hydrogen (e.g., 99.999% and higher) is required. The PSA cyclic operation is based on adsorption of gases at high pressure and desorption at lower pressure by a plurality of adsorbent beds loaded with zeolites or AC. Figure 17.8 outlines the mechanism of gas separation by the PSA method.

Technological variations in the PSA process include VSA, in which vacuum is used instead of high pressure, temperature swing adsorption (TSA), which involves adsorption at low temperature and desorption at high temperature, and electric swing adsorption (ESA), in which electric current is used for regeneration (Global CCS Institute, 2009). PSA and TSA are commercially practiced technologies used in

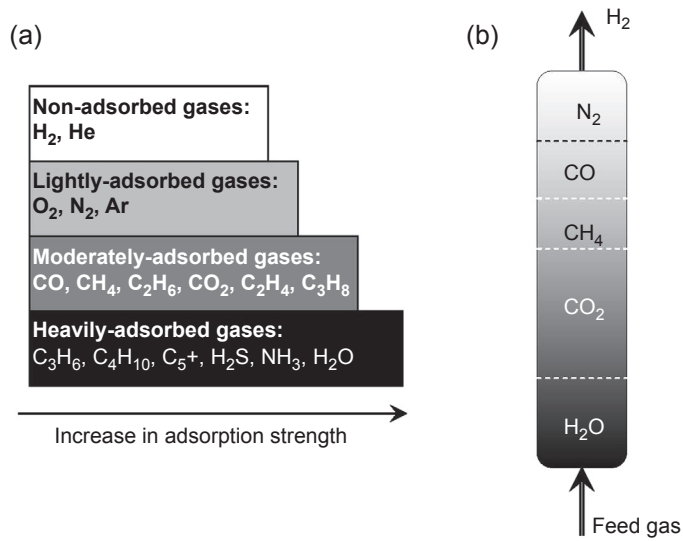

Figure 17.8 Separation of gases by pressure swing adsorption (PSA) technique. A, Relative strength of adsorption of typical impurities in syngas. B, Schematic of the operation of a single adsorbent bed in a PSA unit.
Cortes et al. (2009).

hydrogen manufacturing plants (e.g., SMR) and in CO_2 removal from subquality NG (Global CCS Institute, 2009); VSA and ESA are at the demonstration (e.g., APC plant) and early stages of development, respectively. Emerging technologies for CO_2 capture via physical adsorption processes involve MOF and nanostructured carbon-based sorbents. MOF have high porosity and adjustable chemical functionality that can be tailored to increase the CO_2 adsorption capacity (Millward & Yaghi, 2005).

Gas Separation Membranes. Considerable R&D efforts are focused on the development of efficient and selective membranes for CO_2 separation from industrial gaseous streams (Ciferno, Fout, Jones, & Murphy, 2009; Lin, Merkel, & Baker, 2007; US DOE/NETL 2003). In general, gas separation can be accomplished using polymeric or inorganic membranes. Polymeric membranes are effective (owing to a large surface to volume ratio) and inexpensive, but they are subject to gradual degradation (especially at elevated temperatures). Polymeric membranes are based on polymers such as cellulose acetate, polyimides, polyamides, and polysulfone. Inorganic membranes are stable at high temperatures and corrosive environments but are more expensive than polymeric ones. Among inorganic materials used for the membrane separation of H_2 and CO_2 are Pd alloys, perovskites, silica, carbon, zeolite, and glass. Among new developments are membranes containing amines, dendrimers, potassium carbonate, and polyelectrolytes (Du et al., 2011; Garcia Cortes et al., 2009). A detailed discussion on inorganic membrane reactors for pure hydrogen production and CO_2 separation is presented in Chapter 23.

Cryogenic Separation. Cryogenic CO_2 separation methods are based on differences in boiling points of CO_2 and other components of the gaseous mixture (US DOE/NETL, 2012). The cryogenic method is currently widely used commercially in processes involving the liquefaction and purification of CO_2. Typically, three different cooling loops involving three different refrigerants (R32, ethylene, and methane) form the cooling system (Garcia Cortes et al., 2009). The technology has good economy of scale and the possibility of direct production of liquid CO_2 that can be transported in liquid form or stored at high pressure as liquid. Main shortcomings of the cryogenic method relate to its high energy intensity and the need to remove components with a relatively high freezing point (e.g., water, NO_2) before cooling.

17.2.4.2 Carbon dioxide capture from diluted CO_2 streams

The capture of CO_2 from diluted CO_2 streams (e.g., flue gases) is significantly more challenging than that from shifted syngas, tail gas, and other streams with relatively high CO_2 content. The main technical difficulties can be attributed to the low CO_2 concentration in flue gases (3−15 vol%) and its low pressure (close to atmospheric), resulting in large-capacity equipment and significant energy penalties. Although in general many CO_2 capture methods discussed in the previous section could be applied to diluted CO_2 streams, there might be some limitations to the economic feasibility of their application, mainly owing to substantially lower CO_2 concentrations in the gas streams. Main (preferred) technological options for CO_2 capture from diluted streams are outlined in Figure 17.9.

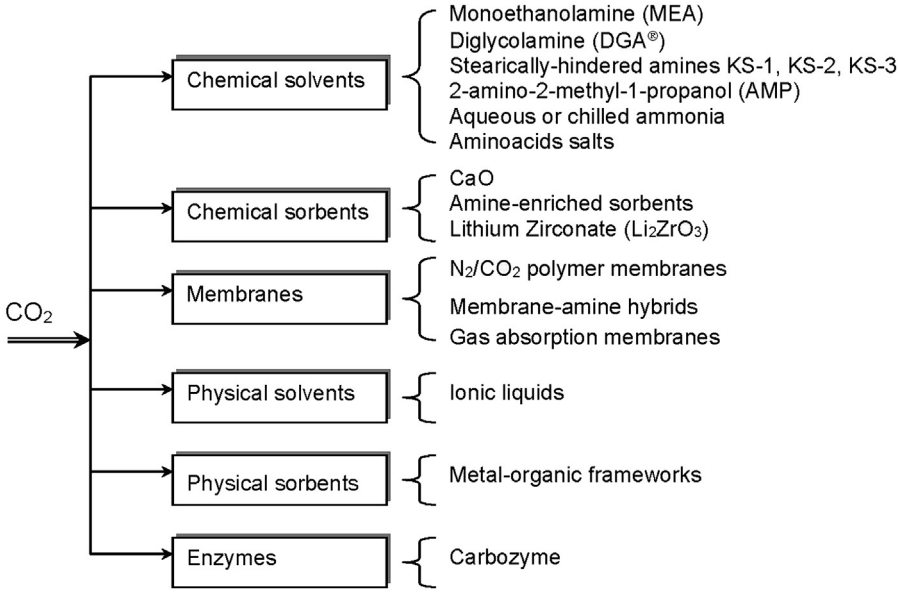

Figure 17.9 Carbon dioxide capture technologies from flue gases and other streams with a relatively low CO_2 content.
Global CCS Institute (2009), US DOE (2007), Fauth & Hoffman (2004), Feron & Asbroek (2004).

17.2.5 Carbon dioxide storage options

Carbon dioxide storage is a final stage in the multistep CCS process. Practically all existing CO_2 storage projects relate to the gas-processing industry and coal-fired power plants. Among the few CCS demonstration and commercialization projects applied to hydrogen production is APC's plant in Port Arthur (see Section 17.2.2). In principle, all potential CO_2 storage options could be applicable to hydrogen production plants, in particular:

- Geological storage
- Ocean storage
- Mineral sequestration
- Biological storage
- Industrial use of CO_2

17.2.5.1 Geological CO_2 storage

Geological carbon storage (sometimes called geosequestration) is the most mature CO_2 storage technology; it is carried out by injection of CO_2 into deep geological formations (e.g., porous rocks or saline formations) that isolate CO_2 from the atmosphere by thick layers of impermeable rock. The first geological CO_2 storage projects were performed by gas companies and dealt with NG fields with high CO_2 content, such

as the Sleipner project in Norway and In Salah project in Algeria. As the technology improved, power generation and other industries started showing an interest in geological storage as a carbon mitigation option. Main criteria for a particular geological CO_2 storage formation to be considered a suitable storage site are sufficient storage capacity, a reliable confining unit, and a stable geological environment, among others (Bachu, 2003). The following geological formations are considered suitable for CO_2 storage:

- Deep saline formations
- Depleted oil and gas reservoirs
- Unminable coal beds and abandoned mines
- Salt caverns
- Basalts and organic-rich shales

More detailed information on this topic can be found in the following sources: IPCC, 2005, 2007.

17.2.5.2 Beneficial CO_2 reuse applications

The term "beneficial CO_2 reuse" relates to energy resource recovery applications in which CO_2 is used to generate additional revenue from the sale of crude oil or NG that is recovered as a result of CO_2 storage. EOR is the most widely used beneficial CO_2 reuse application; it aims to increase the amount of extracted crude oil that would otherwise remain stranded. In a typical EOR operation, CO_2 is compressed to dense-phase CO_2 and injected through an injection well into an oil reservoir, where it is mixed with crude oil. This makes oil in the reservoir less viscous and more mobile and forces it to flow to a series of production wells. EOR offers an advantage of substantially increasing the oil production through CO_2 flooding of an oil well. As a tertiary oil recovery operation, EOR recovers between 6.7% and 23% of original oil in place (Ferguson, Van Leeuwen & Kuuskraa, 2008). For the US, with an average recovery rate of 14.6%, this translates into additional 87.1 billion barrels of oil (based on the estimated 595.7 billion barrels of oil in place) (Global CCS Institute, 2009). Examples of the large EOR projects are the Rangely Project (Colorado, US) and the Weyburn−Midale Project (Saskatchewan, Canada). The EOR provides opportunities for the most cost-effective way and earliest opportunities to introduce CCS projects to the market.

17.2.6 Economics of fossil-based hydrogen production with CCS

Techno-economic assessment of hydrogen production by SMR coupled with CCS has been extensively reported in the literature. Among early publications, Audus et al. (1996) analyzed the concept of coupling the SMR process with CO_2 capture and disposal in a saline aquifer. The authors concluded that the inclusion of CCS would add about 25−30% to the cost of hydrogen production. In another study conducted by the US National Research Council (NRC), the estimates of the cost of centralized hydrogen production by SMR without and with added CO_2 capture were reported as \$1.03 kg^{-1} and \$1.22 kg^{-1} H_2, respectively (an increase of 18.5%) (NRC 2004).

The cost of pipeline transport and distribution of hydrogen would add \$0.96 kg^{-1} H_2 (NRC, 2004).

Simbeck (2005) estimated that CO_2 capture would add 32.5% to the unit cost of H_2 production by SMR. A reduction in net CO_2 emissions per unit H_2 product was estimated at 72−83% (after factoring in CO_2 emissions from imported electricity) (NRC 2004; Simbeck, 2005). The cost of H_2 production is sensitive to NG prices, so the variation in the latter may greatly affect the costs of H_2 production and CO_2 capture. For coal-based H_2 production, the US NRC study reported about an 8% increase in the unit cost of H_2 and 83% reduction in CO_2 emissions per unit H_2. Steinberger-Wilckens, Trumper, Madsen, and Norgaard (2008) estimated that the addition of CCS to hydrogen plants would cause a relatively small increase in H_2 production costs (15−35%) compared with power plants (up to 60%), which would make H_2 production more attractive for CCS applications. The difference can be attributed to the CO_2 separation stage, which is already integrated into the H_2 production process, whereas it has to be added in the case of power plants.

The International Energy Agency (IEA) report provided the range of total costs for CO_2 capture, transport, and geological storage (based on current technology) for a new hydrogen plant (IPCC, 2005). Figure 17.10 compares the costs of fossil-based hydrogen production for three cases: (1) an H_2 plant without CCS, (2) an H_2 plant with CO_2 capture and geological storage, and (3) an H_2 plant with CO_2 capture and EOR.

The results obtained indicate that if the baseline H_2 plant is integrated with CCS (assuming a geological storage option), H_2 production cost would increase by 6−54% (an average of 30%) with a carbon mitigation cost of \$3−\$75 per t CO_2 avoided (IPCC, 2005). But if EOR is included in the scheme, the H_2 production

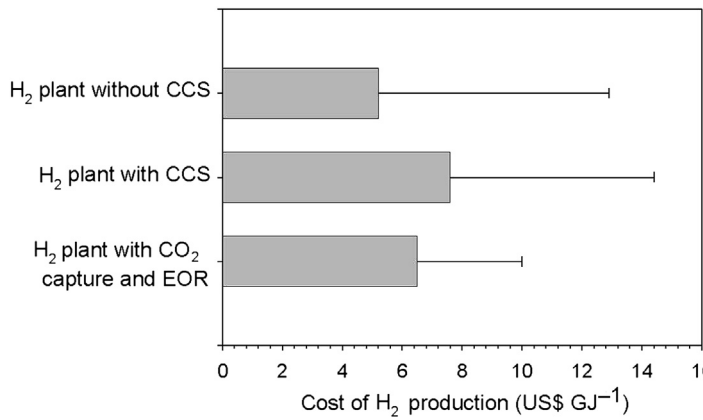

Figure 17.10 Range of total costs for CO_2 capture, transport, and geological storage (based on current technology) for a new hydrogen plant. Three scenarios are considered: (1) H_2 plant without CCS, (2) H_2 plant with CO_2 capture and geological storage, and (3) H_2 plant with CO_2 capture and enhanced oil recovery (EOR).
IPCC (2005).

cost increase varies from−28% (i.e., decrease in H_2 cost) to +28% with a carbon mitigation cost in the range of US$(−14) to US$49 per t CO_2 avoided (IPCC, 2005). This analysis clearly demonstrates the economical advantages of H_2 production integrated with beneficial CO_2 reuse.

More detailed discussion on different aspects of CCS technology is beyond the scope of this chapter. For interested readers, we recommend the following sources: International Energy Agency (2012, 2013a, 2013b), IPCC (2005, 2007), Muradov (2014), Muradov and Veziroğlu (2012), Wilcox (2012).

17.3 Carbon dioxide-free hydrogen production via methane decomposition

Because of the high cost of CO_2 capture and long-term ecological uncertainties regarding CO_2 storage, there have been proposals to produce H_2 via dissociation of methane as an alternative to the SMR-CCS approach owing to its potential to do away completely with CO_2 production. This promising environmentally friendly approach to hydrogen production from NG was promoted in the early works of Muradov (2001, 2009), Steinberg (1998), and other researchers. In contrast to multistage SMR, methane decomposition is a simple one-step process:

$$CH_4 \rightarrow C + 2H_2 \qquad \Delta H^\circ = 75.6 \text{ kJ/mol} \tag{17.1}$$

In this moderately endothermic reaction, the energy requirement per mole of hydrogen produced (37.8 kJ/mol H_2) is substantially lower than that in the SMR process (63.3 kJ/mol H_2). Advantageously, the methane decomposition process produces a valuable by-product: clean carbon that can be marketed and used in a variety of traditional and novel application areas, or it can be securely stored for future use in a less carbon-constrained world (it is environmentally much safer to store solid carbon than gaseous or supercritical CO_2). Marketing the carbon product would substantially reduce the cost of hydrogen production by methane decomposition; in contrast, adding CCS to SMR would significantly increase the cost of H_2 production (see Section 17.2.6).

The major problem with methane decomposition reaction is that, because of strong C−H bonds ($E_{dis.} = 436$ kJ/mol) and the lack of polarity, methane is one of the most stable organic molecules. As a consequence, carrying out reaction (17.1) at a reasonable rate would require an energy input in the form of either very high-temperature heat (>1,200 °C), or electrical discharge (plasma). Existing and emerging technological options for methane decomposition into hydrogen and carbon are summarized in Figure 17.11.

17.3.1 Thermal decomposition of methane

The thermal decomposition of methane is not a new process. The thermal black process has been practiced since the 1930s to manufacture carbon black (CB) via thermal

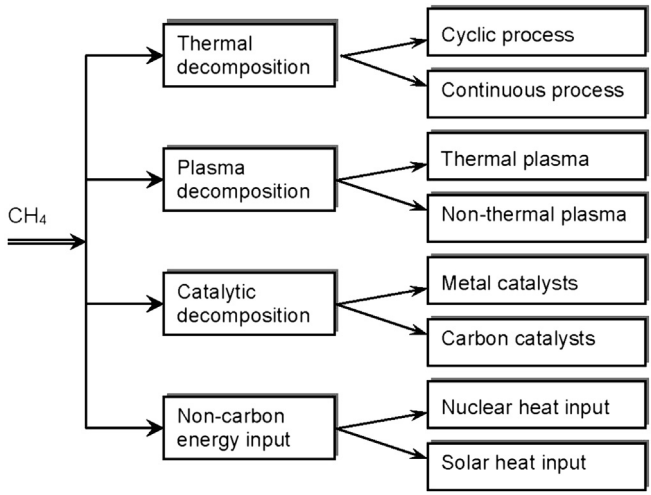

Figure 17.11 Technological options for the thermocatalytic decomposition of methane.

decomposition of NG in a semicontinuous process using two tandem reactors operating at high temperatures (up to 1,400 °C). Hydrogen was a by-product of the process and was used as supplemental fuel. Later, the thermal black process was supplanted by the more efficient oil furnace process based on partial oxidation of heavy petroleum feedstocks.

Several new approaches to thermal decomposition of methane have been developed. Shpilrain, Shterenberg, and Zaichenko (1999) reported a high-temperature regenerative heater-reactor for NG decomposition into hydrogen and CB. In this process, thermal decomposition of NG was conducted in a "free volume" of the reactor using a carrier gas (N_2 or H_2) that was heated to 1,627−1,727 °C. Steinberg (1999) studied a methane decomposition reactor consisting of a molten metal bath. Methane was decomposed while bubbling through a molten tin or copper bath at a temperature of 900 °C and higher. Main advantages of this system relate to the ease of CB separation from the liquid metal surface and efficient heat transfer to the methane stream.

17.3.2 Plasma-assisted methane decomposition

Thermal plasma systems. In thermal plasma reactors, the energy required to accomplish an endothermic methane decomposition reaction is provided by high-temperature (5,000−10,000 °C) plasma. Kvaerner Company of Norway developed the Kvaerner CB&H process to produce hydrogen and CB by the thermal plasma decomposition of NG (Lynum & Gaudernack, 1996). More detailed discussion on the Kvaerner process can be found in Chapter 12 of this book. Fulcheri and Schwob (1995) studied thermal plasma decomposition of methane to hydrogen and CB. The authors estimated electric energy consumption of the plasma pyrolyzer to be 4−7 kWh/kg of CB and 1−1.9 kWh/m^3 H_2. Bromberg, Cohn, Rabinovich, O'Brien, and Hochgreb (1998) reported plasma pyrolysis of methane in a plasmatron using a cathode with a zirconium tip and a copper tubular anode. Average specific power consumption was measured in the range of 200−250 MJ/kg H_2.

Nonthermal plasma systems. The advantage of nonthermal plasma (NTP) systems is that NTP stimulates chemical reactions employing an amount of energy much less than that required by thermal plasma devices. In NTP systems, most of the applied energy is directed toward the production of high-energy electrons, radicals, ions, and other active species that initiate a variety of reactions leading to the efficient conversion of feedstocks at much lower temperatures compared with thermal plasma. Czernichowski, Czernichowski, and Ranaivosolarimanana (1996) investigated NTP pyrolysis of NG in a gliding arc reactor with voltage and current varying in the range of 0.5−10 kV and 0.1−5 A (per discharge), respectively. Nozaki, Kimura, and Okazaki (2002) used a barrier discharge plasma reactor for the simultaneous production of hydrogen and carbon nanotubes (CNT) via the decomposition of methane. Babaritskiy (2000) studied microwave plasma-catalyzed decomposition of methane in an experimental setup consisting of two blocks: a gas heater and a plasma block.

The main problem with plasma-assisted methane decomposition processes (especially thermal plasma systems) is that they require a relatively large amount of electricity. Thus, the overall amount of CO_2 emissions from the plasma-assisted process is tied to the fuel mix used in the power generation sector, and it may be high in countries with a large share of coal-fired power plants (in 2009 the global average rate of CO_2 emission was 500 kg CO_2 per MWh electricity) (International Energy Agency, 2011).

17.3.3 Metal-catalyzed methane decomposition

The methane decomposition process lends itself to the use of catalysts to reduce maximum temperature and facilitate its kinetics. Thermocatalytic decomposition (TCD) of methane over a number of supported transition metal (e.g., Fe, Ni, Co, Pt, Mo, Cr) catalysts using different types of reactors was reported by many groups of researchers (e.g., Aiello, Fiscus, Loye, & Amiridis, 2000; Ashok, Kumar, Venugopal, Kumari, & Subrahmanyam, 2007; Choudhary, Sivadinarayana, Chusuei, Klinghoffer, & Goodman, 2001; Reshetenko, Avdeeva, Ismagilov, Chuvilin, & Ushakov, 2003; Sueleves, Lazaro, Moliner, Corbella, & Palacios, 2005). Koerts, Deelen, and van Santen (1992) demonstrated that the rate of methane activation in the presence of transition metals followed the order: Ni, Co, Ru, Rh > Pt, Re, Ir > Pd, Cu, W, Fe, Mo. Recently, intensive R&D efforts have focused on the development of a process for the simultaneous production of hydrogen and high-value forms of carbon such as CNT, nanofibers, graphene, and other carbon nanostructures via the metal-catalyzed methane decomposition process (e.g., Piao, Chen, Chang, & Lin, 2002; Takenaka, Shigeta, Tanabe, & Otsuka, 2003). For example, Li, Chen, Qin, and Cheng (2000) reported the production of hydrogen and CNT by the decomposition of methane on Ni and Ni−Cu catalysts. The authors demonstrated the production of hydrogen with purity of 80 vol% and 180 g of nanotubes per 1 g of catalyst over 10 h. Production of H_2 and CNT via methane TCD over silica- and zeolite-supported Ni catalysts was reported by Choudhary et al. (2001) and Aiello et al. (2000). Coproduction of graphene sheets and hydrogen by the decomposition of methane using cobalt-based catalysts was reported by Jana, O'Shea, Coronado, and Serrano (2011). Ermakova and Ermakov (2002) studied Ni/SiO_2 and Fe/SiO_2 catalysts for

the production of hydrogen and CNT via methane decomposition using high-loaded, silica-supported Ni and Fe (85–90 wt.% of the metal) at 550–700 °C.

Technical challenges with regard to catalyst deactivation and the separation of carbon product from catalyst still present a major roadblock to practical implementation of the metal-catalyzed methane decomposition process. More detailed discussion on metal-catalyzed TCD of methane can be found in reviews by Abbas and Wan Daud (2010) and Yan and Hoekman (2014).

17.3.4 Carbon-catalyzed methane decomposition

The use of carbon-based catalysts offers certain advantages over metal catalysts owing to their durability and low cost. In contrast to metal-based catalysts, carbon catalysts are sulfur- and temperature-resistant and may not require a catalyst-carbon separation stage (Muradov, 1998). A variety of carbon materials were screened by Muradov et al. (2001, 2005), who demonstrated that efficient catalytic methane decomposition can be accomplished over disordered high-surface area carbons (e.g., AC, CBs) at a temperature range typical of the SMR process (800–900 °C). The results indicated, however, that the initial reaction rate of carbon-catalyzed methane decomposition could not be sustained, and it gradually dropped as a result of the buildup of catalytically inactive turbostratic carbon.

The production of hydrogen by TCD of methane in a fluidized-bed reactor using a CB catalyst was reported by Dunker, Kumar, and Mulawa (2006). Kim et al. (2004) and Bai, Chen, Li, and Li (2005) conducted a kinetic study of methane catalytic decomposition over AC. Moliner, Suelves, Lazaro and Moreno (2005) investigated the effect of textural properties and surface chemistry of AC on the TCD of methane. Serrano et al. studied methane decomposition over ordered mesoporous carbons (2008) as well as a variety of commercial carbon materials (2009).

Several approaches to improving the sustainability of the methane TCD process have been investigated, in particular, by adding small amounts of oxidizing agents (e.g., steam, oxygen, CO_2) to the methane feedstock (Dufour et al., 2008) or by partially gasifying carbon in a continuous process involving carbon particles circulating between a TCD reactor and a heater/regenerator in a fluidized state (Muradov, Chen, & Smith, 2005). Muradov, Smith, Bockerman, and Scammon (2009) proposed a sustainable TCD process involving continuously generated catalytically active carbon aerosols produced by a nonthermal plasma device integrated with a TCD reactor.

17.4 Use of nuclear heat input for fossil-based hydrogen production

17.4.1 Integration of SMR with high-temperature nuclear reactors

Because of the high endothermicity of SMR, coal gasification, and other fossil fuel-based hydrogen production processes, significant part of CO_2 emissions originate

from the combustion of fuels (for example, in the case of SMR, about a third of the overall CO_2 produced). Therefore, significant research effort has been focused on using alternative noncarbon energy sources to provide energy input to endothermic processes. This could potentially lead to a dramatic reduction in CO_2 emissions and conservation of NG and other valuable fossil resources. From this viewpoint, the potential of using high-temperature nuclear heat has long attracted the interest of researchers.

According to several early technical evaluations, the SMR process has great potential for integration with a high-temperature nuclear heat source (Jiacoletti, 1977; Peterma, 1975). Researchers at General Atomic company have been conducting feasibility studies on a nuclear-heated methane reforming plant since the 1970s (Peterma, 1975). According to the proposed concept, helium (He) is heated to 950 °C in a high-temperature gas-cooled nuclear reactor (HTGR) and circulated in indirectly heated heat exchangers countercurrent to methane and steam flowing through the reformer tubes, releasing its sensible heat and being cooled from 950 °C to about 600 °C. In the preferred reformer tube design, the reformed gas flows through an inner helical catalyst-filled tube. The nuclear-heated system can potentially reach an efficiency of 85%, which substantially exceeds that of the SMR process with the conventional heat input (74%). These reactors (called EVA reactors) can be used to produce hydrogen from syngas or, in conjunction with a methanation reactor, to transfer heat for long distances (the latter option is termed the ADAM-EVA system).

Researchers at the US DOE Idaho National Laboratory (INL) conducted technical and economic evaluation of integrating HTGR with SMR (Gandrik, Wood, Patterson, & Mills, 2010). In the studied system, the HTGR provides steam and high-temperature heat (with an outlet temperature of 750 °C) for SMR (for more mature HTGR, temperatures up to 950 °C are anticipated). Two options for the HTGR-integrated SMR hydrogen production plant were analyzed: without and with CO_2 capture. Figure 17.12 depicts a block diagram of an HTGR-integrated SMR with CO_2 capture.

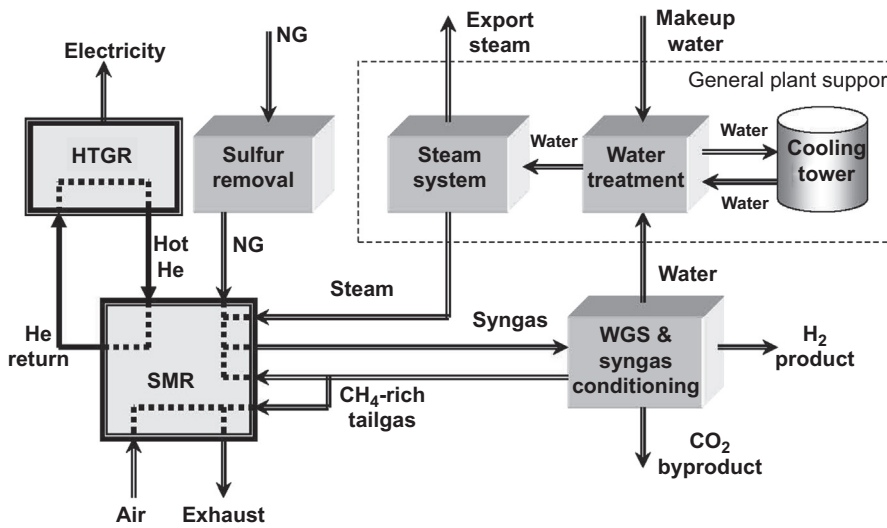

Figure 17.12 Block flow diagram of an HTGR-integrated SMR with CO_2 capture. Gandrik et al. (2010).

Main conclusions of the INL study are as follows. Integrating HTGR with an SMR plant is economically viable: Hydrogen can be produced for less than $2.50/kg (at the internal rate of return of 15%). Assuming an NG price of $6.50 per 1,000 standard cubic feet (or 28.3 m^3), an HTGR-SMR plant without carbon capture can produce H_2 for less than conventional SMR when a carbon tax of $20/ton CO_2 or higher is imposed. For the case of an HTGR-SMR plant with carbon capture (with the same assumption), a carbon tax of $75/ton CO_2 or higher should be imposed. Evidently, HTGR-SMR integration appears to be more advantageous for cases in which no carbon capture is included. However, the analysis shows that the HTGR-SMR-CCS scenario becomes preferable when a carbon tax of $35/ton CO_2 is imposed. The amounts of CO_2 captured and emitted from the HTGR-SMR plant for different cases are shown in Table 17.2 (for comparison, data for a stand-alone SMR plant with and without carbon capture are also included in the table).

De Falco, Salladini, Palo, and Iaquanello (2011) analyzed the integration of a high-temperature nuclear reactor with a steam methane reformer membrane module. The advantage of the proposed membrane reformer configuration is that the presence of the integrated Pd membrane results in the removal of produced H_2 and shifting chemical equilibrium, thus enhancing the final product yield and decreasing the operational temperature. The process may thus be operated at 600−650 °C (compared with 850−880 °C in conventional SMR plants) and using a lower-temperature nuclear heat source.

17.4.2 Use of nuclear heat input for methane decomposition

There have also been studies on the potential application of HTGR as a heat input source for methane thermal decomposition. Serban, Lewis, Marshall, and Doctor (2003) proposed the concept of using Generation IV high-temperature nuclear reactors to provide process heat for producing hydrogen and carbon by methane direct contact

Table 17.2 Amount of CO_2 captured and emitted by conventional SMR and HTGR-SMR with and without carbon capture option

Analyzed case	Amount of CO_2 captured, t CO_2/t H_2	Amount of CO_2 emitted, t CO_2/t H_2
Conventional SMR without carbon capture	–	9.77
Conventional SMR with carbon capture	6.53	2.61
HTGR-integrated SMR without carbon capture	–	8.27
HTGR-integrated SMR with carbon capture	6.47	1.60

Gandrik et al. (2010).

pyrolysis. According to the concept, high-temperature heat is transferred from a nuclear reactor to a methane thermal cracking unit. Methane is bubbled through a bed of low-melting point metals (Pb or Sn) at a temperature range of 600−900 °C. The advantage of the proposed system is the ease of separating the carbon product from the heat transfer media (by buoyancy owing to differences in densities) and contact with the liquid metal coolant. However, because of the low catalytic activity of the used metals, the methane conversion was low (at 750 °C, methane conversion was only 9%).

17.5 Solar-powered hydrogen production from hydrocarbons

17.5.1 Solar reforming of methane

Solar concentrating systems can provide process heat at a wide range of temperatures depending on the solar flux concentration ratio, which is determined by the type of a concentrator: trough, tower, or dish systems (Steinfeld & Meier, 2004). The application of solar concentrators to SMR has been extensively studied by many research teams using different irradiation sources (solar furnaces, concentrators, and simulators), solar-receiver designs, reactor configurations (e.g., with indirect and direct irradiation), and reforming catalysts (e.g., Aristov, Fedoseev, & Parmon, 1997; Tamme, Epstein, Fisher, Sugarmen, & Buck, 2001; Yokota et al., 2000). Researchers at ETH (Switzerland) studied an indirectly irradiated solar reforming reactor consisting of a pentagonal cavity receiver containing a set of Inconel tubes filled with Rh (2%)/Al_2O_3 catalyst (Steinfeld & Meier, 2004). Although the system had the advantage of eliminating the transparent window, its shortcomings relate to limitations imposed by the construction materials. A volumetric-type solar reactor in which an absorber consisted of an array of ceramic pins, and which included alumina-supported Ru promoted with La and Mn oxides as catalyst, was tested in SMR and CO_2-methane reforming reactions in the temperature range of 500−1,100 °C (Berman, Karn, & Epstein, 2006).

Direct-irradiated solar reactors have the advantages of providing efficient radiation heat transfer directly to the reaction zone and, in some cases, photochemically stimulating the reaction kinetics. Experimental studies of solar-heated SMR under direct illumination of a catalyst by concentrated light was reported by researchers from the Boreskov Institute of Catalysis (Aristov et al., 1997). It was demonstrated that with this type of the reactor-receiver with a transparent wall, both the specific power density of the device (measured at 50−100 W/cm^3) and the specific rate of hydrogen production (measured at 130 Ndm^3/h per 1 g of catalyst) increased significantly compared with an indirectly radiated stainless-steel reactor. The authors attributed the increase in reaction rate to the significant intensification of energy absorption by the catalyst bed. Yokota et al. (2000) investigated SMR over an Ni/Al_2O_3 catalyst using a Xe lamp as a solar simulator and found that at 850 °C and $H_2O/CH_4 = 1/1$ molar ratio, methane conversion exceeded 85%.

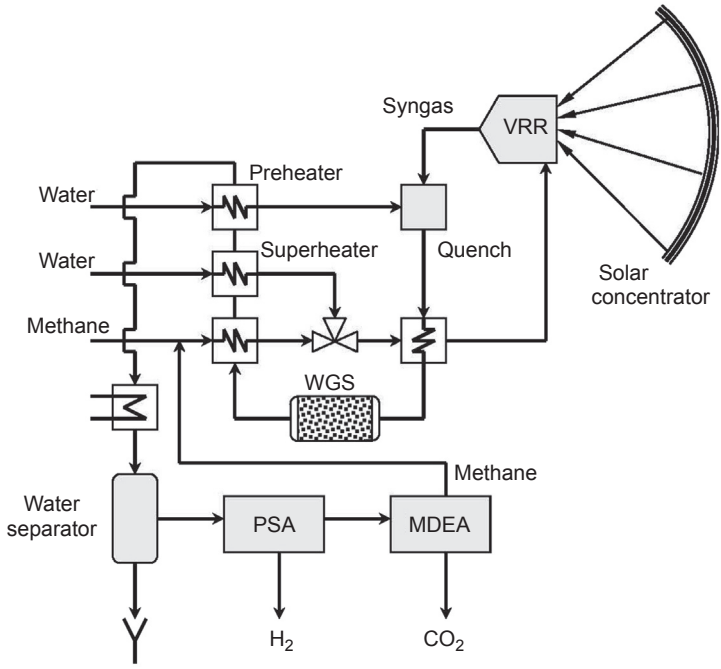

Figure 17.13 Block diagram of the solar methane reforming process. VVR, volumetric reactor receiver; MDEA, methyldiethanol amine. Temperature in VVR is 900 °C. H_2O:CH_4 = 1.5. Moller et al. (2006).

A team of researchers from DLR (Deutsches Zentrum für Luft- und Raumfahrt e.V.) and the University of Flensburg (Germany) analyzed solar-powered SMR using an innovative volumetric reactor receiver (VRR) in the framework of the EU project SOLREF (Moller, Kaucic, & Sattler, 2006). Figure 17.13 shows a block diagram of the proposed solar-SMR system.

Concentrated solar energy is absorbed in the VRR with heat transferred to the SOLASYS reformer vessel, where steam and methane (at an H_2O:CH_4 ratio of 1.5−3.0) react at about 900 °C, producing syngas. After the WGS unit, CO_2 and remaining methane are separated in PSA and subsequently in MDEA scrubber. The CO_2 yield was measured at 0.25 mol per mol H_2 at a reforming efficiency of 87%. The cost of hydrogen produced was estimated at €4.5−4.7/kWh H_2 (LHV), which is about 20% higher than the cost of conventional SMR-produced hydrogen.

Han et al. studied solar reforming of NG with the objective of cogenerating hydrogen and electricity with CO_2 removal (Han, Jin, & Lin, 2011). The authors of the study considered a heat input provided by a solar tower and a cavity-type solar reformer-receiver consisting of a series of vertical tubes filled with catalyst. Carbon dioxide was separated by the PSA system and liquefied. The system shows the potential to generate both hydrogen and electricity at a net overall power efficiency of 39.2%, and it can achieve 92% CO_2 removal.

17.5.2 Solar-powered decomposition of methane

Because the decomposition of methane is a high-temperature endothermic process, it lends itself to integration with a solar concentrating solar source. Steinfeld et al. (1997) demonstrated the technical feasibility of solar-powered methane decomposition using a reactor-receiver containing a fluidized bed of catalyst particulates. Experiments conducted at the Paul Scherrer Institute (Switzerland) 15-kW solar furnace involved a quartz reactor with a fluidized bed of Ni (90%)/Al_2O_3 catalyst and alumina grains positioned in the focus of the furnace. The catalyst particles were directly irradiated, which enabled efficient heat transfer to the reaction zone maintained at 577 °C and below (to prevent rapid catalyst deactivation). The system achieved 40% conversion of methane to H_2 in a single pass. The TCD of gaseous hydrocarbons CH_4 and C_4H_{10} into hydrogen and filamentous carbon using concentrated solar radiation was reported by Meier et al. (1999). At an average 30% conversion rate of CH_4 to H_2, two forms of filamentous carbon were produced in the solar experiments, depending on the nature of the catalyst: nanotubes were produced using Co/MgO catalyst and nanofibers were formed over Ni/Al_2O_3.

Kogan, Kogan, and Barak (2005) studied solar-driven decomposition of methane to hydrogen and carbon using a volumetric solar reactor-receiver. It was demonstrated that the efficient volumetric absorption of solar radiation could be achieved by adding a cloud of fine CB particles (about 0.1 g of CB particles per 1 m^3 of irradiated gas) to the reaction chamber. Solar thermal methane decomposition in a fluid-wall aerosol-flow reactor-receiver was reported by Dahl, Buechler, Weimer, Lewandowski, and Bingham (2004). The use of carbon aerosol particles for the efficient absorption of concentrated solar energy was also studied by Maag, Zanganeh, and Steinfeld (2009). Solar methane decomposition was carried out in a 5-kW directly radiated solar chemical reactor tested in a solar furnace in the temperature range of 1,300−1,600 K. Methane conversion of 95% was achieved at the residence time of 2 s with solar-to-chemical energy conversion efficiency measured at 16%. Patrianakos, Kostoglou, and Konstandopoulos (2012) analyzed the effect of seeding on the solar methane decomposition rate in a 10-MW solar thermal reactor with an indirect heating option. A modeling study of the effect of carbon particles seeding on solar reactors performance was conducted by Ozalp and Kanjirakat (2010). The application of solar aerosol technology to hydrogen production from liquid hydrocarbons (C7−C8) was reported by Ma, Lall, Aronhime, and Zachariah (2010). The highest hydrogen yield of 81% was obtained for *n*-octane at 1050 °C.

Abanades and Flamant (2005) reported a nozzle-type solar reactor for thermal methane decomposition. In the solar reactor, a nozzle made of graphite absorbed concentrated radiation provided by a 2-m-diameter solar furnace, and the absorbed heat was then transferred to the reagents. Methane-to-H_2 conversion was in the range of 30−90%. The team also studied a fluid-wall solar reactor (Abanades & Flamant, 2008). Thermal methane decomposition conducted in a medium-scale (10-kW) indirectly heated solar reactor containing four graphite tubular reaction zones was reported by Rodat, Abanades, and Flamant (2011). The solar reactor represented a cubic cavity receiver that absorbed concentrated solar radiation through a 9-cm quartz window.

Almost quantitative methane conversion to H_2 and CB was achieved at the temperature range of 1740−2070 K with some appreciable amount (up to 7%) of acetylene by-product.

17.5.3 Photoreforming of hydrocarbons to hydrogen

Photoreforming of hydrocarbons to hydrogen and CO_2 is a potentially attractive approach to converting solar photon energy to chemical energy of hydrogen because it can be carried out at near-ambient conditions, thus avoiding expensive solar concentrating systems. Because hydrocarbons absorb irradiation in a vacuum ultraviolet (UV) region (which are not present in the solar spectrum), production of hydrogen by direct solar photolysis of hydrocarbons is not feasible. The use of photocatalysts enables the conversion of hydrocarbons to H_2 under exposure to near-UV irradiation (wavelengths of 300−380 nm) that are present in the solar spectrum (about 4−5% of the total spectrum).

There is scarce information in the literature on photoreforming of hydrocarbons to H_2 or H_2-rich gases. Hashimoto, Kawai, and Sakata (1984) studied photoreforming of aliphatic and aromatic hydrocarbons to an H_2−CO_2 mixture using a Pt/TiO_2 photocatalyst suspended in deaerated water. The hydrocarbon−water−photocatalyst system was exposed to near-UV irradiation (wavelengths of 320 nm and greater) from a 500-W Xe lamp at 40−50 °C. Photoreforming of *n*-hexadecane ($C_{16}H_{34}$) can be represented as follows:

$$C_{16}H_{34} + 32H_2O + \text{light} \rightarrow 49H_2 + 16CO_2 \qquad \Delta G^o = 1{,}232\ \text{kJ/mol} \quad (17.2)$$

In particular, 4.14 mmol of H_2 was produced from 85 μmol of *n*-$C_{16}H_{34}$, which is close to the theoretical yield. The photocatalytic production of hydrogen with simultaneous functionalization of alkanes in a liquid phase in the presence of heteropolycompounds of Mo and W exposed to UV light ($\lambda > 260$ nm) was reported by Renneke and Hill (1986). Muradov and Rustamov (1988) reported a photocatalytic system based on aqueous solutions of isopolytungstates that, upon exposure to near-UV light, converted light alkanes (C3−C6) to hydrogen and functionalized hydrocarbons.

17.6 Conclusions

Intensive worldwide efforts are under way to tackle man-made CO_2 emissions and their potentially devastating impact on our planet's biosphere and climate. Currently, practically all industrial manufacturing of hydrogen is based on fossil fuels: primarily NG and coal. Paradoxically, based on the amount of CO_2 produced per unit of product, hydrogen plants are among the most carbon-intensive industrial facilities; even the "cleanest" of H_2 production processes: SMR produces close to 10 kg CO_2 per kilogram of H_2. This fact may diminish the environmental appeal of hydrogen as an environmentally clean fuel. There are three main approaches to low-carbon production of

hydrogen from fossil fuels: (1) the integration of hydrogen plants with CCS, (2) the production of CO_2-free hydrogen via dissociation (decomposition) of methane, and (3) the combination of hydrogen production processes with noncarbon energy sources such as nuclear or solar.

The deployment of CCS systems would prevent CO_2 emissions from reaching the atmosphere by capturing and securely storing CO_2 in such sinks as geologic formations, the ocean, and terrestrial ecosystems. However, the wide-scale implementation of CCS technologies currently faces three major challenges: (1) a significant reduction in cost, (2) understanding of storage reservoir options (e.g., its permanence, potential leakage rates), and (3) assessment of key risk factors associated with long-term ecological consequences of this approach (potential environmental impact, possible health hazard, public acceptance, etc.). Coupling of hydrogen plants with CCS is still at an early stage of commercial deployment; Air Products and Chemicals, Inc., with the support of US DOE, is working on retrofitting its two steam methane reformers located within the Valero refiner in Port Arthur (Texas) to capture and sequester CO_2.

Because of the high cost and long-term environmental uncertainties of the CCS approach, there have been proposals to produce H_2 via dissociation of methane or other light hydrocarbons in an oxidant-free environment. This single-step approach would not only avoid direct CO_2 production but produce a value-added product: clean carbon, which could substantially improve the process economics. The major problem with practical realization of the methane dissociation process is that owing to strong C−H bonds, methane is one of the most stable organic molecules, and thus the process would require energy input in the form of either very high-temperature heat or electrical discharge (or plasma) energy. The use of metal- or carbon-based catalysts could significantly reduce the methane decomposition temperature, but this technological approach is still in the early R&D stage.

It has been recognized that the use of carbon-free (i.e., nonfossil) energy sources as a means of energy input to H_2 manufacturing processes would result in a dramatic reduction in the amount of CO_2 emissions and substantial conservation of fossil resources. From this viewpoint, the use of high-temperature nuclear and solar heat sources has long attracted the interest of researchers. A number of feasibility and techno-economic studies on the technological use of high-temperature nuclear reactors (e.g., Generation IV reactors) pointed out that the SMR process has the greatest potential for near-term integration with a nuclear heat source.

Similarly, the use of high-temperature solar heat source (e.g., by means of solar concentrators) can potentially provide the necessary energy input to endothermic methane steam (or CO_2) reforming, coal gasification, or methane decomposition processes. Advantageously, solar concentrators can achieve much higher temperatures than nuclear reactors (e.g., temperatures of 1270 °C and higher at a concentration ratio of 5000 and higher can be achieved using a cavity receiver-type reactor configuration). Solar reforming of methane has been extensively studied in solar furnaces as well as in solar simulators using different reactor configurations and catalysts. The use of a high-temperature solar source could be especially advantageous for a methane decomposition reaction because it could provide temperatures up to

1500−2000 °C, which could make the use of catalysts unnecessary (thus avoiding catalyst deactivation and other related problems). Because of the lack of a CO_2 by-product, solar methane decomposition could provide a means of zero-CO_2 production of hydrogen from NG.

17.7 Future trends and outlook

It is widely acknowledged that to eliminate or drastically reduce carbon emissions from H_2 manufacturing processes, extensive deployment of CCS systems in the hydrogen industry will be a critical target. However, to date, CCS technology has a high financial barrier with no economic stimuli or regulatory drivers; thus, the integration of H_2 production with EOR or other beneficial reuse options could provide a substantial economic payback, facilitating its introduction to the market.

The wide-scale deployment of the CCS technology in hydrogen plants requires significant improvements in SMR performance through the development of novel, more active, and durable catalysts (in particular, WGS catalysts) and efficient reactors. There is also room for improvements in the CO_2 capture stage by introducing innovative membranes, adsorbents, and absorbents with higher CO_2-capturing capacity and better durability. In particular, the development and implementation of new efficient (so-called "second-generation") solvents would make it possible to remove both CO_2 and SO_2 from flue gases, thus significantly improving the process economics. Longer-term technological developments in CO_2 capture from diluted streams will most likely involve ionic liquids, phase change solvents, and high-capacity adsorbents that are currently at the R&D stage. Process optimization and integration on component and system levels should also be pursued to facilitate the market penetration of hydrogen plants coupled with CO_2 capture.

The advantages of thermocatalytic methane decomposition as a CO_2-free alternative to SMR are that it is technologically simple (a one-step process) and does not require an expensive CCS system. However, the competitiveness of this approach will depend on solving two main problems: (1) the development of an energy-efficient sustainable methane decomposition process operating at temperatures below 800−900 °C with minimal electricity input, and (2) finding sufficiently large markets for carbon coproducts. Thus, future work will probably focus on developing active and stable catalysts and engineering aspects of the technology, as well as expanding carbon products to new markets, such as advanced composites and construction and building materials.

Nuclear energy does not inherently involve the direct production of CO_2; thus, it has the potential to make significant contributions to low-to-zero carbon production of hydrogen. Emerging Generation IV nuclear reactors will be capable of providing high-temperature heat for endothermic SMR and TCD processes. Future progress in this direction will likely relate to the development of novel types of reformer-reactors optimally integrated with a nuclear source, including membrane-type reactors.

The use of concentrating solar energy is another promising technological option for curbing carbon emissions. Concentrating solar energy is becoming increasingly cost-competitive with traditional energy sources in many countries around the globe. Although most applications of solar concentrators are now concerned with power generation, one can expect their penetration into the hydrogen production market. Of particular importance is the capacity of solar concentrating systems to provide long-term storage of thermal energy in a wide range of temperatures (400−1,000 °C), which can be advantageous for the SMR and TCD processes. Future developments in this area will focus on efficient solar-receiver reactors with improved solar radiation absorption characteristics and integrated thermal storage systems.

17.8 Sources of further information

Hydrogen Fuel. Production, Transport and Storage. Ram Gupta (ed.). CRC Press, Boca Raton, 2009. This book is a good introduction to hydrogen production technologies, including comprehensive overviews of H_2 production from hydrocarbons and coal. It contains chapters on nuclear and solar H_2 production and CO_2 sequestration.

Hydrogen and Syngas Production and Purification Technologies. K. Liu, C.Song and V.Subramani (Eds.). John Wiley & Sons, Inc., 2010. This book contains chapters on steam methane reforming and CO_2-selective membranes for hydrogen fuel processing.

Carbon-Neutral Fuels and Energy Carriers. Nazim Muradov and Nejat Veziroğlu (Eds.). CRC Press, Boca Raton, 2012. This book is a reference on carbon-neutral technologies, including low-carbon production of H_2 from different sources. Special emphasis is on electricity and H_2 production integrated with CO_2 capture and storage.

Nazim Muradov. *Liberating Energy From Carbon: Introduction to Decarbonization*. Springer, NY, 2014. This book is a comprehensive introduction to fossil fuel decarbonization. A detailed discussion on CO_2 capture, use, and storage technologies is provided.

IPCC Special Report on Carbon Dioxide Capture and Storage. Prepared by Working Group III of the Intergovernmental Panel on Climate Change. Intergovernmental Panel on Climate Change. In: Metz B, Davidson O, de Coninck H et al. (eds). Cambridge University Press, Cambridge, UK and NY, USA. This book is an excellent reference book on CO_2 capture and storage technologies.

International Energy Agency. *Energy Technology Perspectives 2012.* This book by IEA provides up-to-date information on the status of clean energy technologies, including carbon-free electricity, hydrogen, and advanced biofuels.

Hydrogen Economy. Opportunities and Challenges. Michael Ball, Martin Witschel (eds.). Cambridge Univ. Press, Cambridge, 2009. The book provides a broad overview of hydrogen production, storage, and use systems. It contains chapters on fossil H_2 production and carbon capture and sequestration technologies.

List of acronyms

AC	Activated carbon
APC	Air Products and Chemicals, Inc.
CB	Carbon black

CCS	Carbon capture and storage
CNT	Carbon nanotubes
DLR	Deutsches Zentrum für Luft- und Raumfahrt e.V. (Germany)
DOE	US Department of Energy
EOR	Enhanced oil recovery
ESA	Electric swing adsorption
GWP	Global warming potential
HTGR	High-temperature gas-cooled nuclear reactor
IEA	International Energy Agency
IGCC	integrated gasification combined cycle
INL	Idaho National Laboratory (USA)
MDEA	Methyldiethanolamine
MEA	Monoethanolamine
MOF	Metal organic frameworks
NETL	National Energy Technology Laboratory (USA)
NG	Natural gas
NRC	National Research Council (USA)
NTP	Nonthermal plasma
PSA	Pressure swing adsorption
SMR	Steam methane reforming
TCD	Thermocatalytic decomposition
TSA	Temperature swing adsorption
UV	Ultraviolet
VRR	Volumetric reactor-receiver
VSA	Vacuum swing adsorption
WGS	Water gas shift

References

Abanades, S., & Flamant, G. (2005). Production of hydrogen by thermal methane splitting in a nozzle-type laboratory-scale solar reactor. *International Journal of Hydrogen Energy, 30*, 843−853.

Abanades, S., & Flamant, G. (2008). Hydrogen production from solar thermal dissociation of methane in a high-temperature fluid-wall chemical reactor. *Chemical Engineering and Processing: Process Intensification, 47*, 490−498.

Abbas, H., & Wan Daud, W. (2010). Hydrogen production by methane decomposition: a review. *International Journal of Hydrogen Energy, 35*, 1160−1190.

Aiello, R., Fiscus, J., Loye, H., & Amiridis, M. (2000). Hydrogen production via the direct cracking of methane over Ni/SiO_2: catalyst deactivation and regeneration. *Applied Catalysis A, 192*, 227−234.

Aristov, Y., Fedoseev, V., & Parmon, V. (1997). High-density conversion of light energy via direct illumination of catalyst. *International Journal of Hydrogen Energy, 22*, 869−874.

Ashok, J., Kumar, S., Venugopal, A., Kumari, V., & Subrahmanyam, M. (2007). CO_x free H_2 production via catalytic decomposition of CH_4 over Ni supported on zeolite catalysts. *Journal of Power Sources, 164*, 809−814.

Audus, H., Kaarstad, O., & Kowal, M. (1996). Decarbonization of fossil fuels: hydrogen as an energy vector. In *Proc. 11th world hydrogen energy conf.* Stuttgart, Germany.

Baade, W., Farnand, S., Hutchinson, R., & Welch, K. (2012). *CO_2 capture from SMRs: A demonstration project*. Hydrocarbon Processing http://www.hydrocarbonprocessing.com/article/3081308/co2-capture-from-smrs-a-demonstration-project.html. Accessed 27.12.13.

Babaritskiy, A. (2000). Plasma catalysis processes for hydrogen and syngas production from hydrocarbons. In *Proc. 13th world hydrogen energy conf., Beijing, China, 2000*.

Bachu, S. (2003). Screening and ranking of sedimentary basins for sequestration of CO_2 in geological media. *Environmental Geology, 44*, 277−289.

Bai, Z., Chen, H., Li, B., & Li, W. (2005). Catalytic decomposition of methane over activated carbon. *Journal of Analytical and Applied Pyrolysis, 73*, 335−341.

Berman, A., Karn, R., & Epstein, M. (2006). *Steam reforming of methane on Ru-catalysts for solar hydrogen production*. Abstracts of 232 ACS National Meeting, Paper: FUEL-140. San Francisco, CA.

Brennecke, J., & Gurkan, B. (2010). Ionic liquids for CO_2 capture and emission reduction. *The Journal of Physical Chemistry Letters*, 3459−3464.

Bromberg, L., Cohn, D., Rabinovich, A., O'Brien, C., & Hochgreb, S. (1998). Plasma reforming of methane. *Energy & Fuels, 12*, 11−18. http://dx.doi.org/10.1021/ef9701091.

Choudhary, T., Sivadinarayana, C., Chusuei, C., Klinghoffer, A., & Goodman, D. (2001). Hydrogen production via catalytic decomposition of methane. *Journal of Catalysis, 199*, 9−18.

Ciferno, J., Fout, T., Jones, A., & Murphy, J. (2009). Capturing carbon from existing coal-fired power plants. *Chemical Engineering Progress*, 33−47. April.

Collodi, G. (2010). *Hydrogen production via steam reforming with CO_2 capture*. Viewed 10.02.13 http://www.audic.it/CICAP4/webpapers/7Collodi.pdf.

Cortes, G., Tzimas, E., & Peteves, S. (2009). Technologies for coal based hydrogen and electricity co-production power plants with CO_2 capture. *European Commission Joint Research Centre Institute for Energy*. http://dx.doi.org/10.2790/23969. Viewed 05.03.10 http://www.energy.eu/publications/a05.pdf.

Czernichowski, A., Czernichowski, P., & Ranaivosolarimanana, A. (1996). Plasma pyrolysis of natural gas in gliding arc reactor. In *Proc. 11th world hydrogen energy conf.* Stuttgart, Germany.

Dahl, J., Buechler, K., Weimer, A., Lewandowski, A., & Bingham, C. (2004). Solar thermal dissociation of methane in a fluid-wall aerosol flow reactor. *International Journal of Hydrogen Energy, 29*, 725−736.

De Falco, M., Salladini, A., Palo, E., & Iaquanello, G. (2011). Reformer and membrane modules (RMM) for methane conversion powered by a nuclear reactor. In P. Tsvetkov (Ed.), *Nuclear power − Deployment, operation and sustainability*, ISBN: 978-953-307-474-0.

DOE/NETL. (2010). Assessment of hydrogen production with CO_2 capture. In *Baseline state-of-the-art plants* (Vol. 1) US DOE National Energy Technology Laboratory. DOE/NETL Final report 2010/1434. http://www.netl.doe.gov/energy-analyses/pubs/H2_prod_vol1_2010.pdf

Dufour, A., Celzard, A., Fierro, V., Martin, E., Broust, F., & Zoulalian, A. (2008). Catalytic decomposition of methane over a wood char concurrently activated by a pyrolysis gas. *Applied Catalysis, A: General, 346*, 164−173.

Dunker, A., Kumar, S., & Mulawa, P. (2006). Production of hydrogen by thermal decomposition of methane in a fluidized bed reactor- effect of catalyst, temperature and residence time. *International Journal of Hydrogen Energy, 31*, 473−484.

Du, N., Park, H., Robertson, G., Gal-Cin, M., Visser, T., Scoles, L., et al. (2011). Polymer nanosieve membranes for CO_2-capture applications. *Nature Materials, 10*, 372−375.

Ermakova, M., & Ermakov, D. (2002). Ni/SiO_2 and Fe/SiO_2 catalysts for production of hydrogen and filamentous carbon via methane decomposition. *Catalysis Today, 77*, 225−235.

Fauth, D., & Hoffman, J. (2004). CO_2 scrubbing with novel lithium zirconate sorbents. *Preprint Paper − American Chemical Society, 49*(1), 310−311.

Ferguson, R., Van Leeuwen, T., & Kuuskraa, V. (2008). Storing CO_2 with enhanced oil recovery. In *7th Annual conf. carbon capture and sequestration*, *May 5−8, Pittsburgh, PA*.

Feron, H., & Asbroek, N. (2004). New solvents based on aminoacid salts for CO_2 capture from flue gases. In *7th Intern. conf. greenhouse gas technologies, Sept. 5−9, Vancouver, Canada*.

Fulcheri, L., & Schwob, Y. (1995). From methane to hydrogen, carbon black and water. *International Journal of Hydrogen Energy, 20*, 197−202.

Gandrik, A., Wood, R., Patterson, M., & Mills, P. (2010). *HTGR-integrated hydrogen production via steam methane reforming (SMR) economic analysis*. Idaho National Laboratory. Doc. ID TEV-954. Project # 23843, 9/15/2010.

Global CCS Institute. (2009). *Strategic analysis of the global status of carbon capture and storage*. Final report http://www/globalccsinstitute.com/downloads/reports/2009/worley/foundation-report-1-rev0.pdf. Viewed 03.08.10.

Global CCS Institute. (2013). Status of carbon capture and storage update. *Carbon Capture Journal*. March−April, no.32. Viewed 19.09.13.

Gray, D., & Tomlinson, G. (2003). Hydrogen from coal. *Mitretek Technical Paper MTR-2003-13* (prepared for US DOE NETL).

Han, W., Jin, H., & Lin, R. (2011). A novel multifunctional energy system for CO_2 removal by solar reforming of natural gas. *Journal of Solar Energy Engineering, 133*. pp. 041004−04101 − 041004−04108.

Hashimoto, K., Kawai, T., & Sakata, T. (1984). Photocatalytic reactions of hydrocarbons and fossil fuels with water. Hydrogen production and oxidation. *Journal of Physical Chemistry, 88*, 4083−4088.

He, H., Li, W., Zhong, M., Konkolewicz, D., Wu, D., & Yaccato, K. (2013). Reversible CO_2 capture with porous polymers using the humidity swing. *Energy & Environmental Science, 6*, 488−493. http://dx.doi.org/10.1039/c2ee24139k.

International Energy Agency. (2007). *Hydrogen production and distribution: IEA energy technology essentials*. Paris: OECD/IEA.

International Energy Agency. (2011). *CO_2 emissions from fuel combustion*. Paris, France: IEA Report.

International Energy Agency. (2012). *Energy technology perspectives. Pathways to a clean energy system*. Paris, France: IEA/OECD.

International Energy Agency. (2013a). *Tracking clean energy progress. IEA input to the clean energy ministereal*. Paris: IEA. www.iea.org/publications/TCEP_web.pdf. Viewed 10.09.13.

International Energy Agency. (2013b). *International energy agency. Technology roadmap. Carbon capture and storage*. http://www.iea.org/publications/freepublications/publication/TechnologyRoadmapCarbonCaptureandStorage.pdf. Viewed 05.09.13.

International Energy Agency. (March 1996). *Decarbonization of fossil fuels*. IEA Report PH2/2. Cheltenham, UK: IEA Greenhouse Gas R&D Programme.

IPCC. (2005). IPCC special report on carbon dioxide capture and storage. Prepared by working group III of the intergovernmental panel on climate change. In B. Metz, O. Davidson, H. de Coninck, et al. (Eds.), *Intergovernmental panel on climate change*. Cambridge, UK and NY, USA: Cambridge University Press.

IPCC. (2007). *The intergovernmental panel on climate change 4th assessment report, climate change 2007. The physical science basis*. Cambridge and NY: Cambridge University Press.

Jana, P., O'Shea, V., Coronado, J., & Serrano, D. (2011). Co-production of graphene sheets and hydrogen by decomposition of methane using cobalt based catalysts. *Energy & Environmental Science, 4*, 778−783. http://dx.doi.org/10.1039/C0EE00490A.

Jiacoletti, R. (1977). Hydrogen from nuclear energy. In K. Cox, & K. Williamson (Eds.), *Hydrogen: Its technology and applications* (Vol. 4, pp. 119−144). Boca Raton, chap: CRC Press.

Kim, M., Lee, E., Jun, J., Kong, S., Han, G., & Kwon, B. (2004). Hydrogen production by catalytic decomposition of methane over activated carbons: kinetic study. *International Journal of Hydrogen Energy, 29*, 187−193.

Koerts, T., Deelen, M., & van Santen, R. (1992). Hydrocarbon formation from methane by a low-temperature two-step reaction sequence. *Journal of Catalysis, 138*, 101−114.

Kogan, A., Kogan, M., & Barak, S. (2005). Production of hydrogen and carbon by solar thermal methane splitting. III. Fluidization, entrainment and seeding powder particles into a volumetric solar receiver. *International Journal of Hydrogen Energy, 30*, 35−43.

Kreutz, T., Williams, P., Chiesa, P., & Consonni, S. (2005). Co-production of hydrogen, electricity and CO_2 from coal with commercially ready technology. *International Journal of Hydrogen Energy, 30*, 769−784.

Li, Y., Chen, J., Qin, Y., & Cheng, L. (2000). Simultaneous production of hydrogen and nanocarbon from decomposition of methane on nickel-based catalyst. *Energy & Fuel, 14*, 1188−1194. http://dx.doi.org/10.1021/ef0000781.

Lin, H., Merkel, T., & Baker, R. (2007). The membrane solution to global warming. In *6th Annual conf. carbon capture and sequestration, Pittsburgh, PA*.

Lynum, S., & Gaudernack, B. (1996). Hydrogen from natural gas without release of CO_2 to the atmosphere. In *Proc. 11th world hydrogen energy conf., Stuttgart, Germany*.

Maag, G., Zanganeh, G., & Steinfeld, A. (2009). Solar thermal cracking of methane in a particle-flow reactor for the co-production of hydrogen and carbon. *International Journal of Hydrogen Energy, 34*, 7676−7685.

Ma, X., Lall, A., Aronhime, N., & Zachariah, M. (2010). Catalytic decomposition of liquid hydrocarbons in an aerosol reactor: a potential route to hydrogen production. *International Journal of Hydrogen Energy, 35*, 7476−7484.

Meier, A., Kirillov, V., Kuvshinov, G., Mogilnykh, Y., Reller, A., & Steinfeld, A. (1999). Solar thermal decomposition of hydrocarbons and carbon monoxide for the production of catalytic filamentous carbon. *Chemical Engineering and Science, 54*, 3341−3348.

Millward, A., & Yaghi, O. (2005). Metal-organic frameworks with exceptionally high capacity for storage of carbon dioxide at room temperature. *Journal of the American Chemical Society, 127*, 17998−17999.

Moliner, R., Suelves, I., Lazaro, M., & Moreno, O. (2005). Thermocatalytic decomposition of methane over activated carbons: influence of textural properties and surface chemistry. *International Journal of Hydrogen Energy, 30*, 293−300.

Moller, S., Kaucic, D., & Sattler, C. (2006). Hydrogen production by solar reforming of natural gas: a comparison study of two possible process configurations. *Transactions of the ASME, 128*, 16−23.

Muradov, N. (1998). CO_2-free production of hydrogen by catalytic pyrolysis of hydrocarbon fuel. *Energy & Fuel, 12*, 41−48.

Muradov, N. (2001). Catalysis of methane decomposition over elemental carbon. *Catalysis Communications, 2*, 89−94.

Muradov, N. (2005). Catalytic activity of carbon for methane decomposition reaction. *Catalysis Today, 102-103*, 225−233.

Muradov, N. (2009). Production of hydrogen from hydrocarbons. In R. Gupta (Ed.), *Hydrogen fuel. Production, transport and storage* (pp. 33−102). Boca Raton: CRC Press (Chapter 2).

Muradov, N. (2014). *Liberating Energy from Carbon: Introduction to decarbonization*. NY: Springer.

Muradov, N., Chen, Z., & Smith, F. (2005). Fossil hydrogen production with reduced CO_2 emission: modeling thermocatalytic decomposition of methane in a fluidized bed of carbon particles. *International Journal of Hydrogen Energy, 30*, 1149−1158.

Muradov, N., & Rustamov, M. (1988). Photocatalytic activation of low alkanes in aqueous solutions of polyoxocomplexes of tungsten. *Accounts of USSR Academy of Sciences, 303*, 656−659 (in Russian).

Muradov, N., Smith, F., Bockerman, G., & Scammon, K. (2009). Thermocatalytic decomposition of natural gas over plasma-generated carbon aerosols for sustainable production of hydrogen and carbon. *Applied Catalysis A: General, 365*, 292−300. http://dx.doi.org/10.1016/j-apcata.2009.06.031.

Muradov, N., & Veziroğlu, N. (Eds.). (2012). *Carbon-neutral fuels and energy carriers*. Boca Raton: CRC Press.

NETL. (2010). *Worldwide gasification database online*. Pittsburgh, PA: National Energy Technology Laboratory. www.netl.doe.gov/coalpower/gasification/models/dtbs.pdf. Viewed 05.07.12.

Nozaki, T., Kimura, Y., & Okazaki, K. (2002). Carbon nanotubes and hydrogen co-production from methane using atmospheric pressure non-equilibrium plasma. In *Proc. 16th ESCAMPIG and 5th ICRP joint conf. (Grenoble, France)*.

NRC. (2004). The hydrogen economy: Opportunities, costs, barriers and R&D needs (239 pp). Washington DC: National Research Council and National Academy of Engineering, National Academies Press.

Ozalp, N., & Kanjirakat, A. (2010). A CFD study on the effect of carbon particle seeding for the improvement of solar reactors performance. *ASME Journal of Heat Transfer, 132*, 122901−122908. http://dx.doi.org/10.1115/1.4002173.

Patrianakos, G., Kostoglou, M., & Konstandopoulos, A. (2012). Effect of seeding on hydrogen and carbon particle production in a 10 MW solar thermal reactor for methane decomposition. *International Journal of Hydrogen Energy, 37*, 16570−16580.

Peterma, D. (1975). Studies of the use of high temperature nuclear heat from an HTGR for hydrogen production. *General Atomic Company Report GA-A11391* (San Diego, CA, USA).

Piao, L., Chen, J., Chang, L., & Lin, J. (2002). Methane decomposition to carbon nanotubes and hydrogen on an alumina supported nickel aerogel catalyst. *Catalysis Today, 74*, 145−155.

Renneke, R., & Hill, C. (1986). Homogeneous catalytic photochemical functionalization of alkanes by polyoxometalates. *Journal of the American Chemical Society, 108*, 3528−3529.

Reshetenko, T., Avdeeva, L., Ismagilov, Z., Chuvilin, A., & Ushakov, V. (2003). Carbon capacious Ni−Cu−Al_2O_3 catalysts for high-temperature methane decomposition. *Applied Catalysis A: General, 247*, 51−63.

Resnick, K., Yeh, J., & Pennline, H. (2004). Aqua ammonia process for simultaneous removal of CO_2, SO_2 and NOx. *International Journal of Environmental Technology and Management, 4*(1/2), 89−104.

Rochelle, G. (2009). Amine scrubbing for CO_2 capture. *Science, 325*, 1652−1654.

Rodat, S., Abanades, S., & Flamant, G. (2011). Co-production of hydrogen and carbon black from solar thermal methane splitting in a tubular reactor prototype. *Solar Energy, 85*, 645−652.

Scholz, W. (1993). Processes for industrial production of hydrogen and associated environmental effect. *Gas Seperation & Purification, 7*, 131−139.

Serban, M., Lewis, M., Marshall, C., & Doctor, R. (2003). Hydrogen production by direct contact pyrolysis of natural gas. *Energy Fuels, 17*(3), 705−713. http://dx.doi.org/10.1021/ef020271q.

Serrano, D., Botas, J., & Guil-Lopez, R. (2009). H_2 production from methane pyrolysis over commercial carbon catalysts: kinetic and deactivation study. *International Journal of Hydrogen Energy, 34*, 4488−4494.

Serrano, D., Botas, J., Pizarro, P., Guil-Lopez, R., & Gomez, G. (2008). Ordered mesoporous carbons as highly active catalysts for hydrogen production by CH_4 decomposition. *Chemical Communications*, 6585−6587.

Shpilrain, E., Shterenberg, V., & Zaichenko, V. (1999). Comparative analysis of different natural gas pyrolysis methods. *International Journal of Hydrogen Energy, 24*, 613−624. http://dx.doi.org/10.1016/S0360-3199(98)00114-1.

Simbeck, D. (2005). Hydrogen costs with CO_2 capture. In *7th Intern. conf. greenhouse gas control technologies* (Vol. II, pp. 1059−1066). Oxford, UK: Elsevier Science.

Spath, P., & Mann, M. (2000). Life cycle assessment of hydrogen production via natural gas steam reforming. *Technical Report*. NREL/TP-570-27637 Golden, CO.

Steinberg, M. (1998). Production of hydrogen and methanol from natural gas with reduced CO_2 emission. *International Journal of Hydrogen Energy, 23*, 419−425.

Steinberg, M. (1999). Fossil fuel decarbonization technology for mitigating global warming. *International Journal of Hydrogen Energy, 24*, 771−777.

Steinberger-Wilckens, R., Trumper, S., Madsen, A., & Norgaard, P. (2008). Potential of emerging and future CO_2-neutral hydrogen sources on the European scale. *Roads2HyCom*. Report number: R2H2008PU.1. http://www.roads2hy.com/r2h_downloads/roads2hycom%20r2h2008pu%20-%20potential%20of%20co2-neutral%20h2%20sources%20in%20europe.pdf. Viewed 10.12.13.

Steinfeld, A. (1997). Production of filamentous carbon and hydrogen by solar thermal catalytic cracking of methane. *Chemical Engineering and Science, 52*, 3599−3603.

Steinfeld, A., & Meier, A. (2004). Solar fuels and materials. *Encyclopedia of Energy, 5*, 623−637.

Sueleves, I., Lazaro, M., Moliner, R., Corbella, B., & Palacios, J. (2005). Hydrogen production by thermo catalytic decomposition of methane on Ni-based catalysts: Influence of operating conditions on catalyst deactivation and carbon characteristics. *International Journal of Hydrogen Energy, 30*, 1555−1567.

Takenaka, S., Shigeta, Y., Tanabe, E., & Otsuka, K. (2003). Methane decomposition into hydrogen and carbon nanofibers over supported Pd-Ni catalysts. *Journal of Catalysis, 220*, 468−477.

Tamme, R., Epstein, M., Fisher, U., Sugarmen, C., & Buck, R. (2001). Solar upgrading of fuels for generation of electricity. *Journal of Solar Energy Engineering, 123*, 160−163. http://dx.doi.org/10.1115/1.1353177.

US DOE. (2005). Roadmap for the hydrogen economy. In *Workshop on manufacturing R&D for the hydrogen economy*. Washington, DC: US Department of Energy.

US DOE. (2007). *Carbon sequestration technology roadmap*. Washington, DC: US Department of Energy.

US DOE/NETL. (2003). Carbon sequestration. Technology roadmap and program plan. In *US department of energy, office of fossil energy*. Morgantown, West Virginia: National Energy Technology Laboratory.

US DOE/NETL. (2012). *Cryogenic carbon capture*. US Department of Energy. ARPA-E project DE-AR0000101 http://www.netl.doe.gov/publications/proceedings/12/co2capture/

presentations/5-Posters/D%20Frankman-SES-Cryogenic%20Carbon%20Capture.pdf. Viewed 20.01.13.

Wilcox, J. (2012). *Carbon capture*. NY: Springer.

Wilson, E., & Gerard, D. (2007). *Carbon capture and sequestration. Integrating technology, monitoring and regulation*. Ames, Iowa: Blackwell Publishing.

Yan, W., & Hoekman, S. (2014). Producion of CO_2-free hydrogen from methane dissociation. *Environmental Progress & Sustainable Energy, 33*, 213−219.

Yokota, O., Oku, Y., Arakawa, M., Hasegawa, N., Matsunami, J., Kaneko, H., et al. (2000). Steam reforming of methane by using a solar simulator controlled by $H_2O/CH_4 = 1/1$. *Applied Organometallic Chemistry, 14*, 867−870. http://dx.doi.org/10.1002/1099-0739(200012)14: 12<867::AID-AOC99>3.0.CO;2-X.

Index

Note: Page numbers followed by "f" and "t" indicate figures and tables respectively.

This page intentionally left blank